Alexander G. Volkov *Editor*

Plant Electrophysiology

Methods and Cell Electrophysiology

Springer

Plant Electrophysiology

Alexander G. Volkov
Editor

Plant Electrophysiology

Methods and Cell Electrophysiology

Springer

Editor
Alexander G. Volkov
Department of Chemistry
Oakwood University
Adventist Blvd. 7000
Huntsville, AL 35896
USA

ISBN 978-3-642-29118-0 ISBN 978-3-642-29119-7 (eBook)
DOI 10.1007/978-3-642-29119-7
Springer Heidelberg New York Dordrecht London

Library of Congress Control Number: 2012937217

Printed on acid-free paper

Springer is part of Springer Science+Business Media (www.springer.com)

Preface

Plant electrophysiology is the study of the electrochemical phenomena associated with biological cells and tissues in plants. It involves measurements of electrical potentials and currents on a wide variety of scales from single ion channels to whole plant tissues. Electrical properties of plant cells mostly derive from the electrochemical properties of their membranes. Electrophysiological study of plants includes measurements of the electrical activity of the phloem, xylem, plasmodesmata, stomata, and particularly the electrical signals, propagation along the plasma membrane. Action potentials are characteristic responses of excitation that can be induced by stimuli such as: applied pressure, chemical substances, thermal stimuli, electrical or magnetic stimuli, and mechanical stimuli.

There are two major divisions of electrophysiology: intracellular recording and extracellular recording.

The electrical phenomena in plants have attracted researchers since the eighteenth century and have been discussed in a variety of books (Baluška et al. 2006; Bertholon 1783; Bose 1907, 1913, 1918, 1926, 1928; Lemström 1902; Ksenzhek and Volkov 1998; Volkov 2006; Volta 1816). The identification and characterization of bioelectrochemical mechanisms for electrical signal transduction in plants would mark a significant step forward in understanding this under-explored area of plant physiology. Although plant mechanical and chemical sensing and corresponding responses are well known, membrane electrical potential changes in plant cells and the possible involvement of electrophysiology in transduction mediation of these sense-response patterns represent a new dimension of plant tissue and whole organism integrative communication. Plants continually gather information about their environment. Environmental changes elicit various biological responses. The cells, tissues, and organs of plants possess the ability to become excited under the influence of certain environmental factors. Plants synchronize their normal biological functions with their responses to the environment. The synchronization of internal functions, based on external events, is linked with the phenomenon of excitability in plant cells. The conduction of bioelectrochemical excitation is a fundamental property of living organisms.

Electrical impulses may arise as a result of stimulation. Once initiated, these impulses can propagate to adjacent excitable cells. The change in transmembrane potential can create a wave of depolarization which can affect the adjoining resting membrane. Action potentials in higher plants are the information carriers in intracellular and intercellular communication during environmental changes.

The conduction of bioelectrochemical excitation is a rapid method of long distance signal transmission between plant tissues and organs. Plants promptly respond to changes in luminous intensity, osmotic pressure, temperature, cutting, mechanical stimulation, water availability, wounding, and chemical compounds such as herbicides, plant growth stimulants, salts, and water potential. Once initiated, electrical impulses can propagate to adjacent excitable cells. The bioelectrochemical system in plants not only regulates stress responses, but photosynthetic processes as well. The generation of electrical gradients is a fundamental aspect of signal transduction.

The first volume entitled "Plant Electrophysiology—Methods and Cell Electrophysiology" consists of a historical introduction to plant electrophysiology and two parts. The first part introduces the different methods in plant electrophysiology. The chapters present methods of measuring the membrane potentials, ion fluxes, trans-membrane ion gradients, ion-selective microelectrode measurements, patch-clamp technique, multi-electrode array, electrochemical impedance spectroscopy, data acquisition, and electrostimulation methods. The second part deals with plant cell electrophysiology. It includes chapters on pH banding in Characean cells, effects of membrane excitation and cytoplasmic streaming on photosynthesis in Chara, functional characterization of plant ion channels, and mechanism of passive permeation of ions and molecules through plant membranes.

The second volume entitled "Plant Electrophysiology—Signaling and Responses" presents experimental results and theoretical interpretation of whole plant electrophysiology. The first three chapters describe electrophysiology of the Venus flytrap, including mechanisms of the trap closing and opening, morphing structures, and the effects of electrical signal transduction on photosynthesis and respiration. The Venus flytrap is a marvelous plant that has intrigued scientists since the times of Charles Darwin. This carnivorous plant is capable of very fast movements to catch insects. The mechanism of this movement has been debated for a long time. The Chap. 4 describes the electrophysiology of the Telegraph plant. The role of ion channels in plant nyctinastic movement is discussed in Chap. 5. Electrophysiology of plant-insect interactions can be found in Chap. 6. Plants can sense mechanical, electrical and electromagnetic stimuli, gravity, temperature, direction of light, insect attack, chemicals and pollutants, pathogens, water balance, etc. Chapter 7 shows how plants sense different environmental stresses and stimuli and how phytoactuators respond to them. This field has both theoretical and practical significance because these phytosensors and phytoactuators employ new principles of stimuli reception and signal transduction and play a very important role in the life of plants. Chapters 8 and 9 analyze generation and transmission of electrical signals in plants. Chapter 10 explores bioelectrochemical aspects of the plant-lunisolar gravitational relationship. The authors of Chap. 11

describe the higher plant as a hydraulic-electrochemical signal transducer. Chapter 12 discusses properties of auxin-secreting plant synapses. The coordination of cellular physiology, organ development, life cycle phases and symbiotic interaction, as well as the triggering of a response to changes in the environment in plants depends on the exchange of molecules that function as messengers. Chapter 13 presents an overview of the coupling between ligands binding to a receptor protein and subsequent ion flux changes. Chapter 14 summarizes data on physiological techniques and basic concepts for investigation of Ca^{2+}-permeable cation channels in plant root cells.

All chapters are comprehensively referenced throughout.

Green plants are a unique canvas for studying signal transduction. Plant electrophysiology is the foundation of discovering and improving biosensors for monitoring the environment; detecting effects of pollutants, pesticides, and defoliants; monitoring climate changes; plant–insect interactions; agriculture; and directing and fast controlling of conditions influencing the harvest.

We thank the authors for the time they spent on this project and for teaching us about their work. I would like to thank our Acquisition Editor, Dr. Cristina Eckey, and our Production Editor, Dr. Ursula Gramm, for their friendly and courteous assistance.

Prof. Alexander George Volkov Ph.D.

References

Baluška F, Mancuso S, Volkmann D (2006) Communication in plants. Neuronal aspects of plant life. Springer, Berlin

Bertholon M (1783) De l'electricite des vegetaux: ouvrage dans lequel on traite de l'electricite de l'atmosphere sur les plantes, de ses effets sur leconomie des vegetaux, de leurs vertus medico. P.F. Didot Jeune, Paris

Bose JC (1907) Comparative electro-physiology, a physico-physiological study. Longmans, Green & Co., London

Bose JC (1913) Researches on irritability of plants. Longmans, London

Bose JC (1918) Life movements in plants. B.R. Publishing, Delhi

Bose JC (1926) The nervous mechanism of plants. Longmans, Green and Co., London

Bose JC (1928) The motor mechanism of plants. Longmans Green, London, UK.

Ksenzhek OS, Volkov AG (1998) Plant energetics. Academic, San Diego

Lemström S (1902) Elektrokultur. Springer, Berlin

Stern K (1924) Elektrophysiologie der Pflanzen. Springer, Berlin

Volkov AG (ed) (2006) Plant electrophysiology. Springer, Berlin

Volta A (1816) Collez ione dell' opera del cavaliere Conte Alessandro Volta. Nella stamperia di G. Piatti, Firence, Vol. 1.

Contents

Contributors

Elisa Azzarello Department of Plant, Soil and Environment, University of Florence, Viale delle Idee 30, 50019 Sesto Fiorentino, Firenze (FI), Italy

Mary J. Beilby School of Physics, The University of New South Wales, Sydney, NSW 2052, Australia, e-mail: m.j.beilby@unsw.edu.au

Mary A. Bisson Department of Biological Sciences, University at Buffalo, Buffalo, NY 14260, USA

Jayakumar Bose School of Agricultural Science, University of Tasmania, Private Bag 54, Hobart, TAS 7001, Australia

François Bouteau Sorbonne Paris Cité, Laboratoire d'Electrophysiologie des Membranes, Institut de Biologie des Plantes, Université Paris Diderot-Paris 7, Orsay 91405, France, e-mail: francois.bouteau@univ-paris-diderot.fr

Alexander A. Bulychev Department of Biophysics, Biology, Moscow State University, Moscow 119991, Russia, e-mail: bulychev@biophys.msu.ru

J. Theo M. Elzenga Plant Ecophysiology, University of Groningen, Nijenborgh 7, 9747 AG Groningen, The Netherlands, e-mail: j.t.m.elzenga@rug.nl

Emil Jovanov Electrical and Computer Engineering Department, University of Alabama, Huntsville, AL 35899, USA, e-mail: jovanove@uah.edu

Roger R. Lew Department of Biology, York University, Toronto, ON, Canada, e-mail: planters@yorku.ca

Stefano Mancuso Department of Plant, Soil and Environment, University of Florence, Viale delle Idee 30, 50019 Sesto Fiorentino, Firenze (FI), Italy, e-mail: stefano.mancuso@unifi.it

Vladislav S. Markin Department of Neurology, University of Texas Southwestern Medical Center, Dallas, TX 75390-8833, USA; Department of Chemistry, Oakwood University, 7000 Adventist Blvd, Huntsville, AL 35896, USA

Elisa Masi Department of Plant, Soil and Environment, University of Florence, Viale delle Idee 30, 50019 Sesto Fiorentino, Firenze (FI), Italy

Veronica A. Murphy Department of Chemistry, Oakwood University, 7000 Adventist Blvd, Huntsville, AL 35896, USA

Anthony J. Miller Department of Disease and Stress Biology, John Innes Centre, Norwich Research Park, Norwich NR4 7UH, UK, e-mail: tony.miller@jic.ac.uk

Ian Newman School of Mathematics and Physics, University of Tasmania, Private Bag 37, Hobart, TAS 7001, Australia

Lana Shabala School of Agricultural Science, University of Tasmania, Private Bag 54, Hobart, TAS 7001, Australia

Sergey Shabala School of Agricultural Science, University of Tasmania, Private Bag 54, Hobart, TAS 7001, Australia, e-mail: Sergey.Shabala@utas.edu.au

Virginia A. Shepherd Department of Biophysics, School of Physics, The University of NSW, Sydney, NSW 2052, Australia, e-mail: vas@phys.unsw.edu.au

Daniel Tran Sorbonne Paris Cité, Laboratoire d'Electrophysiologie des Membranes, Institut de Biologie des Plantes, Université Paris Diderot-Paris 7, Orsay 91405, France

Alexander G. Volkov Department of Chemistry, Oakwood University, 7000 Adventist Blvd, Huntsville, AL 35896, USA

Yi Wang College of Biological Sciences, China Agricultural University, #2 West Yuan Ming Yuan Rd., Beijing 100193, China

Part I
Methods of Plant Electrophysiology

Chapter 1
At the Roots of Plant Neurobiology

V. A. Shepherd

Abstract If biology throughout the nineteenth and twentieth centuries was dominated by the metaphor of the machine, the metaphor underlying twenty first century biology is that of the network or web. A rapid proliferation of molecular data coupled with increased computational power has revealed that gene regulation, protein interaction, the topology of metabolism and signal-transduction in and between cells, tissues, organs and organisms can all be described as robust, resilient and modular networks. Such small-world networks are characterised by rapid signal propagation, a capacity for computation and for synchronisation between the same, or different, hierarchic levels. Organelles, cells, tissues, organisms and ecosystems are not mere aggregations of components, but are hierarchies of interacting systems or modules, each possessing a degree of autonomy, and each a degree of interdependence. Into this metaphor of the network has emerged the discipline of integrative plant electrophysiology, called by its adherents, plant neurobiology. This field aims to understand how plants perceive, recall and process experience, coordinating behavioural responses via integrated information networks that include molecular, chemical and electrical levels of signalling. Integrative plant electrophysiology rejects the long standing view of plants as passive insensate automata that react to the environment with mechanical simplicity. The controversial use of the word 'neurobiology' as applied to plants signifies that long-distance electrical signals, such as action potentials, convey meaningful information from the site of initiation to a distant site, where the signal is interpreted and evaluated, and an adaptive behavioural

V. A. Shepherd (✉)
Department of Biophysics, School of Physics, The University of NSW,
Sydney, NSW 2052, Australia
e-mail: vas@phys.unsw.edu.au

V. A. Shepherd
Department of Biophysics, School of Physics, University of Western Sydney,
Blacktown Nirimba Campus, Quakers Hill, NSW 2762, Australia

A. G. Volkov (ed.), *Plant Electrophysiology*,
DOI: 10.1007/978-3-642-29119-7_1, © Springer-Verlag Berlin Heidelberg 2012

response is mounted. Such inter-module communication is 'nervous' in the sense that it is adaptive, thereby implying capacities for memory, learning, anticipating the future and for generating novel responses. By itself a touch stimulus is meaningless, and by itself a behaviour (e.g. *Mimosa* leaf folding) is meaningless. Meaning lies in the network of processes that associate and integrate these events. Communication processes within, and between plants and associated organisms, can therefore be considered as biosemiotic, involving as they do the interpretation and evaluation of stimuli. This review traces historical aspects of the development of integrative plant electrophysiology and the methods that inform it, with a special emphasis on the work of Indian biophysicist Sir J. C. Bose (1858–1937), who, in an impressive body of published research, proposed that plants and animals share essentially similar fundamental physiological mechanisms. The first scientist to appreciate that responses in plants (e.g. leaf folding in the sensitive plant *Mimosa*) constitute behaviour reliant on integrative electrical signals; Bose argued further that all plants co-ordinate their movements and integrate their responses to the world through electrical signalling. Despite their sessile habits, plants are to be regarded as sensate, active, intelligent explorers of the world. Bose identified a fundamental physiological motif that interlinked measurable pulsations or oscillations in cellular electric potentials with oscillations in cell turgor pressure, cellular contractility and growth. All plants respond to the world and to other living things through adaptations of this pulsatile motif, an electromechanical pulse that underlies electro-osmotically enacted behaviour. J.C. Bose's conclusions that all plants possess a nervous system, a form of intelligence, and a capacity for remembering and learning, were poorly received by prominent electrophysiologists of his time. Experiments devoted to plant responsiveness, inter-organism communication, kin-recognition, foraging, intelligence and learning as mediated by electrical signalling, are now published and debated in the mainstream literature as aspects of integrative plant electrophysiology.

1.1 Introduction: It's a Small World

> The two acts which seem to constitute the excitatory process, viz. excitation and response, are not continuous, but are joined together by a non-measurable link…. It is, in short, something which is involved in organism, for which the most proper designation is organismal. (Sir John Burdon-Sanderson 1904, cited by Haldane 1912).

In an emerging 'biosemiotic' understanding of life (Kauffman et al. 2008; Riofrio 2008) a living system processes, interprets and evaluates information that is meaningful in the sense that it is *about* the state of the external and internal worlds, requires interpretation by the system, and impels a response that propagates the organisation of the system. Thus, according to Kauffman et al. (2008), bio-information is semiotic or meaningful, and is therefore distinguishable from Shannon-type information, which, being non-semantic is inapplicable to biological systems.

> As part of the propagating organization within living cells, the cell operates as an information-processing unit, receiving information from its environment, propagating that information through complex molecular networks, and using the information stored in its DNA and cell-molecular systems to mount the appropriate response (Kauffman et al. 2008, p. 28).

In the early twentieth century plant electrophysiological research focused on entire and complex behaviours, such as trap closure in the Venus flytrap *Dionaea*, or leaf movements in *Mimosa* (the sensitive plant). Much subsequent electrophysiological research was impelled by mechanistic materialist philosophies of science, with a mission to deconstruct complex behaviours into the simpler properties of components, beginning with cells, and continuing into further minute levels of ion channels and genes. At the same time prominent scientists drew attention to the problem of integration that such studies pose. For example, Peters (1969) postulated a network theorem of cell function, and argued for the existence of a cell cytoskeleton that we now take for granted.

> There still remains the puzzle as to how the cell is integrated on a molecular basis, and adjusted to environmental stimuli and otherwise. Every change in the individual reactions of a cell is based upon some phase of chemistry or physical chemistry. Can we still believe, however, that the whole living cell is merely an extremely complex chemical equilibrium or have we still to look for some tenuous coordinating structure, fulfilling the role the nervous system does in the animal? (Peters 1969).

Peter's comments apply to other hierarchical levels of living systems, such as the whole plant. At the close of the twentieth century, increased computing power and the expansion of the World-Wide Web, coupled with the pursuit of genes and plant genomes, has enabled us to recognise the systems or network level of gene regulatory and metabolic networks, for example in *Arabidopsis* (reviewed, Yuan et al. 2008). If biology from the mid-nineteenth century and throughout the twentieth century had been dominated by the metaphor of the machine, as argued persuasively by Koestler (1978), the symbolism underlying twenty-first century biology has become that of the network or Web.

The proliferation of molecular data and rapid increase in computational power confirms that cells, organisms and ecosystems behave as networks of a special kind, the so-called small-world, or scale-free network (Strogatz 2001, 2003). These are not purely scale-free networks, but contain a hierarchy of modules (Ravasz et al. 2002) such as sets of genes, metabolons, cell groups or modules, tissues, organs interlinked by communication pathways and so on. Protein interaction networks, gene regulation networks, signal-transduction pathways, the large-scale topology of metabolism and cellular interactions, can all be described mathematically as modular small-world networks (reviewed, Albert 2005). In the 1990s cell biology began its ongoing shift from a molecular to a modular approach (reviewed by Hartwell et al. 1999) and this has revealed many surprising similarities between animals and plants. For example, defects in homologous modular gene networks common to *Arabidopsis* and humans leads in one instance to disrupted negative gravitropism in the plant, and neural crest defects resulting in craniofacial disease in humans (McGary et al. 2010).

Small-world networks seem to be inherent in the way living systems are organised. Not only protein to protein interactions, gene regulation, the topology of metabolism, but the human nervous system, gossip networks, networks of scientific collaboration and citation, Internet and peer group connectivity, and the structure of language behave as small-world networks (Strogatz 2001).

Small-world networks are collectives of nodes and the edges or paths that connect them as conduits for the flow of bio-information. On a cellular level, paths can be directed from one node to another, as in substrate to product, or non-directed, in which mutual interactions occur, such as the binding of one protein by another. Some nodes (hubs) are highly clustered, meaning that they connect to many or even all other nodes, whilst others are poorly connected. The power-law distribution of node connectivity makes these networks extremely robust and resilient with inbuilt redundancy. A key point is that the mathematical structure of small-world networks endows them with

> enhanced signal propagation speed, computational power and synchronisability (Watts and Strogatz 1998).

The deconstruction of the behaviours of organisms and cells into the simpler properties of component molecules has culminated in the elucidation of genomes. So successful has this approach been that it has begun, like the ouroborus, to devour its own tail. The vast extent of networked epigenetic regulation has now been recognised, and the emerging concept of 'a gene' is now 'a field of possibility' (reviewed by Jorgensen 2011). Nucleic acid sequences are the foci of alternative chromatin states, which are responsive to developmental or environmental circumstances. Barbara McClintock's concept of a genome that can be rapidly reorganised in response to specific or novel challenges (Keller 1983) has moved to the forefront.

In plants, gene expression is responsive to environmental stimuli transmitted via electrical signals between distant tissues. As a classic example, a flame wound activates proteinase inhibitor genes in distant tissues via an electrical signal (Wildon et al. 1992), called by them an action potential, but which was probably a variation or slow-wave potential (Davies 2004, 2006). Gene expression in plants is responsive to stimuli including light, osmotic conditions, and gravity, through the cellular calcium signalling network that Trewavas and Malho (1998) have called 'the big network'.

The root–shoot polarity is fundamental to plant life. At the level of integrative signalling, the neural system of plants (reviewed by Barlow 2008) embraces the vascular tissues; phloem, now widely acknowledged as the living conduit through which fast-moving long-distance action potentials are transmitted, and xylem, through which the slow-wave or variation potentials stimulated by wounding may travel; as well as a postulated integrative centre or "root-brain" at the root apex transition zone (Baluska et al. 2004), whose cells emit synchronised electrical spikes (Masi et al. 2009). In terms of small-world network theory, this would be less a 'command centre' than a hub, a node which connects to most or all other nodes in the network.

The medium (network) is truly the message. Events perceived at the level of roots translate into adaptive action at the leaves. For example, water-stressed maize responds to onset of watering with root-initiated action potentials transmitted via the phloem to the leaves, where the rates of CO_2 and H_2O exchange subsequently increase (Fromm and Fei 1998). The guard cells regulating this gas exchange behave as networks. For example, conductance of stomata is 'patchy' in that coherent groups of stomata can independently adjust their conductance, and stomatal patches can oscillate in phase with distant patches on the same leaf, implying long-distance interaction (reviewed by Mott and Buckley 2000). Similarly, foraging by roots and leaves (now commonly referred to as 'foraging strategy') is plastic and adaptive and involves integration of local and systemic responses (reviewed by de Kroon et al. 2009). The plant is

> …an interconnected network of modules, each with the ability to sense and respond to its environment (de Kroon et al. 2009).

Decisions about branching frequency are made locally and involve local signals within a module such as shoots or roots, but can be modified by signals emerging from other connected modules, resulting in

> …integrated and adaptive response at the level of the whole plant to its whole environmental context (de Kroon et al. 2009, p. 705).

Although once controversial, it is now fully accepted that plants employ electrical signals in the integration of their responses to the world. Stimuli such as changes in light, temperature, water potential (or turgor pressure from a cell's point of view), touch, wounding, sound (Telewski 2006) or volatile chemical signals, can induce electrical signals including receptor potentials, rapidly propagated action potentials and slow wave or variation potentials (reviewed Fromm and Lautner 2007).

In this age of networks, signal propagation, synchronisation and computation (in loose terms, a capacity for acquiring and assessing information, or decision making) have emerged as research priorities in integrative plant electrophysiology. These issues are central to our understanding of how, for example, roots may succeed in mining for mineral nutrients in the same place for hundreds or even thousands of years (Frommer 2010), and how, at the same time, leaves may position themselves for harvesting the light energy that is the portal for energy to enter the biosphere, whilst moderating the rate of photosynthesis according to water status of different regions of the root system (Fromm and Fei 1998).

Controversy over the use of terminologies usually not associated with plants (such as 'intelligence', learning', 'memory' or 'nervous system') is resolvable within the context of Living Systems Theory (Barlow 2008) where each level of biological organisation (e.g. cell, tissue, organ, organism and ecosystem) is supported by a set of critical subsystems, which repeat at each level, building a 'self-similar organisational hierarchy' (Barlow 2008). This concept endows the small-world network with the aspect that is critical to life- meaning. It removes the

loaded word ‘intelligence’ and considers instead information processing by living systems and their subsystems.

This returns us to the study of complex plant behaviours that began in the nineteenth and early twentieth centuries. Informed by the twenty first century concepts of the behaviour of networks, and with an impetus towards integration, we can employ the techniques of vast computational power, multiple electrode systems, faster data acquisition and analysis, and advanced imaging in an attempt to grasp the behavioural complexity of plants.

Histories are relational. As genes may be fields of possibility, existing in alternative states according to the circumstances surrounding them, histories unfold differently according to the focus of the compiler. The review that follows does not attempt to cover the rich and complex history of plant electrophysiology but takes as its focus the position of integrative plant electrophysiology. It includes a brief history of the research of Jagadis Chandra Bose, who had at the turn of the last century had so controversially argued that plants are integrated by the functional equivalent of a nervous system. In so doing the review refers to current and past advances in the electrophysiology of complex plant behaviours.

1.2 A Short History of ‘Animal and Vegetable Electricity’

1.2.1 The Discovery of Animal Electricity: Galvani and Volta

> “I am attacked by two opposite sects- the scientists and the know-nothings”, wrote Luigi Galvani, “Both laugh at me, calling me the ‘frog’s dancing master’. Yet I know that I have discovered one of the greatest forces in nature” (cited by Verkhratsky et al. 2006).

Electrophysiology can be approached from two directions, the integrative and the reductive. Perhaps neither is complete without the other. The last in Galvani’s famous series of experiments with twitching frog’s legs can be called integrative, for he showed that muscles contracted when a frog’s leg was touched with the long sciatic nerves of the animal’s exposed spinal cord (Verkhratsky et al. 2006). In his 1791 publication, De Viribus Electricitatis in Motu Musculari Commentarius, Galvani regarded this ‘animal electricity’ or ‘electric fluid’ as the force integrating animal behaviour. His viewpoint, and perhaps his growing fame, led to a long-lasting and acrimonious scientific dispute with his compatriot, Volta.

In Galvani’s earlier series of experiments the frog leg muscles had contracted when an electrical circuit was made between nerve, two dissimilar metals in series, and another part of a frog’s body. Volta, sceptical and competitive, insisted that the electric current was reducible to the metallic interface in the circuit, and had nothing to do with ‘animal electricity’. Through sustained efforts to refute Galvani, Volta discovered bimetallic electrical conduction, and he invented the Voltaic battery in 1880 (Verkhratsky et al. 2006). After refusing to support Napoleon’s takeover of Bologna, Galvani suffered political persecution, lost his home,

his university position and his fortune. Volta, on the other hand, presented the battery to Napoleon, accepted a gold medal and became a successful politician.

Although criticised as a quasi-mystical vitalist by Volta and others, Galvani's explanation for 'animal electricity' (as the result of accumulated positive and negative charges on the inner and outer surfaces of nerve and muscle, where water-filled pores facilitated current flow; Piccolino 2006), anticipated Bernstein's later Membrane Theory of bioelectric potentials. The controversy over the existence of 'animal electricity' was resolved in 1779, shortly before Galvani's death, when von Humboldt proved the existence of both Galvani's 'animal electricity' and Volta's 'bimetallic electricity' (Becker and Marino 1982). Galvani and Volta were both partly right and partly wrong.

By the mid-nineteenth century, German mechanistic materialist philosophies had begun to influence the science of physiology, and hierarchically organised and bureaucratised research institutes began to emerge, in which scientists operated, in today's jargon, as technologists, managers and entrepreneurs (Veit-Brause 2002). The analytic–summative philosophy of science (Agutter et al. 2000) imbued the discipline of physiology with the idea that organisms are machines—Descartes' 'bete machine' (Drack et al. 2007). As a tenet of Descartes, philosophy, cells, tissues and organisms respond passively to the physical and chemical features of their environments as

> …flotsam on a physico-chemical ocean… (Agutter et al. 2000).

The New Physicalist School, including Du-Bois-Reymond and his student Bernstein, focussed on the nerve action potential with the aim of dispelling 'Naturphilosophie' and what they perceived to be the fog of vitalism, seeking a purely physico-chemical explanation for 'animal electricity' (Veit-Brause 2002).

Nobili's 1858 invention of the galvanometer, an instrument that could detect the flow of electrical currents, enabled Du Bois-Reymond to show that stimulation of a nerve resulted in a propagated electrical disturbance (depolarisation) that provoked muscle contraction. Du-Bois-Reymond's student Julius Bernstein took this discovery further, inventing the 'rheotome' or 'current slicer', a galvanometer with a timer and sampling device with which, in 1868, he produced the first true recordings of nerve action potentials, measuring their velocity at 25–30 ms^{-1} (Seyfarth 2006). In 1902, Bernstein formulated his Membrane Theory, incorporating Nernst's equations describing electrocatalytic theory, and Ostwald's concept of a semi-permeable lipid membrane. The Membrane Theory in essence described a cell as an electrolytic solution bounded by a selectively permeable membrane. This physico-chemical theory provided a satisfying mechanistic explanation for 'animal electricity', and it was widely accepted from the mid-1930s.

In 1873, a few years after the first measurement of animal action potentials, Sir John Burdon-Sanderson proved that trap closure in the Venus flytrap was brought about electrically, via action potentials that could travel at 20 cm s^{-1}. Later, Bose (1913) published detailed evidence that leaf movements in the sensitive plant *Mimosa* were induced by action potentials, propagated through the phloem, which he controversially argued was the plant equivalent of a nervous system.

This concept of nerve-like electrical signalling in *Mimosa* was unpopular at a time when many scientists sought to construct a purely physico-chemical theory of life (Agutter et al. 2000), exorcising vitalism, Romantic notions like Gustav Fechner's 'soul of plants' and interpretations of plant response that were reminiscent of animal behaviour.

The field of plant cellular electrophysiology was born within a theoretical scaffolding of membrane biophysics in the same era that saw acceptance of Bernstein's Membrane Theory. In 1930, Umrath succeeded in using intracellular microelectrodes to record action potentials from single giant *Nitella* cells, and continued improvements in electrometers, pen recorders and glass microelectrodes enabled the field of membrane biophysics to burgeon (reviewed by Hope and Walker 1975). The pace at which new techniques appeared and were applied accelerated (reviewed by Verkhratsky et al. 2006). Cole developed voltage-clamping in 1939; Hodgkin and Huxley applied it almost immediately, and produced the H–H membrane theory of excitation with indications of ion channel activity. Ling and Gerard developed a minimally invasive microelectrode technique in 1949, and Neher and Sakmann introduced patch-clamping of single ion channels in the 1980s. The techniques emerging from animal cell physiology were widely adapted and contemporaneously applied by plant cell electrophysiologists (reviewed by Hope and Walker 1975).

Whilst some researchers continued to focus on the electrophysiology of complex plant behaviours (reviewed, Sibaoka 1969, 1991; Pickard 1973; Davies 1987a; Wayne 1994), application of the patch-clamp technique had by the 1980s revealed the existence of plant ion channels underlying action potentials and other electrical signals (reviewed by Hedrich and Schroeder 1989), and a plethora of plant ion channels was identified. The molecular biology revolution pursued genes and plant genomes that specify such proteins, and the first complete genome sequence (*Arabidopsis*) was published in 2000.

1.2.2 The Discovery of Vegetable Electricity: Enter J.C. Bose

The discovery of 'vegetable electricity', in the sense of propagated electrical signals as integrative signals in all plants, took place in circumstances equally as contentious as the dispute between Galvani and Volta.

At the beginning of the twentieth century the Indian biophysicist Jagadis Chandra Bose (Fig. 1.1) was already well known and respected for his ingenuity and perspicacity in the field of microwave physics. In a prolific 5 years, from 1894 to 1899, Bose performed and published innovative research into the physics of electromagnetic waves. Between 1985 and 1900, Bose published ten papers in the *Proceedings of the Royal Society*, all of them communicated by Lord Rayleigh, and others in the "Philosophical Magazine" and "The Electrician" (Sengupta et al. 1998). This work was admired by distinguished physicists of the time, including Lord Rayleigh and J.J. Thompson. Many of Bose's inventions, including

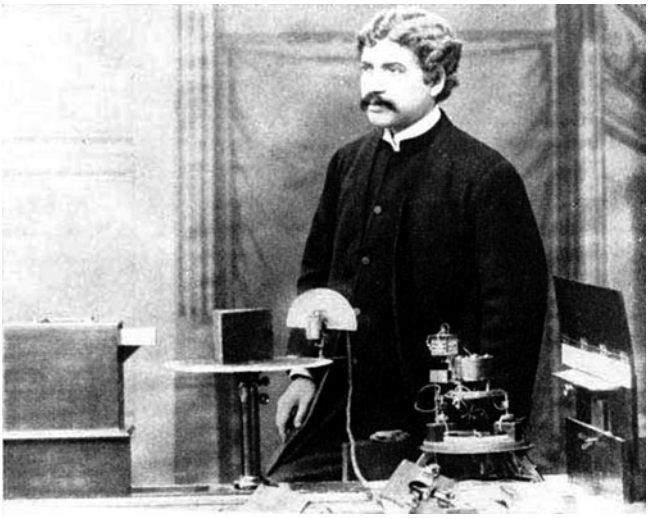

Fig. 1.1 J. C. Bose at the Royal Institution, London, with his radio equipment. The date is 1897, prior to his plant research

the world's first solid-state semi-conductor diode, are now devices taken for granted in contemporary microwave technology. Bose invented the 'coherer', a semiconducting diode device, which was adapted by Marconi for use in trans-atlantic wireless signalling.

Over a decade of research had established for Bose an enduring reputation as an inventor and physicist of extraordinary originality and perspicacity. Not only had he discovered millimetre waves, using ingenious devices of his own invention to generate them, but he laid bare most of their properties, and invented the 'eye' ('coherer') or receiver that would detect them (Engineer 2009). In the process, Bose published increasingly daring, original and inspired papers (Engineer 2009) in prestigious journals including *Proceedings of the Royal Society*, the "Philosophical Magazine" and "The Electrician" (Engineer 2009; Sengupta 2009; Sengupta et al. 1998; Bondyopadhyay 1998; Emerson 1997; Mitra 1997; Ramaseshan 1996).

This research, applauded in its time, continues to inspire today. Concepts from Bose's 1897 Royal Society paper were incorporated into the design of a 1.3 mm multibeam receiver, part of a 12 m telescope at the National Radio Astronomy Observatory in Tucson, Arizona (Emerson 1997) and Bose's one patented invention, the Detector for Electrical Disturbances, was the world's first solid-state semiconductor diode detector, a galena crystal detector sensitive to microwave/millimetre and optical waves (Engineer 2009; Bondyopadhyay 1998; Bose 1904).

Without semiconductors, today's networked world is truly unimaginable.

In around 1900, J.C. Bose began his plant electrophysiological research, becoming in the process one of the earliest biophysicists. He pursued this research

until his death in 1937 (Shepherd 1999, 2005). His hard-won reputation as a physicist of originality and insight was almost immediately overwritten, in Western botanical and electrophysiological circles, by a kind of notoriety, an image as mystic, maverick and outsider. Nonetheless, he established a nascent field of integrative plant biophysics.

Bose has been criticised for holding vitalist views (Nandy 1995), but he was actually critical of vitalism. Whilst the vitalists had asserted a dualism between living and non-living things, in which the former were animated by a non-material force, an entelechy or *vis viva* that some had equated with 'animal electricity', Bose argued against 'vital forces' on the basis that there existed no sharp demarcation between the realms of the living and non-living—these were parts of a continuum. Life did not emerge de novo from the physico-chemical realm, but rather its properties were pre-figured and already inherent in matter. In this, Bose was allied more closely with the later process philosophers, including Alfred North Whitehead.

Bose began by applying delicate instrumentation he had invented in his semiconductor research to deliver electrical stimuli and record electrical responses from various plant parts, including leafy stalks of horse chestnut, plane tree, celery, turnip, cauliflower and Eucharis lily, the storage roots of carrot and radish, the flower stalk of the Arum lily and the fruit of the eggplant (Bose 1902). He discovered that both living animal and plant tissues exhibited a diminution of sensitivity after continuous stimulation, recovery after rest, a 'staircase' or summation of electrical effects following mechanical stimulation, abolition of current flow after applying poisons and reduced sensitivity at low temperature. Strong and feeble mechanical stimuli produced bioelectrical responses of opposite polarity in the mechanically stimulated radish. The published record clearly shows what today would be called receptor potentials, small touch-induced transient depolarisations that precede an action potential. Furthermore, the form and polarity of these potentials depended on the condition and history of the plant and upon viability. Responsiveness disappeared when the tissue was killed with steam.

Having reported his results at numerous prestigious meetings and institutions, including the Friday Evening Discourse of the Royal Institution, May 1901, and at the Royal Society in June 1901, Bose wrote

> … the wave of molecular disturbance in a living animal tissue under stimulus is accompanied by a wave of electrical disturbance; … in certain types of tissue the stimulated region is relatively positive to the less disturbed, while in others it is the reverse; … this characteristic of exhibiting electrical response under stimulus is not confined to animal, but extends also to vegetable tissues. In these the same electrical variations as in nerve and muscle were obtained … (Bose 1902).

In the audience for the 1901 lecture at the Royal Society were the two prominent electrophysiologists, Sir John Burdon-Sanderson and Auguste Waller, each now poised to become a professional nemesis to Bose, who stated

> …every plant, and even the organ of every plant, is excitable and responds to stimulus by electric response… (Bose 1913),

and postulated the existence of a 'vegetable electricity' as the counterpart of 'animal electricity'.

It was in this lecture that Bose also drew analogies between the semiconducting characteristics of metals, and the changes in electric potentials he had measured following mechanical stimulation of plant tissues. Eager to prove his non-vitalist stance (that there exists no sharp demarcation between the living and the non-living), Bose drew analogies between changes in semiconducting properties of metals following 'stimuli' (such as fatiguing and poisoning) and the responses of living tissues to similar stimuli—as if matter (the metals), had, in some sense, proto life-like properties. This attempt to reconcile the difficulties inherent in explaining the meaningful nature of a plant's response to stimulation in terms of physico–chemical theory (biology's central problem, according to Bose's contemporary J.S Haldane, the son of Burdon-Sanderson) was poorly received.

The professional conflicts that subsequently arose between Waller and Bose have been eloquently reconstructed and analysed in Dasgupta's comprehensive article (Dasgupta 1998). Whilst Burdon-Sanderson, the first to have measured action potentials in the Venus flytrap, maintained that excitation was restricted to such strange and exceptional plants and strongly objected to the use of the physiological word 'response' in connection with metals, Waller, although hostile, made no comment. However, in November 1901 Waller published his own paper, 'Electrical response of vegetable protoplasm to mechanical excitation' in the *Journal of Physiology*, reporting, amongst other things, electropositive (depolarisation) responses to mechanical stimulus in parts of ordinary plants (e.g. the vine-shoot), exactly as Bose had done.

Both Waller and Bose then claimed priority for the discovery of 'vegetable electricity'. Professors Vines and Howes of the Linnaean Society, who had read proofs of Bose's 'vegetable electricity' manuscript, archived without publication by the Royal Society 5 months before Waller's claim to priority, established a committee of inquiry of the Linnaean Society (Geddes 1920). The inquiry granted Bose priority, but the damage was done. The roots of a professional conflict were deeply established.

Burdon-Sanderson later scathingly reviewed and recommended rejection of a *Mimosa* paper submitted by Bose to the *Philosophical Transactions of the Royal Society of London*. Paul Simons, describing the incident, writes,

> …The attitude of Burdon-Sanderson, the pioneer of plant electrophysiology, was altogether more baffling. He too refused to believe Bose's results. Why he was so antagonistic amazes me. Was it professional jealousy because he himself had not investigated the Mimosa?' Was it because Bose did not cite Burdon-Sanderson's paper on the Venus Flytrap?

Simons (1992) writes that doubt was cast on Bose's professional competence. Bose was controversial, he had said that there was no demarcation between life and non-life (had he actually said that metals are alive?), and furthermore the Victorian science establishment in England was not well-disposed towards mavericks. To Bose, the problem was more easily understood:

> …I had unwittingly strayed into the domain of a new and unfamiliar caste system, and so offended its etiquette…, he wrote, '…an unconscious theological bias was also present…. To the theological bias was added the misgivings about the inherent bend of the Indian mind towards mysticism and unchecked imagination…. Thus no conditions could have been more desperately hopeless than those which confronted me for the next twelve years…' (Bose 1917).

1.3 Bose's Research: The Biophysics of Plant Behaviour and Response

> I once did not know that these trees have a life like ours…they eat and grow…face poverty, sorrows and suffering. This poverty may…induce them to steal and rob…they also help each other, develop friendships, sacrifice their lives for their children… (JC. Bose cited in Nandy 1995, p. 46).

Seeking unifying principals underlying apparent disparities between animal and plant responses, Bose invented original and ingenious instruments that enabled him to simultaneously measure bioelectric potentials and to quantify very small movements in plants.

> But since plants for the most part seem motionless and passive….. limited in their range of movement, special apparatus of extreme delicacy had to be invented, which should magnify the tremor of excitation and also measure the perception period of a plant to a thousandth part of a second. Ultra-microscopic movements were measured and recorded, the length measured being often smaller than a fraction of a single wave-length of light (Bose 1918).

From amongst the numerous plants with which Bose worked, this review concentrates on the suite of experiments employing touch-sensitive plants, including *Mimosa pudica*, plants that perform spontaneous movements, such as the Indian telegraph plant *Desmodium*, as well as some 'ordinary' plants (e.g. *Phoenix dactylifera*, the Praying Palm of Faridpur, or *Musa*, the banana palm) that were neither dramatically touch-sensitive nor spontaneously motile.

Bose viewed each of the experimental plants as an individual whose history determined the nature of its response to the environment. He noted that seedlings germinated from the same batch of seed and raised under three different environmental conditions responded differently to application of a poison—the first batch was killed, the second recovered and a third batch was stimulated. Therefore, Bose did not pool his experimental data or subject it to statistical analysis. Rather, he was interested in the individually variable behaviour of each plant. Whilst contemporary plant physiological experiments strive to control and make consistent the environmental conditions, Bose regarded constant environment change as being essential for plant behaviour to reveal itself;

> …the continuance of normal functions depends on external stimulus…deprivation of stimulus reduces plants to an atonic condition in which all life-activities are brought to a standstill…rhythmic activities are maintained…by stimulus… (Bose 1923, p. 245).

The velocity of the transmitted electrical excitation in *Mimosa* depended on the tonic condition of the plant. A plant in optimum condition showed a rapid velocity of excitation, but excessive stimulation also resulted in rapid fatiguing of the response. A subtonic plant responded to stimulus with an excitation of slower velocity, but excessive stimulation actually enhanced the response. This dependence on the strength and duration of previous stimulations indicated a form of learning that had to be considered when interpreting experiments.

> A plant carefully protected under glass from outside shocks looks sleek and flourishing, but its higher nervous function is then found to be atrophied. But when a succession of blows is rained on this effete and bloated specimen, the shocks themselves create nervous channels and arouse anew the deteriorated nature… (Bose 1917).

Thus, the velocity of electrical transmission was modified by

> …individual vigour…temperature, and by the season. In summer, the velocity in thick petioles is 30 mm/s, in winter, as low as 5 mm/s…" (Bose 1926, p. 63). The age of organs was also influential; "…It is impossible to dissociate from the consideration of the age of a leaf its previous history as regards the stimulus of sunlight…the uppermost or youngest leaf of Mimosa [is] pre-optimum and less sensitive…the sensitiveness…[reaches a] maximum as we descend lower…continuing to descend…excitability [is] progressively decreased… (Bose 1913, p. 267).

The standardised conditions of many plant physiological experiments, with constant light period, constant temperature, uniform watering, may not only produce the effete and bloated specimens Bose deplored, but the application of statistical analyses to such experiments will conceal the subtleties of individual plant behaviours that were a focus of Bose's research.

Many of Bose's experiments were published in books, probably because the research papers he submitted to prominent journals were archived for years, without publication. Of hundreds of intricate experiments using original and ingenious apparatus, reported in books, research papers and essays, I confine myself to a brief overview of those studies where Bose coupled specific plant behaviours with electrical and hydraulic signals. Four books are considered here; "Researches into the Irritability of Plants" (1913), "Life Movements in Plants" (1918), "The Ascent of Sap" (1923) and "The Nervous Mechanisms of Plants" (1926).

Bose (1913, 1918, 1923, and 1926) aimed to compare and contrast three kinds of responses. These were:

1. *Contractility* (plant movements, following a stimulus). For example, the *Mimosa* or "touch-me-not" plant folds its leaflets and dips the entire leaf as a response to being touched.

2. *Rhythmicity* (plant movements taking place automatically, analogous to a heartbeat: Bose 1913, p. 202). The Indian Telegraph Plant *Desmodium* (Bon Charal or "forest churl") has a trifoliate leaf, whose two small lateral leaflets make mysterious spontaneous gyrations of regular periods. Bose found that *Biophytum* was capable of both contractile and rhythmic responses. Stimulus-induced and spontaneous movements both took place in the same plant, depending on the strength of the stimulus and the individual's history (Bose 1913, p. 289). All plants showed rhythmic or pulsatile growth.
3. *Conductivity* (transmission of electrical excitation associated with plant movements).

Bose also investigated ordinary plants that made no obvious dramatic movements. These included *Chrysanthemum*, trees such as *Ficus*, *Nauclea*, the mango, monocotyledons including the banana (*Musa*), palms, and fruits and other organs, including the tomato, turnip, carrot and potato.

Bose invented unique instruments for simultaneously measuring bioelectric potentials and for quantifying very small movements in plants (Figs. 1.2a–d, 1.3a–e). Many of these instruments are still in working order, and housed in the Museum of the Bose Institute in Kolkata, India. With its frictionless jewelled bearings, and lightweight aluminium lever connected to the leaf, the delicate Resonant Recorder (Bose 1913) used a vertical lever to 'write' leaf movements (plant response) on a smoked glass plate that moved at a regular rate using a clockwork mechanism. The problem of friction of the writer against the smoked glass plate was solved by having the writer vibrate or resonate, making intermittent contacts with the plate (Bose 1926, p. 55). Leaf movements were recorded with precision (at intervals of 1/100th of a second)—and "the record is thus its own chronogram" (Bose 1913, p. 22).

Other extraordinary delicate instruments included the High Magnification Crescograph, which magnified increments of growth up to ten thousand times. A plant holder was connected via a series of gear wheels driven by a falling mass and controlled by a fan governor, and descended at various rates, compensating for the growth of the plant. When the rate of growth was exactly balanced with the movement of the plant holder, the record showed a horizontal line. An increase or decrease in the growth rate was reflected in a rise or fall in the record. Bose wrote that the Crescograph could detect and plot a change in growth rate as small as one in 27,000.

The Electric Probe, an early microelectrode, consisted of a fine platinum wire enclosed in a glass capillary, except at the tip. In circuit with a galvanometer, the probe could be advanced into plant tissue at fine intervals of 0.1 mm.

In addition to these instruments for measuring and plotting plant movements and changes in electrical polarity, Bose introduced techniques for electrical stimulation of different intensity. An induction coil, using a slide (potentiometer) to generate feeble (0.5–8 μA) or strong (100 μA) currents could be appended to any of the instruments so that movements or changes in electric potential could be monitored whilst stimulation from electric current was applied. Bose reported that

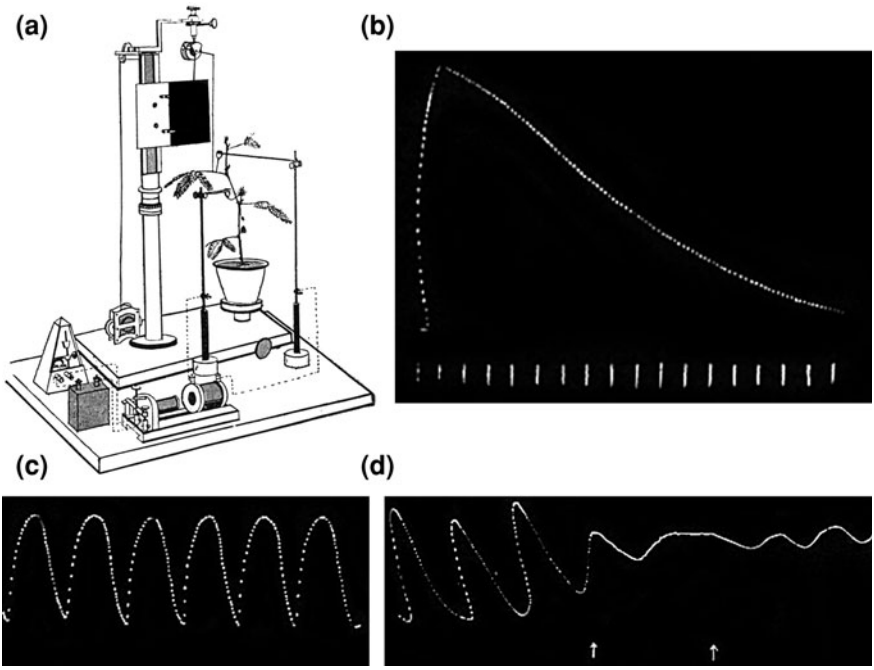

Fig. 1.2 Some of Bose's equipment and some measurements he made with it. **a** The resonant recorder (reproduced from Fig. 4, Bose 1913). This device had "frictionless" jewelled bearings, a fine lightweight *horizontal* lever connected to the pulvinus or leaf, and a *vertical* lever for writing the response on a smoked glass plate, which moved at a uniform rate using a clockwork mechanism. In this configuration, the duration of an "induction shock" applied to *Mimosa* was determined by a metronome, which completed the electric circuit. The illustration shows a *Mimosa* plant ready for measurement of leaf movements. **b** The record shows the leaf-dropping response in *Mimosa* measured with the resonant recorder (reproduced from Fig. 14, Bose 1913). Dots are at 1/10 s intervals during the "contractile" or leaf-dropping phase and at 10 s intervals during recovery. *Vertical marks*, 1 min intervals. **c**. The rhythmic gyrations of the leaflets of the telegraph plant *Desmodium* (reproduced from Fig. 145, Bose 1913). Individual dots are 2 s apart. This leaf was measured in summer and the whole period is about a minute, although in winter this increased to 4–5 min. **d.** Arrest of spontaneous movements in *Desmodium* by a cut applied at the first arrow. The pulsatile movement was revived by an electric shock at the second arrow. An electrical stimulus could substitute for a mechanical one. (Reproduced from Fig. 145, Bose 1913)

plants were in some cases more sensitive to electrical currents than animals. *Biophytum* responded to a feeble stimulating current of about 0.5 μA (Bose 1913, p. 27), which was too feeble for his own tongue to detect (Bose 1923). The

> ..sensitiveness of Mimosa to electrical stimulation is high and may exceed that of a human subject. (Bose 1913, p. 51).

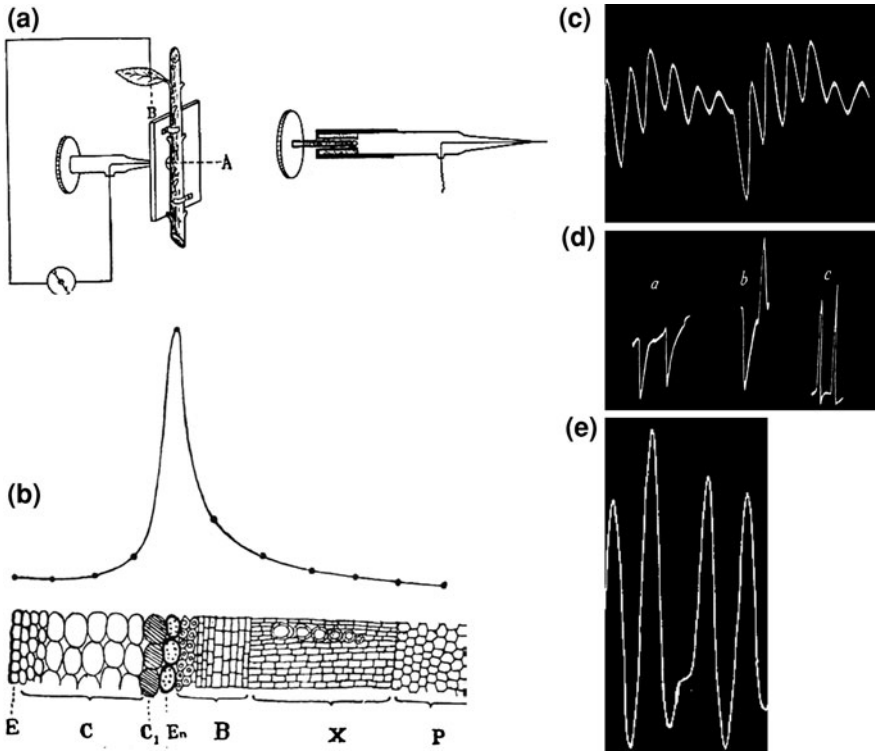

Fig. 1.3 **a**. The Electric Probe (reproduced from Fig. 75, Bose 1923). The tip of the Probe was in circuit with either a sensitive or Einthoven galvanometer, and the device could be driven, by small (0.1 mm) increments into the tissue by turning the screw. Bose achieved remarkable precision of measurement—a deflection of 1 mm PD between electrodes was equivalent to a 1 mV deflection of the galvanometer. In some cases, he measured potentials as small as 0.1 mV. The tip of the probe enters at A, and a reference contact is made with a distant or dead leaf. The micrometric screw enables the probe to be gradually introduced. **b**. A section of a *Brassica* petiole showing the relative cellular activity in terms of electromechanical pulsations, measured with the electric probe. The pulsations occur mainly in the inner cortical layer abutting the endodermis. Reproduced from Fig. 77, Bose 1923. **c**. Regular electromechanical pulsations in the cortical cells of *Musa*, the banana. Bose used an Einthoven galvanometer to measure the amplitude of these pulsations in *Nauclea* as *0.4 mV, and lasting *13.5 s. Reproduced from Fig. 71, Bose 1913. **d**. Three kinds of electrical response to electrical stimulus in *Musa*, the banana. The *first* (a) shows hyperpolarisation following indirect stimulus (feeble stimulus applied at a distance from the responding point), and this was coupled with the leaf erectile response. The *second* (b) shows biphasic response with stronger stimulus—a hyperpolarisation followed by a depolarisation. The *third* (c) shows the depolarisation response with direct stimulus, applied close to the responding point, and accompanied by turgor decrease. Reproduced from Fig. 80, Bose 1918. **e**. Periodic groupings of the electrical oscillations in the pulvinus of *Desmodium* (reproduced from Fig. 69, Bose 1923), which accompanied the mechanical oscillations of leaflet position

His numerous experimental set-ups enabled Bose to perform complex experiments, which would be challenging to execute today. He could simultaneously measure plant movements and electric potentials, measure very small electrical oscillations, apply mechanical stimuli and electrical stimuli, vary hydrostatic pressures, apply chemical inhibitors or poisons (e.g. KCN, HCl, NH_4, H_2S, NO_2, SO_2, anaesthetics such as chloroform and ether), suddenly modify temperature, vary light conditions and measure tiny growth increments over very short time intervals.

1.3.1 Plant Nervous Systems: The Mimosa and Desmodium Work

1.3.1.1 Intimate Coupling of Hydraulic and Electrical Signalling

Bose interpreted his results as constituting evidence that plants possess the equivalent of a well-defined nervous system. All plants co-ordinate their movements and integrate their responses to the environment via propagated electrical signals. All plants have an electromechanical pulse, and are capable of intelligent behaviour, memory and learning. Plants have receptors for stimuli, conductors (plant nerves), which electrically code and propagate the stimulus, and effectors, or terminal motor organs. The

> …physiological mechanism of the plant is identical with that of the animal… (Bose 1926, p. 9).

> …All plants and their organs are excitable, the state of excitation being manifested by an electric response of galvanometric negativity [relative depolarisation] (Bose 1926, p. 95).

> It can only be in virtue of a system of nerves that the plant constitutes a single organised whole, each of whose parts is affected by every influence that falls on any other (Bose 1913, p. 121).

Bose's contemporaries Pfeffer and Haberlandt had reasoned that the collapse of leaves following touch stimulus in *Mimosa* was not a true excitation, but rather a sort of 'hydraulic lift', 'a disturbance of hydrostatic equilibrium within the transmitting elements', which were situated within the leptome, or phloem (reviewed, Haberlandt 1928). Haberlandt reasoned that the shock-induced movement of a leaflet exerted pressure on these transmitting cells, and succeeding pressure waves then acted as shock or touch stimuli on other leaflets. Scalding, he reported, was without effect and so this was not a true, protoplasmic excitation.

Bose (1914, 1926) reported to the contrary. In *Mimosa,* the excitatory response could be induced by touch, sudden temperature change, by initiation or cessation of a constant current and by induction shock. Crucially, the mechanical (touch) stimulus could be substituted for by an electrical one, the onset or cessation of an electric current. The excitation was bipolar, moving both with and against the

direction of the transpiration stream, unlike the non-discriminative hydromechanical model. The action potentials travelled at rates of 20–29 mm s^{-1}, at similar rates to Bernstein's measurements of the nerve impulse. Bose concluded that electrical signals (including action potentials) controlled the leaf movements.

> Transmission of excitation in the plant is a process fundamentally similar to that which takes place in the animal, in the one case as in the other, a propagation of protoplasmic charge (Bose 1913).

Bose determined that the type of response depended on the strength of the stimulus. A non-electrical stimulus (light) applied to the upper half of the leaf produced either of two responses—an increase of turgor (and leaf lifting) if the light stimulus was moderate or short-lived, and an abrupt leaf-dropping response (loss of turgor on the lower half) if the light stimulus was strong.

The former response (leaf lifting) was associated with increased turgor pressure, expansion of cells, and "galvanometric positivity" [relative hyperpolarisation]. The latter (leaf-folding) involved a true excitation, a propagated wave of "galvanometric negativity" [relative depolarisation], cell contraction and abrupt loss of turgor pressure. The range of electrical responses showed a hyperpolarisation with mild stimulus, a biphasic response—both depolarisation and hyperpolarisation—with moderate stimulus, and a depolarisation with a strong stimulus, as in *Musa* (Fig. 1.3d). Bose determined that there are two forms of travelling signal, the first hydraulic and associated with leaf-lifting and turgor increase, the second a true propagated excitation, associated with turgor decrease and collapse of leaves. The first involved a

> "…quick absorption of water which causes a hydrostatic impulse; this travelling with great rapidity delivers a mechanical blow at the distant responding point…" to cause the second, true propagated excitation, "… the excitatory response of contraction and galvanometric negativity [depolarisation]…." (Bose 1923, p. 205).

The motor organ in both *Desmodium* and *Mimosa* is the pulvinus, a joint-like thickening at the base of a petiole, which supports the leaf. Increase or decrease of turgor pressure in pulvinar cells causes the leaf to collapse or rise. One of Bose's remarkable discoveries was that only the electrical or excitatory response decreased turgor pressure in the *Mimosa* pulvinus sufficiently to collapse the leaves. The hydraulic and electrical systems of a plant cell were intimately coupled, Bose reasoned, and the plant nervous system was complex, with both sensory and motor components. A mild unilateral stimulus was conducted only on the stimulated side. However, if repeated, or if the stimulus was increased to a critical intensity, the slow sensory or hydraulic impulse associated with it was converted into a fast motor impulse, a true excitation, in the pulvinus. The ascending hydraulic impulse was converted into a descending, true excitation after crossing over at the apex of the stem (Bose 1926, p. 42, p. 204).

Thus, there were two forms of signal, and

> …stimulation causes local contraction of the excited cells, with expulsion of water which gives rise to a hydraulic wave, the velocity of which is generally greater than the propagation of the excitatory protoplasmic change constituting the nervous impulse….. [In Mimosa]…the hydraulic wave gives rise to the preliminary erectile response; the subsequent excitatory fall is brought about by the nervous impulse (Bose 1923, p. 250).

Electrical propagation depended on living cells, and the major conduction pathway or nerve (established with the Electric Probe), was, in agreement with Haberlandt's view, situated in the phloem. Safranin and haemotoxylin staining showed two phloem bundles, one internal and one external to the xylem, and the Probe measured markedly different velocities of excitations propagating through them. Bose considered these phloem bundles to be the equivalent of animal sensory and motor nerves, with the inner phloem conducting a fast motor impulse, and the outer, a slower sensory impulse (Bose 1926, p. 189).

The electric signal was propagated in a preferential direction—from stem to pulvinus. Moderate stimulation of the pulvinus alone was not accompanied by collapse of the leaves (Bose 1923, p. 44). Bose argued that this proved the presence of a "synapse" between the pulvinus and the stem.

> The typical experiments…prove that conduction is irreciprocal. They also indicate the existence of a synapsoidal membrane, which by their valve-like action, permit propagation [small to moderate stimulus] in one direction only (Bose 1926, p. 48).

Transmission of the electric signal, a propagated protoplasmic excitation, as in the nerve of an animal (Bose 1926, p. 20), was arrested by applying a blocking constant current (two electrodes placed 5 mm apart in between the pulvinus and the point of stimulation, with a constant current maintained between them; Bose 1926, p. 29). In

> …the contractile cells of the pulvinus…a wave of excitatory contraction passes from cell-to-cell at a rate slower than the nervous impulse. I distinguished this as cellular propagation of excitation. The phenomenon is not unlike the propagation of a wave of contraction from cell-to-cell in the muscles of the animal heart (Bose 1913, p. 91).

Applying similar methods to the spontaneous leaf-movements in *Desmodium*, Bose found that these mysterious gyrations were due to rhythmic alternations between "galvanometric negativity"[relative depolarisation] and "galvanometric positivity" [relative hyperpolarisation] of pulvinar cell electric potential. These electrical oscillations or pulsations were of identical periods to the changes in cell turgor pressure and coupled with it. "Galvanometric negativity" (depolarisation) was associated with loss of turgor and leaf folding. "Galvanometric positivity" (hyperpolarisation) was associated with increased turgor and leaf lifting. Clearly, the hydraulic and electrical systems of the leaflets were coupled to drive *Desmodium*'s curious behaviour.

The leaflet gyrations were strongly temperature dependent, with a period of $\sim$4 min in winter, and much faster, with a period of about 1 min, in summer. The pulsations were "…alternately rendered active or inactive above and below the critical temperature" (Bose 1923, p. 69), influenced by light-levels, depressed

or arrested if turgor pressure was reduced, inhibited by strong or repeated stimulus, arrested by large doses of anaesthetic or poisons. Repeated stimuli led to fatigue and loss of response. Furthermore, the pulsations were arrested by short-length Hertzian waves or radio waves (Bose 1923, p. 106).

The excitatory response in *Mimosa*, and rhythmic leaf movements in *Desmodium* were both blocked by metabolic poisons such as KCN, $CuSO_4$, by sudden temperature change, and by anaesthetics such as chloroform. Just as strong electric stimulus of the pulvinus made *Mimosa* leaves fold, without mechanical stimulation, a cut in the *Desmodium* stalk prevented the rhythmic leaf movements, but these were restored by an electric current passing through the pulvinus (Fig. 1.2d).

1.3.1.2 The Electromechanical Pulse of Mimosa and Desmodium

From this comprehensive suite of experiments, Bose (1913, p. 94) generalised:

1. All forms of significant direct stimulation produced a decrease in turgor pressure, a contraction of cells, a transient diminution of growth rate, a negative mechanical response (such as dropping of leaves) and a "galvanometric negativity" [relative depolarisation].
2. Subtle stimuli, on the other hand, produced directly opposite effects. Turgor pressure increased, cells expanded, and the growth rate transiently increased and a "galvanometric positivity" [relative hyperpolarisation] was measured.
3. All plants showed coupled pulsations of turgor pressure and electric potential; these occurred at the levels of whole plant tissues (e.g. in living cells of the phloem) to individual cells.
4. Growth itself was pulsatile. The High Magnification Crescograph showed that *Desmodium* and other plants grew in rhythmic pulses, which corresponded to electrical pulsations.

The electromechanical pulsations became a central motif at the heart of all plant behaviours. A strong or injurious stimulus of leaf or stem in *Mimosa* induced a wave of protoplasmic, electrotonic excitation (electrical depolarisation, an action potential), transmitted through the phloem to the pulvinus, where it caused turgor pressure to decrease, and the leaves to fold. However, subtle stimulus had the opposite effect, causing turgor pressure to increase, and leaves to lift. There existed two nervous systems, a sensory (slow) conduction pathway, and a fast, motor pathway. In *Desmodium*, subtle light stimulus induced rhythmic leaf gyrations, through alternate contraction and expansion (turgor pressure changes) of the pulvinar cells, associated with a corresponding electrical pulsation or oscillation.

Bose reasoned that the expansive phase was hydraulic, and the contractile, depolarising phase was nervous and electrical, a true excitation. The two were antagonistic (Bose 1923, p. 255). As did animals, plants employed sensory and motor conduction pathways. Of these two forms of signalling, the sensory pathway was essentially hydro-mechanical, and the second, involved true, propagated excitation. The first could be converted into the second by a strong enough stimulus.

1.3.1.3 All Plants have an Electromechanical Pulse

Plants such as *Mimosa* or *Desmodium* make striking and dramatic movements that easily catch the attention of a human observer. However, Bose concluded that *all* plants employ electromechanical pulsations in their active responses to the world. Thus,

> …the characteristics of the transmitted impulse as ascertained from the mechanical response of motile, sensitive plants find an exact parallel in the electric response of ordinary non-motile plants. They are in fact common to all plants… (Bose 1913, p. 103).

Bose found that cortical cells abutting the endodermis of ordinary plants (those not making obvious and dramatic movements) also exhibited electric pulsations or oscillations (Bose 1923, p. 219). Using the Electric probe, he measured electrical pulsations in field-grown tomato, vines, and potatoes, *Chrysanthemum*, banana, *Canna*, and trees including the mango and the Cadamba, *Nauclea* (Bose 1923, p. 225).

He found "periodic mechanical pulsations corresponding to electric pulsations, as in Desmodium" (Bose 1923, p. 214). These pulsations he recorded on a photographic plate driven by clockwork, resulting in a galvanograph (Figs. 1.3c, d). The "galvanonegative" part of the pulsation Bose associated cellular contraction and turgor decrease, whilst the "galvanopositive" part was accompanied by cellular expansion and increased turgor.

In an extraordinary experiment, Bose connected the Electric Probe (and reference electrode) to trees 30 m tall, wiring the signals to an Einthoven galvanometer, and measuring electric fluctuations of variable amplitude and period in *Nauclea*. The period of the pulsations changed with temperature (Bose 1923, p. 214). Pulsations were subtle on cold mornings, maximal at noon and changed in amplitude during the course of a day. The period depended on environmental conditions. It increased with sudden irrigation, when warm water was applied to the banana plant, and changed with passage of a constant electric current. The pulsation amplitudes increased with increased hydrostatic pressure, moderate constant current and increased temperature. They were arrested by a large dose of chloroform, plasmolysis of the roots, a sudden, large drop in temperature and poisons such as KCN.

What was the explanation for these electric and hydraulic pulsations in plants making no obvious behavioural movements? Bose rejected the tension-cohesion hypothesis proposed by Dixon and Joly in 1894, which still remains the widely accepted explanation of the ascent of the transpiration stream. He interpreted the electromechanical pulsations of cortical cells as a kind of pulse, a rhythmic electrical oscillation accompanied by turgor increase and decrease in living cells, which propelled water upwards in the xylem. The xylem was a reservoir into which water was injected or from which it was withdrawn, according to the conditions, time of day and temperature (Bose 1923, p. 222).

Fluid was injected into the xylem by expulsive contraction of cortical cells, but this was impossible if all the cells pulsed together at the same time. There had to

be a phase difference of pulsations along the length of the stem. That is, the electromechanical pulsations must be peristaltic. The physicist Bose approached the problem by making a fixed electric contact with a stem, and then bringing the Electric Probe progressively closer to it. Indeed, he found a critical distance at which the potential difference between electrodes was maximal, and another critical distance between electrodes where the PD was cancelled out. The distance at which the maximum PD was found equated to half the pulse width. Thus, the pulse width was about 100 mm in *Chrysanthemum*, 50 mm in banana and 40 mm in *Canna* (Bose 1923, p. 225).

Bose generalised "…any agent affecting the pulsations induced corresponding effects in the ascent of sap…" (Bose 1923, p. 258). His theory of the ascent of sap, put simply, stated that successive periodic hydraulic waves (propagated waves of contraction preceded by waves of expansion) squeezed water upwards.

Thus, Bose argued, all plants employed a universal mechanism involving coupled electrical and mechanical oscillations, protoplasmic contraction and expansion, turgor increase and decrease.

He summarised his results:

> …expulsion of sap by cells of the pulvinus on stimulation is an essential part of its motile mechanism, and this applies also to the pulvinule of the leaflet of Desmodium in its 'spontaneous oscillation'…evidence has been accumulated…. that the active expulsion of sap by living cells is an essential part, not only of the mechanisms of movement, but also…for the distribution of fluid throughout the plant…" (Bose 1923, p. 144).

Plants used a universal mechanism coupling electrical and mechanical oscillations, protoplasmic contraction and expansion, to respond to the world. Plants possessed a means for rapidly transmitting information about an urgent or injurious event as well as for navigating the physical aspects of the world through subtle and exploratory growth movements.

How was the local linked to the systemic in a plant's body? Again, this was through coupled mechanical and electrical pulsations. Bose compared a plant to a bar magnet, its two poles located at root and shoot, with an apparently neutral region in between. However, as the two parts of a divided bar magnet both then show a north and a south pole, so it was with the plant, all the way down to the individual pulsating cell. There were thus whole plant pulsations, the pulsations of organs and tissues, and the pulsations of individual cells. Each level of organisation was responsive to its own surroundings and to those of the greater whole.

All cells pulsed, and each "must exhibit polarity, [one] end absorbing water, [the other] end excreting it" (Bose 1926, p. 192). The polar plant was divisible into quadrants, making movements not only up or down, but also clockwise and anticlockwise. In the case of heliotropic movements, the motor organ had four effectors, one for each of these directions. Plants were highly sensitive to light and could locomote into favourable postures using the sensitivity of the four quadrants as reference points: "a beam of light falling on the left flank of the pulvinus of Mimosa induces an anticlockwise torsion [and vice versa]" (Bose 1926, p. 156).

Light applied to one side of the stem caused turgor to increase at the diametrically opposite point (Bose 1926, p. 165).

Heliotropic movements in the sunflower *Helianthus*, where the entire petiole was the motor organ, were due to the interplay between contraction and expansion of each side of the plant in relation to the direction and intensity of light. In terms of a leaf,

> …the leaf is…thus adjusted in space by the co-ordinated action of four reflexes, equilibrium being attained when the leaf is perpendicular to the incident light (Bose 1926, p. 172).

Bose (1918) investigated the curious case of the "Praying Palm of Faridpur" (in Bengal), a date palm (*Phoenix dactylifer*) that had been displaced by a storm, and the trunk of which inclined about 60° to the vertical. This tree had been regarded as miraculous, bowing down in the evening as temple bells were ringing, and raising its crown again at dawn. Adapting the Resonance Recorder for use with the praying palm, Bose showed that the plant indeed underwent an active diurnal movement along its entire length, the fall of the highest point of the trunk being approximately one metre. A continuous record with a modified Resonance Recorder showed that in addition to the "bowing" movements the tree was never at rest, but in a state of continuous rhythmic movement, day after day. Bose then made similar measurements on ordinary palm trees, and found less dramatic but similar oscillatory movements. These were coupled, not with light conditions, but with diurnal changes in temperature. As temperature steadily increased, the date palms moved downwards by small increments. Similar movements were found in *Basella cordifolia*, *Mimosa pudica* and *Arenga saccharifera*. Bose attributed these movements to a complex interaction between geotropic and temperature responses.

From his numerous experiments, Bose formulated a holistic concept of plant responsiveness in which all plants actively explore the world, and respond to it through a fundamental, pulsatile, motif involving coupled oscillations in electric potential, turgor (hydraulic) pressure, contractility and growth. All plants have an electromechanical pulse, a nervous system whose major conduits are located in the phloem tissue. Plants coordinate their responses to the world through electrical signalling. An injurious, drastic stimulus or an abrupt change in conditions activated a fast, motor response via travelling depolarising waves that we would today call action potentials. Ordinary stimuli were interpreted and transmitted through a hydro-electromechanical sensory system, involving coupled pulsations in electric potential and turgor pressure.

Advancing the view that plants are active, capable of learning from experience and modifying their behaviour accordingly, Bose believed that his experiments had proved the

> ..unity of physiological mechanism in all life. For we find, in the plant and in the animal, similar contractile movement in response to stimulus, similar cell-to-cell propagation of pulsatile movement, similar circulation of fluid by pumping action, a similar nervous

> mechanism for the transmission of excitation, and similar reflex movements at the distant effectors (Bose 1923, p. 271).

According to Simons (1992), failure to accept Bose's *Mimosa* experiments stalled research into plant electrical signalling for many years. At the time of Bose's death in 1937, and afterwards, electrical signalling in plants had become a topic of minor interest, or even an untouchable one. The discovery of auxin in the 1930s led to intense research on plant hormones or growth regulators, and to the idea that plants were coordinated primarily by chemical diffusion. Since plants did not move rapidly, had no eyes, ears, or obvious brain, since they were simple automata stuck in the ground, chemical diffusion was an adequate mechanism for signalling and coordination, and a nervous system was unnecessary. Other contributory factors included the use of plants in parapsychology, and institutional nationalism, racism and sexism (Wayne 1994). Publication of a best-selling popular book, The Secret Life of Plants in 1973, critiqued by Galston and Slayman (1979), apparently made research into plant electrical signals "…untouchable in the eyes and minds of funding agencies" (Davies 2004).

1.4 Some Current Aspects of Plant Neurobiology

Plant neurobiology (Baluska et al. 2006; Brenner et al. 2006; Barlow 2008), as a relatively new and somewhat controversial addition to the discipline of plant sciences, aims to provide both a forum and a context for investigating the means by which plants perceive features of the world, transduce this information into electrical, hydraulic and chemical signals, and subsequently respond physiologically, morphologically and behaviorally.

Rather than the traditional emphasis on differences between animals and plants, plant neurobiology is inclusive, focusing on similarities. Indisputably, animals and plants share major biochemical pathways, some neurotransmitters (including glutamate receptor-like genes), reproduce by similar fusion of gametes, develop immunity, and employ similar molecules and pathways to drive circadian/chronobiological rhythms (Baluska et al. 2006).

Plant neurobiology goes further still, asserting that the complexity of plants, whose capacities include making integrated responses to the environment, decision making (e.g. the onset of dormancy or flowering, selection of prey by the parasite dodder), social learning, behavioural inheritance and employing complex plant–plant, plant–insect and plant–animal communications, implies a far more sophisticated sensory perception than has hitherto been acknowledged (Baluska and Mancuso 2007). As did Bose over a century ago, current plant neurobiology regards plants as active and exploratory organisms, capable of learning from experience and modifying their behaviour accordingly. Integral to this form of plant intelligence is the equivalent of a nervous system. Bose was the first person

to use the term ‘plant nerve’, locating the nervous route for long-distance electrical signalling in the vascular tissue, specifically the phloem.

The use of terms such as ‘plant nervous system’, ‘plant brain’, ‘plant synapses’, ‘plant intelligence’ by plant neurobiologists has provoked controversy (e.g Alpi et al. 2007) and the contention that such concepts contradict the parsimony principal of Ockham’s Razor (Struik et al. 2008). Barlow (2008) proposes adopting Living Systems Theory as a means for reconciling neural homoplasies between plants and animals. This enables a network understanding that incorporates semiotics, or the processing of meaningful biological information. As Kauffman et al. (2008) reason, even a minimal living system (constituting a boundary between self/not-self, a capacity to perform at least one thermodynamic work cycle, and to reproduce itself), processes meaningful information in the sense that it responds to information in such a way as to propagate its own organisation.

According to the Miller’s Living Systems Theory each level of biological organisation (e.g. cell, tissue, organ, organism or ecosystem) is supported by a set of critical subsystems, which repeat at each level (Barlow 2008). The subsystems and the information they embed together assemble a particular level of biological organisation. At each of these levels the tasks of the subsystem are equivalent, but the elements that make up the subsystem and the means by which the tasks are accomplished differ, becoming more complex at higher organisational levels. Most of the 20 information processing subsystems are appropriate to plants, and at the organism level, the ‘channel and net’ subsystem, with its criterion of transmitting electrical signals (action potentials) throughout the body, is appropriate to plant phloem tissues (Bose’s ‘nerves’) and animal nervous tissues (Barlow 2008). In this way, the adaptive behaviours of animals and plants can be understood by identifying common principals.

In a series of thoughtful reviews, Trewavas (2003, 2005a, b, 2006, 2009) shows us how biased is the widely employed concept of intelligence. Adopting D. Stenhouse’s definition of intelligence, as *adaptively variable behaviour during the lifetime of an individual*, Trewavas gives numerous examples of plant intelligence that involve growth and development. For example, roots navigate the maze of the soil, constructing a perspective of local space. A root that is gravitropically growing downwards and encounters an obstacle begins to grow horizontally, but continues to attempt downward growth, thereby assessing its situation (Massa and Gilroy 2003). The so-called tropisms of plants in fact require an integration and evaluation of numerous stimuli such as light, water status, temperature, gravitational vector, mechanical perturbation and so on, a form of perceptual feedback that results in phenotypic plasticity (Barlow 2010b).

‘Intelligence’, with its embedded anthropocentric associations, is particularly difficult to define. As Cvrckova et al. 2009 reason, even if intelligence exists as a continuum throughout biology it requires selective and accessible memory. Under the terms of their ‘memory test’, root navigation and host choice by dodder do not constitute intelligent behaviour, although auxin canalisation based on experience and involving active cell participation may so do. On the other hand, Calvo et al. (2011) argue for an inclusive concept of intelligence and postulate the existence of

embodied cognition or disseminated intelligence that does not require a central organiser or brain. The ongoing debate is valuable in that it may extend the range of experimental approaches employed in plant physiology.

In the terms of Kauffman et al. (2008), integration and coordination of responses serve to propagate the organisation of a living system through the processing of meaningful information. Plant behaviour involves active phenotypic changes, rather than the obvious movements made by animals, although it is the latter that we have come to exclusively associate with intelligence (Trewavas 2005a). If the 'green intelligence' of plants, as comprehensively assessed by Trewavas (2003, 2005a, b, 2006, 2009) is granted, then plants may constitute a form of minimal embodied cognitive system (Calvo et al 2011). Barlow (2010) argues eloquently that the autopoietic nature of living systems implies cognition, in the sense of a capacity to perceive, acquire and respond to information, and cognition provides impulses for change. The argument that only animals with brains can be intelligent is a form of brain chauvinism, argues Trewavas (2005a, b) and it endows animal nerves with a kind of vitalist quality.

Plant roots recognise kin (Dudley and File 2007, 2008) and self, whilst aggressively competing with non-kin for resources (Novoplansky 2009). Plant roots actively forage, using strategies comparable to those used by foraging animals. Whilst an animal is a single foraging unit with 1 mouth, the roots of an individual plant are repeated foraging units, capable of performing different behaviours simultaneously (McNickle et al. 2009). Plant mouths, as it were, are numerous and can act independently (McNickel et al. 2009). Plants learn through trial and error, have goals, assess and modify their growth behaviour, and are enabled by a form of memory to anticipate difficulties, and to grow around them (reviewed, Baluska and Mancuso 2007; Barlow 2010b). We must ask to what extent plant behaviour is intentional, or instinctual (Barlow 2010a).

In the presence of attacking herbivores, plants 'cry for help' (reviewed, Dicke 2009) and can enlist other organisms in complex behavioural strategies (reviewed, Karban 2008). For example, egg deposition by the pine sawfly induces a gymnosperm plant to release volatile chemicals that attract an egg parasitoid wasp (Hilker et al. 2002). Plants also communicate with each other via airborne chemicals, as in the now well-known example of prey selection by the parasitic vine, dodder (Mescher et al. 2006). In the context of adaptive plant behaviours, the phytochrome pigments are now regarded as central organisers in phenotypic decision-making during shade avoidance (Ballare 2009). Photosensory systems sensitive in the blue and red regions of the spectrum involve phototropin, cryptochrome and phytochrome pigment systems, and illumination with these wavelengths results in action potentials of 0.3 ms duration and 60 mV amplitude (Volkov et al. 2004).

Trewavas (2005a, b) argues that modular plants resemble social insect colonies. Both, he says, "…gather information, evaluate, deliberate, form a consensus, make choices and implement decisions…", and plant intelligence resembles the swarm

intelligence of a bee colony, evocatively called, by Seeley and Levien (1987), a colony of mind. A bee colony as a cognitive entity collects up-to-date information about the world, assesses this in relation to its own internal state (thereby performing simple reasoning), and makes decisions promoting its well-being. Swarm intelligence enables division of labour, morphogenesis and collective decision-making without the necessity for a central controller or supervisor (Garnier et al. 2007) or brain.

1.5 How does Bose's Work Stand Up in Light of Current Research?

Against the background of contemporary plant neurobiological research, the conclusions reached by J.C. Bose seem far less outlandish than they did in the early twentieth century, when the Royal Society archived his submitted papers without publication. In the following paragraphs, I briefly measure some of Bose's conclusions against more recent research.

1.5.1 Plants are Individuals, and Their Behavior Manifests in Their Natural Habitat, Rather than Under Controlled Conditions

Trewavas (2003) presents detailed arguments: first, that the widespread application of controlled conditions, where only a single variable is manipulated, obscures intelligent behaviour by plants, as this requires the appropriate environmental context to be expressed. The application of statistics to experimental results in plant physiology produces a mean, which is fallaciously assumed to reflect the behaviour of all individuals in the population—it is similarly fallacious to assume that variations from the mean are due to experimental error. If we seek evidence for adaptive and intelligent behaviour in plants, we need to pay attention to the complex behaviours of individuals, as did J.C. Bose, and seek this evidence under conditions that are as natural as possible. The emerging concept of genes as fields of possibility (Jorgensen 2011) has as a focus the epigenetic regulation of chromatin states. We may expect that controlled conditions will obscure or eliminate epigenetic repertoires or innovation by individual plants, or even produce plants adapted to the artificial experimental situation.

1.5.2 All Plants Employ Electrical Signalling as a Means of Transmitting Information About the World and Responding to it

At the time of Bose's death in 1937 electrical signalling in plants had become a marginalised topic. Went's identification of auxin (indole-acetic acid) in 1928 focussed attention on diffusive chemical signalling, the slowness of which matched the slow movements and passivity expected of plants.

By the 1970 and 1980s some plant electrophysiologists had built strong experimental and theoretical frameworks supporting the ubiquity of electrical signalling in plants. Action potentials, they argued (e.g. Pickard 1973; Davies 1987a, b, 2006; reviewed Wayne 1994; Davies 2004), are multi-functional electrical signals employed by plants in actively constructing responses to the world. However, not until the 1990s, nearly a hundred years after Bose's research, did plant scientists widely embrace this view (Roberts 1992). The critical role of electrical signalling was validated by Wildon et al. (1992) who demonstrated that a flame wound activated proteinase inhibitor genes in distant tissues—not chemically, but electrically. The electrical signal was a slow-wave potential or variation potential, initiated by a hydraulic surge, rather than an action potential (Davies 2004, 2006). A similar flame-induced electrical signal transiently halts photosynthesis in *M. pudica* (Koziolek et al. 2004).

In 2011 it is understood that most, and perhaps all plant cells are excitable, responding to stimuli such as heat, cold, wounding, touch and changes in extracellular osmotic pressure with electrical signals. Signals may be restricted to a single cell (receptor potentials), transmitted over relatively short distances (variation or slow-wave potentials) or transmitted over long distances (action potentials). Plants, with their sessile habits, are fundamentally tactile organisms. As Bose had asserted over a hundred years ago, mechano-perception underlies many subtleties of plant behaviour, including responses to gravity, temperature, osmolarity, and turgor-controlled growth and development (reviewed by Baluska et al. 2003a, b; Shimmen 2006).

Action potentials are electrotonically transmitted at rates of at least 10–70 mm s^{-1} (Stahlberg and Cosgrove 1997; Wayne 1994) and possibly much faster. Along with aliasing and other experimental errors in sampling rates, the individual variations Bose reported in *Mimosa* (modified by a plant's history, by temperature, season and age), may account for the variability in reported rates of action potential transmission, as noted by Volkov et al. (2010). For example, the uncoupler FCCP, surely a drastic stimulus, induces action potentials propagated an order of magnitude faster, at 40 ms^{-1} (Volkov et al. 2004).

An action potential is understood to be an abrupt depolarisation, induced by release of Ca^{2+} into the cell cytoplasm, activating Cl^- ion channels and voltage-dependent potassium K^+ channels. The result is an efflux of Cl^- and K^+ (Oda 1976; Wayne 1994), water efflux, transitory loss of turgor pressure (Zimmermann

and Beckers 1978) and a transitory contraction of the cell (Oda and Linstead 1975).

This motif (Ca^{2+} influx, K^+ and Cl^- efflux, contraction and turgor change) is fundamental to the osmotic machinery that enables plant movements (Hill and Findlay 1981). In action, it mirrors Bose's electromechanical 'pulsations', which played an intrinsic role in plant behaviour. As Volkov et al. (2010) put it, voltage-gated K^+ and Cl^- channels are the electrical starter of the osmotic motor in the *Mimosa* pulvinus.

1.5.3 Plants have Nervous Systems

What of the two nervous systems, sensory and motor, that Bose had proposed? Plant neurobiology acknowledges the existence of three kinds of neural-like pathways. First, as proposed by Bose, there is a pathway comprising phloem sieve tubes and their companion cells (reviewed by Davies and Stankovic 2006), through which electrical action potentials are transmitted.

Second, is the pathway comprising (non-living) xylem elements and their accompanying living xylem parenchyma, where occur the variation (slow-wave) potentials—initiated by hydrostatic signals or pressure waves in the xylem (Pickard 1973). This contrasts with Bose's view that hydraulic signals travelled in a second phloem bundle. Variation potentials may result from Ca^{2+} influx through mechano-sensitive channels (Davies and Stankovic 2006). It is often difficult to distinguish the effects of variation potentials from those of action potentials, especially since the former can initiate the latter (Stankovic et al. 1998). Similarly, the so-called receptor potential is a small depolarisation brought about by mechanosensory ion channels, and occurs in response to touch stimulus (Shimmen 2001). It is graded according to stimulus intensity, and does not travel from cell-to-cell. When a critical depolarisation threshold is reached, the receptor potential initiates an action potential, which then moves intercellularly. Reducing turgor pressure does not alter the threshold for the action potential but it does alter the magnitude of the receptor potential for a given stimulus (Shepherd et al. 2001, 2002, 2008). With reduced turgor, a cell is more sensitive to stimulus and more likely to respond with an action potential.

It can be so difficult to distinguish between action and variation potentials, that they may have been frequently confused in published work (Mancuso 1999). In the grapevine, the variation potential involves a hydraulic wave transmitted in the xylem, as it is accompanied by a transient decrease and subsequent increase in shoot diameter, and it disappears at saturating humidity (Mancuso 1999). On the other hand, action potentials were not affected by saturating humidity, failed to travel through dead tissue and did not involve changes in shoot diameter (Mancuso 1999). Both however, involve changes in the activity of the electrogenic proton pump in living cells.

According to Stahlberg and Cosgrove (1997), the variation potential is not an electric long-distance signal per se. It is, rather, a hydraulic surge almost instantaneously propagated in the xylem, which creates an axial pressure gradient resulting in slow local depolarisations of living cells, and thereby giving the impression of a propagating electrical signal. According to a recent publication (Vodeneev et al. 2011), a variation potential provoked by drastic stimuli such as cutting or burning, involves transient inhibition of the proton pump and activation of Ca^{2+}-activated Cl^{-} channels. Following injury, the variation potential develops by an increase in xylem pressure/appearance of a 'wound substance', activation of mechanosensitive and/or ligand-activated Ca^{2+} channels, activation of Ca^{2+}-activated Cl^{-} channels, and inactivation of the proton pump, giving the mechanisms underlying cell depolarisation a certain universality (Vodeneev et al. 2011).

The third neural-like pathway in plants, as postulated by Baluska et al. (2005), is the 'plant brain', the transition zone of roots, where actin-enriched fields of cell-to-cell communication channels (plasmodesmata) at the end-poles of cells act as synaptic connections. Synapses in this region confer on the root apex the properties of a 'brain', or command centre, where incoming sensory signals are processed (Baluska et al. 2004; Barlow 2006, 2008). 'Higher plants show neuronal-like features in that the end-poles of elongating plant cells resemble chemical synapses' (Baluska et al. 2003a, b). It is here that synchronised electrical 'spikes' are measured, which are proposed to reflect integration of internal and external signals (Masi et al. 2009).

Bose had argued for the necessity of such synaptic polarity in cell-to-cell signalling in plants, comparing a tree to a bar magnet, with two poles at root and shoot. In plant neurobiological terms, plants stand upon their heads (Baluska et al. 2006). The root apex contains plant command centres, or the 'plant brain', or an extremely well-connected hub in the information network, whilst the shoot apex, with its respiratory and reproductive organs (leaves and flowers) is the posterior pole of the body. Complex social interactions between plants, plants and fungi and plants and bacteria, are mediated primarily through the roots (Baluska et al. 2004, 2006; Bais et al. 2004).

Ironically, the plant growth regulator auxin (indole-acetic acid) that dominated the field of plant chemical signalling, is now regarded as a potential plant neurotransmitter. Polar auxin transport has much in common with synaptic signal transmission in excitable animal tissues (e.g. Baluska et al. 2005; Baluska and Mancuso 2007). Plants show neuronal-like features in that the end-poles of elongating cells resemble chemical synapses. Thus, auxin is thought to be secreted from cell-to-cell, neurotransmitter-like, via vesicle trafficking. The end-to-end polarities of root apical cells, the enrichment of the end-poles with the cytoskeletal protein actin, and the cell-to-cell communication channels (plasmodesmata) at end-pole walls linking adjoining cells, constitute the synapse-enriched brain-equivalent of the root.

1.5.4 Plants Remember and Learn: The Basis of Plant Learning

Even if one argues that plants have neither neuronal equivalents nor the capacity for learning, it seems clear that memory (regarded as an ability to store and recall information) operates in *Bidens* seedlings (Thellier et al. 1982; Tafforeau et al. 2006). In a thoughtful article, Calvo-Garzon and Keijzer (2011) propose that a capacity for what they call offline processing, or memory, is necessary if we are to consider plants as systems with embodied minimal cognition. How is it possible for plants, which lack an obvious brain and the capacity for rapid movement, to foresee, remember, plan and respond? A current view is that calcium signalling, involving transmitted electrical signals such as action potentials, underlies plant responsiveness (Bothwell and Ng 2005). This involves chemical signalling also, as calcium is either an agonist or antagonist of all plant growth regulators, including auxin, as proposed in the 1980s (Ettlinger and Lehle 1988). How can calcium, a mere divalent ion, control such complex processes? Trewavas (1999a, b) and Bose and Karmekar (2003) propose a neural net concept of Ca^{2+} signalling as the basis of plant learning and intelligence. Electrical signalling systems (e.g. action potentials) that release calcium confer on plants the potential for computation, learning and memory. Changes in cytoplasmic Ca^{2+} are the basis of the intelligent system, not through Ca^{2+} diffusion, but through propagated waves of Ca^{2+} release. Plant cells potentially compute, remember and learn, through a Ca^{2+}-based neural net system (Trewavas 1999a, b; Bose and Karmekar 2003) that constitutes the 'big network' of cellular signalling (Trewavas and Malho 1998). These authors argue that this Ca^{2+}-based neural net is a means for computing, remembering and learning that is unique to plants. It accelerates information transfer and it can be reinforced. Repeated signals make the path more sensitive whilst too many signals inhibit it. A similar Ca^{2+} signal can have different effects in different cells, which thereby remember previous experience, and know where and what, they are.

The Venus flytrap electrical memory, whereby two touch stimuli must be received within 30 s. for trap closure to occur, is a short-term electrical memory (Volkov et al. 2008). However, there is evidence that such 'offline' processing or memory can be intergenerational. As one example, *Arabidopsis* plants stressed by UV light or flagellin, a defence elicitor, showed somatic homologous rearrangement of a transgenic reporter that was passed on to the next generation of untreated plants (Molinier et al. 2006). The untreated generations retain flexibility of their genomes and a wide literature is now devoted to the inheritance of other epigenetic traits (e.g. reviews by Bond and Finnegan 2007; Boyko and Kovalchuk 2010).

1.5.5 Mimosa and Desmodium Literature Today

That the phloem tissue is the major conduction pathway for action potentials is now strongly supported by contemporary *Mimosa* researchers (e.g. Volkov

et al. 2010; Fromm and Lautner 2007). The classic papers of Fromm and Eschrich (1998a, b, c; reviewed 2007) demonstrated conduction of excitation within the phloem, and furthermore, that decreased pulvinar turgor is accompanied by phloem depolarisation and expulsion of Cl^- and K^+ as well as a sudden unloading of sucrose (Fromm and Eschrich 1998a, b, c). Three types of electric signals can be identified in *Mimosa*; the m wave or action potential, which cannot pass the pulvinus, and is propagated at 15–40 mms^{-1}, the s wave or variation potential, which can pass the pulvinus, and travels at 2–5 mms^{-1}, and the r wave, travelling at 60–120 mms^{-1}, whose role is unknown (reviewed, Shimmen 2006).

The contractile actin-myosin system is involved in the collapse of *Mimosa* leaves, and in the spontaneous movements of *Desmodium* (reviewed, van den Driessche 2000). Motor cell movements in *Mimosa* are inhibited by drugs that affect the actin-myosin system involved in cytoplasmic streaming in plants. Recently, Volkov et al. (2010) proposed a model of a biologically closed circuit that embraces aspects of the osmotic motor, chemical (Ricca factor or turgorin) and so-called muscular hypotheses of *Mimosa* seismonastic movements. In this model, stimulation activates mechanosensory channels, resulting in receptor potentials, action potentials (when above threshold), signal transduction via the phloem to the pulvinus, activation of voltage-gated Cl^- and K^+ channels, activation of the proton pump and redistribution of water between flexor and extensor sides of the pulvinus, as well as phosphorylation of actin-tyrosine and finally actin fragmentation and hydroelastic shape change with increased volume on the flexor side.

In the 1990s, elegant experiments of Antkowiak et al. (1991) and Antkowiak and Engelmann (1995) proved *Desmodium* leaflet gyration is coupled with rhythmic changes of pulvinar cell turgor pressure, and these in turn are coupled with rhythmic oscillations of membrane potential difference. Using ion-sensitive H^+ and K^+ extracellular microelectrodes as well as intracellular microelectrodes, they showed that the leaflet downstroke was coupled with depolarisation of pulvinar motor cells, and increased apoplastic K^+ concentration. The cells contracted, losing turgor. Leaflet lifting occurred when pulvinar motor cells were hyperpolarised, apoplastic K^+ concentration declined, the external PD was positive, the cell expanded and turgor pressure increased. Like Bose, these researchers found that an anaesthetic, enflurane, abolished the movements, and increased temperature shortened the period of the oscillations. Pulsed radio-frequency fields do transiently alter the amplitude, period and phase of the leaflet rhythms in *Desmodium* (Ellingsrud and Johnsson 1993).

Although he did not apply the concept of ion channels and preferred to view the entire plant as comprising semiconducting circuits, Bose's concept of a slow-moving signal (variation potential) that could be converted into a fast-moving propagated electrical signal seems to have been vindicated. Are these indeed the equivalents of sensory and motor nervous systems?

1.5.6 The Hydro-Electrochemical Pulse of Plants

What of Bose's conclusion that *all* plants employ a fundamental behavioural motif, a hydro-electrochemical pulse, involving coupled pulsations or oscillations in turgor pressure, membrane potential, expansion/contraction and growth? Many researchers have confirmed the links between rhythmic changes in cell volume, influx and efflux of water, and rhythmic changes in cell electric potential difference. Mitsuno and Sibaoko (1989) found that inhibiting the electrogenic ion pump or oxidative phosphorylation in *Desmodium* arrests its pulsations, and suggested that an electrogenic pump is rhythmically altering its activity. Electric oscillations are coupled with growth oscillations (or pulses) in roots (Souda et al. 1990), where oscillatory patterns of H^+, K^+, Ca^{2+} and Cl^- influx (Shabala and Knowles 2002) represent ultradian oscillations in nutrient acquisition. These authors argue that the plant proton pump must therefore operate rhythmically. This implies that energy metabolism is itself rhythmic.

Careful analysis of time-lapse photographic records coupled with precise measurements of stem elongation in long and short day forms of *Chenopodium* species show unequivocally that stem extension growth and leaf movements are indeed rhythmic, and change their phase relationship in a coordinated way upon induction of flowering (Normann et al. 2007). Furthermore, there is a diurnal rhythm in surface membrane potentials and a probable involvement of timed action potentials or frequency coded electric signals in stem growth and rhythmic leaf movements (Wagner et al. 2006, reviewed Normann et al. 2007). These authors regard

> …the circadian oscillation as a hydro-electrochemical phenomenon at the cellular and organismic level… (Normann et al. 2007, p. 203)

that depends on calcium-based signal transduction. They write

> ..proton translocation and concomitant ion movements would give rise to a circadian rhythm in electric potential, paralleled by circadian rhythms in growth, like leaf movements and stem extension rates as universal markers of systemic behaviour (Normann et al. p. 215).

Using a similar experimental set-up as Bose, Gensler and Diaz-Munoz (1983) and Gensler and Yan (1998) measured electrical pulsations in ordinary crop plants. With a palladium electrode inserted in the stem, and a reference palladium electrode in the root zone of tomato plants, they measured a large, stable and reproducible potential difference (~ -400 mV) and recorded characteristic potential/time fluctuations, which they called electrophytograms (Gensler and Yan 1998). These strongly resemble Bose's galvanographs. The authors commercialised the method as a means for predicting changes in water status or determining optimum times for watering.

The Gensler pulsations changed according to the condition of the plant, its water status, atmospheric changes, and the time of day and did appear to be related to transpiration. With an electrode in the stem, and a reference electrode in the root

zone of cotton plants, these researchers simultaneously measured apoplastic electropotentials and stem diameter before and after rainfall and irrigation. Stems contracted during the day and expanded at night, coupled with a decrease and increase of electropotential. Following irrigation stems expanded and the electropotential declined.

In mature trees, variations of electric potential in the bole of trees are linked not only with daily photoperiods, but also as 'stem tides', with mysterious lunar periodicities (Holzknecht and Zurcher 2006). This correlation suggests that the Moon is influencing the flow of water between different parts of the trees (Zurcher et al. 1998, 2009), although it is not known how plants might detect lunar periodicities. The measured electrophysiological oscillations or noise spectra also bear a strong resemblance to Bose's galvanographs.

A diurnal rhythm in surface potential fluctuations may indeed represent integration of the metabolic activities of plants on a hydraulic-electrochemical level (Wagner et al. 2006). Hydraulic changes at the shoot apex prior to initiation of flowers imply hydro-electrochemical communication between leaves, the shoot, and the root system and a specifically timed electrical signal could substitute for photoperiodic flower induction (Wagner et al. 2006).

As to the question of whether living cells are involved in the flow of the transpiration stream, as Bose proposed, mainstream opinion on the whole concludes not. Are electro-mechanical pulsations associated with transpiration? According to Laschimke et al. (2006), water may travel through the xylem in peristaltic waves, and gas bubbles behave as a hydro-pneumatic system that cyclically stores and releases energy. The function of the electrical pulsations coupled with changes in stem diameter, as measured by Bose and others, remains unknown.

1.6 Conclusion

A great gulf separated Bose's philosophy of science from that of the leading electrophysiologists of his day. At least three philosophical movements, mechanistic materialism, vitalism and organicism, informed the Western science and its experimental methodology at that time. As adherents of emerging mechanistic materialism, Bose's detractors, Burdon-Sanderson and Waller, favoured reductionist experimental methods and a definite separation between the physiologies of animal and plant.

Bose's insistence on the unity of the living and non-living may have arisen from his deeply held philosophical position (Dasgupta 1998), Vedanta in inspiration, a monism that regarded the world as a single unified entity (Chakrabarti 2004). From this standpoint, matter and mind were not separated, intelligence existed as a continuum, in which plants and animals participated, and the physiology of plants was in principal similar, albeit differently elaborated, to the physiology of animals. As attempts at uncovering this unity, Bose's investigations demonstrated that

plants integrate their movements and responses to the environment through electrical signals transmitted through the equivalent of a nervous system. All plants explore and perceive their world, and respond to it through a fundamental, rhythmic, motif involving coupled oscillations in electric potential, turgor pressure, contractility and growth. Plants have a hydro-electrochemical pulse, a nervous system, the capacity for remembering and learning. In the preface to his book Life Movements in Plants (Bose 1918), Bose wrote "…. the complex mechanism of the animal … that has long baffled us, need not remain inscrutable for all time, since the intricate problems of animal life would naturally find their solution in the simpler vegetable life," which would mean "very great advance in the sciences of general physiology, of Agriculture, of medicine and even of psychology…". Whether the concept of intelligence remains a metaphor as applied to plants, or is applied inclusively, embracing a continuum from quorum sensing in bacteria to plant behaviour, the complexities of animal behaviour and human social systems, is much debated. It is clear however, that some conceptual framework is needed in which the integration and coordination of plant behaviour can be studied (Struik et al. 2008). There have been calls for a shift in agriculture from a functional genomics approach towards 'crop systems biology' (Keurentjes et al. 2011), which incorporates ecological relationships and the phenotypic plasticity of plants that is regarded as an aspect of green intelligence.

From the perspective of the twenty first century plant neurobiology, plants are no longer to be viewed as passive automata but as agents with a capacity for recalling, predicting and operating in the world with some innovation. According to Bellare and Trewavas (2009), the study of plant behaviour has now not only come of age, but understanding its complexity will be the most important task of plant biologists in this century.

Acknowledgments I thank the members of the Indian Institute of Science, Bangalore, and of the Bose Institute in Kolkata for their generous hospitality. Especially, I thank Debi Sengupta, for his friendship and lively discussions.

References

Agutter PS, Malone PL, Wheatley DN (2000) Diffusion theory: a relic of mechanistic materialism. J Hist Biol 33:71–111

Albert R (2005) Scale-free networks in cell biology. J Cell Sci 118:4947–4957

Alpi A et al (2007) Plant neurobiology: no brain no gain. Trends Plant Sci 12:135–136

Antkowiak B, Engelmann W (1995) Oscillations of apoplasmic K^+ and H^+ activities in *Desmodium motorium* (Hout) Merril. pulvini in relation to the membrane potential of motor cells and leaflet movements. Planta 196:350–356

Antkowiak B, Mayer WE, Engelmann W (1991) Oscillations of the membrane potential of pulvinar motor cells in situ in relation to leaflet movements of *Desmodium motorium*. J Exp Bot 42:901–910

Bais HP, Park SW, Weir TL, Callaway RM, Vivanco JM (2004) How plants communicate using the underground information superhighway. Trends Plant Sci 9:26–32

Ballare CL (2009) Illuminated behaviour: Phytochrome as a key regulator of light foraging and plant anti-herbivore defence. Plant, Cell Environ 32:713–725
Ballare CL, Trewavas AJ (2009) Plant behaviour, special issue introduction. Plant, Cell Environ 32:605
Baluska F, Mancuso S (2007) Plant neurobiology as a paradigm shift not only in the plant sciences. Plant Sign Behav 2:205–207
Baluska F, Samaj J, Wojtaszek P, Volkmann D, Menzel D (2003a) Cytoskeleton-plasma membrane-cell wall continuum in plants: emerging links revisited. Plant Physiol 133:482–491
Baluska F, Samaj J, Menzel D (2003b) Polar transport of auxin: carrier-mediated flux across the plasma membrane or neurotransmitter-like secretion? Trends Cell Biol 13:282–285
Baluska F, Mancuso S, Volkmann D, Barlow PW (2004) Root apices as plant command centres: the unique 'brain-like' status of the root apex transition zone. Biologia, Bratislava 59(Suppl. 13): 1–13
Baluska F, Volkmann D, Menzel D (2005) Plant synapses: actin-based adhesion domains for cell-to-cell communication. Trends Plant Sci 10:106–111
Baluska F, Volkmann D, Hlavacka A, Mancuso S, Barlow PW (2006) Neurobiological view of plants and their body plan. In: Baluska F, Mancuso S, Volkmann D (eds) Communication in plants: Neuronal aspects of plant life. Springer, Berlin, pp 19–35
Barlow PW (2006) Charles Darwin and the plant root apex: closing a gap in living systems theory as applied to plants. In: Baluska F, Mancuso S, Volkmann D (eds) Communication in plants: neuronal aspects of plant life. Springer, Berlin, pp 37–51
Barlow PW (2008) Reflections on plant neurobiology. Biosystems 92:132–147
Barlow PW (2010a) Plant roots: autopoietic and cognitive constructions. Plant Root 4:40–52
Barlow PW (2010b) Plastic, inquisitive roots and intelligent plants in the light of some new vistas in plant biology. Plant Biosyst 144:396–407
Becker RO, Marino AA (1982) Electromagnetism of life. State University of New York Press, Albany
Bond DM, Finnegan EJ (2007) Passing the message on: inheritance of epigenetic traits. Trends Plant Sci 12:211–216
Bondyopadhyay PK (1998) Sir J.C. Boses's diode detector received Marconi's first transatlantic wireless signal of December 1901 (The "Italian Navy Coherer" Scandal Revisited). Proc IEEE 86:259–285
Bose JC (1902) Response in the living and non-living. Longmans, Green and Co, London
Bose JC (1904) Patent for Detector for Electrical Disturbances. reprinted in Trans IEEE 1998 86: 230–234
Bose JC (1913) Researches on irritability of plants. Longmans, Green and Co, London
Bose JC (1917) The voice of life. In: Acharya JC (ed) Bose: The scientific legacy, Bose Inst Kolkata 2004, pp 1-11
Bose JC (1918) Life movements in plants. Trans Bose Res Inst Calcutta, Bengal Government Press, Calcutta
Bose JC (1923) The physiology of the ascent of sap. Longmans, Green and Co, London
Bose JC (1926) The nervous mechanisms of plants. Longmans, Green and Co, London
Bose I, Karmakar R (2003) Simple models of plant learning and memory. Phys Script T106:9–12
Bothwell JHF, Ng CY-K (2005) The evolution of Ca^{2+} signalling in photosynthetic eucaryotes. New Phytol 166:21–38
Boyko A, Kovalchuk I (2010) Transgenerational response to stress in *Arabidopsis*. Plant Signal Behav 5:995–998
Brenner E, Stahlberg R, Mancuso S, Vivanco J, Baluska F, van Volkenburgh E (2006) Plant neurobiology: an integrated view of plant signalling. Trends Plant Sci 11:413–419
Calvo Garzon P, Keijzer F (2011) Plants: Adaptive behaviour, root-brains, and minimal cognition. Adapt Behav 19:155–171
Chakrabarti P (2004) Western science in modern India: metropolitan methods, colonial practices. Orient, Longman Ltd, India

Cvrckova F, Lipavska H, Zarsky V (2009) Plant Intelligence: why, why not or where? Plant Signal Behav 4:394–399
Dasgupta S (1998) Jagadis Bose, Augustus Waller and the discovery of 'vegetable electricity'. Notes Rec Roy Soc Lond 52:307–322
Davies E (1987a) Action potentials as multifunctional signals in plants: a unifying hypothesis to explain apparently disparate wound responses. Plant, Cell Environ 10:623–631
Davies E (1987b) Plant responses to wounding. In: Stumpf PK, Conn EE (eds) The biochemistry of plants, vol 12. Academic, New York, pp 243–264
Davies E (2004) New functions for electrical signals in plants. New Phytol 161:607–610
Davies E (2006) Electrical signals in plants: facts and hypotheses. In: Volkov AG (ed) Plant electrophysiology-theory and methods. Springer, Berlin, pp 407–422
Davies E, Stankovic B (2006) Electrical signals, the cytoskeleton, and gene expression: a hypothesis on the coherence of the cellular responses to environmental insult. In: Baluska F, Mancuso S, Volkmann D (eds) Communication in plants—neuronal aspects of plant life. Springer-Verlag, Berlin, pp 309–320
de Kroon H, Visser EJW, Huber H, Mommer L, Hutchings MJ (2009) A modular concept of plant foraging behaviour: the interplay between local responses and systemic control. Plant, Cell Environ 32:704–712
Dicke M (2009) Behavioural and community ecology of plants that cry for help. Plant, Cell Environ 32:654–665
Drack M, Apfalter W, Pouvreau D (2007) On the making of a system theory of life: Paul A. Weiss and Ludwig von Bertalanffy's conceptual connection. Q Rev Biol 82:349–373
Dudley SA, File AL (2007) Kin recognition in an annual plant. Biol Lett 3:435–438
Dudley SA, File AL (2008) Yes, kin recognition in an annual plant! Biol Lett 4:69–70
Ellingsrud S, Johnsson A (1993) Perturbations of plant leaflet rhythms caused by electromagnetic radio-frequency radiation. Bioelectromag 14:257–271
Emerson DT (1997) Jagadis Chandra Bose: millimetre wave research in the nineteenth century. IEEE Trans Microwave Theory Tech 45:2267–2273
Engineer M (2009) The millimetre wave researches of J.C. Bose. In: Sen Gupta DP, Engineer MH, Shepherd VA (eds) Remembering Sir J.C. Bose. IISc Press, World Scientific, New Jersey, London, Singapore, Beijing, Shanghai, Hong Kong, Taipai, Chennai
Ettlinger C, Lehle L (1988) Auxin induces rapid changes in phosphatidylinositol metabolites. Nature 331:176–178
Fromm J, Eschrich W (1998a) Transport processes in stimulated and non-stimulated leaves of *Mimosa pudica*. I. The movement of ^{14}C-labelled assimilates. Trees 2:7–17
Fromm J, Eschrich W (1998b) Transport processes in stimulated and non-stimulated leaves of *Mimosa pudica*. II. Energesis and transmission of seismic stimulations. Trees 2:18–24
Fromm J, Eschrich W (1998c) Transport processes in stimulated and non-stimulated leaves of *Mimosa pudica*. III. Displacement of ions during seismonastic leaf movements. Trees 2:65–72
Fromm J, Fei H (1998) Electrical signaling and gas exchange in maize plants of drying soil. Plant Sci 132:203–213
Fromm J, Lautner S (2007) Electric signals and their physiological significance in plants. Plant, Cell Environ 30:249–257
Frommer W (2010) Grand opportunities in physiology to address the grand challenges facing the planet. Front Physiol 1:1–3
Galston AW, Slayman CL (1979) The not-so-secret life of plants. Am Sci 67:337–344
Garnier S, Gautrais J, Theraulaz G (2007) The biological principals of swarm intelligence. Swarm Intell 1:3–31
Geddes P (1920) The life and work of Sir Jagadis C. Bose. An Indian pioneer of science. Longmans and Green, London
Gensler W, Diaz-Munoz F (1983) Simultaneous stem diameter expansions and apoplastic electropotential variations following irrigation or rainfall in cotton. Crop Sci 23:920–923
Gensler W, Yan T-L (1998) Investigation of the causative reactant of the apoplast electropotentials of plants. J Electrochem Soc Electrochem Sci Tech 135:2991–2995

Haberlandt G (1928) Physiological plant anatomy. MacMillan and Co, London
Haldane JS (1912) Burdon-Sanderson and vitalism. Nature 89:215–216
Hartwell LH, Hopfield JJ, Leibler S, Murray AW (1999) From molecular to modular cell biology. Nature 402:C47–C52
Hedrich R, Schroeder JI (1989) The physiology of ion channels and electrogenic pumps in higher plants. Ann Rev Plant Physiol Plant Mol Biol 40:539–569
Hilker M, Kobs C, Varama M, Schrank K (2002) Insect egg deposition induces *Pinus sylvestris* to attract egg parasitoids. J Exp Bot 205:455–461
Hill BS, Findlay GP (1981) The power of movement in plants: the role of osmotic machines. Q Rev Biophys 14:173–222
Holzknecht K, Zurcher E (2006) Tree stems and tides- a new approach and elements of reflexion. Schweiz Z Forstwes 157:185–190
Hope AB, Walker NA (1975) The physiology of giant algal cells. Cambridge University Press, London
Jorgensen RA (2011) Epigenetics: biology's quantum mechanics. Front Plant Sci 2:1–4
Karban R (2008) Plant behaviour and communication. Ecol Lett 11:727–739
Kauffman S, Logan RK, Este R, Goebel R, Hobill D, Shmulevich I (2008) Propagating organization: an enquiry. Biol Philos 23:27–45
Keller EF (1983) A feeling for the organism: the life and work of Barbara McClintock. WH Freeman and Co, New York
Koestler A (1978) The ghost in the machine. Pan Books, London
Koziolek C, Grams TEE, Schreiber U, Matyssek R, Fromm J (2004) Transient knockout of photosynthesis mediated by electrical signals. New Phytol 161:715–722
Laschimke R, Burger M, Vallen H (2006) Acoustic emission analysis and experiments with physical model systems reveal a peculiar nature of the xylem tension. J Plant Physiol 163: 996–1007
Mancuso S (1999) Hydraulic and electrical transmission of wound-induced signals in *Vitis vinifera*. Aust J Plant Physiol 26:55–61
Masi E, Ciszak M, Stefano G, Renna L, Azzarello E, Pandolfi C, Mugnai S, Baluska F, Arecchi FT, Mancuso S (2009) Spatiotemporal dynamics of the electrical network activity in the root apex. Proc Nat Acad Sci 106:4048–4053
Massa GD, Gilroy S (2003) Touch modulates gravity sensing to regulate the growth of primary roots of *Arabidopsis thaliana*. Plant J 33:435–445
McGary KL, Park TJ, Woods JO, Cha HJ, Wallingford JB, Marcotte EM (2010) Systematic discovery of nonobvious human disease models through orthologous phenotypes. Proc Nat Acad Sci 107:6544–6549
McNickel GG, Cassady St Clair C, Cahill JF (2009) Focusing the metaphor: plant root foraging behaviour. Trends Ecol Evol 24:419–426
Mescher M, Runyon JB, De Moraes CM (2006) Plant host finding by parasitic plants. A new perspective on plant-to-plant communication. Plant Signal Behav 1:284–286
Mitra AP (1997) J.C. Bose: at the dawn of radio science. Sci Cult 63:6–8
Mitsuno T, Sibaoka T (1989) Rhythmic electrical potential change of motor pulvinus in lateral leaflet of *Codariocalyx motorius*. Plant Cell Physiol 30:1123–1127
Molinier J, Ries G, Zipfel C, Hohn B (2006) Transgenerational memory of stress in plants. Nature 442:1046–1049
Mott KA, Buckley TN (2000) Patchy stomatal conductance: emergent collective behaviour. Trends Plant Sci 5:258–262
Nandy A (1995) Alternative sciences. Creativity and authenticity in two Indian scientists. Oxford University Press, Delhi
Normann J, Vervleit-Scheebaum M, Albrechtova J, Wagner E (2007) Rhythmic stem extension growth and leaf movements as markers of plant behaviour: the integral output from endogenous and environmental signals. In: Mancuso S, Shabala S (eds) Rhythms in plants: phenomenology, mechanisms, and adaptive significance. Springer, Berlin, pp 200–217

Novoplansky A (2009) Picking battles wisely: plant behaviour under competition. Plant, Cell Environ 32:726–741
Oda K (1976) Simultaneous recording of potassium and chloride efflux during an action potential in *Chara corallina*. Plant Cell Physiol 17:1085–1088
Oda K, Linstead PJ (1975) Changes in cell length during action potentials in *Chara*. J Exp Bot 26:228–239
Peters R (1969) The problem of cytoplasmic integration. Proc Roy Soc Lond Ser B Biol Sci 173:11–19
Piccolino M (2006) Luigi Galvani's path to animal electricity. CR Biologie 329:303–318
Pickard BG (1973) Action potentials in higher plants. Bot Rev 39:172–201
Ramaseshan S (1996) The centennial of the discovery of millimetre waves by Jagadis Chandra Bose (1858–1937). Curr Sci 70:172–175
Ravasz E, Somera AL, Mongru DA, Oltvai ZN, Barabasi A-L (2002) Hierarchial organization of modularity in metabolic networks. Science 297:1551–1555
Riofrio W (2008) Understanding the emergence of cellular organisation. Biosemiotics 1:361–377
Roberts K (1992) Potential Awareness of Plants. Nature 360:14–15
Seeley TD, Levien RA (1987) A colony of mind. The beehive as thinking machine. Sciences 27:38–43
Sen Gupta DP (2009) Jagadish Chandra Bose: the man and his time. In: Sen Gupta DP, Engineer MH, Shepherd VA (eds) Remembering sir J.C. Bose. IISc Press, WSPC Publications, New Jersey, London, Singapore
Sengupta D, Sarkar TK, Sen D (1998) Centennial of the semiconductor diode detector. Proc IEEE 86:235–243
Seyfarth CA (2006) Julius Bernstein (1839–1917): pioneer neurobiologist and biophysicist. Biol Cybernet 94:2–8
Shabala SN, Knowles A (2002) Rhythmic patterns of nutrient acquisition by wheat roots. Funct Plant Biol 29:595–605
Shepherd VA (1999) Bioelectricity and the rhythms of sensitive plants- the biophysical research of Jagadis Chandra Bose. Curr Sci 77:189–195
Shepherd VA (2005) From semi-conductors to the rhythms of sensitive plants: the research of J.C Bose. Cell Mol Biol 51:607–619
Shepherd VA, Shimmen T, Beilby MJ (2001) Mechanosensory ion channels in *Chara*: the influence of cell turgor pressure on touch-activated receptor potentials and action potentials. Aust J Plant Physiol 28:551–566
Shepherd VA, Beilby MJ, Shimmen T (2002) Mechanosensory ion channels in charophytes: the response to touch and to salinity stress. Eur Biophys J 31:341–355
Shepherd VA, Beilby MJ, Al Khazaaly SAA, Shimmen T (2008) Mechanoperception in *Chara* cells: the influence of salinity and calcium on touch-activated receptor potentials, action potentials, and ion transport. Plant, Cell Environ 31:1575–1591
Shimmen T (2001) Involvement of receptor potentials and action potentials in mechano-perception in plants. Aust J Plant Physiol 28:567–576
Shimmen T (2006) Electrophysiology of mechanosensing and wounding response. In: Volkov AG (ed) Plant electrophysiology-theory and methods. Springer, Berlin, pp 319–339
Sibaoka T (1969) Physiology of rapid movements in higher plants. Ann Rev Plant Physiol 20: 165–184
Sibaoka T (1991) Rapid plant movements triggered by action potentials. Bot Mag Tokyo 104:73–95
Simons P (1992) The action plant. Movement and nervous behaviour in plants. Blackwell, Oxford, Cambridge
Souda M, Toko K, Hayashi K, Fujiyoshi T, Ezaki S, Yamafuji K (1990) Relationship between growth and electric oscillations in bean roots. Plant Physiol 93:532–536
Stahlberg R, Cosgrove DJ (1997) The propagation of slow wave potentials in pea epicotyls. Plant Physiol 113:209–217

Stanković B, Witters DL, Zawadzki T, Davies E (1998) Action potentials and variation potentials in sunflower: an analysis of their relationships and distinguishing characteristics. Physiol Plant 103:51–58

Strogatz SH (2001) Exploring complex networks. Nature 410:268–276

Strogatz SH (2003) Sync: the emerging science of spontaneous order. Hyperion, USA

Struik PC, Yin X, Meinke H (2008) Plant neurobiology and green plant intelligence: science, metaphors and nonsense. J Sci Food Agric 88:363–370

Tafforeau M, Verdus MC, Norris V, Ripoll C, Thellier M (2006) Memory processes in the response of plants to environmental signals. Plant Sign Behav 1:9–14

Telewski FW (2006) A unified hypothesis of mechanoperception in plants. Am J Bot 93:1466–1476

Thellier M, Desbiez MO, Champagnat P, Kergosien Y (1982) Do memory processes occur in plants? Physiol Plant 56:281–284

Trewavas AJ, Malho R (1998) Ca^{2+} signalling in plant cells: the big network! Curr Opin Plant Biol 1:428–433

Trewavas AJ (1999a) How plants learn. Proc Natl Acad Sci USA 96:4216–4218

Trewavas AJ (1999b) Le calcium, c'est la vie: calcium makes waves. Plant Physiol 120:1–6

Trewavas AJ (2003) Aspects of plant intelligence. Ann Bot 92:1–20

Trewavas AJ (2005a) Plant intelligence. Naturwiss 92:401–403

Trewavas AJ (2005b) The green plant as an intelligent organism. Trends Plant Sci 10:413–419

Trewavas AJ (2006) The green plant as an intelligent organism. In: Baluska F, Mancuso S, Volkmann D (eds) Communication in plants: neuronal aspects of plant life. Springer, Berlin, pp 1–18

Trewavas AJ (2009) What is plant behaviour? Plant, Cell Environ 32:606–616

Van den Driessche T (2000) Nutations in shoots and in *Desmodium* lateral leaflets, nyctinastism and seismonastism in *Mimosa pudica*. Comparison and evolution of morphology and mechanism. Biol Rhythm Res 31:451–468

Veit-Brause I (2002) The making of a modern scientific personae: the scientist as a moral person? Emil Du-Bois Reymond and his friends. Hist Hum Sci 15:19–49

Verkhratsky A, Krishtal OA, Petersen OH (2006) From Galvani to patch-clamp: the development of electrophysiology. Pflugers Arch Eur J Physiol 453:233–247

Vodeneev VA, Akinchits EK, Orlova LA, Sukhov VS (2011) The role of ions Ca^{2+}, H^+ and Cl^- in generation of variation potential in pumpkin plants. Russ J Plant Physiol 58:974–981

Volkov AG, Dunkley TC, Morgan SA, Ruff D, Boyce YC, Labady AJ (2004) Bioelectrochemical signalling in green plants induced by photosensory systems. Bioelectrochem 63:91–94

Volkov AG, Carrell H, Adesina T, Markin VS, Jovanov E (2008) Plant electrical memory. Plant Signal Behav 3:490–492

Volkov AG, Foster JC, Markin VS (2010) Signal transduction in *Mimosa pudica*: biologically closed electrical circuits. Plant, Cell Environ 33:816–827

Wagner E, Lehner L, Normann J, Weit J, Albrechtova J (2006) Hydro-electrochemical integration of the higher plant- basis for electrogenic flower induction. In: Baluska F, Mancuso S, Volkmann D (eds) Communication in plants: neuronal aspects of plant life. Springer, Berlin, pp 369–389

Watts DJ, Strogatz SH (1998) Collective dynamics of small-world networks. Nature 393:440–442

Wayne R (1994) The excitability of plant cells: with a special emphasis on characean internodal cells. Bot Rev 60:265–367

Wildon DC, Thain JF, Minchin PEH, Gubb IR, Reilly AJ, Skipper YD, Doherty HM, O'Donnell PJ, Bowles DJ (1992) Electrical signalling and systemic proteinase inhibitor induction in the wounded plant. Nature 360:62–65

Yuan JS, Galbraith DW, Dai SY, Griffin P, Neal Stewart C (2008) Plant systems biology comes of age. Trends Plant Sci 13:165–171

Zimmermann U, Beckers F (1978) Generation of action potentials in *Chara corallina* by turgor pressure changes. Planta 138:173–179

Zurcher E, Cantiani M-G, Sorbett-Guerri F, Michel D (1998) Tree stem diameters fluctuate with tide. Nature 392:665–666

Zurcher E, Schlaepfer R, Conedara M, Giudici F (2009) Looking for differences in wood properties as a function of felling date: lunar phase correlated variations in the drying behaviour of Norway spruce (*Picea alba* Karst) and sweet chestnut (*Castaneae sativa)*. Trees 30:249–257. doi:10.1007/

Chapter 2
Plant Electrostimulation and Data Acquisition

Emil Jovanov and Alexander G. Volkov

Abstract Plant electrostimulation is a very efficient method for evaluation of biologically closed electrical circuits in plants. The information gained from plant electrostimulation can be used to elucidate and observe the intracellular and intercellular communication in the form of electrical signals within plants. Monitoring the electrical signaling in higher plants represents a promising method to investigate fast electrical communication during environmental changes. Here we discuss DC methods of plant electrostimulation and describe a new Charge Stimulation Method in plant electrophysiology. It is often convenient to represent the real electrical and electrochemical properties of biointerfaces with idealized equivalent electrical circuit models consisting of discrete electrical components. Biologically closed electrical circuits in plants can be investigated using the Charge Stimulation Method.

2.1 Introduction

The electrical phenomena in plants have attracted researchers since the eighteenth century (Bertholon 1783; Bose 1907, 1913, 1918, 1926, 1928; Burdon-Sanderson 1873; Davies 2006; Keller 1930; Ksenzhek and Volkov 1998; Lemström 1904;

E. Jovanov (✉)
Electrical and Computer Engineering Department,
University of Alabama in Huntsville, Huntsville, AL 35899, USA
e-mail: emil.jovanov@uah.edu

A. G. Volkov
Department of Chemistry, Oakwood University,
7000 Adventist Blvd, Huntsville, AL 35896, USA
e-mail: agvolkov@yahoo.com

A. G. Volkov (ed.), *Plant Electrophysiology*,
DOI: 10.1007/978-3-642-29119-7_2, © Springer-Verlag Berlin Heidelberg 2012

Sinukhin and Britikov 1967; Volkov 2006a, b). Biologically closed electrical circuits (Nordestrom 1983) operate over large distances in biological tissues. The activation of such electrical circuits can lead to various physiological and biochemical responses. The cells of many biological organs generate electric potentials that can result in the flow of electric currents (Volkov et al. 1998). Electrical impulses may arise as a result of stimulation. Once initiated, these impulses can propagate to adjacent excitable cells. The change in transmembrane potential can create a wave of depolarization which affects the adjoining, resting membranes. Thus, while the plasma membrane is stimulated at any point, the action potential can propagate over the entire length of the cell membrane and along the conductive bundles of tissue with constant amplitude, duration, and speed (Volkov 2006b). Characteristic length of action potentials is defined as the propagation speed multiplied by the duration of the action potential. To detect the real action potentials, the distance between electrodes should exceed the characteristic length of an action potential. Graded, electrotonic, and variation potentials propagate with decreasing amplitude. Electrical signals can propagate along the plasma membrane on short distances in plasmodesmata, and on long distances in conductive bundles. Action potentials in higher plants hold promise as the information carriers in intracellular and intercellular communication during environmental changes (Volkov 2000, 2006b).

Measurement of plant electrical activity and evoked potentials raise a number of challenging issues, including type and position of electrodes, reference potentials, methodology of measurement, and synchronization with external events. Omissions and mistakes in methodology may lead to incorrect conclusions about the nature of underlying processes. One of the typical mistakes is creating direct analogies between standard electrical circuits and electrical circuits in plants. Electrical circuits have clearly defined reference potential ("common ground") and all potentials are measured relative to the ground potential. Most potentials in computer systems are digital and exhibit high immunity to noise. In contrast, plants exhibit a hierarchical structure with no common ground potential, many signals are nonlinear, and have poor signal to noise ratio.

Scientific hypotheses could be tested using electrical stimulation of plants and monitoring of biological effects caused by the stimulation.

In this chapter we present methods for monitoring and stimulation of plant's electrical activity. In addition to fundamental theoretical concepts we present our experience in the configuration and development of the custom data acquisition and plant DC stimulation systems, and results from plant experiments.

2.2 Data Acquisition

Although many processes in plants are slow enough for direct observation, a number of processes are too quick and require additional instrumentation for scientific study. Typical example is mechanical closing of carnivorous plants, such as the Venus

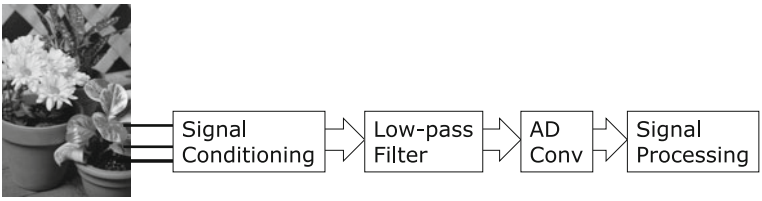

Fig. 2.1 Block diagram of the data acquisition system

flytrap, that can close lobes and capture small insects in a fraction of the second (Markin et al. 2008; Volkov et al. 2007, 2008a, b). In addition to fast cameras, it is necessary to monitor electrical activity and plant signaling during closing.

Data acquisition is the process of converting analog physical signals into digital numeric values that can be stored, processed, and visualized by a computer. Data acquisition systems are often represented by the acronyms DAS or DAQ. Recent development of embedded computer systems and standard data acquisition boards lead to the development of virtual instrumentation that allows use of common hardware with custom software to represent virtual instruments for a variety of applications.

Typical components of data acquisition systems include:

- *Sensors* that convert physical parameters to electrical signals that can be processed by the data acquisition system,
- *Signal conditioning circuits* to convert sensor signals into a form that can be converted to digital values,
- *Analog-to-digital converters*, which convert conditioned sensor signals to digital values,
- *Microprocessor-based controller* that performs the following functions:
  - user interface and control,
  - file access and storage,
  - networking for distributed systems,
  - signal processing and analysis, and
  - result presentation and visualization

For example, a digital thermometer might use thermistor as *sensor* to convert temperature to variable resistance; *signal conditioning circuit* (such as voltage divider or amplifier) to convert variable resistance to variable voltage, amplify and filter signal; *analog-to-digital converter* can be used to convert the voltage to digital values that are read and processed by the microcontroller, and displayed to the user.

Analog-to-digital conversion assumes analog voltages relative to the reference voltage.

Data acquisition applications are typically controlled by application-specific programs that provide custom user-interfaces, processing, and presentation of results (Fig. 2.1).

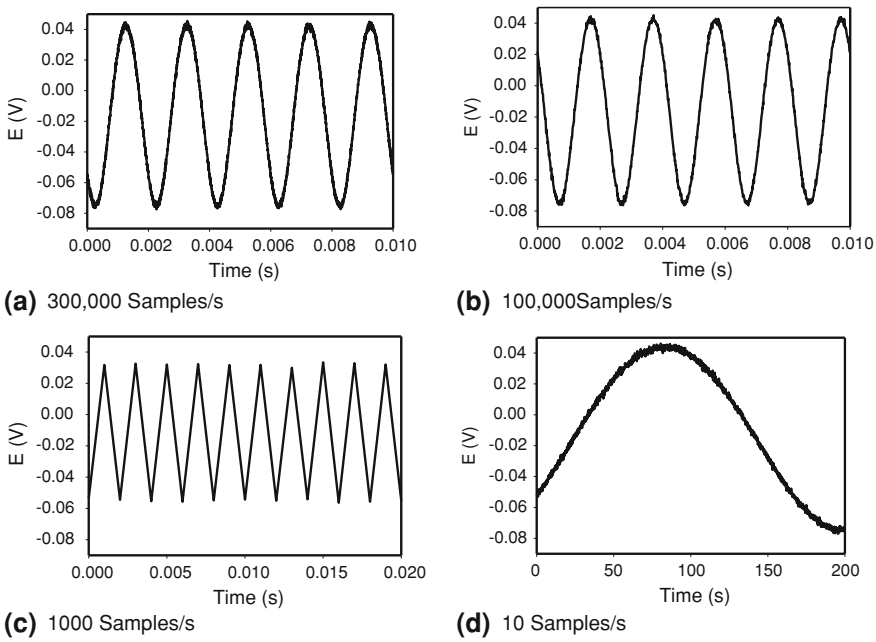

Fig. 2.2 Reconstructed 500 Hz sinusoidal signal from the digitized signal sampled at **a** 300,000 samples/second, **b** 100,000 samples/second, **c** the Nyquist rate of 1,000 samples/second; **d** aliased 500 Hz signal due to under sampling at 10 samples/second

2.2.1 Sampling

Sampling represents the process of converting continuous analog signals with unlimited time and amplitude resolution to discrete samples equivalent to the instantaneous value of the continuous signal at the desired time points. Typical sampling of the analog signal is represented in Fig. 2.2. Sampling involves time and amplitude discretization, as described in the following sections.

2.2.1.1 Time Discretization

Continuous analog signal is converted to a sequence of discrete samples in discrete time points that could be uniform or variable. Uniform sampling is commonly used, where the sampling interval T_s determines sampling frequency or sampling rate F_s:

$$F_s = \frac{1}{T_s} \tag{2.1}$$

Sampling frequency determines the number of samples obtained in one second, represented in samples per second or expressed in Hertz (Hz). For example,

sampling frequency $F_s = 100$ Hz means that we will collect 100 samples of the signal per second.

Fundamental limitation of sampling is represented by Nyquist–Shannon sampling theorem (Shannon 1949) which shows that a sampled analog signal can be perfectly reconstructed from an infinite sequence of samples if the sampling rate exceeds $2 \cdot F_{max}$ samples per second, where F_{max} represents the highest frequency of the original signal, also known as Nyquist frequency:

$$F_s \geq 2 F_{max} \tag{2.2}$$

Therefore, data acquisition systems must satisfy two conditions:

- The signal conditioning circuit must limit maximum frequency of the signal to $F_{s\ max}$ [Hz]; typically, this is implemented as a low pass or band pass filter with maximum cutoff frequency of $F_{s\ max}$ [Hz]. Please note that even without periodic high-frequency components, fast changing signals have wide spectrum (theoretically infinite spectrum) that must be limited for correct data acquisition.
- The data acquisition card must sample signals with sampling rate of at least $2 \cdot F_{max}$ [Hz]. However, lower cutoff frequency of the low pass filter may distort the signal in the presence of fast changing signals (see previous condition); hence, cutoff frequency of the low pass filter is usually selected close to $F_s/2$.

Consequently:

> Sampling frequency F_s is selected to preserve most of the frequency content and shape of the signal, and data acquisition systems must use low pass filter with cutoff frequency not higher than $F_s/2$.

Figure 2.3 represents an example of inadequate sampling frequency and wrong conclusions that might be drawn from the measurement. A sequence of fast regular pulses sampled at low frequency might generate the impression that the underlying phenomenon is a single, slow changing pulse, as represented in the lower plot of Fig. 2.3.

General purpose voltmeters typically represent slow data acquisition systems with sampling rate in the order of few samples per second. Therefore, some high speed changes might generate false impression of the underlying phenomena, as represented in Fig. 2.3.

2.2.1.2 Quantization and Coding

Analog samples are converted to digital values using Analog-to-Digital or AD Converters. AD converter represents a quantizer with a number of discrete levels against which the sampled amplitude is compared to generate a binary code representing amplitude of the current sample. The number of levels is defined by the resolution or number of bits (nb) of the AD converter. The value of the

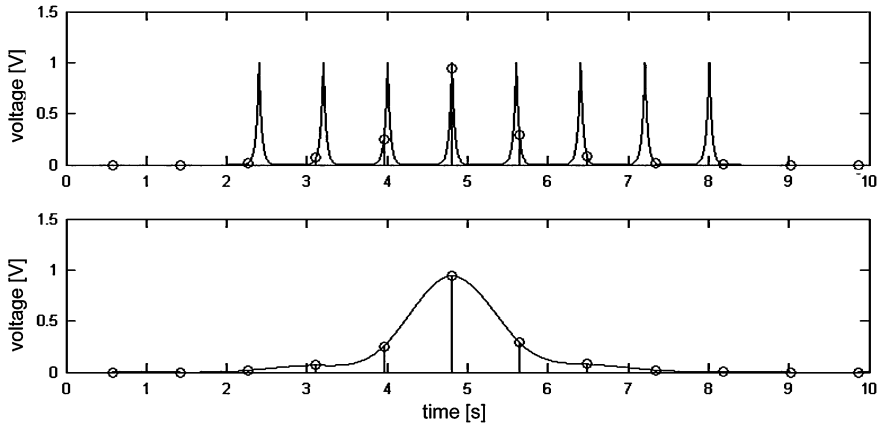

Fig. 2.3 Illustration of data acquisition with inadequate sampling frequency; *upper plot* synthetic signal as a sequence of pulses; *lower plot* reconstructed signal sampled with low sampling frequency

quantization step Δ depends on the range and resolution of the AD converter and can be represented as:

$$\Delta = \frac{V^+ - V^-}{2^{\text{nb}}} \tag{2.3}$$

where V^+ and V^- represent positive and negative reference voltages, and $V_{\text{range}} = V^+ - V^-$. For example, a 12-bit AD converter with $V^+ = 5$ V and $V^- = 0$ V has quantization step of:

$$\Delta = \frac{5\,\text{V} - 0\,\text{V}}{2^{12}} = \frac{5\,\text{V}}{4096} = 1.22\,\text{mV} \tag{2.4}$$

Error generated by the quantization can be represented as a noise generated by conversion. For the truncation quantizer the maximum error can be represented as:

$$0 \leq \varepsilon \leq \Delta = \frac{V_{\text{range}}}{2^{\text{nb}}} \tag{2.5}$$

Therefore, signal to noise ratio and maximum noise can be controlled by the resolution of the AD converter. Quantization and coding are represented in Fig. 2.4.

If a single AD converter is used for multiple signals (multichannel configuration), individual channels might use separate references (*differential input*) or a single reference for all channels (*single ended*). Noise immunity is much better with differential input, while single ended recording allows two times more channels in the same data acquisition setup.

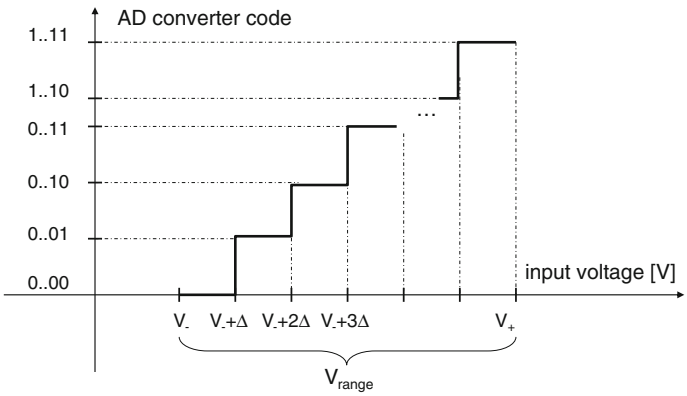

Fig. 2.4 Quantization and coding

2.2.2 Signal Conditioning

Monitoring of electrical activity of plants creates several unique challenges:

- plant's electrical activity generates very small voltages, typically in the order of mV or tens of mV
- sources of plant's electrical activity are very weak and must be amplified to improve noise immunity of the signals
  - amplifiers also need a reference point (referenced as "GROUND" in typical electrical systems); however, choice of the reference point may significantly influence signal generation and signal quality. The most convenient reference point is soil around the plant; however, in many applications this configuration is inadequate due to large resistance between sources of plant activity and root/soil around the plant.
  - separate source ground and measurement system grounds create difference in ground potentials and ground loops, visible mostly as power line interference (50 Hz in Europe or 60 Hz in America).
- long wires typically require differential acquisition or optical isolation of sources of plant activity.

2.2.3 Impedance Matching

Sources of plant electrical activity can be represented as ideal voltage source with series resistance, as represented in Fig. 2.5. Measured voltage (V_m) will depend on the resistance of electrodes (R_e), as well as input resistance of the measurement device (R_{in}) and can be represented as:

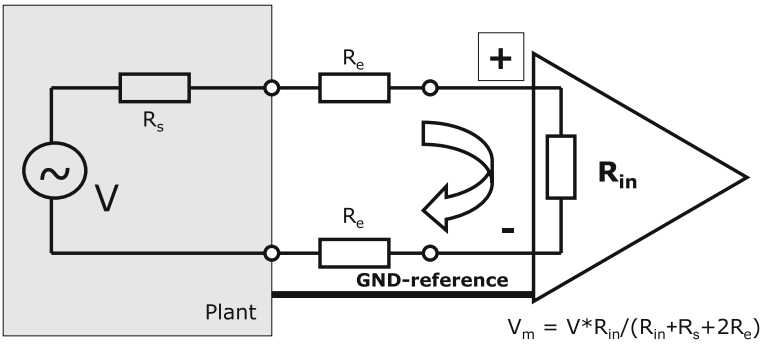

Fig. 2.5 Measured potential as a function of the internal resistance of the measurement equipment; R_e—electrode impedance, R_s—source impedance, R_{in}—input impedance of the measurement system

$$V_m = V_s \frac{R_{in}}{R_{in} + R_s + 2R_e} = V_s \frac{1}{1 + \frac{R_s}{R_{in}} + \frac{2R_e}{R_{in}}} \tag{2.6}$$

For very large values of the input resistance $(R_{in} \to \infty)$, $V_m \approx V_s$.

Typical values for R_e are in the order of a few kΩ for Ag/AgCl electrodes and tens of MΩ for ion selective electrodes with membranes, while R_s is often in the order of hundreds or thousands of kΩ. Therefore, input resistance of the data acquisition system must be at least in the order of GΩ to accurately represent the signal. That is the reason why low input resistance oscilloscopes cannot be used without signal conditioning and amplification of the signal.

2.3 DC Methods of Electrostimulation

There are a few "methods" of plant electrostimulation such as using DC source of voltage or electrical current (Houwink 1935, 1938; Jonas 1970; Mizuguchi et al. 1994; Volkov et al. 2007), function generator (Volkov et al. 2012), charge stimulation method (Volkov et al. 2008a, b, c, 2009a, b, 2010a, b, c, d, 2011a, b, c, d) or AC method of electrical impedance (Inaba et al. 1995; Laarabi et al. 2005; Wang et al. 1994; Zhang and Willison 1991).

2.3.1 Function Generator

Function generators are routinely used for stimulation of the general purpose electrical circuits. The function generator gives many options for the electrostimulation: shapes, duration, frequency of stimulation, and offset voltage U_{offset}, but it cannot regulate the electrical charge or electrical current during the plant electrostimulation.

Function generator actively drives all states of the generated signal. For example, for a square wave signal, function generator will generate inactive states as voltage equal to 0 V and active state at a certain voltage (e.g., 1 V output). This means that the function generator connected to the plant will actively force 0 V voltage even during inactive state that will in most cases interfere with the resting state of the plant (approximately 20–60 mV generated by the plant). Similarly, when a function generator is used to apply pulses with a given potential, it generates a potential of zero volts when the pulse is not being applied. For example, when the generator applies a 100 mV pulse lasting for 1 s, the function generator will generate a 0 mV output before and after the pulse. This means that the native plant potential will be forced to zero during periods of no stimulation, which interferes with the normal plant signaling mechanism and electrical recovery of the plant.

Therefore, stimulation using function generator interferes with the electrical recovery of the plant. That is the reason why we used charge stimulation method.

2.3.2 Charge Stimulation Method

Charged capacitor applies electrical potential between two electrodes decreasing gradually to zero during the discharge of a capacitor. A function generator maintains a given high or low potential in the electrodes. For this reason, the electrical response during the potential increase or decrease from a function generator has corresponding positive or negative amplitude. Therefore, in order to estimate the plant's response after stimulation, we have to effectively "disconnect" the function generator from the plant and monitor the plant's electrical response. This feature is not available with standard function generators. We propose the use of the charge stimulation method that allows delivery of an electrical charge and disconnection from the plant. The charge is delivered from a capacitor that is charged at a given potential. When a capacitor with capacitance C is connected to the source with potential voltage U, the total capacitor charge is $Q = CU$, which allows precise regulation of the amount of charge during stimulation by using different capacitors and applying various voltages. A mechanical or electronic switch can instantaneously connect the charged capacitor to the plant and induce a response for a given stimulation period and disconnect the capacitor to monitor the plant's response (Volkov et al. 2010b, 2011a).

We applied a novel electrostimulation method, as presented in Fig. 2.6, to allow separate control of both amplitude and timing of the stimulation pulse and to provide a high-impedance optical isolation when the plant is not stimulated. We used a custom board with microcontroller *Texas Instruments* MSP430F149 to generate logic pulse of the precisely controlled duration on user's request. The pulse triggers a signal conditioning circuit with preset reference voltage through the optocoupler. This approach effectively disconnects the plant from the stimulation system when the pulse is not present. The amplifier allows active driving of

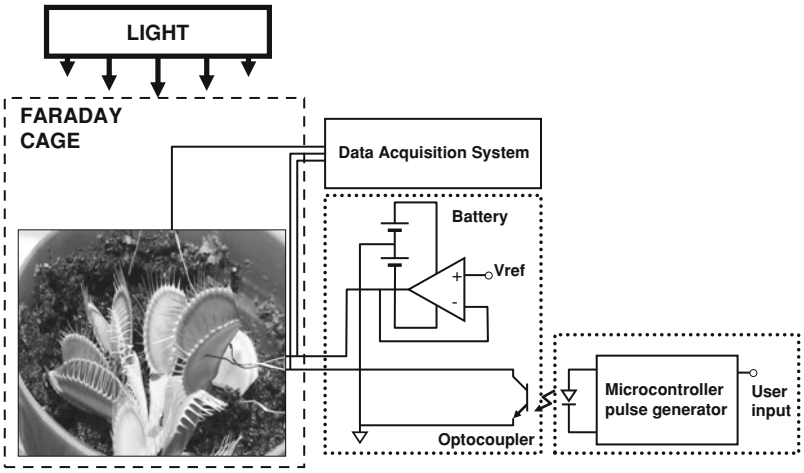

Fig. 2.6 Experimental setup for direct current electrostimulation of a plant with optical isolation

the pulse that results in much faster recharging of the capacitor. A separate battery was used to eliminate high-frequency interference of the pulse generator system.

Using our new DC electrostimulation system, it was evident that the application of an electrical stimulus between the midrib (positive potential) and a lobe (negative potential) causes the Venus flytrap to close the trap without any mechanical stimulation in 0.3 s after electrical stimulation (Volkov et al. 2007). The average stimulation pulse voltage sufficient for rapid closure of the Venus flytrap was 1.50 V (standard deviation is 0.01 V, $n = 50$) for 1 s. The inverted polarity pulse with negative voltage applied to the midrib could not close the plant. We were unable to open the plant by applying impulses in the same voltage range with different polarities for pulses of up to 100 s.

The primary objective of our experiments was to precisely determine the conditions of the charged electrical stimulation that generate a given biological effect. We implemented two types of electrostimulation: a manual switch and a custom made specific controller. Manual stimulation is convenient for single stimulation because it does not require additional equipment. It was implemented using a double pole double throw (DPDT) switch to connect the known capacitor to the voltage source during charging and then to the plant during plant stimulation to induce a response. However, manual switching does not allow precise control of timing of the stimulation. Therefore, we designed and implemented a custom plant stimulator to allow multiple stimulations with precise control of timing and voltage during stimulation. The plant stimulator is a battery-powered portable device controlled by a low-power microcontroller, MSP430F1611 (Texas Instruments, Texas, USA). A specialized PC program allows flexible configuration of the controller and communicates with the controller through optically isolated USB interface. During each stimulation cycle, the controller charges capacitor with

predefined voltage using integrated digital to analog (DA) converter of the microcontroller. A dual integrated analog switch controlled by the microcontroller connects the capacitor to DA converter during charging and to the plant during stimulation, allowing stimulation with microsecond resolution.

Each pulse can be controlled with resolution of 30 μs. The stimulation voltage can be set in steps of 0.6 mV to maximum voltage of 2.5 V. After charging, the capacitor with capacitance C charged with voltage V_s contains the amount of charge equal to $Q_1 = C\ V_s$ if the voltage after stimulation falls to V_{ps} the remaining charge will be $Q_2 = C\,V_{ps}$. Therefore, the stimulation delivered charge $\Delta Q = Q_1 - Q_2 = C(V_s - V_{ps})$. A dual integrated SPDT analog switch is controlled by the microcontroller and connects the capacitor to DA converter during charging and to the plant during stimulation. After N stimulations, the total amount of charge delivered is equal to $Q_s = C \cdot \sum_{i=1}^{N} (V_i - V_{pi})$. The proposed approach can therefore precisely define stimulation timing and charge. For a given capacitance of the stimulation capacitor, the user can select the number of stimulations N and the stimulation period.

For each stimulation, the capacitor was connected to electrodes in the plant until complete discharge and then disconnected from the electrodes. The following experiments with different conditions were performed at least 5 min later, although there was no noticeable difference in response for different time periods between stimulations. Voltage in the plant was measured between experiments, but no additional effects were detected between experiments. Electrodes remained in the plant between experiments.

It is possible to estimate charge $Q = UC$, electrical current $I = -\mathrm{d}Q/\mathrm{d}t$, work $W = U^2C/2$, power $P = UI$, and resistance $R = U/I$ from the time dependence of a capacitor discharge in a plant tissue as it is shown in Fig. 2.7 for a capacitor discharge in the Venus flytrap.

The charge stimulation method (Volkov et al. 2008a, b, 2009a, b, 2010a, b, c, d) was used to estimate, with high precision, the amount of electrical energy necessary to induce a response.

2.3.2.1 Mathematical Treatment of a Capacitor Discharge in Passive Electrical Circuits in Plants Developed by Professor V. S. Markin

If a capacitor of capacitance C with initial voltage U_0 is discharged during time t through a resistor R (Fig. 2.8a), the voltage across the capacitor decreases exponentially with time t:

$$U(t) = U_0 \cdot e^{-t/\tau} \tag{2.7}$$

where $\tau = \mathrm{RC}$ denotes the time constant and U_0 is the initial voltage of a capacitor (Feynman et al. 1963). Equation 2.7 in logarithmic form reads:

$$\log_{10} U(t) = \log_{10} U_0 - t/2.3 \tag{2.8}$$

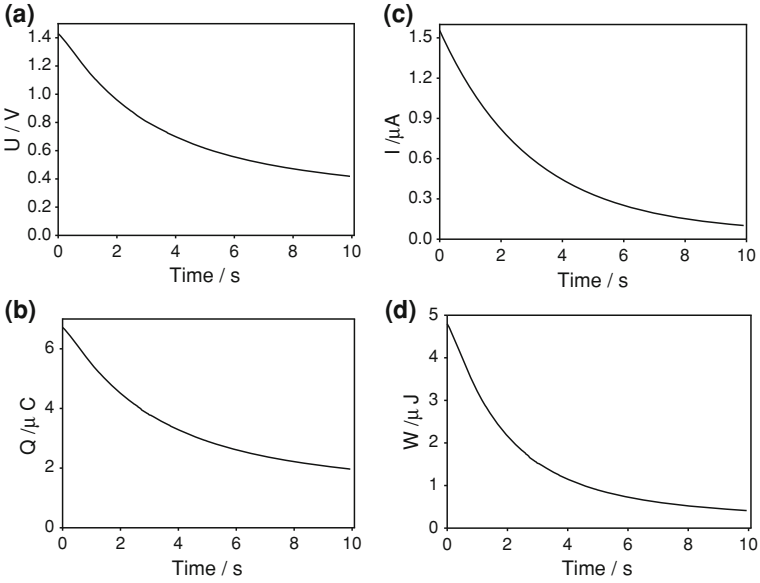

Fig. 2.7 Time dependencies of voltage U **a** charge Q **b** electrical current I **c**, and electrical energy W **d** during electrostimulation of the Venus flytrap upper leaf by 4.7 μF charged capacitor with initial voltage U_0 of 1.5

The time constant τ can be determined from the slope of this linear function. At $\tau = RC$, the capacitor charge is reduced to CU_0e^{-1}, which is about 37% of its initial charge. The voltage across the capacitor decreases exponentially from the initial value U_0 to zero. As the capacitance or resistance increases, the time of the capacitor discharge increases according to Eq. 2.7.

Professor V. S. Markin developed a mathematical treatment of a capacitor discharge in passive electrical circuits in plants (Volkov et al. 2010c). It was observed that capacitor discharge through the *Mimosa pudica* petiole has a two-exponential character (Volkov et al. 2010c). Therefore, the electrical circuit can be modeled as it is shown in Fig. 2.8b. In our experiment the capacitor C_1 was charged to voltage U_0 and the circuit was closed.

After closing the circuit, the electrical potentials U_1 and U_2 at capacitors C_1 and C_2 depend on time according to the equations:

$$\begin{cases} C_1 \frac{dU_1}{dt} = -\frac{1}{R_1}(U_1 - U_2) \\ C_2 \frac{dU_2}{dt} = -\frac{1}{R_1}U_1 - \left(\frac{1}{R_1} + \frac{1}{R_2}\right)U_2 \end{cases} \tag{2.9}$$

with initial conditions

$$U_1[0] = U_0, \quad U_2[0] = 0 \tag{2.10}$$

It is convenient to introduce parameters of time:

$$\theta_1 = R_1 C_1, \quad \theta_2 = R_2 C_2, \quad \theta_3 = R_2 C_1 \tag{2.11}$$

Voltage U_2 can be excluded from the system of Eq. 2.9 giving the single equation for U_1:

$$\theta_1 \theta_2 \frac{\mathrm{d}^2 U_1}{\mathrm{d}t^2} + (\theta_1 + \theta_2 + \theta_3) \frac{\mathrm{d}U_1}{\mathrm{d}t} + U_1 = 0 \tag{2.12}$$

Solving this equation one can find the time course of U_1:

$$\begin{aligned} U_1(t) = U_0 \Bigg\{ & \left[\frac{-\theta_1 + \theta_2 - \theta_3}{\sqrt{-4\theta_1\theta_2 + (\theta_1 + \theta_2 + \theta_3)^2}} + 1 \right] \\ & \times \mathrm{Exp}\left[-\frac{t\left(\theta_1 + \theta_2 + \theta_3 + \sqrt{-4\theta_1\theta_2 + (\theta_1 + \theta_2 + \theta_3)^2} \right)}{2\theta_1\theta_2} \right] \\ & + \left[\frac{\theta_1 - \theta_2 + \theta_3}{\sqrt{-4\theta_1\theta_2 + (\theta_1 + \theta_2 + \theta_3)^2}} + 1 \right] \\ & \times \mathrm{Exp}\left[-\frac{t\left(\theta_1 + \theta_2 + \theta_3 - \sqrt{-4\theta_1\theta_2 + (\theta_1 + \theta_2 + \theta_3)^2} \right)}{2\theta_1\theta_2} \right] \Bigg\} \end{aligned} \tag{2.13}$$

If the experimental dependence can be approximated with function

$$U(t) = A_1 \, \mathrm{e}^{-\frac{t}{\tau_1}} + A_2 \, \mathrm{e}^{-\frac{t}{\tau_2}} \tag{2.14}$$

and parameters A_1, A_2, τ_1, and τ_2 can be determined from the experiment, then one can evaluate the elements of the equivalent circuit in Fig. 2.8b.

To find parameters θ_1, θ_2, θ_3 simultaneously, Markin solved the set of nonlinear equations derived from comparison of Eqs. 2.13 and 2.14:

$$\begin{aligned} A_1 &= U_0 \left[\frac{-\theta_1 + \theta_2 - \theta_3}{\sqrt{-4\theta_1\theta_2 + (\theta_1 + \theta_2 + \theta_3)^2}} + 1 \right] \\ \frac{1}{\tau_1} &= \frac{\theta_1 + \theta_2 + \theta_3 + \sqrt{-4\theta_1\theta_2 + (\theta_1 + \theta_2 + \theta_3)^2}}{2\theta_1\theta_2} \\ \frac{1}{\tau_2} &= \frac{\theta_1 + \theta_2 + \theta_3 - \sqrt{-4\theta_1\theta_2 + (\theta_1 + \theta_2 + \theta_3)^2}}{2\theta_1\theta_2} \end{aligned} \tag{2.15}$$

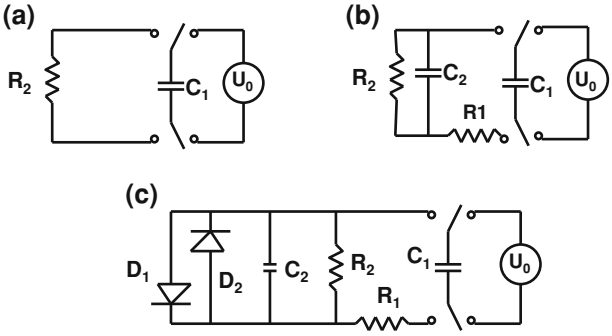

Fig. 2.8 Electrical equivalent schemes of a capacitor discharge in a plant tissue. Abbreviations: C_1 charged capacitor from voltage source U_0; C_2 capacitance of plant tissue; R resistance in plant tissue; D diode as a model of a voltage-gated channel

Finding from here θ_1, θ_2, and θ_3 and using the set of Eq. 2.11, one can determine the value of elements C_2, R_1, R_2 in the equivalent circuit shown in Fig. 2.8b. Volkov et al. (2010c) estimated these parameters in the *M. pudica* petiole.

Another interesting parameter is input resistance that can be defined as

$$R_{\text{input}} = -\frac{U_1}{C_1 \frac{\mathrm{d}U_1}{\mathrm{d}t}} \tag{2.16}$$

This parameter is also often analyzed in electrical impedance spectroscopy studies of biological tissues (Laarabi et al. 2005; Zhang and Willison 1991; Wang et al. 1994). However, there is a problem with interpretation of electrical impedance method, because a few different equivalent circuit models can have identical impedances (McAdams and Jossinet 1996).

2.3.3 Patch Clamp and Electrochemical Impedance Methods

The most frequently used methods for the evaluation of electrical circuits in plants are patch clamps, electrochemical impedance measurement, and electric charge stimulation. The patch clamp method can be used to study electrical characteristics of individual ionic channels in a biological membrane in vitro. Pipette-based recording of membrane currents is the mainstay in the characterization of cellular ion channels. Traditional patch clamp recording is accomplished by using a micromanipulator to position the tip of a glass pipette against the membrane of a cell. In voltage clamp mode, the membrane is clamped to a preset potential, and the current required maintaining this potential is recorded. Current recordings with different electrical protocols and in the presence of different reagents are used to characterize ion channel properties.

The electrochemical impedance method measures static electrical parameters, such as resistance and capacitance, at high-frequency alternative currents (AC). However, different electrochemical circuits can have the same electrochemical impedance.

The description of equivalent electrical circuits based on electrochemical impedance AC measurements is based on the researcher's intuition and can lead to various mistakes (McAdams and Jossinet 1996). Moreover, this method cannot characterize dynamic changes and nonlinear events, such as ion channel opening and closing.

2.4 Plant Electrostimulation

2.4.1 Plant Movements Induced by DC Electrostimulation

Mechanical movements in *M. pudica* were induced by very high applied voltages (Balmer and Franks 1975; Bose 1918; Gardiner 1888; Jonas 1970; Ritter 1811). Balmer and Franks (1975) briefly applied 200–400 V between the soil and the primary pulvinus to measure the contractile characteristics of a petiole. They estimated that the threshold voltage was about 25 V with any electrode polarity. Jonas (1970) used a 0.5 μF capacitor charged by 50, 100, and 150 V for electrostimulation and found that there were oscillations of leaves and fast petiolar movement after the application of an electrical shock. When Yao et al. (2008) applied 9 V to *M. pudica*, the petioles bent downward and the pinnae closed. Volkov et al. (Volkov et al. 2010e) investigated the mechanical movements of the pinnae and petioles in *M. pudica* induced by the electrical stimulation of a pulvinus, petiole, secondary pulvinus, or pinna by low electrical voltage and charge (Fig. 2.9). The threshold value was 1.3–1.5 V of applied voltage and 2–10 μC charge for the closing of the pinnules. Both voltage and electrical charge are responsible for the electrostimulated closing of a leaf (Volkov et al. 2010a, b, c, d).

The electrical stimulus between a midrib and a lobe closes the Venus flytrap leaf by activating motor cells without mechanical stimulation of trigger hairs (Markin et al. 2008; Volkov et al. 2007, 2008a, b, 2009a, b). The closing time of the Venus flytrap by electrical stimulation is 0.3 s, the same as mechanically induced closing. The Venus flytrap can accumulate small subthreshold charges, and when this threshold value is reached, the trap closes. Ion channel blockers such as Ba^{2+} and TEACl as well as uncouplers such as FCCP, 2,4-dinitrophenol and pentachlorophenol dramatically decrease the speed of the trap closing (Volkov et al. 2008c). Electrical stimulation can be used to study mechanisms of fast activity in motor cells of the plant kingdom.

2.4.2 DC Electrostimulation of Plants Can Induce Gene Expression, Enzymatic Systems Activation, Electrical Signaling, and Influences on Plant Growing

Excitability is a fundamental property that plants exhibit at the whole plant, tissue, and cellular levels. This property allows the cells, tissues, and organs of plants to

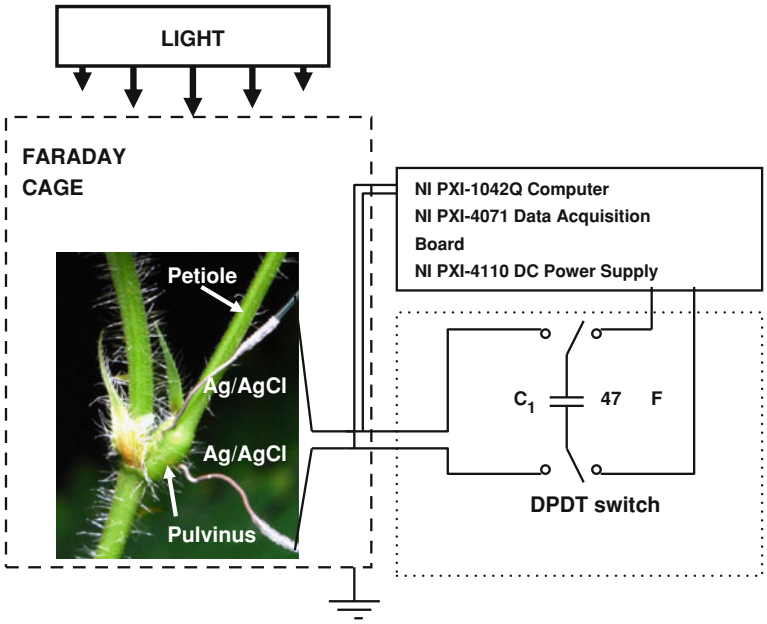

Fig. 2.9 Experimental setup for plant electrostimulation using the charge stimulation method and electrical signal measurements. We used PXI (PCI eXtensions for Instrumentation), a rugged PC-based platform, as a high-performance measurement and automation system (*National Instruments*, *Texas*)

operate in concert to adapt its internal conditions and external reactions in response to environmental stimulants referred to as irritants. The excitation waves, or action potentials, in higher plants are thought to be the mechanism behind intercellular and intracellular communication. Action potentials are signals caused by the depolarization of cellular membranes. Mechanical, physical, or chemical irritants affect not only the location of occurrence, but these irritants may also affect the entire plant as well. In plant species, the velocity of electrical signals depends on many factors, including the intensity of the irritation, temperature, chemical treatment, or mechanical wounding. The excitation reaction may travel between the top of the stem and the root in either direction.

Plant electrostimulation can have influence on the growth of plants (Takamura 2006). Mizuguchi et al. (1994) applied 1 V to the cultured solution and it accelerated by 30% the growth of bean sprouts. Goldsworthy (2006) described in his review how natural and artificial electrical fields stimulate plant growth in the electroculture experiments. Electrical fields can activate growth-promoting genes (Goldsworthy 2006). Electroculture experiments show that electrical fields from the aurora borealis are responsible for green and healthy vegetation in Arctic (Lemström 1904). Goldsworthy (2006) suggested that "plants seem to be using the very strong electrostatic fields associated with thunderstorms as signal to let them make the best use of the rain."

Fromm and Spanswick (1993) measured action potentials induced by electrostimulation of willow shoots. The threshold value of electrical stimulation was function of duration of electrical stimuli (6 V during 1 s, 3–4 V during 2 s or 10 nA in 1 s, 3 nA in 2 s, 2 nA during 4 s). Such dependence on time shows that both voltage and electrical charge are important for the plant electrical response. We can estimate the threshold charge of 6–10 nC by multiplying the threshold current by time of polarization. Amplitude of action potentials was 30–50 mV with velocity of 2 cm/s.

Inaba et al. (1995) applied DC current of 1–3 mA to cucumber (*Cucumis sativus* L.) and found induction of ethylene synthesis and activation of 1-aminocyclopropane-1-carboxylic acid synthase. Inaba et al. (1995) also evaluated parameters of the equivalent electrical circuit of plant tissues.

Herde et al. (1995, 1996) found that electrical current application (10 V, 30 s) activated *pin*2 gene expression in tomato plants and increases endogenous level of abscisic acid.

Stanković and Davies (1996, 1997) demonstrated that electrical stimulation of tomato plants by 9 V during 3–4 s occasionally induces "genuine" action potentials with amplitude of 40 mV and speed of 3.5–4.5 mm/s and elicits systemic *pin*2 gene expression. Propagation of electrical signals in response to electrostimulation was found in 20% of tomato plants only (Stankovic and Davies 1996, 1997). Authors did not analyze the threshold level of a stimulation voltage and possible dependence of action potential on amplitude and polarity of applied voltage. Stankovic and Davies (1996, 1997) found after 9 V electrostimulation that "5-fold or greater increase in *pin*2 mRNA levels occurs within 1 h".

Mishra et al. (2001) studied action potential propagations with velocity of 270 m/s and a latency of 400 μs from root to shoot in *Sorghum bicolor* evoked by electrostimulation. The threshold current was 100 μA during 0.3 ms. These values correspond to the threshold charge of 30 nC. In 7-day-old seedling the threshold charge was 0.45 μC. According to the strength-duration curve of *S. bicolor* seedling the threshold charge varies from 30 to 3 μC (Mishra et al. 2001).

Dziubinska et al. (2001) applied electrical stimuli of 1–2 V during 5 s to the basal part of the stem of *Helianthus annuus* and recorded propagation of action potentials along the stem with an amplitude of 42 mV with speed of 0.18 cm/s. Authors were unable to evoke action potentials by electrical stimulation of leaves (Dziubinska et al. 2001).

Krol et al. (2006) triggered action potentials in the Venus flytrap by electrical stimuli up to 4 V.

Favre and Agosti (2007) described voltage-dependent "action potentials" in *Arabidopsis thaliana* induced by 3–18 V pulses. Amplitude of these "action potentials" was between 10 and 80 mV with an absolute refractory period of 20 min and a speed of propagation of 0.8–1.4 mm/s. Amplitude and velocity of electrical responses was a function of applied voltage.

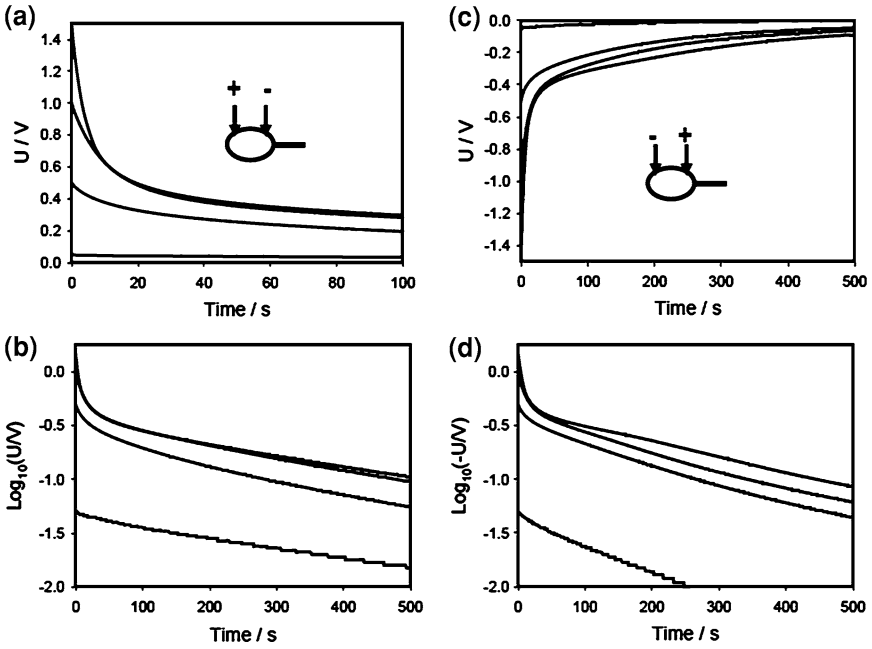

Fig. 2.10 Time dependence of electrical discharge in *M. pudica* pulvinus between electrodes located along the pulvinus and connected to 47 μF charged capacitor (**a**, **c**) Time dependence of electrical discharge in the *M. pudica's* pulvinus between electrodes located along the pulvinus and connected to a charged capacitor in logarithmic coordinates (**b**, **d**)

2.4.3 Anisotropy and Nonlinear Properties of Biologically Closed Electrochemical Circuits in Plants

Electrical circuits in Fig. 2.8a, b are not sensitive to the polarity of applied voltage. We found that after threshold value of electrostimulating potential there is a strong deviation in logarithmic coordinates from Eq. 2.8 predictions and plant electrical responses depend on polarity of applied voltage (Fig. 2.10). The deviation of a capacitor discharge from a linear dependence in logarithmic coordinates can be described by the equivalent electrical schemes shown in Fig. 2.8b, c (Volkov et al. 2009b, 2010a b, c, d). If the capacitor discharge is represented by two-exponential functions and does not depend on polarity of electrodes in the plant tissue, the deviation from linear dependence can be described by Fig. 2.8b. If the response changes with the polarity of stimulation, a rectifier-based model represented in Fig. 2.8c must be used. Kinetics of a capacitor discharge depends on the polarity of electrodes in the *Aloe vera* leaf, Venus flytrap, and *M. pudica* (Figs. 2.10 and 2.11). Figure 2.11 shows the difference in the kinetics of a capacitor discharge as a function of the polarity of stimulation as represented in Fig. 2.10a, c. Dependence of a capacitor discharge on the polarity of electrodes in the *M. pudica* leaf, shown

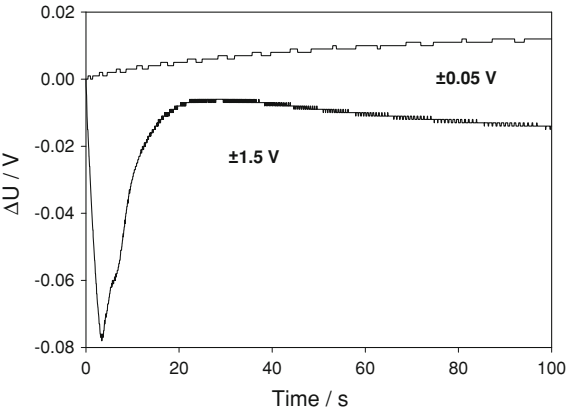

Fig. 2.11 Time dependence of voltage differences (Fig. 2.10a + c) during electrical discharge in the *M. pudica's* pulvinus between electrodes of different polarities located along the *M. pudica* pulvinus and connected to 47 μF charged capacitor

in Figs. 2.10 and 2.11, can be explained by a change in resistivity with applied potential due to opening of ion channels, which can be modeled by diodes in Fig. 2.8c. Opening of voltage-gated channels induce the effect of electrical rectification shown in Fig. 2.11. We found similar rectification effects in the Venus flytrap (Volkov et al. 2009b), *A. vera* (Volkov et al. 2011a, b), and *M. pudica* (Volkov et al. 2010a, b, c, d, e, 2011a). We modeled voltage-gated channels using silicon rectifier diode and reproduced experimental dependencies of a capacitor discharge in plant tissue (Volkov et al. 2009b).

2.4.4 Circadian Variations in Biologically Closed Electrochemical Circuit in Plants

The circadian clock regulates a wide range of electrophysiological and developmental processes in plants. The circadian clock is an endogenous oscillator with a period of approximately 24 h; its rhythm is linked to the light–dark cycle. Molecular mechanism underlying circadian clock function is poorly understood, although it is widely accepted for both plants and animals that are based on circadian oscillators. The circadian clock in plants is sensitive to light, which resets the phase of the rhythm. The circadian clock was discovered by De Mairan (1729) in his first attempt to resolve experimentally the origin of rhythm in the leaf movements of *M. pudica*. This rhythm continued even when *M. pudica* was maintained under continuous darkness. *M. pudica* is a nyctinastic plant that closes its leaves in the evening; the pinnules fold together and the whole leaf droops downward temporarily until sunrise. The leaves open in the morning due to a circadian rhythm, which is regulated by a biological clock with a cycle of about 24 h. During photonastic movement in *M. pudica*, leaves recover their daytime position. During a scotonastic period, the primary pulvini straighten up and pairs of pinnules fold together about the tertiary pulvini. The closing of pinnae depends upon the presence of phytochrome in the far-red absorbing form.

Volkov et al. (2011a,c) found, for the first time, the direct influence of a circadian clock on biologically closed electrochemical circuits in vivo using the Charge Stimulating Method. The electrostimulation of a sensitive plant *M. pudica* and *A. vera* was provided with different timing and different voltages. *A. vera* (L.) is a member of the Asphodelaceae (Liliaceae) family with crassulacean acid metabolism (CAM). In *A. vera*, stomata are open at night and closed during the day. CO_2 acquired by *A. vera* at night is temporarily stored as malic and other organic acids, and is decarboxylated the following day to provide CO_2 for fixation in the Benson-Calvin cycle behind closed stomata.

A. vera is a model for the study of plant electrophysiology with crassulacean acid metabolism.

Resistance between Ag/AgCl electrodes in the leaf of *A. vera* was higher during the day than at night. Discharge of the capacitor in *A. vera* at night was faster than during the day. Discharge of the capacitor in a pulvinus of *M. pudica* was faster during the day. The biologically closed electrical circuits with voltage-gated ion channels in *M. pudica* are also activated the next day, even in the darkness. These results show that the circadian clock can be maintained endogenously and has electrochemical oscillators, which can activate ion channels in biologically closed electrochemical circuits. Initial difference in the speed of the capacitor discharge (faster during the day), can be explained by activation of ion channels, equivalent to the high rectification effect. This effect depends on the applied stimulation voltage.

Isolated pulvinar protoplasts are responsive to light signals in vitro (Coté 1995; Kim et al. 1992, 1993). In the dark period, the closed inward-directed K^+ channels of extensor cells are opened within 3 min by blue light. Conversely, the inward-directed K^+ channels of flexor cells, which are open in the darkness, are closed by blue light. In the light period, however, the situation is more complex. Premature darkness alone is sufficient to close the open channels of extensor protoplasts, but both darkness and a preceding pulse of red light are required to open the closed channels in the flexor protoplasts (Kim et al. 1992, 1993).

The biologically closed electrical circuits with voltage-gated ion channels in *M. pudica* are activated the next day even in the darkness. This phenomenon can be caused by biological clock in *M. pudica*. The nonlinear effect of activation of electrical circuits during the daytime is stronger than during the next day in the darkness.

In contrast to *A. vera* the discharge of the capacitor in a pulvinus of *M. pudica* was faster during the day, because *A. vera* is a CAM plant.

Our results (Volkov et al. 2011a, c) demonstrate that the circadian clock can be maintained endogenously, probably involving electrochemical oscillators, which can activate or deactivate ion channels in biologically closed electrochemical circuits. This circadian rhythm can be related to the differences found in the membrane potentials during the day- and nighttime, which were found in different plants (Kim et al. 1992; 1993; Racusen and Satter 1975; Scott and Gulline 1975; Thomas and Vince-Prue 1997). The expression of many ion transporters in plants is regulated by the circadian rhythm (Lebaudy et al. 2008).

2.5 Conclusion

The information gained from plant electrostimulation can be used to elucidate the intracellular and intercellular communication in the form of electrical signals within plants. Monitoring the electrical signaling in higher plants represents a promising method to investigate electrical communication during environmental changes.

Acknowledgments This work was supported by the grant W911NF-11-1-0132 from the U.S. Army Research Office.

References

Balmer RT, Franks JG (1975) Contractile characteristics of *Mimosa pudica* L. Plant Physiol 56:464–467

Bertholon M (1783) De l'electricite des vegetaux: ouvrage dans lequel on traite de l'electricite de l'atmosphere sur les plantes, de ses effets sur leconomie des vegetaux, de leurs vertus medico. P.F. Didot Jeune, Paris

Bose JC (1907) Comparative electro-physiology, a physico-physiological study. Longmans, Green & Co, London

Bose JC (1913) Researches on irritability of plants. Longmans, London

Bose JC (1918) Life Movements in Plants. B.R. Publishing Corp, Delhi

Bose JC (1926) The Nervous mechanism of plants. Longmans, Green and Co., London

Bose JC (1928) The motor mechanism of plants. Longmans Green, London

Burdon-Sanderson J (1873) Note on the electrical phenomena which accompany stimulation of the leaf of *Dionaea muscipula*. Philos Proc R Soc Lond 21:495–496

Coté GG (1995) Signal transduction in leaf movement. Plant Physiol 109:729–734

Davies E (2006) Electrical signals in plants: facts and hypothesis. In: Volkov AG (ed) Plant electrophysiology—Theory & methods. Springer, Berlin, pp 407–422

De Mairan M (1729) Observation botanique. Histoire de l'Academie Royale de Sciences, Paris, pp 353–356

Dziubinska H, Trebacz K, Zawadzki T (2001) Transmission route for action potentials and variation potentials in *Helianthus annuus* L. J Plant Physiol 158:1167–1172

Favre P, Agosti RD (2007) Voltage-dependent action potentials in Arabidopsis thaliana. Physiol Plant 131:263–272

Feynman RP, Leighton RB, Sands M (1963) The Feynman lectures on physics. Addison Wesley, Reading

Fromm J, Spanswick R (1993) Characteristics of action potentials in willow (*Salix viminalis* L.). J Exp Bot 44:1119–1125

Gardiner W (1888) On the power of contractility exhibited by the protoplasm of certain plant cell. Annals Botany 1:362–367

Goldsworthy A (2006) Effects of electrical and electromagnetic fields on plants and related topics. In: Volkov AG (ed) Plant electrophysiology—Theory and methods. Springer, Berlin, pp 247–267

Herde O, Atzorn R, Fisahn J, Wasternack C, Willmitzer L, Peña-Cortés H (1996) Localized wounding by heat initiates the accumulation of proteinase inhibitor II in abscisic acid-deficient plants by triggering jasmonic acid biosynthesis. Plant Physiol 112:853–860

Herde O, Peña-Cortés H, Fisahn J (1995) Proteinase inhibitor II gene expression induced by electrical stimulation and control of photosynthetic activity in tomato plants. Plant Cell Physiol 36:737–742

Houwink AL (1935) The conduction of excitation in *Mimosa pudica*. Recuril des Travaux Botaniques Neerlandais 32:51–91

Houwink AL (1938) The conduction of excitation in Clematis zeylanica and in *Mimosa pudica*. Annales du Jardin Botanique de Buitenzorg 48:10–16

Inaba A, Manabe T, Tsuji H, Iwamoto T (1995) Electrical impedance analysis of tissue properties associated with ethylene induction by electric currents in cucumber (*Cucumis sativus* L.) fruit. Plant Physiol 107:199–205

Jonas H (1970) Oscillations and movements of *Mimosa* leave due to electric shock. J Interdisciplinary Cycle Res 1:335–348

Keller R (1930) Der elektrische Factor des Wassertransporte in Luhte der Vitalfarbung. Ergeb Physiologie 30:294–407

Kim HY, Coté GG, Crain RC (1992) Effect of light on the membrane potential of protoplasts from Samanea saman pulvini. Involvement of K^+ channels and the H^+-ATPase. Plant Physiol 99:1532–1539

Kim HY, Coté GG, Crain RC (1993) Potasium channels in Samanea saman protoplasts controlled by phytochrome and the biological clock. Science 260:960–962

Krol E, Dziubinska H, Stolarz M, Trebacz K (2006) Effects of ion channel inhibitors on cold- and electrically-induced action potentials in *Dionaea muscipula*. Biol Plantarum 50:411–416

Ksenzhek OS, Volkov AG (1998) Plant energetics. Academic, San Diego

Laarabi S, Kinani KE, Ettouhami A, Limouri M (2005) In vivo impedance of the aerial organs of some mono- and dicotyledonous plants. CR Biol 328:253–262

Lebaudy A, Vavasseur A, Hisy E, Dreyer I, Leonhards N, Thibaud JB, Very AA, Simonneau T, Sentenac H (2008) Plant adaptation to fluctuating environment and biomass production are strongly dependent on guard cell potassium channels. Proc Natl Acad Sci 105:5271–5276

Lemström K (1904) Electricity in agriculture and horticulture. Electrician Publications, London

Markin VS, Volkov AG, Jovanov E (2008) Active movements in plants: mechanism of trap closure by *Dionaea muscipula* Ellis. Plant Signal Behav 3:778–783

McAdams ET, Jossinet J (1996) Problems in equivalent circuit modeling of the electrical properties of biological tissues. Bioelectrochem Bioenerg 40:147–152

Mishra NS, Mallick BN, Sopory SK (2001) Electrical signal from root to shoot in Sorghum bicolor: induction of leaf opening and evidence for fast extracellular propagation. Plant Sci 160:237–245

Mizuguchi Y, Watanabe Y, Matsuzaki H, Ikezawa Y, Takamura T (1994) Grouth acceleration of bean sprouts by the application of electrochemical voltage in a culturing bath. Denki Kagaku 62:1083–1085

Nordestrom BEW (1983) Biologically closed electrical circuits. Clinical, experimental and theoretical evidence for an additional circulatory system. Nordic Medical Publications, Uppsala

Ritter JW (1811) Electrische Versuche an der Mimosa pudica L. In Parallel mit gleichen Versuchen an Fröschen. Denkschr Köningl Akad Wiss (München) 2:345–400

Racusen R, Satter RL (1975) Rhytmic and phytochrome-regulated changes in transmembrane potential in Samanea pulvini. Nature 255:408–410

Scott BIH, Gulline HF (1975) Membrane changes in a circadian system. Nature 254:69–70

Shannon CE (1949) Communication in the presence of noise. Proc Inst Radio Eng 37:10–21

Sinukhin AM, Britikov EA (1967) Action potentials in the reproductive system of plant. Nature 215:1278–1280

Stankovic B, Davies E (1996) Both action potentials and variation potentials induce proteinase inhibitor gene expression in tomato. FEBS Lett 390:275–279

Stankovic B, Davies E (1997) Intercellular communication in plants: electrical stimulation of proteinase inhibitor gene expression in tomato. Planta 202:275–279

Takamura T (2006) Electrochemical potential around the plant root in relation to metabolism and growth acceleration. In: Volkov AG (ed) Plant electrophysiology—Theory & methods. Springer, Berlin, pp 341–374

Thomas B, Vince-Prue D (1997) Photoperiodism in plants. Academic, San Diego

Volkov AG (2000) Green plants: electrochemical interfaces. J Electroanal Chem 483:150–156

Volkov AG (2006a) Electrophysiology and phototropism In: Balushka F, Manusco S, Volkman D (eds) Communication in plants. Neuronal aspects of plant life. Springer, Berlin, pp 351–367

Volkov AG (ed) (2006b) Plant electrophysiology—Theory and methods. Springer, Berlin

Volkov AG, Adesina T, Jovanov E (2008a) Charge induced closing of Dionaea muscipula Ellis trap. Bioelectrochem 74:16–21

Volkov AG, Adesina T, Markin VS, Jovanov E (2007) Closing of Venus flytrap by electrical stimulation of motor cells. Plant Signal Behav 2:139–144

Volkov AG, Adesina T, Markin VS, Jovanov E (2008b) Kinetics and mechanism of *Dionaea muscipula* trap closing. Plant Physiol 146:694–702

Volkov AG, Baker K, Foster JC, Clemmens J, Jovanov E, Markin VS (2011a) Circadian variations in biologically closed electrochemical circuits in *Aloe vera* and *Mimosa pudica*. Bioelectrochem 81:39–45

Volkov AG, Carrell H, Adesina T, Markin VS, Jovanov E (2008c) Plant electrical memory. Plant Signal Behav 3:490–492

Volkov AG, Carrell H, Baldwin A, Markin VS (2009a) Electrical memory in Venus flytrap. Bioelectrochem 75:142–147

Volkov AG, Carrell H, Markin VS (2009b) Biologically closed electrical circuits in Venus flytrap. Plant Physiol 149:1661–1667

Volkov AG, Deamer DW, Tanelian DL, Markin VS (1998) Liquid interfaces in chemistry and biology. Wiley, New York

Volkov AG, Foster JC, Ashby TA, Walker RK, Johnson JA, Markin VS (2010a) *Mimosa pudica*: electrical and mechanical stimulation of plant movements. Plant Cell Environ 33:163–173

Volkov AG, Foster JC, Baker KD, Markin VS (2010b) Mechanical and electrical anisotropy in *Mimosa pudica*. Plant Signal Behav 5:1211–1221

Volkov AG, Foster JC, Jovanov E, Markin VS (2010c) Anisotropy and nonlinear properties of electrochemical circuits in leaves of *Aloe vera* L. Bioelectrochem 81:4–9

Volkov AG, Foster JC, Markin VS (2010d) Signal transduction in *Mimosa pudica*: Biologically closed electrical circuits. Plant, Cell Environ 33:816–827

Volkov AG, Foster JC, Markin VS (2010e) Molecular electronics in pinnae of *Mimosa pudica*. Plant Signal Behav 5:826–831

Volkov AG, Foster JC, Jovanov E, Markin VS (2011b) Anisotropy and nonlinear properties of electrochemical circuits in leaves of *Aloe vera* L. Bioelectrochem 81:4–9

Volkov AG, Pinnock MR, Lowe DC, Gay MS, Markin VS (2011c) Complete hunting cycle of *Dionaea muscipula*: consecutive steps and their electrical properties. J Plant Physiol 168:109–120

Volkov AG, Wooten JD, Waite AJ, Brown CR, Markin VS (2011d) Circadian rhythms in electrical circuits of *Clivia miniata*. J Plant Physiol 168:1753–1760

Volkov AG, O'Neal L, Ebere LC, McIntyre R, Volkova-Gugeshashvili MI, Markin VS (2012) Propagation and collision of nonlinear responses in *Aloe vera* L. and *Arabidopsis thaliana*. Plant Signal Behav 7:5 (in Press)

Wang J, Zimmermann U, Benz R (1994) Contribution of electrogenic ion transport to impedance of the algae *Valonia utricularis* and artificial membranes. Biophys J 67:1582–1593

Yao H, Xu Q, Yuan M (2008) Actin dynamics mediates the changes of calcium level during the pulvinus movement of *Mimosa pudica*. Plant Signal Behav 3:954–960

Zhang MIN, Willison JHM (1991) Electrical impedance analysis in plant tissues: a double shell model. J Exper Bot 42:1465–1475

Chapter 3
Plant Response to Stress: Microelectrode Voltage-Clamp Studies

François Bouteau and Daniel Tran

Abstract Microelectrode voltage-clamp techniques have existed since more than 60 years with the pioneering work on squid axons. In the past decades, the patch-clamp technique became the most widely used voltage-clamp technique for recording macroscopic currents in plant cells and it largely improved the descriptions of the roles and properties of various ion transport systems. However, the necessary removal of the cell wall limits its application to protoplasts. Microelectrode voltage-clamp techniques allow circumventing this problem in working with cells with their intact walls. With these techniques, whole cell currents could be recorded from electrically isolated plant cell types challenged by various environmental stresses that could not be addressed with the patch-clamp technique. In this chapter, we discuss findings concerning different types of ion channel regulations recorded using microelectrode techniques on cells upon challenge by abiotic or biotic stresses; sustained ion channel activities leading to osmotic changes and transient ion channel regulations possibly involved in the signaling process. We further highlight the complex regulations of ion channels observed in host and nonhost cells by harpins from plant pathogenic bacteria.

3.1 Introduction

Plants are sessile organisms that face multiple biotic and abiotic stresses in their natural environment. Abiotic stresses such as drought and salinity greatly affect plant growth and productivity worldwide resulting in billion dollar losses in crop

F. Bouteau (✉) · D. Tran
Laboratoire d'Electrophysiologie des Membranes, Institut de Biologie des Plantes, Université Paris Diderot-Paris 7, Sorbonne Paris Cité, 91405 Orsay, France
e-mail: francois.bouteau@univ-paris-diderot.fr

A. G. Volkov (ed.), *Plant Electrophysiology*,
DOI: 10.1007/978-3-642-29119-7_3,

production around the globe. In addition, nearly one-third of crops and stored food losses are caused by plant pests, and agricultural crops can be injured when exposed to high concentrations of various air pollutants. Injury can range from visible markings to reduced growth and yield, to premature death of the plant. Studying and revealing the mechanisms that plants have evolved to cope with biotic and abiotic stresses is thus, a major issue for plant biologists.

Plants have an outstanding ability to display the optimal responses to stressful environmental conditions. This is the result of an amazingly complex array of physiological mechanisms for signal perception and from multiple cross talk signaling pathways. These signaling mechanisms could include hormones (abscisic acid, salicylic acid, ethylene, jasmonic acid, etc.), chemicals (Ca^{2+}, reactive oxygen species [ROS], etc.), or physical events (e.g. propagating electrical or hydrostatic pressure waves) (Spoel and Dong 2008; Zhang et al. 2008). Recent studies have revealed several molecules, including transcription factors and kinases, as promising candidates for common players that are involved in cross talk between stress signaling pathways, and emerging evidence suggests that both hormonal, as well as ROS signaling pathways play key roles in the cross talk between biotic and abiotic stress signaling that leads to plant responses (Fujita et al. 2006). Ion flux regulations could also be observed in response to most of the stresses a plant could perceive. Such regulations could occur at different levels of signaling pathways or participate directly in the response. Due to its position at the interface between the cytosol and the external medium, the plasma membrane is both, a site of perception of external signals and one of the major vouchers of cell homeostasis. It is therefore an initiation site of signaling pathways eliciting the plant response to biotic or abiotic stress (Jones et al. 1994; Dixon et al. 1996; Batistic and Kudla 2009; Kadono et al. 2010; Hauser et al. 2011), and for pathogens a target which allows alteration of cellular homeostasis for example by disrupting the H^+-ATPase activity (Zhou et al. 2000; Bunney et al. 2002), or by increasing membrane permeability by creating pores (Hutchison et al. 1995; Goudet et al. 1999), or by activating ion channels (El-Maarouf et al. 2001; Errakhi et al. 2008a; Zhang et al. 2008; Jeworutzki et al. 2010).

Concerning biotic stress, a beam of physiological data suggests that pathogen attack is accompanied by an early deregulation of the ion fluxes of the target cell, particularly H^+, Ca^{2+}, K^+, and anions such as NO_3^- (Atkinson et al. 1990; Pike et al. 1998; Wendehenne et al. 2002; Bouizgarne et al. 2006a; Reboutier et al. 2007a, b; Errakhi et al. 2008a, b). The variation of the flow of ions through the plasma membrane could be induced within minutes or even seconds. So this is one of the first events following perception. Given the magnitude of the induced ion efflux, in most cases, it is reasonable to attribute the response to the opening of ion channels (only carriers able to account for the high conductance required). Regulation of the channels following the attack may also represent a factor in the pathogenesis and/or a step in the defense response of the plant. Such events were shown to be associated to other early induced responses (production of ROS, induction of MAP kinase…) and are components of the transduction chains leading to pathogenesis and defense responses (Scheel 1998; Somssich and

Hahlbrock 1998). In this context, the regulation of ion transport systems at the plasma membrane appears to be also an important factor in hypersensitive response (HR) associated with plant programmed cell death (PCD) (Atkinson et al. 1990; Jabs et al. 1997; del Pozo and Lam 1998; Scheel 1998; Somssich and Hahlbrock 1998; Heath 2000; Wendehenne et al. 2002). Recent studies provided genetic evidences positioning cyclic nucleotide-gated channels (CNGC) in the signaling of pathogen attack and the induction of HR (Clough et al. 2000; Balague et al. 2003). Also in vivo recording of CNGC remain scarce, they could be involved in the calcium influx that triggers mechanism of HR (Leng et al. 2002).

Regarding abiotic stress, the rapid regulation of ion channels was also observed in response to hyperosmotic stress such as salinity or nonionic hyperosmotic stress used to mimick dehydration (Teodoro et al. 1998; Zingarelli et al. 1999; Shabala and Newman 2000; Shabala and Lew 2002; Shabala et al. 2007) or drought (Dauphin et al. 2001). In such osmotic stresses, because of the osmotic gradient generated, water flows out of the cell. In response to hypertonic stress, increase or restoration of K^+ uptake through K^+ channels is the major mechanism used in cell osmotic adjustment as reported in various plant tissues (Teodoro et al. 1998; Zingarelli et al. 1999; Shabala and Newman 2000; Dauphin et al. 2001; Shabala and Lew 2002). In response to drought, one of the well-studied systems at cellular level is the stomatal closure and its regulation by abscisic acid (ABA) (Sirichandra et al. 2009; Hauser et al. 2011). Among abiotic stresses, pollutant generated stresses are more and more prevalent and could lead to loss of productivity in plants of agronomic interest. Recent studies highlighted the involvement of ion channels in plant responses to pollutants (Kadono et al. 2006; Vahisalu et al. 2008; Kadono et al. 2010; Tran et al. 2010; Yukihiro et al. 2012). As regards CNGC, genetic evidences position the slow-type anion channel (SLAC1) during plant response to ozone (Vahisalu et al. 2008, 2010), and the guard cell outward rectifying K^+ channel (GORK) in response to oxidative stress (Demidchik et al. 2010).

3.2 Microelectrode Voltage-Clamp Techniques

Much of what we know about the properties of ion channels was provided by voltage-clamp studies developed on the squid giant axon (Cole 1949; Hodgkin et al. 1952). Since these pioneering studies, many derived techniques have evolved and voltage-clamp analysis has been extended to a wide range of cell types, comprising plant cells. The voltage-clamp is a method that allows the measurement of ion flow through a membrane as an electric current. Conventional voltage-clamp using several electrodes has provided the foundations of plant electrophysiology, (Findlay 1961; Gradmann et al. 1978; Beilby 1982). The development of the patch-clamp studies (Neher and Sakmann 1976) has allowed more wide-ranging studies comprising plant cell studies since the initial work of Schroeder et al. (1984) on guard cell protoplasts. During the past decades, the

patch-clamp technique has extended the application of voltage-clamp methods to the recording of ionic currents flowing through single channels, and in its whole cell configuration has also become the most widely used method for recording macroscopic currents in plant cells. Electrophysiological studies have therefore greatly improved the descriptions of both, the properties of various ion channels and ion transport in nutrition, osmoregulation and signalization (Ward et al. 2009). Although the patch-clamp technique presents numerous advantages and notably could in principle allow working on almost any plant cell type, a crucial step in preparing the plant cells is the removal of the cell wall to allow giga-ohm seals. Hence, most patch-clamp studies on plant cells utilize protoplasts after enzymatic digestion of the cell wall. Such protoplasts thus lack their plasma membrane/extracellular matrix connections, and non-physiological osmotic environment in the application of patch-clamp techniques to most plant cells, are unavoidable factors. As a matter of fact, removing the cell wall during protoplast preparation is likely to alter the capacity of the cells to respond to pathogens or elicitors (Klusener and Weiler 1999; Carden and Felle 2003; Humphrey et al. 2007). Moreover, the digestive enzymes used to remove the cell wall (Klusener and Weiler 1999), as cell wall fragments such as oligogalacturonides, could elicit defense responses in plant cells, notably ion fluxes (Reymond et al. 1995), making difficult secondary analysis of pathogen-derived molecules on ion fluxes by patch-clamp. Laser microsurgery techniques have been described to expose the plasma membrane to patch-clamp pipette (Taylor and Brownlee 1992; Kurkdjian et al. 1993; Henriksen et al. 1996), but this approach is not well developed. The use of microelectrode voltage-clamp techniques (MEVC) is an attractive alternative to the whole-cell configuration of the patch-clamp technique. Indeed, with micro-electrode(s) the whole cell voltage-clamp measurements can be conducted in situ on cells with an intact cell wall. It is further noteworthy that the voltage-clamp technique allows studying the activities of ion channels in the environment primarily as physiological [composition not controlled, low perfusion from the pipette (Blatt and Slayman 1983)], which is not provided by the perfusion of the patch-clamp on the protoplasts. These conditions could be important since the activity of ion channels may require cytosolic intermediates for their activation and/or their regulation (Lee et al. 2009). These more physiological conditions are thus best suited to record ion channel activities in cells challenged by environmental stimuli.

A voltage clamp with two electrodes (TEVC) was initially applied to plant cells large and robust enough to tolerate several intracellular electrodes (Findlay 1961; Gradmann et al. 1978; Beilby 1982). A significant advance in TEVC has been the development of double-barreled electrodes allowing working on the smallest plant cells. In this configuration, one barrel of the electrode measures voltage, while current is injected through the other barrel. Numerous studies were performed with TEVC method on stomatal guard cells (Blatt et al. 1987; Blatt 1991, 1992; Roelfsema and Prins 1997; Roelfsema et al. 2001) and on root hairs (Lew 1991; Meharg and Blatt 1995; Lew 1996; Blatt et al. 1997). An alternative to the TEVC technique is the discontinuous single electrode voltage-clamp (dSEVC) technique

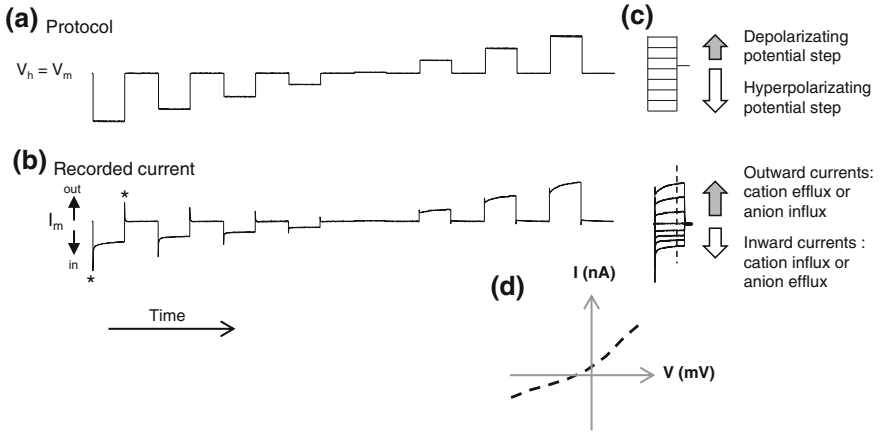

Fig. 3.1 **a** Voltage-clamp protocol: voltage changes in a square fashion from a holding potential (V_h). **b** Typical currents recorded from a voltage-clamped cell when the membrane potential is stepped as shown in **a**. Spikes of capacity current occur at the edges of the pulse (*asterisk*). **c** The voltage steps and recorded currents are then usually represented superimposed. **d** Current–voltage relationship corresponding to the values of current intensity at one defined time of the voltage-clamps (*dashed line*) plot to the corresponding voltages

or "switch-clamp". The main advantage of using only one microelectrode is the lower impact of impalement on cell membrane. In this method, a single electrode performs the current injection and potential measurements, by rapid switching between a current injection mode and potential measuring mode (Brennecke and Lindemann 1974; Finkel and Redman 1984; Halliwell et al. 1994). This method needs microelectrodes with fast settling times and thus takes advantage of a slower time constant of the plasma membrane compared with the electrode. The switching frequency between the current injection- and voltage measuring-mode should thus be high enough to allow any voltage, associated with charging of the electrode capacitance during the current injection cycle to decay before sampling of membrane potential. For a fuller description of the MEVC and their optimization the reader is referred to Finkel and Redman (1984) and Halliwell et al. (1994). The dSEVC has been successfully applied to different plant cell types, Fucus eggs (Taylor and Brownlee 1992), laticifers (Bouteau et al. 1996), guard cells (Forestier et al. 1998; Raschke et al. 2003), root hairs (Bouteau et al. 1999), and cultured cells (Jeannette et al. 1999; El-Maarouf et al. 2001).

During voltage-clamp experiments, the membrane voltage is held at a defined voltage by injecting into the cells, with a feedback amplifier, currents equal in amplitude, and opposite in sign to those that flow through the membrane. Most of the time, the voltage is forced to change from a holding potential (Vh) in a square step fashion as rapidly as possible from one steady state to another (Fig. 3.1a). Upon such protocols, different potential steps are swept allowing the acquisition of information about the ion channel behaviors and their mode of gating (opening and

closure). Indeed, most ion channels are affected by the membrane potential: depolarizing voltage promoting outward currents when hyperpolarizing voltage favoring inward currents (Fig. 3.1b). Therefore, the injected currents provide a measure of ionic and capacitive currents naturally flowing in and out of cells. The instantaneous and transient spikes recorded at each voltage change correspond to the capacitive current flows (asterix in Fig. 3.1b) while at steady-state voltage, the ionic current recorded is free from capacity currents. Currents measured from whole cells are usually called macroscopic currents. The recorded currents are then usually represented as shown in Fig. 3.1c corresponding to potential steps from one side and recorded currents from the other side superimposed. Plotting the values of current intensity at one defined time of the voltage clamps allows presenting a current–voltage relationship or "I–V curve" (Fig. 3.1d). Different parameters, such as speed and isopotentiality (space clamp), should be combined for the voltage clamp of a particular preparation to be efficient. Membrane current should be recorded from an area of uniform potential, so that the current comes from a population of channels that are all submitted to the same voltage. Thus microelectrode clamps, which deliver current at a single point, will be good to space clamp cells which are approximately spherical or are short cylinders. Complications in cells arise for many plant cell types which are electrically coupled to other cells, restricting the application of MEVC. For this reason, only few plant cell types could be used with MEVC. Reliable MEVC experiments were mainly obtained on isolated cultured cells, guard cells, which are symplastically isolated, and root hairs in some specific conditions (Table 3.1). The axial shape of root hairs raises the problem of space clamping, but the choice of small root hairs of about 15 μm in length [1/10 of the length constant for *Arabidopsis thaliana* (Meharg and Blatt 1995) ensured good voltage-clamp conditions (Dauphin et al. 2001); otherwise a cable correction should be applied on the recorded data (Meharg and Blatt 1995).

By using one of the MEVC techniques, TEVC, or dSEVC, mainly potassium and anionic currents were recorded from guard cells, root hairs, and culture cells of various species (Table 3.1). It is also noteworthy that Ca^{2+} currents were never reported from MEVC studies probably because of a weak intensity when compared to K^+ or anion currents in in vivo conditions (internal medium composition not controlled) and/or electrically silent flux probably coupled to compensatory charge movements (Gilliham et al. 2006). Independently of voltage-clamp application, the use of internal microelectrodes also allows following the resting membrane potential of the cells, which represents the integration of the function of the whole transport systems active at the cell membrane.

However, by using MEVC, whole cell macroscopic currents due to anion and/or cation fluxes through various ion channels are recorded. Different typical currents could be discriminated using biophysical and pharmacological characterizations, with more or less specific ion channel blockers. The main biophysical characteristics used for current characterization correspond to the reversal potential (i.e. the voltage value where the current reach zero) which is related to the equilibrium

Table 3.1 Ion channel activities reported from higher plant cells by microelectrode voltage-clamp studies

Currents	Cell type	Organism	Référence
KORC	Guard cells	*Vicia faba*	Blatt (1992); Forestier et al. (1998); Roelfsema et al. (2001)
		Arabidopsis thaliana	Roelfsema and Prins (1997); Forestier et al. (1998)
		Commelina communis	Forestier et al. (1998)
		Nicotiana tabacum	Blatt et al. 1999
	Root hairs	*M. sativa*	Bouteau et al. (1999)
		A. thaliana	Bouteau unpublished
	Cultured cells	*A. thaliana* *N. plombaginifolia*	Jeannette et al. (1999); Bouteau et al.; unpublished
	Laticifer	*Hevea brasiliensis*	Bouteau et al. (1999)
KIRC	Guard cells	*V. faba*	Blatt (1992) Forestier et al. (1998); Roelfsema et al. (2001)
		A. thaliana	Roelfsema and Prins (1997); Forestier et al. (1998)
		N. tabacum	Blatt et al. 1999
		Commelina communis	Forestier et al. (1998)
	Cultured cells	*A. thaliana*	Tran and Bouteau Unpublished
		N. tabacum	Tran and Bouteau Unpublished
	Root hairs	*A. thaliana*	Lew (1991)
		M. sativa	Bouteau et al. (1999)
		A. thaliana	Dauphin et al. (2001) Lew and Shabala 2000
		Vigna unguiculata	Dauphin et al. (2001)
		Phaseolus vulgaris	Dauphin et al. (2001)
	Laticifer	*H. brasiliensis*	Bouteau et al. (1996)
R-type anion current (QUAC)	Guard cells	*V. faba*	Raschke et al. (2003)
S-type anion current (SLAC)	Guard cells	*V. faba*	Forestier et al. (1998)
		A. thaliana	Forestier et al. (1998).
		Commelina communis	Forestier et al. (1998)
		Nicotiana benthamiana	Grabov et al. (1997)
	Cultured cells	*A. thaliana*	Ghellis et al. (2000); Reboutier et al. (2002)
		N. plumbaginifolia	Gauthier et al. (2007)
		N. tabacum	Tran and Bouteau unpublished
		Malus sp.	Reboutier et al. (2007)

(continued)

Table 3.1 (continued)

Currents	Cell type	Organism	Référence
	Root hairs	*M. sativa*	Bouteau et al. (1999)
		A. thaliana	Dauphin et al. (2001); Lew and Shabala 2000
		Vigna unguiculata	Dauphin et al. (2001)
		Phaseolus vulgaris	Dauphin et al. (2001)
IRAC	Root hairs	*M. sativa*	Bouteau et al. (1999)
		A. thaliana	Bouizgarne et al. (2006b)
		Phoenix dactilifera	Bouizgarne and Bouteau unpublished
H^+-ATPase current	Root hairs	*A. thaliana*	Lew (1991)
		M. sativa	Kurkdjian et al. (2000)
		Phoenix dactilifera	Bouizgarne et al. (2004)
	Guard cells	*Vicia faba*	Blatt (1992); Roelfsema et al. (2001)

thermodynamical potential for a given ion ($Ei = \frac{RT}{zF} \ln \frac{[i]int}{[i]ext}$); the rectifying properties (ability for a channel to allow ion flow in only one way) and the kinetics of macroscopic current activation or inactivation at given voltages. For example, macroscopic current dominated by typical K^+ outward rectifying currents (KORC) are shwon in Fig. 3.2a. In this experiment, the voltage was held at the value of membrane potential (around −40 mV) and then stepped from −200 to +80 mV. This current presents rectifying properties since current could only be recorded for voltages positive to $E_K > -40$mV, moreover, the current increases in a time-dependent manner during the more positive voltage pulses with a typical sigmoidal curve. By modifying the value of the holding potential the gating characteristic of channels could be highlighted. Figure 3.2b shows recordings of whole cell macroscopic currents dominated by K^+ inward rectifying currents (KIRC) on the same cell for holding potential at Vm (left); at −100 mV, negative to E_K in our conditions, (center) and +50 mV, positive to E_K. When the voltage was held at a potential negative to E_K, inward rectifying K^+ channels are open and no time-dependent activation of the macroscopic current could be observed for the more negative voltage pulses when deactivation of current, indicative of channel closure, could be observed for the more positive voltage pulses (Fig. 3.2b, center). On the contrary, when the holding potential was held at a voltage far positive to E_K, (Fig. 3.2b, right), a time-dependent activation of the KIRC is observed for voltage values negative to E_K. By modulating the voltage protocols more specific gating characteristics of some channels could be observed. Figure 3.2c presents recordings of whole cell macroscopic current dominated by anion current through slow-type anion channel. The classical protocol (Fig. 3.2c, left) allows recording a nonrectifying current presenting deactivation for the more negative voltage. By using a longer biphasic voltage-clamp protocol, the characteristic slow activation indicative of channel opening at positive voltage and deactivation indicative of channel closure at negative voltage typical of slow-type anion current (SLAC) (Schroeder and Keller 1992) could be observed

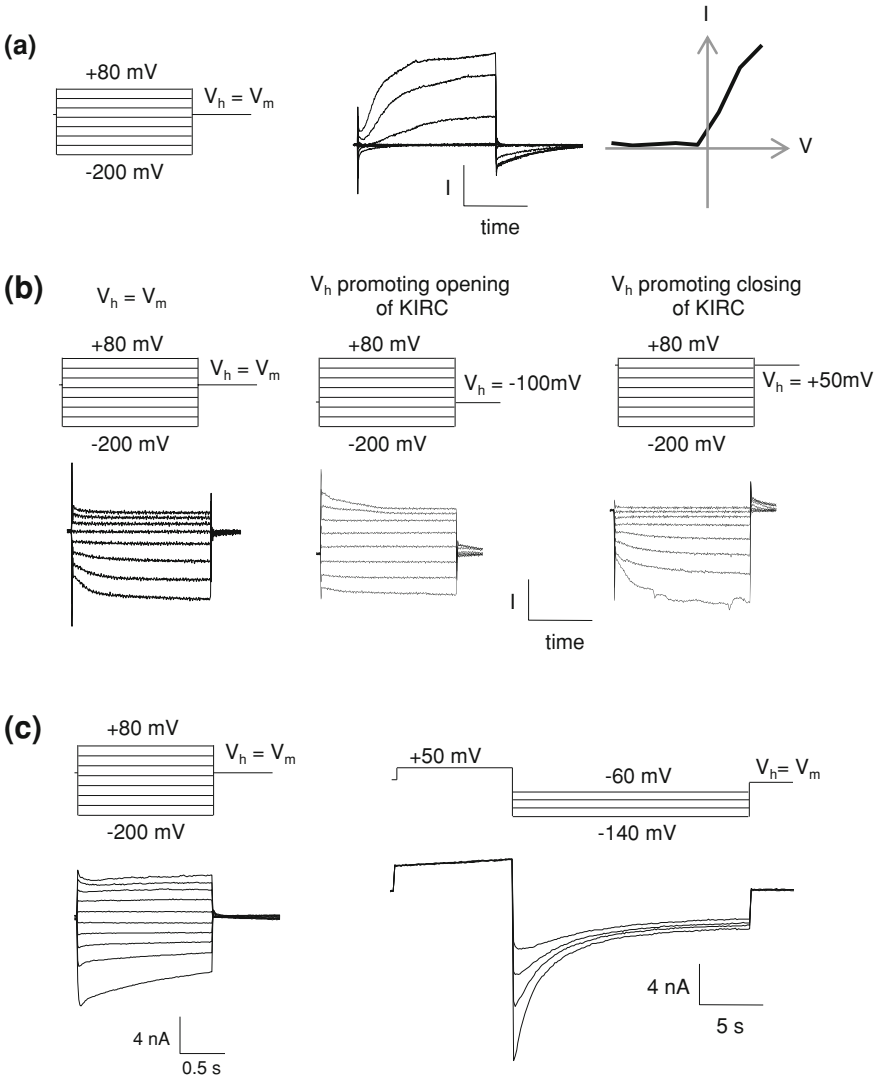

Fig. 3.2 **a** Typical K^+ outward rectifying currents (KORC) elicited from a holding potential (V_h) equal to the running membrane potential (V_m) by voltages stepped from −200 to +80 mV. **b** K^+ inward rectifying currents (KIRC) elicited from a holding potential (V_h) equal to the running membrane potential (V_m) by voltages stepped from −200 to +80 mV (*left*). Same current elicited with the same protocol but from holding potential promoting opening (*center*) or closure of KIRC (*right*). **c** Typical slow type anion current (SLAC) elicted from a holding potential (V_h) equal to the running membrane potential (V_m) by voltages stepped from −200 to +80 mV (*left*) or with a longer biphasic voltage-clamp protocol (*right*) allowing to display slow activation at postive voltage and slow deactivation at negative voltage

(Fig. 3.2c, right). The H^+-ATPases activity is virtually constant over the voltage range of –200 to 50 mV (Spanswick 1981; Lohse and Hedrich 1992; Taylor and Assmann 2001). Thus, using MEVC, voltage-independent variations of macroscopic currents resulting in the shift in the background I–V-curve could correspond to H^+-ATPase activity (Blatt 1992; Kurkdjian et al. 2000; Roelfsema et al. 2001), consistently with their modulation by H^+-ATPase pharmacology (Kurkdjian et al. 2000).

3.3 Plant Response to Stress: Sustained Ion Channel Activation

3.3.1 Stomatal Closure

The main studies on plant cells using MEVC concern guard cell behavior (e.g. Blatt 1987, 1992; Roelfsema and Prins 1997; Forestier et al. 1998; Roelfsema et al. 2001). The stomatal guard cells are specialized epidermal cells, located in the aerial organs of plants. By changing ion and water fluxes across the plasma membrane, they regulate the aperture of stomatal pores. Guard cells therefore play a major role in controlling gas exchange and plant-water relations which is of peculiar importance during drought conditions (Sirichandra et al. 2009; Kim et al. 2010; Roelfsema and Hedrich 2010; Lee and Luan 2011; Mori and Murata 2011). Stomatal closure was also observed in response to the air pollutant ozone (Vahisalu et al. 2008, 2010). Open stomata are also a major route of pathogen entry into the plant. Thus, plants have evolved mechanisms to regulate stomatal aperture as a response to abiotic stress such as drought and ozone but also as an immune response against bacterial invasion (Kim et al. 2010; Zeng et al. 2010; Lee and Luan 2011). In the case of drought, ABA serves as a chemical signal that induces stomatal closure (Sirichandra et al. 2009; Kim et al. 2010). Recent studies demonstrate that ABA plays an important role also in response to ozone and pathogens, suggesting a large overlap of the signaling pathways induced in response to pathogens and abiotic stress (Lee and Luan 2011). Although numerous data were obtained from the patch-clamp technique (see Ward et al. 2009), guard cells being unconnected to adjacent epidermal cells by plasmodesmata and thus electrically isolated, consist for a long time in an attractive cellular model for MEVC. Ion channels were recorded in guard cells from peeled epidermis from the abaxial side of the leaf (Blatt 1992; Roelfsema and Prins 1997; Forestier et al. 1998; Raschke et al. 2003) and even on guard cells in an intact plant (Roelfsema et al. 2001). The data obtained with MEVC allowed to demonstrate/confirm in living cells that ABA-induced stomatal closure occurs through second messengers, such as ROS, nitric oxide, Ca^{2+}, followed by activation and inactivation of protein kinases/phosphatases that further target the ion channels (Grabov and Blatt 1998, 1999; Garcia-Mata and Lamattina 2003; Sokolovski and Blatt 2004; Sokolovski et al. 2005). For stomatal control, guard cell turgor is a major parameter that is regulated

by ion fluxes across the plasma membrane through K^+ and anion channels. Under favorable conditions, stomatal pores are open to allow CO_2 uptake from the atmosphere and then photosynthesis. The osmotic opening of stomatal pores is performed by increasing the K^+ uptake through inward-rectifying K^+ channels, by activation of plasma membrane H^+-ATPases, the organic acid (mainly malate) concentrations and the uptake of inorganic anions. Under stress conditions such as drought or pathogen invasion, ABA-induced stomatal closure could be mediated by the release of K^+ and anions from guard cells, resulting in guard cell turgor reduction and guard cell volume decrease. Depolarization due to plasma membrane SLAC (Grabov et al. 1997) was proposed to drive K^+ efflux through activation of channels driving KORC, whereas KIRC are inactivated (Armstrong et al. 1995) resulting in cellular export of K^+ and anions driving water efflux (Fig. 3.3a). Ozone triggers rapid stomatal closure controlled by the guard cell slow-type anion channel SLAC1 (Vahisalu et al. 2008, 2010) probably also in an ABA-dependent manner (Geiger et al. 2009; Lee et al. 2009; Vahisalu et al. 2010).

To counteract stomatal closure as a defense response, pathogens may have evolved virulence factors to actively counter stomatal closure to facilitate invasion (Zeng et al. 2010). In a study using *Nicotiana tabacum* haboring the Cf-9 transgene encoding an extracytosolic leucine-rich repeat (LRR) protein that confers resistance in tomato to races of the fungus *Cladosporium fulvum* expressing the corresponding avirulence gene Avr9, Grabov, and Blatt (1997) showed that exposure of intact guard cells in epidermal peels to Avr9 resulted in stimulation of KORC and almost complete suppression of KIRC compatible with stomatal closure. Thus further studies are needed to check for the effect of pathogen-derived molecules on guard cell ion current allowing stomatal closure or opening.

3.3.2 Plasmolysis and PCD

Suspension cells are a convenient system for identifying early physiological events induced by pathogens or their derived elicitors (Cessna et al. 2000; Wendehenne et al. 2002; Samadi and Shahsavan Behboodi 2006) and abiotic stress (Sano et al. 2006; Kadono et al. 2006). It is further noteworthy that *A. thaliana* cultured cells respond to ABA in the same way as guard cells, i.e., by activating KORC and SLAC in a ROS- and Ca^{2+} dependent manner (Jeannette et al. 1999; Brault et al. 2004; Trouverie et al. 2008; Meimoun et al. 2009), so far suggesting that guard cell and cell culture shared principles in stress signaling. They show physiological responses to various stimuli similar to cells within tissues, especially the morphological features of dying cells during PCD (van Doorn and Woltering 2005). This is of particular interest since during nonhost interaction pathogenic microorganisms induce PCD process during HR (Heath 2000; van Doorn et al. 2011). This model is currently used to analyze events that occur during PCD (Krause and Durner 2004; Swidzinski et al. 2004; Doyle et al. 2010).

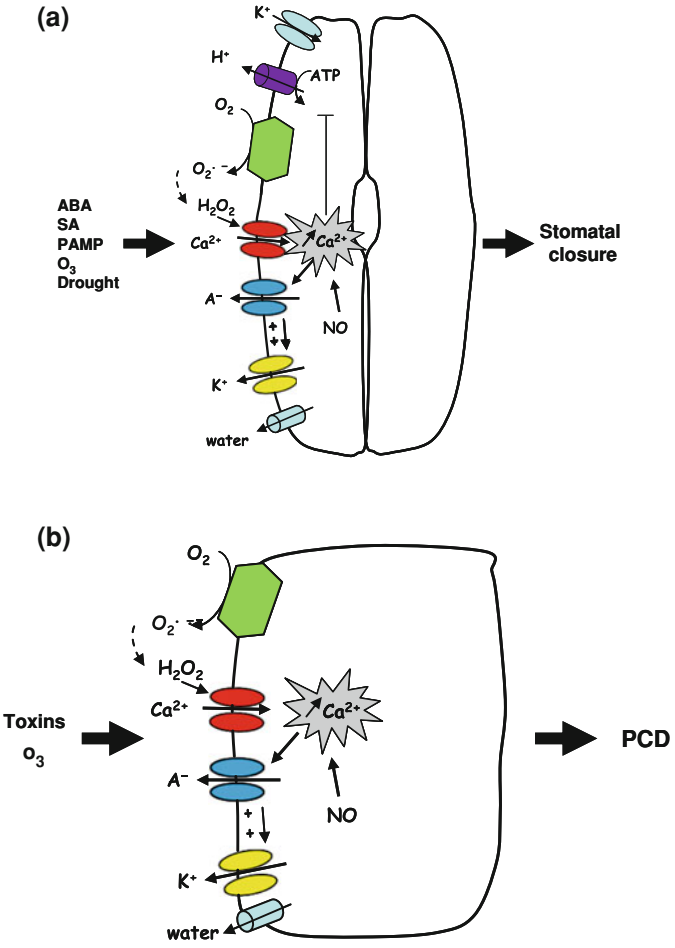

Fig. 3.3 **a** Model for regulation and activity of plasma membrane transporters during stomatal closure. **b** Model for regulation and activity of plasma membrane transporters upon stress induced PCD

In plants, ion effluxes are among the earliest responses of plant cells to elicitors and commonly precede the HR (Heath 2000). Using cultured cells as a model and dSEVC, our team studied the effect of various microbe-derived molecules, such as harpins (El-Maarouf et al. 2001; Reboutier et al. 2005; 2007a, b), considered as a PAMP (*Pathogenesis Associated Molecular Pattern*) (Nurnberger and Brunner 2002) or toxins produced by various pathogens, such as fusaric acid (Bouizgarne et al. 2006a), cryptogein (Gauthier et al. 2007), oxalic acid (Errakhi et al. 2008a) or thaxtomine (Errakhi et al. 2008b), on ion channel regulations and cell death. Our results highlight the complex involvement of ion channels in transduction mechanisms leading to cell death since various ion channels and various regulations likely participate in both the activation and execution of PCD.

We have shown that the inhibition of anion channel mediated NO_3^- efflux, an early prerequisite to the cryptogein-triggered HR on tobacco cells, prevents plasma membrane depolarization and Ca^{2+} influx, and suppresses vacuolar collapse; hallmarks of PCD (Gauthier et al. 2007). Such events were also observed on *A. thaliana* cells in response to the toxins oxalic acid (Errakhi et al. 2008b) but also in response to abiotic stress such as ozone (Kadono et al. 2010). Delayed activation of KORC was also recorded upon addition of cryptogein on tobacco or ozone on *A. thaliana* cells (unpublished data). Moreover, we have shown that increase in SLAC activity probably promotes the accumulation of transcripts encoding a vacuolar processing enzyme (VPE) (Gauthier et al. 2007; Kadono et al. 2010) that belongs to a family of proteases displaying a caspase 1-like activity and were reported to contribute to the disruption of vacuole integrity that was observed during HR (Hatsugai et al. 2006). Ion channel inhibitors counteract PCD induced by different stress in cultured cells (Gauthier et al. 2007; Errakhi et al. 2008b; Kadono et al. 2010) which reinforce the alteration of ion channel activity as key elements of PCD development.

These ion channel regulations are reminiscent of altered activity of ion channels that may promote apoptosis in animal cells (Yu and Choi 2000; Bortner and Cidlowski 2007). Effectively during apoptosis, a well-described form of animal PCD, ion channels contribute to cell shrinkage, also termed as apoptotic volume decrease (AVD), and modify intracellular ion composition. Potassium effluxes through K^+ channels contribute to cell shrinkage and decreases intracellular K^+ concentration. This in turn promotes caspase-induced apoptotic cell death. Nuclease and caspase activities were effectively shown to be dependent on low intracellular K^+ concentrations and are restricted to shrunken cells. Chloride channels have also been shown in various apoptotic model systems to play a critical role during cell death in both the signaling and control of AVD (Yu and Choi 2000; Bortner and Cidlowski 2007). Thus, as in animal cells during apoptosis or, in plant cells during stomatal closure or PCD ongoing, activation of anion channel allowing long-term anion effluxes and activation of KORC allowing K^+ effluxes result in cell turgor reduction and plasmolysis (Fig. 3.3b). Data obtained on different PCD-inducing stress (Wendehenne et al. 2002; Gauthier et al. 2007; Errakhi et al. 2008a; Kadono et al. 2010) point toward a probable early interplay between slow-type anion channel regulation and a subset of well-established second messengers involved in cell death but also in guard cell closure (Fig. 3.3a, b), notably Ca^{2+} and ROS (Garcia-Brugger et al. 2006; Gauthier et al. 2007; Ahlfors et al. 2009; Kadono et al. 2010). Knowing why guard cells submitted to repetitive cell shrinkage did not undertake PCD process could be raised. During animal apoptosis, some caspases are activated only when the K^+ internal concentration reach a minimal threshold consisting thus in a nonreturn point crucial for the cell fate (Bortner and Cidlowski 2007). Although during guard cells closure, they could lose half of their volume which is important but perhaps not sufficient to reach the threshold necessary to induce PCD. Another possibility could be that the machinery necessary to this form of PCD could be constitutively inactivated in guard cells.

3.4 Plant Response to Stress: Transient Ion Channel Activations

Involvement of ion channels in response to stress leading to osmotic adjustment necessiates sustained ion channels' activation such as those observed for guard cell closure or cultured cell plasmolysis during PCD. However, transient regulations of ion channel activities were also observed, mainly using MEVC, because cytosolic intermediates are needed to modulate ion channel activities in vivo. For example, the well-known NOD factor-induced depolarization, early event of the interaction between the soil bacteria *Rhizobium* and legume root hairs resulting in the development of nitrogen-fixing nodules (Kurkdjian 1995), is due to the increase of the inward ion current and to the inhibition of the H^+ -ATPases. It involved an instantaneous inward anion current (IRAC) and/or a KIRC. These two ion currents are then downregulated while the H^+ -pump is stimulated allowing the long-term rectification of the membrane potential (Kurkdjian et al. 2000). The same type of response was observed in response to the indolic compound hyphaphorine produced by ectomycorrhizal fungus (Reboutier et al. 2002). It induces a rapid and transient membrane depolarization in root hairs and cultured cells, due to the modulation of anion and K^+ channel. Downregulation of the ion channel activated by symbiosis signals could participate to the lowered defense responses induced by symbiotic microorganisms, since signal transduction of symbiotic and pathogenic microorganisms could proceed via similar pathways, leading to overlaps in the response reaction (Baron and Zambryski 1995).

In addition, we could observe that some toxins such as thaxtomin from *Streptomyces scabies* or fusaric acid secreted by fungi from the genus *Fusarii* also induced a transient variation of the plant cell membrane potential. Fusaric acid induced a hyperpolarization due to transient decrease in SLAC and increase in KORC (Bouizgarne et al. 2006a). It is noteworthy that fusaric acid induced the same hyperpolariztion in root hairs and cultured cells (Bouizgarne et al. 2006a, b). Thaxtomin induced a transient depolarization due to transient increase in SLAC and decrease in KORC (Errakhi et al. 2008b). It is not known whether these early transient ion channel regulations consist in specific regulations participating in signaling pathways or consist more in side effects of the toxins. But the early transient modulation of ion currents induced by these toxins was not involved to induce cell death (Bouizgarne et al. 2006a; Errakhi et al. 2008b).

3.5 Ion Channel Regulations and the Harpins-PAMPs, a Complex Situation

In this last part, we want to consider the effect of harpins, effectors from the type III secretion system (TTSS) present in most plant and animal pathogenic Gram-negative bacteria. Harpins constitute a unique family of TTSS effectors that are not

found in mammalian pathogens. They are considered as PAMPs, and known to induce HR and associated defense responses in nonhost plants (He et al. 2004). As cell wall is important in the plant cell responses to pathogen and notably to harpins (Hoyos et al. 1996; Humphrey et al. 2007), MEVC studies were performed to analyze harpin-induced ion current on intact cultured cells. Our results (El-Maarouf et al. 2001; Reboutier et al. 2005, 2007a, b; Reboutier and Bouteau 2008) obtained with different harpins and different cultured cell types (host and non host), highlight the complex involvement of ion channels in transduction mechanisms leading to harpin-induced effects.

$HrpN_{ea}$, a harpin from *Erwinia amylovora,* induced as expected nonhost cell death. The cell death observed seems to be dependent on a decrease in SLAC although $HrpN_{ea}$ also increase KORC (El Maarouf et al. 2001; Reboutier et al. 2005, 2007a). Moreover, $HrpW_{ea}$, another harpin secreted by *E. amylovora*, at subnanomolar concentrations could antagonize cell death and ROS production induced by $HrpN_{ea}$, as a result of inhibition ion channel regulations triggered $HrpN_{ea}$ (Reboutier et al. 2007a). However, $HrpW_{ea}$, at higher concentrations, was reported to induce HR on tobacco (Kim and Beer 1998) and a cell death concomitant with strong anion channels activation on *A. thaliana* cells (Reboutier et al. 2007a). This strong activation of anion channels could be responsible for an anion efflux and the cell death triggered by $HrpW_{ea}$ could be similar to cell death activated in response to ozone or other toxins (Reboutier and Bouteau 2008). Another set of experiments performed on host apple cells allow to show that $HrpN_{Ea}$ induces anion currents (Reboutier et al. 2007b) opposed of its effect on nonhost *Arabidopsis* cells. Interestingly, $HrpZ_{Pto}$ derived from the compatible pathovar was also able to induce anion currents in the *Arabidopsis* cells, whereas $HrpZ_{Pph}$, derived from an incompatible pathovar, did not induce anion currents (Haapalainen et al. 2012). These data suggest that the anion currents triggered by harpin in a host context might be connected with the virulence function of the harpin. It remains difficult to determine in vivo the exact timings and concentrations of secreted harpins at the host cell surface, but since the bacteria secretes these proteins through a thin needle-like pilus structure (Li et al. 2002), the local concentration could be very high at the pilus tip. It is obvious that the role of ion channel regulations by harpins (and more generally PAMPs) needs further studies to understand their place in transduction mechanisms leading to harpin-induced responses.

3.6 Concluding Remarks

Although MEVC only allow working on few cell types, the highly differentiated guard cells and root hairs by their localization and specific roles in plants consist in very powerful models as ascertained by the numerous studies performed on guard cells (Sirichandra et al. 2009; Kim et al. 2010; Roelfsema and Hedrich 2010; Lee and Luan 2011; Mori and Murata 2011). If plant root hairs are at the moment less studied, they are interesting models to understand plant biology at the level

of a single cell and is of significant interest owing to their unique properties and functions (Libault et al. 2010). On the contrary, dedifferentiated cultured cells consist in a very convenient system for identifying the numerous mechanisms in complex signaling networks leading to plant cell response to stress. By using complementary techniques and tools, such as patch clamp, ion selective microelectrodes, multielectrode array, and fluorescent probes, this should warrant future elaborate use of MEVC in analyzing ion channel roles in plant response to stress.

References

Ahlfors R, Brosché M, Kollist H, Kangasjärvi J (2009) Nitric oxide modulates ozone induced cell death, hormone biosynthesis and gene expression in Arabidopsis thaliana. Plant J 58: 1–12

Armstrong F, Leung J, Grabov A, Brearley J, Giraudat J, Blatt MR (1995) Sensitivity to abscisic acid of guard-cell K+ channels is suppressed by abi1-1, a mutant arabidopsis gene encoding a putative protein phosphatase. Proc Natl Acad Sci U S A 92:9520–9524

Atkinson MM, Keppler LD, Orlandi EW, Baker CJ, Mischke CF (1990) Involvement of plasma membrane calcium influx in bacterial induction of the K+/H+ and hypersensitive responses in tobacco. Plant Physiol 92:215–221

Balague C, Lin BQ, Alcon C, Flottes G, Malmstrom S, Kohler C, Neuhaus G, Pelletier G, Gaymard F, Roby D (2003) HLM1, an essential signaling component in the hypersensitive response, is a member of the cyclic nucleotide-gated channel ion channel family. Plant Cell 15:365–379

Baron C, Zambryski P (1995) The plant response in pathogenesis, symbiosis, and wounding: variations on a common theme? Annu Rev Genet 29:107–129

Batistic O, Kudla J (2009) Plant calcineurin B-like proteins and their interacting protein kinases. Biochim Biophys Acta 1793:985–992

Beilby MJ (1982) Cl^- channels in chara. Philos Trans Roy Soc Lond Ser B-Biol Sci 299:435–445

Blatt MR (1991) Ion channel gating in plants: physiological implications and integration for stomatal function. J Membr Biol 124:95–112

Blatt MR (1992) K^+ channels of stomatal guard cells. Characteristics of the inward rectifier and its control by pH. J Gen Physiol 99:615–644

Blatt MR, Slayman CL (1983) KCl leakage from microelectrodes and its impact on the membrane parameters of a nonexcitable cell. J Membr Biol 72:223–234

Blatt MR, Rodriguez-Navarro A, Slayman CL (1987) Potassium-proton symport in *Neurospora*: kinetic control by pH and membrane potential. J Membr Biol 98:169–189

Blatt MR, Maurousset L, Meharg AA (1997) High-affinity NO3–H+ cotransport in the fungus *Neurospora*: induction and control by pH and membrane voltage. J Membr Biol 160:59–76

Bortner CD, Cidlowski JA (2007) Cell shrinkage and monovalent cation fluxes: role in apoptosis. Arch Biochem Biophys 462:176–188

Bouizgarne B, Brault M, Amiar Z, Rona JP, Ouhdouch Y, El Hadrami I, Bouteau F (2004) Electrophysiological responses of root hairs from seedlings of date palm to fusaric acid: potential relation with resistance to the vascular wilt caused by *Fusarium oxysporum albedinis*. J Phytopath 152:321–324

Bouizgarne B, El-Maarouf-Bouteau H, Frankart C, Reboutier D, Madiona K, Pennarun AM, Monestiez M, Trouverie J, Amiar Z, Briand J, Brault M, Rona JP, Ouhdouch Y, El Hadrami I, Bouteau F (2006a) Early physiological responses of *Arabidopsis thaliana* cells to fusaric acid: toxic and signalling effects. New Phytol 169:209–218

Bouizgarne B, El-Maarouf-Bouteau H, Madiona K, Biligui B, Monestiez M, Pennarun AM, Amiar Z, Rona JP, Ouhdouch Y, El Hadrami I, Bouteau F (2006b) A putative role for fusaric

acid in biocontrol of the parasitic angiosperm Orobanche ramosa. Mol Plant Microbe Interact 19:550–556

Bouteau F, Bousquet U, Pennarun AM, Convert M, Dellis O, Cornel D, Rona JP (1996) Time dependent K^+ currents through plasmalemma of laticifer protoplasts from *Hevea brasiliensis*. Physiol Plant 98:97–104

Bouteau F, Pennarun AM, Kurkdjian A, Convert M, Cornel D, Monestiez M, Rona JP, Bousquet U (1999) Ion channels of intact young root hairs from *Medicago sativa*. Plant Physiol Biochem 37:889–898

Brault M, Amiar Z, Pennarum AM, Monestiez M, Zhang Z, Cornel D, Dellis O, Knight H, Bouteau F, Rona JP (2004) Plasma membrane depolarization induced by ABA in Arabidopsis thaliana suspension cells involves inhibition of H+ -pump in addition to anion channel activation cells which are both Ca2+ dependent. Plant Physiol 135:231–243

Brennecke R, Lindemann B (1974) Design of a fast voltage-clamp for biological membranes, using discontinuous feedback. Rev Sci Instrum 45:656–661

Bunney TD, van den Wijngaard PW, de Boer AH (2002) 14-3-3 protein regulation of proton pumps and ion channels. Plant Mol Biol 50:1041–1051

Carden DE, Felle HH (2003) The mode of action of cell wall-degrading enzymes and their interference with Nod factor signalling in *Medicago sativa* root hairs. Planta 216:993–1002

Cessna SG, Sears VE, Dickman MB, Low PS (2000) Oxalic acid, a pathogenicity factor for Sclerotinia sclerotiorum, suppresses the oxidative burst of the host plant. Plant Cell 12: 2191–2200

Clough SJ, Fengler KA, Yu IC, Lippok B, Smith RK, Bent AF (2000) The Arabidopsis *dnd1* "defense, no death" gene encodes a mutated cyclic nucleotide-gated ion channel. Proc Nat Acad Sci U S A 97:9323–9328

Cole KS (1949) Some physical aspects of bioelectric phenomena. Proc Natl Acad Sci U S A 35:558–566

Dauphin A, El-Maarouf H, Vienney N, Rona JP, Bouteau F (2001) Effect of desiccation on potassium and anion currents from young root hairs: implication on tip growth. Physiol Plant 113:79–84

del Pozo O, Lam E (1998) Caspases and programmed cell death in the hypersensitive response of plants to pathogens. Curr Biol 8:R896

Demidchik V, Cuin TA, Svistunenko D, Smith SJ, Miller AJ, Shabala S, Sokolik A, Yurin V (2010) Arabidopsis root K^+-efflux conductance activated by hydroxyl radicals: single-channel properties, genetic basis and involvement in stress-induced cell death. J Cell Sci 123: 1468–1479

Dixon MS, Jones DA, Keddie JS, Thomas CM, Harrison K, Jones JD (1996) The tomato Cf-2 disease resistance locus comprises two functional genes encoding leucine-rich repeat proteins. Cell 84:451–459

Doyle SM, Diamond M, McCabe PF (2010) Chloroplast and reactive oxygen species involvement in apoptotic-like programmed cell death in Arabidopsis suspension cultures. J Exp Bot 61: 473–482

El-Maarouf H, Barny MA, Rona JP, Bouteau F (2001) Harpin, a hypersensitive response elicitor from *Erwinia amylovora,* regulates ion channel activities in *Arabidopsis thaliana* suspension cells. FEBS Lett 497:82–84

Errakhi R, Dauphin A, Meimoun P, Lehner A, Reboutier D, Vatsa P, Briand J, Madiona K, Rona JP, Barakate M, Wendehenne D, Beaulieu C, Bouteau F (2008a) An early Ca^{2+} influx is a prerequisite to thaxtomin A-induced cell death in *Arabidopsis thaliana* cells. J Exp Bot 59: 4259–4270

Errakhi R, Meimoun P, Lehner A, Vidal G, Briand J, Corbineau F, Rona JP, Bouteau F (2008b) Anion channel activity is necessary to induce ethylene synthesis and programmed cell death in response to oxalic acid. J Exp Bot 59:3121–3129

Findlay GP (1961) Voltage-clamp experiments with Nitella. Nature 191:812

Finkel AS, Redman S (1984) Theory and operation of a single microelectrode voltage-clamp. J Neurosci Methods 11:101–127

Forestier C, Bouteau F, Leonhardt N, Vavasseur A (1998) Pharmacological properties of slow anion currents in intact guard cells of Arabidopsis. Application of the discontinuous single-electrode voltage-clamp to different species. Pflugers Arch 436:920–927

Fujita M, Fujita Y, Noutoshi Y, Takahashi F, Narusaka Y, Yamaguchi-Shinozaki K, Shinozaki K (2006) Crosstalk between abiotic and biotic stress responses: a current view from the points of convergence in the stress signaling networks. Curr Opin Plant Biol 9:436–442

Garcia-Brugger A, Lamotte O, Vandelle E, Bourque S, Lecourieux D, Poinssot B, Wendehenne D, Pugin A (2006) Early signaling events induced by elicitors of plant defenses. Mol Plant Microbe Interact 19:711–724

Garcia-Mata C, Lamattina L (2003) Abscisic acid, nitric oxide and stomatal closure—is nitrate reductase one of the missing links? Trends Plant Sci 8:20–26

Gauthier A, Lamotte O, Reboutier D, Bouteau F, Pugin A, Wendehenne D (2007) Cryptogein-induced anion effluxes: electrophysiological properties and analysis of the mechanisms through which they contribute to the elicitor-triggered cell death. Plant Signal Behav 2:89–98

Geiger D, Scherzer S, Mumm P, Stange A, Marten I, Bauer H, Ache P, Matschi S, Liese A, Al-Rasheid KA, Romeis T, Hedrich R (2009) Activity of guard cell anion channel SLAC1 is controlled by drought-stress signaling kinase-phosphatase pair. Proc Natl Acad Sci U S A 106:21425–21430

Ghelis T, Dellis O, Jeannette E, Bardat F, Cornel D, Miginiac E, Rona JP, Sotta B (2000) Abscissic acid specific expression of RAB18 involves activation of anion channels in Arabidopsis thaliana suspension cells. FEBS Lett 474:43–47

Gilliham M, Sullivan W, Tester M, Tyerman SD (2006) Simultaneous flux and current measurement from single plant protoplasts reveals a strong link between K^+ fluxes and current, but no link between Ca^{2+} fluxes and current. Plant J 46:134–144

Goudet C, Benitah JP, Milat ML, Sentenac H, Thibaud JB (1999) Cluster organization and pore structure of ion channels formed by beticolin 3, a nonpeptidic fungal toxin. Biophys J 77:3052–3059

Grabov A, Blatt MR (1998) Membrane voltage initiates Ca^{2+} waves and potentiates Ca^{2+} increases with abscisic acid in stomatal guard cells. Proc Natl Acad Sci U S A 95:4778–4783

Grabov A, Blatt MR (1999) A steep dependence of inward-rectifying potassium channels on cytosolic free calcium concentration increase evoked by hyperpolarization in guard cells. Plant Physiol 119:277–288

Grabov A, Leung J, Giraudat J, Blatt MR (1997) Alteration of anion channel kinetics in wild-type and abi1-1 transgenic Nicotiana benthamiana guard cells by abscisic acid. Plant J 12:203–213

Gradmann D, Hansen UP, Long WS, Slayman CL, Warncke J (1978) Current-voltage relationships for the plasma membrane and its principal electrogenic pump in *Neurospora crassa*: I. Steady-state conditions. J Membr Biol 39:333–367

Haapalainen M, Dauphin A, Li CM, Bailly G, Tran D, Briand J, Bouteau F, Taira S (2012) HrpZ harpins from different pseudomonas syringae pathovars differ in molecular interactions and in induction of anion channel responses in arabidopsis thaliana suspension cells. Plant Physiol Biochem 51:168–174

Halliwell JV, Plant TD, Robbins J, Standen NB (1994) Voltage-clamp techniques. In: Microelectrode techniques, The plymouth workshop handbook (Ogden DC, ed), vol 2nd edn, Cambridge, UK, p 270

Hatsugai N, Kuroyanagi M, Nishimura M, Hara-Nishimura I (2006) A cellular suicide strategy of plants: vacuole-mediated cell death. Apoptosis 11:905–911

Hauser F, Waadtl R, Schroeder JI (2011) Evolution of abscisic acid synthesis and signaling mechanisms. Curr Biol 21:R346–R355

He SY, Nomura K, Whittam TS (2004) Type III protein secretion mechanism in mammalian and plant pathogens. Biochim Biophys Acta 1694:181–206

Heath MC (2000) Hypersensitive response-related death. Plant Mol Biol 44:321–334

Henriksen GH, Taylor AR, Brownlee C, Assmann SM (1996) Laser microsurgery of higher plant cell walls permits patch-clamp access. Plant Physiol 110:1063–1068

Hodgkin AL, Huxley AF, Katz B (1952) Measurement of current-voltage relations in the membrane of the giant axon of Loligo. J Physiol 116:424–448

Hoyos ME, Stanley CM, He SY, Pike S, Pu XA, Novacky A (1996) The interaction of $Harpin_{Pss}$ with plant cell walls. Mol Plant-Microbe Interact 9:608–616

Humphrey TV, Bonetta DT, Goring DR (2007) Sentinels at the wall: cell wall receptors and sensors. New Phytol 176:7–21

Hutchison ML, Tester MA, Gross DC (1995) Role of biosurfactant and ion channel-forming activities of syringomycin in transmembrane ion flux: a model for the mechanism of action in the plant-pathogen interaction. Mol Plant Microbe Interact 8:610–620

Jabs T, Tschope M, Colling C, Hahlbrock K, Scheel D (1997) Elicitor-stimulated ion fluxes and O_2^- from the oxidative burst are essential components in triggering defense gene activation and phytoalexin synthesis in parsley. Proc Nat Acad Sci U S A 94:4800–4805

Jeannette E, Rona JP, Bardat F, Cornel D, Sotta B, Miginiac E (1999) Induction of RAB18 gene expression and activation of K^+ outward rectifying channels depend on an extracellular perception of ABA in *Arabidopsis thaliana* suspension cells. Plant J 18:13–22

Jeworutzki E, Roelfsema MRG, Anschutz U, Krol E, Elzenga JTM, Felix G, Boller T, Hedrich R, Becker D (2010) Early signaling through the Arabidopsis pattern recognition receptors FLS2 and EFR involves Ca^{2+}-associated opening of plasma membrane anion channels. Plant J 62:367–378

Jones DA, Thomas CM, Hammond-Kosack KE, Balint-Kurti PJ, Jones JD (1994) Isolation of the tomato Cf-9 gene for resistance to *Cladosporium fulvum* by transposon tagging. Science 266:789–793

Kadono H, Shimizu N, Toyooka S (2006) Statistical interferometry and application to monitoring of biological activity of plant. SPECKLE06: Speckles, From Grains to Flowers 6341: U282–U286

Kadono T, Tran D, Errakhi R, Hiramatsu T, Meimoun P, Briand J, Iwaya-Inoue M, Kawano T, Bouteau F (2010) Increased anion channel activity is an unavoidable event in ozone-induced programmed cell death. PLoS ONE 5:e13373

Kim JF, Beer SV (1998) HrpW of *Erwinia amylovora*, a new harpin that contains a domain homologous to pectate lyases of a distinct class. J Bacteriol 180:5203–5210

Kim TH, Bohmer M, Hu H, Nishimura N, Schroeder JI (2010) Guard cell signal transduction network: advances in understanding abscisic acid, CO_2, and Ca^{2+} signaling. Annu Rev Plant Biol 61:561–591

Klusener B, Weiler EW (1999) Pore-forming properties of elicitors of plant defense reactions and cellulolytic enzymes. FEBS Lett 459:263–266

Krause M, Durner J (2004) Harpin inactivates mitochondria in Arabidopsis suspension cells. Mol Plant Microbe Interact 17:131–139

Kurkdjian A (1995) Role of the differentiation of root epidermal cells in Nod-factor (from *Rhizobium meliloti)* induced root hair depolarization of *Medicago sativa*. Plant Physiol 107:783–790

Kurkdjian A, Leitz G, Manigault P, Harim A, Greulich KO (1993) Nonenzymatic access to the Plasma-Membrane of medicago root hairs by laser microsurgery. J Cell Sci 105:263–268

Kurkdjian A, Bouteau F, Pennarun AM, Convert M, Cornel D, Rona JP, Bousquet U (2000) Ion currents involved in early Nod factor response in *Medicago sativa* root hairs: a discontinuous single-electrode voltage-clamp study. Plant J 22:9–17

Lee SC, Luan S (2011) ABA signal transduction at the crossroad of biotic and abiotic stress responses. Plant, Cell Environ

Lee SC, Lan W, Buchanan BB, Luan S (2009) A protein kinase-phosphatase pair interacts with an ion channel to regulate ABA signaling in plant guard cells. Proc Natl Acad Sci U S A 106:21419–21424

Leng Q, Mercier RW, Hua BG, Fromm H, Berkowitz GA (2002) Electrophysiological analysis of cloned cyclic nucleotide-gated ion channels. Plant Physiol 128:400–410

Lew RR (1991) Substrate regulation of single Potassium and Chloride-Ion channels in Arabidopsis plasma-membrane. Plant Physiol 95:642–647

Lew RR (1996) Pressure regulation of the electrical properties of growing *Arabidopsis thaliana L.* root hairs. Plant Physiol 112:1089–1100

Li CM, Brown I, Mansfield J, Stevens C, Boureau T, Romantschuk M, Taira S (2002) The Hrp pilus of *Pseudomonas syringae* elongates from its tip and acts as a conduit for translocation of the effector protein HrpZ. EMBO J 21:1909–1915

Libault M, Brechenmacher L, Cheng J, Xu D, Stacey G (2010) Root hair systems biology. Trends Plant Sci 15:641–650

Lohse G, Hedrich R (1992) Characterization of the Plasma-Membrane H^+-Atpase from *Vicia-Faba* Guard-Cells - Modulation by Extracellular Factors and Seasonal-Changes. Planta 188:206–214

Meharg AA, Blatt MR (1995) NO_3^- transport across the plasma membrane of *Arabidopsis thaliana* root hairs: kinetic control by pH and membrane voltage. J Membr Biol 145:49–66

Meimoun P, Vidal G, Bohrer AS, Lehner A, Tran D, Briand J, Bouteau F, Rona JP (2009) Intracellular Ca2+ stores could participate to abscisic acid-induced depolarization and stomatal closure in Arabidopsis thaliana. Plant Signal Behav 4:830–835

Mori IC, Murata Y (2011) ABA signaling in stomatal guard cells: lessons from Commelina and Vicia. J Plant Res 124:477–487

Neher E, Sakmann B (1976) Single-channel currents recorded from membrane of denervated frog muscle fibres. Nature 260:799–802

Nürnberger T, Brunner F (2002) Innate immunity in plants and animals: emerging parallels between the recognition of general elicitors and pathogen-associated molecular patterns. Curr Opin Plant Biol 5:318–324

Pike SM, Adam AL, Pu XA, Hoyos ME, Laby R, Beer SV, Novacky A (1998) Effects of *Erwinia amylovora* harpin on tobacco leaf cell membranes are related to leaf necrosis and electrolyte leakage and distinct from perturbations caused by inoculated *E-amylovora*. Physiol Mol Plant Pathol 53:39–60

Raschke K, Shabahang M, Wolf R (2003) The slow and the quick anion conductance in whole guard cells: their voltage-dependent alternation, and the modulation of their activities by abscisic acid and CO2. Planta 217:639–650

Reboutier D, Bouteau F (2008) Harpins and ion channels modulations: many ways to die. Plant Signal Behav 3:5

Reboutier D, Bianchi M, Brault M, Roux C, Dauphin A, Rona JP, Legué V, Frédéric Lapeyrie Bouteau F (2002) The indolic compound hypaphorine produced by ectomycorrhizal fungus interferes with auxin action and evokes early responses in non-host *Arabidopsis thaliana*. Mol Plant Microb Interact 15:932–938

Reboutier D, Frankart C, Vedel R, Brault M, Duggleby RG, Rona JP, Barny MA, Bouteau F (2005) A CFTR chloride channel activator prevents $HrpN_{ea}$-induced cell death in *Arabidopsis thaliana* suspension cells. Plant Physiol Biochem 43:567–572

Reboutier D, Frankart C, Briand J, Biligui B, Laroche S, Rona JP, Barny MA, Bouteau F (2007a) The $HrpN_{ea}$ harpin from *Erwinia amylovora* triggers differential responses on the nonhost *Arabidopsis thaliana* cells and on the host apple cells. Mol Plant Microbe Interact 20:94–100

Reboutier D, Frankart C, Briand J, Biligui B, Rona JP, Haapalainen M, Barny MA, Bouteau F (2007b) Antagonistic action of harpin proteins: HrpWea from Erwinia amylovora suppresses HrpNea-induced cell death in Arabidopsis thaliana. J Cell Sci 120:3271–3278

Reymond P, Grunberger S, Paul K, Muller M, Farmer EE (1995) Oligogalacturonide defense signals in plants—large fragments interact with the Plasma-Membrane in Vitro. Proc Nat Acad Sci U S A 92:4145–4149

Roelfsema MRG, Hedrich R (2010) Making sense out of Ca^{2+}signals: their role in regulating stomatal movements. Plant, Cell Environ 33:305–321

Roelfsema MRG, Prins HBA (1997) Ion channels in guard cells of *Arabidopsis thaliana (L) Heynh*. Planta 202:18–27

Roelfsema MRG, Steinmeyer R, Staal M, Hedrich R (2001) Single guard cell recordings in intact plants: light-induced hyperpolarization of the plasma membrane. Plant J 26:1–13

Samadi L, Shahsavan Behboodi B (2006) Fusaric acid induces apoptosis in saffron root-tip cells: roles of caspase-like activity, cytochrome c, and H2O2. Planta 225:223–234

Sano T, Higaki T, Handa K, Kadota Y, Kuchitsu K, Hasezawa S, Hoffmann A, Endter J, Zimmermann U, Hedrich R, Roitsch T (2006) Calcium ions are involved in the delay of plant cell cycle progression by abiotic stresses. FEBS Lett 580:597–602

Scheel D (1998) Resistance response physiology and signal transduction. Curr Opin Plant Biol 1:305–310

Schroeder JI, Keller BU (1992) Two types of anion channel currents in guard cells with distinct voltage regulation. Proc Natl Acad Sci U S A 89:5025–5029

Schroeder JI, Hedrich R, Fernandez JM (1984) Potassium-selective single channels in guard-cell protoplasts of *Vicia-Faba*. Nature 312:361–362

Shabala SN, Lew RR (2002) Turgor regulation in osmotically stressed Arabidopsis epidermal root cells. Direct support for the role of inorganic ion uptake as revealed by concurrent flux and cell turgor measurements. Plant Physiol 129:290–299

Shabala S, Newman I (2000) Salinity effects on the activity of plasma membrane H^+ and Ca^{2+} transporters in bean leaf mesophyll: masking role of the cell wall. Ann Bot 85:681–686

Shabala S, Cuin TA, Pottosin I (2007) Polyamines prevent NaCl-induced K^+ efflux from pea mesophyll by blocking non-selective cation channels. FEBS Lett 581:1993–1999

Sirichandra C, Wasilewska A, Vlad F, Valon C, Leung J (2009) The guard cell as a single-cell model towards understanding drought tolerance and abscisic acid action. J Exp Bot 60: 1439–1463

Sokolovski S, Blatt MR (2004) Nitric oxide block of outward-rectifying K^+ channels indicates direct control by protein nitrosylation in guard cells. Plant Physiol 136:4275–4284

Sokolovski S, Hills A, Gay R, Garcia-Mata C, Lamattina L, Blatt MR (2005) Protein phosphorylation is a prerequisite for intracellular Ca^{2+} release and ion channel control by nitric oxide and abscisic acid in guard cells. Plant J 43:520–529

Somssich IE, Hahlbrock K (1998) Pathogen defence in plants—a paradigm of biological complexity. Trends Plant Sci 3:86–90

Spanswick RM (1981) Electrogenic ion pumps. Ann Rev Plant Physiol Plant Mol Biol 32: 267–289

Spoel SH, Dong X (2008) Making sense of hormone crosstalk during plant immune responses. Cell Host Microbe 3:348–351

Swidzinski JA, Leaver CJ, Sweetlove LJ (2004) A proteomic analysis of plant programmed cell death. Phytochemistry 65:1829–1838

Taylor AR, Assmann SM (2001) Apparent absence of a redox requirement for blue light activation of pump current in broad bean guard cells. Plant Physiol 125:329–338

Taylor AR, Brownlee C (1992) Localized patch clamping of Plasma Membrane of a polarized plant cell: laser microsurgery of the fucus Spiralis rhizoid cell wall. Plant Physiol 99: 1686–1688

Teodoro AE, Zingarelli L, Lado P (1998) Early changes of Cl^- efflux and H^+ extrusion induced by osmotic stress in *Arabidopsis thaliana* cells. Physiol Plant 102:29–37

Tran D, Kadono T, Meimoun P, Kawano T, Bouteau F (2010) TiO_2 nanoparticles induce ROS generation and cytosolic Ca^{2+} increases on BY-2 tobacco cells: a chemiluminescence study. Luminescence 25:140–142

Trouverie J, Vidal D, Zhang Z, Sirichandra C, Madiona K, Amiar Z, Prioul JL, Jeannette E, Rona JP, Brault M (2008) Anion channel activation and proton pumping inhibition involved in the plasma membrane depolarization induced by ABA in Arabidopsis thaliana suspension cells are both ROS dependent. Plant Cell Physiol 49:1495–1507

Vahisalu T, Kollist H, Wang YF, Nishimura N, Chan WY, Valerio G, Lamminmaki A, Brosche M, Moldau H, Desikan R, Schroeder JI, Kangasjarvi J (2008) SLAC1 is required for plant guard cell S-type anion channel function in stomatal signalling. Nature 452:487–491

Vahisalu T, Puzõrjova I, Brosché M, Valk E, Lepiku M, Moldau H, Pechter P, Wang YS, Lindgren O, Salojärvi J, Loog M, Kangasjärvi J, Kollist H (2010) Ozone-triggered rapid

stomatal response involves the production of reactive oxygen species, and is controlled by SLAC1 and OST1. Plant J 62:442–453

van Doorn WG, Woltering EJ (2005) Many ways to exit? Cell death categories in plants. Trends Plant Sci 10:117–122

van Doorn WG, Beers EP, Dangl JL, Franklin-Tong VE, Gallois P, Hara-Nishimura I, Jones AM, Kawai-Yamada M, Lam E, Mundy J, Mur LA, Petersen M, Smertenko A, Taliansky M, Van Breusegem F, Wolpert T, Woltering E, Zhivotovsky B, Bozhkov PV (2011) Morphological classification of plant cell deaths. Cell Death Differ 18:1241–1246

Ward JM, Maser P, Schroeder JI (2009) Plant ion channels: gene families, physiology, and functional genomics analyses. Ann Rev Physiol 71:59–82

Wendehenne D, Lamotte O, Frachisse JM, Barbier-Brygoo H, Pugin A (2002) Nitrate efflux is an essential component of the cryptogein signaling pathway leading to defense responses and hypersensitive cell death in tobacco. Plant Cell 14:1937–1951

Yu SP, Choi DW (2000) Ions, cell volume, and apoptosis. Proc Natl Acad Sci U S A 97: 9360–9362

Yukihiro M, Hiramatsu T, Bouteau F, Kadono T, Kawano T (2012) Peroxyacetyl nitrate-induced oxidative and calcium signaling events leading to cell death in ozone-sensitive tobacco cell-line. Plant Sig Behav 7(1):113–120

Zeng W, Melotto M, He SY (2010) Plant stomata: a checkpoint of host immunity and pathogen virulence. Curr Opin Biotechnol 21:599–603

Zhang W, He SY, Assmann SM (2008) The plant innate immunity response in stomatal guard cells invokes G-protein-dependent ion channel regulation. Plant J 56:984–996

Zhou F, Andersen CH, Burhenne K, Fischer PH, Collinge DB, Thordal-Christensen H (2000) Proton extrusion is an essential signalling component in the HR of epidermal single cells in the barley-powdery mildew interaction. Plant J 23:245–254

Zingarelli L, Marre MT, Massardi F, Lado P (1999) Effects of hyper-osmotic stress on K^+ fluxes, H^+ extrusion, transmembrane electric potential difference and comparison with the effects of fusicoccin. Physiol Plant 106:287–295

Chapter 4
Application of Non-invasive Microelectrode Flux Measurements in Plant Stress Physiology

Sergey Shabala and Jayakumar Bose

Abstract Non-invasive microelectrode flux measurement (the MIFE^{TM} technique) is a convenient tool to study membrane-transport processes in plants in situ. Over the last 20 years, many papers have been published elucidating the critical role of membrane-transport processes in response to a variety of abiotic and biotic stresses including salinity, osmotic stress, temperature extremes, acidity, oxygen deprivation, nutritional disorders, oxidative stress, and pathogens and elicitors. In this review, we summarize some of these findings and illustrate how the application of ion-selective microelectrodes may be combined with other techniques to address some fundamental issues related to mechanisms of plant nutrient acquisition and stress signaling and adaptation.

Abbreviations

abi1	Abscisic acid-insensitive1
akt1	*Arabidopsis* K^+ transporter1
ALMT	Aluminum-activated malate transporter
AM	Arbuscular mycorrhiza
AtCNGC10	*Arabidopsis* cyclic nucleotide-gated channel10
AtHELPS	*Arabidopsis* DExD/H box RNA helicase
ATP	Adenosine triposphate
CED-9	Cell death defective-9
Cu/a	Cu^{2+}/ascorbate
$[Ca^{2+}]_{cyt}$	Cytosolic free calcium
Em	Membrane potential
GORK	Guard cell outward-rectifying K^+ channel
HR	Hypersensitive response

S. Shabala (✉) · J. Bose
School of Agricultural Science, University of Tasmania,
Private Bag 54, Hobart, TAS 7001, Australia
e-mail: Sergey.Shabala@utas.edu.au

A. G. Volkov (ed.), *Plant Electrophysiology*,
DOI: 10.1007/978-3-642-29119-7_4, © Springer-Verlag Berlin Heidelberg 2012

Kcv	Viral-encoded K^+ channel
KIR	K^+ inward-rectifying channel
KOR	K^+ outward-rectifying channel
LIX	Liquid ion exchanger
MATE	Multidrug and toxic efflux transporter
MBS	Marine bioactive substances
NORC	Nonspecific outward-rectifying channel
NSCC	Non-selective cation channel
O_2	Oxygen
PAMPs	Pathogen-associated molecular patterns
PA	Polyamines
PBCV-1	*Paramecium bursaria* chlorella virus
PCD	Programmed cell death
PM	Plasma membrane
PMV	Papaya mosaic virus
PVX	Potato virus X
ROS	Reactive oxygen species
SAC	Stretch-activated channels
SIET	Scanning ion-selective electrode technique
TEA	Tetraethylammonium
TUNEL	Terminal deoxynucleotidyl dUTP nick end labeling
ucu2-2/gi2	*ultracurvata2-2/gigantea-2*
UV-C	Ultraviolet-C
zVAD-fmk	Benzyloxycarbonyl-Val-Ala-Asp (OMe)—uoromethylketone

4.1 Introduction

The idea of measuring a specific ion flux non-invasively using ion-selective microelectrodes that move between two positions near the tissue was proposed as early as in 1985 (Lucas and Kochian 1986). Following the initial development stage (Newman et al. 1987; Kochian et al. 1989), two automated systems were developed for computer-controlled electrode movement and data recording, independently at the University of Tasmania and at the MBL (Marine Biological Laboratory, Woods Hole, MA)(Newman et al. 2012). These two systems are now known as MIFE^{TM} (Microelectrode ion flux measurement) and SIET (Scanning ion-selective electrode technique), accordingly.

Since the mid-90s our laboratory has pioneered application of non-invasive ion flux measuring (the MIFE technique) in plant stress physiology. This technique provides an impressive capability to link genetic/genomic data to cellular physiological behavior, thus providing a valuable contribution to functional genome/phenome research. Over

100 papers have been published by both us and other researchers using MIFE (or its equivalent) technique for elucidating the critical role of membrane-transport processes in response to a variety of abiotic and biotic stresses including salinity, osmotic stress, temperature extremes, acidity, oxygen deprivation, nutritional disorders, oxidative stress, and pathogens and elicitors. In this review, we summarize some of these findings and illustrate how the application of ion-selective microelectrodes may be combined with other techniques to address some fundamental issues related to mechanisms of plant nutrient acquisition and stress signaling and adaptation.

4.2 Nutrient Acquisition and Transport

The non-invasive vibrating microelectrode technique has been used widely to decipher nutrient deficiency, acquisition, and transport mechanisms in plants. The following section summaries pilot studies undertaken in this area of research.

Upon iron (Fe) limitation, plants use two strategies to improve Fe acquisition: Strategy I plants (all plants except grasses) upregulate H^+-ATPase (H^+ efflux) in order to acidify the rhizosphere thereby increasing solubility/reduction of Fe in the rhizosphere, and strategy II plants excrete phytosiderphores which form stable Fe-chelates for transport into the plant (Walker and Connolly 2008). Rice presents a special case: being a strategy II plant, it also possess a strategy I mechanism to take up reduced Fe(II) from flooded-hypoxic environment. In this regard, a recent study isolated a vesicle-related protein OsSEC27P from rice and demonstrated enhanced H^+ secretion in transgenic tobacco roots under Fe deficiency conditions (Yang et al. 2010).

Magnesium(Mg) deficiency-induced inhibition of photosynthesis is a widely accepted phenomenon. However, such inhibition occurs only after prolonged growth (few weeks to months) in Mg-deficient media. Thus early detection is critical for adopting corrective measures. In this regard, Hariadi and Shabala (2004) found that light-induced changes in leaf surface electric potential can be used as the early (within two weeks of emergence) detection tool for Mg-deficiency, with a 2-fold difference in the magnitude of leaf bioelectric response between Mg-deficient (10 ppm) and optimal (50 ppm) treatments. This difference in leaf surface electric potential was explained by the difference in Mg^{2+} movement across the plasma membrane. Subsequent analysis of Mg^{2+} transport revealed that two kinds of Mg^{2+} transporters viz., Mg^{2+}/H^+ exchanger (at $\leq$30 μM range) and non-selective cation channel (>300 μM range) were involved in Mg^{2+} uptake across the plasma membrane of bean mesophyll cells (Shabala and Hariadi 2005).

Nodulation and mycorrhizal symbiosis are the effective strategies employed by the plants to fix atmospheric nitrogen and increase soil nutrient uptake, respectively. Though a number of anatomical (e.g. increase in the nutrient absorbing area) and physiological mechanisms (e.g. synthesis and exudation of organic compounds, exoenzymes to solubilize nutrients) are clearly involved, the exact mechanism by which host recognition and enhanced nutrient uptake are achieved is poorly understood (Ramos et al. 2009). To shed light on this issue, Ramos et al. (2008) traced the

pre-symbiotic development of the arbuscular mycorrhizal (AM) fungi, and found that H^+ flux "signature" was involved in host recognition. Particularly, AM fungi showed increase in H^+ efflux and hyphal growth rate when the fungus was growing close to clover roots or was pre-treated with root exudates (Ramos et al. 2008). In a separate study, ectomycorrhizal roots of *Eucalyptus* showed 6-fold increase in H^+ efflux and concomitant rhizophere acidification at the elongation zone (Ramos et al. 2009). Similarly, Ding et al. (2011) inoculated soybean with nodule forming rhizobia and AM fungus and observed 3 to 8-fold increase in H^+ efflux during synergistic interaction in the plant-nodules-hyphae-rhizosphere continuum. Thus, elevated H^+ efflux and accompanied rhizophere acidification is the key determinant for enhanced nutrient uptake during nodule and/or symbiosis formation.

Soil or foliar application of marine bioactive substances (MBS; a biostimulant) extracted from sea weed received considerable attention, due to their potential use in organic and sustainable agriculture as a means to avoid excessive fertilizer application and to improve mineral absorption (Mugnai et al. 2008). It is believed that MBS improves crop growth through the enhanced supply of major and minor nutrients, amino acids, vitamins, and also cytokinins, auxin, and absicisic acid-like growth substances (see Mugnai et al. 2008). Recent studies from Mancuso's laboratory showed that MBS enhance NH_4^+, K^+, and Ca^{2+} uptake into *Vitis vinifera* roots, with beneficial effects for plant growth (Mancuso et al. 2006; Mugnai et al. 2008).

Based on anatomy and growth pattern, plant roots are divided into five distinct zones along the longitudinal axis viz., root cap, meristem (zone of active cell division), distal elongation zone or transition zone (zone of slow cell growth in length and width), elongation zone (zone of rapid cell growth in length without growth in width), and mature zone (zone of root hairs) (Verbelen et al. 2006). It is hypothesized that these root zones may differ distinctly in nutrient acquisition and plant signaling in response to environmental stimuli. From this perspective, non-invasive vibrating microelectrodes form the only technique available to provide the required spatial resolution along the longitudinal axis. It has been demonstrated now that H^+, K^+ (Bose et al. 2010b), NH_4^+, NO_3^- (Hawkins et al. 2008), Ca^{2+}, and Mg^{2+} (Guo et al. 2010) fluxes differ between different root zones. Moreover, this technique can be used to do functional analysis for individual transporters at the molecular level. For example, (Guo et al. (2010) demonstrated that *AtCNGC*10 transporter (*Arabidopsis* cyclic nucleotide-gated channel) is involved in transporting Ca^{2+} and Mg^{2+} ions. Similarly, functional analysis of *AtHELPS*, an *Arabidopsis* DExD/H box RNA helicase revealed that *AtHELPS* is a negative regulator of high affinity K^+ transporters (e.g. *AKT1- Arabidopsis* K^+ *transporter1*), required during K^+ deprivation (Xu et al. 2011).

4.3 Salinity

Salinity is a major environmental problem affecting crop production around the world, with up to 7% of the total land surface on earth being saline (Flowers and Yeo 1995). The economic penalties are in the range of billions of dollars. To tackle

the problem, large-scale soil amelioration has to be complemented by efficient breeding programs to increase the salt tolerance of plants, by either traditional breeding or genetic manipulation technologies (Tester and Davenport 2003).

Salt tolerance in plants is conferred by a large number of adaptive mechanisms, most of which are related to membrane-transport processes. Not surprisingly, application of the MIFE technique has allowed us to address many of the fundamental issues related to salinity stress signaling and tolerance in both glycophyte and halophyte species.

4.3.1 Revealing Osmotic and Na-Specific Components of Salt Stress Signaling

The two principal adverse effects of salinity in non-tolerant plants are osmotic stress and specific ion (Na^+ or Cl^-) toxicity (Zhu 2003; Tester and Davenport 2003). We have shown that the ionic basis of plant adaptive responses to each of these components of salinity is strikingly different (Shabala 2000; Chen et al. 2005). While NaCl promotes a net K^+ efflux, isotonic mannitol treatment induces a gradual increase in the net K^+ uptake leading to turgor recovery. This difference is explained by the specificity of effects of "ionic" and "osmotic" components of the salt stress on cell membrane potential, affecting K^+ transport via voltage-gated inward- and outward-rectifying K^+ channels (Shabala and Cuin 2008). K^+ efflux is mediated essentially by depolarization-activated K^+ outward-rectifying channels (KOR), while inward-rectifying channels (KIR) are responsible for K^+ uptake in response to non-ionic hyperosmotic treatment. Thus, two oppositely directed signals appear to initiate K^+ fluxes from salinity-stressed plant cells: (1) K^+ efflux resulting from NaCl-induced plasma membrane depolarization, and (2) K^+ uptake resulting from an as yet unknown "osmosensing mechanism". Under mild salinities, the latter component would dominate, while at higher NaCl levels, the result would be a net loss of K^+.

4.3.2 Revealing Essentiality of Cytosolic K^+ Retention as a Key Determinant of Plant Salinity Tolerance

Na^+ toxicity occurs as a result of its competition with K^+ for enzyme activation and protein biosynthesis. From this point of view, it is not the absolute quantity of Na^+ per se, but rather the cytosolic K^+/Na^+ ratio that determines cell metabolic competence and ultimately, the ability of a plant to survive in saline environments (Shabala and Cuin 2008). Thus, efficient cytosolic K^+ retention is absolutely essential for plant salinity tolerance. A strong positive correlation between shoot K^+ concentration and genotype's salinity tolerance was reported for a wide range

of plant species (Cuin et al. 2003; Colmer et al. 2006; Chen et al. 2005, 2007; Cuin et al. 2010).

Of 75 K^+-permeable transporters found in plants (Very and Sentenac 2002; Shabala 2003), depolarization-activated outward-rectifying K^+ (KOR) channel and non-selective cation (NSCC) channel play the dominant role in maintaining the optimal cytosolic K^+ homeostasis and controlling salinity-induced K^+ leak (Shabala and Cuin 2008). Under saline conditions, the root plasma membrane is strongly depolarized as a consequence of a massive influx of positively charged Na^+ ions. This makes K^+ uptake through KIR channels thermodynamically impossible, and plants must rely exclusively on K^+ uptake via high affinity transport systems (which is much less efficient). Even more importantly, the observed depolarization not only makes K^+ uptake more problematic but also causes a massive K^+ efflux through KOR channels. Taken together, these two factors result in a massive depletion in the cytosolic K^+ pool (Cuin et al. 2003; Shabala et al. 2006).

The potassium retention trait seems to be highly heritable (Chen et al. 2005, 2008; Cuin et al. 2011b), opening prospects of using MIFE for plant seedling screening in breeding programs. Simple protocols have been developed to screen plant accessions for salinity tolerance in this species (Chen et al. 2005, 2007b). These could be used by plant breeders in order to achieve their aim of developing salinity tolerant crop varieties.

4.3.3 Resolving the Role of the Plasma Membrane H^+-Pump in Salinity Responses

A salinity-induced increase in H^+-pump activity can provide a driving force for a plasma membrane Na^+/H^+ exchanger to move Na^+ from the cytoplasm into the apoplast and has been reported in many halophytic species (Ayala et al. 1996; Vera-Estrella et al. 1999; Vera-Estrella et al. 2005). However, in *Aster tripolium* NaCl-induced stimulation of P-ATPase activity was observed only after one day of salt treatment and was followed by a pronounced decline of the P-ATPase activity (Ramani et al. 2006). In *Plantago maritima*, such treatment caused a decrease in the plasma membrane H^+-ATPase activity in leaves (Bruggemann and Janiesch 1989). Is higher H^+-ATPase activity essential for salinity stress tolerance, and is there any difference between halophyte and glycophyte species?

Using the MIFE technique we have shown that NaCl application induces vanadate-sensitive H^+ efflux from both leaf (Shabala 2000) and root (Shabala et al. 2005b) tissues in a range of glycophyte species. Furthermore, higher H^+-pump activity correlated significantly with a cultivar's tolerance (Chen et al. 2007b). More tolerant varieties were able to maintain more negative membrane potential values under saline conditions and, thus, were able to prevent (or significantly reduce the magnitude of) NaCl-induced K^+ leak from the cytosol. With plasma membrane (PM) H^+-ATPase being a major determinant of membrane potential (Em; Michelet

and Boutry 1995; Palmgren 2001), more negative E_m values in salt-tolerant genotypes under steady-state conditions could be a direct consequence of a more active H^+ pump. However, in contrast to some other species (Elkahoui et al. 2005; Yang et al. 2006), Western blot analysis revealed no difference in the amount of protein present between different cultivars (Chen et al. 2007b). This suggests that the 5-fold difference in H^+-ATPase activity observed between contrasting cultivars was due to post-translational modulation of the ATPase.

4.3.4 *Understanding Ameliorative Effects of Ca^{2+} and Divalent Cations*

The application of Ca^{2+} significantly ameliorates salinity stress in many species (LaHaye and Epstein 1969; Cramer et al. 1987; Reid and Smith 2000; Shabala et al. 2003). Given the fact that such amelioration is also observed in hydroponically grown plants, the beneficial effects of supplemental Ca^{2+} are not related to changes in the soil structure and result from direct interaction between Ca^{2+} and root ion transporters. It has traditionally been accepted that the dominating mechanism behind this was the Ca^{2+} restriction of Na^+ uptake via non-selective cation channels (NSCC), the likely main pathway for Na^+ uptake into the cell (Tyerman et al. 1997; Demidchik and Tester 2002). Using MIFE, we have shown that supplemental Ca^{2+} also efficiently reduces or even prevents NaCl-induced K^+ efflux through GORK (Guard cell outward-rectifying K^+ channel) channels (Shabala et al. 2003, 2005b, 2006). The concurrent blockage by supplemental Ca^{2+} of both Na^+ uptake via NSCC and K^+ loss via efflux channels will have beneficial effect on the cytosolic K/Na ratio and cell metabolism under saline conditions. Importantly, not only Ca^{2+} but other divalent cations such as Mg^{2+} and Ba^{2+} were capable of inhibiting Na^+-induced K^+ efflux (Shabala et al. 2005b), and these effects were observed not only in root but also in shoot tissues.

4.3.5 *Elucidating the Role of Polyamines in Plant Adaptive Responses to Salinity*

Polyamines (PAs; putrescine, spermidine, and spermine) are plant growth regulators, critical for a number of developmental processes, including cell division, somatic embryogenesis, root growth, floral initiation, and flower and fruit development (Evans and Malmberg 1989; Galston and Kaur-Sawhney 1990). In addition to their role in plant development, PA may also play an important role in plant stress responses and, specifically, responses to salinity. A positive correlation between the level of unconjugated polyamines and plant salinity tolerance has been reported (Basu and Ghosh 1991; Erdei et al. 1990)

The specific details of how PA may mediate plant adaptation to salinity remain elusive. Reduced Na^+ accumulation in leaves and higher K^+/Na^+ ratios in the shoot of PA treated plants grown in the presence of NaCl have been reported at the whole-plant level (Lakra et al. 2006; Ndayiragije and Lutts, 2006). This phenomenon was explained by the ability of PA to control permeability of both non-selective, NSCC (Shabala et al. 2007a) and outward-rectifying K^+ (Pandolfi et al. 2010) channels and, hence, directly affect the intracellular K^+/Na^+ ratio. Indirect effects are also possible. First, PA blockage of NSCC will restrict inward Na^+ flux and a subsequent membrane depolarization, reducing NaCl-induced K^+ leak from the cytosol. Second, PA may regulate the activity of plant H^+-ATPases through enhancing their interaction with 14-3-3 proteins (Garufi et al. 2007), also affecting plasma membrane potential and, by doing this, channel permeability.

PAs have been also shown to possess the ability to influence reactive oxygen species (ROS) scavenging. This may be achieved directly, via increasing the activities of antioxidant systems, both enzymatic (APX, SOD) and non-enzymatic (glutathione and carotenoids) (Tang and Newton 2005; Verma and Mishra 2005). Indirect control is also very likely. Very recently, we have shown that PAs act as cofactors in the ROS-induction of PM Ca^{2+} -permeable ion channels and can also induce active Ca^{2+} efflux from the cell by activating PM-based Ca^{2+}-ATPase (Zepeda-Jazo et al. 2011).

4.3.6 Revealing Mechanisms of Ion Loading into the Xylem

Among the multiple physiological mechanisms contributing to plant salinity tolerance, reducing Na^+ loading into the xylem is often named as one of the most crucial features (Tester and Davenport 2003; Munns and Tester 2008). This can be achieved either by minimization of Na^+ entry to the xylem from the root symplast, or by maximization of retrieval back out from the xylem before it reaches sensitive tissues in the shoot.

Application of a range of biophysical and physiological kinetics of Na^+ and K^+ loading into the xylem was studied in barley varieties contrasting in their salt tolerance (Shabala et al. 2010b). It was found that restricting Na^+ loading into the xylem is not essential for conferring salinity tolerance in barley, with tolerant varieties showing xylem Na^+ concentrations at least as high as sensitive ones. At the same time, tolerant genotypes were capable of maintaining higher xylem K^+/Na^+ ratios and efficiently sequestering the accumulated Na^+ in leaves (Shabala et al. 2010b). The former was achieved by more efficient loading of K^+ into the xylem, and evidence was presented that K^+-permeable voltage-sensitive channels in parenchyma cells are involved in xylem loading and that they operate in a feedback manner to maintain a constant K^+/Na^+ ratio in the xylem sap. As for Na^+ loading, two possibilities exist: (1) passive loading mediated by Na^+-permeable ion channels located at the xylem-parenchyma interface, or (2) active loading mediated by SOS1 Na^+/H^+ exchangers (Shabala 2007).

Both MIFE measurements on isolated stellar tissues (Shabala et al. 2010b) and *in planta* measurements using multifunctional xylem pressure probes (Wegner et al. 2011) favor an active Na^+ loading concept. The most likely candidate for this active loading is the Na^+/H^+ antiporter SOS1. Such antiporters were shown to be preferentially expressed at the xylem symplast boundary of roots (Shi et al. 2002) and use H^+-ATPase energy to pump Na^+ against its electrochemical gradient existing between the parenchyma cell cytosol and the xylem (Shabala and Mackay 2011). When cytosolic Na^+ content in xylem parenchyma cells becomes higher (e.g. above 100 mM as was suggested in some works; e.g. Flowers and Colmer 2008), and xylem Na^+ content is low, NORC (Nonspecific outward-rectifying) channels (Wegner and Raschke 1994) may be responsible for the passive Na^+ loading into the xylem. However, such a situation is likely to happen only after very prolonged NaCl exposures. In all other cases, plants favor active Na^+ loading to achieve quick osmotic adjustment in the shoot.

4.3.7 *Quantifying Kinetics of Na^+ Transport in Salinity-Stressed Plants*

Measurements of net Na^+ fluxes from salinized plant tissues are significantly handicapped by two factors. One is the unfavorable flux signal to noise ratio observed under saline conditions; the other one is poor selectivity of all available commercial Na^+ LIX (Liquid ion exchanger; Carden et al. 2003; Chen et al. 2005). The latter problem is manifested by the fact that Na^+ LIX has an almost ideal Nernst response when calibrated in a set of K^+ or Ca^{2+} standards (Chen et al. 2005). Thus, any apparent Na^+ flux recorded after the imposition of NaCl is confounded by the massive efflux of K^+ (see above) and Ca^{2+} (the result of Donnan exchange in the cell wall; Ryan et al. 1992; Shabala and Newman 2000) that occur in response to salinity treatment. In consequence, the net Na^+ uptake will be substantially underestimated.

To overcome the above limitations, a new method defined as a "recovery protocol" was developed (Cuin et al. 2011a) involving recording the net efflux of Na^+ in a Na^+-free medium, immediately after the removal of NaCl. This method was successfully used to show that a more salinity tolerant wheat variety has a far superior ability to export Na^+ out of the plant root than more susceptible varieties (Cuin et al. 2011a). Pharmacological experiments, as well as experiments on a range of Na^+ transport mutants, have revealed that this flux is mediated by the SOS1-like Na^+/H^+ antiporters located in root epidermal cells. Evidence for high inheritance of this trait has been presented (Cuin et al. 2011b). Thus, the developed MIFE protocols provide a relatively reliable and straightforward method for rapidly assessing a plant's ability to actively export Na^+ and, thus, can be used in breeding programs to select varieties with high Na^+ extruding capacity.

4.4 Osmotic Stress

4.4.1 Osmotic Adjustment in Plants

Osmotic stress is ubiquitous in nature and can be manifested by a range of environmental conditions such as drought or salinity. It results in severe disturbance to cell metabolism, plant growth and survival and severely limits global agricultural productivity, resulting in multibillion dollar penalties. To adjust to increased external osmolality, cells in all three kingdoms accumulate a variety of molecules in the cytoplasm to counteract the external osmotic pressure. Two major avenues are available for plants.

First, cells can achieve osmotic adjustment by accumulation (de novo synthesis) of so-called *compatible solutes*—small water-soluble molecules that may be accumulated in cells at high concentrations without affecting metabolic reactions in either the cytosol or major organelles (Hasegawa et al. 2000). Four major classes of osmolytes are usually distinguished (Delauney and Verma 1993): (1) sugars (e.g. sucrose or trehalose); (2) polyoles (e.g. glycerol, sorbitol, or mannitol); (3) amino acids (e.g. glutamate or proline); (4) quaternary ammonium compounds (e.g. glycine betaine). According to the classical view, accumulation of these non-toxic (thus *compatible*) osmotically active solutes will result in an increase in cellular osmolarity leading to the influx of water into, or at least reduced efflux from, cells, thus providing the turgor necessary for cell expansion (Delauney and Verma 1993; Hare et al. 2002).

4.4.2 Are Compatible Solutes Actually Involved into Osmotic Adjustment?

The above concept became a dogma and has dominated the literature for the last two decades (Shabala and Shabala 2011). Improving crop resistance to osmotic stresses by overexpressing genes responsible for biosynthesis of various compatible solutes has long been an attractive and widely popular option (Bohnert et al. 1995; Bray 1997; Bohnert and Shen 1999; Serrano et al. 1999; Bajaj et al. 1999). However, despite all efforts, the progress is disappointingly slow, and an increase in the osmotic tolerance in a field situation is only marginal (Bohnert and Shen 1999; Bajaj et al. 1999). Several major reasons may explain this:

1. Concentrations are always far too low (Williamson and Slocum 1992; Peng et al. 1996; Igarashi et al. 1997; Shen et al. 1997; Garg et al. 2002) and not enough to account for maintenance of the cell turgor under hyperosmotic conditions. As the very best, organic osmolytes may be accountable for osmotic adjustment in the cytosol and/or plastids.

2. With a possible exception for the food-dwelling microorganisms, concentration of organic osmolytes in the external environment is usually far too low to rely upon for osmotic adjustment. Hence, plants and bacteria have to synthesize these compatible solutes de novo. This comes at a very high cost to the organism, as between 30 and 109 molecules of ATP (Adinosine triposphate) appear to be required for the autotrophic biosynthesis of one molecule of the different compatible solutes (Raven 1985; Oren 1999).
3. Synthesis of compatible solutes is a rather slow process, operating in a time-scale of hours and days. At the same time, many organisms may experience much faster fluctuations in media osmolality and, hence, require more quick ways for osmotic adjustment.
4. The last and, arguably, most important controversy is the lack of consistent correlation between osmotic stress tolerance and accumulation of organic osmolytes. *Arabidopsis rss* mutant with reduced salt sensitivity showed much less capacity for proline accumulation under both salinity and osmotic stresses compared with wild type (Werner and Finkelstein 1995). Salt-sensitive genotypes often accumulate much more organic osmolytes compared with tolerant varieties (Lutts et al. 1999; Colmer et al. 2006; Chen et al. 2007a).

4.4.3 Inorganic Ion Uptake and Plant Osmotic Adjustment

A viable alternative to the energetically expensive and rather slow (see above) process of osmolyte biosynthesis is osmotic adjustment by means of inorganic ions (Shabala and Shabala 2011). Indeed, from a thermodynamical point of view, water retention within the cell may be achieved equally well by increased concentration of both organic and inorganic molecules. The idea that changed ion fluxes in response to osmotic stress may provide quick (within a few minutes) osmotic adjustment and maintain normal turgor is rather old (e.g. Wyn Jones and Pritchard 1989). However, direct experimental evidence is rather scant and mostly based on theoretical calculations of changes in cell osmotic potential caused by measured fluxes of inorganic ions (Okazaki et al. 1984; Teodoro et al. 1998). The first direct support at the cellular level came from concurrent measurements of net ion fluxes in osmotically stressed *Arabidopsis thaliana* epidermal root cells (measured by the MIFE technique) and cell turgor changes (measured by the pressure-probe technique) (Shabala and Lew 2002). It was shown that over 90% of cell turgor was recovered by uptake of three major inorganic ions (K^+, Na^+, and Cl^-) within 40 min after onset of hyperosmotic stress. Very similar numbers were obtained for bean mesophyll cells (Shabala et al. 2000).

The above conclusions made for higher plants were later confirmed also for bacterial (Shabala et al. 2009a) and fungal (Lew et al. 2006; Shabala et al. 2009a) species. MIFE microelctrode ion flux measurements on a marine protist thraustochytrid have suggested that almost complete osmotic adjustment was achieved

in thraustochytrid cells by changes in the rate of Na^+, Cl^-, and K^+ fluxes within the first 30 min upon stress onset (Shabala et al. 2009b). A direct comparison between cell turgor recovery and kinetics of net ion fluxes was conducted in the filamentous fungus *Neurospora crassa* in response to hyperosmotic stress (Lew et al. 2006). The turgor recovery was completed within 60 min and occurred concurrently with net K^+ and Cl^- uptake. The magnitude of the ion uptake was more than sufficient to account for the osmotic gradients required for turgor, ruling out a need for any organic osmolyte involvement.

4.4.4 On a Quest for Osmosensors

Specific ionic mechanisms involved in osmotic stress perception are still elusive. Lew (1996) suggested that *Arabidopsis* root hair cells possess an osmosensing but not a turgor-sensing mechanism. At least two mechanisms by which a plant can sense osmotic conditions have been suggested by Brownlee et al. (1999). First, the changes in cell volume could be sensed by mechanosensitive, or stretch-activated, channels (SAC) at the plasma membrane (Cosgrove and Hedrich 1991; Pickard and Ding 1993; Ramahaleo et al. 1996). However, most reported evidence of SAC was obtained by using the patch-clamp technique; there is thus a need for more experimental observations of SAC effects at the tissue or organ level. Appearance of the additional 2-min component in ion flux oscillations measured from hyperosmotically stressed plant roots (Shabala and Newman 1998) may provide such evidence. Another option is that the intracellular osmosensing mechanisms may detect the degree of cytosol hydration (Brownlee et al. 1999). Alterations in cytoplasmic Ca^{2+} concentrations were suggested as a part of the turgor signal-transduction chain for *Lamprothamnium* (Okazaki and Tazawa 1990) and *Chara* (Bisson et al. 1995).

A ubiquitous component of osmotic adjustment in higher plants is modulation of the proton-pumping activity (Reinhold et al. 1984; Reuveni et al. 1987; Li and Delrot 1987). Palmgren (1991) suggested that the relaxation of the stretched status of the membrane might directly activate the plasma membrane H^+-ATPase, as the activity of this enzyme is strictly dependent on the lipid environment. If this is the case, then osmotically induced increase in net K^+ uptake under hyperosmotic stress conditions caused by non-ionic osmotica (e.g. Shabala and Lew 2002; Chen et al. 2007b) can be explained by enhanced K^+ uptake via voltage-gated K^+ inward-rectifying channels or, alternatively, by reduced K^+ efflux through outward K^+ channels. Indeed, hyperosmotically induced membrane hyperpolarization has been reported in direct experiments on plant (Shabala and Lew 2002), fungal (Lew et al. 2006), and bacterial (Shabala et al. 2009a) species, and the role of inward-rectifying K^+ channels in root osmotic adjustment was directly shown in MIFE experiments using *Arabidopsis akt1* mutants (Shabala and Cuin 2008). It still remains, however, to be answered whether the plasma membrane H^+- pump is a primary target (a receptor) of osmotic stress (Reinhold et al. 1984), or merely a component of the

complex signaling network controlling the activity of the plasma membrane transporters for other ions (Kinraide and Wyse 1986; Li and Delrot 1987).

4.4.5 Multiple Roles of Organic Osmolytes

What is then the role of organic osmolytes, and why does their content increase dramatically under osmotic stress conditions? Multiple functions have been suggested, including their roles as low-molecular-weight chaperones, for membrane integrity maintenance, protecting the structure of enzymes and proteins, PSII protection and repair, redox potential buffering, and ROS scavenging (Smirnoff and Cumbes 1989; McCue and Hanson 1990; Bohnert et al. 1995; Shen et al. 1997; Hasegawa et al. 2000). Importantly, these functions do not require high amounts of organic osmolytes and, hence, do not come at high energetic cost to the organism.

Recent experiments in our laboratory have shown that compatible solutes are very efficient in reducing the extent of K^+ loss from cytosol in response to both salinity (Cuin and Shabala 2005, 2007a) and oxidative stress (Cuin and Shabala 2007b). Exogenously supplied physiologically relevant (5 mM) concentrations of proline and glycine betaine rapidly ameliorated NaCl-induced K^+ efflux from barley roots (Cuin and Shabala 2005). Further experiments have shown that 21 (of 26) protein- and non-protein- amino acids caused significant mitigation of NaCl-induced K^+ efflux, although two amino acids (valine and ornithine) substantially *enhanced* the detrimental effects of salinity on K^+ homeostasis (Cuin and Shabala 2007a). It is possible, therefore, that compatible solutes may indeed assist in plant osmotic adjustment not directly (by retaining water; which is thermodynamically impossible) but rather via retaining K^+. Importantly, the above mitigating effects were obtained *in situ* at physiologically relevant (0.1–1 mM) concentrations (Cuin and Shabala 2007a). Hence, plants do not need to synthesize substantial quantities of organic osmolytes to control intracellular ionic homeostasis and, ultimately, achieve osmotic adjustment via better K^+ retention. It should be added that, to the best of our knowledge, all previous reports of stabilizing effects of amino acids on membrane permeability and enzymatic activity were obtained in vitro and for physiologically unrealistic (e.g. 100–500 mM; Heber et al. 1971; Nash et al. 1982) concentrations. In addition, K^+ retention seems to be crucial for preventing ROS-induced programmed cell death (PCD; see section 4.7.3).

4.5 Soil pH

It is estimated that up to 70%, of the world's arable land is acidic (von Uexkull and Mutert 1995). Soil acidification is a natural process that occurs as the result of weathering of acidic parent material and leaching of basic cations. Other factors such as intensive agriculture, cultivation of legumes, use of acid-forming

fertilizers, and acid rain can also increase soil acidity. Thus, both the severity and the extent of soil acidity increase with time (Rengel 2004).

In acidic soils, plant growth may be limited by various toxicities (H^+, Al^{3+}, Mn^{2+}) and deficiencies (NH_4^+-N, P, Ca^{2+}, Mg^{2+}, and MoO_4^{2-}) (see Kidd and Proctor 2001). In the complex acid-soil syndrome, aluminum toxicity poses a major threat to plant growth by inhibiting root growth (Kochian et al. 2004). Al^{3+} ion is the most rhizotoxic form (Kochian 1995); its activity peaks at around pH 4.2–4.3 (Kinraide 1993; Taylor et al. 2000). Therefore, Al^{3+} toxicity is always studied in combination with low-pH stress (H^+ toxicity). While these two stresses normally occur together, the mechanisms of plant tolerance to each of these may be strikingly different. It was shown that H^+ toxicity causes irreversible damage to primary and lateral roots in *Arabidopsis*, with the pattern of damage being different from the one caused by Al^{3+} rhizotoxicity (Koyama et al. 1995; Koyama et al. 2001). Furthermore, an *Arabidopsis* QTL analysis suggested that Al^{3+} tolerance and H^+ tolerance are controlled by different genes (Ikka et al. 2007).

A comprehensive functional characterization of *Arabidopsis* root responses to low-pH and combined low-pH/Al^{3+} stresses have been recently undertaken using the MIFE technique. In the absence of Al^{3+}, low-pH stress-induced H^+ influx thereby causing rhizosphere alkalization, while the presence of Al^{3+} inhibited H^+ influx and resulted in lesser rhizosphere alkalinization (Bose et al. 2010b). Moreover, aluminum sensitive *Arabidopsis* mutant *als5* grew well under low-pH stress and poorly under Al^{3+} stress, whereas *als3* was sensitive and *alr104* tolerant to both stresses. Ability of *Arabidopsis* mutants to alkalinize the rhizosphere and take up H^+ from a low-pH environment is linked to the tolerance to low-pH and combined low-pH/Al^{3+} stresses (Degenhardt et al. 1998; Bose et al. 2010a). Another MIFE study compared an acid-soil tolerant conifer (*Pseudotsuga menziesii*) with the acid-soil sensitive soybean (*Glycine max*). The results proved that ability of *P. menziesii* roots to maintain higher H^+ efflux and NH_4^+ influx than *G. max* at pH 4.0 is the key trait responsible for acid-soil tolerance in the former species (Hawkins and Robbins 2010).

Al^{3+} has a strong affinity for the plasma membrane surface (Akeson et al. 1989). To prevent such binding, plants evolved several Al^{3+} exclusion mechanisms; the best-described one is the root exudation of low-molecular-weight organic acid anions to increase the rhizosphere pH and reduce Al^{3+} solubility (Ryan et al. 2001; Kochian et al. 2004; Kochian et al. 2005). Also, organic acid anions with a large number of carboxylate groups may directly chelate Al^{3+} (Kochian et al. 2004). Depending on the plant species, Al^{3+} activates exudation of various organic acid anions such as malate, citrate, oxalate, pyruvate, and/or succinate (Larsen et al. 1998; Ryan et al. 2001; Kochian et al. 2005). This extrusion seems to be species-specific and mediated by organic-anion-permeable plasma membrane channels (Pineros and Kochian 2001; Zhang et al. 2001; Sasaki et al. 2004). Both aluminum-activated malate (ALMT) and citrate (MATE- Multidrug and toxic efflux) transporters have been identified in a range of plant species (reviewed in Bose et al. 2011a). Some plant species can release more than one organic acid anion in response to Al^{3+} exposure (Hoekenga et al. 2006; Liu et al. 2009).

The above release of Al^{3+}-induced organic anions from plant roots is accompanied by K^+ efflux to account for electroneutrality (Ryan et al. 1995). As most studies used excised root apices and relatively short treatment times, it has remained unclear whether a similar response operates in intact roots and if it is sustained over long periods of Al^{3+} exposure. Using near-isogenic wheat lines that differ in Al^{3+} tolerance (ET8 and ES8), Wherrett et al. (2005) showed that addition of 50 μM $AlCl_3$ to the bathing solution stimulated an increase in K^+ efflux in ET8 but not in ES8. The differences between the genotypes were sustained for 24 h and were observed only at the elongating zone and not the meristematic zone. These results provide new temporal and spatial information on the Al^{3+}-activated efflux of K^+ from intact wheat plants. It was further shown that membrane depolarization caused by organic-anion efflux is the mechanism behind the stimulation of K^+ efflux in wheat (Wherrett et al. 2005).

The action spectrum of Al^{3+} appears to be much broader than just activation of anion channels. Particularly, the interaction between Al^{3+} and Ca^{2+} uptake received considerable attention because symptoms of severe Al^{3+} toxicity resemble Ca^{2+} deficiency in plants (see Foy 1988; Rengel and Elliott 1992 for references) and exogenous application of relatively high (millimolar) concentrations of Ca^{2+} alleviated Al^{3+} toxicity in many plant species (Brady et al. 1993; Keltjens and Tan 1993; Kinraide et al. 2004). Al^{3+} might inhibit Ca^{2+} influx into intact root cells (Huang et al. 1992; Ryan and Kochian 1993), protoplasts (Rengel and Elliott 1992; Rengel 1994), and membrane vesicles (Huang et al. 1996; White 1998) through binding of Al^{3+} on the plasma membrane surface. Such binding of Al^{3+} to the surface may block Ca^{2+}-permeable channels in the plasma membrane. Indeed, both the hyperpolarization-activated Ca^{2+}-permeable channels (Ding et al. 1993; Kiegle et al. 2000; Very and Davies 2000) and depolarization-activated Ca^{2+} channels (Rengel et al. 1995; Pineros and Tester 1997) are sensitive to Al^{3+}. The Ca^{2+} influx inhibition following Al^{3+} exposure precedes root growth inhibition (Huang et al. 1992; Ryan and Kochian 1993) and, thus, is one of the potential primary causes of Al^{3+} phytotoxicity in plants (Rengel 1992; Rengel and Zhang 2003). However, further studies revealed that low concentration of Al^{3+} can also inhibit root growth without affecting Ca^{2+} influx, and addition of ameliorating cations (Mg^{2+} and Na^+) improved root growth, even though the net Ca^{2+} influx remained inhibited (Ryan and Kochian 1993; Ryan et al. 1997). Similarly, Al^{3+} caused root hair growth inhibition without affecting Ca^{2+} influx in *Limnobium stoloniferum* (Jones et al. 1995). Poor correlation between Al-induced Ca^{2+} influx inhibition and elongation growth of *Chara* (Reid et al. 1995) indicated that Al-induced inhibition of Ca^{2+} influx alone cannot be a critical factor in triggering Al toxicity in plants.

K^+ is essential for cell division (Alberts et al. 1994) and turgor-dependent cell elongation. Though K^+ efflux during low-pH alone is well established (Babourina et al. 2001; Bose et al. 2010b), there is no causal relationship between Al^{3+} toxicity and K^+ nutrition in plants. Both Al^{3+} induced inhibition (Matsumoto and Yamaya 1986; Nichol et al. 1993) and stimulation (Lee and Pritchard 1984; Lindberg 1990; Tanoi et al. 2005) in K^+ uptake have been reported. A possible explanation for this

controversy could come from MIFE experiments. Future studies involving specific K^+ transport *Arabidopsis* mutants would pave way for identification of specific K^+ transporters responsible for observed phenomena during low-pH and combined low-pH/Al^{3+} stress.

4.6 Waterlogging and Oxygen Deprivation

Waterlogging is a major constraint affecting crop growth in many agricultural regions around the world. Approximately 10% of the global land area is affected by waterlogging (Setter and Waters 2003). In Australia alone, 3.8 million ha of duplex soils in Victoria and 60% of similar soils in Western Australia experience surface and subsurface waterlogging (Greenway and Gibbs 2003). The overall loss in crop production due to waterlogging is second largest after drought (Boyer 1982). As the yield loss varies considerably (several fold) depending on the crop species, crop growth stage at which waterlogging is experienced, and stress duration (Zhou 2010), understanding the physiological mechanisms mediating plant adaptive responses to waterlogging is essential for breeding tolerant varieties.

Higher plants require continuous supply of O_2 to support respiration and oxidation reactions. When the soil is saturated with water, all the air from soil pore spaces is replaced by water resulting in either hypoxia or anoxia. This O_2 shortage for root respiration causes inhibition of root growth and decline in acquisition of major nutrients such as N, P, K, Ca, and Mg (Colmer and Greenway 2011). This form of O_2 deficiency is further aggravated by soil microorganisms which use residual O_2 in the rhizosphere (Shabala 2011). Plants usually switch from aerobic respiration to fermentation during hypoxia (low O_2 supply) or anoxia (absence of O_2) to produce ATP during waterlogging stress. Prolonged O_2 deprivation also results in accumulation of ethanol as the end product of fermentation and, thus, results in cytotoxicity to plants. Also, energy yield per mol of glucose is much lower (just three ATP molecules) in fermentation when compared to aerobic respiration (36 ATP molecules). As a result, plants experience significant (up to 97%; Greenway and Gibbs 2003) reduction in the rate of energy production under waterlogged conditions and, thus, have much less to invest into their growth.

Given the above importance of oxygen, it is not surprising that preventing O_2 loss or improving its transport to, or storage in the root, have always been central to breeding programs dealing with plant waterlogging stress tolerance. Tolerant varieties were able to maintain higher net influx of O_2 in the mature root zone compared with their sensitive counterparts, as revealed by O_2-selective microelectrode flux measurements in barley (Pang et al. 2006) and *Vitis* (Mancuso and Boselli 2002). Moreover, under anoxia stress, waterlogging tolerant *Vitis* species prevented O_2 loss from adventitious roots (Mancuso and Boselli 2002).

In addition to O_2 deficiency, accumulation of potentially toxic manganese, iron, hydrogen sulfide, various organic acids, CO_2, and ethylene can also pose serious

challenges to root growth in waterlogged soils (Colmer and Greenway 2011; Shabala 2011). Despite being diverse in their chemical nature, all the above factors affect membrane integrity and thus membrane transport in plants (Pang et al. 2006; Pang et al. 2007). For example, non-specific loss of K^+ was reported soon after onset of anoxia (Greenway et al. 1992; Colmer et al. 2001) or root exposure to secondary metabolites associated with anaerobic soils (e.g. monocarboxylic acids; (Pang et al. 2007). Thus, maintenance of membrane integrity is considered as a key factor in survival of plant cells under waterlogging stress (Rawyler et al. 1999). From this point of view, non-invasive ion flux measurements give an excellent opportunity to look at underlying mechanisms associated with membrane responses to O_2 deprivation. Comparison of genotypes contrasting in waterlogging tolerance, suggested that avoiding K^+ loss or reducing K^+ leakage during hypoxia or anoxia stress is the key mechanism responsible for waterlogging tolerance in plants (Mancuso and Marras 2006; Pang et al. 2006; Pang et al. 2007; Mugnai et al. 2011). K^+ flux measurements along the longitudinal axis of barley roots under hypoxia revealed that hypoxia-induced K^+ flux responses are mediated by both KIR and NSCC channels in the elongation zone, while in the mature zone KOR channels are likely to play a vital role (Pang et al. 2006). Moreover, closure of KOR channels by rapid restoration of the membrane potential to values more negative than the K^+ diffusion potential may result in better K^+ homeostasic regulation during O_2 deprivation (Greenway and Gibbs 2003). Reggiani (1997) also provided evidence for cAMP-triggered KOR closure under anoxia. This is in line with a hypothesis proposed by Greenway and Gibbs (2003) that in anoxia-tolerant tissues, energy flow during anoxia must be directed toward essential nutrient transport.

Elucidating the signaling events associated with hypoxia-anoxia remains one of the great challenges. Changes in cytosolic pH (Ratcliffe 1997; Greenway and Gibbs 2003) and free calcium, $[Ca^{2+}]_{cyt}$ (Subbaiah et al. 1998) are thought to be part of the signal-transduction pathway. As cytosolic acidification was an early response observed within 5 min of anoxia (Gout et al. 2001), it was considered as the primary signal of an O_2 deprivation (Felle 2001). Inhibition of H^+-pump activity by O_2 deprivation was suggested as the mechanism responsible for cytoplasmic acidification (Gout et al. 2001; Tazawa 2003). However, other evidence suggests that the H^+-pump may in fact be upregulated (i.e. net H^+ extrusion increases) when cytosolic pH falls under hypoxic-anoxic conditions (Xia and Roberts 1996; Pang et al. 2006; Koizumi et al. 2011). The above controversy remains to be resolved.

Similar to cytosolic acidification, elevation of $[Ca^{2+}]_{cyt}$ is also an early response to O_2 deprivation. Both plasma membrane (Tamura et al. 2001; Pang et al. 2007) and endomembrane (Subbaiah and Sachs 2003a) Ca^{2+} transporters seem to be involved in $[Ca^{2+}]_{cyt}$ elevation, while the resting level of $[Ca^{2+}]_{cyt}$ upon signal termination is restored by Ca^{2+}-ATPase (CAP1) (Subbaiah and Sachs 2003a; b).

4.7 Oxidative Stress

Reactive oxygen species (ROS) are produced as a by-product of cellular metabolic pathways. The major sources of ROS production are cell wall peroxidise and amine oxidase, plasma membrane NADPH oxidase, and intracellular oxidases and peroxidises in mitochondria, chloroplasts, and peroxisomes. High concentrations of ROS are detrimental to plant cells because of their ability to cause lipid peroxidation in cellular membranes, DNA damage, protein denaturation, carbohydrate oxidation, pigment breakdown, and an impairment of enzymatic activity (Noctor and Foyer 1998; Santos et al. 2001; Lee et al. 2004). However, it became increasingly clear that, in addition to being potentially hazardous products of metabolic imbalance, ROS play a very important signaling and regulatory role in plant growth, development, and adaptation. Indeed, ROS were shown to be involved in the regulation of gravitropism, stomatal aperture, cell expansion and polar growth, leaf and flower development, and programmed cell death (Cervantes 2001; Hoeberichts and Woltering 2003; Casolo et al. 2005; Wang and Song 2008). Additionally, ROS produced during abiotic stresses act to signal change and regulate gene expression (Mittler et al. 2004; Miller et al. 2008; Qiao and Fan 2008). Upstream of this signaling is ROS-induced activation of ion channels.

4.7.1 Revealing the Role of Compatible Solutes in Ameliorating Detrimental ROS Effects

Detrimental effects of ROS on membrane permeability are usually attributed to non-specific effects such as oxidation of sulphydryl groups located on the ion transport proteins, peroxidation of membrane phospholipids, inhibition of membrane-bound regulatory enzymes, and disruption to oxidative phosphorylation and ATP levels (Kourie 1998). Application of a hydroxyl radical ($OH^{\bullet}$)-generating Cu^{2+}/ascorbate (Cu/a) mixture to plant roots results in a massive, dose-dependent efflux of K^+ from various plant tissues (Demidchik et al. 2003; Cuin and Shabala 2007b; Demidchik et al. 2010). The $OH^{\bullet}$-induced efflux of K^+ is not instantaneous but develops gradually; reaching peak values 6–15 min after treatment. In *Arabidopsis* roots, both the magnitude and time of peak K^+ efflux showed a strong dose-dependency on the amount of Cu/a applied (Cuin and Shabala 2007b). The $OH^{\bullet}$-induced K^+ efflux was sensitive to tetraethylammonium (TEA^+) and correlated with depolarization of the membrane potential, suggesting that it was largely mediated by depolarization-activated outward-rectifying K^+ channels.

Keeping in mind the requirement for strict K^+ homeostasis in the cell cytosol (Leigh 2001), such a massive K^+ efflux has a major impact on growth, metabolic performance, and survival of the plant. A large number of enzymatic and non-enzymatic antioxidants contribute to detoxication of ROS species to prevent the

above effect (Mittler et al. 2004). Among non-enzymatic antioxidants, the ability of compatible solutes to scavenge free radical species is widely reported (Smirnoff and Cumbes 1989; Bohnert et al. 1995; Shen et al. 1997; Noctor and Foyer 1998; Hong et al. 2000). Most of these results, however, were obtained from in vitro experiments. In addition, such scavenging was reported for relatively high concentrations of compatible solutes (e.g. 100 mM; Henle and Linn 1997; Shen et al. 1997; Noctor and Foyer 1998). Using the MIFE technique, we have provided the first evidence for an in situ mitigating effect of much lower (5 mM) concentrations of compatible solutes on ROS-induced ion fluxes across the plasma membrane. Interestingly, not only known free radical scavenging compatible solutes such as mannitol, myo-inositol, and proline but also glycine betaine, previously shown to be non-effective in ROS scavenging in vitro (Halliwell and Grootveld 1988; Smirnoff and Cumbes 1989) were effective in reducing the $OH^{\bullet}$-induced K^+ efflux. A significant difference in $OH^{\bullet}$-induced K^+ flux kinetics in roots pre-incubated in a range of compatible solutes and the fact that a large reduction in $OH^{\bullet}$-induced K^+ efflux was recorded in plants pre-incubated in glycine betaine could indicate different mechanisms of protection, such as direct transporter protection or a channel blocking role, in addition to, or as an alternative to ROS scavenging.

4.7.2 *Revealing Identity and Roles of ROS-Activated Cation Channels in Plant Roots*

In addition to causing massive K^+ efflux across the plasma membrane of *Arabidopsis* root cells, $OH^{\bullet}$ application also induced rapid Ca^{2+} influx into root epidermis (Demidchik et al. 2003). This effect was mediated by ROS control upon the activity of at least two different types of plasma membrane channels. While ROS-induced increase in cytosolic Ca^{2+} was mediated by a novel population of NSCC that differ in selectivity and pharmacology from those involved in toxic Na^+ influx (Demidchik and Tester 2002), ROS-induced K^+ efflux was due to $OH^{\bullet}$ stimulation of an outward-rectifying potassium (KOR) channel. Experiments with *abi1* (*Abcisic acid-insensitive1*) mutant suggested that the phosphorylation state is critical to such KOR activation.

Potassium efflux is known to be one of the earliest events observed in response to a variety of stresses such as salinity (Shabala 2000; Babourina et al. 2001; Shabala et al. 2003, 2005a), acidity (Babourina et al. 2001), chilling (Shabala and Shabala 2002), and hypoxia (Pang et al. 2006). Traditionally, these effects were attributed to membrane depolarization (Shabala et al. 2003). The above finding of ROS-induced K^+ efflux from plant roots demonstrates that stress-induced K^+ efflux can be mediated by a previously unknown mechanism–activation of KOR by $OH^{\bullet}$. K^+ channels harbor reactive groups and thus are expected to be sensitive to ROS (Kohler et al. 2003). Importantly, flux amplitude and the time-course of K^+ flux responses to ROS treatment varied between species, suggesting species-specific

"flux signatures" in response to $OH^{\bullet}$ (Demidchik et al. 2003). This also suggests that H_2O_2 is not the sole oxygen-derived species capable of signaling and regulation in plants. The response to $OH^{\bullet}$ was tissue-specific and stronger in cells which directly interact with the environment (e.g. root epidermis *vs* pericycle). Based on the above results, two major functions for ROS activation of cation channels were proposed: initialization/amplification of stress signals and control of cell elongation in root growth (Demidchik et al. 2003).

We have also shown that not only $OH^{\bullet}$ but also exogenous H_2O_2 application to *A. thaliana* root epidermis results in dose-dependent transient increases in net Ca^{2+} influx (Demidchik et al. 2007). The magnitude and duration of the transients were greater in the elongation zone than in the mature epidermis at all concentrations tested (10 μM to 10 mM). Application of 10 mM H_2O_2 to the external plasma membrane face of elongation zone epidermal protoplasts resulted in the appearance of a hyperpolarization-activated Ca^{2+}-permeable conductance. In contrast, in mature epidermal protoplasts a plasma membrane hyperpolarization-activated Ca^{2+}-permeable channel was activated only when H_2O_2 was present at the intracellular membrane face (Demidchik et al. 2007). Overall, these results suggest spatial heterogeneity and differential sensitivity of Ca^{2+} channel activation by reactive oxygen species in the root that could underpin signaling.

4.7.3 ROS and Programmed Cell Death

Programmed Cell Death (PCD) plays an important role in mediating plant adaptive responses to the environment, and was experimentally proved to occur in response to salinity, cold stress, waterlogging, and hypoxia (Katsuhara and Kawasaki 1996; Pennell and Lamb 1997; Huh et al. 2002). While the regulatory mechanisms of PCD in animals are fairly well known and mostly depend on caspase activity (Lam et al. 2001), the apoptotic machinery and signal-transduction pathways of PCD in plants remain unclear. A key role for caspase-like proteases has been suggested (Hatsugai et al. 2004; Chichkova et al. 2004), and several reports of plant proteases with caspase-like properties that functionally mimic caspase activity in animals have been published (Watanabe and Lam 2004; Rojo et al. 2004).

While membrane-transport processes were shown to play a pivotal role in PCD in animal tissues (Gulbins et al. 2000; Panayiotidis et al. 2006), only few studies have been undertaken to investigate PCD-related membrane-transport processes in plants. In order to fill this gap, we investigated specific ion flux "signatures" in *Nicotiana benthamiana* plants transiently expressing CED-9 (Cell death defective-9) anti-apoptotic gene and undergoing oxidative stress. We showed that expression of CED-9 increased plant oxidative stress tolerance by altering K^+ and H^+ flux patterns across the plasma membrane (Shabala et al. 2007b). PVX (Potato virus X)/CED-9 plants were capable of preventing stress-induced K^+ efflux through outward-rectifying depolarization-activating K^+ channels (KOR) and non-selective cation channels (NSCC), so maintaining intracellular K^+ homeostasis. A mechanistic model for PCD

linking changes in cytosolic K^+ homeostasis with activation of plant proteases was suggested (Shabala 2009).

The above work, conducted on tobacco leaf mesophyll tissue, was then complemented by a comprehensive electrophysiological study on *Arabidopsis* roots (Demidchik et al. 2010). It was shown that prolonged (2–3 days) $OH^\bullet$ treatment resulted in appearance of PCD symptoms in root epidermal cells. Importantly, $OH^\bullet$- induced PCD was absent, or significantly delayed, in *gork1-1* mutants lacking functional outward-rectifying depolarization-activated GORK potassium channels (Demidchik et al. 2010). Consistent with these observations, PCD protease activation, measured by fluorescently labeled protease inhibitor zVAD-fmk (Benzyloxycarbonyl-Val-Ala-Asp (OMe)—uoromethylketone), was about three to four times lower in *gork1-1* compared with the WT. *Gork1-1* plants also revealed about four times less TUNEL (Terminal deoxynucleotidyl dUTP nick end labeling) staining after 15 h exposure to stress implying that $OH^\bullet$-activated K^+-efflux channels are likely to be involved in endonuclease activation caused by oxidative stress (Demidchik et al. 2010).

4.7.4 ROS in Stress Cross-Protection

Cross-tolerance is the synergistic co-activation of non-specific stress-responsive pathways, referring to a situation when an organism's exposure to one stress increases its tolerance to another (Mittler 2006). In most cases, induced cross-tolerance was attributed to reactive oxygen species (ROS) production during the so-called "oxidative burst"–the rapid release of H_2O_2—and was linked primarily with plant biotic stress responses. This oxidative burst always follows stress-induced elevation in $[Ca^{2+}]_{cyt}$ (Cessna et al. 2003) and, thus, was related to stress-induced activation of plasma membrane Ca^{2+} permeable channels (Pei et al. 2000; Mori and Schroeder 2004). However, although transient increases in $[Ca^{2+}]_{cyt}$ are essential for plant responses to a variety of environmental stimuli, long-lasting elevations in $[Ca^{2+}]_{cyt}$ are harmful for cells (Bose et al. 2011b). Hence, the basal conditions must be restored back to the resting level after the signal is completed, enabling cells to react to further signals (Sanders et al. 1999; Beffagna et al. 2005). Surprisingly, the molecular identity and operating modes of active Ca^{2+} efflux systems mediating this process are poorly understood.

Using *N. benthamiana* plants we have recently demonstrated that plants infected with *Potato virus X* (PVX) had a superior oxidative [UV-C (Ultraviolet-C) and H_2O_2] stress tolerance (Shabala et al. 2011a). These plants were able to maintain lower levels of cytosolic free Ca^{2+} under stress conditions, and this effect was attributed to more active plasma membrane Ca^{2+} efflux systems in PVX-inoculated plants. Pharmacological experiments coupled with biochemical and molecular assays suggested that plasma membrane Ca^{2+}/H^+ exchangers but not plasma membrane Ca^{2+}-ATPases mediate net Ca^{2+} efflux under oxidative stress conditions (Shabala et al. 2011a). Also affected was H^+-ATPase activity, with ~40% increase in

ATP-dependent proton pumping observed in plasma membrane vesicles isolated from plants pre-treated with UV light (Shabala et al. 2011a). However, the amount of plasma membrane H^+-ATPase was not different between treatments, suggesting that the plasma membrane H^+-ATPase had been activated at the post-translational level.

So far, Ca^{2+}/H^+ antiporter activity has been characterized only for the tonoplast (Sanders et al. 1999; Hirschi 2001). Our data (above) provide electrophysiological evidence for the presence of such Ca^{2+}/H^+ exchangers also at the plasma membrane. Furthermore, using biochemical and electrophysiological approaches, we reveal that, in addition to PM Ca^{2+}/H^+ exchangers, both endomembrane P_{2A} and P_{2B} Ca^{2+}-ATPases play significant roles in adaptive responses to oxidative stress, and that their functional expression is significantly altered in PVX-inoculated plants (Shabala et al. 2011b). Taken together, these findings highlight the crucial role of Ca^{2+} efflux systems in acquired tolerance to oxidative stress and open up prospects for practical applications in agriculture.

4.8 Biotic Stresses

4.8.1 Plant Responses to Pathogens

Plants respond to attack from pathogens by activating a variety of defense mechanisms, including synthesis of phytoalexins and hypersensitive cell death, which restricts growth of pathogens at the site of infection (Kadota et al. 2004). These responses are preceded by the interaction between pathogen-associated molecules (elicitors) and putative plant receptors (Vera-Estrella et al. 1994; Blumwald et al. 1998). Some of the earliest detectable signaling events in plant defense responses include plasma membrane depolarization and transmembrane ion fluxes, followed by production of ROS (Zimmermann et al. 1998; Clough et al. 2000). These are sequentially followed by defense gene activation and phytoalexin accumulation (Jabs et al. 1997). Most papers suggest elicitor-induced Ca^{2+} and H^+ influx and effluxes of Cl^- and K^+ (Nurnberger et al. 1994; Jabs et al. 1997; Kadota et al. 2004).

Of particular importance in early recognition between the host and pathogen is the role of Ca^{2+} as a second messenger that triggers a downstream cascade of defense responses (Blumwald et al. 1998; Zimmermann et al. 1999). Fungal elicitors rapidly enhanced expression of the plasma membrane Ca^{2+} pump in soybean (Chung et al. 2000). Ca^{2+} influx and the transient increase in $[Ca^{2+}]_{cyt}$ levels after elicitor treatment have been shown to be necessary and sufficient for the induction of an oxidative burst and thus, plant defense responses (Clough et al. 2000). The important role of Ca^{2+} signaling in response to pathogen infection was observed in a wide range of species (Nurnberger et al. 1994; Jabs et al. 1997; Blume et al. 2000; Lecourieux et al. 2002; Kadota et al. 2004). It was suggested that calcium influx is required for hypersensitive response (HR) initiation and that HR, once initiated, requires sustained Ca^{2+} influx (Atkinson et al. 1990). Surprisingly, despite the great bulk of literature

reporting the critical role of Ca^{2+} in the early recognition between the host and pathogen, direct measurements of Ca^{2+} flux into a single infected cell in vivo are lacking. This is largely due to the lack of appropriate techniques being used.

To address the above issue, we have applied the MIFE technique to characterize early signaling events associated with thaxtomin A (a dipeptide phytotoxin produced by all plant pathogenic *Streptomyces* sp. responsible for common scab disease) toxicity in *Arabidopsis* and tomato roots and pollen tubes. Our results indicate that thaxtomin A treatment causes Ca^{2+}-channel-mediated rapid Ca^{2+} influx across the plasma membrane, triggering further Ca^{2+}-induced Ca^{2+} release from some internal store (Tegg et al. 2005). We also showed that thaxtomin A was more effective in young, physiologically active tissues, suggesting higher density of toxin-binding sites in these regions, as well as suggesting a possible interaction between thaxtomin A and plasma membrane auxin receptors, as revealed from experiments on the auxin sensitive *ucu2-2/gi2* (*ultracurvata2-2/gigantea-2*) *Arabidopsis* mutant (Tegg et al. 2005).

The signaling role of Ca^{2+} was further investigated in experiments using a model plant *N. benthamiana* in response to a challenge with HR-causing pathogen, *Pseudomonas syringae* (Nemchinov et al. 2008). Addition of bacterial inoculum to the measuring chamber caused a rapid and transient elevation in net Ca^{2+} uptake by leaf mesophyll which peaked at ~ 1 min after treatment. The quickness of this response may suggest either direct association of Ca^{2+} -permeable channels with plasma membrane PAMPs (Pathogen-associated molecular patterns)-recognition receptors or a very short signaling pathway from the receptors to the channels. This initial "receptor-type" Ca^{2+} uptake was short-lived and disappeared within 6–10 min after the challenge (Nemchinov et al. 2008). More importantly, however, this initial calcium uptake was then followed by a well-defined calcium efflux initiated 12–48 h after the challenge. As passive Ca^{2+} efflux from the cell cytosol is thermodynamically impossible, some active Ca^{2+} efflux system must be involved. Given Ca^{2+} flux sensitivity to cyclopiazonic acid (a known inhibitor of Ca^{2+}-ATPase), Ca^{2+}-ATP pump involvement was suggested (Nemchinov et al. 2008).

In the light of the above, calcium signaling in response to pathogens is most likely a multi-step process and consists of several phases. It appears that calcium acts not only as an important second messenger in the activation of resistance responses (Grant et al. 2000, Balagué et al. 2003) but also as a downstream mediator of later cell death acceleration, inhibition of the spread of invading pathogens and completion of defense reaction. Accordingly, it was suggested that the existing model of HR should be amended to include such Ca^{2+} pumps (Nemchinov et al. 2008).

4.8.2 Plant Responses to Viral Infection

While the role of membrane-transport processes in plant-pathogen interaction is well defined (see above), electrophysiological events mediating plant responses to viral infection are essentially unexplored. In a rare report on non-host hypersensitive response (HR) to papaya mosaic virus (PMV), Schvarzstein (1997)

described a decrease in the average inward currents and an increase in the outward currents from protoplasts isolated from *Gomphrena globosa* leaf tissue, using the patch-clamp technique. It was suggested that several ions such as K^+, Cl^-, gluconate, and Ca^{2+} may contribute to the above currents, and that cell membrane damage is required for viral infection (Schvarzstein 1997).

In our recently published work, we used the MIFE technique to measure net ion fluxes from mesophyll tissue from a range of host and non-host plants in response to infection with *Potato virus X*, PVX (Shabala et al. 2010a). Addition of the purified PVX preparation to the tobacco mesophyll tissue caused no changes in the rate of Ca^{2+} transport across the plasma membrane. Also, no significant changes in $[Ca^{2+}]_{cyt}$ were detected for at least 50 min after PVX treatment suggesting that Ca^{2+} release from internal stores was also not a part of the signal-transduction mechanism in plant-viral interaction. Thus, it appears that, contrary to bacterial pathogens, rapid Ca^{2+} signaling may not be essential for the viral perception and initiation of downstream transduction pathway. Instead, a massive K^+ efflux was measured as early as 10 min after PVX inoculation (Shabala et al. 2010a). This efflux was absent in non-host species, suggesting high host-specificity of the process. This may suggest that viral infections trigger ionic currents associated with plant defense signaling that differ from ion fluxes induced by other microbes.

Pharmacological and membrane potential data in our experiments point out that a significant part of measured K^+ flux was mediated by depolarization-activated outward-rectifying K^+ channels. Recently, the phenomenon of rapid K^+ release from host cells during the early phase of viral infection was reported for *Chlorella* cells infected by PBCV-1 (*Paramecium bursaria* chlorella virus) (Neupartl et al. 2008); this phenomenon was explained by incorporation of viral-encoded K^+ channels (Kcv) into the host membrane. It remains to be answered whether the same scenario is also applicable for higher plants.

Acknowledgements This work was supported by the Grain Research and Development Corporation and Australian Research Council grants to Prof Sergey Shabala. The authors are grateful to Dr Ian Newman for his critical reading and valuable suggestions on this manuscript.

References

Akeson MA, Munns DN, Burau RG (1989) Adsorption of Al^{3+} to phosphatidylcholine vesicles. Biochim Biophys Acta 986:33–40

Alberts B, Bray D, Lewis J, Raff M, Roberts K, Watson JD (1994) Molecular biology of the cell, 3rd edn. Garland Publishing Inc, New York

Atkinson MM, Keppler LD, Orlandi EW, Baker CJ, Mischke CF (1990) Involvement of plasma membrane calcium influx in bacterial induction of the K^+/H^+ and hypersensitive responses in tobacco. Plant Physiol 92:215–221

Ayala F, Oleary JW, Schumaker KS (1996) Increased vacuolar and plasma membrane H^+-ATPase activities in *Salicornia bigelovii* Torr in response to NaCl. J Exp Bot 47:25–32

Babourina O, Hawkins B, Lew RR, Newman I, Shabala S (2001) K^+ transport by *Arabidopsis* root hairs at low pH. Austral J Plant Physiol 28:635–641

Bajaj S, Targolli J, Liu LF, Ho THD, Wu R (1999) Transgenic approaches to increase dehydration-stress tolerance in plants. Mol Breeding 5:493–503

Balague C, Lin B, Alcon C, Flottes G, Malmstrom S, Kohler C, Neuhaus G, Pelletier G, Gaymard F, Roby D (2003) HLM1, an essential signalling component in the hypersensitive response, is a member of the cyclic nucleotide-gated channel ion channel family. Plant Cell 15: 365–379

Basu R, Ghosh B (1991) Polyamines in various rice (*Oryza sativa*) genotypes with respect to sodium-chloride salinity. Physiol Plant 82:575–581

Beffagna N, Buffoli B, Busi C (2005) Modulation of reactive oxygen species production during osmotic stress in *Arabidopsis thaliana* cultured cells: Involvement of the plasma membrane Ca^{2+}-ATPase and H^+-ATPase. Plant Cell Physiol 46:1326–1339

Bisson MA, Kiegle E, Black D, Kiyosawa K, Gerber N (1995) The role of calcium in turgor regulation in *Chara longifolia*. Plant Cell Environ 18:129–137

Blume B, Nürnberger T, Nass N, Scheel D (2000) Receptor-mediated increase in cytoplasmic free calcium required for activation of pathogen defense in parsley. Plant Cell 12:1425–1440

Blumwald E, Aharon GS, Lam C-H (1998) Early signal transduction pathways in plant-pathogen interactions. Trends Plant Sci 3:342–346

Bohnert HJ, Shen B (1999) Transformation and compatible solutes. Sci Hort 78:237–260

Bohnert HJ, Nelson DE, Jensen RG (1995) Adaptation to environmental stresses. Plant Cell 7:1099–1111

Bose J, Babourina O, Shabala S, Rengel Z (2010a) Aluminium-induced ion transport in *Arabidopsis*: the relationship between Al tolerance and root ion flux. J Exp Bot 61:3163–3175

Bose J, Babourina O, Shabala S, Rengel Z (2010b) Aluminum-dependent dynamics of ion transport in *Arabidopsis*: specificity of low pH and aluminum responses. Physiol Plant 139:401–412

Bose J, Babourina O, Rengel Z (2011a) Role of magnesium in alleviation of aluminium toxicity in plants. J Exp Bot 62:2251–2264

Bose J, Pottosin II, Shabala SS, Palmgren MG, Shabala S (2011b) Calcium efflux systems in stress signalling and adaptation in plants. Front. Plant Sci. 2:85. doi: 10.3389/fpls.2011.00085

Boyer JS (1982) Plant productivity and environment. Science 218:443–448

Brady DJ, Edwards DG, Asher CJ, Blamey FPC (1993) Calcium amelioration of aluminum toxicity effects on root hair development in soybean [*Glycine max* (L) Merr]. New Phytol 123:531–538

Bray EA (1997) Plant responses to water deficit. Trend Plant Sci 2:48–54

Brownlee C, Goddard H, Hetherington AM, Peake L-A (1999) Specificity and integration of responses: Ca^{2+} as a signal in polarity and osmotic regulation. J Exp Bot 50:1001–1011

Bruggemann W, Janiesch P (1989) Comparison of plasma membrane ATPase from salt-treated and salt-free grown *Plantago maritima* L. J Plant Physiol 134:20–25

Carden DE, Walker DJ, Flowers TJ, Miller AJ (2003) Single-cell measurements of the contributions of cytosolic Na^+ and K^+ to salt tolerance. Plant Physiol 131:676–683

Casolo V, Petrussa E, Krajnakova J, Macri F, Vianello A (2005) Involvement of the mitochondrial K^+-ATP channel in H_2O_2- or NO-induced programmed death of soybean suspension cell cultures. J Exp Bot 56:997–1006

Cervantes E (2001) ROS in root gravitropism: the auxin messengers? Trends Plant Sci 6:556

Cessna SG, Kim J, Taylor ATS (2003) Cytosolic Ca^{2+} pulses and protein kinase activation in the signal transduction pathways leading to the plant oxidative burst. J Plant Biol 46:215–222

Chen Z, Newman I, Zhou M, Mendham N, Zhang G, Shabala S (2005) Screening plants for salt tolerance by measuring K^+ flux: a case study for barley. Plant, Cell Environ 28:1230–1246

Chen ZH, Cuin TA, Zhou MX, Twomey A, Naidu BP, Shabala S (2007a) Compatible solute accumulation and stress-mitigating effects in barley genotypes contrasting in their salt tolerance. J Exp Bot 58:4245–4255

Chen ZH, Pottosin II, Cuin TA, Fuglsang AT, Tester M, Jha D, Zepeda-Jazo I, Zhou MX, Palmgren MG, Newman IA, Shabala S (2007b) Root plasma membrane transporters controlling K^+/Na^+ homeostasis in salt-stressed barley. Plant Physiol 145:1714–1725

Chen ZG, Shabala S, Mendham N, Newman I, Zhang GP, Zhou MX (2008) Combining ability of salinity tolerance on the basis of NaCl-induced K^+ flux from roots of barley. Crop Sci 48:1382–1388

Chichkova NV, Kim SH, Titova ES, Kalkum M, Morozov VS, Rubtsov YP, Kalinina NO, Taliansky ME, Vartapetian AB (2004) A plant caspase-like protease activated during the hypersensitive response. Plant Cell 16:157–171

Chung WS, Lee SH, Kim JC, Heo WD, Kim MC, Park CY, Park HC, Lim CO, Kim WB, Harper JF, Cho MJ (2000) Identification of a calmodulin-regulated soybean Ca^{2+}-ATPase (SCA1) that is located in the plasma membrane. Plant Cell 12:1393–1407

Clough SJ, Fengler KA, Yu IC, Lippok B, Smith RK, Bent AF (2000) The *Arabidopsis dnd1* "defense, no death" gene encodes a mutated cyclic nucleotide-gated ion channel. Proc Natl Acad Sci USA 97: 9323–9328

Colmer TD, Greenway H (2011) Ion transport in seminal and adventitious roots of cereals during O_2 deficiency. J Exp Bot 62:39–57

Colmer TD, Huang SB, Greenway H (2001) Evidence for down-regulation of ethanolic fermentation and K^+ effluxes in the coleoptile of rice seedlings during prolonged anoxia. J Exp Bot 52:1507–1517

Colmer TD, Flowers TJ, Munns R (2006) Use of wild relatives to improve salt tolerance in wheat. J Exp Bot 57:1059–1078

Cosgrove DJ, Hedrich R (1991) Stretch-activated chloride, potassium, and calcium channels coexisting in plasma membranes of guard cells of *Vicia faba* L. Planta 186:143–153

Cramer GR, Lynch J, Lauchli A, Epstein E (1987) Influx of Na^+, K^+, and Ca^{2+} into roots of salt-stressed cotton seedlings. Effects of supplemental Ca^{2+}. Plant Physiol 83:510–516

Cuin TA, Shabala S (2005) Exogenously supplied compatible solutes rapidly ameliorate NaCl-induced potassium efflux from barley roots. Plant Cell Physiol 46:1924–1933

Cuin TA, Shabala S (2007a) Amino acids regulate salinity-induced potassium efflux in barley root epidermis. Planta 225:753–761

Cuin TA, Shabala S (2007b) Compatible solutes reduce ROS-induced potassium efflux in *Arabidopsis* roots. Plant Cell Environ 30:875–885

Cuin TA, Miller AJ, Laurie SA, Leigh RA (2003) Potassium activities in cell compartments of salt-grown barley leaves. J Exp Bot 54:657–661

Cuin TA, Parsons D, Shabala S (2010) Wheat cultivars can be screened for NaCl salinity tolerance by measuring leaf chlorophyll content and shoot sap potassium. Funct Plant Biol 37:656–664

Cuin TA, Bose J, Stefano G, Jha D, Tester M, Mancuso S, Shabala S (2011a) Assessing the role of root plasma membrane and tonoplast Na^+/H^+ exchangers in salinity tolerance in wheat: in planta quantification methods. Plant, Cell Environ 34:947–961

Cuin TA, Zhou MZ, Parsons D, Shabala S (2011b) Genetic behaviour of physiological traits conferring cytosolic K^+/Na^+ homeostasis in wheat. Plant Biol doi: 10.1111/j.1438-8677.2011.00526.x

Degenhardt J, Larsen PB, Howell SH, Kochian LV (1998) Aluminum resistance in the *Arabidopsis* mutant *alr-104* is caused by an Aluminum-induced increase in rhizosphere pH. Plant Physiol 117:19–27

Delauney AJ, Verma DPS (1993) Proline biosynthesis and osmoregulation in plants. Plant J 4:215–223

Demidchik V, Tester M (2002) Sodium fluxes through nonselective cation channels in the plasma membrane of protoplasts from *Arabidopsis* roots. Plant Physiol 128:379–387

Demidchik V, Shabala SN, Coutts KB, Tester MA, Davies JM (2003) Free oxygen radicals regulate plasma membrane Ca^{2+} and K^+- permeable channels in plant root cells. J Cell Sci 116:81–88

Demidchik V, Shabala SN, Davies JM (2007) Spatial variation in H_2O_2 response of *Arabidopsis thaliana* root epidermal Ca^{2+} flux and plasma membrane Ca^{2+} channels. Plant J 49:377–386

Demidchik V, Cuin TA, Svistunenko D, Smith SJ, Miller AJ, Shabala S, Sokolik A, Yurin V (2010) *Arabidopsis* root K^+-efflux conductance activated by hydroxyl radicals: single-channel properties, genetic basis and involvement in stress-induced cell death. J Cell Sci 123: 1468–1479

Ding X et al. (2011) Synergistic interactions between *Glomus mosseae* and *Bradyrhizobium japonicum* in enhancing proton release from nodules and hyphae. Mycorrhiza:1–8 (DOI:10.1007/s00572-00011-00381-00573)

Ding JP, Badot PM, Pickard BG (1993) Aluminium and hydrogen ions inhibit a mechanosensory calcium-selective cation channel. Aust J Plant Physiol 20:771–778

Elkahoui S, Carvajal M, Ghrir R, Limam F (2005) Study of the involvement of osmotic adjustment and H^+-ATPase activity in the resistance of *Catharanthus roseus* suspension cells to salt stress. Plant Cell Tiss Org 80:287–294

Erdei L, Trivedi S, Takeda K, Matsumoto H (1990) Effects of osmotic and salt stresses on the accumulation of polyamines in leaf segments from wheat-varieties differing in salt and drought tolerance. J Plant Physiol 137:165–168

Evans PT, Malmberg RL (1989) Do polyamines have roles in plant development? Annu Rev Plant Physiol Plant Mol Biol 40:235–269

Felle H (2001) pH: signal and messenger in plant cells. Plant biology 3:577–591

Flowers TJ, Colmer TD (2008) Salinity tolerance in halophytes. New Phytol 179:945–963

Flowers TJ, Yeo AR (1995) Breeding for salinity resistance in crop plants: Where next? Austral J Plant Physiol 22:875–884

Foy CD (1988) Plant adaptation to acid, aluminum-toxic soils. Commun Soil Sci Plant Anal 19:959–987

Galston AW, Kaur-Sawhney R (1990) Polyamines in plant physiology. Plant Physiol 94:406–410

Garg AK, Kim JK, Owens TG, Ranwala AP, Do Choi Y, Kochian LV, Wu RJ (2002) Trehalose accumulation in rice plants confers high tolerance levels to different abiotic stresses. Proc Natl Acad Sci USA 99:15898–15903

Garufi A, Visconti S, Camoni L, Aducci P (2007) Polyamines as physiological regulators of 14-3-3 interaction with the plant plasma membrane H^+-ATPase. Plant Cell Physiol 48:434–440

Gout E, Boisson AM, Aubert S, Douce R, Bligny R (2001) Origin of the cytoplasmic pH changes during anaerobic stress in higher plant cells. Carbon-13 and phosphorous-31 nuclear magnetic resonance studies. Plant Physiol 125:912–925

Grant M, Brown I, Adams S, Knight M, Ainslie A, Mansfield J (2000) The RPM1 plant disease resistance gene facilitates a rapid and sustained increase in cytosolic calcium that is necessary for the oxidative burst and hypersensitive cell death. Plant J 23:441–450

Greenway H, Gibbs J (2003) Mechanisms of anoxia tolerance in plants. II. Energy requirements for maintenance and energy distribution to essential processes. Funct Plant Biol 30:999–1036

Greenway H, Waters I, Newsome J (1992) Effects of anoxia on uptake and loss of solutes in roots of wheat. Aust J Plant Physiol 19:233–247

Gulbins E, Jekle A, Ferlinz K, Grassme H, Lang F (2000) Physiology of apoptosis. Amer J Physiol Renal Physiol 279: F605–F615

Guo KM, Babourina O, Christopher DA, Borsic T, Rengel Z (2010) The cyclic nucleotide gated channel AtCNGC10 transports Ca^{2+} and Mg^{2+} in *Arabidopsis*. Physiol Plant 139:303–312

Halliwell B, Grootveld M (1988) Methods for the measurement of hydroxyl radicals in biochemical systems–deoxyribose degradation and aromatic hydroxylation. Methods Biochem Analisis 33:59–90

Hare PD, Cress WA, van Staden J (2002) Disruptive effects of exogenous proline on chloroplast and mitochondrial ultrastructure in *Arabidopsis* leaves. South African J Bot 68:393–396

Hariadi Y, Shabala S (2004) Screening broad beans (*Vicia faba*) for magnesium deficiency. II. Photosynthetic performance and leaf bioelectrical responses. Funct Plant Biol 31:539–549

Hasegawa PM, Bressan RA, Zhu JK, Bohnert HJ (2000) Plant cellular and molecular responses to high salinity. Annu Rev Plant Physiol Plant Mol Biol 51:463–499

Hatsugai N, Kuroyanagi M, Yamada K, Meshi T, Tsuda S, Kondo M, Nishimura M, Hara-Nishimura I (2004) A plant vacuolar protease, VPE, mediates virus-induced hypersensitive cell death. Science 305:855–858

Hawkins BJ, Robbins S (2010) pH affects ammonium, nitrate and proton fluxes in the apical region of conifer and soybean roots. Physiol Plant 138:238–247

Hawkins B, Boukcim H, Plassard C (2008) A comparison of ammonium, nitrate and proton net fluxes along seedling roots of Douglas fir and lodgepole pine grown and measured with different inorganic nitrogen sources. Plant Cell Environ 31:278–287

Heber U, Tyankova L, Santarius KA (1971) Stabilization and inactivation of biological membranes during freezing in presence of amino acids. Biochim Biophys Acta 241:578–592

Henle ES, Linn S (1997) Formation, prevention, and repair of DNA damage by iron hydrogen peroxide. J Biol Chem 272:19095–19098

Hirschi K (2001) Vacuolar H^+/Ca^{2+} transport: who's directing the traffic? Trend Plant Sci 6: 100–104

Hoeberichts FA, Woltering EJ (2003) Multiple mediators of plant programmed cell death: interplay of conserved cell death mechanisms and plant-specific regulators. BioEssays 25:47–57

Hoekenga OA et al (2006) *AtALMT1*, which encodes a malate transporter, is identified as one of several genes critical for aluminum tolerance in *Arabidopsis*. Proc Natl Acad Sci USA 103:9738–9743

Hong ZL, Lakkineni K, Zhang ZM, Verma DPS (2000) Removal of feedback inhibition of Δ^1-pyrroline-5-carboxylate synthetase results in increased proline accumulation and protection of plants from osmotic stress. Plant Physiol 122:1129–1136

Huang JW, Shaff JE, Grunes DL, Kochian LV (1992) Aluminum effects on calcium fluxes at the root apex of aluminum-tolerant and aluminum-sensitive wheat cultivars. Plant Physiol 98:230–237

Huang JW, Pellet DM, Papernik LA, Kochian LV (1996) Aluminum interactions with voltage-dependent calcium transport in plasma membrane vesicles isolated from roots of aluminum-sensitive and-resistant wheat cultivars. Plant Physiol 110:561–569

Huh GH, Damsz B, Matsumoto TK, Reddy MP, Rus AM, Ibeas JI, Narasimhan ML, Bressan RA, Hasegawa PM (2002) Salt causes ion disequilibrium-induced programmed cell death in yeast and plants. Plant J 29:649–659

Igarashi Y, Yoshiba Y, Sanada Y, YamaguchiShinozaki K, Wada K, Shinozaki K (1997) Characterization of the gene for Δ^1-pyrroline-5-carboxylate synthetase and correlation between the expression of the gene and salt tolerance in *Oryza sativa* L. Plant Mol Biol 33:857–865

Ikka T et al (2007) Natural variation of *Arabidopsis thaliana* reveals that aluminum resistance and proton resistance are controlled by different genetic factors. Theor Appl Genet 115: 709–719

Jabs T, Tschope M, Colling C, Hahlbrock K, Scheel D (1997) Elicitor-stimulated ion fluxes and O_2^- from the oxidative burst are essential components in triggering defense gene activation and phytoalexin synthesis in parsley. Proc Natl Acad Sci USA 94:4800–4805

Jones DL, Shaff JE, Kochian LV (1995) Role of calcium and other ions in directing root hair tip growth in *Limnobium stoloniferum*. Planta 197:672–680

Kadota Y, Goh T, Tomatsu H, Tamauchi R, Higashi K, Muto S, Kuchitsu K (2004) Cryptogein-induced initial events in tobacco BY-2 cells: Pharmacological characterization of molecular relationship among cytosolic Ca^{2+} transients, anion efflux and production of reactive oxygen species. Plant Cell Physiol 45:160–170

Katsuhara M, Kawasaki T (1996) Salt stress induced nuclear and DNA degradation in meristematic cells of barley roots. Plant Cell Physiol 37:169–173

Keltjens WG, Tan K (1993) Interactions between aluminium, magnesium and calcium with different monocotyledonous and dicotyledonous plant species. Plant Soil 155–156:485–488

Kidd PS, Proctor J (2001) Why plants grow poorly on very acid soils: are ecologists missing the obvious? J Exp Bot 52:791–799

Kiegle E, Gilliham M, Haseloff J, Tester M (2000) Hyperpolarisation-activated calcium currents found only in cells from the elongation zone of *Arabidopsis thaliana* roots. Plant J 21:225–229

Kinraide TB (1993) Aluminum enhancement of plant growth in acid rooting media–a case of reciprocal alleviation of toxicity by 2 toxic cations. Physiol Plant 88:619–625

Kinraide TB, Wyse RE (1986) Electrical evidence for turgor inhibition of proton extrusion in sugar beet taproot. Plant Physiol 82:1148–1150

Kinraide TB, Pedler JF, Parker DR (2004) Relative effectiveness of calcium and magnesium in the alleviation of rhizotoxicity in wheat induced by copper, zinc, aluminum, sodium, and low pH. Plant Soil 259:201–208

Kochian LV (1995) Cellular mechanisms of aluminum toxicity and resistance in plants. Annu Rev Plant Physiol Plant Mol Biol 46:237–260

Kochian LV, Shaff JE, Lucas WJ (1989) High affinity K^+ uptake in maize roots. A lack of coupling with H^+ efflux. Plant Physiol 91:1202–1211

Kochian LV, Hoekenga OA, Piñeros MA (2004) How do crop plants tolerate acid soils? Mechanisms of aluminum tolerance and phosphorous efficiency. Annu Rev Plant Biol 55:459–493

Kochian LV, Pineros MA, Hoekenga OA (2005) The physiology, genetics and molecular biology of plant aluminum resistance and toxicity. Plant Soil 274:175–195

Kohler B, Hills A, Blatt MR (2003) Control of guard cell ion channels by hydrogen peroxide and abscisic acid indicates their action through alternate signalling pathways. Plant Physiol 131:385–388

Koizumi Y, Hara Y, Yazaki Y, Sakano K, Ishizawa K (2011) Involvement of plasma membrane H^+ ATPase in anoxic elongation of stems in pondweed (*Potamogeton distinctus*) turions. New Phytol 190:421–430

Kourie JI (1998) Interaction of reactive oxygen species with ion transport mechanisms. Amer J Physiol 44:1–24

Koyama H, Toda T, Yokota S, Dawair Z, Hara T (1995) Effects of aluminum and pH on root growth and cell viability in *Arabidopsis thaliana* strain Landsberg in hydroponic culture. Plant Cell Physiol 36:201–205

Koyama H, Toda T, Hara T (2001) Brief exposure to low-pH stress causes irreversible damage to the growing root in *Arabidopsis thaliana*: pectin-Ca interaction may play an important role in proton rhizotoxicity. J Exp Bot 52:361–368

LaHaye PA, Epstein E (1969) Salt tolerance in plants: enhancement with calcium. Science 166:395–396

Lakra N, Mishra SN, Singh DB, Tomar PC (2006) Exogenous putrescine effect on cation concentration in leaf of *Brassica juncea* seedlings subjected to Cd and Pb along with salinity stress. J Env Biol 27:263–269

Lam E, Kato N, Lawton M (2001) Programmed cell death, mitochondria and the plant hypersensitive response. Nature 411:848–853

Larsen PB, Degenhardt J, Tai C-Y, Stenzler LM, Howell SH, Kochian LV (1998) Aluminum-resistant *Arabidopsis* mutants that exhibit altered patterns of aluminum accumulation and organic acid release from roots. Plant Physiol 117:9–17

Lecourieux D, Mazars C, Pauly N, Ranjeva R, Pugin A (2002) Analysis and effects of cytosolic free calcium increases in response to elicitors in *Nicotiana plumbaginifolia* cells. Plant Cell 14:2627–2641

Lee J, Pritchard M (1984) Aluminium toxicity expression nutrient uptake, growth and root morphology of *Trifolium repens* L. cv. 'Grasslands Huia'. Plant Soil 82:101–116

Lee SH, Singh AP, Chung GC (2004) Rapid accumulation of hydrogen peroxide in cucumber roots due to exposure to low temperature appears to mediate decreases in water transport. J Exp Bot 55:1733–1741

Leigh RA (2001) Potassium homeostasis and membrane transport. J Plant Nutrit Soil Sci 164:193–198

Lew RR (1996) Pressure regulation of the electrical properties of growing *Arabidopsis thaliana* L root hairs. Plant Physiol 112:1089–1100

Lew RR, Levina NN, Shabala L, Anderca MI, Shabala SN (2006) Role of a mitogen-activated protein kinase cascade in ion flux-mediated turgor regulation in fungi. Eukaryot Cell 5:480–487

Li Z-S, Delrot S (1987) Osmotic dependence of the transmembrane potential difference of broad bean mesocarp cells. Plant Physiol 84:895–899

Lindberg S (1990) Aluminium interactions with K^+ ($^{86}Rb^+$) and $^{45}Ca^{2+}$ fluxes in three cultivars of sugar beet (*Beta vulgaris*). Physiol Plant 79:275–282

Liu J, Magalhaes JV, Shaff J, Kochian LV (2009) Aluminum-activated citrate and malate transporters from the MATE and ALMT families function independently to confer *Arabidopsis* aluminum tolerance. Plant J 57:389–399

Lucas WJ, Kochian LV (1986) Ion transport processes in corn roots: an approach utilizing microelectrode techniques. In: Gensler WG (ed) Advanced agricultural instrumentation: design and use. Martinus Nijhoff, Dordrecht, pp 402–425

Lutts S, Majerus V, Kinet JM (1999) NaCl effects on proline metabolism in rice (*Oryza sativa*) seedlings. Physiol Plant 105:450–458

Mancuso S, Boselli M (2002) Characterisation of the oxygen fluxes in the division, elongation and mature zones of *Vitis* roots: influence of oxygen availability. Planta 214:767–774

Mancuso S, Marras AM (2006) Adaptative response of *Vitis* root to anoxia. Plant Cell Physiol 47:401–409

Mancuso S, Azzarello E, Mugnai S, Briand X (2006) Marine bioactive substances (IPA extract) improve foliar ion uptake and water stress tolerance in potted *Vitis vinifera* plants. Adv Hortic Sci 20:156–161

Matsumoto H, Yamaya T (1986) Inhibition of potassium uptake and regulation of membrane-associated Mg^{2+} -ATPase activity of pea roots by aluminum. Soil Sci Plant Nutr 32:179–188

McCue KF, Hanson AD (1990) Drought and salt tolerance–towards understanding and application. Trends Biotechnol 8:358–362

Michelet B, Boutry M (1995) The plasma membrane H^+-ATPase: a highly regulated enzyme with multiple physiological functions. Plant Physiol 108:1–6

Miller G, Shulaev V, Mittler R (2008) Reactive oxygen signaling and abiotic stress. Physiol Plant 133:481–489

Mittler R (2006) Abiotic stress, the field environment and stress combination. Trends Plant Sci 11:15–19

Mittler R, Vanderauwera S, Gollery M, Van Breusegem F (2004) Reactive oxygen gene network of plants. Trends Plant Sci 9:490–498

Mori IC, Schroeder JI (2004) Reactive oxygen species activation of plant Ca^{2+} channels. A signalling mechanism in polar growth, hormone transduction, stress signaling, and hypothetically mechanotransduction. Plant Physiol 135:702–708

Mugnai S, Azzarello E, Pandolfi C, Salamagne S, Briand X, Mancuso S (2008) Enhancement of ammonium and potassium root influxes by the application of marine bioactive substances positively affects *Vitis vinifera* plant growth. J Appl Phycol 20:177–182

Mugnai S, Marras AM, Mancuso S (2011) Effect of hypoxic acclimation on anoxia tolerance in *Vitis* roots: Response of metabolic activity and K^+ fluxes. Plant Cell Physiol 52:1107–1116

Munns R, Tester M (2008) Mechanisms of salinity tolerance. Annu Rev Plant Biol 59:651–681

Nash D, Paleg LG, Wiskich JT (1982) Effect of proline, betaine and some other solutes on the heat stability of mitochondrial enzymes. Aust J Plant Physiol 9:47–57

Ndayiragije A, Lutts S (2006) Exogenous putrescine reduces sodium and chloride accumulation in NaCl-treated calli of the salt-sensitive rice cultivar I Kong Pao. Plant Growth Reg 48:51–63

Nemchinov LG, Shabala L, Shabala S (2008) Calcium efflux as a component of the hypersensitive response of *Nicotiana benthamiana* to *Pseudomonas syringae*. Plant Cell Physiol 49:40–46

Neupartl M, Meyer C, Woll I, Frohns F, Kang M, Van Etten JL, Kramer D, Hertel B, Moroni A, Thiel G (2008) Chlorella viruses evoke a rapid release of K^+ from host cells during the early phase of infection. Virology 372:340–348

Newman IA, Kochian LV, Grusak MA, Lucas WJ (1987) Fluxes of H^+ and K^+ in corn roots—characterization and stoichiometries using ion selective microelectrodes. Plant Physiol 84:1177–1184

Newman I, Chen SL, Porterfield DM, Sun J (2012) Non-invasive flux measurements using microsensors: theory, limitations and systems. In: Shabala S, Cuin TA (eds) Methods in molecular biology–plant salt tolerance. Humana Press, Clifton (in press)

Nichol BE, Oliveira LA, Glass ADM, Siddiqi MY (1993) The effects of aluminum on the influx of calcium, potassium, ammonium, nitrate, and phosphate in an aluminum-sensitive cultivar of barley (*Hordeum vulgare* L.). Plant Physiol 101:1263–1266

Noctor G, Foyer CH (1998) Ascorbate and glutathione: Keeping active oxygen under control. Annu Rev Plant Physiol Plant Mol Biol 49:249–279

Nurnberger T, Nennsteil D, Jabs T, Sacks WR, Hahlbrock K, Scheel D (1994) High affinity binding of a fungal oligopeptide elicitor to parsley plasma membranes triggers multiple defence responses. Cell 78:449–460

Okazaki Y, Tazawa M (1990) Calcium ion and turgor regulation in plant cells. J Membrane Biol 114:189–194

Okazaki Y, Shimmen T, Tazawa M (1984) Turgor regulation in a brackish Charophyte, *Lamprothamnium succinctum*. II. Changes in K^+, Na^+ and Cl^- concentrations, membrane potential and membrane resistance during turgor regulation. Plant Cell Physiol 25:573–581

Oren A (1999) Bioenergetic aspects of halophilism. Microbiol Mol Biol Rev 63:334–348

Palmgren MG (1991) Regulation of plasma membrane H^+-ATPase activity. Physiol Plant 83:314–323

Palmgren MG (2001) Plant plasma membrane H^+-ATPases: powerhouses for nutrient uptake. Annu Rev Plant Biol 52:817–845

Panayiotidis MI, Bortner CD, Cidlowski JA (2006) On the mechanism of ionic regulation of apoptosis: would the Na^+/K^+-ATPase please stand up? Acta Physiol 187:205–215

Pandolfi C, Pottosin I, Cuin T, Mancuso S, Shabala S (2010) Specificity of polyamine effects on NaCl-induced ion flux kinetics and salt stress amelioration in plants. Plant Cell Physiol 51:422–434

Pang JY, Newman I, Mendham N, Zhou M, Shabala S (2006) Microelectrode ion and O_2 fluxes measurements reveal differential sensitivity of barley root tissues to hypoxia. Plant Cell Environ 29:1107–1121

Pang JY, Cuin T, Shabala L, Zhou MX, Mendham N, Shabala S (2007) Effect of secondary metabolites associated with anaerobic soil conditions on ion fluxes and electrophysiology in barley roots. Plant Physiol 145:266–276

Pei ZM, Murata Y, Benning G, Thomine S, Klusener B, Allen GJ, Grill E, Schroeder JI (2000) Calcium channels activated by hydrogen peroxide mediate abscisic acid signalling in guard cells. Nature 406:731–734

Peng Z, Lu Q, Verma DPS (1996) Reciprocal regulation of Δ^1-pyrroline-5-carboxylate synthetase and proline dehydrogenase genes controls proline levels during and after osmotic stress in plants. Mol Gen Genetics 253:334–341

Pennell RI, Lamb C (1997) Programmed cell death in plants. Plant Cell 9:1157–1168

Pickard BG, Ding JP (1993) The mechanosensory calcium-selective ion channel: key component of a plasmalemma control centre? Austral J Plant Physiol 20:439–459

Pineros MA, Kochian LV (2001) A patch-clamp study on the physiology of aluminum toxicity and aluminum tolerance in maize. Identification and characterization of Al^{3+}-induced anion channels. Plant Physiol 125:292–305

Pineros M, Tester M (1997) Calcium channels in higher plant cells: Selectivity, regulation and pharmacology. J Exp Bot 48:551–577

Qiao WH, Fan LM (2008) Nitric oxide signaling in plant responses to abiotic stresses. J Integrat Plant Biol 50:1238–1246

Ramahaleo T, Alexandre J, Lassalles J-P (1996) Stretch activated channels in plant cells. A new model for osmoelastic coupling. Plant Physiol Biochem 34:327–334

Ramani B, Reeck T, Debez A, Stelzer R, Huchzermeyer B, Schmidt A, Papenbrock J (2006) *Aster tripolium* L. and *Sesuvium portulacastrum* L.: two halophytes, two strategies to survive in saline habitats. Plant Physiol Biochem 44:395–408

Ramos AC, Façanha AR, Feijó JA (2008) Proton (H^+) flux signature for the presymbiotic development of the arbuscular mycorrhizal fungi. New Phytol 178:177–188

Ramos AC, Lima PT, Dias PN, Kasuya MCM, Feijó JA (2009) A pH signaling mechanism involved in the spatial distribution of calcium and anion fluxes in ectomycorrhizal roots. New Phytol 181:448–462

Ratcliffe RG (1997) *In vivo* NMR studies of the metabolic response of plant tissues to anoxia. Ann Bot 79:39–48

Rawyler A, Pavelic D, Gianinazzi C, Oberson J, Braendle R (1999) Membrane lipid integrity relies on a threshold of ATP production rate in potato cell cultures submitted to anoxia. Plant Physiol 120:293–300

Raven JA (1985) Regulation of pH and generation of osmolarity in vascular plants: a cost-benefit analysis in relation to efficiency of use of energy, nitrogen and water. New Phytol 101:25–77

Reid RJ, Smith FA (2000) The limits of sodium/calcium interactions in plant growth. Austral J Plant Physiol 27:709–715

Reid RJ, Tester MA, Smith FA (1995) Calcium/aluminium interactions in the cell wall and plasma membrane of *Chara*. Planta 195:362–368

Reinhold L, Seiden A, Volokita M (1984) Is modulation of the rate of proton pumping a key event in osmoregulation? Plant Physiol 75:846–849

Reggiani R (1997) Alteration of levels of cyclic nucleotides in response to anaerobiosis in rice seedlings. Plant Cell Physiol 38:740–742

Rengel Z (1992) Role of calcium in aluminium toxicity. New Phytol 121:499–513

Rengel Z (1994) Effects of Al, rare earth elements, and other metals on net $^{45}Ca^{2+}$ uptake by *Amaranthus* protoplasts. J Plant Physiol 143:47–51

Rengel Z (2004) Aluminium cycling in the soil-plant-animal-human continuum. Biometals 17:669–689

Rengel Z, Elliott DC (1992) Mechanism of aluminum inhibition of net $^{45}Ca^{2+}$ uptake by amaranthus protoplasts. Plant Physiol 98:632–638

Rengel Z, Zhang WH (2003) Role of dynamics of intracellular calcium in aluminium toxicity syndrome. New Phytol 159:295–314

Rengel Z, Pineros M, Tester M (1995) Transmembrane calcium fluxes during Al stress. Plant Soil 171:125–130

Reuveni M, Colombo R, Lerner HR, Pradet A, Polyakoff-Mayber A (1987) Osmotically induced proton extrusion from carrot cells in suspension culture. Plant Physiol 85:383–388

Rojo E, Martin R, Carter C, Zouhar J, Pan SQ, Plotnikova J, Jin HL, Paneque M, Sanchez-Serrano JJ, Baker B, Ausubel FM, Raikhel NV (2004) VPE gamma exhibits a caspase-like activity that contributes to defense against pathogens. Curr Biol 14:1897–1906

Ryan PR, Kochian LV (1993) Interaction between aluminum toxicity and calcium uptake at the root apex in near-isogenic lines of wheat (*Triticum aestivum* L.) differing in aluminum tolerance. Plant Physiol 102:975–982

Ryan PR, Newman IA, Arif I (1992) Rapid calcium exchange for protons and potassium in cell walls of Chara. Plant Cell Environ 15:675–683

Ryan PR, Delhaize E, Randall PJ (1995) Characterisation of Al-stimulated efflux of malate from the apices of Al-tolerant wheat roots. Planta 196:103–110

Ryan PR, Reid RJ, Smith FA (1997) Direct evaluation of the Ca^{2+}-displacement hypothesis for Al toxicity. Plant Physiol 113:1351–1357

Ryan PR, Delhaize E, Jones DL (2001) Function and mechanism of organic anion exudation from plant roots. Annu Rev Plant Physiol Plant Mol Biol 52:527–560

Sanders D, Brownlee C, Harper JF (1999) Communicating with calcium. Plant Cell 11:691–706

Santos CLV, Campos A, Azevedo H, Caldeira G (2001) *In situ* and *in vitro* senescence induced by KCl stress: nutritional imbalance, lipid peroxidation and antioxidant metabolism. J Exp Bot 52:351–360

Sasaki T et al (2004) A wheat gene encoding an aluminum-activated malate transporter. Plant J 37:645–653
Schvarzstein M (1997) Changes in host plasma membrane ion fluxes during the *Gomphrena globosa*–Papaya Mosaic Virus interaction. M Sci Thesis, Department of Botany. University of Toronto, Canada
Serrano R, Culianz-Macia FA, Moreno V (1999) Genetic engineering of salt and drought tolerance with yeast regulatory genes. Sci Hort 78:261–269
Setter TL, Waters I (2003) Review of prospects for germplasm improvement for waterlogging tolerance in wheat, barley and oats. Plant Soil 253:1–34
Shabala S (2000) Ionic and osmotic components of salt stress specifically modulate net ion fluxes from bean leaf mesophyll. Plant Cell Environ 23:825–837
Shabala S (2003) Regulation of potassium transport in leaves: from molecular to tissue level. Ann Bot 92:627–634
Shabala S. (2007) Transport from root to shoot. In: Yeo AR, Flowers TJ (ed) Plant solute transport. Blackwell Publishing, Oxford. pp. 214–234
Shabala S (2009) Salinity and programmed cell death: unravelling mechanisms for ion specific signalling. J Exp Bot 60:709–711
Shabala S (2011) Physiological and cellular aspects of phytotoxicity tolerance in plants: the role of membrane transporters and implications for crop breeding for waterlogging tolerance. New Phytol 190:289–298
Shabala S, Cuin TA (2008) Potassium transport and plant salt tolerance. Physiol Plant 133: 651–669
Shabala S, Hariadi Y (2005) Effects of magnesium availability on the activity of plasma membrane ion transporters and light-induced responses from broad bean leaf mesophyll. Planta 221:56–65
Shabala S, Lew RR (2002) Turgor regulation in osmotically stressed *Arabidopsis* epidermal root cells. Direct support for the role of inorganic ion uptake as revealed by concurrent flux and cell turgor measurements. Plant Physiol 129:290–299
Shabala S, Mackay A (2011) Ion transport in Halophytes. Adv Bot Res 57:151–199
Shabala S, Newman IA (1998) Osmotic sensitivity of Ca^{2+} and H^+ transporters in corn roots–effect on fluxes and their oscillations in the elongation region. J Membrane Biol 161:45–54
Shabala S, Newman I (2000) Salinity effects on the activity of plasma membrane H^+ and Ca^{2+} transporters in bean leaf mesophyll: Masking role of the cell wall. Ann Bot 85:681–686
Shabala S, Shabala L (2002) Kinetics of net H^+, Ca^{2+}, K^+, Na^+, NH_4^+, and Cl^- fluxes associated with post-chilling recovery of plasma membrane transporters in *Zea mays* leaf and root tissues. Physiol Plant 114:47–56
Shabala S, Shabala L (2011) Ion transport and osmotic adjustment in plants and bacteria. BioMol Concepts 2:407–419
Shabala S, Babourina O, Newman I (2000) Ion-specific mechanisms of osmoregulation in bean mesophyll cells. J Exp Bot 51:1243–1253
Shabala S, Shabala L, Van Volkenburgh E (2003) Effect of calcium on root development and root ion fluxes in salinised barley seedlings. Funct Plant Biol 30:507–514
Shabala L, Cuin TA, Newman IA, Shabala S (2005a) Salinity-induced ion flux patterns from the excised roots of *Arabidopsis sos* mutants. Planta 222:1041–1050
Shabala S, Shabala L, Van Volkenburgh E, Newman I (2005b) Effect of divalent cations on ion fluxes and leaf photochemistry in salinized barley leaves. J Exp Bot 56:1369–1378
Shabala S, Demidchik V, Shabala L, Cuin TA, Smith SJ, Miller AJ, Davies JM, Newman IA (2006) Extracellular Ca^{2+} ameliorates NaCl-induced K^+ loss from *Arabidopsis* root and leaf cells by controlling plasma membrane K+-permeable channels. Plant Physiol 141:1653–1665
Shabala S, Cuin TA, Pottosin I (2007a) Polyamines prevent NaCl-induced K^+ efflux from pea mesophyll by blocking non-selective cation channels. FEBS Let 581:1993–1999
Shabala S, Cuin TA, Prismall L, Nemchinov LG (2007b) Expression of animal CED-9 anti-apoptotic gene in tobacco modifies plasma membrane ion fluxes in response to salinity and oxidative stress. Planta 227:189–197

Shabala L, Bowman J, Brown J, Ross T, McMeekin T, Shabala S (2009a) Ion transport and osmotic adjustment in *Escherichia coli* in response to ionic and non-ionic osmotica. Environ Microbiol 11:137–148

Shabala L, McMeekin T, Shabala S (2009b) Osmotic adjustment and requirement for sodium in marine protist thraustochytrid. Environ Microbiol 11:1835–1843

Shabala S, Babourina O, Rengel Z, Nemchinov LG (2010a) Non-invasive microelectrode potassium flux measurements as a potential tool for early recognition of virus-host compatibility in plants. Planta 232:807–815

Shabala S, Cuin TA, Pang JY, Percey W, Chen ZH, Conn S, Eing C, Wegner LH (2010b) Xylem ionic relations and salinity tolerance in barley. Plant J 61:839–853

Shabala S, Baekgaard L, Shabala L, Fuglsang A, Babourina O, Palmgren MG, Cuin TA, Rengel Z, Nemchinov LG (2011a) Plasma membrane Ca^{2+} transporters mediate virus-induced acquired resistance to oxidative stress. Plant Cell Environ 34:406–417

Shabala S, Baekgaard L, Shabala L, Fuglsang AT, Cuin TA, Nemchinov LG, Palmgren MG (2011b) Endomembrane Ca^{2+}-ATPases play a significant role in virus-induced adaptation to oxidative stress. Plant Signal Behav 6:135–138

Shen B, Jensen RG, Bohnert HJ (1997) Mannitol protects against oxidation by hydroxyl radicals. Plant Physiol 115:527–532

Shi HZ, Quintero FJ, Pardo JM, Zhu JK (2002) The putative plasma membrane Na^+/H^+ antiporter SOS1 controls long-distance Na^+ transport in plants. Plant Cell 14:465–477

Smirnoff N, Cumbes QJ (1989) Hydroxyl radical scavenging activity of compatible solutes. Phytochem 28:1057–1060

Subbaiah CC, Sachs MM (2003a) Calcium-mediated responses of maize to oxygen deprivation. Russ J Plant Physiol 50:752–761

Subbaiah CC, Sachs MM (2003b) Molecular and cellular adaptations of maize to flooding stress. Ann Bot 91:119–127

Subbaiah CC, Bush DS, Sachs MM (1998) Mitochondrial contribution to the anoxic Ca^{2+} signal in maize suspension-cultured cells. Plant Physiol 118:759–771

Tamura S, Kuramochi H, Ishizawa K (2001) Involvement of calcium ion in the stimulated shoot elongation of arrowhead tubers under anaerobic conditions. Plant Cell Physiol 42:717–722

Tang W, Newton RJ (2005) Polyamines reduce salt-induced oxidative damage by increasing the activities of antioxidant enzymes and decreasing lipid peroxidation in Virginia pine. Plant Growth Reg 46:31–43

Tanoi K, Junko H, Kazutoshi S, Yoshitake H, Hiroki N, Tomoko MN (2005) Analysis of potassium uptake by rice roots treated with aluminum using a positron emitting nuclide, ^{38}K. Soil Sci Plant Nutr 51:715–717

Taylor GJ et al (2000) Direct measurement of aluminum uptake and distribution in single cells of *Chara corallina*. Plant Physiol 123:987–996

Tazawa M (2003) Cell physiological aspects of the plasma membrane electrogenic H^+ pump. J Plant Res 116:419–442

Tegg RS, Melian L, Wilson CR, Shabala S (2005) Plant cell growth and ion flux responses to the *Streptomycete* phytotoxin thaxtomin-A: calcium and hydrogen flux patterns revealed by the non-invasive MIFE technique. Plant Cell Physiol 46:638–648

Teodoro AE, Zingarelli L, Lado P (1998) Early changes of Cl^- efflux and H^+ extrusion induced by osmotic stress in *Arabidopsis thaliana* cells. Physiol Plant 102:29–37

Tester M, Davenport R (2003) Na^+ tolerance and Na^+ transport in higher plants. Ann Bot 91: 503–527

Tyerman SD, Skerrett M, Garrill A, Findlay GP, Leigh RA (1997) Pathways for the permeation of Na^+ and Cl^- into protoplasts derived from the cortex of wheat roots. J Exp Bot 48:459–480

Vera-Estrella R, Barkla BJ, Higgins VJ, Blumwald E (1994) Plant defence response to fungal pathogens. Activation of host-plasma membrane H^+-ATPase by elicitor-induced enzyme dephosphorylation. Plant Physiol 104:209–215

Vera-Estrella R, Barkla BJ, Bohnert HJ, Pantoja O (1999) Salt stress in *Mesembryanthemum crystallinum* L cell suspensions activates adaptive mechanisms similar to those observed in the whole plant. Planta 207:426–435

Vera-Estrella R, Barkla BJ, Garcia-Ramirez L, Pantoja O (2005) Salt stress in *Thellungiella halophila* activates Na^+ transport mechanisms required for salinity tolerance. Plant Physiol 139:1507–1517

Verbelen JP, De Cnodder T, Le J, Vissenberg K, Baluška F (2006) The root apex of *Arabidopsis thaliana* consists of four distinct zones of cellular activities: meristematic zone, transition zone, fast elongation zone, and growth terminating zone. Plant Signal Behav 1:296–304

Verma S, Mishra SN (2005) Putrescine alleviation of growth in salt stressed Brassica juncea by inducing antioxidative defense system. J Plant Physiol 162:669–677

Very A–A, Davies JM (2000) Hyperpolarization-activated calcium channels at the tip of *Arabidopsis* root hairs. Proc Natl Acad Sci USA 97:9801–9806

Very AA, Sentenac H (2002) Cation channels in the *Arabidopsis* plasma membrane. Trend Plant Sci 7:168–175

von Uexkull HR, Mutert E (1995) Global extent, development and economic impact of acid soils. Plant Soil 171:1–15

Walker EL, Connolly EL (2008) Time to pump iron: iron-deficiency-signaling mechanisms of higher plants. Curr Opin Plant Biol 11:530–535

Wang PT, Song CP (2008) Guard-cell signalling for hydrogen peroxide and abscisic acid. New Phytol 178:703–718

Watanabe N, Lam E (2004) Recent advance in the study of caspase-like proteases and Bax inhibitor-1 in plants: their possible roles as regulator of programmed cell death. Mol Plant Pathol 5:65–70

Wegner LH, Raschke K (1994) Ion channels in the xylem parenchyma of barley roots–a procedure to isolate protoplasts from this tissue and a patch- clamp exploration of salt passageways into xylem vessels. Plant Physiol 105:799–813

Wegner LH, Stefano G, Shabala L, Rossi M, Mancuso S, Shabala S (2011) Sequential depolarization of root cortical and stelar cells induced by an acute salt shock–implications for Na^+ and K^+ transport into xylem vessels. Plant Cell Environ 34:859–869

Werner JE, Finkelstein RR (1995) Arabidopsis mutants with reduced response to NaCl and osmotic-stress. Physiol Plantar 93:659–666

Wherrett T, Ryan PR, Delhaize E, Shabala S (2005) Effect of aluminium on membrane potential and ion fluxes at the apices of wheat roots. Funct Plant Biol 32:199–208

White PJ (1998) Calcium channels in the plasma membrane of root cells. Ann Bot 81:173–183

Williamson CL, Slocum RD (1992) Molecular-cloning and evidence for osmoregulation of the Δ^1-pyrroline-5-carboxylate reductase (proC) gene in pea (*Pisum sativum* L). Plant Physiol 100:1464–1470

Wyn Jones RG, Pritchard J (1989) Stresses, membranes and cell walls. In: Jones HG, Flowers TJ, Jones MB (eds) Plants under stress: biochemistry, physiology, and ecology and their application to plant improvement. University Press, Cambridge, pp 95–114

Xia JH, Roberts JKM (1996) Regulation of H^+ extruction and cytoplasmic pH in maize root tips acclimated to a low-oxigen environment. Plant Physiol 111:227–233

Xu RR, Qi SD, Lu LT, Chen CT, Wu CA, Zheng CC (2011) A DExD H box RNA helicase is important for K deprivation responses and tolerance in *Arabidopsis thaliana*. FEBS J 278:2296–2306

Yang Y, Zhang F, Zhao M, An L, Zhang L, Chen N (2006) Properties of plasma membrane H+-ATPase in salt-treated *Populus euphratica* callus. Plant Cell Rep 26:229–235

Yang G et al (2010) Vesicle-related OsSEC27P enhances H^+ secretion in the iron deficient transgenic tobacco root. Chin Sci Bull 55:3298–3304

Zepeda-Jazo I, Velarde-Buendía A-M, Enríquez-Figueroa R, Bose J, Shabala S, Muñiz-Murguía J, Pottosin I (2011) Polyamines interact with hydroxyl radicals in activating Ca^{2+} and K^+ transport across the root epidermal plasma membranes. Plant Physiol 157:2167–2180

Zhang WH, Ryan PR, Tyerman SD (2001) Malate-permeable channels and cation channels activated by aluminum in the apical cells of wheat roots. Plant Physiol 125:1459–1472
Zhou M (2010) Improvement of plant waterlogging tolerance. In: Mancuso S, Shabala S (eds) Waterlogging signalling and tolerance in plants. Springer, Berlin
Zhu JK (2003) Regulation of ion homeostasis under salt stress. Curr Opin Plant Biol 6:441–445
Zimmermann S, Frachisse JM, Thomine S, Barbier-Brygoo H, Guern J (1998) Elicitor-induced chloride efflux and anion channels in tobacco cell suspensions. Plant Physiol Biochem 36:665–674
Zimmermann S, Ehrhardt T, Plesch G, Muller-Rober B (1999) Ion channels in plant signalling. Cell Mol Life Sci 55:183–203

Chapter 5
Intracellular Measurements of the Electrical Properties of Walled Cells

Roger R. Lew

Abstract The electrical properties of plant (and other walled) cells have a tremendous impact on the transport of ions into or out of the cell. Ion transport is necessary for plant growth and survival. Thus, the electrical properties of the plant cell are crucial to the survival and growth of the plant. The most direct way to measure the electrical properties of the cell is intracellular impalement with a microelectrode. A range of techniques, their execution, and potential pitfalls are described in this chapter. Special attention is paid to dual impalement techniques to measure current–voltage relations of the cell.

5.1 Intracellular Measurements in Intact, Turgid Walled Cells

The foundation of the 'electrical' plant is the electrical nature of individual cells. To measure the electrical properties of walled cells, the most direct technique is to impale the cell with a microelectrode so that the electrical potential inside of the cell can be compared with the outside potential: The *transmembrane* potential. Impalements can be done relatively easily on large cells, such as Characean giant algal cells, that have dimensions of 1.5 mm by 3 cm. They are far more challenging to perform on small cells of higher plants —20 by 40 μm— and fungi with hyphal diameters of <15 μm. Etherton and Higinbotham (1960) and Slayman and Slayman (1962) successfully measured the potentials of barley and fungal cells, respectively. They showed that respiratory inhibitors depolarized the negative

R. R. Lew (✉)
Department of Biology, York University, Toronto, Canada
e-mail: planters@yorku.ca

A. G. Volkov (ed.), *Plant Electrophysiology*,
DOI: 10.1007/978-3-642-29119-7_5, © Springer-Verlag Berlin Heidelberg 2012

inside potential of the cell, demonstrating that the *transmembrane* potential required cellular metabolic energy, that is, the potential is actively generated. Since these pioneering measurements, the electrophysiological properties of numerous walled cells have been studied. Because the *transmembrane* potential strongly influences ion uptake and release, it is fundamental to transport energetics and kinetic mechanisms. Even the transport of uncharged solutes is often coupled with transport of charged ions (usually H^+). Ion and solute transport are crucial to the survival and growth of the organism because of their impact on nutrition. Therefore, the electrical properties of a cell are crucial for survival and growth.

In this chapter, I will describe methods for intracellular measurements used to characterize the *transmembrane* potential and other electrical properties of walled cells. I will introduce the technique and then describe the electrical properties of the cell. Finally, I will explore more sophisticated techniques, such as voltage clamp, which reveals the voltage dependence of *transmembrane* ionic currents.

5.1.1 The Basics of Intracellular Measurements

There are a number of books that describe intracellular measurements of the electrical properties of cells. Microelectrode construction and use are described by Thomas (1978), Purves (1981) and Blatt (1991). Ion-selective microelectrodes are described by Ammann (1986). The Plymouth Workshop Handbook (Ogden 1994) includes contributed chapters describing a variety of experimental techniques and analysis.

Impaling a cell with a microelectrode first requires fabrication of the micropipette. Details of fabrication techniques have been described extensively by Purves (1981). The micropipette tip must be sharp, with a diameter small enough so that it can penetrate the wall and plasma membrane with minimal damage to the cell. Micropipettes are fabricated using pipette pullers. These are commercially available from a number of vendors. A schematic of the technique is shown in Fig. 5.1. Briefly, a short length of capillary tubing is held at both ends (the upper end is fixed, the lower end is attached to a heavy weight), and a localized region at the center of the tube heated until the glass has softened. The weight slowly drops, stretching the glass tube, followed by a fast pull using a solenoid that separates the two ends of the capillary. The resulting tip is quite sharp, with dimensions in the range of 200–500 nm. Once pulled, the inside of the micropipette is filled with electrolyte (3 M KCl is commonly used). The electrolyte creates an electrically conductive pathway that is required for electrical measurements. Capillary tubing for micropipette fabrication contains an internal fiber that improves the ability to fill the very small bore at the sharp tip of the micropipette with the salt solution—avoiding air bubbles that would block electrical conductivity. The chloride ions in the KCl backfill solution function as part of an Ag–AgCl half-cell to connect the micropipette to an electrometer to measure the voltage. Silver chloride coating on the silver wire reacts *reversibly* with chloride ions in solution ($Ag + Cl^- <—> AgCl + e^-$) to create the electrical connection to the

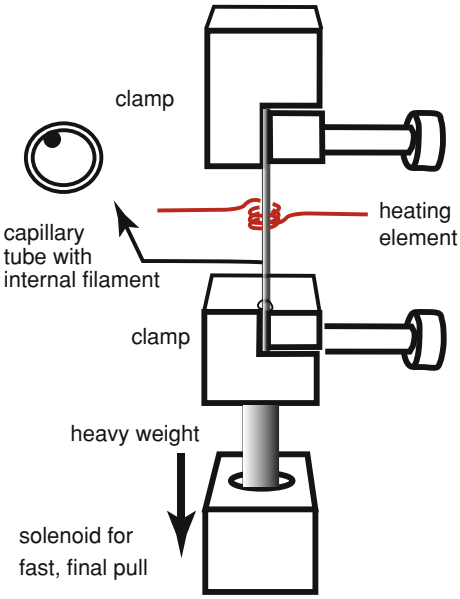

Fig. 5.1 Construction of a single barrel micropipette. A schematic of a typical setup for pulling a micropipette is shown. The capillary glass is clamped in a stationary clamp above, and a moveable clamp below a heating element. As the glass melts, the lower clamp drops down, initially by gravity alone, then with a strong pull (by activating a solenoid) to produce a sharp-pointed micropipette. The glass is borosilicate glass tubing with an internal filament; the internal filament assists filling with a conductive salt solution (usually 3 M KCl)

electrometer. A similar half-cell is connected to the extracellular solution with a salt bridge (usually 3 M KCl in agar) to form an electrical ground that completes the circuit to the electrometer.

Because of the small dimensions of the micropipette tip, its resistance is very high (in the range of 20–40 $\times$ 10^6 Ω). At such a high resistance, electrical noise from external sources can obscure the measured potentials, which is why the measuring apparatus is usually shielded from the external environment by a grounded metal enclosure known as a Faraday cage. The high resistance also requires that the voltage be measured with a high input impedance electrometer.

Impaling a small cell requires micromanipulators and isolation from mechanical vibration. Micromanipulators use mechanical, hydraulic, or piezoelectric mechanisms to allow fine positional control of the microelectrode tip at resolutions less than 1 micron. Both commercial and 'home-made' vibration isolation systems rely on a heavy (high inertia) tabletop made of metal or granite resting on top of 'shock absorbers' (pressurized air cylinders are commonly used).

Examples of impalements into algal, fungal, and plant cells are shown in Fig. 5.2. The cell diameters range from 8 to 100 μm. In all cases, the tip must puncture the wall, shown in Fig. 5.2a, where the micropipette tip bends before it 'pops' into the cell (the green alga *Eremosphaera viridis*). In Fig. 5.2b, the fact that the puncture site

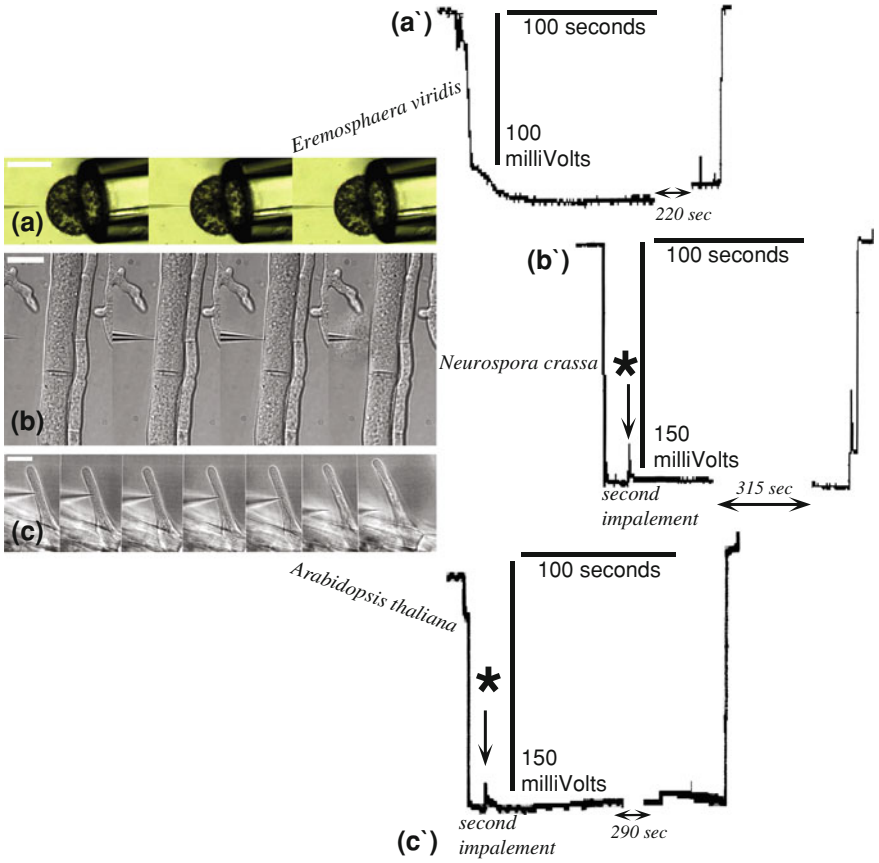

Fig. 5.2 Examples of intracellular impalements to measure the electrical properties of the cell. The three examples come from protists (**a** the chlorophyte *E. viridis*, bar = 100 μm), fungi (**b** the ascomycete *N. crassa*, bar = 20 μm), and a higher plant (**c** *A. thaliana*, bar = 20 μm). Examples of the electrical responses to impalement are also shown. In the impalement of *E. viridis* (**a′**), the voltage rapidly becomes negative, and then slowly becomes even more hyperpolarized, probably due to slow sealing at the impalement site. The examples for *N. crassa* (**b′**) and *A. thaliana* (**c′**) are both dual impalements. The second impalements (*starred arrows*) have no effect on the measured voltage. This indicates the high resistance at the impalement site, so high that shunt leakage does not cause a depolarized potential. Additional evidence for the electrical integrity of the seal at the impalement site is demonstrated in the micropipette removal from the *N. crassa* hypha. The high turgor causes blowout of cytoplasm from the hypha, but only after removal. Thus the seal at the impalement site resists pressures as high as about 600 kPa

is sealed against high pressure is demonstrated by the burst of cytoplasm out of the cell when the tip is removed (the fungus *Neurospora crassa*). That cells survive impalement quite well is demonstrated in Fig. 5.2c, in which the root hair (the higher plant *Arabidopsis thaliana*) continues growing after impalement. For the fungal and plant impalements, the electrical traces demonstrate another property of the

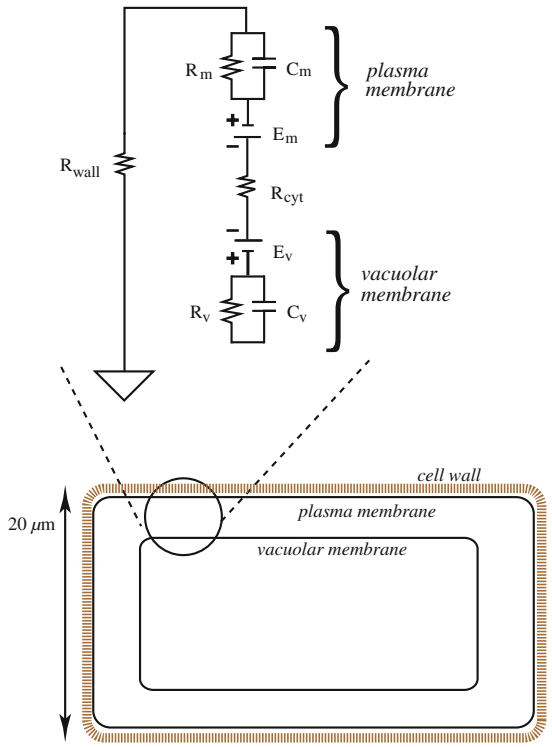

Fig. 5.3 Idealized electrical network of a walled cell. Resistances and capacitance and the potential are shown for both the plasma membrane and vacuole. The potential of the plasma membrane is usually in the range of 100–200 mV, negative inside. The vacuole is about 20 mV, positive inside. Capacitance of either membrane depends on the area; specific capacitance is about 10^{-2} μF m^{-2} for biological membranes

impalement. In both cases, the cell was impaled with a *second* micropipette at the vertical arrows. The second impalement had no effect on the measured potential (after a transient and small depolarization), indicating how well the micropipettes are sealed electrically. If there were significant damage and ion leakage at the impalement sites, the potential would have become depolarized, and remained depolarized.

Having Impaled the Cell, What are the Electrical Properties?

5.1.2 Electrical Network of a Walled Cell

The terms common to electronics —voltage, current, resistance, and capacitance— also describe the electrical properties of cells. The electrical network for an idealized walled cell incorporating these elements is shown in Fig. 5.3. Voltage, current, and resistance are related through Ohm's Law: $V = IR$, where V is the voltage (in Volts), I is the current (in Amperes), and R is the resistance (in Ohms, Ω). Typical values for a walled cell are a 'resting potential' of −0.15 V (negative inside). The 'resting potential' indicates that the net current is zero. This means that, although ion fluxes will be occurring, there is no *net* charge movement across the membrane. A typical cell resistance is in the range of 10–20 × 10^6 Ω. Larger cells have lower resistance

compared to smaller cells because the specific resistance is fairly constant (about 1.5 kΩ cm^2). Capacitance is a more complicated property. In simple terms, it is the ability (or capacity) of the cell to hold a net charge, similar to a battery. Cell capacitance is directly related to the area of plasma membrane at the cell boundary: the larger the cell, the higher the capacitance. The impact of capacitance is 2-fold. It affects how much net charge imbalance between the inside and outside of the cell is required to create the transmembrane potential. Net charge (Q, in Coulombs) is the product of the capacitance (C, Farads, or coulombs $volt^{-1}$) and the potential difference (ΔE, volts): $Q = C \cdot \Delta E$. For biological membranes, specific capacitance is about $10^{-2}\,F\,m^{-2}$; the specific capacitance is multiplied by cell area to obtain the capacitance. The charge can also be defined by the concentration of net charges. That is, the net charge (Q) is the product of the cell volume (V, in m^3), the net concentration of the ion (c_{ion}, in mole m^{-3}), and the Faraday constant (F, 96480 coulombs $mole^{-1}$, to convert coulombs to moles): $Q = V \cdot c_{ion} \cdot F$. Combining the two equations and solving for the net ion concentration: $c_{ion} = (C \cdot \Delta E)/(V \cdot F)$. For a typical cell with dimensions of $20 \times 20 \times 80$ μm, a net charge concentration of 3.5×10^{-3} mol m^{-3} (3.5 μM) will create a potential of 150 mV. This is a very small charge difference compared to the usual ion concentrations of the cell (about 200 mM). The other effect of capacitance is related to the time it takes to charge the membrane capacitance. The higher the capacitance, the longer it takes for the potential to change in response to net ion flow into or out of the cell. This places limits on the measurability of fast events. Capacitance can be harnessed in some techniques that use a single micropipette to measure *both* the potential and resistance of the cell plasma membrane. For example, the discontinuous voltage clamp (described below) relies on differences in the capacitances of the electrode and cell (and therefore the time responses) to separate the resistance of the cell from the resistance of the microelectrode impaled into the cell.

To measure the full range of electrical properties of the cell, it is necessary to have some means of both injecting current and monitoring voltage (so that two of the three terms of Ohm's Law are known). One such method is the patch clamp technique (Hamill et al. 1981). Patch clamp revolutionized the study of ion transport in cells, including animal, fungal, algal, and higher plant cells. The two major discoverers, Erwin Neher and Bert Sakmann, were awarded the Nobel Prize in 1991. The power of the patch clamp technique was 2-fold. First, it allowed individual ion channels to be measured in situ, in their natural state in the membrane. Second, with the whole cell mode, it enabled the experimenter to extend the range of possible measurements: to examine the voltage and time dependence of ionic currents, and use this information to identify the specific ions contributing to the current. With patch clamp, a wealth of information has been uncovered about the molecular foundations of ionic transport in cells.

There is a drawback to the use of patch clamping of plants, algae, and fungi. When the patch clamp technique is used to measure ionic currents in walled cells, the wall must first be removed to expose the plasma membrane to the patch pipette. To avoid lysis, the cell must be held in a solution of osmolarity high enough to induce plasmolysis. This is necessary whether the wall is removed by enzymatic digestion or some other technique, such as laser ablation. This means

that the advantage of patch clamp —to examine the voltage and time dependence of ion transport across the plasma membrane— is offset by the non-physiological condition of the cell: plasmolyzed and probably attempting turgor recovery. Certainly not growing, certainly in an abnormal physiological state, the plasmolyzed cell is a technical problem that can obscure the relevance of patch clamp measurements. The ideal way to overcome this is to perform measurements of the voltage and time dependence of ionic currents in intact, turgid, possibly even growing cells. But how can this be done in an intact cell?

5.2 Voltage Clamping Intact Turgid Cells

Voltage clamp is the technique of choice to measure the voltage and time dependence of ionic currents across the plasma membrane. There are three ways to voltage clamp intact turgid cells: discontinuous voltage clamp, dual impalements, and double barrel micropipettes. In all instances, the intent is to measure the voltage and time dependence of the plasma membrane ionic currents separate from any contribution of the micropipette itself. The micropipette resistance is a significant problem, because the resistance at the tip of the micropipette is often similar in magnitude to the resistance of the plasma membrane. This can cause an inability to separate the voltage and time dependence of ionic currents through the micropipette tip from the ionic currents through the plasma membrane.

5.2.1 Discontinuous Voltage Clamp: A Single Barrel Used for Both Current Injection and Voltage Monitoring

Finkel and Redman (1984) described the discontinuous single microelectrode voltage clamp technique. The technique has been used successfully in intact higher plant cells. The basic idea is that the time dependence of electrical currents at the microelectrode tip is very different from those of the plasma membrane because the capacitance of the micropipette tip is much lower than the capacitance of the cell membrane. This will cause a much faster time response, τ, defined as resistance (R) · capacitance (C): $\tau = R \cdot C$. By rapidly switching between current injection and voltage measurements, it is possible to separate *temporally* the contribution of the micropipette from the contribution of the plasma membrane, as long as $\tau_{electrode} < \tau_{cell}$. A set of papers using the discontinuous single electrode voltage clamp technique illustrates the technique and problems. Forestier et al. (1998) explored the use of the technique to identify slow anion currents in guard cells. The advantage of the technique was that measurements could be done in intact cells. Since guard cells change their turgor in response to different stimuli to control stomata aperture in the epidermis of the leaf, intact cells offer much greater

insight into ion transport required for turgor changes compared to the turgor-less protoplasts used for patch clamp. In the discontinuous single electrode voltage clamp technique, it is necessary to electronically compensate for the capacitance of the electrode. Roelfsema et al. (2001) raised doubts about the applicability of the discontinuous single electrode voltage clamp technique in small cells, like guard cells, because the low capacitance of small cells would be similar to the capacitance of the electrode ($\tau_{electrode} \sim \tau_{cell}$); thus, a clear separation of the contribution of the electrode and cell would be difficult. Raschke et al. (2003) confirmed the results of Forestier et al. (1998), noting that it is crucial to use micropipettes that possess a linear current–voltage relation to assure that their capacitance can be compensated electronically. That is, the resistance must be voltage independent to assure $R \cdot C$ is constant for all clamped voltages. Although others have used this technique, the three papers cited above give a flavor of the doubts associated with the method. There are two issues: whether it is electronically possible to compensate for the electrode capacitance (or more accurately, time response, $R \cdot C$) consistently, and whether the properties of the microelectrode tip are the same before and during insertion into the cell. In fact, Etherton et al. (1977) explored the latter question by directly comparing membrane resistance measurements obtained using two electrodes impaled separately into the same cell with single electrode impalements. They expressed the concern that the properties of the single electrode change upon impalement, rendering the technique questionable. Guard cells do not lend themselves to multiple impalements, so the discontinuous voltage clamp technique remains a useful technique to avoid the protoplasting required to patch clamp the cell, with caveats regarding the quality of the data. Supporting evidence, such as inhibitor effects (Forestier et al. 1998; Bouteau et al. 1999), bolsters interpretation of the data.

5.2.2 Dual Impalements

Etherton et al. (1977) assumed that dual impalements with a voltage monitoring electrode and a current-injecting electrode were the "standard by which the accuracy" of single electrode techniques "could be judged". Since the two processes, voltage monitoring and current injection, are separate, this is a likely assumption. One concern exists that multiple impalements may affect the resistance of the plasma membrane due to membrane damage caused by the impalements, but Lew (2000) presented evidence discounting this possibility, at least in root hairs, by showing that multiple impalements do not cause a decrease in the potential, which means that the impalement site is not a source of significant ionic leakage. Supporting evidence is shown in Fig. 5.2. Multiple impalements are technically difficult. The cells must be accessible, and good imaging is very helpful, to ensure the micropipettes are impaled into the same cellular compartment. Indeed, the 'standard' to assure where the tips are located is fluorescent dye injection (Holdaway-Clarke et al. 1996). Because only a single impalement into

the cell is required, double barrel micropipettes offer technical advantages, while retaining separation of the voltage and current-injecting microelectrodes.

5.2.3 Double Barrel Micropipettes

A number of researchers have used double barrel micropipettes over the years. In fungi, Michael Blatt and others used them to perform voltage clamping of the filamentous fungus *N. crassa* (Blatt and Slayman 1983, 1987). Blatt subsequently used the technique in guard cells (Blatt 1987) and wrote a primer on double barrel micropipettes and other electrophysiological techniques (Blatt 1991) that I recommend highly for new and experienced electrophysiologists.

5.3 Double Barrel Micropipette Fabrication

The fabrication of double barrel micropipettes involves a sequential set of steps that are best performed by fabricating a batch of micropipettes at the same time. Borosilicate capillaries with internal filaments are first cut to an appropriate length (about 7 cm). We use 1 mm OD, 0.58 mm ID tubing. The two capillaries are inserted into a micropipette puller in which one of the two clamps on either side of the heating filament can be rotated (Fig. 5.4). When the heating filament has softened the glass, the capillaries are rotated 360° to create a twist in the glass. Then standard pulling protocols are used to pull the micropipette. Once pulled, a small amount of fast-setting epoxy is applied just above the twist to strengthen the fused joint between the two capillaries. Finally, one of the barrels is heated and pulled away to form a Y-shape. This eases insertion of one of the barrels of the micropipette into a holder, and insertion of a chlorided silver wire into the other barrel. Photographs of the fabrication steps are shown in Fig. 5.4c.

Typically, we fabricate 8–10 of the double barrel micropipettes at the same time. First, all are pulled. Then epoxy is applied. When hardened, one barrel is pulled away to form a Y. Then they are stored in a covered dish until used. Fabrication takes about 1–2 h.

One problem that can arise is crack formation in one of the glass barrels, probably during the twisting if the glass has not softened enough during heating. The cracks are not visible (except as a stress crack under magnification), but reveal themselves when the micropipettes are being tested for tip resistance and crosstalk just prior to impalements. At this time, the crack causes an extremely low resistance in one of the barrels, far less than the normal 20 MΩ.

Filling of the micropipette barrels with electrolyte is done as with a single barrel electrode. A small amount of electrolyte is injected into the blunt end of capillaries; 10 min later, the tip would have filled due to capillary action of the internal filament. Even the glass twist would have filled. Backfilling of the bent barrel requires a fine gauge needle, so that it can be easily inserted past the bend right up to the twist.

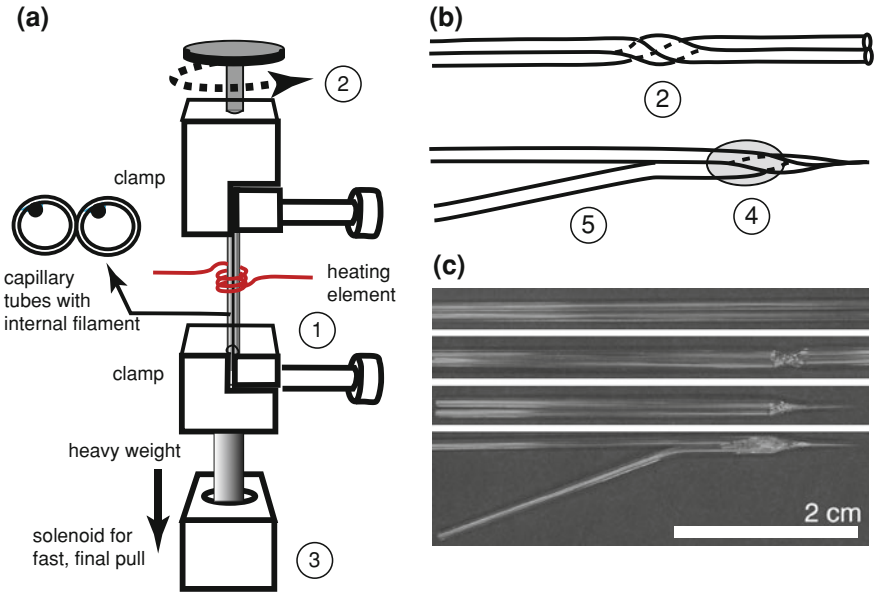

Fig. 5.4 Construction of a double barrel micropipette. **a** First, the two capillaries—held together by clamps above and below a heating element *1*—are heated in a localized region. When the glass has softened, the two capillaries are twisted by rotating one of the clamps 360° *2*. The two capillaries are then pulled to form the sharp tip *3*, and removed from the pipette puller. **b** A drop of fast-setting epoxy is applied to the joint between the two barrels at the fused twist to strengthen the joint *4*. Finally, one of the capillaries is softened by localized heating and pulled away to produce a Y-shape *5*. The photo inset **c** shows the two capillaries, twisted together in the second panel, pulled in the third panel, and after final fabrication in the fourth panel. Bar = 2 cm

5.3.1 Limitations

There are limitations to the use of double barrel micropipettes due to crosstalk and the localized nature of the current injection and voltage monitoring.

5.3.1.1 Crosstalk Between Barrels

In a double barrel micropipette, the glass wall separating the two barrels is twice the thickness of the outer glass walls (Fig. 5.5a). However, there is a possibility of some current 'leakage' across the wall. The response of both barrels to a current injected through one barrel is shown in Fig. 5.5b. There are voltage deflections in the second barrel. Initially, there is a capacitance spike due to capacitative coupling between the two barrels (Fig. 5.5c), followed by a steady-state deflection of very small magnitude. The deflection, expressed as a % coupling ($100 \cdot (\Delta E_2/\Delta E_1)$) is about 1–2% (Fig. 5.5d).

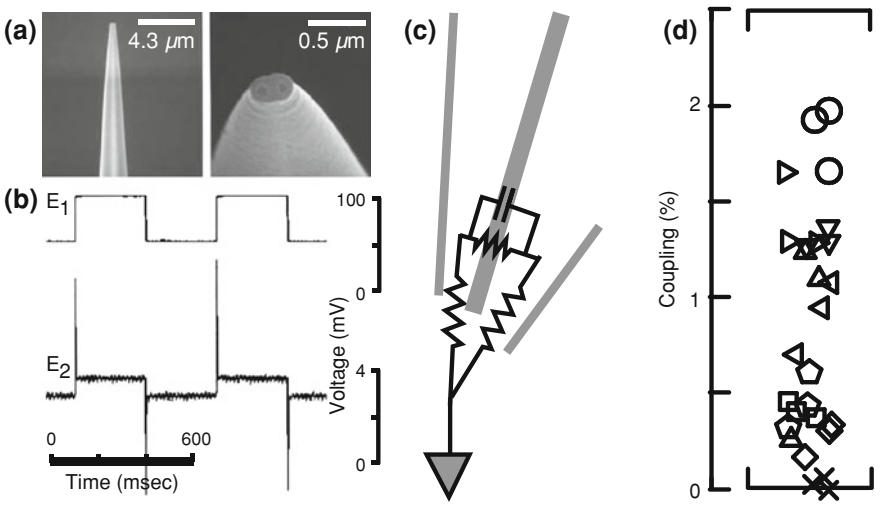

Fig. 5.5 Electrical properties of the double barrel micropipette. **a** Scanning electron microscopy of double barrel micropipette tip (*left* tip shape; *right* tip apertures). Note the double thickness of glass between the two apertures. Bars 4.3 and 0.5 μm, as shown. **b** Voltage response of the two barrels (E_1 and E_2) to a 2 nA peak to peak current injected into the first barrel (E_1). The large voltage deflection in the first barrel is due to the resistance of the micropipette tip, 25 MΩ in this example. Some of the current 'leaks' across the glass barrier between the two barrels, causing a much smaller voltage deflection in the second barrel (E_2, about 1 mV). Spikes at each step transition in the current injection are caused by the capacitance of the glass barrier between the two barrels. The measurements were performed with 3 M KCl filling the barrels, and 150 mM KCl in the external solution to mimic the ionic conductivity of the cytoplasm. Grounding was with a chlorided silver wire. The resistive network is shown in **c**. By measuring the resistance of each barrel, and the amount of 'coupling' between the barrels ($100 \cdot (\Delta E_2/\Delta E_1)$)(**d**), it was possible to estimate the value of the resistance of the glass barrier between the two barrels. The value ranged from 500 MΩ to 100 GΩ, the median value was 3 GΩ. This is consistent with the known resistivity of borosilicate glass, about 10^{15} Ω · cm. With an estimated barrier thickness of 100 nm, the calculated resistance would be 10 GΩ

5.3.1.2 Maximal Current Injection

As a consequence of the crosstalk between the two barrels, double barrel micropipettes are not suitable for measurements requiring large current injections. A 2 nA current causes a very small voltage deflection in the second barrel, but a μA current will cause a deflection large enough to affect measurements in walled cells, whose membrane potentials range from −50 to −200 mV. Thus, double barrel micropipettes are not suitable for measurements, where μA currents are required, such as the large green algae *Chara* and *Nitella*, although larger micropipette apertures may be a solution.

5.3.1.3 Space Clamping

Another problem associated with large cells is the incomplete 'spread' of voltage throughout the cell. When voltage clamping, the cell may not attain the specified voltage, this is incomplete space clamping. It is a problem for double barrel microelectrodes, because current injection and voltage monitoring occur in the same region within the cell. Incomplete space clamping should not be a problem for small, electrically isolated cells (such as guard cells). However, with large cells, or when there is electrical coupling between cells, the problem is pervasive. Under these conditions, quantitation requires multiple impalements, and correction depends upon assumptions about current spread and cell geometry. There is no simple authoritative solution. Examples of space clamping problems are shown for different cell types later in the chapter.

5.4 Use: Electronics and Computer Control

There are many resources describing electronics and computer control of experiments. Purves (1981) is a classic, still timely today. Ogden (1994) includes very useful contributions on microelectrodes, voltage clamping techniques, and computer control. For versatility, we use digital oscilloscopes to monitor experiments and print a copy of recordings. For computer control: Analog/digital converters for measuring voltage and clamping currents, digital/analog converters for controlling the clamped voltage, digital input/output to switch voltage clamping on, and timers to control the duration of the voltage clamp are all supplied by a Labmaster board from Scientific Solutions (Solon, Ohio). The required software is written in C, compiled and run on a DOS computer. While this may seem anachronistic, the advantage for us is complete control of the experimental environment, including the CPU cycles of the computer. The technical specifications for hardware control have not changed, so newer systems offer little advantage. For new or experienced electrophysiologists, writing the software programs may be too daunting. If this is so, turnkey systems are available from many vendors at a significant cost. The latest development is the inclusion of a DSP (digital signal processor) chip in a stand alone system for performing measurements and voltage clamp.

5.4.1 Electrometers and Voltage Clamp Circuit

Any electrometer with sufficiently high input impedance ($>10^{11}$ Ω) will work. It is important to assure that the time responses of the voltage and current-injecting headstages are the same; thus, the input impedances should be matched. A voltage clamp circuit is connected to the electrometers. A schematic of the electronic circuit is shown in Fig. 5.6.

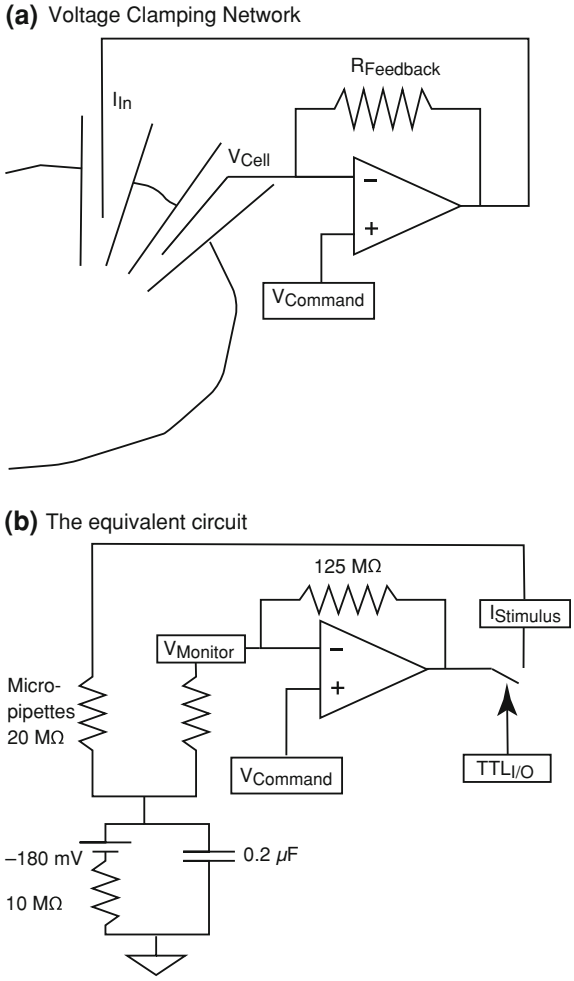

Fig. 5.6 Voltage clamping schematic. **a** If we specify $V_{Command,}$ the operational amplifier will drive whatever current is necessary into the feedback system (the cell and feedback resistor $R_{Feedback}$) to maintain V_{Cell} at $V_{Command}$. **b**. A more detailed equivalent circuit. The $TTL_{I/O}$ is a switch relay controlled by the computer to turn on the voltage clamping circuit. The V_{Cell} is measured at the electrometer ($V_{Monitor}$). The current is injected via the $I_{Stimulus}$ input of another electrometer. The feedback resistor in this example is very high (125 MΩ) and assures a fast response by the operational amplifier so that V_{Cell} is rapidly clamped with high fidelity

5.5 Examples of Measurements

Examples of measurements in walled cells can include any situation, where current injection and voltage measurements must be kept separate. A variety of types of measurements in walled cells are described below. It is important to emphasize

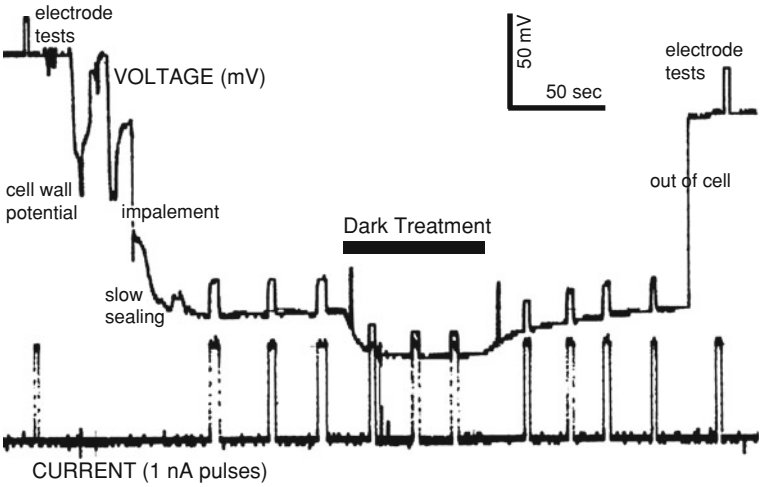

Fig. 5.7 Input resistance measurements from a mesophyll cell of *C. richardii*. Both voltage (*top trace*) monitored with one barrel of the double barrel micropipette and current (*lower trace*) injected through the other barrel are shown. Prior to and after the experiment, electrode tests were conducted to assure there was no electrical crosstalk between the voltage monitoring and current-injecting electrodes. Current injection through the voltage monitoring electrode causes a voltage deflection as expected, but current injection through the current-injecting electrode caused no visible deflection in the voltage monitoring electrode. Immediately following impalement, confirmed visually, a transient negative spike is followed by a slow sealing event that is characterized by a gradual hyperpolarization to a stable potential. After impalement, current injection through one barrel of the double barrel micropipette causes a voltage deflection in the other barrel due to the resistance of the plasma membrane. This confirmed that the impalement was successful. The response of the cell to changes in photosynthesis is documented in this experiment. Removal of the pipette from the cell results in a rapid depolarization to a value similar to what was observed before the cell was impaled

that, like any technique, double barrel micropipettes may not be sufficient to resolve the electrical properties of a cell. Some of these issues are outlined in the following examples.

5.5.1 Input Resistance

By injecting a known current through one barrel, the magnitude of the voltage deflection in the other barrel can be used to calculate the resistance of the cell. If the geometry of the cell is known, then the specific resistance can be calculated. An example of such a measurement is shown in Fig. 5.7, from a mesophyll cell of a *Ceratopteris richardii* gametophyte. In these cells, dye injected into the cell was distributed throughout the cytoplasm and did not migrate into adjacent cells, indicating that the impalement was cytoplasmic, and that cell-to-cell coupling was minimal. Having measured the mesophyll cell dimensions, the specific resistance could be calculated: about 1.5 $k\Omega \cdot cm^2$.

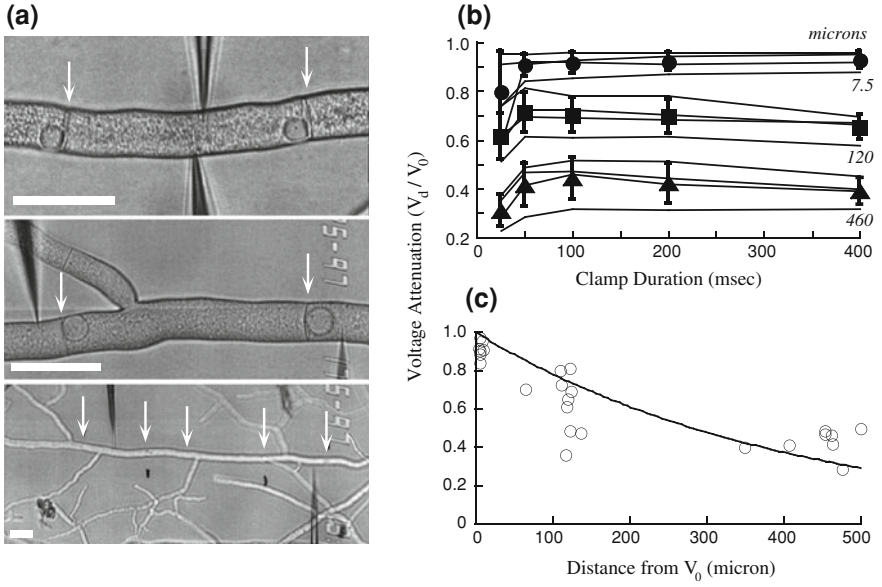

Fig. 5.8 Current–Voltage measurements: The effect of cable properties. The example is for hyphal trunks of the fungus *N. crassa*. **a** Examples of impalements with varying distances between impalement sites (Bars = 20 μm). One of the micropipettes was double barreled, the other single barreled. Voltage clamping was performed with the double barrel microelectrode, and voltage deflections in the single barrel microelectrode were used to determine the magnitude of voltage attenuation (V_d/V_0 where V_d is the voltage measured with the single barrel microelectrode and V_0 the voltage measured with the double barrel microelectrode). **b** Time-dependent changes in clamping current were complete within 100 ms. **c** The voltage attenuation can be fit to an exponential function to determine the length constant for the hypha —the degree of voltage attenuation, which will depend upon the extent of current leakage out of the hypha as distance increases: $V_d/V_0 = e^{(x/-\lambda)}$, where x is the separation distance and λ is the length constant. To correct for current attenuation and obtain current density (I_m in units of A m^{-2}), the cable current (i_m in units of A m^{-1}) is calculated ($i_m = I/2\lambda$, where I is the current, and the term 2λ accounts for the current attenuation in both directions), then the current density ($I_m = i_m/(\pi d)$, where πd accounts for the effect of hyphal diameter) (Rall 1977; Lew 2007)

5.5.2 Current–Voltage Relations

An example of a current–voltage measurement using voltage clamping is shown in Fig. 5.8, using trunk hyphae of the fungus *N. crassa*. The measurement illustrates not only the voltage clamp technique, but also the issue of space clamping and time dependence. A hyphal compartment was impaled with a double barrel micropipette, and the same hypha impaled with a single barrel microelectrode at various distances from the first impalement. Although voltage fidelity was observed when the two micropipettes were within 10 μm of each other, current

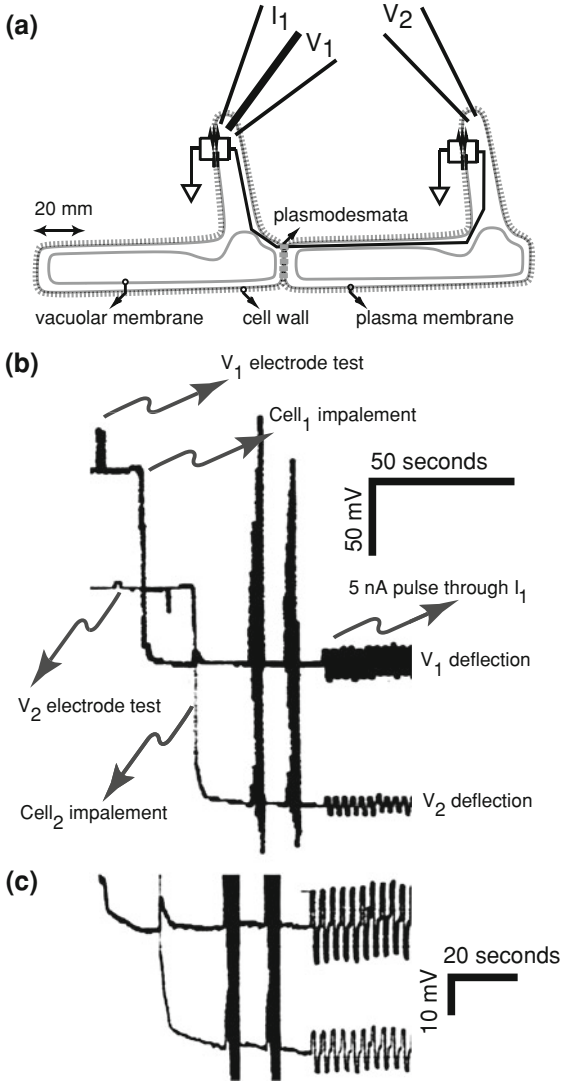

Fig. 5.9 Example of cell-to-cell coupling measurement. This example is for two root hairs adjacent to each other on a longitudinal file of an *A. thaliana* root. **a** Diagrammatic representation of cell-to-cell coupling through plasmodesmata. **b** As marked, $Cell_1$ is impaled with a double barrel electrode, followed by a separate impalement into $Cell_2$. A 5 nA pulse through the current-injecting electrode in $Cell_1$ results in a voltage deflection in both $Cell_1$ and in $Cell_2$, due to coupling through plasmodesmata. **c** A higher magnification segment of the traces shown in **a** Regulation of cell-to-cell coupling between root hairs was described by Lew (1994)

leakage through the plasma membrane causes an attenuated voltage clamp along the hypha. Cable theory can be used to correct for current attenuation in fungal hyphae (Gradmann et al. 1978; Lew 2007).

5.5.3 Cell-to-Cell Coupling

An example of the use of double barrel micropipettes to measure electrical coupling through plasmodesmata is shown in Fig. 5.9. The example is adjacent root hairs on an *A. thaliana* root. Analogous to fungal hyphae, electrical connections between cells results in significant current passage into adjacent cells, resulting in an overestimate of the clamping current in voltage clamp measurements.

5.6 Summary

Electrophysiological analyses of ion transport in walled cells are essential to our understanding of the life of the cell. Ion transport plays crucial roles in regulating the intracellular milieu of the cell, in signal transduction, osmotic regulation, and cellular growth. A detailed characterization of the electrical properties of the cells relies upon multiple techniques, among them, voltage clamping is very useful. Voltage clamping with double barrel micropipettes is especially important given the 'physiology problem' associated with patch clamp measurements on plasmolyzed protoplasts. Technical constraints and accessibility of the cell make voltage clamping a challenging endeavor, but double barrel micropipettes offer increased technical ease, simplifying the challenges faced by the researcher when working with intact cells. However, it should be clear from the examples presented in this chapter that double barrel micropipettes are not an absolute solution, but instead another step in our efforts to discover the roles of ion transport in cellular functions.

References

Ammann D (1986) Ion-selective microelectrodes. Principles, design and application. Springer, Berlin, pp 1–346

Blatt MR, Slayman CL (1983) KCl leakage from microelectrodes and its impact on the membrane parameters of a nonexcitable cell. J Memb Biol 72:223–234

Blatt MR, Slayman CL (1987) Role of "active" potassium transport in the regulation of cytoplasmic pH by nonanimal cells. Proc Natl Acad Sci USA 84:2737–2741

Blatt MR (1987) Electrical characteristics of stomatal guard cells: the ionic basis of the membrane potential and the consequence of potassium chloride leakage from microelectrodes. Planta 170:272–287

Blatt MR (1991). A primer in plant electrophysiological methods. In: Hostettmann K (ed) Methods in plant biochemistry. Volume 6. Assays for bioactivity. Academic Press, London. (xi and 360 pages), pp 281–321 (ISBN: 0124610161)

Bouteau F, Pennarun A-M, Kurkdjian A, Convert M, Cornel D, Monestiez M, Rona J-P, Bousquest U (1999) Ion channels of intact young root hairs from *Medicago sativa*. Plant Physiol Biochem 37:889–898

Etherton B, Higinbotham N (1960) Transmembrane potential measurements of cells of higher plants as related to salt uptake. Science 131:409–410

Etherton B, Keifer DW, Spanswick RM (1977) Comparison of three methods for measuring electrical resistances of plant cell membranes. Plant Physiol 60:684–688

Finkel AS, Redman S (1984) Theory and operation of a single microelectrode voltage clamp. J Neurosci Meth 11:101–127

Forestier C, Bouteau F, Leonhardt N, Vavasseur A (1998) Pharmacological properties of slow anion currents in intact guard cells of *Arabidopsis*. Application of the discontinuous single-electrode voltage-clamp to different species. Pflügers Arch 436:920–927

Gradmann D, Hansen U-P, Long WS, Slayman CL, Warncke J (1978) Current-voltage relationships for the plasma membrane and its principal electrogenic pump in *Neurospora crassa*: steady-state conditions. J Memb Biol 39:333–367

Hamill OP, Marty A, Neher E, Sakmann B, Sigworth FJ (1981) Improved patch-clamp techniques for high-resolution current recording from cells and cell-free membrane patches. Pflügers Arch 391:85–100

Holdaway-Clarke TL, Walker NA, Overall RL (1996) Measurement of the electrical resistance of plasmodesmata and membranes of corn suspension-culture cells. Planta 199:537–544

Lew RR (1994) Regulation of electrical coupling between *Arabidopsis* root hairs. Planta 193:67–73

Lew RR (2000) Electrobiology of root hairs. In: Ridge RW, Emons AMC (eds) Root hairs. Cell and molecular biology. Springer, Tokyo, pp 115–139

Lew RR (2007) Ionic currents and ion fluxes in *Neurospora crassa* hyphae. J Exp Bot 58:3475–3481

Ogden D (ed) (1994) Microelectrode techniques. The plymouth workshop handbook. The company of biologists, Cambridge. p 448

Purves RD (1981) Microelectrode methods for intracellular recording and ionophoresis. Academic, London, p 146

Raschke K, Shabahang M, Wolf R (2003) The slow and quick anion conductance in whole guard cells: their voltage-dependent alternation, and the modulation of their activities by abscisic acid and CO_2. Planta 217:639–650

Rall W (1977) Core conductor theory and cable properties of neurons. In: Kandel ER (ed) Handbook of physiology. Vol. 1 (Cellular Biology of Neurons, Part 1). American Physiological Society. Bethesda. pp 39–97

Roelfsema MRG, Steinmeyer R, Hedrich R (2001) Discontinuous single electrode voltage-clamp measurements: assessment of clamp accuracy in *Vicia faba* guard cells. J Exp Bot 52:1933–1939

Slayman CL, Slayman CW (1962) Measurements of membrane potentials in Neurospora. Science 136:876–877

Thomas RC (1978) Ion-sensitive intracellular microelectrodes. How to make and use them. Academic Press, London, New York, San Francisco. xiii and p 110

Chapter 6
Making Contact and Measuring Cellular Electrochemical Gradients

Electrochemical Methods and Ion-Selective Electrodes in Plant Physiology

Anthony J. Miller

Abstract Reporting a voltage requires an electrical circuit that includes a voltmeter with contact to the biological material provided by an electrode. These electrodes can be metal or glass pipettes filled with a conducting salt solution. An ion-selective electrode contains a membrane in the tip of the glass pipette and is responsive to the activity (not concentration) of the ion sensed by the selective membrane. These electrodes can be made with tips of around 10^{-6} m diameter suitable for insertion measurements inside the cells of intact tissues and plants. This chapter describes how to make and use the electrodes for intracellular measurements in plants. Four stages of ion-selective microelectrode fabrication can be defined, and these are: (1) pulling of glass micropipettes, (2) silanization of the inside of surface of the ion-selective electrode or barrel, (3) backfilling and (4) calibration. Like all methods, there are both advantages and disadvantages in using microelectrodes to measure cellular electrochemical gradients and these are compared and discussed in relation to other available techniques.

6.1 Methods for Electrical Recordings From Plants

6.1.1 Making Contact

The reporting of a voltage requires a complete electrical circuit or ring that includes the measuring device, a voltmeter, or electrometer. The electrical contact to the biological material is provided by an electrode. This interface between the plant

A. J. Miller (✉)
Department of Metabolic Biology, John Innes Centre,
Norwich Research Park, Norwich, NR4 7UH, UK
e-mail: tony.miller@jic.ac.uk

A. G. Volkov (ed.), *Plant Electrophysiology*,
DOI: 10.1007/978-3-642-29119-7_6, © Springer-Verlag Berlin Heidelberg 2012

tissue and electrometer is very important as ideally it should provide a low electrical resistance pathway that does not interfere with the cells being measured. The word microelectrode is commonly used to describe a glass micropipette which is pulled into a fine tip at one end and filled with an aqueous salt solution. The junction between the salt solution inside the microelectrode and the input to the electrometer amplifier is provided by a half-cell. There are different types of half-cells, but usually the metal contact electrode is AgCl-coated Ag wire and the salt solution is 0.1 M KCl (e.g. World Precision Instruments, Sarasota, FL http://www.wpiinc.com/). The micropipette provides a salt bridge between the inside of a living cell and the metal contact in the half-cell. The simplest microelectrodes measure voltage and when inserted into cells measure the membrane potential between the inside and outside of the cell. Typically, a plant cell membrane potential is between −100 and −200 mV, but the value depends on the solution bathing the cell. The metal contact can be made directly to the cell or tissue surface, but this type of electrode can be subject to various types of interference as the surface can be coated by plant material that will influence the stability and size of the electrical potential reported. This problem is much less likely to occur when the tip is constructed from glass that has been heated and pulled into a small fine tipped microelectrode. A small tip also provides less intrusion and interference for the biological tissue or cells being examined.

An *ion-selective* microelectrode contains an ion-selective membrane in the tip of the glass micropipette and is responsive both to the membrane potential and the activity (not concentration) of the ion sensed by the selective membrane. To make intracellular measurements it is also necessary to simultaneously measure the membrane potential either by insertion of a second electrode or, for small cells, by combining the ion-selective and voltage measuring electrodes into a *double-barreled microelectrode* (see Fig. 6.1). To be able to measure several different ions it may be necessary to combine together several different electrodes to make multibarreled electrodes (e.g., Walker et al. 1995).

Solid metal electrodes have been used to directly report from plant material and for some types of specialist uses such as measurements of electrical current in oxygen electrodes. Metal electrodes are usually made from Ag or platinum and these solid-state electrodes have been used to make ion-selective microelectrodes (see Sect. 6.2.2). Metal electrodes have also been used for direct recording from the surface of plants to measure extracellular transient electrical signals such as those elicited by external signals, e.g. wounding. The interface between the plant material and a metal recording electrode may also be made by a salt bridge using a wick electrode. The wick can be made of fiber, for example, paper or cotton thread soaked in salt solution (e.g., Wildon et al. 1992).

6.1.2 Recording from Plants

Electrophysiology recordings require solid anchoring of the plant material while at the same time preserving the normal state and environment of the material as far as

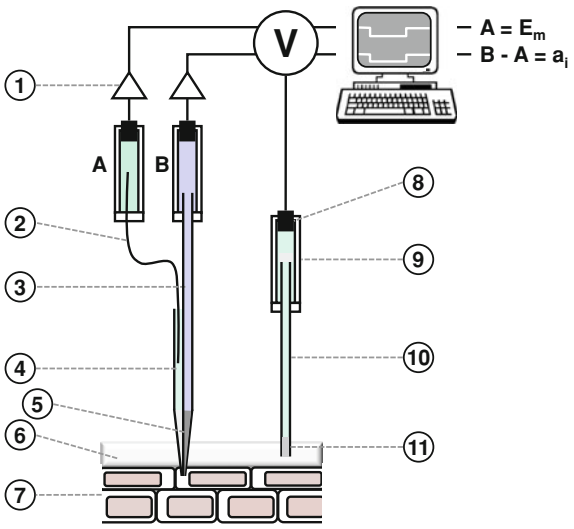

Fig. 6.1 Diagrammatic representation of the circuit required for double-barreled ion-selective microelectrode measurements. Key: *1* headstage signal amplifier, *2* Ag/AgCl coated Ag wire, *3* glass ion-selective barrel, *4* glass cell membrane potential barrel filled with 0.1 M KCl, *5* ion-selective sensor plug in the tip, *6* nutrient solution bathing plant, *7* plant tissue with microelectrode tip in a cell (cytoplasm), *8* Ag/AgCl chloride coated pellet, *9* half-cell, *10* salt bridge, *11* porous glass frit or agar plug

possible. It is best to avoid dissecting the plant material as this is likely to lead to local wounding that is known to have major effects on gene expression (Zeller et al. 2009). Plants grown in hydroponic culture can be easily transferred to the microscope stage for electrode impalements of either root or leaf tissue. The hydroponic environment for roots is easily maintained on the stage of a microscope, but leaves are more difficult requiring some wet contact between the tissue and the bathing solution. Microelectrode impalements are usually made under a microscope using long working distance objectives that allow sufficient space for microelectrode access. Although they are generally used for patch-clamp experiments, inverted microscopes are not so suitable for this type of work. Dissecting microscopes can be used for microelectrode impalements but they usually do not have sufficient magnification to see individual cells. They can be used for impalements by letting the electrical recording show when tissue contact has been made, and a successful impalement can be gaged by the size of the membrane potential measured. Microelectrodes are mounted on micromanipulators for cellular impalement to allow the delicate movement of the tip into a cell. There are a range of different types and hand control of tip movement is achieved by either joystick or rotational manipulation. The size and fine movement axis should be chosen so that the micromanipulator can be conveniently positioned alongside the microscope stage for tissue impalement.

Plant tissue is usually mounted in a purpose-built chamber for microelectrode impalements. The chamber is usually made from Plexiglass and is constructed so that the tissue can be perfused with nutrient solution throughout the experiment. This perfusion through the chamber helps prevent large local concentration gradients (unstirred layers) of ions developing around cells. Treatments can be applied to the tissue during a recording by changing the composition of the nutrient solution bathing the tissue. The chamber design is very important and it is worth investing time in this aspect of the experimental system. If the tissue is not well anchored in position it is impossible to achieve good electrical recordings. Each type of tissue usually requires a purpose built chamber but published work often does not report the details of this key aspect of the experimental system. The general principles of chamber construction have been reviewed previously (see Blatt 1991) and a chamber for leaf measurements has been described (Miller et al. 2001).

The diagram in Fig. 6.1 shows some of the equipment needed for microelectrode recording and the more complete list is as follows:

- Voltmeter (also known as an electrometer)
- Microscope (with long working distance objectives)
- Micromanipulator
- Tissue chamber (for holding and perfusion)
- Data logging system (e.g., computer or chart recorder)
- Vibration-free table (for microscope and micromanipulator to avoid interference from external vibration sources)
- Faraday cage (electrical screening around the microscope and micromanipulator especially necessary for high resistance electrodes)
- Oscilloscope (not essential but useful for fixing recording noise problems).

6.2 Manufacture and Use of Ion-Selective Electrodes

Ion-selective microelectrodes are used to measure ion gradients across membranes. These measurements can be made outside and inside cells. For example, ion fluxes at the surface of roots can be measured using ion-selective microelectrodes (Henriksen et al. 1990) or by using a vibrating ion-selective probe (Kochian et al. 1992). Intracellular measurements have been used to give important information on the compartmentation of nutrients, dynamics of cellular ion activities (e.g., in intracellular signaling) and transport mechanisms, particularly the energy gradients for ion transport. The main criticism of intracellular measurements made with microelectrodes is that they report the ion activity at a single point within the cell. This will result in incomplete information if there are significant ion gradients within the cytoplasm of a single cell. The chief advantages of using ion-selective microelectrodes are that:

- They offer a nondestructive method of measuring ions within cells
- They do not change the activity of the ion being measured
- They permit simultaneous measurement of the electrical and chemical gradients across membranes
- They are relatively cheap when compared to other methods for measuring intracellular ions and once purchased the same equipment can be used to measure a range of different ions.

6.2.1 Theory of Ion Selective Electrodes

The theoretical background has already been described by many authors (e.g., Ammann 1986, and references therein) and will only be outlined here. The properties of an ion-selective microelectrode are defined by several characteristics:

- Detection limit
- Selectivity
- Slope
- Response time.

The ideal relationship between electrode output (mV) and the activity (a_i) of the ion of interest (1) is log-linear and is described mathematically by the Nernst equation. Calibration of the electrode against a range of standard solutions should ideally yield a slope (s) of 59 mV (at 25 C) per decade change in the activity of a monovalent ion. In practice, however, the situation is more complicated than this because no ion-selective electrode (ISE) has ideal selectivity for one particular ion and under most conditions there is more than one ion present in the sample solution. Hence, contributions to the overall electro-motive force (EMF) made by each interfering ion j, must be taken into account. In this situation, the Nicolsky–Eisenman equation, a modified Nernst equation, describes the EMF:

$$\text{EMF} = E + s \cdot \log\left[a_i + K_{ij}^{\text{pot}}\left(a_j\right)^{\text{zi/zj}}\right] \tag{6.1}$$

where K_{ij}^{pot} is the selectivity coefficient of the electrode for the ion i with respect to ion j. This term expresses, on a molar basis, the relative contribution of ions i and j to the measured potential.

The parameters s and K_{ij}^{pot} are the two main characteristics defining any type of ion-selective electrode. The slope should be a near ideal Nernstian response when an electrode is calibrated against ion activity, but s is temperature sensitive (see Sect. 6.2.4). The selectivity coefficient measures the preference of the sensor for the detected ion i relative to the interfering ion j. It can be determined by the separate solution method, the fixed interference method or the fixed primary ion method. For ideally selective membranes, or for samples containing no other ions with the same net charge as the ion in question, K_{ij}^{pot} must be zero. A log selectivity coefficient <1 indicates a preference for the measuring ion i relative to

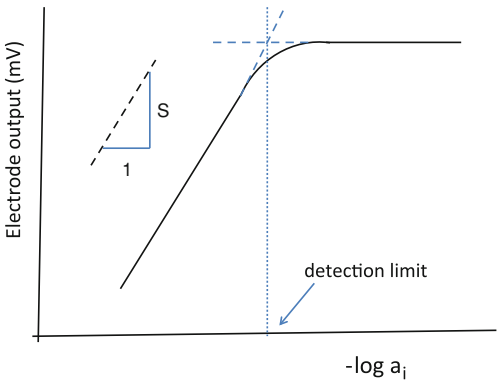

Fig. 6.2 Calibration of an ion-selective microelectrode to show how the slope and detection limit are calculated

the interfering ion *j*, and vice versa for a selectivity coefficient >1. The K_{ij}^{pot} values should not be considered to be constant parameters that characterize membrane selectivity under all conditions; the values are dependent on both the method used for determination, and on the conditions under which the calibrations are made. The fixed interference method is commonly used to calculate the selectivity coefficient and it is the method recommended by the International Union of Pure and Applied Chemistry (Inczédy et al. 1998). Whichever type of method is chosen the one used should always be quoted.

A schematic representation showing an ideal ion-selective microelectrode calibration curve is given in Fig. 6.2. The slope *s*, is the change in EMF per decade change in activity of a monovalent anion *i*, which is equivalent to 59.2 mV at 25°C; the limit of detection is defined as described in the text and is also indicated.

Another important parameter of an ion-selective microelectrode is the detection limit, which is the lowest ion activity that can be detected with confidence and is defined by the intercept of the two asymptotes of the Nicolsky response curve (see Fig. 6.2). In practice, the detection limit seems to depend on the tip geometry and composition of the microelectrode's ion-selective membrane. Finer or smaller diameter tips have higher detection limits; while composition affects detection in ways that can only be determined experimentally (see Sect. 6.2.4). The presence of interfering ions alters the detection limit (e.g., chloride for nitrate-selective microelectrodes, see Miller and Zhen 1991). Electrodes provide no useful information below their detection limits and for maximum benefit should be used in the linear portion of their calibration curves. The response time of ISEs can be important when measuring changes in ion activities (Fig. 6.3). This microelectrode parameter is dependent on many factors, including tip geometry, membrane composition, and resistance. Response time can be measured during the calibration as the time taken for the voltage to adjust when ion activity at the tip is changed (see Fig. 6.3 for an example recording).

The response time has a chemical and electrical component and for ion-selective electrodes the former is usually much slower than the latter. The sensor composition can be varied to improve response times (see Sect. 6.2.3.4 additives),

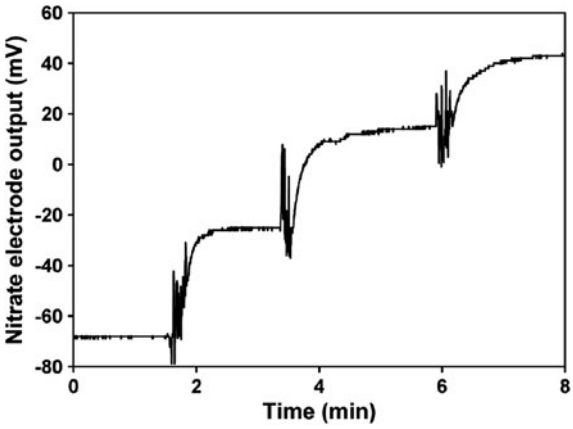

Fig. 6.3 Calibration response times obtained from a typical nitrate-selective microelectrode. This recording shows the changing response times of the electrode as the tip was exposed to decreasing activities of nitrate from 100–10 mM to 1–0.1 mM nitrate

but this is often at a cost as the detection limit and selectivity may be influenced. Chemical response times depend on the concentration of the ion being reported and this is shown in Fig. 6.3; with an inverse relationship, as the concentration of nitrate decreased the response time increased. Response times may be too slow to detect rapid changes in the intracellular concentrations of some ions like Ca^{2+} (see Sect. 6.4.2). When recording transient changes in intracellular ion concentrations it is important to check the response time of the actual electrode; for microelectrodes the half-times may be several minutes. This is much less of a problem for larger pore diameter tips and microelectrodes when a larger surface area of the ion sensing membrane is exposed and response times are much faster.

6.2.2 Types of ISEs

There are three major types of ISE, all of which can be miniaturized for use in plant cells. These are solid state, glass, and liquid-(or fluid) membrane electrodes. Solid-state microelectrodes have been used to measure pH or Cl^- inside plants cells (e.g., Coster 1966) and recessed tip glass microelectrodes have been made using pH-selective glass (Sanders and Slayman 1982). These two types of microelectrode have largely been superseded for intracellular measurements by liquid membrane electrodes so only the latter will be described here. Liquid ion-selective membranes are composed of the sensor molecule dissolved in a plasticizer (membrane solvent). The membrane may also contain a lipophilic additive and a matrix. Liquid membrane sensors are commercially available for a wide range of ions (e.g., see Sigma http://www.sigmaaldrich.com/).

To make an ion-selective microelectrode, the tip of the glass electrode is filled with an ion-sensing chemical cocktail which gives a voltage output of different values when placed in solutions containing varying activities of the ion. Therefore, when an electrode is inserted into a cell, the voltage measured gives a direct

indication of the intracellular ion activity. This situation is complicated by the voltage across the cell membrane; the ion-selective electrode will sense this in addition to voltage due to the activity of the ion of interest. To obtain the output for the ion alone, the cell membrane potential must be subtracted. This is done by using either two single electrodes or a double-barreled electrode in which the ion-sensing electrode is combined with a cell-voltage-measuring electrode (see Fig. 6.1). Both output voltages are measured against a reference ground electrode in the external solution. The ion activity is determined from the calibration curve after subtracting the membrane potential.

6.2.3 Making ISEs

The preparation of ion-selective microelectrodes can be divided into four main stages:

1. pulling of glass micropipettes
2. silanization of the inside of surface of the ion-selective electrode or barrel
3. backfilling
4. calibration.

The preparation of a nitrate-selective cocktail for backfilling microelectrodes is described by Miller and Zhen (1991) and a generalized method which is suitable for all different types of ion-selective microelectrode has been described previously (Miller 1995). The background to each stage is described here.

6.2.3.1 Pulling of Glass Micropipettes

Microelectrodes should be prepared to give dimensions suitable for impaling the target cell type. Double-barreled microelectrodes can be prepared by twisting together two single pieces of filamented glass tubing or using glass which is already fused. Filamented glass has a glass fiber attached to the inner wall; this fiber assists backfilling by providing a hydraulic conduit along which the solution can flow by capillarity. Twisting is done using an electrode puller which both heats the glass and pulls it in a way predetermined by the operator. The heating is paused for the two barrels to be twisted around one another and then the heating and pulling continues. There are various different types of microelectrode puller and the most important feature is reproducibility; this ensures that when an optimum microelectrode shape for a particular cell type has been prepared, it can be exactly duplicated many times. Before or after pulling, glue or heat shrink tubing can be used to provide support and additional strength to hold together the two or three pieces of glass.

Microelectrodes are usually made from borosilicate glass although sometimes the harder aluminosilicate glass can be used. Multibarreled glass of varying dimensions that is fused together lengthwise is available from suppliers

(e.g., Hilgenberg http://www.hilgenberg-gmbh.de/). This type of glass is best for ion-selective microelectrode work. An alternative type of double-barreled glass called "theta" glass can be used; this has a single thin glass wall between the two preformed barrels. Adjacent ion-selective barrels may mutually interfere because the thin glass walls at the electrode tip have electrical impedance that may be as low as the impedances of the liquid ion exchangers, so that the measured potential depends on the potential across the glass as well as the potential across the liquid ion exchanger. This problem is more acute when "theta" glass is used because the final glass partition in the tip is much thinner. Both barrels of glass should have an internal filament to assist with backfilling. Identification of the different barrels can be done by using different diameter glass, marking with a pen, cutting to various lengths, or bending the blunt end of one barrel to give an obvious angle. The advantage of each of the latter two methods is that they make it easier to insert Ag wire (see Fig. 6.1). Wear safety glasses at all times when pulling and breaking glass.

Before preparing the ion-selective microelectrode it is important to determine that glass microelectrodes filled with 0.1 M KCl can be used to impale cells and measure stable resting membrane potentials sensitive to metabolic inhibitors (in the usual range for the cell type, in the bathing solution used). An estimate of the tip geometry of the microelectrode is provided by measuring its electrical resistance when filled with KCl, larger tips having lower resistances. For tips of 2–0.1 μm diameter the electrical resistances of ion-selective microelectrodes are usually in the GΩ range, while microelectrodes filled with 0.1 M KCl have 10^3 smaller resistances in the MΩ range. Electrical resistance does depend on the salt concentration of the backfilling solution. The dimensions of the microelectrodes are usually a compromise between obtaining a stable membrane potential and a good calibration response (detection limit).

6.2.3.2 Silanization of Glass Surface

The inside of the glass micropipettes must be given a hydrophobic coating to allow the formation of a high resistance seal between the glass and the hydrophobic ion-selective membrane. The barrel designated to be ion selective is heat dried then silanized by placing a few drops of a solution of 2% (w/v) silanizing agent in chloroform on its blunt open end. There are a range of different silanizing agents which can be used at this concentration, but dimethyldichlorosilane or trimethylchlorosilane are most commonly used. Care must be taken to ensure that the reagent does not enter the membrane potential measuring barrel. Beware silanizing agents are highly corrosive and toxic, protective glasses and gloves must be worn and glass must be treated in a fume hood. The microelectrode is placed under a heating lamp giving a temperature of 140°C at the glass surface. After 30 min drying the silanizing solution is added and quickly vaporizes giving the ion-selective barrel a hydrophobic coating. There should be no visible residue remaining in the microelectrode tip before the next step, backfilling.

6.2.3.3 Backfilling

There are actually two steps to backfilling, the first uses a cocktail to form the ion-selective membrane in the microelectrode tip, and the second step, usually a minimum of 48 h later, uses an aqueous salt solution to provide contact between this membrane and the Ag/AgCl metal electrode (in the base of the microelectrode holder). Both steps are made much simpler by using filamented glass to make the microelectrodes and can be achieved using a syringe and fine all metal needle.

Electrodes are backfilled with a sensor cocktail containing several different components:

- An ion-selective molecule, sensor, or exchanger
- Membrane solvent or plasticizer
- Additives, e.g., lipophilic cation/anion
- A membrane matrix to solidify the ion-selective membrane. This is essential for measurements in cells possessing turgor.

For many ions, the membrane cocktail can be purchased already mixed and it is advisable to start by using the commercial mixture. However, preparing the cocktail from the individual components is cheaper and these can be bought from chemical suppliers. For commercially available liquid membrane cocktails the membrane matrix is not normally included. A matrix is needed if microelectrodes are to be used in plant cells because turgor will displace a liquid membrane from the electrode tip, thereby changing, or eliminating the sensitivity to the measuring ion (Miller 1995). The matrix used is normally a high molecular weight poly(vinyl chloride) (PVC) polymer, but can also include nitrocellulose for additional strength.

6.2.3.4 Cocktail Components

The various components of an ion-selective membrane are mixed together to form a sensor cocktail. Many premixed cocktails for a range of different ions are available commercially (e.g., the Fluka Selectophore® range sold by Sigma http://www.sigmaaldrich.com/). If a matrix is present, the cocktail is usually dissolved in a solvent such as tetrahydrofuran. If the cocktail does not include a solvent, it can be introduced to the tip of a micropipette for immediate use. Membranes formed from solubilized cocktails are produced by solvent casting. The mixture is introduced into a micropipette and the solvent is allowed to slowly evaporate to leave a solid or semi-solid membrane at the micropipette tip. The choice and relative proportions of the components of a cocktail determine the properties of the ion-selective membrane. Cocktails are optimized by a process of informed experimental trial and error, adjusting components, and proportions until the desired properties are achieved. It is important to note that the precise composition of the cocktail is important for ion selectivity. If the mixture is modified the ion selectivity must be tested and cannot be assumed.

Of all of the components, the ion-selective sensor is the main factor determining electrode characteristics (e.g., slope, selectivity, and limit of detection); however, the plasticizer can alter properties such as lifetime, stability, and selectivity. Additionally, membrane additives, such as lipophilic ions, can be used to improve the performance of microelectrodes. Sometimes these additives can introduce changes in ion selectivity, for example, the plasticizer can introduce nitrate sensitivity (Cuin et al. 1999). The final optimum cocktail is found by varying the composition of each component to find electrodes with the best performance. Good electrodes should have a low detection limit, a near ideal slope, and a small selectivity coefficient for physiologically important interfering ions. The roles played by each cocktail component are now described in more detail.

Ion-selective sensor The sensor is the most important component of the membrane in determining electrode characteristics (Miller 1995). Sensor molecules employed in ion-selective membranes may be ion exchangers or neutral or charged carriers. The discovery of the ion-selective ionophores has lead to the development of a large range of sensors for ion-selective microelectrodes. Sensors are now available for a wide range of cations and anions (see Miller 1995) and improved sensors are always being reported (e.g., for Na^+, Carden et al. 2001; Jayakannan et al. 2011).

Plasticizer The plasticizer forms the bulk of an ion-selective membrane (typically 60–90 wt %), and can substantially influence membrane properties such as selectivity and lifetime (Ammann 1986). The main function of the plasticizer is to solubilize the ion-selective sensor and lipophilic additives. Other important properties include lipophilicity, viscosity, and the ability to plasticize the matrix material. Commonly used plasticizers include: dibutyl sebacate, bis(2-ethylhexyl) sebacate, and 2-nitrophenyl octyl ether.

Additives The performance of cation-selective neutral carrier membranes can be enhanced by the addition of lipophilic additives. Common additives are alkali metal salts of lipophilic anions such as sodium tetraphenylborate and potassium tetrakis(4-chlorophenyl) borate. These chemicals introduce mobile cation exchange sites into the membrane which can produce many useful effects. They reduce or remove any interference from lipophilic anions in the sample, decrease electrode response time, lower the electrical membrane resistance, and improve cation sensitivity and selectivity (Ammann 1986). A lipophilic cation (methyltriphenylphosphonium bromide) was used to improve the properties of an nitrate-selective membrane based on a charged carrier (Miller and Zhen 1991).

Matrix The membrane matrix provides mechanical stability to a liquid membrane. The most widely used matrix is PVC, but many other compounds have been used, including: silicone rubber, polyurethane, polystyrene, poly(methyl methacrylate), and nitrocellulose. Some matrix materials can be polymerized using uv light but the reactive ligands produced by this reaction can interfere with the ion-selective sensor (Miller unpublished). If a microelectrode is to be used for recording from a cell with turgor the inclusion of a matrix in the membrane is essential to prevent dislodging the sensor from the electrode tip.

6.2.4 Calibration and Storage

Ion-selective microelectrodes can be calibrated using concentration or activity although they actually respond to changes in activity (see Sect. 6.1.2). Furthermore, activity is actually the important parameter for all biochemical reactions. Calibrating with ion activity gives a microelectrode output which can be used directly without any assumptions of the intracellular activity coefficient for the ion. For these reasons the calibration of microelectrodes generally uses solutions which resemble the intracellular environment in terms of interfering ions, and ionic strength. Calibration of pH microelectrodes is easy because standard pH buffers can be used and simply checked with a pH meter. For other types of ion-selective microelectrode the calibration solutions may need to contain a pH buffer and a background salt solution to give an ionic strength approximately equivalent to that inside the cell. Care must be taken in the choice of these additional ions; they must not give significant interference over the range of measurements. In other words, the microelectrodes must have very small selectivity coefficients for these background ions. Calibration solutions are usually chosen to be approximately 0.14 M ionic strength. There are very few examples of detailed whole cell sap analysis to suggest what an appropriate figure might be, but for giant algal cells this value would seem reasonable (Okihara and Kiyosawa 1988). The use of computer programs to calculate ion activity and the availability of a wide range of ion-selective microelectrodes make it easier to prepare calibration solutions for all types of ion-selective microelectrodes. Furthermore, calibration solution recipes have been published for some ion-selective microelectrodes, (Ca^{2+}, Tsien and Rink 1981; Mg^{2+}, Blatter and McGuigan 1988; Na^{+} Carden et al. 2001; NO_3^- Miller and Zhen 1991). Some calibration solutions use concentration not activity, and also the term "free" ion usually means concentration of unbound ion and not activity, particularly for Ca^{2+} and Mg^{2+}. The calibration of calcium selective microelectrodes for intracellular measurements requires the use of calcium buffering agents such as EGTA because of the very low concentrations being measured (Tsien and Rink 1981).

Ion-selective microelectrodes can be calibrated in the microscope chamber where intracellular measurements will be made or in a U-shaped glass funnel alongside the microscope. The slope of the calibration curve is temperature sensitive and both calibrations and intracellular measurements should be done at the same temperature. If the temperature of the calibration solutions is 4°C and the cell is at 20°C, the slope of the electrode calibration for a monovalent ion will be 55 mV per decade change in activity, not the 58 mV expected at 20°C.

Curve fitting software such as the Marquardt curve-fitting algorithm within Sigmaplot (SPSS, http://www.spss.com/) can be used to fit the experimental data to an equation of the form:

$$\mathrm{EMF} = \mathrm{P1} + \mathrm{P2} \cdot \log(a_i + \mathrm{P3}) \tag{6.2}$$

where P1, P2, and P3 are constants. Equation 6.1 can be simplified to (6.2) and it is then apparent that P2 represents the Nernstian slope s, and that P3 represents $K_{ij}^{pot}.(a_j)^{zi/zj}$. The term K_{ij}^{pot} is defined as $a_i'/(a_j)^{zi/zj}$ and therefore P3 is equivalent to a_i', the activity at the intersection of the two linear portions of the response curve in Fig. 6.2—the IUPAC definition of detection limit (Inczédy et al. 1998). Constants P2 and P3 from Eq. 6.2 can thus be used to determine the slope, detection limit, and selectivity coefficient (if a_j is known) of ion-selective microelectrodes without recourse to graphical techniques.

Ideally, the detection limits for ion-selective microelectrodes should be calculated using calibration solutions approximating to the cytosolic composition. In practice, this is not so easy because our knowledge of the ionic environment within a cell is very limited. Although we do have some information on sap collected from giant algal cells (e.g., Okihara and Kiyosawa 1988). The detection limit of some microelectrodes is very small with values of around only 10^{-9} M for some types of ion (Bakker and Pretsch 2005). These limits are quoted by chemists developing new types of sensor molecules but the practical limits for microelectrodes are likely to be several orders of magnitude greater because values depend on the tip diameter and interfering ion concentrations. This means that lower detection limits are possible for extracellular measurements where larger tip diameters can be used.

For long-term storage, ion-selective microelectrodes should be stored without backfilling, in a silica gel dried sealed container in the dark. This can be done in a screw-cap glass jar containing dry silica gel, with the microelectrodes attached to the inner wall using plasticine or Blu®-tack (Bostik, Stafford, UK). Some types of ion-selective microelectrodes can be stored this way for several years and will still give a reasonable performance when backfilled.

6.3 Data Analysis, Interpretation, and Presentation

The high electrical resistance of ion-selective microelectrodes requires the use of a high input impedance ($>10^{15}$ Ω) electrometer to measure electrode voltages. In contrast, the electrometer output is of much lower impedance and can thus be monitored and recorded using less specialized equipment. The simplest method is to use a chart recorder, but this requires laborious subsequent processing and it is more convenient to collect data via an analog to digital (A/D) converter connected to a personal computer. Most modern A/D converters are compatible with software that allows real-time display of the recorded data, reproducing the functionality of a chart recorder while storing the raw data in a format that can be easily exported to statistical and graphing software. A useful feature of any data collection software is the ability to fit calibration curves and use the fitted parameters to display real-time ion activities as the data are being collected.

Ion-selective microelectrodes have a lower resistance and can be used with lower input impedance ($\sim 10^{12}$ Ω) devices such as benchtop pH/mV meters. The output

from such meters can again be recorded using an A/D converter and PC or alternatively a simple data logger may be used. Connecting a battery-powered amplifier to a data logger creates a portable system. Portable microelectrodes can be used for extracellular measurements in the field (Clark et al. 2005) and allow uptake studies to be made in controlled environment conditions rather than the laboratory.

One point regarding statistical analysis of data concerns the calculation of mean values. These should be calculated using the data which is distributed normally, that is using the log activity or output voltages not the actual activities (Fry et al. 1990). Therefore, when mean activity value is used it can only be expressed within 95% confidence limits, whereas log (activity) can be given standard errors or standard deviations.

When measuring changes in intracellular ion concentrations, artifacts can be caused by the differential response times of the two barrels; the ion-selective barrel usually has a slower response time than the membrane potential-sensing barrel. Response of the membrane potential barrel is almost instantaneous whilst that of the ion selective is usually in the order of 5–20 s depending on the measured activity range and the type of sensor (Fig. 6.3). As ion activity is calculated from the voltage difference between the two barrels, an incorrect activity can be reported for this time, limiting detection of rapid changes in ion activity. This can be corrected for when the response time of the electrode is known (Sanders and Slayman 1982).

6.4 Fixing Problems with Ion-Selective Microelectrodes and a Comparison with Other Methods

6.4.1 Trouble Shooting Guide

The best approach is to solve problems by a process of elimination. First, establish whether a problem occurs in the circuitry or is specific to the ion-selective microelectrodes. The circuitry can be tested by putting a broken-tipped KCl-filled microelectrode in place of the ion-selective microelectrode. The broken tipped should give a stable zero output. It may be necessary to recoat Ag/AgCl contact in the half cell or there may be a wiring problem. Noisy recordings can be caused by air bubbles in backfilling solutions or poor earthing. If the circuitry has no problems then the ion-selective microelectrode must be the cause. When the ion-selective microelectrode does not respond to the calibration solutions then the membrane can be checked by deliberately breaking the tip to expose a larger area of ion-selective membrane. Breaking the tip can displace the ion-selective membrane from the tip so it is important to measure the resistance to check it is still in the GΩ range. If the broken tip gives a good response to changes in ion activity then the problem is independent of the composition of the membrane. When the microelectrode tip diameter becomes too fine the output from the ion-selective electrode will no longer respond to changes in ion activity.

Several criteria for acceptable measurements can be defined. After impalement the ion-selective microelectrode should be recalibrated and should give a very similar response to that shown before the cell impalement particularly at activities similar to those measured in vivo. Sometimes the detection limit of the ion-selective microelectrode has changed but provided the measurement was on the linear response range of the electrode calibration curve this is not usually a reason to disregard the result. The performance of the ion-selective microelectrode can even improve with the detection limit actually becoming lower. For this reason, it may be best to quickly impale a cell with a new tip before calibrating prior to measuring the activity in the cell. A comparison between the electrical resistance of the ion-selective microelectrode before and after impalement provides a good indicator of whether the tip will recalibrate. If the resistance decreases below 1 GΩ, the ion-selective membrane has probably been displaced during impalement and the electrode will not recalibrate. Throughout the recording the state of the cell can be assessed by monitoring the membrane potential (which should remain stable unless deliberately perturbed) or processes like cytoplasmic streaming.

In plant cells, identifying in which internal cell compartment (cytoplasm or vacuole) the microelectrode tip is located can be a problem for some ions and it may be necessary to grow the plant under conditions in which two populations of measurements can be identified. Alternatively, a triple-barreled microelectrode can be used where one barrel is pH or Ca^{2+} selective. Large gradients of these two ions are known to exist across the tonoplast, with the cytoplasm maintained at relatively constant values (pH 7.2, Ca^{2+} 100 nM) so compartment identification is possible. Another approach is to use tissues where the two major cell compartments can be identified under the microscope for example, root hairs, or cell cultures which have no large vacuole. However, identifying which compartment the electrode is in can still be problematic, particularly if the electrode indents the tonoplast but does not penetrate it.

Leakage of salts from the tip of the membrane potential-sensing barrel has been reported (Blatt and Slayman 1983) and this may particularly be a problem in small cells. Diffusion of ions from the membrane potential-sensing barrel could give high local gradients of ions at the tip of a double-barreled microelectrode. It may be important to try measurements where different types of backfilling solution are used in the reference barrel. Large leaks should affect membrane potential and monitoring this should indicate possible problems.

The Ag/AgCl junctions of electrodes have been found to respond directly to light (Janz 1961) and problems with obtaining stable recordings can result from a poor chloride coating on the Ag of the half cell. For stable recording, both the metal electrode part of half cells and the Ag wire contacts (see Fig. 6.1) require regular recoating with AgCl.

A further possible problem can arise when using ion-selective microelectrodes with inhibitors. Some inhibitor chemicals are highly lipophilic and will readily dissolve in the sensor membrane and can poison the response, but this will be demonstrated during the recalibration of the ion-selective microelectrode. It is also

best to avoid exposing all types of electrodes to very low ion concentrations as most types of ion-selective membrane respond badly to such treatment.

6.4.2 Comparison with Other Methods

No method is ideal for measuring transmembrane ion gradients as all involve some perturbation of the tissue that may directly influence the parameters being measured. Extracellular measurements and biological samples can use ISEs. The various analytical methods for measuring trace elements in biological samples compared potentiometry (ISEs), voltammetry, atomic spectrometry (e.g., ICP-MS, inductively coupled plasma mass spectrometry), and nuclear techniques have been compared (Brown and Milton 2005). For example, ICP-MS and ISE measurement of lead concentrations in the same samples gave excellent agreement. Typically, ISEs compare well, providing moderate throughput at a low cost but the detection limits were often higher than other methods, typically an order of magnitude ($\times 10$) different.

There are several different nondestructive methods for measuring transmembrane ion gradients. Ion-selective microelectrodes have an advantage over most other methods because they can be used to report the ion activities in single cells and within the vacuole and cytoplasm. Compartmental tracer ion efflux analysis has frequently been used to measure the cytoplasmic concentrations of ions within living cells (MacRobbie 1971). This technique depends on the fact that the labeled ion or compound is in equilibrium with the unlabeled form in all parts of the cell. The method treats all the different cells and tissues of an organ like the root as a single entity even though the transport properties of each may be different. For the calculation of the intracellular ion concentrations it is necessary to make assumptions about the volume of each cellular compartment (see Miller and Smith 1996). Nuclear magnetic resonance can also be used to measure transmembrane ion gradients of some ions (e.g., pH and phosphate) in intact whole organs like roots, but is more commonly used for metabolite molecules (reviewed by Ratcliffe and Shachar-Hill 2001).

Energy dispersive X-ray microanalysis (EDAX) is a destructive method for measuring intracellular ion concentrations and the method requires chemical fixation of the tissue prior to the measurement. This treatment may lead to changes in transmembrane ion gradients before the fixation is complete. The precise area of tissue sampled for this analysis is difficult to control and so compartmental assignment of the measurement can be difficult. The method gives total elemental analysis of the tissue and for many ions this figure may be very different from the more biologically relevant value, the ion activity. Another example of a destructive technique is cell fractionation; this involves breaking the tissue into protoplasts and then vacuoles and measuring the concentrations of ions in each fraction. Unfortunately, the preparation of the cell fractions requires incubation for several hours in tissue degrading enzymes that might lead to changes in transmembrane ion gradients.

Dyes can be used to measure intracellular ion concentrations or activities but they first require some method for introducing the dye into the cell. Microinjection, ionophoresis (using electrical current flow to carry charged molecules) and in some cases the cell's transport systems can be used to take up ion reporter dyes (Negulescu and Machen 1990). Once inside the cell, dyes are usually used to monitor ion concentrations in the cytoplasm. The presence of the dye in the cell may influence normal cell processes. In addition, the dyes themselves must bind the ion being detected to function as a reporter and may therefore be influencing the parameter that they are measuring. Dyes have most commonly been used for cations, like H^+, K^+, and Ca^{2+}.

The best performance Ca^{2+}-selective electrodes use the ligand ETH 129 and have detection limits around 1 nM (Schefer et al. 1986). In the past Ca^{2+}-selective electrodes have been used concomitantly with absorption indicators such as arsenazo-III, but their use has been eclipsed by the introduction of a many different types of fluorescent calcium probes with calcium sensitivities varying from the nanomolar to the micromolar range such as fura-2, indo-1, fluo-4, and many others (Hove-Madsen et al. 2010). Reporter calcium probes can be microinjected into cells. Plants can be genetically engineered to express foreign proteins that are sensitive to changes in the local ion environment and these can be used to measure in both the apoplast and the cytoplasm (e.g., Gao et al. 2004). The quantitative use of these reporter proteins requires in vitro calibration and to obtain sufficient signal for the detection system expression is driven by a strong promoter (e.g., CaMV 35S). The use of this promoter gives expression of the reporter protein in many different types of tissue. These proteins, like the dyes, require physical interaction with the ion and their presence in the cell may cause modifications to normal cellular function. The cameleon calcium reporter protein, has be used to analyze changes in Ca^{2+} in specialized plant tissues like stomatal guard cells (Allen et al., 1999) root hairs (Miwa et al. 2006). Binding of Ca^{2+} causes a conformational change in the chimeric fluorescent cameleon protein, increasing the efficiency of fluorescent resonance energy transfer (FRET) from the cyan fluorescent protein (CFP) to the yellow fluorescent protein (YFP); thus as the Ca^{2+} concentration increases, fluorescence from CFP decreases and fluorescence from YFP increases.

Microelectrode measurements have been criticized because the insertion of a micropipette tip may cause cellular damage or induce wound responses. Point contacts on the surface of the plant have been proposed to represent signals related to fungal penetration or herbivore attack (Hardham et al. 2008). In Arabidopsis roots mechanical stimulation elicited a cytoplasmic acidification and an apoplastic alkalinization and reactive oxygen species production (Monshausen et al. 2009). Mechanically perturbing root epidermal cells or root hairs with a glass micropipette elicited an increase in cytosolic Ca^{2+} at the site of touch within 1–18 s after initiation of the stimulus. These stimulation elicited changes were transient and had dissipated completely after 90 s.

There are very few comparisons of techniques for intracellular measurements. Intracellular ion-selective microelectrode measurements of vacuolar nitrate have been compared with whole tissue analysis and single cell sap sampling methods

(Zhen et al. 1991). In a more recent paper, nitrate-selective microelectrode measurements of cytosolic nitrate were compared with values obtained using NMR on the same tissue (Radcliffe et al. 2005). In both these examples, there was good agreement between the different methods employed. The best approach to making intracellular measurements of ion concentrations is to use several different methods to obtain a consensus value.

6.5 Transport and Transmembrane Ion Gradients

Ion-selective microelectrode data give information on both electrical gradients and intracellular activities across the plasma membrane and tonoplast. These intracellular electrochemical gradients can be used to determine the likely mechanisms of transport across membranes. One example is the use of pH and nitrate-selective microelectrode measurements to determine the thermodynamics of nitrate transport systems across the plasma membrane (Miller and Smith 1996) and tonoplast (Miller and Smith 1992). Compartmental measurements of the transmembrane ion gradients of NO_3^- and H^+ enabled the energetic feasibility of different co-transporter stoichiometries to be calculated. This type of measurement can also be used to show the activity of proton-coupled transport systems at the plasma membrane as an acidification of cytosolic pH can be measured when nitrate is supplied outside the cell.

The distribution of NH_4^+ in an internodal cell of the freshwater alga *Chara corallina* measured using NH_4^+-selective microelectrodes (Wells and Miller 2000). Published data for vacuolar and cytoplasmic pH allows a calculation of the compartmental concentrations of NH_3 using the Henderson–Hasselbalch equation. Microelectrodes also measure the transtonoplast and plasma membrane potentials, allowing the mechanism of transport of the two forms of ammonium to be modeled. The Nernstian equilibrium voltage for the observed distribution of NH_4^+ across the plasma membrane is -50 mV, lower than the -115 mV measured, suggesting the passive uptake of NH_4^+ at this external concentration. Similarly, the observed vacuolar levels of NH_4^+ may be explained by passive transport driven by the transtonoplast potential. Calculated NH_3 concentration based on the experimental data is higher in the cytoplasm than either the vacuole or the external solution. NH_3 is freely diffusible across biological membranes and passive diffusion of NH_3 along this concentration gradient will thus be out of the cytoplasm into both the vacuole and the external solution.

Ion-selective microelectrodes can be used to directly measure the ion concentrations in other biological situations such as depletion from a nutrient solution for net uptake studies or on very small samples such as plant exudates. Micro- and macro-electrodes can also be used directly in soil where they provide a direct measure of the nutrient concentration that is available at the surface of plant roots and allow mapping of spatial and temporal nutrient heterogeneity. Soil electrode data can also be used to shed light on important soil processes such as N

mineralization, which can be quantified by the simultaneous use of nitrate- and ammonium-selective electrodes. Combining field data with laboratory measurement of apoplastic and intracellular ion concentrations allows models of transport to be developed.

Acknowledgments John Innes Centre is grant-aided by the Biotechnology and Biological Sciences Research Council (BBSRC) of the UK.

References

Allen GJ, Kwak JM, Chu SP, Llopis J, Tsien RY, Harper JF, Schroeder JI (1999) Cameleon calcium indicator reports cytoplasmic calcium dynamics in *Arabidopsis* guard cells. Plant J 19:735–747

Ammann D (1986) Ion-selective microelectrodes, principles, design and application. Springer, Berlin

Bakker E, Pretsch E (2005) Potentiometric sensors for trace level analysis. Trends Anal Chem 24:199–207

Blatt MR (1991) A primer in plant electrophysiological methods. In: Dey PM, Harbourne JB (eds) Methods in plant biochemistry, vol 6. Academic, San Diego, pp 281–356

Blatt MR, Slayman CL (1983) KCl leakage from microelectrodes and its impact on the membrane parameters of a non-excitable cell. J Memb Biol 72:223–234

Blatter LA, McGuigan JAS (1988) Estimation of the upper limit of the free magnesium concentration measured with Mg-sensitive microelectrodes in ferret ventricular muscle: (1) use of the Nicolsky-Eisenmann equation and (2) in calibrating solutions of the appropriate concentrations. Magnesium 7:154–165

Brown RJC, Milton MJT (2005) Analytical techniques for trace element analysis: an overview. Trends Anal Chem 24:266–274

Carden DE, Diamond D, Miller AJ (2001) An improved Na^+-selective microelectrode for intracellular measurements in plant cells. J Exp Bot 52:1353–1359

Clark LJ, Gowing DJG, Lark RM, Leeds-Harrison PB, Miller AJ, Wells DM, Whalley WR, Whitmore AP (2005) Sensing the physical and nutritional status of the root environment in the field: a review of progress and opportunities. J Agric Sci 143:347–358

Coster HGL (1966) Chloride in cells of *Chara australis*. Aust J Biol Sci 19:545–554

Cuin TA, Miller AJ, Laurie SA, Leigh RA (1999) Nitrate interference with potassium-selective microelectrodes. J Exp Bot 50:1709–1712

Fry CH, Hall SK, Blatter LA, McGuigan JAS (1990) Analysis and presentation of intracellular measurements obtained with ion- selective microelectrodes. Exp Physiol 75:187–198

Gao D, Knight MR, Trewavas AJ, Sattelmacher B, Plieth C (2004) Self-reporting *Arabidopsis* expressing pH and $[Ca^{2+}]$ indicators unveil ion dynamics in the cytoplasm and in the apoplast under abiotic stress. Plant Physiol 134:898–908

Hardham AR, Takemoto D, White RG (2008) Rapid and dynamic subcellular reorganization following mechanical stimulation of *Arabidopsis* epidermal cells mimics responses to fungal and oomycete attack. BMC Plant Biol 8:63

Henriksen GH, Bloom AJ, Spanswick RM (1990) Measurement of net fluxes of ammonium and nitrate at the surface of barley roots using ion-selective microelectrodes. Plant Physiol 93:271–280

Hove-Madsen L, Baudet S, Bers DM (2010) Making and using calcium-selective mini- and microelectrodes. In: Whitaker M (ed) Calcium in living cells, vol 99. Elsevier Academic Press Inc., San Diego, pp 67–89

Inczédy J, Lengyel Y, Ure AM (1998) Compendium of analytical nomenclature: definitive rules 1997, 3rd edn. Blackwell Science, Oxford

Janz GJ (1961) Silver-silver halide electrodes. In: Ives DJG, Janz GJ (eds) Reference electrodes: theory and practice. Academic, NY, pp 218–220

Jayakannan M, Babourina O, Rengel Z (2011) Improved measurements of Na^+ fluxes in plants using calixarene-based microelectrodes. J Plant Physiol 168:1045–1051

Kochian LV, Shaff JE, Kuhtrieber WM, Jaffe L, Lucas WJ (1992) Use of extracellular, ion-selective, vibrating microelectrode system for the quantification of K^+, H^+ and Ca^{2+} fluxes in maize roots and maize suspension cells. Planta 188:601–610

MacRobbie EAC (1971) Fluxes and compartmentation in plant cells. Annu Rev Plant Physiol 22:75–96

Miller AJ (1995) Ion-selective microelectrodes for measurement of intracellular ion concentrations. Methods Plant Cell Biol 49:273–289

Miller AJ, Cookson SJ, Smith SJ, Wells DM (2001) The use of microelectrodes to investigate compartmentation and the transport of metabolized inorganic ions in plants. J Exp Bot 52:541–549

Miller AJ, Smith SJ (1992) The mechanism of nitrate transport across the tonoplast of barley root cells. Planta 187:554–557

Miller AJ, Smith SJ (1996) Nitrate transport and compartmentation in cereal root cells. J Exp Bot 47:843–854

Miller AJ, Zhen R-G (1991) Measurement of intracellular nitrate concentration in *Chara* using nitrate-selective microelectrodes. Planta 184:47–52

Miwa H, Sun J, Oldroyd JED, Downie A (2006) Analysis of calcium spiking using a cameleon calcium sensor reveals that nodulation gene expression is regulated by calcium spike number and the developmental status of the cell. Plant J 48:883–894

Monshausen GB, Bibikova TN, Weisenseel MH, Gilroy S (2009) Ca^{2+} regulates reactive oxygen species production and pH during mechanosensing in *Arabidopsis* roots. Plant Cell 21: 2341–2356

Negulescu PA, Machen TE (1990) Intracellular ion activities and membrane transport in parietal cells measured with fluorescent dyes. In: Fleischer S, Fleischer B (eds) Methods in enzymology, vol 192. Academic, San Diego, pp 38–81

Okihara K, Kiyosawa K (1988) Ion composition of the chara internode. Plant Cell Physiol 29: 21–25

Radcliffe SA, Miller AJ, Ratcliffe RG (2005) Microelectrode and ^{133}Cs NMR evidence for variable cytosolic and cytoplasmic nitrate pools in maize root tips. Plant Cell Environ 28:1379–1387

Ratcliffe RG, Shachar-Hill Y (2001) Probing plant metabolism with NMR. Annu Rev Plant Physiol Plant Mol Biol 52:499–526

Sanders D, Slayman CL (1982) Control of intracellular pH. predominant role of oxidative metabolism, not proton transport, in the eukaryotic microorganism *Neurospora*. J Gen Physiol 80:377–402

Schefer U, Ammann D, Pretsch E, Oesch U, Simon W (1986) Neutral carrier based Ca^{2+}-selective electrode with detection limit in the sub-nanomolar range. Anal Chem 58: 2282–2285

Tsien RY, Rink TJ (1981) Ca^{2+} selective electrodes: a novel PVC- gelled neutral carrier mixture compared with other currently available sensors. J Neurosci Methods 4:73–86

Walker DJ, Smith SJ, Miller AJ (1995) Simultaneous measurement of intracellular pH and K^+ or NO_3^- in barley root cells using triple-barreled, ion-selective microelectrodes. Plant Physiol 108:743–751

Wells D, Miller AJ (2000) Intracellular measurement of ammonium in *Chara corallina* using ion-selective microelectrodes. Plant Soil 221:105–108

Wildon DC, Thain JF, Minchin PEH, Gubb IR, Reilly AJ, Skipper YD, Doherty HM, O'Donnell PJ, Bowles DJ (1992) Electrical signalling and systemic proteinase inhibitor induction in the wounded plant. Nature 360:62–65

Zeller G, Henz SR, Widmer CK, Sachsenberg T, Rätsch G, Weigel D, Laubinger S (2009) Stress-induced changes in the *Arabidopsis thaliana* transcriptome analyzed using whole-genome tiling arrays. Plant J 58:1068–1082

Zhen R-G, Koyro H-W, Leigh RA, Tomos AD, Miller AJ (1991) Compartmental nitrate concentrations in barley root cells measured with nitrate-selective microelectrodes and by single-cell sap sampling. Planta 185:356–361

Chapter 7
Studying Membrane Transport Processes by Non-invasive Microelectrodes: Basic Principles and Methods

Sergey Shabala, Lana Shabala and Ian Newman

Abstract Non-invasive microelectrode flux measurement is a convenient tool to study membrane transport processes in plants in situ. Its high resolution (a few microns in space and several seconds in time) enables real-time studies of membrane transport processes at various levels of plant structural organization, from intact organs to various tissues, single cells or protoplasts derived from these cells. Being noninvasive, the technique allows flux measurements over several hours or days, even from rapidly moving tissues such as growing or nutating plant axial organs. Importantly, fluxes of several ions and neutral molecules can be measured concurrently, enabling not only quantitative estimates of rates of measured processes, but also providing some valuable information about the stoichiometry between activities of various membrane transporters and their time dependence. In this review, we revise the principles of non-invasive ion and neutral molecule flux measurements using the MIFE^{TM} technique and discuss some methodological aspects of manufacturing, calibrating, and using flux measuring microelectrodes.

Abbreviations

LIX Liquid ion exchanger
NMR Nuclear magnetic resonance

S. Shabala (✉) · L. Shabala
School of Agricultural Science, University of Tasmania,
Private Bag 54, Hobart, TAS 7001, Australia
e-mail: sergey.shabala@utas.edu.au

I. Newman
School of Mathematics and Physics, University of Tasmania,
Private Bag 37, Hobart, TAS 7001, Australia

A. G. Volkov (ed.), *Plant Electrophysiology*,
DOI: 10.1007/978-3-642-29119-7_7,

7.1 Introduction: Why Study Membranes?

Plant membranes constitute a barrier to free diffusion of molecules and underlie many essential cell biological processes including nutrient acquisition and compartmentation, pH and ionic homeostasis, turgor generation, metabolite distribution and waste excretion, energy transduction and signaling. According to Ward (2001), 43% of over 25,000 protein sequences in the *Arabidopsis* genome have at least one transmembrane spanning domain with 18% proteins having more than two, thus indicating association with cellular membranes. Electrophysiological and molecular genetic studies have revealed the crucial role of plasma membrane transporters in perception and signaling in response to virtually every known environmental factor (Zimmermann et al. 1999). In many organisms, changes in plasma membrane potential or modulation of ion flux are among the earliest cellular events in response to light, temperature, osmotic stress, salinity, hormonal stimuli, elicitors, and mechanical stimulation (Blumwald et al. 1998; Sanders et al. 1999; Zimmermann et al. 1999; Spalding 2000; Knight and Knight 2001; De Angeli et al. 2007; Laohavisit and Davies 2009; Dietrich et al. 2010; Grefen et al. 2011). For many, if not all of the stresses mentioned above, the receptors involved were suggested to be located at one of the cellular membranes.

In addition to hosting various receptors mediating plant-environment interactions, membrane transporters always act as the ultimate effectors of plant adaptive responses. In the case of salt tolerance, this may be by excluding toxic Na^+ from the cytosol via either the SOS1 plasma membrane Na^+/H^+ antiporter (Zhu 2003) or by compartmentalizing it into the vacuole by the NHX tonoplast Na^+/H^+ antiporter (Apse et al. 1999). In the case of Al^{3+} toxicity, the adaptive response includes activation of anion channels responsible for malate or citrate efflux and changes in the rhizosphere pH (Ryan et al. 2011). Osmotic adjustment includes rapid increase in the uptake of inorganic ions (Shabala and Lew 2002), while plant adaptive responses to low temperature include dramatic changes in membrane fluidity (Ruelland and Zachowski 2010). Such a central role of plant membranes and membrane transport processes in plant adaptive responses to environmental conditions makes them important targets for genetic manipulations aimed to improve tolerance to a particular stress. To enable this, causal links between membrane transport processes and other metabolic or physiological processes in the cell need to be understood.

Gaining such an understanding is not an easy task. It is complicated not only by the large number of transporters involved (for cations, 46 unique families are known, containing approximately 880 members in *Arabidopsis*; Maser et al. 2001), but also by the myriad of interactions and cross-talk between various transporters and signaling components. Over the last two decades, various state-of-the-art molecular and biophysical techniques (such as patch-clamp or fluorescence imaging) have been used to reveal some of these interactions. These techniques have been the subject of many comprehensive reviews and thus are mentioned only briefly here. However, at the same time, the inevitable consequence of such "in-depth" approaches was a decrease in the physiological reality of the transporters' environment (Tester 1997).

There are many reports (some of which are discussed in another chapter in this volume) showing that activity of a particular transporter differs dramatically when expressed in a heterologous system compared with *in planta* conditions. This makes it very difficult (and often even impossible) to transfer the results obtained by these advanced techniques to *real* plants in their natural habitats. The more advanced the technique, the bigger the gap between physiologists/molecular biologists and the agronomists interested in plant behavior in the field.

Non-invasive microelectrode flux measurements have gradually emerged as a convenient tool to study membrane transport processes in plants in situ. Some of their key features (non-invasiveness, high spatial and temporal resolution, etc.) allow us to establish and quantify causal links between membrane transport processes and other metabolic or physiological processes in the cell. This chapter briefly highlights basic techniques to study membrane transport in plants, and discuss the *pros* and *cons* of their application. Then the basic principles of the MIFE technique for non-invasive microelectrode flux measurements are reviewed, and methodological aspects of application of this technique are discussed. Finally, future prospects for the MIFE application (in combination with other advanced techniques) are canvassed.

7.2 Basic Techniques for Studying Membrane Transport in Plants

Many techniques are available to study ionic relations and transport of nutrients and ions across cell membranes. They range from whole-plant methods (depletion experiments, radioactive tracers) to those applicable at cellular (fluorescence microscopy; intracellular microelectrode measurements) or molecular (patch-clamp studies on single channels) levels. Their *pros* and *cons* are briefly summarized below.

1. *Destructive sampling* At the whole-plant level, basic chemical analysis of the elemental content in plant samples is still the most popular and widely used method. An appropriate plant sample is collected, dried, ground, and digested in a strong acid (Handson and Shelley 1993). Then the elemental content of the plant sample is analyzed using an appropriate technique (ICP-AES or AA spectroscopy, X-ray fluorescence spectroscopy, flame photometry etc.). The advantage of this method is its simplicity. The major problem is a very low time resolution (usually, several days or more), as there is an obvious limit on how often the samples may be taken. As a result, this method is mostly used to address some basic agronomical issues, rather than for fundamental physiological research.
2. *Growth solution depletion experiments* This is another basic method used for many decades for studies on plant nutrition. Plants are grown hydroponically, and the rate of nutrient uptake is determined by periodically taking small

volumes of the growth solution for chemical analysis (as above). Once again, the method has very low time resolution. The latter may be partially resolved by using conventional ion-selective electrodes placed in the growth solution to monitor concentration changes. Even then, however, the sensitivity of the method is rather low.

3. *Radioactive tracers* Various radioisotopes have been successfully used to study membrane transport processes in plants (Abbott and Fraley 1991; Tester and Davenport 2003). The method is relatively straightforward and allows quantification of the unidirectional fluxes of a specific ion. The main limitation is the spatial resolution of the method, as well as the relatively limited number of ions that can be studied.
4. *Nuclear magnetic resonance spectroscopy* NMR spectroscopy is a non-destructive tool enabling quantitative analysis of metabolites from cell suspensions, tissues, and whole plants (Ratcliffe 1997). As NMR detects atoms with magnetic moments only, not every nutrient can be studied. Taking nitrogen metabolism as an example, ^{14}N is naturally abundant (99.6%) but not useful for NMR studies due to extremely broad signals for almost all nitrogenous metabolites (Mesnard and Ratcliffe 2005). So, plant samples have to be enriched with ^{15}N before analysis, which significantly complicates the procedure. Again, a low time resolution (several hours; Rokitta et al. 2004) is a problem.
5. *Fluorescence microscopy* Ion imaging by fluorescence microscopy is based on fluorescence probes that accumulate inside cells and change their fluorescence properties when bound to distinct ions (Roos 2000). There is a relatively wide range of commercially available probes (both ratiometric and single-wavelength), enabling quantification and kinetic studies of changes in H^+, Ca^{2+} and, to lesser extent, K^+ and Mg^{2+} in plant cells. The method has high temporal and spatial resolution (especially when confocal microscopy is used) and, being non-invasive, has a great potential for studying cellular adaptive responses to the environment. There are several pitfalls, however, that severely restrict its application, of which the most important is probe loading. As not every tissue can be loaded with ester-bound probes, acid loading procedures are often used (Roos 2000). This imposes additional stress on the plant and might affect the overall plant response to the stimuli studied. Other problems include photobleaching, interaction of ion probes with cell metabolism, difficulties of calibration, poor discrimination of some probes (e.g. between K^+ and Na^+), and the limited range of ions that can be measured by this technique (Roos 2000).
6. *Single cell sampling* This technique has been developed by Tomos and coworkers as an extension of pressure-probe measurements at the single cell level (Tomos and Leigh 1999). By using a fine oil-filled glass microcapillary mounted on a micromanipulator, the cell sap is sampled from individual plant cells. Ion concentrations in these samples can then be analyzed using a range of physical and chemical methods such as X-ray microdroplet analysis or capillary electrophoresis (Tomos and Leigh 1999). The method has very high spatial resolution. Two main obstacles limiting its application are (1) the issue of

mixing of vacuolar and cytosolic content and (2) impossibility of kinetics study by this method.

7. *Patch-clamp* The patch-clamp technique is the most advanced method of studying ion-transport processes at the molecular level (Tester 1997) and can provide comprehensive information about the kinetics and properties of specific transport proteins at cell membranes. The method is based on a tight attachment of a plasma membrane patch to a microelectrode glass pipette, thus establishing a so-called "giga seal" (with up to 10^9 Ω resistance), enabling measurements of very low (pA range) currents through the prepared isolated plasma membrane patch in response to a series of voltage clamps. Ultimately, membrane ion channels may be characterized with respect to the ion they conduct (and their specificity for that ion), the conductance value of their open state, their gating properties, and their sensitivity to various pharmacological agents (Garrill and Davies 1994). However, patch-clamp is a rather sophisticated method that requires high level technical and data interpretation skills. Quite often, conditions that enable seal formation are rather nonphysiological (e.g., high amount of Ca^{2+} in the pipette). As a result, it is not always possible to extrapolate patch-clamp data onto ion channel behavior *in planta*.
8. *Impaled microelectrodes* Traditionally, microelectrode impalement has been applied to measure plasma membrane potential (MP). Significant membrane depolarization is observed in response to various environmental stresses such as salinity (Shabala et al. 2003), chilling (Clarkson et al. 1988), acidity (Babourina et al. 2001), and hypoxia (Zhang et al. 1992). As transport of all nutrients is directly or indirectly linked to MP values, the more substantial is the membrane depolarization, the more severe is the disturbance to cell ionic homeostasis. A more sophisticated method involves a microelectrode tip being filled with a specific ionophore, sensitive to a particular ion (Miller et al. 2001). As the MP electrode also has to be impaled alongside the ion-selective microelectrode, multibarreled electrodes are often used for these purposes (Carden et al. 2003). This technique thus makes it possible to monitor changes in cytosolic ion homeostasis and therefore to provide answers to some fundamental questions about ionic mechanisms underlying stress tolerance in plant cells. However, this technique is extremely technical and skill-demanding and is thus not likely to be used routinely.

7.3 Non-invasive Flux Measurements

7.3.1 Historical Context

In recent years, non-invasive microelectrode measurements of ion and neutral molecule fluxes have become a popular tool in studying adaptive responses of plant cells and tissues to a large number of abiotic and biotic stresses. A couple of

dozen laboratories around the world employ this technique, and their number is growing.

The idea of using slowly vibrating ion-selective microprobes to measure net ion fluxes noninvasively was first proposed by Lucas (Lucas and Kochian 1986). The microelectrodes were proposed to measure ion concentration *gradients* (strictly, electrochemical potential differences between two positions) in solution outside the organism tissues, and to use those gradients to calculate the *net fluxes* of the ions crossing the membrane. The first application of the theory was to measure the stoichiometry of H^+ and K^+ fluxes near corn roots (Newman et al. 1987; Kochian et al. 1989). The National Vibrating Probe Facility at Woods Hole MA in the USA, which is widely used for electrophysiological research in medical and animal physiology, adapted the vibrating probe (Jaffe and Nuccitelli 1974) to include ion flux measuring capability (Jaffe and Levy 1987). Two automated systems were then developed and are available commercially. The Massachusetts system has come to be called SIET (Scanning Ion Electrode Technique; Messerli et al. 2006, and other chapters in this volume). The system developed at the University of Tasmania, largely by Ian Newman and co-workers (Newman 2001) is named MIFE™ (Microelectrode Ion Flux mEasurement), which is also used as a trade mark for the system. Since the mid-1990s MIFE systems have been applied successfully to the study of various aspects of membrane transport processes in a broad range of plant (see other chapters in this volume), bacterial (Shabala et al. 2006, 2009a), fungal (Levina et al. 2002; Lew et al. 2006; Shabala et al. 2009b), and animal (Shabala et al. 2008; Valencia-Cruz et al. 2009) systems, resulting in over 100 publications. Each system also allows measurement of neutral molecule fluxes (Pang et al. 2006; Porterfield 2007; McLamore et al. 2010; McLamore et al. 2011).

7.3.2 Advantages of Non-invasive Flux Measurements

There are at least five major features that, taken together, provide a significant advantage of the MIFE or SIET approach over other methods (see previous section) for flux measurements. This chapter focuses on the MIFE. The particular advantages of the approach include:

1. *Non-destructiveness* In contrast to many other methods, the technique allows in situ measurements of net fluxes, in physiologically realistic conditions.
2. *High spatial resolution* The electrode tip is typically 2–3 μm in diameter, which makes it possible to measure net ion fluxes from single cells (Babourina et al. 2000; Shabala et al. 2001) or protoplasts derived from plant cells (Shabala et al. 1998; Tyerman et al. 2001). Moreover, for some ionophores (such as H^+) with high signal-to-noise ratio, the electrode tip diameter can be further reduced to 0.8–1.0 μm. As a result, the cell surface can be "mapped" (Shabala et al.

1998; Tegg et al. 2005), providing information about spatial distribution and functional expression of specific ion transporters.

3. *High temporal resolution* The typical MIFE settings assume electrode movement with 10 s period. This could be reduced without difficulty to 2 or 3 s in some cases. Such high temporal resolution is crucial in studying rapid signaling events at plant membranes. Most other non-invasive techniques operate on a time scale at least one order of magnitude slower. This gives the MIFE technique an opportunity to provide insights into very early (and fast) events associated with plant responses to environmental changes.
4. *Duration of measurements is not restricted* The technique is non-invasive, and its application is practically limited only by the lifetime of the ion-selective electrode (typically 15–20 h). Moreover, electrodes may be replaced easily, and measurements resumed only after a few minutes' break. The other techniques having similar time resolution (e.g., patch-clamp or fluorescence imaging) do not provide this opportunity. Due to dye bleaching, fluorescence measurements are usually restricted to a limited number of images being taken. Maintaining a 'gigaseal' for several hours is also a big problem in every patch-clamp study. The use of impaled ion-selective microelectrodes is limited by the clogging of the electrode by the dense cytosol after some time.
5. *Simultaneous measurements of several ions and neutral molecules* The possibility of measuring flux kinetics of several ions or neutrals simultaneously, and essentially at the same spot, is important for understanding the underlying ionic mechanisms of cell adaptive responses. By assessing stoichiometry ratios between various fluxes, valuable information can be gained about the membrane transporters involved.

7.4 The MIFE Technique for Non-invasive Flux Measurements

7.4.1 Theory

The theory of non-invasive MIFE ion flux measurements was given in detail by Newman (2001). The theory has also been extended to include neutral molecule fluxes (Pang et al. 2006). The basic principles and useful conclusions are summarized here.

Substances in solution diffuse due to forces acting on their molecules. If a substance is being taken up by tissue, depleting the nearby solution concentration, it will diffuse in from the higher distant concentration. The diffusion force depends on the rate of change with distance of the logarithm of concentration. For ions there is an additional force due to the electric field. The rate of movement of the substance across an area, or the net flux J (mol m^{-2} s^{-1}), is given by the flux equation:

$$J = cD/RT(\Delta\mu/\Delta x).$$

When applied to a surface just outside some tissue in solution, x is the distance from the tissue surface, with Δx a small change in that distance. J is the net flux *into* the surface (opposite to x). c is the local concentration of the substance, with D its diffusion coefficient. R is the gas constant and T the temperature. The electrochemical potential is μ, with $\Delta\mu$ its change over the small Δx, and it is given by the equation:

$$\mu = \mu_0 + RT\ln(\gamma c) + zFV_b.$$

The reference level for μ is μ_0 and it has a chemical term with ln(c) and an electrical term that incorporates local bath electric potential V_b. The Nernst equation for electrochemical equilibrium between two points is derived from this equation. The chemical activity coefficient for the substance is γ and z is the valence, with F the Faraday number. For an uncharged molecule, $\gamma = 1$ and $z = 0$, so the flux equation reduces to Fick's law of diffusion.

Ions Theory For an ion, an ion-selective microelectrode measures the electrochemical potential μ in terms of an output voltage V. To calibrate the electrode, it is placed in turn into solutions of known concentration (with no electric field). The resulting calibration graph of V against $\log_{10}(c)$ is (ideally) a straight line whose slope is called the "Nernst slope" for the electrode. The Nernst slope describes the performance of the electrode in practice and it allows the flux equation to be rewritten:

$$J = cD(F/RT)\,(\text{Nernst slope})\,(\Delta V/\Delta x).$$

During measurements, the electrode tip is moved repeatedly in a slow square-wave cycle between two positions, near to (position 1), and far from (position 2) the sample surface (Fig. 7.1), and the voltage change ΔV is recorded. The concentration c is calculated from the average V at the two positions using the calibration graph. This equation, which is used in the MIFE software, gives the net flux through a plane surface close to the tissue. It is inferred that this is exactly the flux of interest that is crossing the adjacent tissue surface. It is assumed that convection and water uptake are negligibly small and that unstirred layer conditions are met.

If the actual tissue geometry is not a plane surface, but is a cylinder (as for a root) or sphere (as for a protoplast) having a radius r, the flux equation can still be used if Δx is replaced by $\Delta x = r^2[1/(r+x) - 1/(r+x+\Delta x)]$ for the cylinder, or by $\Delta x = r\ln[(r+x+\Delta x)/(r+x)]$ for the sphere.

Neutrals theory The theory for measuring fluxes of electrically neutral molecules is given in Pang et al. (2006), who applied it to measure O_2 fluxes at hypoxic barley roots. Much work has also been done by Porterfield's group on developing amperometric and other kinds of sensors to measure a range of neutral molecule fluxes using an equivalent technique (McLamore and Porterfield 2011).

In the flux equation, the electrochemical potential depends only on the concentration c. Hence the equation can be written as Fick's Law:

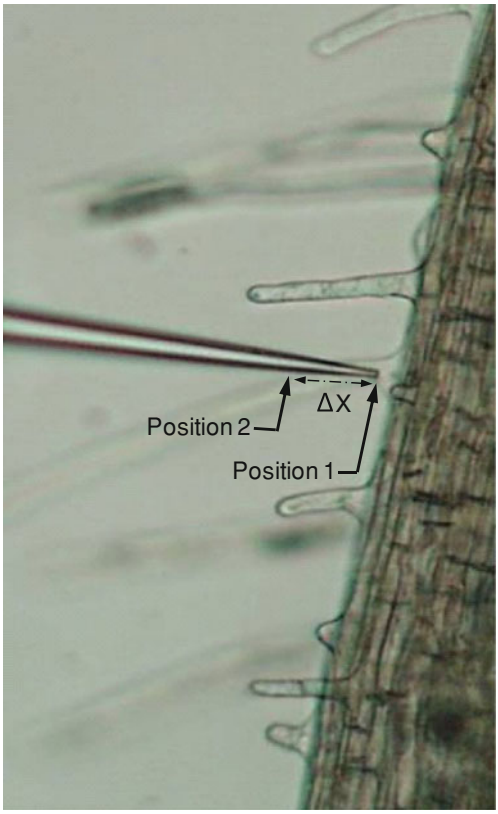

Fig. 7.1 Basic principles of the MIFE flux measurements. The ionselective microelectrode is moved repeatedly between two positions near the root surface. A voltage difference (ΔV) is measured by the electrometer between two positions over the travel range Δx

$$J = D(\Delta c/\Delta x).$$

The output from the electronics of the amperometric, or other, sensor is a voltage that is proportional to the concentration. Hence the flux equation can be written in terms of this voltage as:

$$J = D(\Delta V/\Delta x)/S,$$

where S is the slope of the calibration graph of output voltage against concentration. This is the equation that the MIFE software uses to calculate neutral molecule fluxes. The other issues, including geometry, are the same as for ion fluxes.

7.4.2 MIFE Hardware

The MIFE setup is built around a microscope system with long distance objectives and 100–400x total magnification. There are several basic MIFE configurations

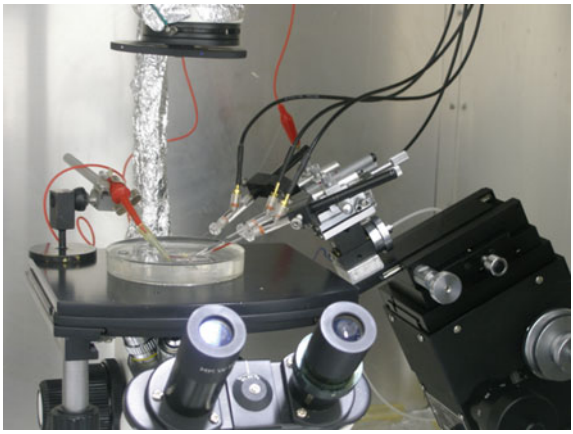

Fig. 7.2 The MIFE setup using inverted microscope configuration. The plant specimen is immobilised in a holder at the *bottom* of a standard Petri dish. Three MIFE microelectrodes come *down* from the *right*. The reference electrode is on the *left*, where a patch pipette could also be mounted

used in our laboratory. When fluxes are to be measured from small specimens (single cells; protoplasts; bacterial monolayers, etc.), an inverted microscope is used (Fig. 7.2). For the ion-selective electrode holders, typically we use WPI 64-0918 electrode holders (SDR Clinical Technology, Middle Cove, Australia). Up to three of these are mounted on an SM-17 or MMT-5 (Narishige, Tokyo, Japan) multi-micromanipulator that allows fine positioning of the electrode tips close together and near the specimen surface. The SM-17 (or MMT-5) manipulator is supported on a stepper motor-driven 3-axis hydraulic micromanipulator (Narishige WR-88 or MHW-3 models). The support is a 30 or 45° wedge to tilt the electrodes to come down at an angle to the stage. This arrangement enables the square-wave electrode movement in the plane of the stage to measure the electrochemical potential of the ions at the two positions in solution close to a tissue surface. Additional flexibility in electrode positioning is achieved by mounting the ensemble on a Narishige MX-2 mechanical micromanipulator. Instead of the MHW-3, a single axis MHW-4 may be used.

The measured specimen is held at the bottom of the open experimental chamber that is placed on the microscope stage. A standard non-polarizing Ag/AgCl reference electrode is positioned in the chamber. The electrodes are oscillated by the computer-controlled stepper motor at the chosen rate (typically 0.1–0.3 Hz) between the two positions. The near one is usually 20–30 μm from the surface and the far one 50–80 μm. The voltage output from the electrodes is amplified by the MIFE electronics and digitized for storage and for display on the computer screen to guide the experiment.

This voltage display allows the experimenter to observe how quickly the electrode voltages settle to their new values after each move between the two positions. The movement cycle time must be long enough so that there is a portion of time, at the end of each half-cycle, when each electrode voltage has settled. This is the "valid time" for calculating the average voltage at that position. The ΔV

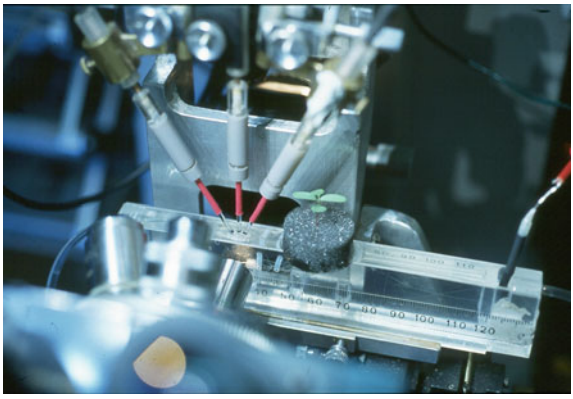

Fig. 7.3 The MIFE setup in a "classic electrophysiology" configuration, having a compound microscope on its back with horizontal optical axis. The three MIFE electrodes are mounted on the coarse manipulator (fixed to the microscope body) that brings them down vertically. (Photo: T Garnett, *Eucalyptus nitens* seedling)

values are calculated from these averages. This analysis is given in detail by Newman (2001).

For studies on plant roots, it is convenient to use the classic electrophysiology configuration, which has a compound microscope on its back with horizontal optical axis (Fig. 7.3). The stage is replaced by a narrow, long, vertical sample chamber (Fig. 7.4). To provide the 3-axis adjustment and the square-wave movement relative to the tissue, the chamber is mounted on a PatchMan NP2 manipulator (Eppendorf) or on a Narishige MHW-3. The MMT-5, holding the three electrodes, is rigidly fixed onto the microscope stand, bringing the electrodes down vertically into the chamber. The main advantage of this arrangement (Shabala and Newman 1997a) is the convenience of electrode positioning (much further from the chamber's bottom—thus, less danger for electrodes to be broken).

7.4.3 The MIFE Software

The CHART software package (University of Tasmania, Hobart, Australia), running under DOS on a Windows 98 or ME platform, is used to control data acquisition by the MIFE hardware system. This software allows automated and interactive real-time control of the amplifier configuration and the micromanipulator while the data are being collected and written to disk (Shabala et al. 1997; Newman 2001). The system configuration is recorded together with the data, and all modifications during data acquisition are recorded in a log file which can also include annotations typed during the experiment. The recorded voltage traces are displayed on the screen in a real-time scale (Fig. 7.5), with a possibility of expanding or contracting some selected data segment without interrupting the measurements. More details are available at http://www.mife.com.

Flux calculations are performed subsequently from the calibration, data, and log files by the MIFEFLUX software (University of Tasmania, Hobart, Australia), as

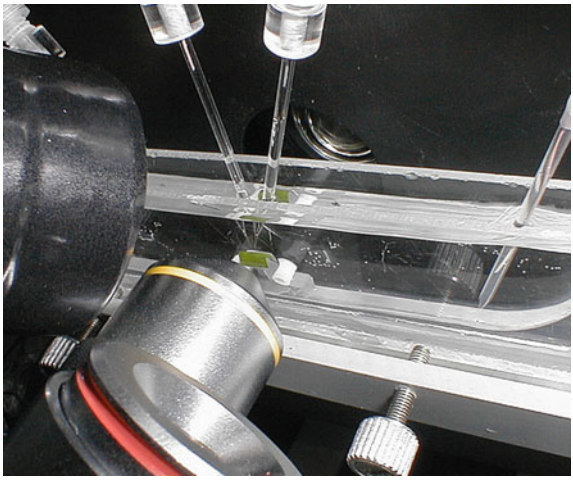

Fig. 7.4 A close-up look at a plant specimen and electrode positioning in a *narrow* chamber used in the MIFE setup with a horizontal optical axis arrangement. Reference electrode on the *right*

described by Newman (2001). Calculated ion fluxes (in nmol m^{-2} s^{-1}) and concentrations are saved as a tab-delimited text file for importing into a spreadsheet.

7.5 Methodological Aspects

7.5.1 Microelectrode Fabrication

Good ion-selective microelectrode fabrication is a crucial step in MIFE measurements. Several different approaches for microelectrode preparation are available in the literature (Smith et al. 1999; Shabala and Newman 1997a, b; Newman 2001). The procedure accepted in our laboratory includes several distinct steps:

- pulling out electrode blanks;
- baking and silanizing the blanks;
- filling the electrodes with an appropriate liquid ion exchanger (LIX);
- electrode calibration.

Pulling out electrode blanks The electrode blanks are made using 1.5 mm (OD) non-filamentous borosilicate glass capillaries (GC150-10, Harvard Apparatus Ltd, Kent, UK). The blanks are pulled to <1 μm diameter tips using a vertical pipette puller (PP 830, Narishige, Japan).

Baking and silanizing the blanks Electrode blanks are placed upright, base down, in a stainless steel rack and oven dried at 220°C overnight. Before silanization, electrodes are covered by a steel lid that creates a closed container with the blanks. Ten to fifteen minutes later ~50 μL of tributylchlorosilane (90,796, Fluka Chemicals) is injected under the lid. The lid is removed after

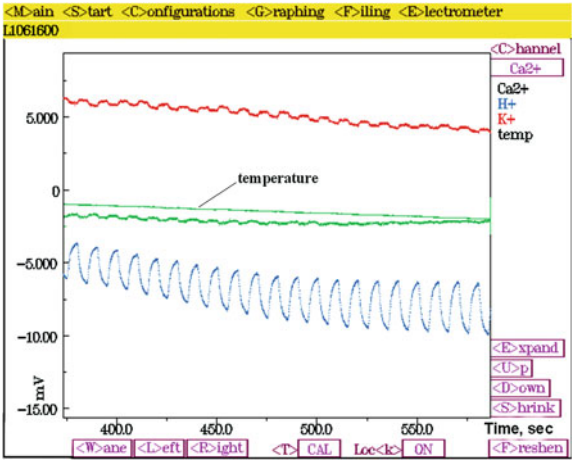

Fig. 7.5 Computer screen display of the MIFE recordings. A (reverse colour) screen is pictured showing four concurrent voltage records for Ca^{2+}, H^+, K^+, and temperature. Fluxes of ions were calculated from the recorded and displayed voltage changes (ΔV). H^+ and K^+ concentrations are decreasing slowly. K^+ and H^+ fluxes are nearly steady, while Ca^{2+} flux decreases to zero. The 10 s cycle time is not long enough for the H^+ electrode to settle at each position. Temperature (reversed scale) increases slowly

10 min and electrode blanks are baked at 220°C for a further 30 min. By this procedure, the surface of the electrode is made hydrophobic. Freshly pulled electrodes are hydrophilic due to the surface hydroxyl groups. The hydrophobic coating of the electrode blank enables entry of the organic LIX cocktails into the tip of the prepared microelectrode.

Filling the electrodes with an appropriate ion-selective resin (*LIX*) Dried and cooled electrode blanks are then filled with LIX. Details about the commercially available LIXs are given in Table 7.1. A LIX-containing tube is first constructed using a broken-back glass mirocapillary (tip diameter approximately 100 μm), which was dipped into the stock LIX, taking up a column of cocktail of approximately 1 mm. The microelectrode blank is mounted horizontally on a 3D micromanipulator and the electrode tip is broken back to achieve tip diameter of 2–3 μm. To do that, the electrode blank is gently placed against a flat glass surface under a stereo microscope. Blanks with required tip size are back filled with appropriate back-filling solutions using a syringe with a custom made nylon needle. The latter is pulled out from 0.1 mL nylon pipette tip after flaming it. Immediately after back-filling, the electrode tip is front-filled with the corresponding LIX. To do that, the back-filled electrode blank is positioned co-axially with the broken mirocapillary containing the appropriate LIX in its tip. The blank is briefly put in contact with LIX, and resin flows into the electrode tip to a column length of 50–200 μm. Immediately after filling, electrodes are immersed in solution and kept there until use (up to 8–10 h).

Table 7.1 Commercially available ion-selective LIX routinely used in our laboratory (all from Fluka, Buchs, Switzerland)

Ion	Catalogue number	Backfilling solution (mM)
K^+	60031	200 KCl
Na^+	71138	500 NaCl
Ca^{2+}	21048	500 $CaCl_2$
Mg^{2+}	63048	500 $MgCl_2$
H^+	95297	15 NaCl + 40 KH_2PO_4
NH_4^+	09882	500 NH_4Cl
Cl^-	24902	500 NaCl

Electrode calibration Electrodes are fitted to the electrode holder and then calibrated, before or after the experiment, in a set of three standards covering the expected range of concentrations of the ion in question. Details of the composition of back-filling solutions used are given in Table 7.1.

For most physiological conditions, electrode calibration graphs (output voltage $\sim \log_{10}$ concentration) are expected to be linear. The usual responses of electrodes are about 53–56 mV/decade for monovalent ions and 27–28 mV/decade for divalent ions. Electrodes with responses less than 50 mV per decade for monovalent ions and 25 mV per decade for calcium, or with correlation coefficients less than 0.999 are discarded. Both the slope and intercept of the calibration line are used to calculate the concentration c in the flux equation from the value of V measured during the experiment.

In our laboratory, we routinely use the MIFE system to measure net fluxes of H^+, Ca^{2+}, K^+, Na^+, Cl^-, Mg^{2+}, NH_4^+, NO_3^-, and Cd^{2+} from various systems: higher plant tissues and protoplasts; animal tissues (e.g., muscles and neurons); fungi; algae; protists; yeasts; bacterial monolayers, and biofilms. Several more ions (e.g., Zn^{2+}, Cu^{2+}, Cs^+, Pb^{3+}, SO_4^{-2}) can also be measured using commercially available ionophores.

7.5.2 Useful Hints

The same principle is used for measurements of fluxes of all ions, but each ion has some specific features related to fabrication, calibration, and use of ion-selective microelectrodes. Some of these issues are also covered in detail in previous reviews on MIFE (Newman 2001; Shabala et al. 2006) or on alternative systems (Messerli et al. 2006; McLamore and Porterfield 2011). Only the crucial issues are mentioned here.

1. *Reference electrodes for calibrations and flux measurements* Poor reference electrodes can cause signal instability. To make an Ag/AgCl reference electrode, a pulled glass microcapillary is broken back to 50 μm tip diameter and filled with 1 M KCl in 2% agar. A chlorided silver wire (galvanized in

0.25 N HCl for 15 min) is inserted into the microcapillary and sealed with parafilm. The small tip diameter ensures little K^+ leakage from this reference electrode.

2. *Basic ion-selective electrode characteristics* The resistance of the microelectrodes is typically 1–5 GΩ. The values of electrode resistance and the length of the LIX in the tip of the electrode are critical for the quality of the prepared electrode. High values result in an increase in 'noise' of electrode response. If measurements are made at very low concentrations, nonlinearity requires that more than the usual 3 standards should be used.
3. *Electrode "conditioning"* Most of the prepared microelectrodes can be used immediately after preparation, while others (e.g., H^+ and Cl^-) need some conditioning time ($\sim$1 h) to ensure a stable response.
4. *Settling during MIFE measurements* The electrodes are moved repetitively between the two positions. For accurate flux calculations, the LIX must "settle" at each position. In Fig. 7.5, K^+ and Ca^{2+} settle quickly, H^+ does not. From practical experience, settling is quicker if the LIX column length is relatively short. However, in this case there is a danger of a gradual leak of LIX out of the tip and the electrode loosing its sensitivity. The compromise is achieved by optimizing the amount of silane used for electrode fabrication and the amount of LIX used for electrode filling. If slow settling is expected, the cycle period can be increased.
5. *Effect of ionic strength* Variations in ionic strength of solutions might significantly affect characteristics of ion-selective electrodes and result in inaccurate estimates of ionic concentrations and, hence, of net ion fluxes. The actual concentration (and, thus, flux) is overestimated for solutions with ionic strength lower than that of the standard, and is underestimated vice versa (Shabala et al. 2006). For many ions, such a difference may be as big as a factor of 2 in a physiologically relevant range of concentrations (e.g., Na^+ levels of 200 mM). The rule is to make the calibration standards in a background of the solution to be used in experiments.
6. *Flux sensitivity* Due to the thermal electron noise in the high resistance of the electrodes, there is some theoretical lower limit on the magnitude of the flux that can be detected against the background noise (Ryan et al. 1990). There are two practical measures to overcome this problem and to improve the sensitivity of the flux measurements. One is to increase the travel range of the electrode (making voltage changes larger, but settling longer); another is to decrease resistance by increasing electrode tip diameter (Shabala et al. 2006). This noise problem does not apply to the neutral molecule flux sensors, which have low resistance.
7. *Temperature* The theory shows that the Nernst slope is proportional to the Kelvin temperature. This effect is automatically covered if calibration and measurements are done at the same temperature. The effects of temperature changes during an experiment are still open to question. Our experiments in the 4–40°C range suggested that in all cases the Nernst slope remained >50 mV/decade, and the maximum inaccuracy in flux calculation did not exceed 6%

(Shabala et al. 2006). Thus, in practice no compensation is needed. However, at temperatures above 32°C, the LIX often became very "noisy". Thus, the performance of specific LIX should be tested at the high temperatures to be applied in an experiment, to ensure that the signal-to-noise ratio is acceptable, and that net flux responses can be distinguished from background noise.

8. *Confounding effect of inhibitors* Pharmacological experiments are frequent in plant electrophysiology. However, many of the channel blockers and metabolic inhibitors routinely used in patch-clamp experiments may significantly affect LIX characteristics. For example, even micromolar concentrations of CCCP completely "killed" Ca^{2+} LIX, reducing electrode slope from 27 to <3 mV/decade. Therefore, a rigorous test should be undertaken first of LIX performance in the presence of the metabolic agents to be used. Calibration standards should also include the agent.
9. *Selectivity of LIX* Although the chosen LIX may have excellent characteristics for the ion of interest, it may also respond to the concentrations and fluxes of other "interfering" ions. This lack of selectivity is a renowned problem for the LIX available for Na^+ (e.g., Chen et al. 2005). Selectivity ratios for interfering ions are available from the LIX supplier. Those ratios are needed for making any calculation of fluxes, whether by also making a measurement of the interfering ion's actual flux, or by making a Nicolsky-Eisenman analysis (Messerli et al. 2006). In all cases the concentrations of interfering ions should be made as small as is biologically reasonable.

7.6 Prospects and Conclusions

Key features of the MIFE technique such as noninvasiveness, high spatial and temporal resolution, and possibility of concurrent measurements of fluxes of several ions and neutral molecules make it a very useful tool to study membrane transport processes in response to literally every known environmental stress. As fluxes are measured in situ, a direct extrapolation of the results to a variety of "natural" situations (e.g., plant stress response in the field) becomes possible.

The power of the MIFE technique is enhanced many fold when used in combination with other advanced experimental tools. One such example is a combination of the MIFE and patch-clamp techniques (Tyerman et al. 2001; Chen et al. 2007; Demidchik et al. 2007, 2010). Such a combination facilitates better identification of membrane currents and makes it possible to determine stoichiometries of transporter reactions. Another example is a combination of MIFE and fluorescence imaging techniques. By combining MIFE measurements with confocal imaging of Sodium Green distribution in plant tissues, quantification of SOS1 plasma membrane Na^+/H^+ activity has become possible (Cuin et al. 2011). Concurrent use of the Fura-2 dye with non-invasive Ca^{2+} flux measurements revealed

the role of an active Ca^{2+} efflux system in stress cross-tolerant plants (Shabala et al. 2011). Alternatively, impaled ion-selective microelectrodes may be used in combination with MIFE for these purposes. Earlier we used a similar approach to measure net ion fluxes concurrently with membrane potential changes from leaf epidermal and mesophyll cells in response to light (Shabala and Newman 1999). Combination of the MIFE technique with voltage-clamp (Babourina et al. 2001; Shabala and Lew 2002) or pressure-probe (Shabala and Lew 2002) techniques also gave a significant conceptual advance in our knowledge of the ion-transport processes underlying plant adaptive responses to pH and osmotic stresses. It appears that non-invasive flux measurements may play a unique role in filling the gap between fundamental membrane transport studies at the molecular levels and the needs of agronomists who aim to improve plant performance under stress conditions in the field. The technique can probably claim the "best value for money" title in its area. Time will judge if this claim is fully justified.

Acknowledgments This work was supported by an Australian Research Council grant to Prof Sergey Shabala.

References

Abbott ML, Fraley L (1991) Radiotracer methods to determine root distribution—a review. Environ Exp Bot 31:1–10

Apse MP, Aharon GS, Snedden WA, Blumwald E (1999) Salt tolerance conferred by overexpression of a vacuolar Na^+/H^+ antiport in *Arabidopsis*. Science 285:1256–1258

Babourina O, Leonova T, Shabala S, Newman I (2000) Effect of sudden salt stress on ion fluxes in intact wheat suspension cells. Ann Bot 85:759–767

Babourina O, Hawkins B, Lew RR, Newman I, Shabala S (2001) K^+ transport by *Arabidopsis* root hairs at low pH. Aust J Plant Physiol 28:635–641

Blumwald E, Aharon GS, Lam C-H (1998) Early signal transduction pathways in plant-pathogen interactions. Trends Plant Sci 3:342–346

Carden DE, Walker DJ, Flowers TJ, Miller AJ (2003) Single-cell measurements of the contributions of cytosolic Na^+ and K^+ to salt tolerance. Plant Physiol 131:676–683

Chen Z, Newman I, Zhou M, Mendham N, Zhang G, Shabala S (2005) Screening plants for salt tolerance by measuring K^+ flux: a case study for barley. Plant Cell Environ 28:1230–1246

Chen ZH, Pottosin II, Cuin TA, Fuglsang AT, Tester M, Jha D, Zepeda-Jazo I, Zhou MX, Palmgren MG, Newman IA, Shabala S (2007) Root plasma membrane transporters controlling K^+/Na^+ homeostasis in salt-stressed barley. Plant Physiol 145:1714–1725

Clarkson DT, Earnshow MJ, White PJ, Cooper HD (1988) Temperature dependent factors influencing nutrient uptake: an analysis of responses at different levels of organization. In: Plants and temperature. Society for Experimental Botany, Cambridge, pp 281–309

Cuin TA, Bose J, Stefano G, Jha D, Tester M, Mancuso S, Shabala S (2011) Assessing the role of root plasma membrane and tonoplast Na^+/H^+ exchangers in salinity tolerance in wheat: *in planta* quantification methods. Plant Cell Environ 34:947–961

De Angeli A, Thomine S, Frachisse JM, Ephritikhine G, Gambale F, Barbier-Brygoo H (2007) Anion channels and transporters in plant cell membranes. FEBS Lett 581:2367–2374

Demidchik V, Shabala SN, Davies JM (2007) Spatial variation in H_2O_2 response of *Arabidopsis thaliana* root epidermal Ca^{2+} flux and plasma membrane Ca^{2+} channels. Plant J 49:377–386

Demidchik V, Cuin TA, Svistunenko D, Smith SJ, Miller AJ, Shabala S, Sokolik A, Yurin V (2010) *Arabidopsis* root K^+-efflux conductance activated by hydroxyl radicals: single-channel properties, genetic basis and involvement in stress-induced cell death. J Cell Sci 123:1468–1479

Dietrich P, Anschutz U, Kugler A, Becker D (2010) Physiology and biophysics of plant ligand-gated ion channels. Plant Biol 12:80–93

Garril A, Davies JM (1994) Patch clamping fungal membranes: new perspectives on ion transport. Micol Res 98:257–263

Grefen C, Honsbein A, Blatt MR (2011) Ion transport, membrane traffic and cellular volume control. Curr Opin Plant Biol 14:332–339

Handson PD, Shelley BC (1993) A review of plant analysis in Australia. Austral J Exp Agricult 33:1029–1038

Jaffe LF, Levy S (1987) Calcium gradients measured with a vibrating calcium-selective electrode. Proc IEEE/EMBS Conf 9:779–781

Jaffe LF, Nuccitelli R (1974) An ultrasensitive vibrating probe for measuring steady state extracellular currents. J Cell Biol 63:614–628

Knight H, Knight MR (2001) Abiotic stress signalling pathways: specificity and cross-talk. Trend Plant Sci 6:262–267

Kochian LV, Shaff JE, Lucas WJ (1989) High affinity K^+ uptake in maize roots. A lack of coupling with H^+ efflux. Plant Physiol 91:1202–1211

Laohavisit A, Davies JM (2009) Multifunctional annexins. Plant Sci 177:532–539

Levina NN, Dunina-Barkovskaya AY, Shabala S, Lew RR (2002) Blue light modulation of ion transport in the slime mutant of *Neurospora crassa*. J Membr Biol 188:213–226

Lew RR, Levina NN, Shabala L, Anderca MI, Shabala SN (2006) Role of a mitogen-activated protein kinase cascade in ion flux-mediated turgor regulation in fungi. Eukaryot Cell 5:480–487

Lucas WJ, Kochian LV (1986) Ion transport processes in corn roots: an approach utilizing microelectrode techniques. In: Gensler WG (ed) Advanced agricultural instrumentation: design and use. Matinus Nijhoff, Dordrecht, pp 402–425

Maser P, Thomine S, Schroeder JI, Ward JM, Hirschi K, Sze H, Talke IN, Amtmann A, Maathuis FJM, Sanders D, Harper JF, Tchieu J, Gribskov M, Persans MW, Salt DE, Kim SA, Guerinot ML (2001) Phylogenetic relationships within cation transporter families of *Arabidopsis*. Plant Physiol 126:1646–1667

McLamore ES, Porterfield DM (2011) Non-Invasive tools for measuring metabolism and biophysical analyte transport: self-referencing physiological sensing. Chem Soc Rev 40(11):5308–5320. doi:10.1039/C0CS00173B

McLamore ES, Diggs A, Marzal PC, Shi J, Blakeslee JJ, Peer WA, Murphy AS, Porterfield DM (2010) Non-invasive quantification of endogenous root auxin transport using an integrated flux microsensor technique. Plant J 63:1004–1016

McLamore ES, Shi J, Jaroch D, Claussen JC, Uchida A, Jiang Y, Zhang W, Donkin S, Banks K, Buhman KK, Teegarden D, Rickus JL, Porterfield DM (2011) A self referencing platinum nanoparticle decorated enzyme-based microbiosensor for real time measurement of physiological glucose transport. Biosens Bioelectron 26:2237–2245

Mesnard F, Ratcliffe RG (2005) NMR analysis of plant nitrogen metabolism. Photosynth Res 83:163–180

Messerli MA, Robinson KR, Smith PJS (2006) Electrochemical sensor applications to the study of molecular physiology and analyte flux in plants. In: Volkov AG (ed) Plant electrophysiology—theory and methods. Springer, Heidelberg

Miller AJ, Cookson SJ, Smith SJ, Wells DM (2001) The use of microelectrodes to investigate compartmentation and the transport of metabolized inorganic ions in plants. J Exp Bot 52:541–549

Newman IA (2001) Ion transport in roots: measurement of fluxes using ion- selective microelectrodes to characterize transporter function. Plant Cell Environ 24:1–14

Newman IA, Kochian LV, Grusak MA, Lucas WJ (1987) Fluxes of H^+ and K^+ in corn roots. Characterisation and stoichiometries using ion-selective microelectrodes. Plant Physiol 84:1177–1184

Pang JY, Newman I, Mendham N, Zhou M, Shabala S (2006) Microelectrode ion and O_2 fluxes measurements reveal differential sensitivity of barley root tissues to hypoxia. Plant Cell Environ 29:1107–1121

Porterfield DM (2007) Measuring metabolism and biophysical flux in the tissue, cellular and sub-cellular domains: recent developments in self-referencing amperometry for physiological sensing. Biosens Bioelectron (Tier 1) 22:1186–1196

Ratcliffe RG (1997) In vivo NMR studies of the metabolic response of plant tissues to anoxia. Ann Bot 79:39–48

Rokitta M, Medek D, Pope JM, Critchley C (2004) ^{23}Na NMR microimaging: a tool for non-invasive monitoring of sodium distribution in living plants. Funct Plant Biol 31:879–887

Roos W (2000) Ion mapping in plant cells—methods and applications in signal transduction research. Planta 210:347–370

Ruelland E, Zachowski A (2010) How plants sense temperature. Environ Exp Bot 69:225–232

Ryan PR, Newman IA, Shields B (1990) Ion fluxes in corn roots measured by microelectrodes with ion-specific liquid membranes. J Membr Sci 53:59–69

Ryan PR, Tyerman SD, Sasaki T, Furuichi T, Yamamoto Y, Zhang WH, Delhaize E (2011) The identification of aluminium-resistance genes provides opportunities for enhancing crop production on acid soils. J Exp Bot 62:9–20

Sanders D, Brownlee C, Harper JF (1999) Communicating with calcium. Plant Cell 11:691–706

Shabala S, Lew RR (2002) Turgor regulation in osmotically stressed *Arabidopsis* epidermal root cells. Direct support for the role of inorganic ion uptake as revealed by concurrent flux and cell turgor measurements. Plant Physiol 129:290–299

Shabala S, Newman IA (1997a) H^+ flux kinetics around plant roots after short-term exposure to low temperature—identifying critical temperatures for plant chilling tolerance. Plant Cell Environ 20:1401–1410

Shabala S, Newman IA (1997b) Proton and calcium flux oscillations in the elongation region correlate with root nutation. Physiol Plant 100:917–926

Shabala S, Newman I (1999) Light-induced changes in hydrogen, calcium, potassium, and chloride ion fluxes and concentrations from the mesophyll and epidermal tissues of bean leaves. Understanding the Ionic basis of light-induced bioelectrogenesis. Plant Physiol 119:1115–1124

Shabala S, Newman IA, Morris J (1997) Oscillations in H^+ and Ca^{2+} ion fluxes around the elongation region of corn roots and effects of external pH. Plant Physiol 113:111–118

Shabala S, Newman I, Whittington J, Juswono U (1998) Protoplast ion fluxes: their measurement and variation with time, position and osmoticum. Planta 204:146–152

Shabala L, Shabala S, Ross T, McMeekin T (2001) Membrane transport activity and ultradian ion flux oscillations associated with cell cycle of *Thraustochytrium sp*. Austral J Plant Physiol 28:87–99

Shabala S, Shabala L, Van Volkenburgh E (2003) Effect of calcium on root development and root ion fluxes in salinised barley seedlings. Funct Plant Biol 30:507–514

Shabala L, Ross T, McMeekin T, Shabala S (2006) Non-invasive microelectrode ion flux measurements to study adaptive responses of microorganisms to the environment. FEMS Microbial Rev 30:472–486

Shabala L, Sanchez-Pastor E, Trujillo X, Shabala S, Muniz J, Huerta M (2008) Effects of verapamil and gadolinium on caffeine-induced contractures and calcium fluxes in frog slow skeletal muscle fibers. J Membr Biol 221:7–13

Shabala L, Bowman J, Brown J, Ross T, McMeekin T, Shabala S (2009a) Ion transport and osmotic adjustment in *Escherichia coli* in response to ionic and non-ionic osmotica. Environ Microbiol 11:137–148

Shabala L, McMeekin T, Shabala S (2009b) Osmotic adjustment and requirement for sodium in marine protist thraustochytrid. Environ Microbiol 11:1835–1843

Shabala S, Baekgaard L, Shabala L, Fuglsang A, Babourina O, Palmgren MG, Cuin TA, Rengel Z, Nemchinov LG (2011) Plasma membrane Ca^{2+} transporters mediate virus-induced acquired resistance to oxidative stress. Plant Cell Environ 34:406–417

Smith PJS, Hammar K, Porterfield DM, Sanger RH, Trimarchi JR (1999) Self-referencing, non-invasive, ion selective electrode for single cell detection of trans-plasma membrane calcium flux. Microsc Res Techniqe 46:398–417

Spalding EP (2000) Ion channels and the transduction of light signals. Plant Cell Environ 23:665–674

Tegg RS, Melian L, Wilson CR, Shabala S (2005) Plant cell growth and ion flux responses to the *Streptomycete* phytotoxin thaxtomin-A: calcium and hydrogen flux patterns revealed by the non-invasive MIFE technique. Plant Cell Physiol 46:638–648

Tester M (1997) Techniques for studying ion channels: an introduction. J Exp Bot 48:353–359

Tester M, Davenport R (2003) Na^+ tolerance and Na^+ transport in higher plants. Ann Bot 91:503–527

Tomos AD, Leigh RA (1999) The pressure probe: a versatile tool in plant cell physiology. Annu Rev Plant Physiol Plant Mol Biol 50:447–472

Tyerman SD, Beilby M, Whittington J, Juswono U, Newman I, Shabala S (2001) Oscillations in proton transport revealed from simultaneous measurements of net current and net proton fluxes from isolated root protoplasts: MIFE meets patch-clamp. Austral J Plant Physiol 28:591–604

Valencia-Cruz G, Shabala L, Delgado-Enciso I, Shabala S, Bonales-Alatorre E, Pottosin II, Dobrovinskaya OR (2009) K-bg and Kv1.3 channels mediate potassium efflux in the early phase of apoptosis in jurkat T lymphocytes. Am J Physiol, Cell Physiol 297:C1544–C1553

Ward JM (2001) Identification of novel families of membrane proteins from the model plant *Arabidopsis thaliana*. Bioinformatics 17:560–563

Zhang Q, Lauchli A, Greenway H (1992) Effects of anoxia on solute loss from beetroot storage tissue. J Exp Bot 43:897–905

Zhu JK (2003) Regulation of ion homeostasis under salt stress. Curr Opin Plant Biol 6:441–445

Zimmermann S, Ehrhardt T, Plesch G, Muller-Rober B (1999) Ion channels in plant signalling. Cell Mol Life Sci 55:183–203

Chapter 8
Multielectrode Array: A New Approach to Plant Electrophysiology

Elisa Masi, Elisa Azzarello and Stefano Mancuso

Abstract A number of recent technical advances allowed the ideation of the multielectrode array (MEA) technology, a valuable tool to record electrical activity with high information content both in the spatial and temporal dimensions. Microfabricated arrays, recording hardware and software for data acquisition and analysis, are now commercially available and enable continuous, stable recordings. Here, the MEA system and the different arrays available are reviewed with regard to their intrinsic characteristics and performances. Some interesting applications of the MEA approach in plants and in combination with other techniques (e.g. imaging) are mentioned. Due to the emerging demand for novel electrophysiological methods that allows automated recording from cells and tissues, it is expected that the MEA technology will become a widely accepted and used tool in the field of plant electrophysiology.

Abbreviations

MEA	Multielectrode array
PBC	Printed board circuit
S/N	Signal-to-noise
Au	Gold
Pt	Platinum
TiN	Titanium nitride
ITO	Indium tin-doped oxide
IED	Interelectrode distance
pMEA	Perforated MEA

E. Masi · E. Azzarello · S. Mancuso (✉)
Department of Plant, Soil and Environment, University of Florence,
Viale delle Idee 30, 50019 Sesto Fiorentino, Firenze (FI), Italy
e-mail: stefano.mancuso@unifi.it

A. G. Volkov (ed.), *Plant Electrophysiology*,
DOI: 10.1007/978-3-642-29119-7_8, © Springer-Verlag Berlin Heidelberg 2012

PGP	Perfusion ground plate
FlexMEA	Flexible MEA
3D MEA	3D MEA
HD-MEA	High-density MEA
CMOS	Complementary metal–oxide–semiconductor
LAPS	Light addressable potentiometric sensors
AP	Action potential
VP	Variation potential

8.1 Introduction

While considerable progress has been made over the past decades in the understanding of plant electrophysiological processes at the single-channel level, the comprehension of electrophysiological processes at the cellular network level is still in its infancy. This is in large part due to the technical difficulties of recording electrical activity from large numbers of cells simultaneously and for prolonged periods of time. In fact, it is technically difficult to record from and stimulate more than three cells concurrently using standard intracellular microelectrodes; moreover, these cells usually die within minutes or, rarely, hours (Mancuso 1999; Volkov 2006).

Optical techniques using voltage-sensitive dyes, although showing good spatial resolution, sometimes suffer from a low signal-to-noise (S/N) ratio (Kerr and Denk 2008). Furthermore, as it was recently demonstrated by Flickinger et al. (2010), in a study on the use of voltage-sensitive dyes in protoplasts of *Nicotiana spp*., in comparison with animal cells, the field-strength-dependence of the protoplast's transmembrane potential shows strong asymmetric saturation characteristics due to the influence of the higher resting potential. Nevertheless, they were able to measure high-resolution time-courses of the transmembrane potential following an external field pulse.

In recent years, enormous progress has been made in the field of the electrophysiological application of cellular systems with direct surface multielectrode coupling, notably in the core areas of medical research and pharmaceutical drug discovery. More recently, the pioneering work of Masi et al. (2009) in plant roots opened the way to the use of this multi-site recording technique for the analysis and detection of electrical activity in plant tissues, mainly in root apices.

The interdisciplinary integration of microelectronics—specifically in the field of microelectrode arrays (MEAs)—with modern tissue engineering, has meant the combination of two promising technologies and has determined great innovations in plant electrophysiology by developing new products and applications. In fact, the possibility to study intact plant tissues, where structural relationships among cells are preserved, provides fruitful information about the cellular networks.

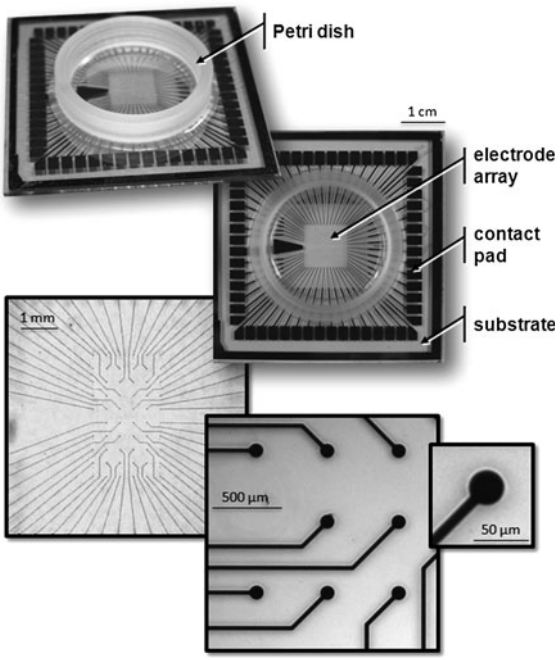

Fig. 8.1 Standard microelectrode array (*MEA*) with 60 electrodes (diameter of 30 µm, IED of 500 µm) arranged in 6 × 10 matrix at different magnifications

Here, we give an overview on selected MEA applications. Additionally, biophysical considerations on generation, spread, and recording of field potentials and concepts for the analysis of extracellular electrical signals are presented.

8.2 History of MEA Development

Traditionally, the excitable properties of cells have been studied using glass micropipette electrodes. Because each electrode must be held and tediously positioned by a bulky mechanical micromanipulator, it is very difficult to record from or stimulate more than few cells at a time. Multielectrode array (MEA) culture dishes (Fig. 8.1) allow simultaneous recording from and stimulation of over a hundred sites, greatly expanding our field of view, while keeping the single cell in sharp focus. These wired Petri dishes are most often referred to as MEAs (multielectrode arrays or microelectrode arrays), but have also been called multimicroelectrode plates, planar electrode arrays, and multielectrode dishes. MEA technology enables the study of distributed patterns of electrical activity in cultured networks via noninvasive extracellular electrodes built into the substrate. These electrodes can also be used to stimulate samples extracellularly and nondestructively (Regehr et al. 1989; Gross et al. 1993), allowing a long-term two-way connection between them and a computer.

MEAs have been around for a while; Thomas and co-workers first described MEAs for monitoring activity in electrically excitable cells in 1972 (Thomas et al. 1972). They recorded field potentials from spontaneously contracting sheets of cultured cardiac myocytes, but could not record activity from single cells. A few years later, Gross (1979) and Pine (1980) independently developed arrays for chronic multi-single-cell recording and electrical stimulation of cultured neuronal networks.

In the following years, custom-made MEAs, hardware, and software were created by each of the labs that dared to get involved in this technically demanding field (for references, see Potter 2001), allowing a remarkable step forward in MEA applications. As a result, MEA technology is now accessible to labs whose research topics do not necessarily focus on computer programming, array microfabrication, or electronics development. Complete MEA systems capable of recording from at least 60 electrodes have been produced first by Multichannel Systems from Germany, Panasonic from Japan, and Plexon Inc from Texas, USA. Starting from these, some other companies (for example, BioCell-Interface SA from Switzerland and Axion Bio Systems from USA) have started to develop complete multielectrode systems and chips.

Since then, the MEA technology and the related methods for electrophysiological cell and tissue assay have been continually improved, with the development of high-quality arrays with novel electrodes suitable for long-term monitoring with a sufficient S/N ratio, the establishment of advanced applications, and the final analysis of the data.

8.3 Extracellular Recording with MEA Technology

With MEAs, extracellular potentials deriving from single cells or tissues are monitored and recorded at the 2D surface of a conductive sheet where a sample with electrogenic cells is put into contact with the planar substrate as sketched in Fig. 8.2.

The electrical activity of cells that can be recorded extracellularly by microelectrodes is due to the movement of ions through the channels that span the membranes of cells in their immediate vicinity and generates a flow of current through the extracellular fluid surrounding the cellular signal sources.

Starting from the studies of Kovacs (1994), many electrical engineers have discussed and modeled the cell/microelectrode interface (for an in-depth description see Fromherz 2003). A simplified model circuit for an electrogenic cell on top of a microelectrode is presented in Fig. 8.3. The local alteration of the ion channel conductance of the cells produces an extracellular field potential with a time course that is approximately equal to the transmembrane current of the active cellular compartments. For fast events, the transmembrane current and therefore the extracellular recording is roughly equal to the first derivative of the transmembrane potential (Johnston and Wu 1995). This was well illustrated by Stett

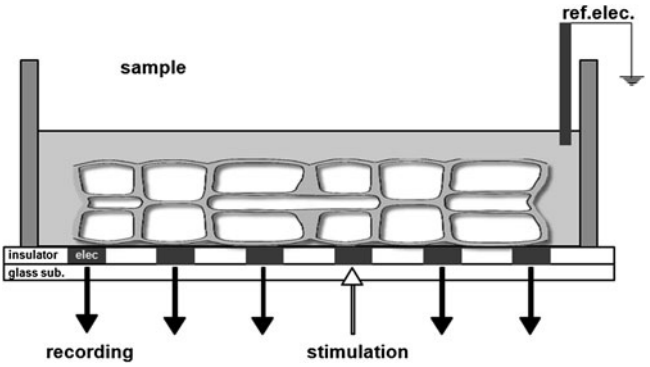

Fig. 8.2 Stimulation and recording of electrical activity in a plant sample with MEA system. The substrate-integrated planar electrodes can be used for both recording and stimulation (elec, electrode; ref.elec., reference electrode)

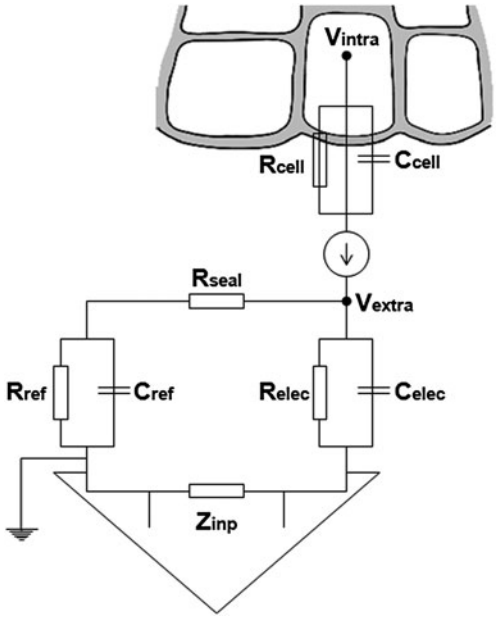

Fig. 8.3 Simplified model circuit for an electrogenic cell on top of a microelectrode. Vintra, intracellular potential; Vextra, extracellular potential; Rseal, sealing resistance (a measure of the quality of a contact between cell and electrode surface); Relec and Celec, resistance and capacitance of the recording electrode, respectively; Rcell and Ccell, resistance and capacitance of the cell membrane, respectively (adapted from Kovacs 1994)

et al. (2003) that measured simultaneously the electrical activity of single cells by using concurrently a conventional impaled microelectrode and a MEA system (Fig. 8.4).

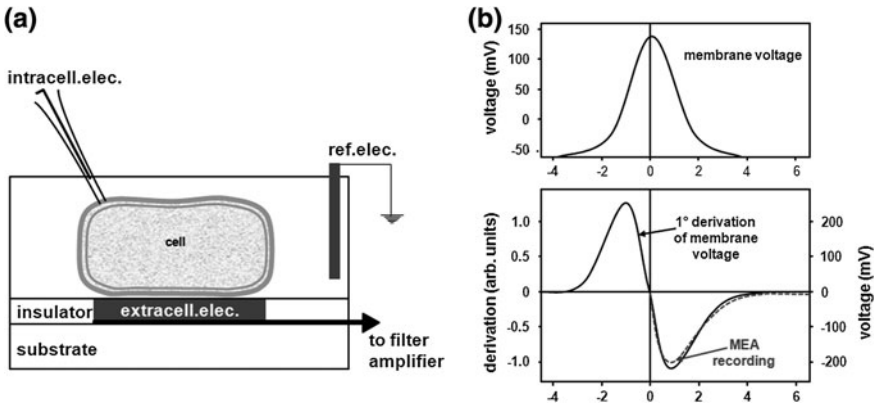

Fig. 8.4 (**a**) A single cell activity is simultaneously detected intracellularly with a conventional microelectrode and extracellularly by a microelectrode: the cell covers completely one single MEA electrode; (**b**) comparison of intracellular and corresponding extracellular voltage is shown: a Gaussian-like membrane voltage clamp (*top trace*) and MEA recording of the corresponding extracellular voltage (*bottom*, *dot grey line*) and first derivative of membrane potential (*black line*) are shown (adapted from Stett et al. 2003)

Nevertheless, no definitive theory of signal transduction is available to interpret or predict signals recorded with planar MEAs. In fact, many parameters remain difficult to quantify; these include differences in the cell-electrode distance, the coverage of the electrode by the cell, differences in the nature, and density of ion channels in the cell membrane.

As a consequence, the signal recorded from a MEA system may, sometimes, exhibit strong variation in amplitude and waveform from one electrode to another. This should be taken in account when analyzing data, while the information available in the timestamps of the signals can be used for statistical analysis without ambiguity on the nature of data.

For example, when recording from single cells cultured on the MEA surface, individual ones may contact partially the planar electrodes. Thus, the cell body is partially covering the electrode surface, and the free electrode area is in contact with the external saline and connected to ground. The amplifier connected to the conducting lane records the sum of the potentials at the surface of the free electrode and the surface of the electrode covered by the membrane. In this case, the amplitude of the recorded signal depends roughly linearly on the ratio of the covered electrode area and the entire electrode area (Fejtl et al. 2006).

When recording from tissue sheets, the signal sources that generate the field potential are compartments of single cells. The electrical activity, recorded with respect to the reference electrode, spreads within the cellular compartments and from cells to cells via plasmodesmata connections. This spread of excitation within cells and the tissue is always accompanied by the flow of ionic current through the extracellular fluid. Related to the current is an extracellular voltage gradient that varies in time and space according to the time course of the temporal activity as

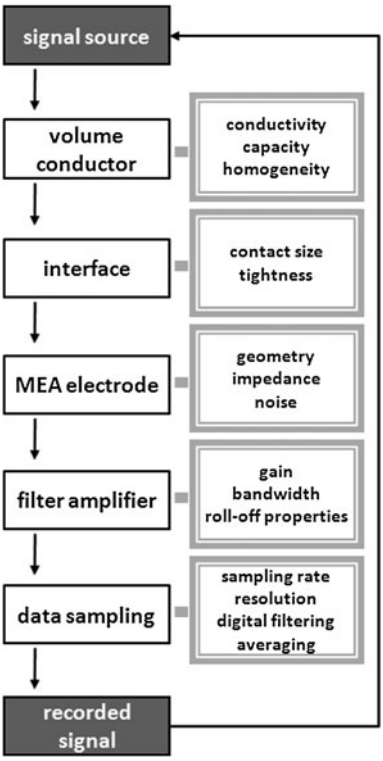

Fig. 8.5 Pathway showing factors and parameters involved in signal recording with a MEA system (adapted from Fejtl et al. 2006)

well as the spatial distribution and orientation of the cells. The MEA system allows the recording of both slow field potentials as well as fast spikes arising from action potentials (AP).

In order to understand the factors affecting the performance of the system, a pathway of the main components of the entire system and involved parameters that have to be considered, has been schematized in Fig. 8.5. The system is basically composed of the cellular signal sources and the tissue allowing spread of ionic current; the contact between the cell and the tissue, respectively, and the electrodes; the substrate and the microelectrodes embedded in an insulator layer; the external hardware with stimulators and filter amplifiers connected to the electrodes (Fejtl et al. 2006).

Besides ensuring tissue vitality (see below) and adequate conditions for cell culture, the probably most critical aspect for successful recording from acute slice preparations with MEAs is establishing and maintaining a very close contact between tissue and electrode. From the perspective of the equivalent circuit, decreasing this distance increases the seal resistance between the electrode tip and the reference electrode, and thus the S/N ratio in the recording. This can be implemented by either carefully pressing the tissue onto the array or, probably less stressful for the tissue, gluing the slice onto the MEA using an adhesive coating, e.g., polyethylenimine (PEI) or cellulose nitrate. As an example, in order to have

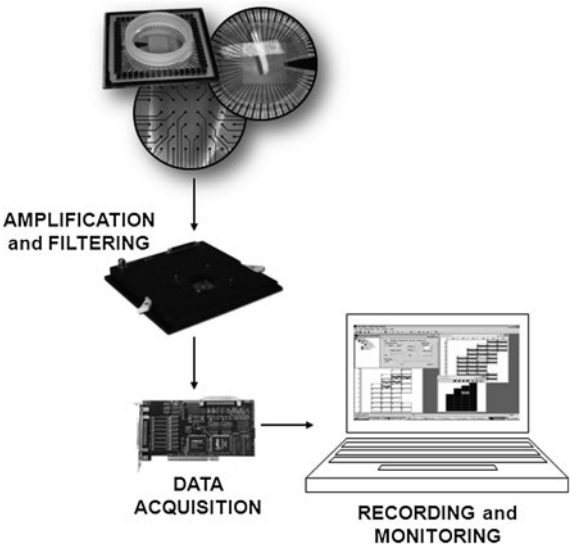

Fig. 8.6 Schematization of a classical MEA system. A longitudinal section of maize root fixed to the MEA array for recording. Is shown on *top*

good adhesion of root section of maize to the array, Masi et al. (2009) used an adhesive water permeable and water resistant tape (3M Micropore Surgical Tape) that mediate close and flat adhesion of the slice to the MEA surface, allowing in the meantime superfusion of the tissue (Fig. 8.6).

8.4 Extracellular Electrical Stimulation with MEA

The MEA system also allows extracellular electrical stimulation by applying either current or voltage impulses to the electrodes. Application of voltage to the electrodes charges the capacity of the electrical double layer of the metal-electrolyte interface. This leads to fast, strong but transient, capacitive currents with opposite sign at the rising and falling edges of voltage pulses resulting in transient hyperpolarization and depolarization of cellular membranes (Stett et al. 2000). Obviously, membrane polarization of the target cell is primarily affected by the voltage gradient generated by the local current density and tissue resistance in the vicinity of the cells. Thus the stimulation efficacy depends on the effective spread of the injected current within the electrode-tissue interface and within the tissue.

8.5 The MEA System

The classical MEA system consists of a data acquisition computer and MEA amplifiers for 60–256 channels recordings from a MEA chip (Fig. 8.6).

Other instruments can be added, such as temperature controller, stimulator, and recirculation system.

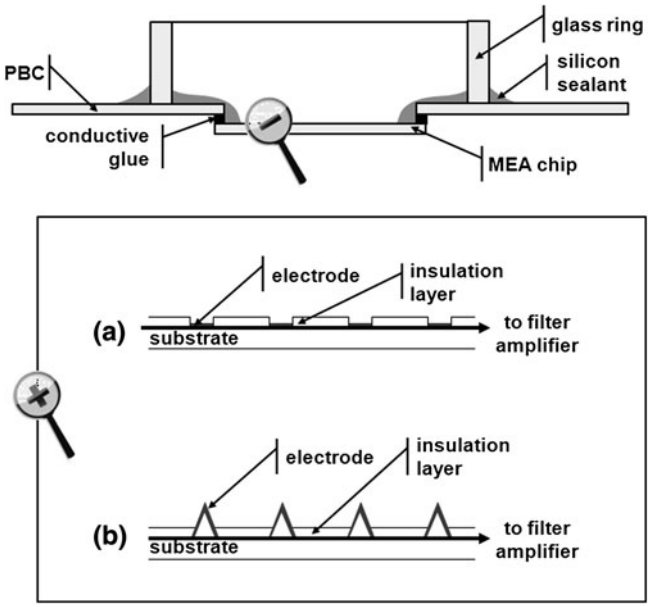

Fig. 8.7 Schematic cross-section of a MEA array (*top*) and MEA chips (*bottom*): (**a**) standard MEA chip; (**b**) 3D MEA chip. The MEA chip is glued under a printed circuit board (*PBC*) for interfacing to signal amplification and data acquisition system. A glass ring, which is fixed on the *top* of the PBC, and sealed to the MEA array using silicone rubber, builds a watertight culture chamber

The core element is the MEA amplifier whose number can range from one to four. Each amplifier can run completely independent experiments. A data acquisition card allows the signals to be recorded and displayed on a computer with a sampling frequency up to 50 kHz.

8.5.1 Multi Electrode Arrays

Most commercially available MEAs consist of a substrate (5 × 5 cm) where a number of cell-sized electrodes are arrayed embedded in an electrode insulation layer and a glass ring building a culture chamber of about 1.5–3 ml, depending on the ring diameter (Figs. 8.1 and 8.7 top). The substrate where microelectrodes are embedded is usually transparent glass to guarantee good chemical and electrical isolation and to allow observations with an inverted microscope. A printed circuit boards (PCB) is used to interface MEA chips to data acquisition systems (Fig. 8.7a).

Microelectrodes must have reasonable low impedance; a high S/N ratio is necessary to allow the detection of small extracellular signals (from 10 to 100 μV).

Low impedance is also requested to allow the propagation of sufficient stimulation current without exceeding the electrochemical breakdown voltage of the medium. Initially, this was achieved with electrodes made of platinized gold (Pt–Au); the electroporation with porous platinum ("Pt black") treatment decreases typical Au impedance even if such electrodes are not stable over a long time period due to the degradation of the Pt layer and thus they have to be replatinized in order to be used again. Furthermore, Pt-black electrodes tend to increase their impedance when reused and even during long-term recordings. The practice to electroporate while sonicating can reduce greatly this problem (Marrese 1987).

In order to have durable MEA electrodes, new low impedance electrode coatings have been developed, starting from the use of indium tin-doped oxide, ITO (Blau et al. 1997), or titanium nitride, TiN (Egert et al. 1998).

Finally, the surface of the array and electrodes are treated with some biocompatible insulator (usually polyimide or silicon nitride/oxyde) that prevents electrical shorting to the bath, and allows sample adhesion after coating with, for example, polyaminoacids or laminin.

Increasing demand for specific MEA layouts based on specific biological questions, has determined an ongoing development of MEAs with custom designed layouts geared toward specific applications. So far, specific MEA layouts have been designed for many applications.

The standard type of MEA comes in a pattern of 8×8 or 6×10 electrodes, whose diameter ranges between 10 and 30 μm and the interelectrode distance (IED) between 100 and 500 μm; with these configurations, the recording area varies from 0.35 to 12.25 mm^2. However, many other arrangements of the electrodes are available.

MEA electrodes have demonstrated to be highly sensitive in detecting signals at distance up to 100 μm from the source of them (experiments performed with array where electrodes of 10–20 μm of diameter were arranged in an 8×8 grid with IED of 100–200 μm). However, signal sources can be better detected within a radius of 30 μm around the MEA electrode center (Egert et al. 2002).

Arrays must be grounded with a reference electrode located in the bath; accordingly most of the MEAs are provided with an internal embedded reference electrode.

Some other types of MEAs and their characteristics are briefly illustrated in the following paragraphs.

- *Thin MEA* The glass substrate is replaced with a thinner one (about 180 μm size as a coverslip glass); it is ideal when high-resolution imaging is combined with MEA technology (Eytan et al. 2004; Molina-Luna et al. 2007).
- *pMEA* (*perforated MEA*) The substrate is manufactured on a thin polyimide foil instead of glass. Around the electrode field there is a circular area where the foil is perforated so that, in combination with a perfusion ground plate (PGP), tissue perfusion from the bottom can be possible while recording. From the openings situated on the substrate, a negative pressure can be also applied that enhances

the contact between the sample and the electrodes thus increasing the magnitude of the recorded signals (Boppart et al. 1992).

- *Flexible/Stretchable MEA* Also known as Flex MEA, in this alternative approach metal electrodes are encased into a more flexible polymeric substrate. Boppart et al. (1992) used a kind of polymidine, fabricating an array that is flexible and able to conform to the surfaces of the sample. In the following years, other technologies were developed, based, for example, on the use of stretchable thin gold films embedded on elastomeric substrates; these fabricated electronic surfaces are capable of both bending and stretching, thus an improvement of the conformability of electro-biological interfaces can be achieved (Tsay et al. 2005). Flexible/Stretchable MEA technologies are frequently associated to perforate ones.
- *3D MEA* In 3D microarrays the number of sites and eventually the surface area is increased by not only using a higher number of electrodes but also by increasing the dimension of the recording area in the z-axis, i.e., height (Fig. 8.7b). This allows a better seal resistance between the tissue and the electrodes that may sometimes be difficult because of the dead cell layers present at the surface of the slice, a consequence of the cutting procedure. The recorded signals are clearer and with higher amplitude when compared to the use of a standard 2D MEA (Heusckel et al. 2002).
- *High-Density MEA* In order to increase the spatial resolution, MEA arrays with a higher density of electrodes (HD-MEA) in respect to standard ones have been developed. The first approach consisted in a layout of 256 electrodes arranged in a square grid pattern utilizing 100 μm as IED distance in the center of the recording area and 200 μm in the periphery. The total recording area was of 2.80 mm^2 (Fejtl et al. 2006). Bucher et al. (2001) used a methodology based on light addressable potentiometric sensors (LAPS) to increase the number of electrodes that could be built on a MEA chip; nevertheless, the technology revealed to be unsuitable for long-term recording due to toxicity problems. A further concept, based on standard complementary metal–oxide–semiconductor (CMOS) technology, was then proposed (Eversmann et al. 2003; Berdondini et al. 2004; Frey et al. 2009). The CMOS-based HD-MEA array consists of 11.011 electrodes (diameter of 7 μm) arranged in a matrix of 2.00 × 1.75 mm: the resulting density is of 3.150 electrodes per mm^2 (Fig. 8.8). The chip has a circuitry channels system that allows the recording (and stimulation) from 126 electrodes simultaneously. Flexibility in the electrode selection is achieved by a switch tool integrated in the electrode array; the spatial resolution of the recordings can thus be chosen depending on the requirements of the experiments. For example, a preliminary scanning phase at lower spatial resolution can be automated all over the recording area for the individuation of "points" of interest of the sample, followed by a second scanning phase at higher resolution. With this setup, recordings can be performed at single-cell or even subcellular level, potentially enabling the characterization of ion channel properties and ion channel distributions in single cells.

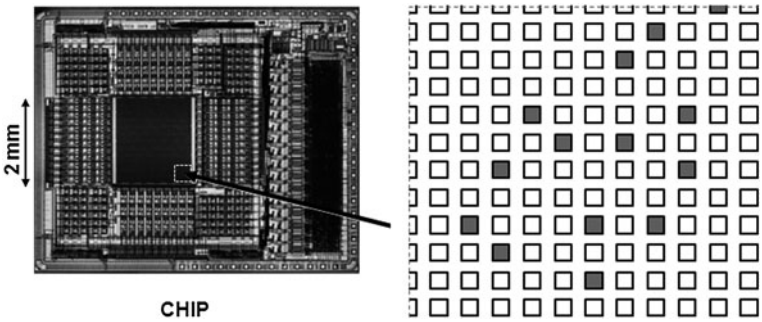

Fig. 8.8 CMOS-based HD-MEA. *Left*: micrograph of the chip where the actual electrode array is visible as the black square in the center. The array is surrounded by three amplification and filtering stages per channel, by the stimulation buffers, the analog-digital converter and the digital core at the right. *Right*: scheme of a magnification of the electrodes arrangement where both active (*grey*) and inactive (*white*) electrodes are shown (adapted from Frey *et al*. 2009)

8.6 Interpretation of Recorded Signal-Data Processing

When interpreting signals, it is important to consider the following aspect:

- the cells size;
- the electrode size;
- the IED;
- the number of layers of cells that insist on the same array/electrode.

The recorded signal may be analyzed for individual spikes (the extracellular signal correlated to an AP) or the spikes correlated to one or more cells. In fact, the electrical signals detected at any single site in the extracellular space must be regarded as the sum of contributions coming from all of the current sources in contact with each electrode and within the recording horizon of the electrode (Egert et al. 2002; Halbach et al. 2003).

In addition to APs, plants also show VPs (variation potentials or slow wave potentials) that can interfere in data interpretation. Depending on the properties of the recording setup, APs and VPs may occur as a mix, which is often separated by appropriate filtering of the raw voltage trace.

Furthermore, the detection area that a single electrode can cover depends on the characteristics of the array. According to what has been said before, each electrode of a standard array has an optimum detection radius of 30 μm around itself. Masi et al. (2009) used standard MEAs to detect the electrical activity of root apices of maize. Using an IED of 500 μm, they reasonably assumed that the electrical signals generated by a single root cell were detected by just one electrode.

It is worth noting that the choice of the recording and processing setup greatly influences the interpretation of signals.

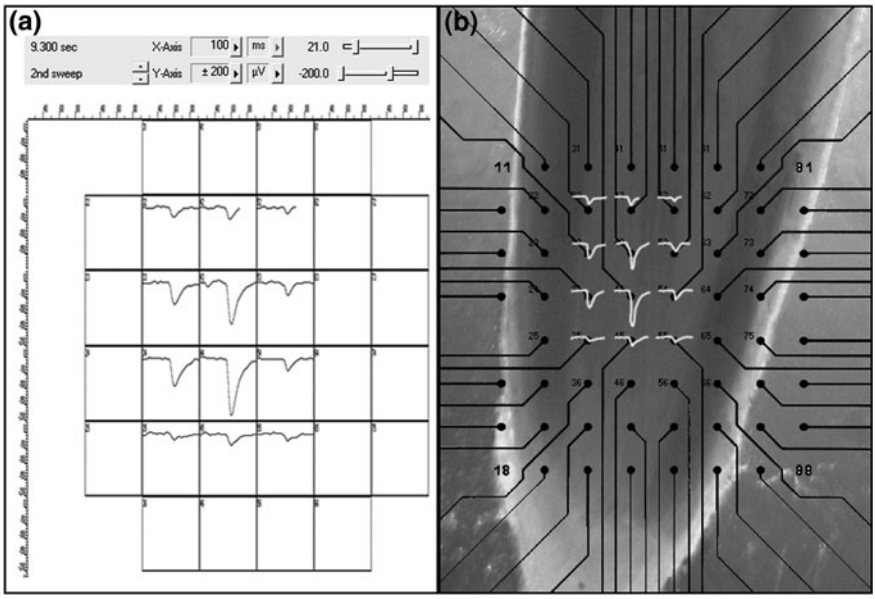

Fig. 8.9 Example of screen shot taken during data post-processing. (**a**) Each box represents the recording area of one electrode; several spikes detected can be seen. (**b**) The image taken with the microscope is superimposed to the matrix of electrodes; spikes detected can be then analyzed in respect to their spatial distribution on the sample

Data processing in all multielectrode recording means processing of a large amount of data acquired in each experiment. For a 60-electrode array, for example, continuous recording at a sampling rate of 20 kHz with a 12-bit AD converter amounts to approximately 1 MB per second.

The analysis process is generally segregated into online and offline steps. During the recording, in fact, the experiment can be monitored and some quick analyses can be performed for important parameters, such as spike rate. Offline analysis may either require more processing time or more of the experimenter's attention than during an experiment. Raw data need, in fact, to be properly filtered in order to remove artifacts and improve S/N ratio. Spike detection is then performed on filtered data using, for example, the threshold method: waveforms that meet the requirements defined are cut out from the raw data and their timestamps and shapes are stored.

Timestamps data can be used for the analysis of the spatial distribution of electrical activity by combining it with histological data, such as cell type or tissue anatomy; for this purpose, images from the microscope showing the position of the sample on the array are routinely taken and superimposed to the data display of the activity (Fig. 8.9). Many other analyses can be done on timestamps data, such as spike rate, spike rate *versus* time, interspike interval histogram, correlation across different recording sites, raster plots, etc.

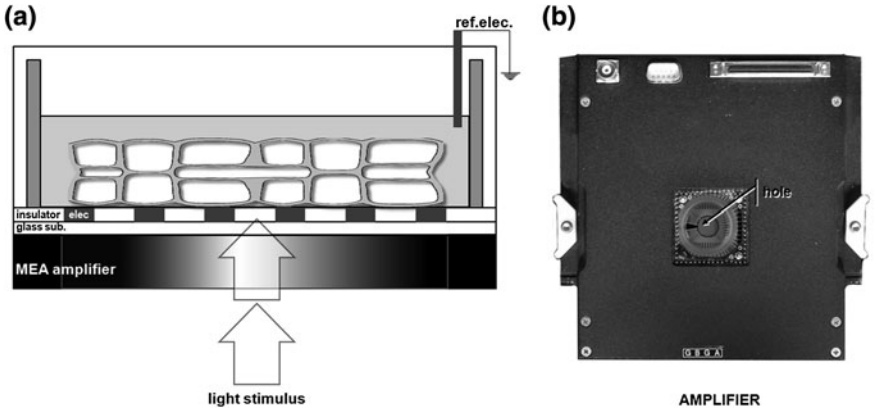

Fig. 8.10 **a** A plant slice placed onto a MEA system can be light stimulated also from the bottom part (cut cell side) due to the presence of an hole on the amplifier that allow the passage of light. **b** View of on amplifier from the top: the center of the MEA array, where the sample is plated, is located in correspondence of a hole

Data on shape can be used for extraction of minima, maxima, and duration of each spike, and for the general analysis on waveforms.

These analyses need automated processing allowing comparisons of the electrical activity recorded by different electrodes within and across experiments. Some commercial software tools are available, and many laboratories have developed their own routines for specific applications and experimental conditions.

8.7 MEA System Applications

In principle, any part of the plant can be placed onto a MEA in order to study cell electrical activity. Masi et al. (2009) applied the MEA technology to the study of the electrical activity of maize root apex. For that purpose, caryopses of *Zea mays* L. were soaked in distilled water and placed between damp paper towels in Petri dishes. After the roots reached a length of about 3 cm, longitudinal and transversal slices from the primary root tip were cut with a tissue slicer and were stored and submerged for 2 h in $CaCl_2$ 5 mM (pH 6.5) at room temperature before recording. Recordings were performed with tissues submerged in bath solution by means of a perfusion system. The perfusion system was also used to screen the effect of increasing concentration of $CaCl_2$ and the effect of L-glutamate on the root electrical activity.

Furthermore, almost any kind of environmental stimuli can be evoked during a recording session. If necessary, light stimulation can be performed as well. The light stimulus is projected from the bottom through the transparent MEA glass insulator and directly reaches the sample (Fig. 8.10).

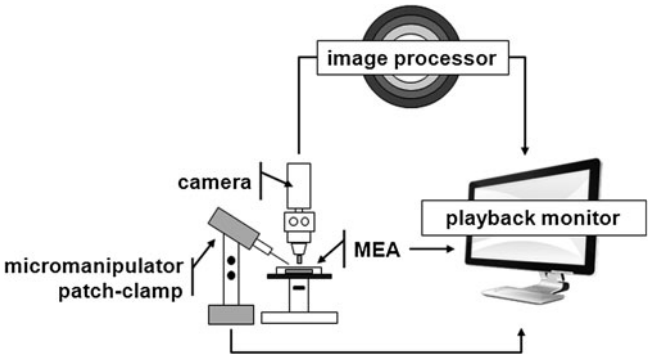

Fig. 8.11 A simple arrangement of the setup for simultaneous recording of the electrical activity with a MEA system, patch-clamp and imaging

The MEA system can be also used in combination with fluorescence imaging and patch-clamping, as numerous applications in the field of neuroscience have already been reported (Fig. 8.11). Takayama et al. (2008), for example, investigated the transition of spontaneous intracellular calcium dynamics and the relationship between calcium transients and electrical activity during the recording of electrical activity of cultured cortical cells by a MEA system. They could observe periodic synchronized calcium transients following synchronized bursting of spikes and speculate on the role of calcium waves in the generation of the electrical network activity of neuronal cells.

Kandler et al. (2010), monitoring the synchronized electrical activity intracellularly and extracellularly with dual patch-clamp electrodes and MEA, gained insight into the underlying network connectivity and the activity dynamics on a single neuron and at population level.

These applications could be also useful to better understand the not completely clear ion mechanisms undergoing the generation of electrical signals in plant cells.

8.8 Conclusion

The present and future significance of MEA technology is entrenched in one or a combination of the following motivations:

- noninvasive multisite recording and stimulation of any kind of cell or tissue: in fact, direct access to cells for electrical stimulation and contemporary recording can be achieved without any damage;
- optimization of the experimental conditions, reducing the time required for an experiment by simultaneously recording at several sites in parallel;
- sampling the distribution of electrophysiological behavior efficiently, which may include comparison of tissue properties at different locations;

- high spatio-temporal dynamics analysis of interactions between electrogenic cells at different locations in the same tissue;
- monitoring the changes of electrical activity over periods of time not accessible with individual conventional electrodes for in vitro experiments;
- setting up controls within the same experimental setup by using one electrode as a control and others as experimental;
- performing functional studies, in vitro but noninvasively, under physiological or induced stress conditions.

The MEA technology, initially developed for the field of animal neuroscience, has been already applied in plants (Masi et al. 2009), and it has revealed a useful tool for the study of the electrical network activity of root apex cells. In fact, both intense spontaneous electrical activities and locally propagating electrical signals were observed. Propagation of the spikes indicates the existence of excitable traveling waves in plants, similar to those observed in non-nerve electrogenic tissues of animals. Obtained data also revealed synchronous electric activities of root cells emerging in a specific root apex region, the transition zone. The study of the dynamic electrochemical activity of root apex cells by means of the MEA technology allowed the authors to speculate on the possible role of the electrical activity in plant's roots as a way to continuously integrate internal and external signaling for developmental adaptations in a changing environment.

It is therefore expected that, similar to what has happened in the field of neuroscience, the technique can become a standard tool also for plant electrophysiology.

References

Berdondini L, van der Wal PD, Guenat O, de Rooij NF, Koudelka-Hep M, Seitz P, Kaufmann R, Metzler P, Blanc N, Rohr S (2004) High-density electrode array for imaging in vitro electrophysiological activity. Biosens Bioelectron 21:167–174

Boppart SA, Wheeler BC, Wallace CS (1992) A flexible perforated microelectrode array for extended neural recordings. IEEE Trans Biomed Eng 39:37–42

Bucher V, Brunner B, Leibrock C, Schubert M, Nisch W (2001) Electrical properties of a light-addressable microelectrode chip with high electrode density for extracellular stimulation and recording of excitable cells. Biosens Bioelectron 16(3):205–210

Egert U, Knott T, Schwarz C, Nawrot M, Brandt A, Rotter S, Diesmann M (2002) MEA-tools: an open source toolbox for the analysis of multi-electrode data with MATLAB. J Neurosci Methods 117:33–42

Egert U, Schlosshauer B, Fennrich S, Nisch W, Fejtl M, Knott Th, Müller T, Hämmerle H (1998) A novel organotypic long-term culture of the rat hippocampus on substrate-integrated multielectrode arrays. Brain Res Protoc 2:229–242

Eversmann B, Jenkner M, Hofmann F, Paulus C, Brederlow R, Holzapfl B, Fromherz P, Merz M, Brenner M, Schreiter M, Gabl R, Plehnert K, Steinhauser M, Eckstein G, Schmitt-Landsiedel D, Thewes R (2003) A 128 × 128 CMOS biosensor array for extracellular recording of neural activity. IEEE J Solid-State Circuits 38(12):2306–2317

Eytan D, Minerbi A, Ziv NE, Marom S (2004) Dopamine-induced dispersion of correlations between action potentials in networks of cortical neurons. J Neurophysiol 92(3):1817–1824

Fejtl M, Stett A, Nisch W, Boven K-H, Möller A (2006) On micro-electrode array revival: its development, sophistication of recording, and stimulation. In: Taketani M, Baudry M (eds) Advances in network electrophysiology. Springer, Berlin

Flickinger B, Berghofer T, Eing C, Gusbeth C, Strassner R, Frey W (2010) Transmembrane-potential, easurements on plant cells using the voltage sensitive dye annine-6. Protoplasma 247:3–12

Frey U, Egert U, Heer F, Hafizovic S, Hierlemann A (2009) Microelectronic system for high-resolution mapping of extracellular electric fields applied to brain slices. Biosens Bioelectron 24:2191–2198

Fromherz P (2003) Neuroelectronic interfacing: semiconductor chips with ion channels, nerve cells, and brain. In: Waser J, Verlag W-VCH (eds) Nanoelectronics and information technology. Wiley VCH Publishing, Berlin

Gross GW (1979) Simultaneous single unit recording in vitro with a photoetched laser deinsulated gold multimicroelectrode surface. IEEE Trans Biomed Eng 26:273–279

Gross GW, Rhoades BK, Reust DL, Schwahn FU (1993) Stimulation of monolayer networks in culture through thin-fihn indium-tin oxide recording electrodes. J Neurosci Methods 50(2):131–143

Halbach MD, Egert U, Hescheler J, Banach K (2003) Estimation of action potential changes from field potential recordings in multi-cellular mouse cardiac myocyte cultures. Cell Physiol Biochem 13:271–284

Heusckel MO, Fejl M, Raggenbass M, Bertrand D, Renaud P (2002) A three dimensional multi-electrode array for multi-site stimulation and recording in acute brain slices. J Neurosci Methods 114:135–148

Johnston D, Wu MS (1995) Extracellular field recordings. In: foundations of cellular neurophysiology. MIT Press, Cambridge, MA

Kandler S, OkujeniS, Reinartz S, Egert U (2010) Networks in dissociated culture follow native corticaldevelopment. In: Stett A (ed) Proceedings MEA meeting 2010, Stuttgart: BIOPRO Baden-Württemberg GmbH 2010, pp 44–45

Kerr JND, Denk W (2008) Imaging in vivo: watching the brain in action. Nat Rev Neurosci 9:195–203

Kovacs G (1994) Introduction to the theory, design and modeling of thin-film microelectrodes for neural interfaces. In: Stenger DA, McKenna T (eds) Enabling technologies for cultured neural networks. Academic, San Diego

Marrese CA (1987) Preparation of strongly adherent platinum black coatings. Anal Chem 59:217–218

Mancuso S (1999) Hydraulic and electrical transmission of wound-induced signals in *Vitis vinifera*. Aust J Plant Physiol 26:55–61

Masi E, Ciszak M, Stefano G, Renna L, Azzarello E, Pandolfi C, Mugnai S, Baluska F, Arecchi T, Mancuso S (2009) Spatiotemporal dynamics of the electrical network activity in the root apex. PNAS 106:4048–4053

Molina-Luna K, Buitrago MM, Hertler B, Schubring M, Haiss F, Nisch W, Schulz JB, Luft AR (2007) Cortical stimulation mapping using epidurally implanted thin-film microelectrode arrays. J Neurosci Methods 161(1):118–125

Pine J (1980) Recording action potentials from cultured neurons with extracellular microcircuit electrodes. J Neunxci Methods 2:19–31

Potter SM (2001) Distributed processing in cultured neuronal networks. Prog Brain Res 130:49–62

Regehr WG, Pine J, Cohan CS, Mischke MD, Tank DW (1989) Sealing cultured invertebrate neurons to embedded dish electrodes facilitates long-term stimulation and recording. J Neurosci Methods 30(2):91–106

Stett A, Barth W, Weiss S, Haemmerle H, Zrenner E (2000) Electrical multisite stimulation of the isolated chicken retina. Vis Res 40:1785–1795

Stett A, Egert U, Guenther E, Hofmann F, Meyer T, Nisch W, Haemmerle H (2003) Biological application of microelectrode arrays in drug discovery and basic research. Anal Bioanal Chem 377:486–495

Takayama Y, Moriguchi H, Jimbo Y (2008) Site-selective stimulation and recording of the electrical activity of cultured neuronal networks using mobile microelectrodes. In: Proceedings of the international symposium on biological and physiological engineering, pp 159–162

Thomas CA, Springer PA, Loeb GE, Berwald-Netter Y, Okun LM (1972) A miniature microelectrode array to monitor the bioelectric activity of cultured cells. Exp Cell Res 74:61–66

Tsay C, Lacour SP, Wagner S, Morrison III B (2005) Architecture, fabrication, and properties of stretchable microelectrode arrays. In: Proceedings of the 4th IEEE conference on sensors, pp 1169–1172

Volkov AG (2006) Plant electrophysiology: theory and methods. Springer, Berlin

Chapter 9
Electrochemical Impedance Spectroscopy

E. Azzarello, E. Masi and S. Mancuso

Abstract Electrochemical impedance spectroscopy (EIS) is a method to study the characteristics of organic and inorganic materials, based on their passive electrical properties, determined by the observation of the tissue electrical response to the passage of external electrical energy. The impedance and phase angles of the materials is measured by a multiple frequency impedance analyzer (impedance meter) that is able to scan each sample at different frequencies. Electrochemical impedance have been widely used to estimate plant health, their nutrient status, mineral deficiency, presence of viruses, fruit damages, structural cellular variation during fruit ripening, freeze or chill damages, sensitivity to salinity, and measurement of root system growth in trees. In all these studies EIS measurements provided a means of nondestructively analyzing variation in intra- and extracellular resistances and in the condition of the membranes.The fundamental studies and some applications of EIS for the field of plant science are described, particularly in relation to root growth and development, seed quality, environmental stresses, and fruits damages or ripening.

9.1 Introduction

An electric circuit is formed by individual electronic components, through which electric current (i) can flow continuously. Voltage (v) is the measure of potential energy present in a circuit capable to move electrons from one point to another

E. Azzarello · E. Masi · S. Mancuso (✉)
Department of Plant, Soil and Environment, University of Florence,
Viale delle Idee 30, 50019 Sesto Fiorentino, Italy
e-mail: stefano.mancuso@unifi.it

A. G. Volkov (ed.), *Plant Electrophysiology*,
DOI: 10.1007/978-3-642-29119-7_9,

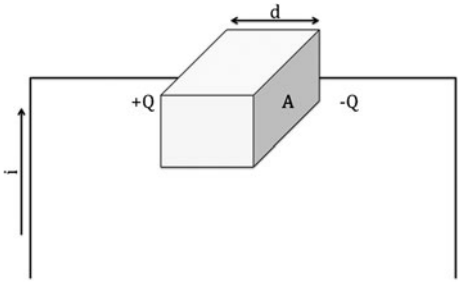

Fig. 9.1 Schematic representation of the parallel-plate structure related with the capacitance phenomenon. i = current, $+Q$=positive charges, $-Q$ = negative charges, d = distance between the two conductive plates, A = area of the plate

one. The opposition to a motion of free electrons in a circuit is called resistance (R) and, similar to voltage, is relative to two points.

Resistance is measured by the ratio between voltage and current (Ohm's law):

$$R = \frac{v}{i}. \tag{9.1}$$

In other words, the Ohm's law bases on a linear relation between voltage and current.

Indeed, the use of this equation is limited to an ideal resistor that must show three properties: (1) it follows Ohm's law at any current and voltage value; (2) resistance value does not depend on frequency; (3) alternate current and voltage signals, through a resistor, are in phase with each other. Charge carriers are able to move in materials that conduct electricity. In materials that do not conduct electricity, called dielectrics, all the charges are fixed. It can therefore be said that the resistance of an ideal conductor is 0 while the resistance of an ideal dielectric is infinite (Ivorra 2003).

The simplest example of a dielectric capacitor consists of two conducting plates placed on either side of a layer of dielectric material, and separated by a distance d (Fig. 9.1). The amount of charge that the dielectric is capable to store depends on its dimension and on a dielectric parameter called permittivity (ε) that indicates the extent to which charge distributions within the material can be distorted or polarized in response to an applied electric field (Martinez 2007). Capacitance is measured as

$$C = \frac{A}{d}\varepsilon, \tag{9.2}$$

where A is the area of the plane electrodes and d the separation distance, while $\varepsilon = \varepsilon_\rho \varepsilon_0$ is the permittivity, with ε_r indicating relative permittivity and ε_0 permittivity of a vacuum. Capacitance measures the relative amount of charge (Q) that can be stored on a pair of parallel plate for a given amount of voltage (v) when a constant voltage is applied between the electrodes.

$$C = \frac{Q}{v} \tag{9.3}$$

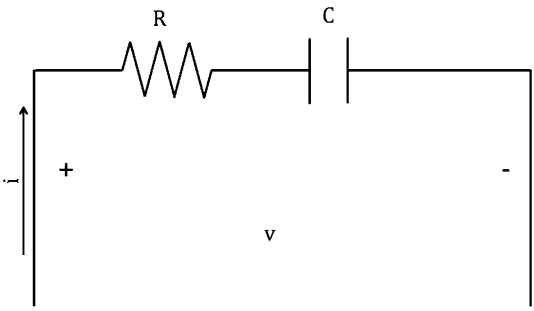

Fig. 9.2 Electrical circuit formed by a resistor and a capacitor in series

If the capacitance increases more charge can be stored when the same potential is applied.

If the capacitance voltage is constant, no current enters or leaves the capacitance. When voltage changes with time, a quantity of current can enter and leave the capacitor, charging or discharging it. In this way it can be assumed that, if a time varying voltage is applied to a capacitor, some current is able to flow through the source (Ivorra 2003).

As described above, resistance obeys the Ohm's law and the relation between voltage and current can be represented as a relation of magnitudes

$$Z = Re = R = \frac{v}{i} \tag{9.4}$$

On the contrary, impedance of a capacitor, called capacitive reactance, depends on frequency (f) and is defined as the relation between the input voltage and the input current for that frequency. It can be calculated as

$$Z = j\frac{1}{(2\pi fC)}, \tag{9.5}$$

where $j^2 = -1$ is the complex unit (indicating an anticlockwise rotation by $\pi/2$ relative to the x-axis) that relates to the phase angle.

At low frequencies the capacitor blocks the current flow, causing a very high impedance modulus. At high frequency, the current is free to flow through the capacitor that is not enough charged, thus causing a minor opposition to the flow (Ivorra 2003).

As a consequence of this, it can be said that the impedance of a circuit (Fig. 9.2) formed by a resistor and a capacitor in series can be calculated as

$$Z = R + j\frac{1}{(2\pi fC)} \tag{9.6}$$

9.2 Impedance Concept

Oliver Heaviside introduced, for the first time, the impedance concept in the 1880s (Filho 2002). Impedance is measured by applying a small alternating current of known frequency and small amplitude to a system, determining the amplitude and phase difference of the associated electrical potential that develops across it (Coster et al. 1996). In many materials impedance varies as the frequency of the applied voltage changes, due to the properties of the material itself. This may be due to its physical structure, to the chemical processes within it, or to the combination of both (Schröder et al. 2004).

Impedance Z is the quotient of the voltage–time function v(t) and the resulting current–time function i(t):

$$Z = \frac{v(t)}{i(t)} = \frac{v_0 \text{sen}(\omega t)}{i_0 \text{sen}(\omega t + \theta)}, \tag{9.7}$$

where v_0 and i_0 are the maximum voltage and current signals, $\omega = 2\pi f$ is the angular frequency, and θ is the phase difference between the voltage and the current (Pänke et al. 2008).

In Cartesian coordinates, impedance becomes a complex number, constituted of two components (Eq. 9.8–9.11):

$$Z(\omega) = \mathrm{Z_r}(\omega) + j\mathrm{Z_i}(\omega), \tag{9.8}$$

where

$$\mathrm{Z_r}(\omega) = |Z| cos(\theta) \tag{9.9}$$

is the real component,

$$\mathrm{Z_i}(\omega) = |Z| sen(\theta) \tag{9.10}$$

is the imaginary component or reactance,

$$\text{and } \theta = tan^{-1} \frac{Zi}{Zr} \tag{9.11}$$

is the impedance phase angle. Phase angle is a linear method for the measurement of the relationship between resistance and reactance in series or parallel circuits. Phase angle can range from 0 to 90°. When the angle is 0° the circuit is only resistive, at 90° the circuit is only capacitive, while at 45° the circuit has an equal amount of capacitive reactance and resistance (Liedtke 1997).

Finally, the relation between impedance and its individual component (resistance and reactance) can be represented as a vector (Fig. 9.3), whose magnitude is:

$$|Z(\omega)| = \sqrt{Z_r^2 + Z_i^2}. \tag{9.12}$$

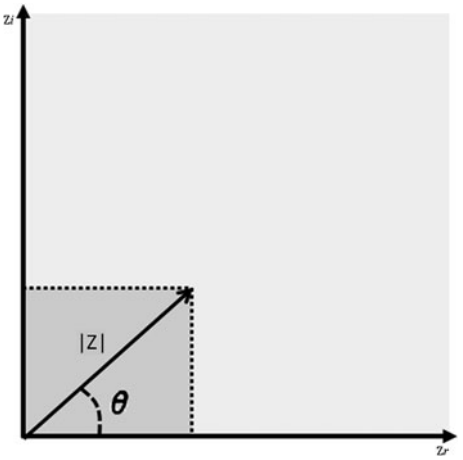

Fig. 9.3 Vector diagram showing relationship between resistance (Zr), reactance (Zi), and impedance

Fig. 9.4 Impedance spectrum (plot of reactance (*imaginary part*) against resistance (*real part*) with frequency as parametric variable)

The real and imaginary parts of Z describe the resistance and reactance, respectively. If the real part is plotted on the X-axis and the imaginary part on the Y-axis, an impedance spectrum, using the frequency as the parametric variable, is obtained (Fig. 9.4).

9.3 Electrochemical Impedance Spectroscopy

Electrochemical impedance spectroscopy (EIS) is a technology that can investigate electrical and electrochemical properties of different materials and systems. One of the most interesting aspects of EIS is the close correlation that exists between the

behavior of a real system and an idealized model circuit with discrete electrical components (Macdonald 1987).

EIS is a very sensitive technique and, although it does not provide a direct measure of the physical phenomena, is a valuable analysis method for materials with high ionic conduction, such as solid and liquid electrolytes, fused salts, ionically conducting glasses, and all materials where conduction involves motion of ion vacant and interstitial. EIS is also valuable in the study of fuel cells, rechargeable batteries, and corrosion (Macdonald 1992).

Of course, the measurements of electrical parameters are also very useful to characterize most events or conditions in human, animal, and plant tissues (Cole 1972; Lewis et al. 1989).

While in metals the electrical charge carriers are represented by electrons, ions are the charge carriers in biological tissues, and conductivity is dependent on their concentration and diffusion coefficients (Ackmann and Sitz 1984). All biological tissues consist of cells and extracellular matrix, an intricate network of macro and small molecules, ions, and water. Both extracellular and intracellular medium can be considered as liquid electrolytes whose viscosity varies with the temperature, decreasing or increasing ions mobility and consequently the resistance. Inside the cell, beside ions and charged molecules (protein, organic acids, etc.), there are numerous membrane structures with a completely different electrical response. Thus, the impedance of the intracellular medium must be a mixture of conductive and capacitive properties (Ivorra 2003).

Cell membranes separate intracellular space from the extracellular ones contributing to make a barrier for the passage of ions and large molecules. They are formed by a lipid bilayer to which is associated proteins, transport organelles, ionic channels, and ionic pumps, the basic elements of the membrane active role. The intrinsic electrical conductance of this structure is very poor and can be approximated to a dielectric (Martinez 2007).

The complete organization composed by the extracellular medium, the lipid bilayer membrane, and the intracellular medium forms the conductor–dielectric–conductor structure schematized in Fig. 9.5.

When an alternating electric field is applied to plant tissues, AC (alternating current) causes polarization and relaxation, leading to changes in amplitude and phase of the applied AC signal (Repo et al. 2000). Based on these changes the impedance of the sample can be determined. This current is usually applied throughout a range of specific frequencies to produce a spectrum of measurements. The polarization of a particular component depends on the sample's tissue properties as well as on the frequency, on the force of the electrical field applied, on the ionic concentration, on the temperature, etc. In general, the smaller the component's dimension, the higher the frequency at which the polarization takes place.

In biological samples, the proportion of current passing through the apoplastic and symplastic spaces in a tissue depends on AC frequency (Repo et al. 2000) (Fig. 9.6). The lipid bilayer of plasma membrane contributes to stop the passage of AC at low frequencies, acting as a capacitor that store energy in an electric field. The only way for current to pass is the apoplast and the total impedance is mostly

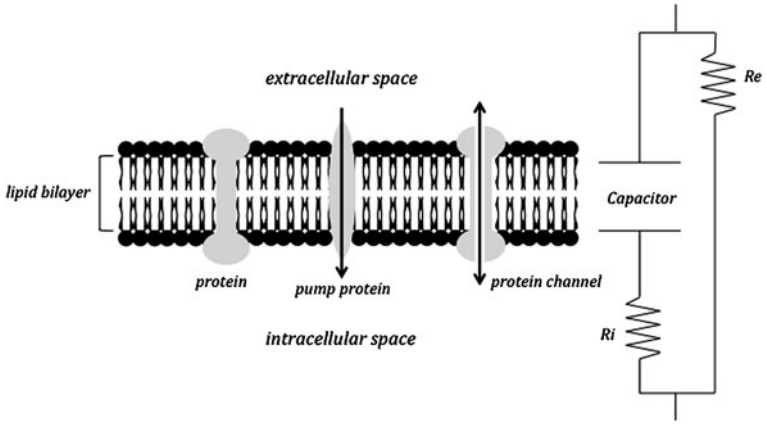

Fig. 9.5 Diagram of the electrical cell model, where the capacitor represents the plasma membrane, while *R*e and *R*i represent the extra cellular and intracellular fluids, respectively

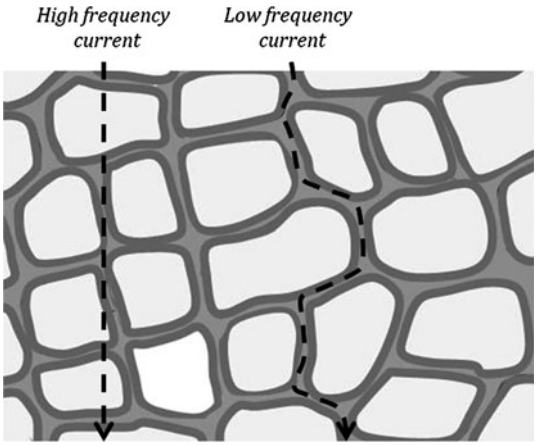

Fig. 9.6 Schematic diagram of *high* and *low* frequencies flowing through a vegetal tissue

due to the resistance of the extracellular space. When frequency increases, also cell membranes become conductive causing a change in impedance that will be composed of a parallel combination of intra-and extracellular resistances (Ozier-Lafontaine and Bajazet 2005).

9.3.1 Data Analysis and Interpretation

Modern impedance analyzers allow measuring impedance and phase angle of materials at different frequencies. Many of these analyzers are integrated with

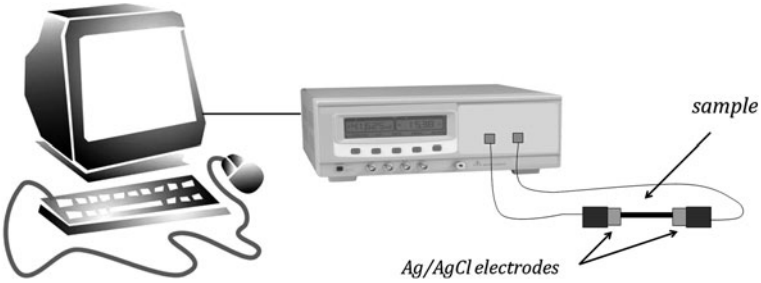

Fig. 9.7 Custom-designed apparatus to measure impedance spectra in plant

software useful in the evaluation and analysis of the data (Panke et al. 2008) (Fig. 9.7).

Before performing the analysis, it is useful to examine IS data graphically, both to search for any outliers and to examine the structure of the data that will usually reflect the physical processes present that led to that data (Macdonald 1992). The step of the graphics examination is very important to estimate some system parameters, but only in the simplest cases. When the cases are more complex the use of complex nonlinear least squares (CNLS) data-fitting of different equivalent circuits is needed.

After that, an equivalent circuit is used to investigate the nature of the samples. An equivalent circuit is a model composed by a certain number of ideal resistors and capacitors connected to each other, which produces a frequency response that is similar to that measured by the impedance experiment (Mancuso and Rinaldelli 1996). If a proper equivalent circuit is chosen, the study of tissue properties, according to the changes in the parameters of the model, becomes possible (Zhang and Willison 1992; Zhang and Willison 1993; Repo et al. 1994; Repo and Pulli 1996; Ryyppö et al. 1998).

9.3.2 How and What Equivalent Circuit Should be Chosen?

The choice of the equivalent model is crucial to understand the characteristics of the materials under investigation. The choice depends on the characteristic of the system under study and on the intuition of the researcher. There can be potential problems caused by the fact that equivalent circuits are rarely unique and several circuit models can have identical or very similar impedances (Lackermeier et al. 1999).

In order to verify the validity of the chosen circuit, the quality of the fit to the experimental curve must be evaluated. Whenever possible, the model should be verified before being used. One way to verify the model is to alter a single cell component and wait for the expected changes in the impedance spectrum (Macdonald 1987).

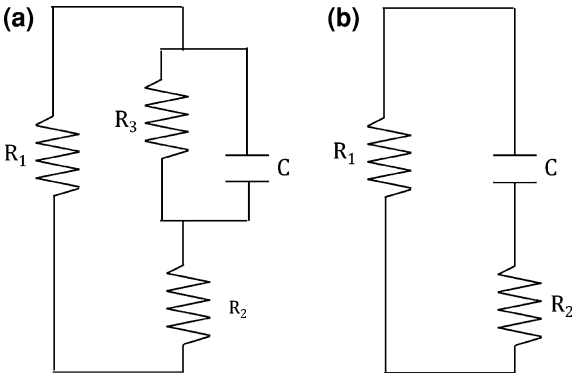

Fig. 9.8 **a** Hayden model: R_1, apoplasmic resistance; R_2, symplasmic resistance; R_3, plasma membrane resistance. **b** Simplifed Hayden model without R_3

When impedance analyses are applied to vegetal tissues, usually two types of equivalent circuits are used: lumped circuit (Cole 1940; Hayden et al. 1969; Zhang and Willison 1991, 1992; Harker and Maindonald 1994; Inaba et al. 1995) and distributed models (Repo and Zhang 1993; Repo et al. 1994). A lumped model consists of limited number of ideal resistors and capacitors. One of the first important lumped model was developed by Cole in 1940 and it characterizes biological tissue into two-branch parallel circuit. In this model R_1 and R_2 represent extracellular and intracellular space resistance, respectively, while C represents membrane capacitance (Fig. 9.8b).

However, the measurement of complex impedance in different vegetal tissues has shown that lumped circuits cannot describe all tissues. Generally, stems and needles of woody plants or other highly differentiated tissues cannot be modeled by a simple lumped circuit, thus distributed circuit elements (DCE) are required (Repo and Pulli 1996; Burr et al. 2001). In fact, impedance spectrum of these tissues has one or more depressed centers that suggest a distribution of time constant (Repo 1994).

DCE-models are more complex than lumped ones; moreover, each component of the model does not necessarily correspond to a biological structure. Nevertheless, they have an excellent fit to the experimental data; thanks to a highly compact mathematical expression (Cole and Cole 1941; Macdonald 1987). These benefits have led to an increasing use of DCE-models compared to the lumped ones (Kanai et al. 1987; Foster and Schwan 1989; Mancuso and Rinaldelli 1996).

9.3.3 Models Examples

9.3.3.1 The Hayden Model

In the Hayden model different intracellular compartments are represented by apoplasmic resistance R_1, symplasmic resistance R_2, and plasma membrane resistance R_3, while plasma membrane capacitance is represented by C (Fig. 9.8a).

Hayden and collaborators measured impedance in potato and alfalfa tissues (Hayden et al. 1969). They estimated apoplasmic resistance at low frequency; for the symplasmic one they approximated that the reactive component of impedance approaches zero at high frequency.

The real part of the impedance of the circuit of the Hayden model is calculated as:

$$X = \frac{R_1(R_2 + R_3)(R_1 + R_2 + R_3) + \omega^2 C^2 R_1 R_2 R_3^2 (R_1 + R_2)}{(R_1 + R_2 + R_3)^2 + \omega^2 C^2 R_3^2 (R_1 + R_2)} \tag{9.13}$$

while the imaginary part is:

$$Y = \frac{-\omega C (R_1 R_3)^2}{(R_1 + R_2 + R_3)^2 \omega^2 C^2 R_3^2 (R_1 + R_2)} \tag{9.14}$$

where ω is the angular frequency.

Actually, the Hayden model can be simplified omitting R_3 from the equations, whenever $R_3 \gg R_1$ and $R_3 \gg R_2$.

$$X = \frac{R_1 \left[R_2 (R_1 + R_2) + \left(\frac{1}{\omega C}\right)^2 \right]}{(R_1 + R_2)^2 + \left(\frac{1}{\omega C}\right)^2} \tag{9.15}$$

and

$$Y = \frac{-R_1^2 \left(\frac{1}{\omega C}\right)}{(R_1 + R_2)^2 + \left(\frac{1}{\omega C}\right)^2} \tag{9.16}$$

Therefore, substituting X and Y in the modulus of $Z = \sqrt{X^2 + Y^2}$, the equation becomes:

$$Z^2 = \left[\frac{R_1 R_2 (R_1 + R_2) + R_1 \left(\frac{1}{\omega C}\right)}{(R_1 + R_2)^2 + \left(\frac{1}{\omega C}\right)^2} \right]^2 + \left[\frac{R_1^2 \left(\frac{1}{\omega C}\right)}{(R_1 + R_2)^2 + \left(\frac{1}{\omega C}\right)^2} \right]^2 \tag{9.17}$$

and R_1 and R_2 values can be calculated (see Zhang et al. 1990).

9.3.3.2 Double-Distributed Electrical Circuit Model

In the distributed electrical circuits, resistance, capacitance, and inductance are distributed continuously throughout the material of the circuit. The distributed element model is more defined and also more complex than the lumped one. The impedance measurements of biological tissues frequently produce impedance spectra composed by two arcs with strongly depressed centers (Repo et al. 2002) (Fig. 9.9); in these cases, a double-distributed model may be used (Paine et al. 2001; Repo et al. 2002). As reported in Fig. 9.9, the resistors (R, R_1, and R_2) of the

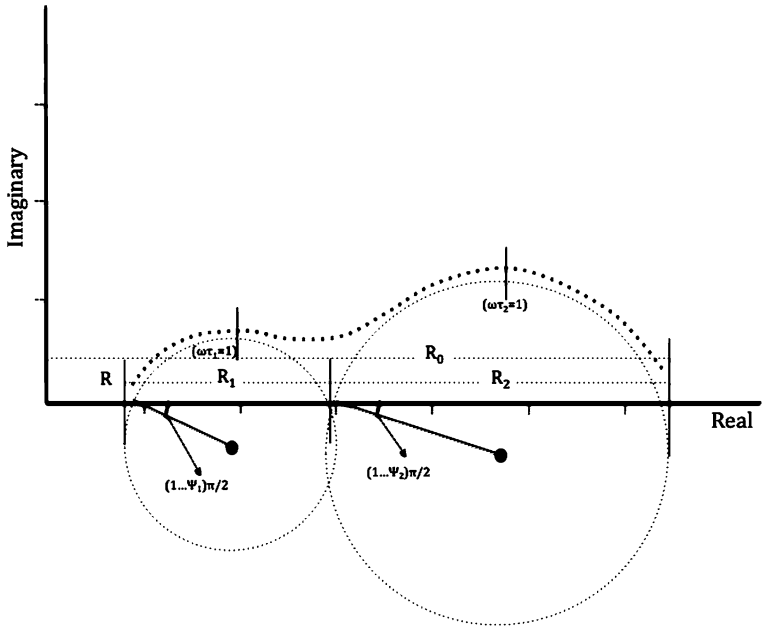

Fig. 9.9 Wessel diagram. Real data plotted along the x-axis and imaginary on the y with frequency as parametric variable (modified by Repo et al. 2005)

model can be calculated from the interceptions of the circles with the x-axis; the relaxation times (τ_1 and τ_2) describe the location of the dispersion range on the frequency and are obtained from the apex of the arcs and plane. The coefficients Ψ_1 and Ψ_2 describe the distribution of the relaxation times (Repo et al. 2002).

The Voigt model is a double-DCE model, composed of two distributed elements (DCE_1 and DCE_2) in series with a resistor (R). Both DCEs are composed by the parallel arrangement of two resistors R_1 and R_2 and two constant-phase elements Z_{CPE1} and Z_{CPE2}. The constant-phase element (CPE) is described as a capacitance that is frequency dependent (Ivorra 2003) and has been introduced to improve the equivalent electrical circuit models to more closely fit the real impedance spectra. The impedance of the constant-phase elements is (Macdonald 1987):

$$Z_{\mathrm{CPE1}} = \frac{1}{(J\omega C_1)^{\Psi^1}} \tag{9.18}$$

and

$$Z_{\mathrm{CPE2}} = \frac{1}{(J\omega C_2)^{\Psi^2}} \tag{9.19}$$

For the impedance of DCEs we get:

$$\frac{1}{Z_{\mathrm{DCE1}}} = \frac{1}{R_1} + \frac{1}{Z_{\mathrm{CPE1}}} \tag{9.20}$$

and

$$\frac{1}{Z_{\mathrm{DCE2}}} = \frac{1}{R_2} + \frac{1}{Z_{\mathrm{CPE2}}} \tag{9.21}$$

Therefore:

$$Z_{\mathrm{DCE1}} = \frac{R_1}{1 + R_1(j\omega C_1)^{\Psi 1}} = \frac{R_1}{1 + \left(j\omega C_1 R_1^{\frac{1}{\Psi 1}}\right)^{\Psi 1}} \tag{9.22}$$

and

$$Z_{\mathrm{DCE2}} = \frac{R_2}{1 + R_2(j\omega C_2)^{\Psi 2}} = \frac{R_2}{1 + \left(j\omega C_2 R_1^{\frac{1}{\Psi 1}}\right)^{\Psi 2}} \tag{9.23}$$

In this way it is possible to define $\tau_1 = C_1 R_1^{\frac{1}{\Psi 1}} \tau_1$ and $\tau_2 = C_2 R_2^{\frac{1}{\Psi 2}}$ and

$$Z_{\mathrm{DCE1}} = \frac{R_1}{1 + (j\omega\tau_1)^{\Psi 1}} \text{ and } Z_{\mathrm{DCE2}} = \frac{R_2}{1 + (j\omega\tau_2)^{\Psi 2}} \tag{9.24}$$

For the total impedance of the double-DCE model we get:

$$Z = R + Z_{\mathrm{DCE1}} + Z_{\mathrm{DCE2}} = R + \frac{R_1}{1 + (j\omega\tau_1)^{\Psi 1}} + \frac{R_2}{1 + (j\omega\tau_2)^{\Psi 2}}, \tag{9.25}$$

where ω = angular velocity = $2\pi f$

9.3.3.3 Complex Nonlinear Least Squares Data-Fitting

Complex nonlinear least squares data-fitting is a fitting technique that can be used for a good characterization of the material-electrode system (Macdonald 1992). Macdonald and Garber (1977) applied this method for the first time to impedance spectroscopy. Thanks to a mathematical model, CNLS shows which parameters are useful for fitting; moreover, it allows fitting very complex models having more than 10 unknown parameters (Macdonald 1987).

The weighted sum of squares of the real and imaginary residual has to be minimized. A residual is the difference between a data value at a given frequency and the corresponding value calculated from the model. The weights are calculated as the inverses of the estimated error variance for a given real data value and for the corresponding imaginary value (Macdonald 1992).

$$S(P) = \sum_{j=1}^{M} w_j \left[Y_j - YC_j(P) \right]^2, \tag{9.26}$$

where:

M	total number of data points;
w_j	weight associated with the jth point;
Y_j	jth data point value to be fitted;
$YC_j(P)$	value calculated fitting function involving the set parameters P.

The initial choice of the parameters is very important: they must be relatively close to the real values. On the contrary CNLS method becomes easily divergent.

9.4 EIS Applications in Plants

9.4.1 EIS, Root Growth, and Development

Although the dynamic of root growth is very difficult to study, EIS technique was interestingly employed in experiments on growth and morphological studies of the root system (Dalton 1995; Van Beem et al. 1998; Ozier-La Fontaine et al. 2001; Matsumoto et al. 2001; Rajkai et al. 2002). The use of EIS is based on the capacitance changes that happen to the system root/soil during root growth. In 2005 Repo and collaborators tried to develop a non-destructive evaluation of plant root growth using EIS. In this study they modeled the IS by a circuit consisting of a resistor, two Zarc-Cole elements, and a constant-phase element in series (Fig. 9.10). In a further research conducted in 2005, Ozier-La Fontaine and Bajazet aimed to verify experimentally the validity of the relationship between root fresh or dry weight and root capacitance. By measuring EIS using two Ag–AgCl electrodes inserted in the plant stem and into the soil, respectively, they demontsrated that the root growth was characterized by a modifications in both electrical capacitance and resistance components.

The complications caused by the different polarization interfaces between conductive mediums and root/soil system, the soil type, and the soil moisture content that can interfere with EIS properties may be overcome with experiment conducted in hydroponic culture. In fact, hydroponic culture, representing a simplified system, is able to standardize some of the confounding factors of soil. In 2011, Cao and collaborators developed equivalent circuits for estimating willow root system size nondestructively using the EIS approach. Willows roots were grown in hydroponic solution and the electrical impedance spectrum was measured inserting one Ag electrode in the middle position of the stem above the solution, and another at the bottom of the narrow solution container. They prepared three different setups (one with all the roots immersed in the solution; another one

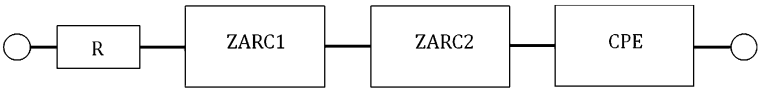

Fig. 9.10 Electrical circuit consisting of a resistor, two ZARC-Cole elements (ZARC1 and ZARC2) and one constant-phase-element (CPE)

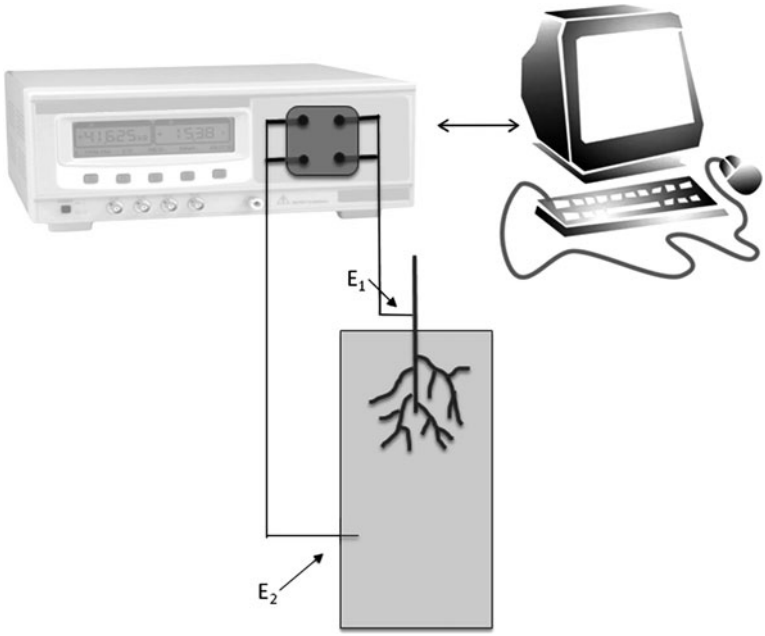

Fig. 9.11 Diagram of the experimental setups for the measurement of the impedance spectra of the root apparatus. E1 and E2 refer to the Ag electrodes (modified by Cao et al. 2011)

with a single root immersed in the solution; and the third one with only the stem immersed in the solution) (Fig. 9.11). For each setup they developed a lumped model as equivalent circuit resulting in a good fit of the measured data.

In the case of the DCE-models a little bit more attention is needed. In fact, even if they have been used many times (Dalton 1995; Ozier-Lafontaine and Bajazet 2005) and with mathematically good fit, the biological interpretation of the data remains more difficult than using lumped model.

9.4.2 EIS and Seed Quality

Electrical impedance spectroscopy was used to evaluate the seed quality (Paine et al. 2001; Repo et al. 2002). Seeds contain different microstructures as the cell

walls, the membranes and the starch grains that are able to modify significantly the ionic transport. The physiological changes of these microstructures, due to the age of the seed, can be followed by corresponding changes in the impedance values. EIS parameters vary between viable and non-viable seeds because of the lost of membranes integrity (Priestley 1986). Conventional techniques used to evaluate seed viability are often time consuming and destructive. Compared to them, EIS offers different advantages thanks to its capacity to evaluate seed quality noninvasively.

9.4.3 EIS and Environmental Stresses

One of the most important applications of EIS is in the study of stress physiology and in particular in the evaluation of damages caused by abiotic stresses.

Many interesting researches have been conducted to evaluate freezing and cold tolerance in different woody and herbaceous plant species in relation to cold acclimation. One of the most sensitive mechanisms to low temperatures in plant is the ionic transport through the cellular membranes, mainly because of alterations of the H^+ and K^+ transporting systems (Levitt 1981; Yoshida 1991, 1994; Palta and Weiss 1993; Shabala and Newman 1997). For that reason, monitoring the state of electrical impedance can be used as a possible indicator of the initial stage of chilling stress in plants (Mancuso 2000).

During cold acclimation several changes in the content of cellular sap and cell membranes occur (Steponkus 1984) that are mirrored in the modification of the electrical level of cellular constituents and consequently can be detected by EIS (Repo et al. 2005; Zhang and Willison 1991; Zhang et al. 1992; Tsarouhas et al. 2000; Vainola and Repo 2000; Luoranen et al. 2004; Repo et al. 2000; Mancuso et al. 2004).

Interestingly, data extrapolated directly from impedance spectra were sufficient to evaluate lethal temperature (LT) in Australian plants (Mancuso et al. 2004). In this research, the impact of temperature injury was estimated as the change in impedance ratio (low/high frequency) before and after the thermal treatment

$$DZ_{\text{ratio}} = \left(\frac{Z_{\text{low}}}{Z_{\text{high}}}\right)_{\text{after}} - \left(\frac{Z_{\text{low}}}{Z_{\text{high}}}\right)_{\text{before}},$$

where DZ_{ratio} is the change in the ratio of the impedance to freezing, $(Z_{\text{low}}/Z_{\text{high}})_{\text{after}}$ the ratio of the impedance at 1 and 20 kHz after freezing, and $(Z_{\text{low}}/Z_{\text{high}})_{\text{before}}$ the ratio of the impedance at 1 and 20 kHz before freezing. The lethal temperature was finally estimated as the inflection point of a logistic sigmoid function, plotting DZ_{ratio} against the temperatures analyzed. This method was also applied to study the answers of plant tissues to other types of stress, such as heat (Mancuso and Azzarello 2002) and salinity (Mancuso and Rinaldelli 1996).

9.4.4 EIS Analysis on Fruits

Many EIS researches have been conducted on the study of the physiological condition and maturity of fruits and on study of ripening of chill-injured fruits (Weaver and Jackson 1966; Zachariah 1976; Furmanski and Buescher 1979; Lougheed et al. 1981; Inaba et al. 1995; Varlan and Sansen, 1996). EIS has the advantage to identify easily and fastly the internal condition of the fruit during ripening and cold storage (Klein 1987; Schoorl and Holt 1977), thanks to the capacity to detect rapid changes associated with physiological dysfunction and membrane damage (Zhang and Willison 1992; Harker and Forbes 1997). Using this method Harker and Maindonald in 1994 were able to assess changes in the condition of the cell wall, cell membranes, and intracellular compartments during ripening of nectarine. Similar studies were conducted in peaches, kiwi, and persimmon with or without chilling injuries (Furmanski and Buescher 1979; Sugiyama et al. 1987; Von Mollendorff et al. 1992; Harker and Maindonald 1994; Harker and Forbes 1997; Bauchot et al. 2000).

9.5 Conclusions

Electrochemical impedance spectroscopy plays an important and fundamental role in electrochemistry and biological science being a simple, quick, repeatable, and non-destructive technique. Modern impedance analyzers, by widening the frequency range from the millihertz to megahertz, have made possible a solid increase in the studies of impedance applied to plant science. All the described applications confirm that EIS is a useful tool to assess physiological changes in vegetal tissues due to the plant development as well as after the exposure to stresses. The choice of the procedures to estimate the best correlation between the electrical measurements and the physiological properties of plant tissues remains crucial for the successful use of this technology.

References

Ackmann JJ, Seitz MA (1984) Methods of complex impedance measurements in biological tissues. CRC Crit Rev Biomed Eng 11:281–311

Bauchot AD, Harker FR, Arnold WM (2000) The use of electrical impedance spectroscopy to assess the physiological condition of kiwifruit. Post Biol Technol 18:9–18

Burr K, Hawkins C, L'Hindorelle S, Binder W, George M, Repo T (2001) Methods for measuring cold hardiness of conifers. In: Bigras FJ, Colombo SJ (eds) Conifer cold hardiness. Kluwer Academic Publishers, Dordrecht, pp 369–401

Cao Y, Repo T, Silvennoinen R, Lehto T, Pelkonen P (2011) Analysis of willow root system by electrical impedance spectroscopy. J Exp Bot 62:351–358

Cole KS (1940) Permeability and impermeability of cell membranes for ions. Cold Spring Harb Symp Quant Biol 8:110–122
Cole KS (1972) Membranes, ions and impulses. University of California Press, Berkeley
Cole KS, Cole RH (1941) Dispersion and adsorption in dielectrics alternating current characteristics. J Chem Phys 9:341–352
Coster HGL, Chilcott TC, Coster ACF (1996) Impedance spectroscopy of interfaces, membranes and ultrastructures. Bioelectrochem Bioenerg 40:79–98
Dalton F (1995) In situ root extent measurements by electrical capacitance methods. Plant Soil 173:157–165
Filho PB (2002) Tissue characterisation using an impedance spectroscopy probe. PhD thesis, Department of Medical Physiscs and Chemical Engineering, University of Sheffield
Foster KR, Schwan HP (1989) Dielectric properties of tissues and biological materials: a critical review. In: Bourne JR (ed) Critical reviews in biomedical engineering. CRC Press, Boca Raton, pp 25–104
Furmanski RJ, Buescher RW (1979) Influence of chilling on electrolyte leakage and internal conductivity of peach fruits. HortSci 14:167–168
Harker FR, Forbes SK (1997) Ripening and development of chilling injury in persimonn fruit: an electrical impedance study. NZ J Crop Hort Sci 25:149–157
Harker FR, Maindonald JH (1994) Ripening of nectarine fruit. Changes in the cell wall, vacuole, and membrane detected using electrical impedance measurements. Plant Physiol 106:165–171
Hayden RI, Moyse CA, Calder FW, Crawford DP, Fensom DS (1969) Electrical impedance studies on potato and alfalfa tissue. J Exp Bot 20:177–200
Inaba A, Manabe T, Tsuji H, Iwamoto T (1995) Electrical impedance analysis of tissue properties associated with ethylene induction by electric currents in cucumber (*Cucumis sativus* L.). Plant Physiol 107:199–205
Ivorra A (2003) Bioimpedance monitoring for physicians: an overview. Centre Nacional de Microelectrònica Biomedical Applications Group
Kanai H, Haemo M, Sakamoto K (1987) Electrical measurements of fluid distribution in legs and arms. Med Prog Technol 12:159–170
Klein JD (1987) Relationship of harvest date, storage conditions, and fruit characteristics to bruise susceptibility of apple. J Am Soc Hort Sci 112:113–118
Lackermeier AH, McAdams ET, Moss GP, Woolfson AD (1999) In vivo ac impedance spectroscopy of human skin: theory and problems in monitoring of passive percutaneous drug delivery. Ann N Y Acad Sci 873:197–213
Levitt J (1981) Responses of plants to environmental stresses. Water, radiation, salt, and other stresses. In: Kozlowski TT (ed) Physiological ecology, vol 2. Academic Press, Toronto, pp 28–53
Lewis GS, Aizinbud E, Leherer AR (1989) Changes in electrical resistance of vulvar tissue in Holstein cows during ovarian cycles and after treatment with prostaglandin F2α. Anim Reprod Sci 18:183–197
Liedtke RJ (1997) Principles of bioelectrical impedance analysis. RJL Systems Inc., Clinton 10
Lougheed EC, Miller SR, Miller BD, Cline R (1981) Electrical impedance of diaminozide and calcium-trated mcIntosh apples. Experimentia 37:835–837
Luoranen J, Tapani R, Lappi J (2004) Assessment of the frost hardiness of shoots of silver birch (Betula *pendula)* seedlings with and without controlled exposure to freezing. Can J For Res 34:1108–1118
Macdonald JR (1987) Impedance spectroscopy. Emphasizing solid materials and systems. John Wiley and Sons, New York
Macdonald JR (1992) Impedance spectroscopy. Ann Biomed Eng 20:289–305
Macdonald JR, Garber JA (1977) Analysis of impedance and admittance data for solids and liquids. J Electroch Soc 124:1022–1030
Mancuso S (2000) Electrical resistance changes during exposure to low temperature and freezing measure chilling tolerance in olive tree (Olea *europaea* L.) plants. Plant, Cell Environ 23:291–299

Mancuso S, Azzarello E (2002) Heat tolerance in olive. Adv Hort Sci 16:125–130
Mancuso S, Rinaldelli E (1996) Response of young mycorrhizal and non-mycorrhizal plants of Olive tree (Olea *europea* L.) to saline conditions. II. dynamics of electrical impedance parameters of shoots and leaves. Adv Hort Sci 10:135–145
Mancuso S, Nicese FP, Masi E, Azzarello E (2004) Comparing fractal analysis, electrical impedance and electrolyte leakage for the assessment of the freezing tolerance in *Callistemon* and *Grevillea* spp. J Hort Sci Biotech 79:627–632
Martinez FS (2007) Electrical bioimpedance cerebral monitoring: fundamental steps towards clinical application, thesis for the degree of doctor of philosophy. School of Engineering, University College of Borås, Sweden. Printed by Chalmers Reproservice Göteborg, Sweden
Matsumoto N, Homma T, Morita S, Abe J (2001) Capacitance as a possible indicator for size of maize root system. In: Proceedings of the 6th symposium of the international society of root research, Nagoya, Japan, pp 578–579
Ozier-Lafontaine H, Bajazet T (2005) Analysis of root growth by impedance spectroscopy (EIS). Plant Soil 277:299–313
Ozier-Lafontaine H, Bajazet T, Cabidoche YM (2001) Electrical capacitance as a tool for non-invasive root size estimation: minimizing soil and electrodes influences. In: Proceedings of the 6th symposium of the international society of root research, Nagoya, Japan, pp 190–191
Paine DH, Repo T, Taylor AG (2001) Noninvasive seed quality test by impedance spectrum analysis. Reprinted Seed Technol 23:187–192
Palta JP, Weiss LS (1993) Ice formation and freezing injury: an overview on the survival mechanisms and molecular aspects of injury and cold acclimation in herbaceous plants. In: Li PH, Christersson L (eds) advances in plant cold hardiness. CRC Press, Inc., Boca Raton, pp 143–176
Pänke O, Balkenhohl T, Kafka J, Schäfer D, Lisdat F (2008) Impedance spectroscopy and biosensing. Adv Biochem Eng Biotechnol 109:195–237
Priestley DA (1986) Seed aging. Cornell University Press, New York
Rajkai K, Végh KR, Nacsa T (2002) Electrical capacitance as the indicator of root size and activity. Agrokémia és Talajtan 51:1–10
Repo T (1994) Influence of different electrodes and tissues on the impedance spectra of scots pine shoots. Electro Magnetobiol 13:1–14
Repo T, Pulli S (1996) Application of impedance spectroscopy for selecting frost hardy varieties of english ryegrass. Ann Bot 78:605–609
Repo T, Zhang MIN (1993) Modelling woody plant tissues using a distributed electrical circuits. J Exp Bot 44:977–992
Repo T, Zhang MIN, Ryyppö A, Vapaavuori E, Sutinen S (1994) Effects of freeze-thaw injury on parameters of distributed electrical circuits of stems and needles of scots pine seedlings at different stages of acclimation. J Exp Bot 45:557–565
Repo T, Zhang G, Ryyppö A, Rikala R (2000) The electrical impedance spectroscopy of Scots pine (*Pinus sylvestris* L.) shoots in relation to cold acclimation. J Exp Bot 51(353):2095–2107
Repo T, Paine D, Taylor A (2002) Electrical impedance spectroscopy in relation to seed viability and moisture content in snap bean (*Phaseolus vulgaris* L.). Seed Sci Res 12:17–29
Repo T, Laukkanen J, Silvennoinen R (2005) Measurement of the tree root growth using electrical impedance spectroscopy. Silv Fenn 39:159–166
Ryyppö A, Repo T, Vapaavuori E (1998) Development of freezing tolerance in roots and shoots of Scots pine seedlings at non freezing temperatures. Can J For Res 51:2095–2107
Schoorl D, Holt JE (1977) The effects of storage time and temperature on the bruising of Jonathan, delicious and granny Smith apples. J Text Stud 8:409–416
Schröder J, Doerner S, Schneider T, Hauptmann P (2004) Analogue and digital sensor interfaces for impedance spectroscopy. Meas Sci Technol 15:1271–1278
Shabala SN, Newman IA (1997) H^+ flux kinetics around plant roots after short-term exposure to low temperature: identifying critical temperatures for plant chilling tolerance. Plant, Cell Environ 10:1401–1410

Steponkus PL (1984) Role of the plasma membrane in freezing injury and cold acclimation. Ann Rev Plant Physiol Plant Mol Biol 35:543–584

Sugiyama J, Hayashi T, Horiuchi H (1987) Electrical impedance of kiwifruit. Nippon Shokuhin Kogyo Gakkaishi 33:725–730

Tsarouhas WA, Kenney L, Zsuffa LZ (2000) Application of two electrical methods for the rapid assessment of freezing resistance in *Salix eriocephala*. Biom Bioener 19(3):165–175

Väinölä A, Repo T (2000) Impedance spectroscopy in frost hardiness evaluation of *Rhododendron* leaves. Ann Bot 86:799–805

van Beem J, Smith ME, Zobel RW (1998) Estimating root mass in maize using a portable capacitance meter. Agron J 90:566–570

Varlan AR, Sansen W (1996) Nondestructive electrical impedance analysis in fruit: normal ripening and injuries characterization. Electro Magnetobiol 15:213–227

von Mollendorff LJ, Jacobs G, de Villiers OT (1992) Cold storage influences internal characteristics of nectarines during ripening. HortSci 27:1295–1297

Weaver GM, Jackson HO (1966) Electric impedance, an objective index of maturity in peach. Can J Plant Sci 46:323–326

Yoshida S (1991) Chilling-induced inactivation and its recovery of tonoplast H + -ATPase in mung bean cell suspension cultures. Plant Physiol 95:456–460

Yoshida S (1994) Low temperatures-induced cytoplasmic acidosis in cultured mung bean (*Vigna radiata* (L.) Wilczek) cells. Plant Physiol 104:1131–1138

Zachariah G (1976) Electrical properties of fruits and vegetables for quality evaluation. In: Gaffney JJ (ed) Quality detection in foods. American Society of Agricultural Engineers, St Joseph, pp 98–101

Zhang MIN, Willison JHM (1991) Electrical impedance analysis in plant tissues: a double shell model. J Exp Bot 42:1465–1475

Zhang MIN, Willison JHM (1992) Electrical impedance analysis in plant tissues: the effect of freeze-thaw injury on the electrical properties of potato tuber and carrot root tissues. Can J Plant Sci 72:545–553

Zhang MIN, Willison JHM (1993) Electrical impedance analysis in plant tissues: impedance measurement in leaves. J Exp Bot 44:1369–1375

Zhang MIN, Stout DG, Willison JHM (1990) Electrical impedance analysis in plant tissues: symplasmic resistance and membrane capacitance in the hayden model. J Exp Bot 41:371–380

Zhang MIN, Stout DG, Willison JHM (1992) Plant tissue impedance and cold acclimation: a re-analysis. J Exp Bot 43:263–266

Chapter 10
Patch Clamp Techniques for Plant Cells

J. Theo M. Elzenga

Abstract The study of electrophysiological processes at the molecular level, with exquisite sensitivity and full control over the experimental conditions, is possible with the patch clamp technique. A concise overview is given of the different configurations that are used with the technique. The patch clamp technique critically depends on the formation of a tight, gigaOhm, seal between the glass tip of the measuring electrode and the cell membrane, which for plant cells means that the cell wall has to be removed. Methods that have been developed specifically to gain access to the membrane, such as laser microsurgery and protoplast release, are discussed. This chapter also provides a review of the factors that influence the interaction between the glass tip of the electrode and cell membrane.

10.1 Introduction

The first plant electrophysiological results obtained with the patch clamp technique were reported in 1984 (Moran et al. 1984; Schroeder et al. 1984). Since that time many different ion channels in the plasma membranes and intracellular membranes of different kinds of plant cells have been characterized (Ward et al. 2009). Only a few years before, the technique was developed for animal cells by Sackmann and Neher (Hamil et al. 1981), who received the Nobel prize for their discovery in 1991. The application of the patch clamp techniques on plant cell membranes has brought us a deeper understanding of the molecular basis of membrane transport in

J. T. M. Elzenga (✉)
Plant Ecophysiology, University of Groningen,
Nijenborgh 7, 9747 AG, Groningen, The Netherlands
e-mail: j.t.m.elzenga@rug.nl

A. G. Volkov (ed.), *Plant Electrophysiology*,
DOI: 10.1007/978-3-642-29119-7_10,

plants, has enabled the identification of ion channel proteins involved in plant responses to abiotic and biotic stresses, and has helped in the characterization of non-channel ion transporter proteins such as H^+-pumping ATPases. This chapter will partly be a basic primer of the patch clamp technique, will touch on some of the technical intricacies of applying the technique to plant cells, will describe new developments, and will try to give an outlook on future uses of the technique.

10.2 A Short Primer of the Patch Clamp Technique

Living cells depend on maintaining conditions in cytoplasm that allow uninterrupted activity of enzymes involved in metabolism and the synthesis of the cells' building blocks, such as proteins, lipids, and secondary metabolites. To maintain homeostasis in the cytoplasm and different specialized cell compartments such as mitochondria, chloroplasts, endoplasmatic reticular vesicles, these compartments are separated from their environment by a lipid membrane. The ionic composition of these compartments is often distinctly different from the surrounding solution. The ionic gradients across the membranes enveloping cell and organelles are being maintained by the relatively low permeability of the lipid bilayer that forms a major part of membranes, and the regulation of passage of ions through the specialized transporter proteins, such as ion channels, ion symporters, and ion pumps. A flow of ions across a membrane requires therefore two things, (1) a driving force and (2) a conductance pathway formed by 'open' ion transporter proteins. Current is defined as a movement of charge (I, measured in amperes A). The driving force, or the measure of the amount of work needed for the movement of a charged particle, is provided by the combination of the electrical potential difference and the concentration gradient of the particle over the membrane and is measured in Volts V, note that the potential of the concentration gradient can be expressed in Volts by applying the Nernst equation $E = RT/zF$. ln[(ion outside cell)/(ion inside cell)].

The conductance pathway for current is most often formed by ion channels and the number of channels, the proportion of open or active channels, and the ease by which ions pass through individual channels determine the conductance, or the inverse, the resistance. As with any current, the relationship between voltage, current, and resistance is defined by Ohm's Law:

$$I = \frac{V}{R}.$$

It is apparent that the larger the driving force (voltage) and the smaller the resistance (R), the larger the current. Ohm's Law also dictates that when the voltage is kept constant, any current changes over time reflect changes in resistance. In a biological membrane resistance changes are the result of changes in the number of active transporter proteins, mainly by changes in the opening state of

ion channels, i.e., the opening and closing of the channels. The patch clamp technique is based on this relationship. Clamping the voltage at a particular value and measuring the current through the system enables the calculation of the resistance for ionic currents across the membrane.

The conductance of ion channels is in the pA range and requires sensitive equipment and minimization of other, interfering, currents. In order to isolate the currents through ion channels from other currents, the membrane that contains the channels being studied is 'sealed' over the tip of the glass micropipette that contains one of the measuring electrodes. When the tightness of this seal is in the order of tens of gigaOhm, currents through individual channels can be reliably measured. Seals with such a high resistance can only form between a 'clean' membrane surface and a clean glass micropipette tip surface. Application of the patch clamp technique to ion channels in membranes of plant cells requires exposure of the 'naked' membrane and thus removing the cell wall. In separate paragraphs the preparation of protoplast in order to expose the membrane surface and the factors that influence the ease of gigaOhm seal formation will be treated.

A typical patch clamp experiment starts by the approaching of the cell membrane with the tip of a glass micropipette fixed to a micromanipulator. In order to monitor the formation of the tight seal between membrane and pipette tip a test voltage pulse is applied between a reference electrode, placed in the bath solution containing the cells, and the measuring electrode, which sits inside the glass micropipette. The resulting current, which is initially flowing between the two electrodes, is determined by the voltage applied and the resistance provided by the solution in the bath, the opening in the tip of the micropipette, and the solution in the glass micropipette will decrease when the tip of the micropipette makes contact with the cell membrane (Fig. 10.1). Occlusion of the tip opening results in an increased resistance, a further increase is often obtained by applying suction to the micropipette, creating an Ω(omega)-shaped membrane bleb in the tip of the micropipette which creates a greater contact area between glass (the inside of the pipette tip) and membrane (the neck of the Ω-shaped bleb). Under favorable conditions this is sufficient for the—often sudden—formation of the desired, essential gigaOhm seal. The suction needed to form the bleb is likely to disrupt the cytoskeletal structure under the membrane patch (Milton and Caldwell 1990).

The physics underlying the tight association between the membrane and the glass in the tip of the micropipette has long been a black box (Milton and Caldwell 1990) and selecting the right conditions for forming a gigaOhm seal has mainly been a process of trial and error. Only recently the biophysics involved in the seal formation is being elucidated and the effect of seal on single channel measurements is coming to light (Suchina et al. 2009). From these studies it has become evident that during the formation of the high resistance membrane-glass adhesion the membrane will be altered and these alterations might affect channel kinetics of many channels. The actual seal is formed by a 1–2 mm long 'neck' of the membrane bleb that is sucked into the pipette tip (Fig. 10.2). From this 'neck' the proteins are excluded, leaving lipids that form the seal. The membrane-glass adhesion energy consists of van der Waals attraction, which is offset against the

repulsive static electrical force between glass and membrane surface. The adhesion energy can be increased by a high ionic strength and a low pH of the pipette solution. It is noteworthy that these positive effects of high ionic strength and low pH on seal strength seem contrary to the seal-promoting properties of a pipette solution that contains no K^+ and has a high pH (Maathuis et al. 1997). The seal itself is negatively charged and the high resistance is probably due to high viscosity glycoproteins. High-resolution optical studies of the seal also indicate that the seal is not static, but might creep up the pipette during the course of an experiment.

All advanced patch clamp systems currently on the market include software modules to control the test pulses, monitor the resulting current, and calculate the resulting seal resistance. The test pulse is often set to 10 (or 5) mV. In the 'open' system, i.e., when the tip of the electrode is not yet covered with a patch of membrane, the resulting currents are typically in the range of around 2 nA, giving a micropipette tip resistance of $(10 \times 10^{-3}\ \text{V})/(2 \times 10^{-9}\ \text{A})$ or around $5 \times 10^6\ \Omega$ or 5 MΩ. After a high resistance seal has been established the currents invoked by the test pulse are reduced to typically around 4 pA and the resulting resistance is therefore then $(10 \times 10^{-3}\ \text{V})/(4 \times 10^{-12}\ \text{A})$ of around $2.5 \times 10^9\ \Omega$ or 2.5 GΩ.

Why is this very high resistance necessary? Any signal that one likes to record and analyze needs to be distinguishable from random fluctuations or noise. The better the signal-to-noise ratio the higher fidelity with which a signal can be recorded. Since the signal (the currents through the channels) is in the picoampere to low nanoampere range, the random noise should be kept as low as 10% of that value. Channels with a relatively low conductance, like for instance most calcium-conducting channels, demand very low noise levels and are therefore technically challenging to study. There are several sources for unwanted currents and noise and several good instruction manuals that give directions on how to prevent the interference from these external sources have been published. However, thermal or Johnson noise originates from any simple resistor, such as membrane patches across the tip of a glass micropipette electrode and therefore is inherent in the very system that is being studied. This noise is described by the following equation:

$$i_n = \sqrt{\frac{4kT\Delta f}{R}}$$

where i_n is thermal current noise, k is the Boltzmann constant, T is the absolute temperature, Δf is the bandwidth over which the noise is being measured in Hz, and R is the resistance. It is immediately clear from the equation that current noise will be reduced by lowering the temperature (often not feasible for a biological preparation), by narrowing the bandwidth (filtering out those frequencies that do not have biological significance and are not relevant to the measurement), or by increasing the resistance. Therefore, the higher the resistance of the seal, the smaller the ion channel currents that can be recorded and analyzed. This was the essential innovation made with the introduction of the patch clamp technique that

enabled the study of the molecular basis of the currents underlying the electrophysiological phenomena exhibited by biological membranes.

Once the GigaOhm seal has formed—later in this chapter it is described how to establish such seals on plant cell membranes—the ion currents can be recorded. A very good overview of the different types of measurements and of the different approaches that can be taken to characterize the transport proteins involved in ion transport across the membrane is given in Ward (1997) while other introductory information can be found in Hamill et al. (1981), Hedrich and Schroeder (1989), Hille (1992), Ogden (1994).

10.2.1 Cell-Attached Patch Mode

The cell-attached patch mode is the starting point of all patch clamp experiments, since this is the situation that results when the gigaOhm seal between the tip of the micropipette and the neck of the membrane bleb sucked into the pipette opening has formed. Currents that leak from bath solution to pipette solution are almost completely blocked by the tight seal. The main conductance pathway is now from pipette solution, through transporter proteins in the membrane patch covering the tip opening, through the cytoplasm, through the transporters in that part of the membrane around the cell that remained outside the electrode tip, and through the bath solution. All of these represent a resistance against the current flowing from the electrode in the micropipette to the electrode in the bath solution and they are connected in series. The resistance of pipette solution, cytoplasm, and bath solution are relatively low compared with the resistance of the membrane patch and the membrane around the cell. Since the number of transporters can be assumed to be proportional to the membrane surface area, there will be several orders of magnitude more transporter proteins present in the membrane around the cell, than in the membrane patch covering the tip of the electrode. Therefore, the resistance of the membrane patch will be much higher than the resistance of the membrane around the cell and dominate the current through the whole series of resistances.

In this configuration the resolution of a current measurement will be determined by the noise generated by the amplifier. The patch clamp amplifiers of the latest generation have noise levels as low as 30–150 fA. In practice, this means that currents of 0.03–0.15 pA could be resolved from the background. A channel with a conductance of 1.5 pS would pass 0.15 pA current at a membrane potential of 100 mV from the equilibrium potential for the ion passing through such a channel. A current of 0.15 pA is equivalent with a flow of 0.95×10^6 monovalent ions per second. From these numbers it is immediately clear that it would be impossible to measure the activity of a single ion pump, like the proton pumping ATPase, that is maximally able to operate at a rate of 100 ions per second. The inherent limitation on the rate of ion transport through a pump is the need for conformational change in the ion pumping protein (complex) during each individual ion transport cycle. Where in ion pumps (and equally so for symporter or antiporter transport proteins)

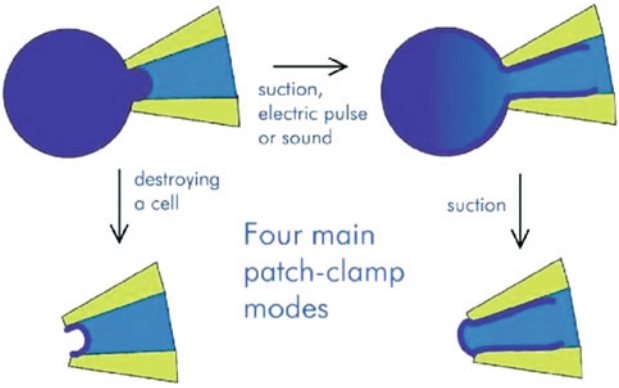

Fig. 10.1 Four modes used with the patch clamp technique and the treatments change the initial cell-attached patch mode (*upper left*) into, respectively, the whole cell mode (*upper right*), outside out (*lower right*) and inside out (*lower left*) mode. See text for explanation of the specific properties of the different modes

such a conformational change is needed for the tranlocation of every single (Na^+/K^+ ATPase in animals, H^+ ATPase is plants) or double charge (Ca^{2+} ATPases), in channels a conformational change is only required for the transition from the closed to the open state. Once in the open state ions, and thus charges, are freely flowing at a rate typically in the order of 10^7 charges per second (1.5 pA) (Gadsby 2009). The single channel conductance of channels found in plant cells range from 1 to 150 pS [the slow vacuolar (SV) channel in Sugar Beet, Tester 2006]. The permeation of ions through channels can adequately be described by simple diffusion for some channels (Latorre and Miller 1983), but in other channels the ion seems to interact with the channel protein at some stage during the passage (Bertl and other references). Since the opening of a channel allows immediate passage of ions, determined by channel conductance, ion concentration, and potential difference across the membrane, and closing of a channel completely limits ion flow, opening and closing events are visible as discrete jumps in the measured current (Fig. 10.3). The current is observed as being 'turned on' and 'turned off' and every switching event is a single conformational change in a single channel protein (complex). The patch clamp technique is thus capable of measuring the activity of a single protein in real time.

In the example of a recording of single channel currents (Fig. 10.2), the membrane potential was varied from −120 to +120 mV. From the analysis of the open channel current, which is obtained by subtracting the current level in the closed state from the current level in the open state, and plotting these against the potential the single channel conductance is found by taking the slope of this relation. Note that the current level in the closed state of the channel is not necessarily zero. The origin of the closed channel current, which can be considered noise, is several: leakage of current through the seal, ion transport through ion symporters and antiporters with unbalanced charge transport (as in the ClC

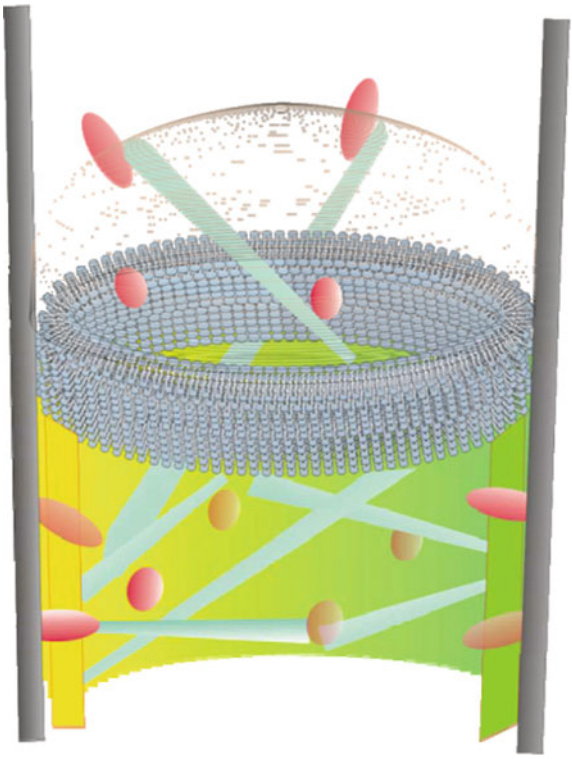

Fig. 10.2 Cartoon showing the channel-free exclusion zone below the domed patch (from: Suchina et al. 2009)

transporter with 2:1 H^+: NO_x^- stoichiometry), and ion pumps. The selectivity of the channel for particular ions can be determined from the obtained *I*/*V* curve. For this we need to find the current reversal potential. This is the potential where the *I*/*V* curve crosses the voltage axis and indicates the potential, where the driving force on the ion passing through the channel is zero. The theoretical potential value where this occurs is derived from the Nernst equation (Hille 1992).

$$E_{\text{Nernst}}, \text{X} = \frac{2.3RT}{mF} . \log \frac{[\text{X}]_\text{o}}{[\text{X}]_\text{i}}$$

where $E_{\text{Nerst,X}}$ is the equilibrium membrane potential in mV, F is Faraday's constant, R is the gas constant, and m is the valence of ion X. The ratio $[X]_o/[X]_i$ represents the concentration gradient of ion X across the membrane. In the case of a monovalent cation, like K^+ and when the experiment is performed at room temperature, substitution of the relevant constants leads a simplified equation:

$$E_{\text{Nernst}}, \text{X} = 5g . \log \frac{[\text{X}]_\text{o}}{[\text{X}]_\text{i}}$$

When the K^+ concentration in the cytosol ($[K^+]_i$) is 10 times higher than in the external solution ($[K^+]_o$), the reversal potential for potassium is −59 mV. We can do this calculation for all the ions present in the solutions and compare the Nernst equations with the current reversal potential found in the experiment. Matching values give a good indication that the channel is selective for the ion we found the match for. From this explanation it is clear that when we are trying to determine the selectivity of a channel the cell-attached patch configuration is not very suitable. The reason for this is the lack of control over the composition of the cytoplasm. We can only assume that most of the commonly present ions such as K^+, Na^+, Ca^{2+}, $Cl^-NO_3^-$and HPO_4^- have a typical order of magnitude value, but these cannot be used for accurate calculation of theoretical Nernst potentials. The configurations that do allow these accurate calculations are the excised patch configurations. The reason why the attached patch configuration is used in some studies, despite this lack of control over the solution at both faces of the membrane, is the loss of some of the factors present in the cytosol that regulate ion channel activity when the membrane patches are excised. Some channels do 'run down' when not in contact with the cytoplasm (this is even the case in the whole cell configuration, where the cytoplasm equilibrates with the pipette solution). For full physiological functioning, these channels need hormones, in particular Ca^{2+} concentrations, second messengers, kinase activity, or other cytosolic factors. In studies that probe the effect of environmental factors on channel activity the cell-attached patch configuration (i.e. the effect of light on channel activation in Elzenga and Van Volkenburgh 1997) is therefore still necessary.

10.2.2 Excised Patch Mode

The excised patch configuration can be used in both the inside-out and outside-out configuration, with cytoplasmic side of the membrane facing the bath solution and the pipette solution, respectively (Fig. 10.1). The excision of a membrane patch is possible because the tight interaction between the membrane and the glass of the micropipette results not only in a very high resistance, but also provides a rather high mechanical strength that resists the forces needed to excise a patch. Inside-out patches are formed from the cell-attached patch configuration by pulling the pipette away from the cell until the membrane around the outside of the micropipette tip breaks. It is assumed that normally the fringe of membrane around the outside of the pipette tip re-anneals and thus forms a second patch of membrane, blocking the tip. By bringing the pipette shortly above the surface of the bath solution and exposing the tip to air, the second, outer, membrane patch is ruptured, exposing the cytoplasmic side of the original membrane patch inside the tip to the bath solution. The outside-out configuration is obtained by first establishing the whole cell configuration (see the next section) and then pulling the pipette away from the cell until the membrane breaks. When the membrane anneals again, forming a patch covering the tip of the micropipette, the desired configuration is

formed: the cytoplasmic face of the patch is in contact with the pipette filling solution, the apoplastic face with the bath solution. Since changing the pipette solution is technically more challenging (Lapointe and Szabo 1987) than changing the bath solution, for which several techniques are available (see for instance the website of HEKA Elektronik, Lambrecht, Germany: www.heka.com), the option to choose either configuration allows freedom in experimental design.

In the excised patch mode the solution composition on both sides is under full experimental control and allows precise calculations, necessary to precisely characterize the selectivity of the channel. Detailed selectivity experiments make use of bi-ionic conditions in which the ions of which their relative selectivity is to be determined are present in the solutions on opposite sides of the membrane. In order to determine the relative selectivity of chloride against nitrate in a typical experiment the micropipette electrode would be filled with 100 mM KCl, while in the bath solution 100 mM KNO_3 would be present. If both anions enter the channel with equal ease, the current reversal potential would be close to 0 mV. A shift in the reversal potential indicates a more easy access of the channel of one of the anions and thus a higher selectivity for that ion. A second type of analysis focuses on the opening and closing dynamics of the channels often as a function of the potential applied to the membrane patch. Good references for this type of analysis are Colquhoun and Hawkes (1995) or Colquhoun and Sigworth (1995).

10.2.3 Analysis of Whole Cell Currents

The patch clamp technique can be used in different modes: the cell-attached mode, the whole cell mode and the excised patch mode (either inside-out or outside-out). The 'whole-cell mode' (extensively described in Hamill et al. 1981; Hille 1992) is obtained by first forming a "giga seal" between the glass and the membrane of a bleb sucked into the micropipette and then rupturing the patch of membrane that spans the opening of the micropipette tip, either by a short, high voltage pulse, or by a sharp pulse of suction applied to the micropipette. Rupturing this patch allows the pipette solution to equilibrate with the cytosol. When the equilibration is complete, a process that is completed for small ions within minutes, the ion composition on both sides of the membrane is under the experimenter's control and fully defined: on the outside of the membrane the bath solution and on the inside the pipette filling solution. Knowing the ionic composition allows determining the ion that carries the current through channels. In the whole cell mode currents across the entire plasma membrane of the cell can be recorded.

With all commonly used patch clamp software-hardware combinations it is possible to set (or 'clamp', hence the name of the technique) the voltage across the membrane according to defined protocols (sequences of step-wise or ramp-wise voltage increases and decreases) and recording the resulting currents. A typical example of a voltage clamp protocol and the data obtained by applying this voltage protocol in the whole cell mode are presented in Fig. 10.4. Normally the

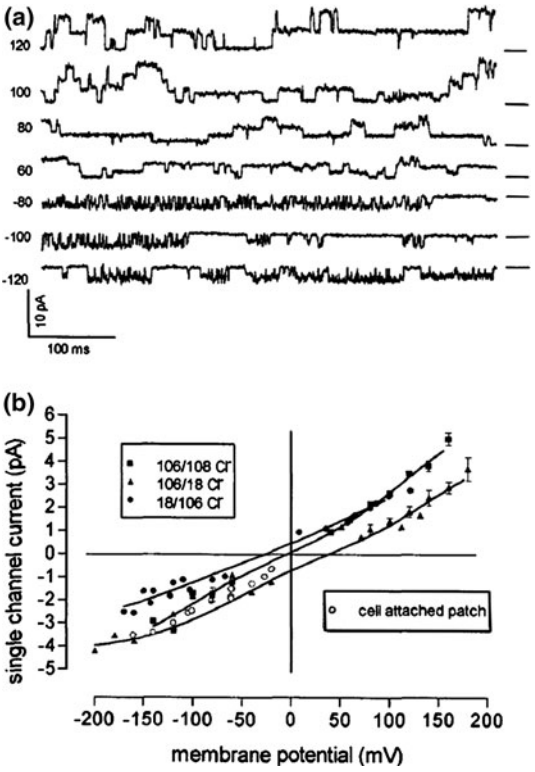

Fig. 10.3 Current–voltage relation of anion channel in the plasma membrane of leaf mesophyll cells of pea. **a** Single channel recording of o/o patch at different holding potentials. The holding potential in mV is indicated at the *left* of the individual traces. The closed channel current is indicated by the horizontal bar at the *right* of the traces. Composition of bath solution was 1 mM $CaCl_2$ 2 mM $MgCl_2$ 100 mM KCl and 10 mM Hepes-BTP, pH 7.0. The pipette solution was 2 mM $MgCl_2$ 100 mM KCl, 10 mM Hepes-BTP, pH 7.0, and 1 mM BAPTA pCa 6. Mannitol was added to adjust the osmolarity to 240 mOsm in the bath solution and to 290 mOsm in the pipette solution. **b** Current–voltage relation of single open channel currents in 100/100 (cytoplasmic/apoplastic concentrations in mM), 10/100, and 100/10 KCl. The different KCl concentrations lead to the Cl^- concentration on the cytoplasmic and apoplastic sides, as indicated in the *inset* (from: Elzenga and Van Volkenburgh 1997)

membrane is held for several seconds at one holding potential between the voltage pulses that are varied, often in a sequence of increasingly negative or increasingly positive pulse potentials. Stepping to a more negative potential normally results in a downward deflection of the currents that are elicited by the voltage pulse. The convention is that downward (more negative) currents are considered to reflect inward currents. Inward currents can be carried by cations moving into the cell or by anions moving out of the cell or a combination of both these fluxes. If the channels in the membrane would be static openings in the membrane and would

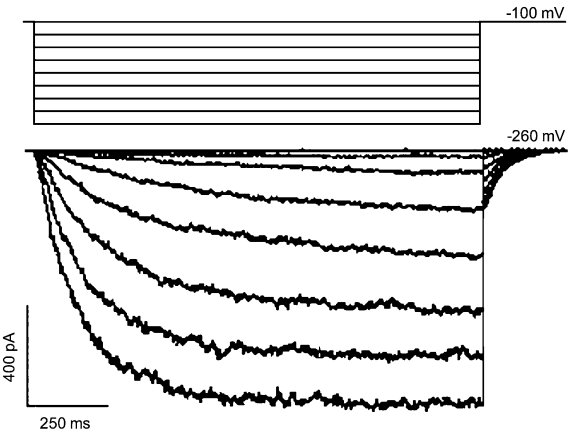

Fig. 10.4 Inward K^+ channel activity in *Arabidopsis* guard cells. The holding potential was −100 mV; voltage steps were applied to potentials ranging between −100 and −260 mV in increments of −20 mV. (from: Lebaudy et al. 2008)

act as a purely Ohmic resistance the square wave voltage pulse would result in a square wave current deflection (for the moment we ignore possible capacitative currents). However, it is obvious that the currents elicited by the test pulse change with time. After an initial instantaneous jump of the current, there is a gradual increase in current that, over the course of about a second, reaches a plateau. The implication is that the population of the channel responsible for passing the ion that carries the current is gradually activated. Activation does not simply mean opening of the channel. In the section above, describing the cell-attached and excised patch mode, it has become clear that even in the fully 'activated' state a channel will still be closed some of the time. Activation of a channel means that the 'open' probability increases. This property of channels, the different open state probability at different voltages, is called voltage gating. The time required to full activation is one of the characteristics used to describe particular channels and sometimes is used in the initial name given to channels [i.e., SLAC, which stands for Slowly Activating Anion Channel (Linder & Raschke)]. Slowly activating channels take seconds to fully activate, while fast channels reach full activation within 0.1 ms. Voltage gated channel can be deactivated by clamping the voltage at the holding potential again. It should be realized that in Fig. 10.4 the pulse voltages and the resulting ion currents are plotted on top of each other and that the pulse voltages were given sequentially each preceded by a period at which the membrane was clamped at the 'holding' potential. The same applies for the current recordings.

By analyzing the current recordings in the whole cell mode several characteristics of the channels responsible for these currents can be determined. Important properties of the conductances are: -activation dynamics (time course of the activation, slowly activating versus fast activating), -activation voltage (the threshold voltage needed for activation, i.e., a channel is only activated at potentials more negative than −140 mV, at values more positive than −140 mV the channels are not activated and this leads to a nonlinear current–voltage

relation, which is another deviation from a purely Ohmic conductance). From these channel properties important conclusions can be drawn with respect to its physiological function.

From pulse protocols that probe the activation kinetics of a channel it is not possible to make inferences about the ions that carry the current. An inward current can be carried by either a cation moving into the cell or an anion moving out of the cell. As described in the previous section, the selectivity of a channel in excised patches can be determined by plotting the open channel current–voltage relation, read from the graph the potential where this current–voltage relation crosses the voltage axis (the current reversal potential) and compare this potential with the Nernst potentials of the ions present in the bath and pipette filling solutions. In the whole cell mode the *I*/*V* relation we obtain by plotting the pulse potentials against the resulting, activated, currents cannot be used for this purpose. In this *I*/*V* relation the open channel conductance is convoluted with the activation state of the channel. Therefore, the apparent current reversal potential often does not reflect the open channel reversal potential and cannot be compared with the theoretical Nernst potential of ions in solution on both sides of the membrane to determine ion specificity of the channels.

To circumvent the interference by voltage activation and deactivation in the accurate measurement of the reversal potential in whole cell mode, we make use of the time dependence of voltage activation and voltage deactivation. In such an experiment a holding potential is selected that activates the current through a channel of interest and the pulse potential protocol is designed in such a manner, that theoretical Nernst potentials of all the ions in the bath and pipette solutions are included. Immediately after the jump from the, activating, holding potential to the, potentially deactivating, pulse potential, the channels will not have had enough time to deactivate and the resulting current will be the result of the driving force equal to the pulse potential minus the Nernst potential for the ion carrying the current and, still, the activated conductance. When we plot the current immediately following the jump, against the pulse voltage, a current–voltage relation is obtained of which the reversal potential can be used to determine the channel selectivity. This method is called tail-current analysis and is described in a very accessible way by Ward (1997).

Associating single channel activities to whole cell activities is often not very straightforward. It should be realized that although it is sometimes possible to reconstruct the time and voltage dependence found in whole cell recordings from voltage-dependent changes in open and closing dynamics in a single channel, the different conditions between the two configurations result in differences: in whole cell mode often larger cell components in the cytoplasm are still present and can affect channel activity and in whole cell mode also the currents that cannot be resolved as single channel openings, like ion pumps and other transporters, are present.

10.3 Using the Patch Clamp Technique on Plant Cells

Using the patch clamp technique on plant cells poses a real challenge, as a 'naked' cell membrane is not directly available since all plant cells are surrounded by a rather sturdy cell wall. To release cell wall-less cells or protoplasts the cell wall integrity has to be compromised in one of three ways:

- Use of hydrolytic enzymes to dissolve or weaken the pectin, cellulose, and hemi-cellulose macromolecules that form the bulk of the cell wall.
- Mechanically disrupting (part of) the cell wall. Plasmolysing the cells in a hyperosmotic solution while still in the tissue and then slicing the tissue will occasionally result in damaging the cell wall structure, while leaving the plasmolysed protoplast or vacuole intact. This is followed by careful isolation of the protoplasts/vacuoles from the debris of the cut up tissue. This method is actually one of the oldest that has been used to release protoplasts and was used by Klercker (1892) more than a century ago. For the isolation of vacuoles this technique has still some use (Davies et al. 1992, Maathuis and Prins 1990, 1991), but is not much used for protoplasts.
- A variation on the second method is cutting a hole in the cell wall with a laser under the microscope after first plasmolysing the cells. When a hole in the cell wall has been formed, gently re-swelling the cells in a more hypo-osmotic solution will release the protoplast from the cell, or the protoplast can be approached with the micropipette through the ablated hole in the cell wall.

10.3.1 Hydrolytic Enzymes

The first successful attempts to isolate protoplast that could be used for the patch clamp technique were done on stomatal guard cells (Schroeder et al. 1984). A strip of epidermis was removed mechanically and treated with enzymes to degrade the cell wall and liberate the protoplasts. Protoplasts were purified by centrifugation to remove debris. The protocol used for guard cells, however, was not successful on other cells types. Until a more or less generally applicable protocol for the protoplast isolation was developed, authors working on plant cells with the patch clamp technique commented on the inability to obtain high resistance seals (Lew 1991; Auerbach and Sachs 1985; Schauf and Wilson 1987a, b), the low success rate of seal formation, which can be 10% or less (Fairley and Walker 1989; Lew 1991; Schauf and Wilson 1987a, b) and the time it takes to form a seal, which is seconds with vacuolar membranes, but can be as long as 0.5 h with plasma membranes (Bush et al. 1988). The recalcitrant nature of plant derived protoplast in forming a gigaseal has been attributed to incomplete cell wall removal, cell wall regeneration, inadequate cleaning of the membrane and lack of cytoskeletal

rigidity (Brownlee 1994). A very recent study indeed indicates that the adhesive energy increases with cytoskeletal rigidity (Suchyna et al. 2009).

Another concern regarding working with protoplasts was the risk of introducing artifacts by the treatment with hydrolytic enzymes, especially when this treatment is prolonged for several hours (Bush et al. 1988; Schauf and Wilson 1987a). Brownlee (1994) summed up the indications that protoplasts, especially when exposed to drastic treatments, may have severely altered properties when compared to *in planta* cells. The membrane potential of tobacco protoplasts was measured to be around −10 to −15 mV, whereas physiologically healthy cells have very negative membrane potentials between −100 and −220 mV. This negative membrane potential reflects the activity of the plasma membrane proton pumping ATPase, which might have a reduced activity in protoplasts. Also the removal of the extracellular matrix and plasma membrane connections with other cells were considered to affect the physiological state of protoplast. In more recent studies, reviewed by Demidchik et al. (2006), enzymatic isolation of protoplasts was shown to induce changes in the physiology of the cell affecting the electrophysiological properties. Treatment of tissue with cellulose does induce an oxidative burst and activation of hydrolytic enzymes (Brudern and Thiel 1999; Kennedy and de Filippis 2004). Demidchik et al. (2006) have found indications that this could result in altered channel behavior and even in the disappearance of channels. Also sudden alteration of the osmotic potential of the external medium can alter the protein composition of the membrane, the proton pumping ATPase activity and the K^+ efflux (Qian et al. 1993). In intact tissue the control over the cytosolic calcium concentration in guard cells is more stringent that in isolated guard cell protoplast (Levchenko et al. 2008).

In quick succession a series of articles appeared between 1991 and 1995 with protocols that yielded protoplasts that were amenable to form gigaseals with a resistance greater than 10 GΩ and that could be used on various tissues from different plant species (Elzenga et al. 1991; Vogelzang and Prins 1992; Blom-Zandstra et al. 1995).

Releasing protoplasts by weakening the cell wall with hydrolytic enzymes has been a technique that has been utilized for decades and has seen a strong development of protocols since protoplasts are not only used for patch clamping experiments, but are used extensively in tissue culture and plant transfection procedures as well (Davey et al. 2005). The reports by Elzenga et al. (1991) and Vogelzang and Prins (1992) focused on minimizing the exposure time of the plant cells to the enzyme cocktail and on the ease and speed of the procedure to produce the protoplasts. The plant tissue is incubated in a solution with a hyperosmotic (>600 mOsm) solution to plasmolyse the cells, the tissue is then transferred to a solution with an enzyme cocktail that minimally contains cellulase, cellulysin and pectolyase and the same osmotic value. At 30°C this treatment only takes 5–10 min, after which the tissue is transferred to a wash solution with again the same osmotic value, which is refreshed once, for 10 min. By dipping the tissue fragments into the patch clamp bath solution that has an osmotic value of around 210 mOsm, the protoplast in the cells will swell, break the cell wall that is

weakened by the hydrolytic enzyme cocktails and are released from the tissue fragment. The protoplasts are then allowed to settle on the bottom of the patch clamp measuring chamber. The bath solution in this chamber is refreshed once to remove tissue and cell wall fragments and protoplasts that do not adhere to the bottom of the chamber. Care is taken that the all the solutions used for flushing the bath solution are filtered through a 0.2 μm filter. With this method is was possible to routinely establish gigaOhm seals on protoplast from pea leaf epidermal and stem cells, oat coleoptile cells, bean leaf mesophyll cells and Arabidopsis cotyledon cells (Elzenga et al. 1991). In the approach taken by Vogelzang and Prins, the initial strong plasmolysis of the tissue and re-swelling in the bath solution to liberate the protoplasts, was replaced by mechanical pressure after the enzyme incubation to release the protoplast. In the method developed by Blom-Zandstra et al. (1995) the focus was on preventing mechanical stress due to either mechanical pressure or osmotic changes. Enzymatic cell wall degradation was performed at relatively low temperature (12°C) for an extended period (16 h) and protoplasts were released by gently moving the fragile tissue section through the bath solution. This method yielded protoplasts from root and mesophyll tissue from tobacco, Arabidopsis and sweet pepper that readily formed gigaOhm seals.

10.3.2 Laser Microsurgery to Gain Access to the Plasmamembrane

Laser ablation was used on plant cells for the first time in 1996 (Henriksen et al. 1996; Henriksen and Assmann 1997). They used the laser to remove a small section of the cell wall to allow placement of the tip of micropipette on the exposed plasma membrane and form a tight seal. Successful single channel recording could be made on guard cells of *Vicia faba*. In a subsequent study, the electrophysiological properties of cells probed with the laser microsurgical method were compared with those of enzymatically released protoplasts. In the 'laser'-treated cells a new category of channels could be recorded that was never observed in the enzyme treated cells (Miedema et al. 1999). Although the technique potentially is superior to the enzymatic digestion technique, the technical complexity has hampered a more general application of this technology.

10.3.3 Factors Affecting Seal Formation

Although the manufacturing of the micropipettes that perform a central role in the patch clamp technique lies outside the scope of this chapter, the geometry and morphology of the pipette tip has been assumed to be important in the seal formation. Comparing newly pulled micropipette tips with, microscopically,

rough and uneven tips, with those that were cut with an ion beam system, creating a smooth and flat tip, revealed that the seal resistance could be doubled by polishing the rim of the pipette opening (Malhoubi et al. 2009). Although this finding seems to support the common practice to heat polish the tip of the micropipette to smooth the rim, it seems in contrast with the results of Suchyna et al. (2009) that indicate that the seal forms in the neck of the membrane bleb that is pulled into the tip of the micropipette and not on the rim. Moreover, that smoothing of the pipette tip is not absolutely needed for the formation of a gigaseal was already demonstrated by Boehle and Benndorf (1994) that used pipette tips after repeated breaking and found these broken tips 'especially appropriate for patch clamping'.

10.4 New Developments

Patch clamping plant cells is still a laborious, complex, and technically demanding activity that all depends on the formation a good gigaseal and low current noise levels. But the technique is well-developed and in numerous laboratories a standard, routine technique. There are a few areas where future development would be desirable. The first area is the selection of specific cell types. Paradoxically, the first successful application of the patch clamp technique on plants was on a very specific cell type, the guard cell (Schoeder et al. 1984). Selection of the guard cell in a preparation is not very difficult. The cells are isolated from a strip of leaf epidermis in which most of the epidermal pavement cells are dead and in case there is a mix of guard cell and pavement cell protoplast, they are easily distinguishable. In phloem strand in *V. faba* the sieve element cells can be recognized by the forisome, a large protein inclusion in the sieve elements of Fabacea (Hafke et al. 2007). In the protoplasts of these cells the forisomes can still be observed and the cell thus selected for. However, in most cases the cell types can no longer be recognized when the cells have lost their cell wall and have become protoplasts, since they lack distinctive characteristics (like presence or absence of chloroplast, as is the case with guard cells and pavement cells). Labeling cells has proved to be a useful technique to select specific cell types for patch clamp studies (Maathuis et al. 1998; Ivashikina et al. 2003). Cell type labeling by fluorescent markers under the control of cell type-specific markers will become more available with the progress that is being made in molecular characterization of cell tissues.

An even greater challenge will be ion channel mapping on cells types that exhibit polarity or regional specialization, like for instance wood forming cells (Arend et al. 2005). The technique is being utilized on animal cells for more than 10 years and involves the combination of patch clamp and scanning ion conductance microscopy (Korchev et al. 2000; Dutta et al. 2008).

References

Arend M, Stinzing A, Wind C, Langer K, Latz A, Ache P, Fromm J, Hedrich R (2005) Polar-localised poplar K^+ channel capable of controlling electrical properties of wood-forming cells. Planta 223:140–148

Auerbach A, Sachs F (1985) High resolution patch-clamp techniques. In: Smith TG, Lecar H, Redman SJ, Gage PW (eds) Voltage and patch clamping with microelectrodes. American Physiological Society, Baltimore, pp 121–149

Blom-Zandstra M, Koot HTM, van Hattum J, Vogelzang SA (1995) Isolation of protoplasts for patch-clamping experiments: an improved method requiring minimal amounts of adult leaf or root tissue from monocotyledonous or dicotyledonous plants. Protoplasma 185:1–6

Boehle T, Benndorf K (1994) Facilitated giga-seal formation with a just originated glass surface. Pflugers Arch 427:487–491

Brownlee C (1994) Microelectrode techniques in plant cells and microorganisms. In: Ogden DC (ed) Microelectrode techniques, the plymouth workshop handbook, 2nd edn. Company of Biologists, Cambridge, pp 347–359

Brudern A, Thiel G (1999) Effect of cell-wall digesting enzymes on physiological state and competence of maize coleoptile cells. Protoplasma 209:246–255

Bush DS, Hedrich R, Schroeder JI, Jones RL (1988) Channel-mediated K^+ flux in barley aleurone protoplasts. Planta 176:368–377

Colquhoun D, Hawkes AG (1995) The principles of the stochastic interpretation of ion-channel mechanisms. In: Sakmann B, Neher E (eds) Single-channel recording, 2nd edn. Plenum Press, New York, pp 397–482

Colquhoun D, Sigworth FJ (1995) Fitting and statistical analysis of single-channel records. In: Sakmann B, Neher E (eds) Single-channel recording, 2nd edn. Plenum Press, New York, pp 483–587

Davey MR, Anthony P, Power JB, Lowe KC (2005) Plant protoplasts: status and biotechnological perspectives. Biotechnol Adv 23:131–171

Davies JM, Poole RJ, Rea PA, Sanders D (1992) Potassium transport into plant vacuoles energized directly by a proton-pumping inorganic pyrophosphatase. Proc Nat Acad Sci USA 89:11701–11705

Demidchik V, Sokolik A, Yurin V (2006) Electrophysiological characterization of plant cation channels. In: Volkov A (ed) Plant electrophysiology: theory and methods. Springer, Berlin, pp 173–183

Dutta AK, Korchev YE, Shevchuk AI, Hayashi S, Okada Y, Sabirov RZ (2008) Spatial distribution of maxi-anion channel on cardiomyocytes detected by smart-patch technique. Biophys J 94:1646–1655

Elzenga JTM, Van Volkenburgh E (1997) Characterization of a light-controlled anion channel in the plasma membrane of mesophyll cells of pea. Plant Physiol 113:1419–1426

Elzenga JTM, Keller CP, Van Volkenburgh E (1991) Patch clamping protoplasts from vascular plants: method for the quick isolation of protoplasts having a high success rate of gigaseal formation 97:1573–1575

Fairley KA, Walker NA (1989) Patch clamping corn protoplasts. Gigaseal frequency is not improved by Congo red inhibition of cell wall regeneration. Protoplasma 153:111–116

Gadsby DC (2009) Ion channels versus ion pumps: the principal difference, in principle. Nat Rev Mol Cell Biol 10:344–352

Hafke JB, Furch ACU, Reitz MU, van Bel AJE (2007) Functional sieve element protoplasts. Plant Physiol 145:703–711

Hamill OP, Marty A, Neher E, Sakmann B, Sigworth FJ (1981) Improved patch-clamp techniques for high-resolution current recording from cells and cell-free membrane patches. Pflügers Arch 391(2):85–100

Hedrich R, Schroeder JI (1989) The physiology of ion channels and electrogenic pumps in higher plants. Annu Rev Plant Physiol Plant Mol Biol 40:539–569

Henriksen GH, Assmann SM (1997) Laser-assisted patch clamping: a methodology. Pfluegers Arch 433:832–841

Henriksen GH, Taylor AR, Brownlee C, Assmann SM (1996) Laser microsurgery of higher plant cell walls permits patch-clamp access. Plant Physiol 110:1063–1068

Hille B (1992) Ion channels of excitable membranes. Sinaur Associates, Sunderland, p 607

Ivashikina N, Deeken R, Sche P, Kranz E, Pommerrenig B, Sauer N, Hedrich R (2003) Isolation of AtSUC2 promoter-GFP-marked companion cells for patch-clamp studies and expression profiling. Plant J 36:931–945

Kennedy BF, De Filippis LF (2004) Tissue degradation and enzymatic activity observed during protoplast isolation in two ornamental *Grevillea* species. In Vitro Cell Dev Biol 40:119–125

Klercker JAf (1892) Eine Methode zur Isolierung lebender Protoplasten. Ofversigt af kong vetenskaps-akademiens forhandlingar 9:463–474

Korchev YE, Negulyaev YA, Edwards CRW, Vodyanoy I, Lab MJ (2000) Functional localization of single active ion channels on the surface of a living cell. Nat Cell Biol 2:616–619

Lapointe J-Y, Szabo G (1987) A novel holder allowing internal perfusion of patch-clamp pipettes. Pfluegers Arch Eur J Physiol 410:212–216

Latorre R, Miller C (1983) Conduction and selectivity in potassium channels. J Membr Biol 71:11–30

Lebaudy A, Vavasseur A, Hosy E, Dreyer I, Leonhardt N, Thibaud J-B, Very AA, Simonneau T, Sentenac H (2008) Plant adaptation to fluctuating environment and biomass production are strongly dependent on guard cell potassium channels. PNAS 105:5271–5276

Levchenko V, Guinot DR, Klein M, Roelfsema MRG, Hedrich R, Dietrich P (2008) Stringent control of cytoplasmic Ca^{2+} in guard cells of intact plants compared to their counterparts in epidermal strips or guard cell protoplasts. Protoplasma 233:61–72

Lew RR (1991) Substrate regulation of single potassium and chloride ion channels in *Arabidopsis* plasma membrane. Plant Physiol 95:642–647

Maathuis FJM, Prins HBA (1990) Patch clamp studies on root cell vacuoles of a salt-tolerant and a salt-sensitive *Plantago* species. Plant Physiol 92:23–28

Maathuis FJM, Prins HBA (1991) Inhibition of inward rectifying tonoplast channels by a vacuolar factor: physiological and kinetic implications. J Membr Biol 122:251–258

Maathuis FJM, Taylor AR, Assmann SM, Sanders D (1997) Seal-promoting solutions and pipette perfusion for patch clamping plant cells. Plant J 11:891–896

Maathuis FJM, May ST, Graham NS, Bowen HC, Jelitto TC, Trimmer P, Bennett MJ, Sanders D, White PJ (1998) Cell marking in *Arabidopsis thaliana* and its application to patch-clamp studies. Plant J 15:843–851

Malhoubi M, Ostadi H, Wang S, Gu Y, Jiang K (2009) Effects of the surface morphology of pipette tip on giga-seal formation. Eng Lett 17:4

Miedema H, Henriksen GH, Assmann SM (1999) A laser microsurgical method of cell wall removal allows detection of large-conductance ion channels in the guard cell plasma membrane. Protoplasma 209:58–67

Milton RL, Caldwell JH (1990) How do patch clamp seals form? A lipid bleb model. Pfluegers Arch Eur J Physiol 416:758–765

Moran N, Ehrenstein G, Iwasa K, Bare C, Mischke C (1984) Ion channels in plasmalemma of wheat protoplasts. Science 226:835–883

Ogden D (ed) (1994) Microelectrodes Techniques. The Plymouth Workshop Handbook. The Company of Biologists Ltd, Cambridge, p 448

Qian YC, Nguyen T, Murphy TM (1993) Effect of washing on the plasma membrane and on stress reactions of cultured rose cells. Plant Cell, Tissue Organ Cult 35:245–252

Schauf CL, Wilson KJ (1987a) Effects of abscisic acid on K^+ channels in *Vicia faba* guard cell protoplasts. Biochem Biophys Res Commun 145:284–290

Schauf CL, Wilson KJ (1987b) Properties of single K^+ and Cl^- channels in *Asclepias tuberosa* protoplasts. Plant Physiol 85:413–418

Schroeder JI, Hedrich R, Fernandez JM (1984) Potassium-selective single channels in guard cell protoplasts of *Vicia faba*. Nature 312:361–362

Suchyna TM, Markin VS, Sachs F (2009) Biophysics and structure of the patch and the gigaseal. Biophys J 97:738–747

Vogelzang SA, Prins HBA (1992) Plasmalemma patch clamp experiments in plant root cells: procedure for fast isolation of protoplasts with minimal exposure to cell wall degrading enzymes. Protoplasma 171:104–109

Ward JM (1997) Patch-clamping and other molecular approaches for the study of plasma membrane transporters delmystified. Plant Physiol 114:1151–1159

Ward JM, Mäser P et al (2009) Plant ion channels: gene families, physiology, and functional genomics analyses. Annu Rev Physiol 71:59–82

Part II
Cell Electrophysiology

Chapter 11
pH Banding in Charophyte Algae

Mary J. Beilby and Mary A. Bisson

Abstract The internodal cells of Characean algal species have long served as a model for membrane processes in plants, because their large size (up to several centimetres in length), simple geometry (cylinder) and clear separation from other cells in the plant have allowed experimental techniques such as multielectrode electrophysiological techniques and cell perfusion. However, the membranes of these cells are not homogeneous, but show distinct differences in their electrophysiological characteristics and transport capabilities. The most obvious example of this non uniformity is the pH difference seen in the external medium surrounding the cells, the "acid bands", with a pH similar or slightly acid to the bulk medium, and "alkaline bands", which can support a pH of 10 or higher. We explore here the transport properties that underlie these differences and their relation to photosynthesis.

Abbreviations

ADP	Adenosine diphosphate
AP	Action potential
APW	Artificial pond water
ATP	Adenosine triphosphate
AZ	Acetazolamide
E_j	Nernst potential for the ion j
DIC	Dissolved inorganic carbon

M. J. Beilby (✉)
School of Physics, University of New South Wales,
Sydney, NSW 2052, Australia
e-mail: m.j.beilby@unsw.edu.au

M. A. Bisson
Department of Biological Sciences, University at Buffalo,
Buffalo, NY 14260, USA
e-mail: bisson@buffalo.edu

A. G. Volkov (ed.), *Plant Electrophysiology*,
DOI: 10.1007/978-3-642-29119-7_11, © Springer-Verlag Berlin Heidelberg 2012

DES	Diethylstilbestrol
DCMU	(3-(3,4-dichlorophenyl)-1,1-dimethylurea
DCCD	N,N′-dicyclohexylcarbodiimide
EZA	Ethoxyzolamide, an inhibitor of carbonic anhydrase
EDAC	1–ethyl -3-(3-dimethylamino-propyl) carbodiimide
E_{vo}	Vacuole to outside potential difference
E_{co}	Cytoplasm to outside potential difference
E_{vc}	Vacuole to cytoplasm potential difference
F	Faraday constant 96,485.3 C/mol in Eqs. 11.1–11.3
F	Fluorescence yield
F'_m	Saturation fluorescence
GHK	Goldman-Hodgkin-Katz equation
g_{bkg}	Background conductance (I/V modelling)
G/*V*	Conductance as a function of voltage
$\Delta\bar{\mu}_H, \Delta\bar{\mu}_{Na}$	Electrical chemical potential difference for H^+ or Na^+, respectively
H^+/OH^- state	State of the membrane whose electrical characteristics are dominated by H^+ or OH^- leak
Hepes	4-(2-hydroxyethyl)-1-piperazineethanesulfonic acid, zwitterionic buffer with pKa = 7.55/OH
I_{bkg}	Background current (I/V modelling)
k^0_{io}, k^0_{oI}, k_{io}, k_{oi}	Proton pump parameters (I/V modelling)
I/*V*	Current as a function of voltage
NEM	N-ethyl maleimide
NPQ	Non-photochemical quenching, a measure of impairment of photosynthesis derived from fluorescence studies
N_XP_X	Number of channels conducting ion X
PCMBS	p-(chloromercuri)benzene sulfonate
PD	Electrical potential difference across a membrane
pH_c	Cytoplasmic pH
pH_o	External pH
P_{o-} and P_{o+}	Open probabilities of a channel at negative and positive potentials, respectively
R	Gas constant 8.314 J/mol.K
R_{co}	Plasma membrane resistance
T	Temperature in Kelvin
V	Transmembrane PD in volts
V_{50}	Half-activation potential (Eqs. 11.2, 11.3)
V_{bkg}	Background current reversal PD (I/V modelling, usually taken as -100 mV)
$[X]_o$, $[X]_i$	Medium and intracellular concentrations, respectively, of ion X (Eq. 11.1)
Y′	Quantum yield, a measure of photosynthesis derived from fluorescence studies
Z	Valency of ion X (Eq. 11.1)
z_g	Charge associated with channel gating (Eqs. 11.2, 11.3)

The internodal cell of the Characean algae, which may have a diameter as large as 1 mm and a length of several centimetres, has long been of great use in electrophysiology. Impalements can be effected easily, without undue harm to the cell, even with early, primitive equipment (Walker 1955). Although microelectrodes usually penetrate into the vacuole, as the cytoplasm is a thin layer pressed up against the cell wall (Hope and Walker 1975), the tonoplast has a high conductance ($\sim$5 S m^{-2}) and small, relatively constant electrical potential difference (PD) of about +10 mV (Findlay and Hope 1964; Coster and Smith 1977). Therefore, the measured potential difference, $E_{vo} = E_{co} + E_{vc}$, essentially tracks the plasma membrane potential, usually more negative than −200 mV (Findlay and Hope 1964). The plasma membrane conductance in proton pump-dominated steady state is usually 0.5–1 S m^{-2}. Thus, the plasma membrane resistance R_{co} can be up to 10× greater than that of the tonoplast. If the voltage clamp is applied to both membranes in series (with the inside electrode in the vacuole), most of the PD appears across the plasma membrane (Beilby 1990).

Other advantages of the large cell include the ability to perfuse away the vacuole (Tazawa 1964) or the cytoplasm (Williamson 1975; Tazawa et al. 1976) in order to determine the components that control membrane processes. Different parts of the cell can be subjected to different environments, allowing such techniques as K^+ anaesthesia, which permits non-invasive measurements of PD (Shimmen et al. 1976). Ca^{2+} and Na^+ fluxes, which for technical reasons are difficult to measure in intact cells, can be determined using different regions of the cell (Reid and Smith 1992; Whittington and Bisson 1994; Kiegle and Bisson 1996). Therefore, important aspects of the plasma membrane potential, including voltage-gated channels and action potentials (AP), are easily determined. Most significantly, it was in *Chara* and *Nitella* that the notion of the chemiosmotic plant plasma membrane was first elucidated, with the membrane being energised by a proton pump that generates an energy gradient for protons, $\Delta\bar{\mu}_H$, that then drives other transport processes (H^+ economy) (Kitasato 1968; Spanswick 1972; Beilby 1984). This form of membrane energisation is similar to but distinct from the animal system, whereby the membrane is energised by an Na^+ pump that generates a $\Delta\bar{\mu}_{Na}$, that drives other transport processes (Na^+ economy). It is likely that this system arose from migration to freshwater, with a low Na^+ concentration that made Na^+ economy less viable. This H^+ economy is widely utilised by vascular plants (Sze et al. 1999), to which Charophytes form a sister group (Karol et al. 2001; McCourt et al. 2004), and which, on land, also grow in what is often an Na^+ poor environment.

However, there are some significant disadvantages to the use of such a large cell. One is the existence of cable properties, the dissipation of injected current along the long cylindrical membrane away from the point of injection. This can result in errors in measuring conductance using point injection of current or the inability to adequately voltage clamp the membrane. These difficulties have long been recognised, and can be dealt with using mathematical correction of resistance measured by point injection, or the use of long, inserted current injection wires to

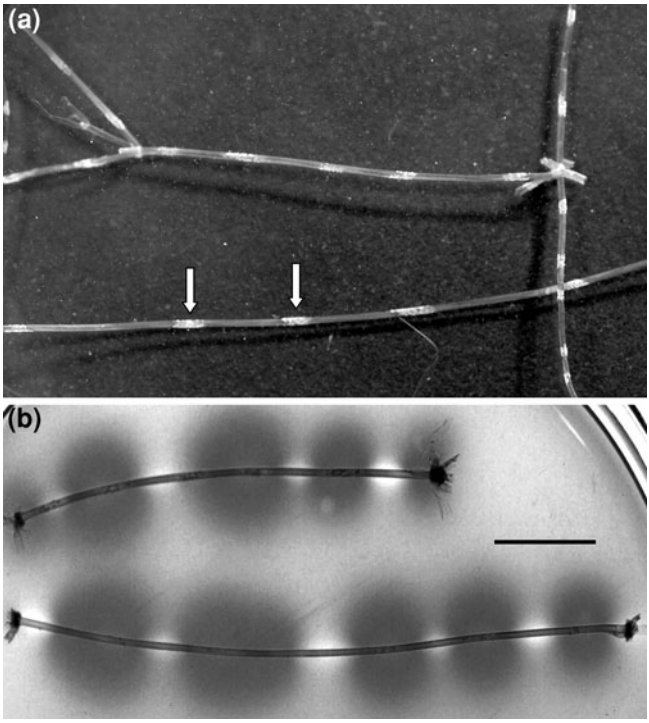

Fig. 11.1 Banding of *Chara australis* cells visualized by: **a** Presence of $CaCO_3$ crystals (light areas, *arrows*) forming on the surface of the cell wall in the alkaline bands. **b** pH indicator phenol red: dark areas are deep red indicating pH above 8.2, light areas are *yellow* in pH below 6.8. Cells were incubated in light in APW with 6.0 mM Sodium bicarbonate and 0.2% agarose to slow the diffusion and accentuate the pH banding. The scale bar is 1 cm for both (**a**) and (**b**)

ensure adequate voltage clamping (Smith 1984; Beilby 1989). However, another possibility that is more difficult to deal with is the inhomogeneities in the electrical properties along the long cylindrical cells. Such inhomogeneities were first recognised by Arens (1939) who noted that calcifications due to $CaCO_3$ precipitation varied in a periodic fashion along the membrane (see Fig. 11.1a). Spear et al. (1969) found that even *Nitella* cells with no visible crystals display pH banding along the cell when exposed to light (see Fig. 11.1b). Large pH differences along the cell can be visualised by pH indicator dyes and measured by scanning pH electrodes.

While the "patchy" membrane might complicate life for Characeae electrophysiologists, it provides interesting insight into an electrophysiological motif that is clearly successful in helping plants to survive in range of environments. pH banding has been adopted by aquatic angiosperms (Prins et al. 1980), roots of land plants (Raven 1991) and pollen tubes (Feijo et al. 1999). There are some

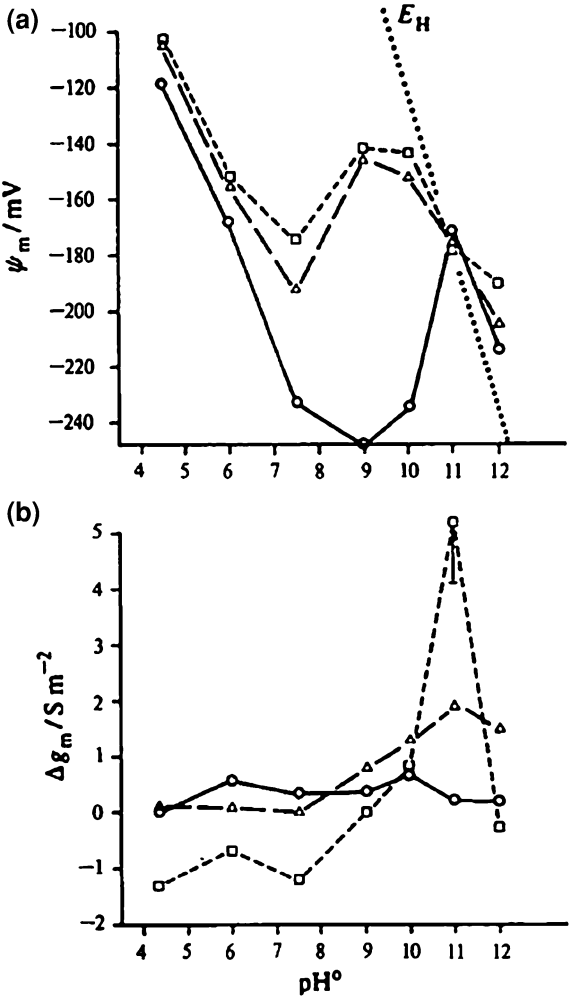

Fig. 11.2 **a** The effect of pH_o on membrane PD and **b** membrane conductance of *C. corallina* (Bisson and Walker 1981). The line labelled E_H represents Nernst PD for H^+ (OH^-) for a cell with pH_i acclimated to pH_o 7.5. However, the cells were pretreated at different pH for 20 min: 4.5 *circles*, 7.5 *triangles*, 9.0 *squares*

indications that similar transporters are involved, confirming Characeae as an important model system.

11.1 The Role of Transporters in Establishing Banding

The banding phenomenon relies on two different transport systems. Acidification of the medium is mediated by the well known H^+-exporting ATPase (Kitasato 1968; Shimmen and Tazawa 1977; Takeshige et al. 1986). But what transport system is responsible for the alkaline band? Bisson and Walker (1980) made a surprising discovery: as the external pH (pH_o) was increased to values between 9

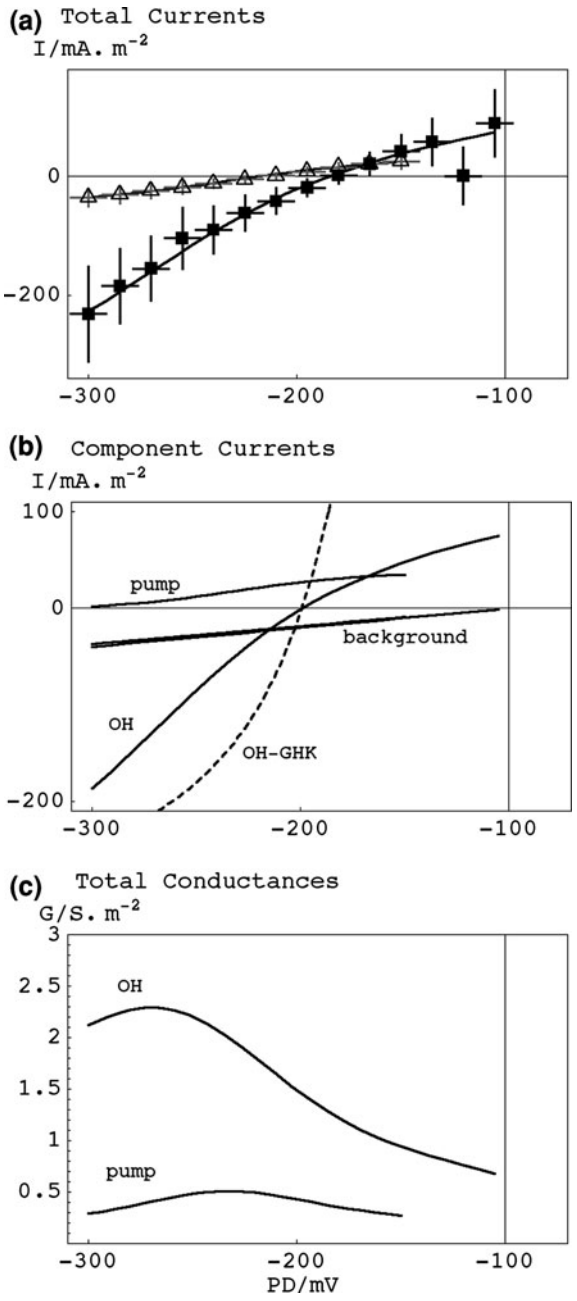

Fig. 11.3 **a** Statistics of 12 *I/V* profiles from 5 cells *Chara australis* in APW of pH_o 7.1 (*open triangles*) compared to statistics of 12 *I/V* profiles from the same 5 cells of at pH_o 11.1 (*filled rectangles*). **b** The fitted OH^-, pump and background currents. No inward or outward rectifiers were fitted to the data. The GHK equation for OH^- current without the Boltzmann distribution is shown by a dotted line. For fit parameters see Table 11.1. **c** The total conductance calculated from the fitted total currents in pump and high pH states (subset of data from Al Khazaaly and Beilby 2012). The pump current was fitted to a two-state model (Hansen et al. 1981; Beilby and Walker 1996) and empirical equation was used for the background current $I_{bkg} = g_{bkg}\ (V–V_{bkg})$

Table 11.1 Fit parameters for Fig. 11.3

(a) Pump and background parameters[a]

Conditions	$k_{io}^{0}(s^{-1})$	$\kappa_{oi}(s^{-1})$	E_p (mV)	Resting PD (mV)	g_{bkg} (S m^{-2})
APW pH 7.1	5,100	20	−334	−218	0.185

(b) OH^- channel parameters[b]

Conditions	$N_{OH}P_{OH} \times 10^{-4}$ (m s^{-1})	$V_{50\text{-}}$(mV)	z_g	pH_i	$E_{H/OH}$ (mV)	Resting PD (mV)	g_{bkg} (S m^{-2})
APW pH 11.1	4.1	−255	0.65	7.75	−199	−185	0.2

[a] The parameters k_{oi}^{0} and κ_{io} were both kept at 0.5 s^{-1}
[b] No inward or outward rectifiers were fitted

and 10, the membrane PD of *Chara corallina* started to follow equilibrium PD for H^+ or OH^- (see Fig. 11.2a, b), which we call the H^+/OH^- state. In some experiments the membrane PD hyperpolarised by −59 mV/pH unit becoming more negative than −200 mV at pH_o 12 (Bisson and Walker 1981). The membrane conductance increased to 5–20 S m^{-2} and the shape of the *I*/*V* characteristics acquired slight downward curvature (Bisson and Walker 1980; Beilby and Bisson 1992). Bisson and Walker (Bisson and Walker 1981; Bisson and Walker 1982; Bisson 1986a; Bisson 1986b) found that the H^+/OH^- conductance can be inhibited by DES, EDAC, DCCD and photosynthesis inhibitors DCMU and darkness. Effects of sulfhydryl reagents (that bind to SH group) NEM and PCMBS were regarded as nonspecific, as they were accompanied by streaming inhibition. Bisson (1984) inhibited H^+/OH^- conductance by exposing *C. corallina* to media lacking Ca^{2+}. The original conductance could be rapidly restored by reintroducing medium with Ca^{2+} or Mg^{2+}.

Beilby and Bisson (1992) investigated the *I*/*V* and *G*/*V* characteristics of H^+/OH^- state in more detail in both intact cells and cytoplasm-enriched fragments of *C. corallina* (Beilby and Shepherd 1989). The currents were fitted by the Goldmann–Hodgkin–Katz (GHK) equation, multiplied by the Boltzmann distribution of open probabilities, $P_{o\text{-}}$ and P_{o+} (Amtmann and Sanders 1999; Beilby and Walker 1996), which make the channel PD-dependence much stronger.

$$I_X = \frac{P_{o+}P_{o-}N_X P_X (zF)^2 V\left([X]_i - [X]_o e^{-\frac{zFV}{RT}}\right)}{RT\left(1 - e^{-\frac{zFV}{RT}}\right)} \tag{11.1}$$

$$P_{o-} = 1 - \frac{1}{1 + e^{-\frac{z_g - F(V - V_{50-})}{RT}}} \tag{11.2}$$

$$P_{o+} = 1 - \frac{1}{1 + e^{-\frac{z_g + F(V - V_{50+})}{RT}}} \tag{11.3}$$

where I_x is the current due to ion *X*. *F*, *R*, *T* have their usual meaning. *V* is the PD across plasma membrane or across both plasma membrane and tonoplast. N_xP_x is the number of channels times the permeability of single channel, treated as a single parameter. The gating charge z_g is designated z_{g-} in Eq. 11.2 and z_{g+} in Eq. 11.3. The half activation potential V_{50} is designated V_{50-} and V_{50+} in Eqs. 11.2 and 11.3, respectively.

The downward curvature of the *I*/*V* profiles at high external pH is quite distinct, conductance dropping between −240 and −100 mV. As can be seen from the dotted line, the GHK equation alone leads to very different *I*/*V* characteristics (see Fig. 11.3 and Table 11.1a and b for fit parameters). The downward curvature was achieved in the model by including Boltzmann distribution (Eq. 11.2), setting V_{50-} at PDs more negative than $E_{H/OH}$ and fractional gating charge (Table 11.1b).

However, the conductance and the reversal PD could be quite variable even over minutes. The conductance at pH_o 12 tended to be less than that at pH_o 10–11.5. Because NaOH was used (with or without Goods buffer of appropriate pK_a) to raise the medium pH, the effect of Na^+ concentration was investigated. However, addition of 20 mM Na^+ decreased rather than increased the membrane conductance (Beilby and Bisson 1992), reinforcing the original hypothesis that it is the high pH_o that activates the channels.

Using H^+ instead of OH^- and the same Boltzmann parameters in the model leads to same *I*/*V* characteristics. However, as the concentration of H^+ in the medium decreases, the N_HP_H parameter (Eq. 11.1) has to be increased by many orders of magnitude to account for the currents and conductances observed in the H^+/OH^- state. On the other hand, $N_{OH}P_{OH}$ of same magnitude can explain observed *I*/*V* characteristics throughout the pH_o range (Beilby and Al Khazaaly 2009). Bisson and Walker (1980) invoked water splitting in the high electric field inside the membrane to provide sufficient protons (Simons 1979) at high pH_o. Beilby and Bisson (1992) suggested that patch-clamping the plasma membrane would distinguish between H^+ and OH^-, as number of H^+ channels and/or their unitary conductance would increase drastically as pH_o increased. This experiment is yet to be performed.

Lucas and Shimmen (1981) found that cytoplasmic perfusion rendered the cells unable to band. As perfusion does not affect the proton pump when ATP is supplied, the authors reason that removal of some cytoplasmic organelle prevents opening of the H^+/OH^- channels. This hypothesis was confirmed by their elegant centrifugation experiment, where only the end of the cell rich in organelles banded normally. Upon later redistribution of cytoplasm throughout the cell, the normal banding pattern was again observed. So far the organelle, responsible for the banding pattern, has not been identified. Beilby et al. (1993) confirmed that H^+/OH^- state was absent in perfused *Nitellopsis* cells at high pH_o. Intact *Nitellopsis* cells did exhibit high conductance at high pH_o and were observed to band under some conditions.

11.2 Range of Topics Involved in Banding

Over the last 50 years the banding phenomenon inspired research into range of important themes: the form of dissolved inorganic carbon species DIC (mainly CO_2 or HCO_3^-) transported across plasma membrane (Smith and Walker 1980; Lucas 1983; Mimura et al. 1993; Walker et al. 1980); the role of charasomes (Lucas and Franceschi 1980; Bisson et al. 1991; Chau et al. 1994); production of external circulating electric currents (Walker and Smith 1977; Lucas and Nuccitelli 1980); biological self-organisation and dissipative structures (Toko et al. 1988; Bulychev et al. 2001b; Bulychev et al. 2003); the role of cytoplasmic streaming (Lucas and Dainty 1977; Yao et al. 1992; Babourina et al. 2004; Dodonova and Bulychev 2010); the effect of centrifugation and perfusion (Lucas and Shimmen 1981); role of photosynthesis (Plieth et al. 1994; Bulychev et al. 2001a; Bulychev and Vredenberg 2003); the effect of excitation (Bulychev et al. 2004; Bulychev et al. 2005; Eremin et al. 2007; Krupenina et al. 2008; Bulychev and Krupenina 2009; Bulychev and Krupenina 2010) and biomineralisation (McConnaughey 1991; McConnaughey and Falk 1991). Some of the topics are beyond the scope of this article, but we will summarise research into most of these aspects. Let us first examine the role of photosynthesis in the phenomenon.

11.3 Relation to Photosynthesis

CO_2 permeates easily across lipid bilayers (Gutknecht et al. 1977). However, aquatic environments of many Characeae offer poor availability of CO_2. Diffusion of CO_2 in water is several orders of magnitude slower than in air and CO_2 equilibration with atmosphere is also slow (Price and Badger 2002). Most pond waters are alkaline ($\sim$pH 8 and higher), tipping the equilibrium between the two main DIC, CO_2 and HCO_3^-, towards the bicarbonate ion (Lucas 1975a; Walker et al. 1980). If the bicarbonate ion is transported across the membrane, it must be converted to CO_2 near the Rubisco enzyme to enter the Calvin cycle for carbon fixation.

The early models suggested a possible bicarbonate pump at plasma membrane with OH^- efflux in alkaline bands (Smith 1968) or an OH^-/HCO_3^- antiport, also in alkaline bands (Lucas and Smith 1973). However, the substitution of HPO_4^{2-} buffer for HCO_3^- sustained the extracellular currents and separated the efflux of OH^- (or equivalent influx of H^+) from HCO_3^- influx (see Lucas 1983 for summary). Walker and co-workers (Walker et al. 1980; Smith and Walker 1980) suggested an alternative hypothesis: active proton pumping produced the acid band with pH sufficiently low in an unstirred layer close to the membrane to generate sufficient CO_2 to diffuse across the membrane. Using a pH microelectrode Bulychev et al. (2001b) measured pH of 5.75 within 0.1 mm from the cell wall surface in unbuffered APW of pH 6.25. Thus, pH levels might be even lower in the

unstirred layer within the cell wall, providing sufficient concentration of CO_2 to explain measured carbon fixation rates (Smith 1968; Lucas 1975a). However, at bulk medium pH 8.2, even pH microelectrodes detected the lowest pH of ~ 7 in the acid band within micrometres from the cell wall (Lucas et al. 1983). Lucas et al. (1983) also reduced the unstirred layer near the cell wall by fast flowing medium and found that carbon fixation at high pH was enhanced rather than reduced as predicted by Walker et al. (1980). Lucas and co-workers suggested that these results supported another model: cotransport of HCO_3^- with H^+ in the acid band. Lucas (1983) proposed that HCO_3^- might cotransport with $2H^+$ and compete for the same transporter with Cl^-. Such HCO_3^--mediated decrease of Cl^- influx was, indeed, observed by Spear et al. (1969). However, the HCO_3^- uptake is at least an order of magnitude greater than Cl^- uptake (Price et al. 1985).

Measuring the rate of photosynthesis as O_2 evolution, (Brechignac and Lucas 1987) found that cells pretreated at high pH exhibited higher affinity for CO_2 than cells pretreated at low pH. However, this difference disappeared if O_2 was kept below 2%. The Warburg effect (increase of photosynthesis rate by lowering O_2 concentration in the medium by inhibiting oxygenase activity in Rubisco) was only observed in the latter group of high CO_2 pretreated cells. On the other hand, cells pretreated at high pH exhibited greater O_2 evolution rates in experiments at high pH if O_2 in the medium was high. The authors suggested that O_2 is required for HCO_3^- utilisation. This is most easily explained if ATP is needed to power transport, either directly or by a chemiosmotic mechanism utilising the H-ATPase to generate $\Delta\bar{\mu}_H$ to drive the transport. The ATP is most likely to come from oxidative phosphorylation, and therefore requires O_2.

Mimura et al. (1993) demonstrated that substantial carbon fixation can be measured in perfused cells (which do not band) in media ranging from pH 5–8.5. As in intact cells, the photosynthetic ^{14}C fixation was diminished at high pH. At both pH levels the rate of carbon fixation dropped when ATP was not included in the perfusion medium or when the proton pump inhibitor sodium orthovanadate was added. On the other hand, to prevent the decrease in ATP and rise in ADP concentrations inside the cell, pyruvate kinase and phosphoenolpyruvate were included in perfusion medium in some experiments. This perfusion medium stimulated greater carbon fixation. In control experiments the cells were perfused with medium containing ^{14}C-labelled bicarbonate. These cells exhibited much greater carbon fixation rates than the cells with DIC added externally. With DIC added internally, there was only a small effect of vanadate or of depletion of ATP using glucose and hexokinase. These results indicate that the mode of inhibition is via the proton pump and transport of DIC from external medium and that chloroplasts themselves were not damaged by perfusion or affected by vanadate or medium without ATP. Thus, banding is not necessary for DIC in external medium to reach the chloroplasts, but import of both HCO_3^- and (surprisingly) CO_2 requires the working of the proton pump.

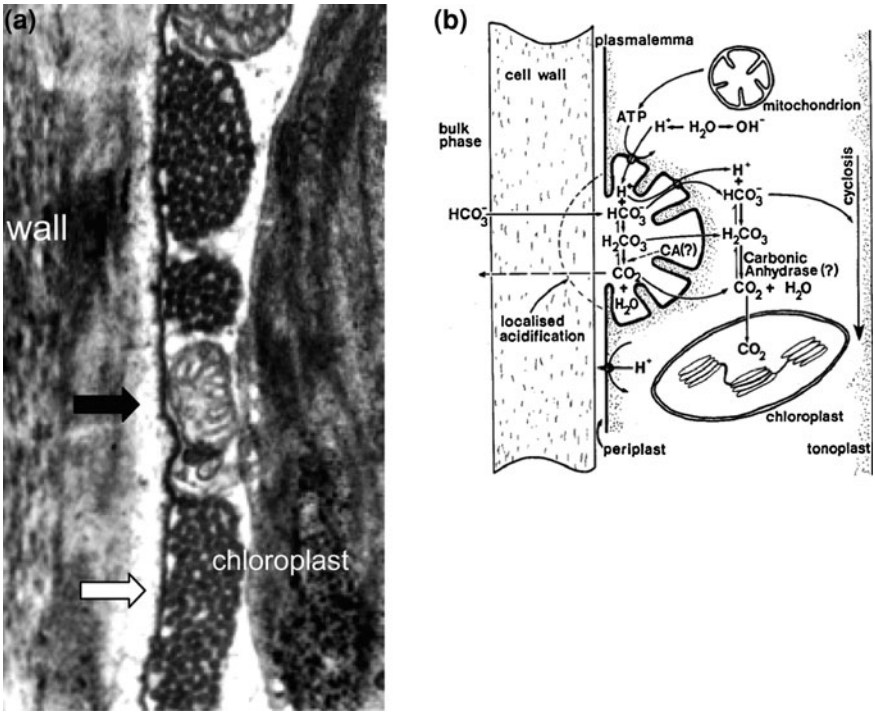

Fig. 11.4 **a** Transmission electron micrograph (×18,000) of charasomes (*white arrows*) from acid band region of *Chara corallina* cultured at pH 7.5 (from Lucas et al. (1986). *Black arrow*: mitochondrion. **b** Schematic diagram of reactions in and near charasome (from Price et al. 1985). *CA* stands for carbonic anhydrase, which is envisaged in both periplasmic space and in the cytoplasm

11.4 Unstirred Layers, Charasomes and Carbonic Anhydrase

The possibility of an unstirred layer that is not accessible to medium flow or stirring emerged with the discovery of charasomes (or plasmalemmasomes). Franceschi and Lucas (1980) described these complex plasma membrane elaborations in *C. corallina* and *Ch. braunii* and started to relate their function to transport. The name charasome became popular when none were found in *Nitella* sp. Price et al. (1985) and Lucas et al. (1986) found a relationship between the density of charasomes and the pH of the culture medium: low at pH near 6 and high at pH 7.5–9.3. More charasomes were found in the acid bands in culture media regardless of pH (see Fig. 11.4a).Price et al. (1985) also established that the pH response is due to the amount of CO_2 in the medium. If the total amount of DIC is increased at high pH, or CO_2 is bubbled through the culture, the charasome density is low despite high pH. Thus, formation of charasomes is inhibited by provision of sufficient free CO_2. Bisson et al. (1991) did not find a correlation

between density of charasomes and acid and alkaline bands in axial internodes of *Chara australis*. Schmolzer et al. (2011) explained these different results by noting that the banding patterns are less stable in the axial internodes than in the leaf internodes, where the charasomes are associated with the acid bands. Charasomes disappear after 1–3 weeks if photosynthesis is inhibited by darkness or DCMU (Bisson et al. 1991; Chau et al. 1994).

Price et al. (1985) detected carbonic anhydrase activity in cells grown in high pH medium. This enzyme catalyses the reaction between carbonic acid and $H_2O + CO_2$, the first rate-limiting step in converting CO_2 to HCO_3^-. It can be inhibited by 20 μM EZA. The rate of photosynthesis (measured by O_2 evolution) was high at low pH (high CO_2 concentration), at high pH (with high concentration of DIC or CO_2 provided by bubbling) and at high pH, when plants contained a large number of charasomes. The last group was sensitive to EZA inhibitor, suggesting that the action of carbonic anhydrase, and hence conversion between CO_2 and HCO_3^-, is important. Similar results were obtained by Shiraiwa and Kikuyama (1989).

Thus, charasomes act by increasing the membrane surface area, particularly in the acid zones, which will multiply transport activity of all kinds. They also provide regions separated from the bulk medium that can be acidified, so the cell can utilise bicarbonate ion by producing easily permeable CO_2 in the charasome or cotransporting bicarbonate ion with protons (see Fig. 11.4b). Price et al. (1985) suggested that carbonic anhydrase can be found inside the periplasm, the convoluted extracellular space within the charasomes, as well as in the cytoplasm. Shiraiwa and Kikuyama (1989) argued that it is mainly found in the cytoplasm. Ray et al. (2003) used the impermeant carbonic anhydrase inhibitor AZ to show conclusively that carbonic anhydrase in the periplasmic space, including charasomes, is important for DIC transport. These authors performed their experiments on *Chara tomentosa* from the brackish Baltic Sea.

As no charasomes were found in *Nitella* sp., they are clearly not necessary for banding or survival. However, there are no reports of *Nitella* sp. growing above pH 9.3 (Price et al. 1985), so charasomes may offer ecological advantage for *Chara* to colonise high pH environments. Further, Lucas et al. (1989) measured a comparatively high rate of photosynthesis upon transfer of low pH pretreated cells into high pH bicarbonate-rich medium before they observed full development of charasomes.

Price and Badger (1985) modelled the inhibition of banding and its effect on carbon fixation by various buffers. They concluded that the buffers penetrate into the periplasmic space and dissipate the H^+ gradient. Also, for media buffered to pH levels below 9, the H^+/OH^- channels would close. Weak bases and acids also affect banding. Bulychev et al. (2001b) observed rapid banding inhibition by 10 mM NH_4Cl, which could be partially reversed by 10 mM sodium acetate. Sodium acetate by itself stimulated band formation even at concentration of 1 mM. The authors suggested that the undissociated forms of the weak base or the weak acid penetrate the plasma membrane and alkalinise or acidify the cytoplasm, respectively. Thus more acid cytoplasm is more likely to encourage banding. Fusicoccin, which is

known to stimulate proton pumping in higher plants (Felle 1982), increased the peak profiles of the banding pattern. On the other hand, banding is suppressed by depolarisation, such as that brought on by 10 mM KCl. From the data on various states, both the pump and the H^+/OH^- channels can be inactivated by high K permeability that is induced by high external concentrations, and impairment of either or both of these systems can disrupt the banding (Beilby 1986).

11.5 Circulating Currents

When the membrane transport activity is dominated by the H^+-ATPase, it usually exhibits more negative membrane PDs, while when it is dominated by the OH^- channel it can be very conductive (see Figs. 11.2, 11.3). In the chimeric banding state, therefore, the membrane should provide spatially separated membrane regions with these different pathways, and since they are close, currents may be driven between them. Walker and Smith (1977) indeed observed small PDs in the medium near the cell and circulating currents up to 75 mA m^{-2} between acid and alkaline zones. Lucas and Nuccitelli (1980) measured somewhat larger currents with the vibrating probe. It is now thought that the source is the proton pump and the sink H^+/OH^- channels, with OH^- efflux rather than H^+ influx (Lucas 1979). The conductance of the alkaline zones was measured as 5–8 S m^{-2} with cable length of 3–5 mm, compared to conductance of the acid zones of $\sim$1 S m^{-2} with longer cable length of 10–15 mm (Ogata et al. 1983; Smith and Walker 1983). Dorn and Weisenseel (1984) followed the circulating currents around *Nitella* cells as function of cell growth. The currents appeared in cells as small as 1 mm in length, and the pattern stabilised as the cell matured. The authors suggested that the circulating currents can provide a mechanism of electrophoretic transport of ions (such as HCO_3^-) through the medium towards the cell surface.

Bulychev et al. (2003) passed current longitudinally through the cell and this led to a decrease in the number of alkaline bands. The AP disrupts the banding pattern, possibly through similar mechanism of extra current flow (see more details later). Bulychev and Krupenina (2009, 2010) found that the high conductance in the alkaline bands dropped transiently after a single AP. Beilby and Bisson (1992) did not observe this effect when the whole cell was in H^+/OH^- state, suggesting that it is the banding pattern, rather than the H^+/OH^- channels that are affected by the AP. This may also be related to the temporary cessation of streaming caused by the AP (see Sect. 11.8).

11.6 The Establishment of Banding

Several researchers have investigated the way the banding pattern develops upon onset of illumination. Since the proton pump continues to work in the dark (Mimura and Tazawa 1986), but the high pH state is inhibited, this measures the

activation of the alkaline band. Lucas (1975b) established that at a threshold light intensity of 0.9 W/m^2 only one alkaline band was activated. As the light intensity increased, more bands appeared until saturation reached near 10 W/m^2. However, as light intensity was reduced, the early appearing bands persisted at levels below the threshold intensity. When dark pretreated cells were illuminated, there was a lag period of several minutes before alkaline band activation. The lag was longer at low light intensities.

Bulychev et al. (2003) obtained a similar progression from a single band to many, by increasing light intensity from 0.4 to 430 μmol m^{-1} s^{-2} PAR (The intensities are difficult to compare, as the wavelength spectrum of Lucas's source is not known. However, for typical light sources, from sunlight to fluorescent lights, 10 W/m^2 is equivalent to between 45 and 50 μmol m^{-1} s^{-2}). The authors confirmed existence of hysteresis: alkaline bands form above threshold intensity when illumination is increased, but persist at dimmer intensities when light is decreased. Lengthwise scans with a pH microprobe that travelled around the cell perimeter indicated that at low light intensities, the periodic closed band structure emerges from irregular spots and unclosed bands. Under these conditions, the evolution of the final regular pattern involves deletions, fusion or widening of pH peaks. Upon illumination with high intensity light the evolution to a regular pattern of full bands is too fast to resolve with pH scans. Bulychev et al. (2001b) experimented with illumination of a small (4 mm) patch of the cell. In this case, a doublet of alkaline bands formed at the edges of the lit area while the rest of the pattern flattened out. When the whole cell was again illuminated, one of the doublet bands disappeared to conform to the pattern of the whole cell. Similar findings were reported by Fisahn and Lucas (1995), who restricted illumination to an acid band and observed evolution of one or more new alkaline bands.

To test the hypothesis that the role of light is photosynthetic, parameters associated with photosynthesis in acid and alkaline bands were measured (Plieth et al. 1994; Bulychev et al. 2001a; Bulychev and Vredenberg 2003). The pulse amplitude modulation (PAM) microfluorimetry technique was used (see Bulychev et al. 2005 for details).

The fluorescence yield F was low in the acid bands and high in alkaline bands. The saturation fluorescence yield, F'$_m$, was also lower in acid bands. The quantum yield Y', on the other hand, reached maximum in the acid band and minimum in alkaline band. Later Bulychev et al. (2005) found that the differences in these parameters were maximised at some light intensities, merging at low and high light intensities. While high Y' suggested high photosynthetic electron transport rate, further information was needed to distinguish between assimilatory (CO_2 fixing) and non-assimilatory electron flows. Bulychev et al. (2001a) also showed that oxygen evolution is greater in the acid bands, confirming these to be the primary locations of carbon fixation. The authors speculate that lack of CO_2 in the alkaline bands favours the radiative losses of the absorbed photons.

As buffers reduce pH banding, Bulychev and Vredenberg (2003) monitored Y' in media buffered by 10 mM Hepes to pH 6.8 and 7.6. They found that while the banding diminished, spatial differences were still resolvable in quantum yield,

especially at lower pH. Upon exposing dark-adapted cell to light, Y' decreased in the alkaline zones within 5–15 min prior to, or synchronously, with the rise of pH. In the acid zones, Y' increased after initial decline. If an alkaline zone was exposed to spot illumination, the photosynthetic parameters changed to those typical of an acid zone. The authors speculated that the events at the chloroplasts might be the cause, rather than the consequence, of the pH banding. They also concluded that banding of the photosynthetic parameters, like the pH banding pattern, is dynamic and not predetermined by structural features.

11.7 Action Potentials and Banding

Bulychev et al. (2004) made an interesting discovery that a single AP transiently suppresses the pH banding system for about 20 min. Following an AP, the pH in the alkaline band dropped by up to 3 units, while pH in the acid band increased slightly ($\sim$0.1 pH unit). The pH measurements suggest transient inhibition of the proton pump as well as closure of H^+/OH^- channels. Maximum fluorescence yield F'_m and quantum yield Y' dropped in the alkaline band, but not in the acid band. The drop in F'_m indicates that non-photochemical quenching (NPQ) of chlorophyll excitation and thermal dissipation of light energy were enhanced. Bulychev et al. (2005) hypothesise that AP response in the alkaline band might be determined by a transient build up of ΔpH at the thylakoid membranes in the chloroplasts. This event is in turn initiated by the increase of Ca^{2+} concentration at the time of AP (Beilby 2007). The increase of Ca^{2+} concentration was also thought to be responsible for the transient pump inhibition (Smith and Beilby 1983). This hypothesis is strengthened by more information available about the proton pump. Ca^{2+} binds to divalent cation-binding site in 14-3-3 protein, altering the interaction of this protein and the proton pump (Sehnke et al. 2002). Thus, while the pH banding transiently smooths out after an AP, the photosynthetic heterogeneity intensifies. This effect seems surprising, as in dark adaptation, both patterns disappear. However, the mechanisms involved are quite different. This interplay between electrical signalling at the plasma membrane and photosynthetic parameters provides a promising subject for further study. An alternative hypothesis, however, is that the effect of the AP is due to its transient inhibition of streaming, which has been shown to be critical for the banding phenomenon (see below).

11.8 The Role of Cytoplasmic Streaming

Lucas and Dainty (1977) found that inhibiting the cytoplasmic streaming by cytochalasin B suppressed the banding pattern, transforming the OH^- efflux to many localised disc-shaped sites. Yao et al. (1992) observed that as the streaming

rate in *C. corallina* was reduced over time by submaximal concentrations of cytochalasin B, the width of alkaline bands became narrower. The distance between the bands decreased, resulting in more bands per length of the cell. The salt-tolerant *Chara longifolia* exhibited similar banding pattern as *C. corallina* in freshwater media, but in saline native medium the bands became narrower and more numerous, with alkaline bands covering more cell surface. The effect was stronger than could be explained by slightly slower cytoplasmic streaming ($\sim$18%), and may be related to the higher H-pump activity in saline-cultured cells. Babourina et al. (2004) used the ion-sensitive vibrating electrode system, MIFE, (Newman 2001) to measure fluxes of H^+, Ca^{2+} and K^+ adjacent to *C. australis* branchlets with basipetal (toward the node) and acropetal (toward branch tip) streaming direction. The pH band amplitude (differences in pH) was greater on acropetal side. Streaming inhibition by cytochalasin D disrupted banding within about two hours. K^+ and Ca^{2+} fluxes were not closely correlated to the pH bands, but showed some correlation to each other. After streaming cessation, both these cations tended to efflux. Dodonova and Bulychev (2010) measured the influence of local illumination (2 mm spot) on downstream and upstream H^+/OH^- transport in a region located on light-shade boundary. Within minutes of illumination, an alkaline band, with an increase in NPQ, was formed on the downstream side. There was an optimal low illumination at which the band formation started and then expanded. The authors suggest that the illuminated chloroplasts produce a mediator substance that is released into the cytoplasm. The mediator is taken by the streaming cytoplasm into the shaded region, where it causes increase in NPQ in the chloroplasts and opening of H^+/OH^- channels in the plasma membrane. Under some lighting regimes, alkaline zone developed without the NPQ increase. Application of cytochalasin B inhibited both the NPQ increase and alkaline band formation. The identity of the mediator is not known. Lucas and Shimmen (1981) centrifuged the bulk of the cell cytoplasm to one side of the cell and then prevented the larger organelles from redistributing into the other half of the cell by weakly applied silk thread ligature. Banding in that side of the cell disappeared and only recovered, when the ligature was removed. Further, perfused cells with the cytoplasm replaced by artificial media, do not band. Thus, the mediator might be a cytoplasmic organelle.

11.9 Summary and Model

How can these various aspects of the banding phenomenon be integrated into a model explaining how the separation of the acid and alkaline bands is initiated and maintained? We summarise our minimal model in Fig. 11.5. The H^+-pumping ATPases and other transport processes occurring with them acidify the exterior and generate the acid band. Simultaneously, they alkalinize the cytoplasm. These processes and their relation to photosynthesis are elaborated in Fig. 11.6, which shows two different models for carbon transport processes occurring in the acid

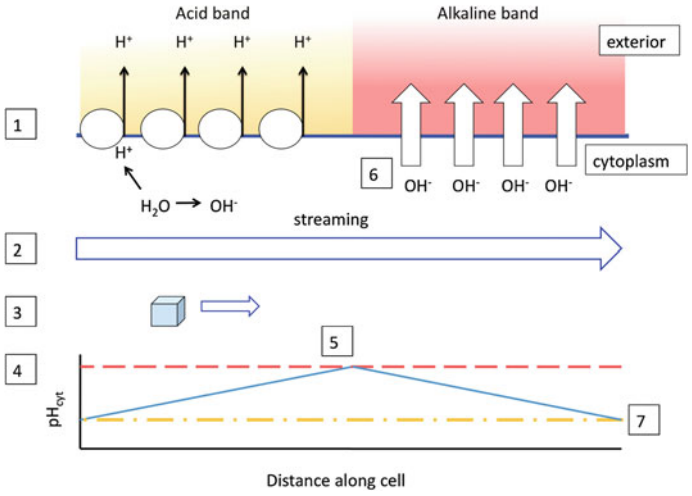

Fig. 11.5 Underlying the acid band are active H^+-pumping ATPases and other transport processes that alkalinize the cytoplasm (see Fig. 11.6 for more details). [*2*] Cytoplasmic streaming carries a voxel of water [*3*] along the cell. [*4*] The longer it stays under the acid band, and therefore the further it moves downstream, the more alkaline it becomes. [*5*] Once it reaches a critical pH level, it signals to the membrane to alter its transport properties in such a way that it allows passive efflux of OH^- [*6*], thus reducing the pH of the cytoplasm. Slower streaming or a higher pumping rate will cause this value to be reached in a shorter distance, and the acid bands will be narrower. Once the pH has been reduced to a lower level [*7*], the plasma membrane is signalled to restore its normal H^+- pumping mode

band. In one (left hand side of the figure) high H^+ in the acid band due to extrusion by the ATPase results in the protonation of bicarbonate. The small, relatively lipophilic H_2CO_3 or CO_2 molecules rapidly move by passive simple diffusion into the cytoplasm and thence to the chloroplast, where they are fixed into carbohydrates and removed from influencing cytoplasmic pH. The net result of this transport is the production of hydroxyls from water, thus increasing cytoplasmic pH. Alternatively, the proton may be returned to the cytoplasm via a H: bicarbonate symporter (right side of figure), which returns a proton to the cytoplasm, neutralising the effect of the H-ATPase. However, a weak base, HCO_3^-, is introduced to the cytoplasm. When CO_2 is extracted for transport to the chloroplast, OH^- is left behind in the cytoplasm. Therefore, both postulated mechanisms have the same effect of introducing hydroxyls into the cytoplasm when carbon dioxide is fixed.

Cytoplasmic streaming carries the cytoplasm along the cell (Fig. 11.5). The longer it stays under the acid band, and therefore the further it moves downstream, the more alkaline it becomes. Once a region of cytoplasm reaches a critical pH level, it signals to the membrane, either directly or via some unidentified second messenger, to alter its transport properties in such a way that it allows passive efflux of OH^-, thus reducing the pH of the cytoplasm and raising the pH in the external medium, generating the alkaline band. Once the pH has been reduced to a

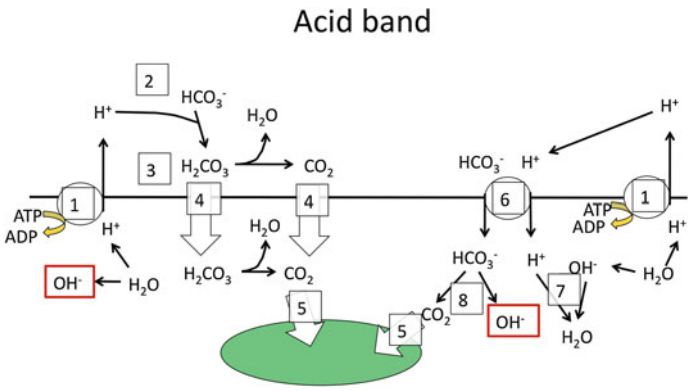

Fig. 11.6 Acid band. [*1*] Medium acidification is due to the active H^+-pumping ATPases. The relationship between carbon assimilation and medium acidification could be due to a number of factors. [*2*] The availability of H^+ in the acid band could result in the protonation of bicarbonate. [*3*] The small, relatively lipophilic H_2CO_3 or CO_2 molecules could rapidly move by passive simple or facilitated diffusion into the cytoplasm [*4*], and diffuse to the chloroplast [*5*], where they are rapidly fixed into carbohydrates and removed from influencing cytoplasmic pH. The net result of this transport is the production of hydroxyl from water, thus increasing pH. Alternatively, the proton may be returned to the cytoplasm via a H: bicarbonate symporter (or the equivalent OH: bicarbonate antiporter) [*6*], which returns a proton to (or removes a hydroxyl from) the cytoplasm, neutralising the effect of the H-ATPase [*7*]. However, a weak base, HCO_3^-, is introduced to the cytoplasm. When CO_2 is extracted for transport to the chloroplast, OH^- is left behind in the cytoplasm. Therefore, both postulated mechanisms have the same effect of introducing hydroxyl into the cytoplasm as DIC is taken up

lower level, the plasma membrane is signalled to restore its normal H^+- pumping mode. The nature of this signalling is not clear. It is related to external pH, however, since imposing high external pH can cause the entire cell to act as an alkaline band. Whether this is due to signalling from external pH, or from alkalinisation of cytoplasmic pH is not clear. It does, however, suggest a mechanism of positive feedback in generating the high OH^- conductance that could contribute to the stability of the banding pattern. If the internal pH begins to fall, influx of OH^- from the external medium would restore the high pH and maintain the H^+/OH^- state. $CaCO_3$ precipitated in the alkaline band can act as a buffer to re-alkalinize the medium if it should dissipate.

This model accommodates a number of the observations described above. Inhibiting the ATPase or inhibiting photosynthesis will decrease the rate of alkalinisation of the cytoplasm, and alkaline bands will not be generated. Slower streaming or a higher pumping rate will cause this value to be reached in a shorter distance, and the acid bands will be narrower. Inhibiting streaming will disrupt the orderly process entirely, resulting in the patchy membranes seen by Lucas and Dainty (1977). It is the simplest explanation for the fact that immersing a normal cell in medium with a pH similar to that found in alkaline bands results in the whole membrane taking on the characteristics of the alkaline band membrane (Bisson and Walker 1980).

What about the evidence for an organelle-situated intermediate (e.g., Lucas and Shimmin 1981)? This model does not rule out an intermediate responding to the pH to control H^+/OH^- permeability. However, perfusion could affect the change in cytoplasmic pH by increasing the volume available to dilute out the photosynthetically derived OH^-, which in the intact cell is limited to the width of the cytoplasmic layer (about 10 μm) but in the perfused cell can range across the diameter of the cell (typically about 0.5 mm). Moreover, since the perfusion medium is typically buffered, this would prevent the increase in pH needed to trigger the H^+/OH^- state. Similarly, the centrifugation studies result in a thinning of the cytoplasm at the upper end of the cell, so that the tonoplast lies closely against the non-streaming chloroplasts. Streaming is disrupted, and cannot move a large volume of cytoplasm. Restoration of streaming brings the organelles back to the upper portion of the cell, but the streaming itself is required for the banding phenomenon.

What about the different photosynthetic rates in the different bands? The ability of the cell to accumulate CO_2 from HCO_3^--containing medium, whether because too little CO_2 is available in a medium at high pH, or because $\Delta\bar{\mu}_H$ is too close to zero and cannot power a symport, would be sufficient to decrease O evolution and increase NPQ in the alkaline band.

The only evidence that counters this hypothesis is the evidence from Bulychev et al. (2003) that NH_4Cl, which alkalinises the cytoplasm, prevents banding, and that sodium acetate stimulates it. This hypothesis predicts the opposite, that alkalinisation should stimulate the formation of alkaline bands. Those results, however, are at odds with the data of Bisson and Walker (1981) (See Fig. 11.2), who showed when cells were preincubated in medium at pH 4.5, it was more difficult to convert the cells to the H^+/OH^- state, requiring a higher external pH. Similar results (Bisson, unpublished) were obtained when the cytoplasm was acidified by incubation in butyric acid. If conversion of the cell to the H^+/OH^- state is a good model for initiation of an alkaline band, this directly contradicts the results of Bulychev et al. (2003). More directly comparable experiments need to be done to resolve this contradiction.

Many questions still remain about this process. What is the nature of the OH^- transport in the alkaline band? Are there channels or some other means of facilitated transport? What is the mechanism that controls and coordinates their activation and inhibition? What signalling intermediates are required for the change?

11.10 Implications for Measurement of Membrane Properties

The chimeric nature of the membrane has been ignored in many descriptions of the electrophysiology of the Charophyte membrane. What are the effects of this phenomenon on overall membrane properties? Neither the membrane potential nor conductance is constant along the length of the membrane. The membrane potential measured will be less negative than the potential under the acid band and more negative than that under the alkaline band. When a single electrode is used to

measure membrane potential, the measured potential will be a complicated function of the relative areas of the acid and alkaline bands, as well as their distances from the electrode. The conductance will also not be constant along the length of the cell, and measuring the overall conductance will be subject to similar problems. The length constant, a measure of how much rapidly injected current propagates along the membrane as opposed to dissipating to the outside, will not be constant, but will be shorter in alkaline bands and longer in acid bands, making cable correction much more complicated.

What can be done to reduce these difficulties? One possibility is to eliminate the alkaline bands. One simple way of doing this is to do experiments in the dark. Rapid inhibition of alkaline band formation may be the underlying cause of the rapid, transient hyperpolarization often reported on the light/dark transition (Bisson 1986b). Alternatively, one can inhibit photosynthesis by DCMU or something similar. These solutions are less than ideal, because the membrane properties one wish to study may be altered by interfering with photosynthesis. Alternatively, since much of the cytoplasmic alkalinisation associated with the acid band is due to carbon assimilation, one could try running the experiments in an inorganic carbon-free state. Unfortunately, since inorganic carbon is ubiquitous—from the atmosphere, from metabolic production, and from dissolving of the deposited carbonate—and since many common materials such as polyethylene are permeable to CO_2, this is easier said than done.

One can also try to suppress the banding by buffering the medium of the cell. However, the efficacy of such buffering should be checked. Even 5 mM buffer may not be sufficient, given the large H^+/OH^- fluxes occurring. Moreover, the buffer must penetrate the periplasmic space of the charasomes in order to be effective.

Alternatively, one can use electrophysiological techniques themselves to minimise this problem. In voltage clamping and conductance determination methods, current can be injected by a wire inserted into the length of the cell rather from a point source. One can also measure PD over a large area of the cell by the "cell anaesthesia" method (Shimmen et al. 1976), although this is an indirect method, it carries with it some uncertainties.

However, reviews by Beilby (1989, 1990) show similar results obtained using a variety of conditions, at least if the medium is well buffered (5 mM buffer), and the cells are relatively short, suggesting that under carefully chosen conditions these difficulties may not alter the measured properties significantly.

References

Al Khazaaly S, Beilby MJ (2012) Zinc ion blocks H^+/OH^- channels in *Chara australis*. Plant Cell Environ (published on line)

Amtmann A, Sanders D (1999) Mechanism of Na^+ uptake by plant cells. Adv Bot Res 29:75–112

Arens K (1939) Physiologische multipolaritat der zelle von *Nitella* der photosynthese. Protoplasma 33:295–300

Babourina O, Voltchanskii K, Newman I (2004) Ion flux interaction with cytoplasmic streaming in branchlets of *Chara australis*. J Exp Bot 55:2505–2512

Beilby MJ, Al Khazaaly S (2009) The role of H^+/OH^- channels in salt stress response of *Chara australis*. J Membr Biol 230:21–34

Beilby MJ, Mimura T, Shimmen T (1993) The proton pump, high pH channels, and excitation: voltage clamp studies of intact and perfused cells of *Nitellopsis obtusa*. Protoplasma 175:144–152

Beilby MJ, Walker NA (1996) Modelling the current-voltage characteristics of Chara membranes. I. the effect of ATP and zero turgor. J Membr Biol 149:89–101

Beilby MJ (1984) Current–voltage characteristics of the proton pump at *Chara* plasmalemma: I. pH dependence. J Membr Biol 81:113–125

Beilby MJ (1986) Potassium channels and different states of *Chara* plasmalemma. J Membr Biol 89:241–249

Beilby MJ (1989) Electrophysiology of giant algal cells. In: Fleischer S, Fleischer B (eds) Methods in enzymology, vol 174. Academic Press, San Diego, pp 403–443

Beilby MJ (1990) Current-voltage curves for plant membrane studies: a critical analysis of the method. J Exp Bot 41:165–182

Beilby MJ (2007) Action potential in charophytes. In: Jeon KW (ed) International review of cytology, vol 257. Elsevier Inc. San Diego, California, pp 43–82

Beilby MJ, Bisson MA (1992) *Chara* plasmalemma at high pH: voltage dependence of the conductance at rest and during excitation. J Membr Biol 125:25–39

Beilby MJ, Shepherd VA (1989) Cytoplasm-enriched fragments of *Chara*: structure and electrophysiology. Protoplasma 148:150–163

Bisson MA (1984) Calcium effects on electrogenic pump and passive permeability of the plasma membrane of *Chara corallina*. J Membr Biol 81:59–67

Bisson MA (1986a) Inhibitors of proton pumping. Effect on passive proton transport. Plant Physiol 81:55–59

Bisson MA (1986b) The effect of darkness on active and passive transport in *Chara corallina*. J Exp Bot 37:8–21

Bisson MA, Siegel A, Chan R, Gelsomino SA, Herdic SL (1991) Distribution of charasomes in *Chara*—banding-pattern and effect of photosynthetic inhibitors. Aust J Plant Physiol 18:81–93

Bisson MA, Walker NA (1980) The *Chara* plasmalemma at high pH. Electrical measurements show rapid specific passive uniport of H^+ or OH^-. J Membr Biol 56:1–7

Bisson MA, Walker NA (1981) The hyperpolarisation of the *Chara* membrane at high pH: effects of external potassium, internal pH, and DCCD. J Exp Bot 32:951–971

Bisson MA, Walker NA (1982) Control of passive permeability in the *Chara plasmalemma*. J Exp Bot 33:520–532

Brechignac F, Lucas WJ (1987) Photorespiration and Internal CO_2 accumulation in *Chara corallina* as inferred from the influence of DIC and O_2 on photosynthesis. Plant Physiol 83:163–169

Bulychev AA, Cherkashin AA, Rubin AB, Vredenberg WJ, Zykov VS, Muller SC (2001a) Comparative study on photosynthetic activity of chloroplasts in acid and alkaline zones of *Chara corallina*. Bioelectrochemistry 53:225–232

Bulychev AA, Kamzolkina NA, Luengviriya J, Rubin AB, Muller SC (2004) Effect of a single excitation stimulus on photosynthetic activity and light-dependent pH banding in *Chara* cells. J Membr Biol 202:11–19

Bulychev AA, Kamzolkina NA, Rubin AB (2005) Effect of plasmalemma electrical excitation on photosystem II activity and nonphotochemical quenching in chloroplasts of cell domains in *Chara corallina*. Dokl Biochem Biophys 401:127–130

Bulychev AA, Krupenina NA (2009) Transient removal of alkaline zones after excitation of *Chara* cells is associated with inactivation of high conductance in the plasmalemma. Plant Signalling Behav 4:727–734

Bulychev AA, Krupenina NA (2010) Inactivation of plasmalemma conductance in alkaline zones of *Chara corallina* after generation of action potential. Biochemistry (Moscow) supplement series A. Membr Cell Biol 4:232–239

Bulychev AA, Polezhaev AA, Zykov SV, Pljusnina TYu, Riznichenko GYu, Rubin AB, Jantos W, Zykov VS, Muller SC (2001b) Light-triggered pH banding profile in *Chara* cells revealed with a scanning pH microprobe and its relation to self-organisation phenomena. J Theor Biol 212:275–294

Bulychev AA, Vredenberg W (2003) Spatio-temporal patterns of photosystem II activity and plasma membrane proton flows in *Chara corallina* cells exposed to overall and local illumination. Planta 218:143–151

Bulychev AA, Zykov SV, Rubin AB, Muller SC (2003) Transitions from alkaline spots to regular bands during pH pattern formation at the plasmalemma of *Chara* cells. Eur Biophys J 32:144–153

Chau R, Bisson MA, Siegel A, Elkin G, Klim P, Strabinger RM (1994) Distribution of charasomes in *Chara*—reestablishment and loss in darkness and correlation with banding and inorganic carbon uptake. Aust J Plant Physiol 21:113–123

Coster HGL, Smith JR (1977) Low-frequency impedance of *Chara corallina*: simultaneous measurements of the separate plasmalemma and tonoplast capacitance and conductance. Aust J Plant Physiol 4:667–674

Dodonova SO, Bulychev AA (2011) Cyclosis-related asymmetry of chloroplast-plasma membrane interactions at the margins of illuminated area in *Chara corallina* cells. Protoplasma 248:737–749

Dorn A, Weisenseel MH (1984) Growth and the current pattern around internodal cells of *Nitella flexilis L.* J Exp Bot 35:373–383

Eremin A, Bulychev AA, Krupenina NA, Mair T, Hauser MJB, Stannarius R, Muller SC, Rubin AB (2007) Excitation-induced dynamics of external pH pattern in *Chara corallina* cells and its dependence on external calcium concentration. Photochem Photobiol Sci 6:103–109

Feijo J, Sainhas J, Hackett GR, Kinkel JG, Hepler PK (1999) Growing pollen tubes possess a constitutive alkaline band in the clear zone and a growth-dependent acidic tip. J Cell Biol 144:483–496

Felle HH (1982) Effects of fusicoccin upon membrane potential, resistance and current-voltage characteristics in root hairs of *Sinapis alba*. Plant Sci Lett 25:219–225

Findlay GP, Hope AB (1964) Ionic relations of cells of *Chara australis*: VII. The separate electrical characteristics of the plasmalemma and tonoplast. Aust J Biol Sci 17:62–77

Fisahn J, Lucas WJ (1995) Spatial organisation of transport domains and subdomains formation in the plasma membrane of *Chara corallina*. J Membr Biol 147:275–281

Franceschi VR, Lucas WJ (1980) Structure and possible function(s) of charasomes; complex plasmalemma-cell wall elaborations present in some characeaen species. Protoplasma 104:253–271

Gutknecht J, Bisson MA, Tosteson DC (1977) Diffusion of carbon dioxide across lipid bilayer membranes. J Gen Physiol 69:779–794

Hansen U-P, Gradmann D, Sanders D, Slayman CL (1981) Interpretation of current-voltage relationship for "active" ion transport systems: I. Steady-state reaction-kinetic analysis of class I mechanisms. J Membr Biol 63:165–190

Hope AB, Walker NA (1975) The physiology of giant algal cells. Cambridge University Press, London

Karol KG, McCourt RM, Cimino MT, Delwiche CF (2001) The closest living relatives of land plants. Science 294:2351–2353

Kiegle EA, Bisson MA (1996) Plasma membrane Na^+ transport in a salt-tolerant charophyte. Plant Physiol 111:1191–1197

Kitasato H (1968) The influence of H^+ on the membrane potential and ion fluxes of *Nitella*. J Gen Physiol 52:60–87

Krupenina NA, Bulychev AA, Roelfsema MR, Screiber U (2008) Action potential in *Chara* cells intensifies spatial patterns of photosynthetic electron flow and non-photochemical quenching in parallel with inhibition of pH banding. Photochem Photobiol Sci 7:681–688

Lucas WJ (1975a) Photosynthetic fixation of ^{14}Carbon by internodal cells of *Chara corallina*. J Exp Bot 26:331–346

Lucas WJ (1975b) The influence of light intensity on the activation and operation of the hydroxyl efflux system of *Chara corallina*. J Exp Bot 26:347–360

Lucas WJ (1979) Alkaline band formation in *Chara corallina*: due to OH^- efflux or H^+ influx? Plant Physiol 63:248–254

Lucas WJ (1983) Photosynthetic assimilation of exogenous HCO_3^- by aquatic plants. Annu Rev Plant Physiol 34:71–104

Lucas WJ, Brechignac F, Mimura T, Oross JW (1989) Charasomes are not essential for photosynthetic utilization of exogenous HCO_3^- in *Chara corallina*. Protoplasma 151:106–114

Lucas WJ, Dainty J (1977) Spatial distribution of functional OH^- carriers along a characean internodal cell: determined by the effect of cytochalasin B on $H^{14}CO_3^-$ assimilation. J Membr Biol 32:75–92

Lucas WJ, Keifer DW, Pescareta TC (1986) Influence of culture medium pH on charasome development and chloride transport in *Chara corallina*. Protoplasma 130:5–11

Lucas WJ, Keifer DW, Sanders D (1983) Bicarbonate transport in *Chara corallina*: evidence for cotransport of HCO_3^- with H^+. J Membr Biol 73:263–274

Lucas WJ, Nuccitelli R (1980) HCO_3^- and OH^- transport across the plasmalemma of *Chara corallina*: spatial resolution obtained using extracellular vibrating probe. Planta 150:120–131

Lucas WJ, Shimmen T (1981) Intracellular perfusion and cell centrifugation studies on plasmalemma transport processes in *Chara corallina*. J Membr Biol 58:227–237

Lucas WJ, Smith FA (1973) The formation of alkaline and acid regions at the surface of *Chara corallina* cells. J Exp Bot 24:1–14

McConnaughey TA (1991) Calcification in *Chara corallina*: CO_2 hydroxylation generates protons for bicarbonate assimilation. Limnol Oceanogr 36:619–628

McConnaughey TA, Falk RH (1991) Calcium- proton exchange during algal calcification. Biol Bull 180:185–195

McCourt RM, Delwiche CF, Karol KG (2004) Charophyte algae and land plant origins. Trends Ecol Evol 19:661–666

Mimura T, Muller R, Kaiser WM, Shimmen T, Dietz K-J (1993) ATP-dependent carbon transport in perfused *Chara* cells. Plant Cell Environ 16:653–661

Mimura T, Tazawa M (1986) Light-induced membrane hyperpolarization and adenine nucleotide levels in perfused characean cells. Plant Cell Physiol 27:319–330

Newman I (2001) Ion transport in roots: measurement of fluxes using ion-selective microelectrodes to characterise transporter function. Plant Cell Environ 24:1–14

Ogata K, Chilcott TC, Coster HGL (1983) Spatial variation of the electrical properties of *Chara australis*. I. External potentials and membrane conductance. Aust J Plant Physiol 10:339–351

Plieth C, Tabrizi H, Hansen U-P (1994) Relationship between banding and photosynthetic activity in *Chara corallina* as studied by the spatially different induction curves of chlorophyll fluorescence observed by an image analysis system. Physiol Plant 91:205–211

Price DP, Badger MR (2002) Advances in understanding how aquatic photosynthetic organisms utilize sources of dissolved inorganic carbon for CO_2 fixation. Funct Plant Biol 29:117–121

Price GD, Badger MR (1985) Inhibition by proton buffers of photosynthetic utilization of bicarbonate in *Chara corallina*. Aust J Plant Physiol 12:257–267

Price GD, Badger MR, Bassett ME, Whitecross MI (1985) Involvement of plasmalemmasomes and carbonic anhydrase in photosynthetic utilisation of bicarbonate in *Chara corallina*. Aust J Plant Physiol 12:242–256

Prins HBA, Snel JFH, Helder RJ, Zanstra PE (1980) Photosynthetic HCO3$^-$ utilization and OH^- excretion in aquatic angiosperms. Plant Physiol 66:818–822

Raven JA (1991) Terrestrial rhizophytes and H^+ currents circulating over at least a millimeter: an obligate relationship? New Phytol 117:177–185

Ray SM, Klenell M, Choo K-S, Pedersen M, Snoeijs P (2003) Carbon acquisition mechanisms in *Chara tomentosa*. Aquat Bot 76:141–154

Reid RJ, Smith FA (1992) Measurement of calcium fluxes in plants using ^{45}Ca. Planta 186:558–566

Schmolzer P, Hoftberger M, Foissner I (2011) Plasma membrane domains participate in pH-banding of *Chara* internodal cells. Plant and cell physiol 52:1274–1288

Sehnke PC, DeLille JM, Ferl RJ (2002) Consummating signal transduction: the role of 14-3-3 proteins in the completion of signal induced transitions in protein activity. Plant Cell 14:S339–S354

Shimmen T, Kikuyama M, Tazawa M (1976) Demonstration of two stable potential states of plasmalemma of *Chara* without tonoplast. J Membr Biol 30:249–270

Shimmen T, Tazawa M (1977) Control of membrane potential and excitability of *Chara* cells with ATP and Mg^{2+}. J Membr Biol 37:167–192

Shiraiwa Y, Kikuyama M (1989) Role of carbonic anhydrase and identification of the active species of inorganic carbon utilised for photosynthesis in *Chara corallina*. Plant Cell Physiol 30:581–587

Simons R (1979) Strong electric field effects on transfer between membrane-bound amines and water. Nature 280:824–826

Smith FA (1968) Rates of photosynthesis in characeaen cells: II. Photosynthetic $^{14}CO_2$ fixation and ^{14}C-bicarbonate uptake by characean cells. J Exp Bot 19:207–217

Smith FA, Walker NA (1980) Photosynthesis by aquatic plants: effect of unstirred layers in relation to assimilation of CO_2 and HCO_3^- and to carbon isotopic discrimination. New Phytol 86:245–259

Smith JR (1984) The electrical properties of plant cell membranes. II. Distortion of non-linear current-voltage characteristics induced by the cable properties of *Chara*. Aust J Plant Physiol 11:211–224

Smith JR, Beilby MJ (1983) Inhibition of electrogenic transport associated with the action potential in Chara. J Membr Biol 71:131–140

Smith JR, Walker NA (1983) Membrane conductance of *Chara* measured in the acid and basic zones. J Membr Biol 73:193–202

Spanswick RM (1972) Evidence for an electrogenic ion pump in *Nitella translucens*: I. The effects of pH, K^+, Na^+, light and temperature on the membrane potential and resistance. Biochim Biophys Acta 288:73–89

Spear DG, Barr JK, Barr CE (1969) Localization of hydrogen ion and chloride ion fluxes in Nitella. J Gen Physiol 54:397–414

Sze H, Li X, Palmgren MG (1999) Energization of plant cell membranes by H^+—pumping ATPases: regulation and biosynthesis. Plant Cell 11:677–689

Takeshige K, Shimmen T, Tazawa M (1986) Quantitative analysis of ATP-dependent H^+ efflux and pump current driven by an electrogenic pump in *Nitellopsis obtusa*. Plant Cell Physiology 27:337–348

Tazawa M (1964) Studies on *Nitella* having artificial cell sap. I Replacement of the cell sap with artificial solutions. Plant Cell Physiol 5:33–43

Tazawa M, Kikuyama M, Shimmen T (1976) Electric characteristics and cytoplasmic streaming of characeae cells lacking tonoplast. Cell Struct Funct 1:165–175

Toko K, Nosaka M, Fujiyoshi T, Yamafuji K, Ogata K (1988) Periodic band pattern as a dissipative structure in ion transport system with cylindrical shape. Bull Math Biol 50:255–288

Walker NA (1955) Microelectrode experiments on *Nitella*. Aust J Biol Sci 8:476–489

Walker NA, Smith FA (1977) Circulating electric currents between acid and alkaline zones associated with HCO_3^- assimilation in *Chara*. J Exp Bot 28:1190–1206

Walker NA, Smith FA, Cathers IR (1980) Bicarbonate assimilation by freshwater charophytes and higher plants: I. membrane transport of bicarbonate ions. J Membr Biol 57:51–58

Whittington J, Bisson MA (1994) Na^+ fluxes in *Chara* under salt stress. J Exp Bot 45:657–665
Williamson RE (1975) Cytoplasmic streaming in *Chara*: a cell model activated by ATP and inhibited by cytochalasin B. J Cell Sci 17:655–668
Yao X, Bisson MA, Brzezicki LJ (1992) ATP-driven proton pumping in two species of *Chara* differing in their salt tolerance. Plant Cell Environ 15:199–210

Chapter 12
Membrane Excitation and Cytoplasmic Streaming as Modulators of Photosynthesis and Proton Flows in Characean Cells

A. A. Bulychev

Abstract Internodal cells of *Chara corallina* represent a unique model system to study interactions between photosynthesis, membrane excitation, and cytoplasmic streaming, as well as the role of these processes in generation and regulation of functional patterns in green cells and tissues. It is established that the inflow of cytoplasm from darkened cell parts promotes photosynthetic activity of chloroplasts residing at intermediate irradiance, whereas the arrival of cytoplasm from illuminated regions suppresses this activity and enhances nonphotochemical quenching. The vectorial movement of the "irradiated" cytoplasm induces functional asymmetry around the light spot (pattern formation) both in the chloroplast layer and in the plasma membrane. The messenger transported between illuminated and shaded cell parts was found to move at the velocity of cytoplasmic streaming. The effects of membrane excitation (action potential) on photosynthesis and membrane H^+ transport are area specific; they are mediated by different mechanisms under physiological conditions and in the presence of some redox-cycling compounds. The influence of action potential on chlorophyll fluorescence under spot illumination appears to involve the activation of Ca^{2+}-mediated pathways and the suppression of metabolite exchange between darkened and illuminated cell parts due to the stoppage of cyclosis. The cytoplasmic flow from darkened to illuminated cell parts seems to enhance interactions between respiratory and light-dependent metabolism, which promotes photosynthesis and protects chloroplasts from photooxidative damage under excess light.

A. A. Bulychev (✉)
Department of Biophysics, Biology, Moscow State University,
Moscow 119991, Russia
e-mail: bulychev@biophys.msu.ru

A. G. Volkov (ed.), *Plant Electrophysiology*,
DOI: 10.1007/978-3-642-29119-7_12,

Abbreviations

AOI	area of inspection where external pH and chlorophyll fluorescence are measured in *Chara* internodal cell;
AP	action potential;
CB	cytochalasin B;
DTT	dithiothreitol;
MV	methyl viologen;
NPQ	nonphotochemical quenching;
pH_c	cytosolic pH;
pH_o	pH near the cell surface in the outer medium;
PM	plasma membrane;
PFD	photon flux density;
PSI and PSII	photosystems I and II;
ROS	reactive oxygen species;
$\Delta F/F_m'$	effective quantum yield of electron transport in PSII

12.1 Introduction

The cells and tissues of green plants can undergo reversible transitions between spatially uniform and patterned distribution of photosynthetic activity upon illumination and darkening. When the dark-adapted leaf is exposed to light, the initial homogeneous images of chlorophyll fluorescence are replaced with the mosaic of patches showing damped oscillations (Siebke and Weis 1995; Schurr et al. 2006; Baker 2008). The origin of pattern emergence in the seemingly uniform system is still far from being clarified. The spatial distribution of photosynthetic activity is tightly related to the formation of nonuniform electrochemical proton gradients across the thylakoid and plasma membranes (PMs) (Bulychev and Vredenberg 2003; Krupenina and Bulychev 2007). Although plant cells possess various photoreceptors (phytochrome, phototropins, etc.), the light responses of membrane transport in green cells are usually mediated by chloroplasts (Marten et al. 2010). Illuminated leaves of aquatic plants acidify the medium adjacent to the lower leaf side, but elevate pH at the opposite leaf side (Prins et al. 1982). This polarity of H^+ transport, beneficial for CO_2 acquisition, indicates that electron- and ion-transport reactions in chloroplasts may activate divergent regulatory pathways resulting in either H^+ influx or efflux at the cell level.

Single cell systems, such as Characean internodes, provide a unique biological model for studying the photosynthetic and H^+ transport patterns. In dark-adapted internodal cells, the potential photosynthetic activity and properties of the PM are spatially uniform. However, the cells exposed to light produce alternating acidic and alkaline bands or asymmetric patches on the outer cell surface. Although the

occurrence of pH bands in Characeae and their possible influence on photosynthesis has been known for almost 40 years (Spear et al. 1969; Lucas 1975a), the first clear-cut evidence for close correlation between the pH banding and photosynthetic activity of chloroplasts in the underlying cell regions was presented much later (Bulychev et al. 2001a). The cell areas producing acid and alkaline pH zones feature high and low photosynthetic rates, respectively (Bulychev et al. 2005), which is clearly evident from imaging of chlorophyll fluorescence and pH bands (Krupenina et al. 2008).

The concerted emergence of pH and photosynthetic bands awaits deeper interpretation. A compelling task is to reveal key factors involved in formation and regulation of these labile patterns. Recent findings emphasized significance of intracellular transport and signaling events. Specifically, the cytoplasmic streaming and electrical excitation of the PM were found engaged in generation and triggered elimination of the pH bands as well as in modulation of chloroplast activity.

Cytoplasmic streaming (cyclosis) enables lateral distribution of substances and vesicles over long distances, at which diffusion is ineffective (Kamiya 1959; Verchot-Lubicz and Goldstein 2010). This function is particularly important for giant cells, such as internodes of Characean algae. The flow of liquid along immobile chloroplasts greatly accelerates the exchange of solutes between organelles and fluids (Pickard 2003; Goldstein et al. 2008). The velocity of cytoplasmic streaming in Characean internodes (up to 100 μm/s) is at the highest limit detected for plant cells. The cytoplasm movement in *Chara* cells is determined by interaction of subcortical actin bundles attached to the inner side of immobile chloroplasts and myosin molecules bound to freely moving organelles in the endoplasm (Shimmen and Yokota 2004). Despite general recognition of vital significance of cyclosis, there is surprisingly scarce data concerning its role in specific cell functions.

Propagation of electric signals in plants has been a matter of numerous studies (Davies 2006; Fromm and Lautner 2007; Krol et al. 2010). Electric signals basically similar to action potentials (AP) of animal cells are obvious in sensitive and carnivorous plants, like *Mimosa* and *Dionaea*, and are also propagated in plants lacking visible movement reactions. The long-distance transmission of electric signals along the conducting bundles after flame injury or mechanical stimulation was found to suppress photosynthesis in leaves (Koziolek et al. 2003; Grams et al. 2009; Pavlovic et al. 2011). The assignment of photosynthesis inhibition to propagation of AP is somewhat obscured by the transmission of both electric and hydraulic signals in response to flame stimuli (Stahlberg and Cosgrove 1997; Fromm 2006). Furthermore, two types of electrical signals can propagate along the conducting tissues after heat injury: AP and variation potentials. Unlike AP, variation potentials are characterized by variable depolarization amplitude, longer duration, and a slower spreading velocity. The inhibitory influence of variation potentials on photosynthesis has long been noted (Van Sambeek and Pickard 1976).

Ambiguity related to different nature of transmitted signals can be avoided by monitoring the photosynthetic activity of individual excitable cells, such as giant

internodes of Characean algae that are capable of generating AP in a controlled and reproducible manner on passing a short pulse of transmembrane electric current. Characean algae are perfectly suitable for studying interrelations between membrane excitability, cytoplasmic streaming, photosynthesis, and pattern formation, because they exhibit all these basic phenomena at the cell level. The essential advantage is that Characean chloroplasts are immobile and produce a densely packed single layer array.

This review outlines current knowledge on relations between the transmembrane H^+ flows and photosynthetic activity and highlights the role of cyclosis and electrical membrane excitation in creation and regulation of external pH pattern and chloroplast functions. Related topics are dealt with in the present volume (Beilby) and were surveyed previously (Bulychev and Krupenina 2008c, 2010).

12.2 Light-Dependent Patterns in Resting *Chara corallina* Cells

12.2.1 Significance of pH Banding

One may wonder why it is important to analyze alkaline zone formation and whether the segregation of alkaline and acid regions is a specific trait of Characean algae, having little relevance to other plant species. Apart from the key role of membrane H^+ transport in regulation of cytoplasmic pH, electrogenesis, and mineral nutrition (Palmgren 1998; Tazawa 2003), several further points should be noted.

1. Spatial separation of H^+-extruding and H^+-absorbing zones is not unique to charophytes and is observed in other systems, e.g., growing pollen tubes (Feijo et al. 1999), root tips (Felle 1998), fungal hyphae (Gow et al. 1984), and leaves of aquatic plants (Prins et al. 1982). The polarity of H^+ fluxes across the PM on different leaf sides is benefit to photosynthesis of aquatic plants inhabiting weakly alkaline stagnant waters, since local acidification shifts the HCO_3^-/CO_2 equilibrium ($pK_1 \sim 6.35$) to higher concentration of permeant neutral species (CO_2) and provides available substrate for photosynthesis (Walker et al. 1980; Prins et al. 1982; Plieth et al. 1994).
2. The elevation of external pH by photosynthesizing cells underlies biogenic calcification (Borowitzka 1987; McConnaughey 1991; Jansson and Northen 2010). At alkaline pH the HCO_3^-/CO_3^{2-} equilibrium ($pK_2 \sim 10.3$) is shifted toward the formation of CO_3^{2-}, which precipitates $CaCO_3$ and depletes Ca^{2+} in the alkaline zones. The resulting variations of Ca^{2+} in the apoplast might be involved in regulation and differentiation of plant growth and development. Mineralization at high pH is documented for cyanobacteria, green algae, e.g., *Halimeda*, and marine plankton algae; it is also important for coral growth.
3. According to the "acid growth theory," the acidic pH of the apoplast weakens cross-linking bonds in cell walls and loosens the cell wall matrix, thus favoring

the plant cell elongation (Rayle and Cleland 1992; Palmgren 1998; Hager 2003). Multiple sites of cell elongation in Characean internodes are restricted to the areas of external acidity (Metraux et al. 1980).

4. The breaking up of uniform pH distribution along the outer cell surface is an early step in formation of cell polarity. The emergence of asymmetry, fixed in ionic and molecular gradients, is a crucial stage in light-dependent morphogenesis, e.g., in developing *Fucus* zygotes (Coelho et al. 2008).
5. The striking heterogeneity of membrane properties in Characean cells was not taken into consideration in many, otherwise excellent, studies concerning light-dependent ion transport, operation of the electrogenic H^+ pump and ion channels in this model system (Tazawa 2003). Clearly, the assumption of homogeneous distribution of ion transport systems over the cell surface is inapplicable in many cases.

12.2.2 Pattern Visualization

The light-dependent pH patterns are readily visualized with indicator dyes phenol red (Spear et al. 1969; Shimmen and Wakabayashi 2008) and thymol blue (Beilby et al. 1993; Eremin et al. 2007). Phenol red is convenient for qualitative detection of alkaline bands. It is unsuitable for evaluation of pH shifts, since its color response is saturated at pH $\geq$ 8, while actual values in the alkaline zones approach pH 10. Therefore, pH changes as large as two pH units can be simply overlooked.

The antimony-based pH microelectrodes, featuring the linear function of pH and high temporal resolution ($\sim$1 s), are perfect for quantitative pH measurements in the regime of scanning along the cell at the velocity of $\sim$10 mm/min (Bulychev et al. 2001b). They are also appropriate for tracking the kinetics of surface pH (pH_o).

Vibrating electrodes proved suitable for mapping the extent and direction of extracellular currents. The routes of electric current correspond to longitudinal pH profiles, with outward current extending from acid zones and the inward current being confined to alkaline zones (Lucas and Nuccitelli 1980). A minor drawback is interference from stirring of external medium by periodic movement of the probe.

Heterogeneous profiles of the membrane potential and the PM conductance were measured with the "water-film electrode" (Ogata et al. 1987). Based on this method, the low-conductance cell regions with the hyperpolarized membrane potential were detected and ascribed to acidic zones. By contrast, the alkaline regions were identified as high-conductance depolarized regions.

Photosynthetic activity in vivo on a microscopic level can be assessed from measurements of chlorophyll fluorescence with the saturation pulse technique [reviewed in (Schreiber 2004)]. The method provides information on the effective quantum yield of electron transport in photosystem II (PSII) ($\Delta F/F_m'$) and on nonphotochemical fluorescence quenching (NPQ), a parameter derived from the Stern–Volmer equation and describing the protective heat dissipation of excess

energy. The actual rate of linear electron flow is proportional to the product of $\Delta F/F_m'$ and the photon flux density (PFD). The longitudinal profiles were measured with point-by-point resolution using Microscopy PAM (pulse-amplitude-modulation) fluorometer (Walz, Germany) and by means of chlorophyll fluorescence imaging (Imaging-PAM Chlorophyll fluorometer, Walz) (Krupenina et al. 2008).

Chlorophyll fluorescence of PSII under weak actinic light is low, since most excitations are spent for charge separations. The saturation light pulse reduces the primary acceptor Q_a, which inhibits the photochemical activity of PSII and enhances fluorescence and energy losses to heat. The effective quantum yield $\Delta F/F_m'$ is calculated from fluorescence measured before and during the saturation pulse (F and F_m', respectively): $\Delta F/F_m' = (F_m' - F)/F_m'$. The parameter NPQ is evaluated from the equation: $NPQ = (F_m - F_m')/F_m'$, where F_m and F_m' designate maximal fluorescence induced by the saturation pulse in the dark-adapted sample and in the same sample exposed to actinic light ($F_m' < F_m$).

The lower values of F_m' compared to F_m reflect the increased thermal losses that are related directly and indirectly to acidification of the thylakoid lumen and ΔpH formation (Finazzi et al. 2004). Thus, NPQ can be used as an indicator of the thylakoid ΔpH. In support of this notion, nonphotochemical quenching in *Chara* cells vanished in the presence of the ionophores nigericin and monensin known to eliminate the thylakoid ΔpH (Bulychev and Kamzolkina 2006). Simultaneous profiling of NPQ and pH_o along *C. corallina* cells revealed their parallel changes, indicating that the thylakoid ΔpH is high in the alkaline cell regions and low in areas with acidic external pH (Krupenina and Bulychev 2007).

Net photosynthetic activity was also assessed amperometrically with glass-insulated platinum electrode whose current is sensitive to O_2 content near the cell surface. When longitudinal profiles of external pH and O_2 concentration were compared, the positions of alkaline peaks coincided with minima of O_2 content, while the acidic regions corresponded to the peaks of O_2 level (Bulychev et al. 2001a). The antiparallel profiles of pH and pO_2, combined with fluorescence data, confirmed the faster rates of PSII electron flow in the acidic cell regions. They might also indicate the electron transport to O_2 in alkaline cell regions.

Cytological studies revealed that cortical mitochondria are relocated under light to photosynthetically active acid regions (Foissner 2004; Braun et al. 2007). Staining *Chara* cells with fluorescent markers of acidic organelles (the PM invaginations charosomes) and with markers of H^+-ATPase revealed their colocalization in the cell regions producing acidic bands (Schmölzer et al. 2011). This confirms the association of the PM H^+-pump with the membrane domains producing acid zones.

Thus, multiple manifestations of spatial heterogeneity in illuminated Characean cells include pH bands or patches, variations in chlorophyll fluorescence and photosynthetic activity, different extents of NPQ and the thylakoid ΔpH, differential conductance and membrane potentials, bands or patches of calcium precipitations, nonuniform distribution of mitochondria, area-specific growth rates, stronger adhesion of water to the cell surface in alkaline regions (Dorn and Weisenseel 1984), and enrichment of acidic cell regions with H^+-ATPase activity.

12.2.3 Coordination of Photosynthetic and pH Patterns

It is generally agreed that photosynthesis is a prerequisite for the band formation; no banding occurs in the presence of diuron, an inhibitor of photosynthetic electron flow. Photosynthesizing chloroplasts act as a source or a sink of some metabolites (e.g., H^+, ATP, Ca^{2+}, or phosphate) during the exchange of these species across the plastid envelope. At low irradiance the cell may exhibit a single band, while the number of bands increases with light intensity (Lucas 1975a; Bulychev et al. 2003).

One hypothesis for coordination of photosynthetic and pH bands is that chloroplasts of acid and alkaline cell regions differ in ATP-synthesizing capacity (Bulychev et al. 2005; Bulychev and Krupenina 2008c). In those regions where the thylakoid ΔpH is not readily utilized for ATP synthesis, higher amounts of protons accumulate in the thylakoid lumen, thus restricting the photosynthetic electron flow (photosynthetic control). The extensive H^+ uptake by thylakoids is supposed to deplete protons in the chloroplast stroma and the cytoplasm (Hansen et al. 1993). The ATP deficiency and high cytoplasmic pH preclude the operation of PM H^+ pump (Hager 2003), which elevates pH on the outer surface (pH_o) and activates the high pH channels whose conductance increases dramatically with the external pH (Bisson and Walker 1980). These channels account for the unusually high area-specific membrane conductance in the alkaline cell regions of illuminated cells (Walker et al. 1980). The downhill H^+ influx through the opened high pH channels will further elevate pH_o, diminish CO_2 content, and suppress the assimilating electron flow.

Conversely, in the regions where chloroplasts rapidly produce ATP for CO_2 fixation, the thylakoid ΔpH is consumed for ATP synthesis and remains low (Finazzi et al. 2004). The cytoplasmic ATP content is not depleted, thus promoting the H^+ pump operation, which creates the acidic external pH. The local acidification near the cell surface converts the membrane-impermeable anion HCO_3^- to the neutral readily permeant species, CO_2. This provides the cell with a carbon substrate and ensures high photosynthetic rates. The sufficiency of ATP for operation of PM H^+-pump in the acidic cell regions is further promoted by gathering of cortical mitochondria in the regions with high photosynthetic activity.

In the above scheme, the PM H^+-ATPase is considered as a generator of outward current, while the inward current in alkaline regions is carried either by H^+ influx or OH^- efflux. Because of the feedback relations, the system homogeneous in darkness can become unstable at light conditions and produce bands with spatially distributed H^+ pumps and H^+ leaks.

Segregated cell areas accommodate hundreds of thousands chloroplasts, which may cast some doubt on the assumption that photosynthetic and pH bands arise from microscopic fluctuations in a spatially uniform distribution. It should be noted, however, that pH zones appear at early stages as numerous minute pH excursions (Bulychev et al. 2001b). These fluctuations transform later to long-lived patches and finally rearrange to radially symmetric bands (Bulychev et al. 2003). Hence, emergence of bands from fluctuations in the originally homogeneous system cannot be excluded.

On the other hand, uniform illumination of the chloroplast layer is hardly ever achieved. Each internode of *C. corallina* contains two helical chloroplast-free narrow lines (equal in width to few chloroplast rows) that separate counter-directed cytoplasmic flows [see, e.g., diagrams in (Verchot-Lubicz and Goldstein 2010)]. At places where these neutral zones intersect the pathway of incident light, they act as transparent windows in the dense chloroplast layer and transmit narrow light beams to the underlying cell side.

If positions of alkaline bands depend on the intracellular pattern of light spots imposed by spiraling chloroplast-free lines and the bands are not structurally fixed (e.g., by calcification or charosomes), the band pattern should be sensitive to angular direction of incident light. Although this possibility remains untested, the role of nonuniform illumination in generation of photosynthetic and pH bands was verified with the use of localized lighting. A narrow beam applied through a thin light guide, can mimic the light spot projected by the chloroplast-free indifferent zone.

12.3 Role of Cyclosis in pH Pattern Formation

The chloroplast–PM interactions outlined above are mediated by the cytoplasm that acts as an intermediary pool of substances transported across PM and the chloroplast envelope upon the onset of photosynthesis and upon activation or inactivation of ion pumps and channels. However, the suggested scheme is static in a sense that rapid cytoplasmic flow is omitted from consideration.

Some mathematical models based on the reaction–diffusion system simulated the appearance of pH bands in *Chara* without implicating the cytoplasmic flow. It was assumed that active and passive H^+ flows across PM depend on the driving force for protons as well as on voltage-controlled operation of the PM H^+-pump and passive H^+ leak (Plyusnina et al. 2005). Other theoretical models comprised cyclosis as an essential element of pattern formation in *Chara* (Bulychev et al. 2001b).

Despite generally recognized role of cyclosis in vital cell functions, little is known about the influence of cytoplasmic streaming on membrane transport and photosynthesis. According to early studies (Lucas and Dainty 1977), the inhibition of streaming with cytochalasin B (CB) had no effect on the rate of photosynthetic CO_2 fixation in *C. corallina* cells exposed to overall illumination. Nevertheless, this conclusion, valid for uniform lighting conditions, may be inapplicable to a more general case of inhomogeneous illumination.

12.3.1 Polarity of pH Patch Formation Around the Light Spot

Application of a narrow light beam, combined with local measurements of pH_o and chlorophyll fluorescence provided new insights into the role of cyclosis in pattern formation (Bulychev and Dodonova 2011; Dodonova and Bulychev 2011).

If chloroplasts in illuminated region release or deplete some functional metabolite, the altered cytoplasm would flow downstream of the illuminated area and may affect the operation of chloroplast and plasmalemma systems in shaded areas. Conversely, in regions located upstream of the lightened area, the cytoplasm composition would be the same as in darkened cell parts. Hence, the cell regions exposed to identical light conditions at equal distances from the light spot might differ in their properties, thus mimicking the pattern formation.

This assumption was verified by measuring the surface pH (pH_o) and chloroplast fluorescence at equal distances on opposite sides from the light spot. For pH_o measurements, the area of inspection (AOI) was selected after checking its ability to generate alkaline zones. The localized beam was applied sequentially upstream and downstream of AOI with regard to the direction of cytoplasmic flow. Light emitted by a diode source (neutral white light, Luxeon, Lumileds, USA) was directed to the cell through a flexible light guide with a core diameter of 2.0 or 0.4 mm. The position of the fiber optics with respect to AOI was adjusted with micrometric screws. The alkaline zone in AOI was first preformed under overall illumination, and then it was allowed to dissipate gradually in darkness. After pH_o dropped to a certain level, the localized illumination was switched on. The subsequent pH changes in AOI differed greatly depending on the position of the light spot upstream or downstream of AOI, while the examined area stayed in the shade at equal distances *d* from the fiber optic core.

When the 2 mm-wide light guide was positioned 1–5 mm downstream of AOI, the onset of local illumination had no effect: the pH_o continued to decrease smoothly toward the bulk pH, with the same kinetics as in darkness (Fig. 12.1). By contrast, when the light guide was placed upstream of AOI at the same distance, a steep formation of alkaline zone was observed. An evident explanation for asymmetric formation of pH patch around the light spot is that illuminated chloroplasts alter the composition of flowing cytoplasm by virtue of ion or metabolite exchange across the envelope membrane, while the flow of modified cytoplasm affects the operation of H^+ (OH^-) transport in the shaded downstream regions. Other possible causes were considered and discarded. In particular, the profiles of residual irradiance against the distance from the light–shade border were identical regardless of the light spot position upstream or downstream of AOI (Dodonova and Bulychev 2011).

12.3.2 Necessity of Dim Light in the Area of Patch Formation

The narrow light beam directed straight to AOI produced no alkaline zone in this area (Bulychev et al. 2001b; Bulychev and Vredenberg 2003). The alkaline patch emerged downstream of the light spot at a short distance from the light–shade border, at a location where irradiance was not zero because of the scattered and reflected stray light. Dim background irradiance at AOI seems essential for generation of the alkaline zone. This notion relies on a series of experiments in which the light beam was directed upstream of AOI through a narrow (0.4 mm) optic

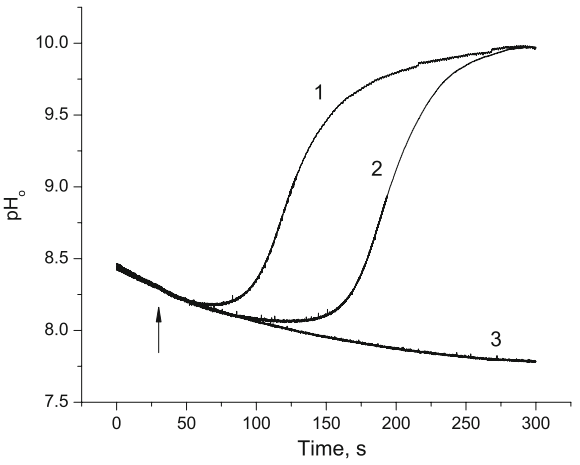

Fig. 12.1 Asymmetric changes of surface pH (pH_o) in response to local illumination applied 2 and 2.5 mm upstream (*curves 1* and *2*, respectively) and 2 mm downstream (*curve 3*) of AOI in *C. corallina* cell. *Arrow* marks the onset of localized illumination (white light, 1,500 μmol m^{-2} s^{-1}, beam width 2 mm). The indicated distances designate the space between AOI and the edge of the light guide core

fiber under the angle of 30° to the horizontal plane to reduce stray light. The irradiance around the light spot was controlled by the background overall illumination that was switched on 60 s prior to localized lighting.

When a narrow beam of intense light (500 μmol m^{-2} s^{-1}) was applied upstream of AOI in addition to dim background light (9 μmol m^{-2} s^{-1}), the alkaline patch was formed in a marked similarity to curve 1 in Fig. 12.1. In the absence of dim background light the application of localized beam did not produce the alkaline patch, and the pH_o declined as in Fig. 12.1, curve 3. The presence of background light without the localized beam was also ineffective.

Apparently, two conditions should be fulfilled for the induction of alkaline patch: (1) AOI should be flushed by "irradiated" cytoplasm and (2) weak background irradiance at AOI is needed. Both conditions are apparently satisfied during unilateral illumination of the whole cell. The transparent spiraling zones create the periodic light pattern at the bottom chloroplast layer, and cyclosis ensures the delivery of cytoplasm across the light–shade interface. The necessity of dim light in AOI indicates that the patch formation involves not only chloroplasts of brightly lit "source area" but also the plastids of shaded "sink" zone. At variance with this notion, the alkaline zone was observed in chloroplast-free cell parts that were obtained by wounding (Shimmen and Yamamoto 2002). Apparently, the mechanisms of alkaline zone formation may differ slightly for intact and wounded cells.

12.3.3 Photosynthesis Versus Photodamage as a Primary Cause of Alkaline Patch Formation

Intensities of local illumination indicated above were severalfold higher than the reported value of 15–20 W/m^2 for saturation of photosynthesis in *C. corallina* (Lucas 1975b). In order to prove that the effects of local illumination were not

caused by injuring action of strong light, the intensity of narrow beam directed through a 2 mm wide fiber optics was lowered to various extents. When PFD was reduced in the range from 1,500 to 190 μmol m^{-2} s^{-1} (in the absence of background overall illumination), alkaline patches with equally high pH_o were formed after the lag periods increasing from 30 to 75 s (Dodonova and Bulychev 2011). The longer lag periods at reduced PFD were probably related to lower intensities of stray light in AOI in the absence of supplemental background illumination. It was concluded that the alkaline zone is formed at a wide range of light intensities and that the high light stress is not essential in this process.

Considering the actual photon flux created by narrow beam in AOI on the lower cell side, it should be noted that the upper chloroplast layer attenuates the transmitted light nearly 3-fold (the absorbance of *C. corallina* internode $\sim$1.0 in the peak of chlorophyll absorption is divided between the upper and lower chloroplast layers). When the light guide was inclined at an angle of 30° to the horizontal plane, the irradiance at the cell bottom diminished additionally at least 2-fold ($\sin 30^\circ = 0.5$). It means that, at PFD of 500 μmol m^{-2} s^{-1}, the chloroplasts in AOI were exposed to 6-fold lower photon flux.

Such flux densities can be considered physiologically relevant, because Characean algae in natural environments may endure PFD up to few hundred micromoles per 1 m^2 per second. The solar radiation on a cloudless summer day is about 2,300 μmol m^{-2} s^{-1} [e.g., (Takakura and Fang 2002)]. In typical freshwater lakes, light is attenuated with depth to 1% at a level of 10 m below the surface (Nobel 2005). Characean algae (e.g., *Nitellopsis*) grow well at about 3 m below the surface, where PFD should be attenuated approximately 4-fold compared to the surface value. The algal cells can apparently cope with negative effects of short exposures to such irradiance.

12.3.4 Effects of Cyclosis Cessation

After the generation of AP, cyclosis stops immediately for about 30 s and fully recovers within about 5 min. When the AP was triggered few seconds before the onset of the local light applied upstream of AOI, the formation of alkaline patch was strongly delayed and pH_o increased insignificantly during the observation period (Dodonova and Bulychev 2011). This finding is consistent with the assumed lateral transfer of a mediator but is not entirely conclusive, because the influence of AP on pH bands may be also caused by the increase in cytosolic Ca^{2+} content and consequent Ca^{2+}-triggered events.

Cytochalasin B is a specific inhibitor of cytoplasmic streaming (Bradley 1973; Foissner and Wasteneys 2007). During incubation in the presence of CB the streaming decelerates and eventually ceases. The alkaline patch formation caused by localized lighting (as shown in Fig. 12.1) was consistently delayed during cyclosis retardation. This delay was quantified by fitting the pH_o changes with the sigmoid curves. Both cyclosis and the light-induced formation of alkaline zone

were restored during the cell wash after the removal of CB from the medium (Dodonova and Bulychev 2011). The streaming velocity and the half-time $t_{1/2}$ of alkaline patch formation changed in opposite directions during and after the CB treatment. The inverse of the time $t_{1/2}$ was taken as a measure of the rate constant of alkaline zone formation. The plot of this rate constant against the streaming velocity was linear, with the slope of straight line $\sim 1\ cm^{-1}$.

12.4 Influence of Cyclosis on Chlorophyll Fluorescence and Photosynthesis

Considering tight relations between photosynthetic and pH patterns, a question arises of how the chloroplasts residing at intermediate irradiance respond to the delivery of cytoplasm from brightly illuminated and shaded areas. This issue was studied by means of localized lighting applied through a thin (0.4 mm) optic fiber inclined at 30° to horizontal plane. Weak background light was permanently imposed on the whole cell to provide controlled PFD on the shaded part of the interface (Bulychev and Dodonova 2011).

12.4.1 Cyclosis-Mediated Polarity of Distant Interactions Between Chloroplasts

Figure 12.2 shows changes of F_m' fluorescence in AOI that were induced by localized light (500 μmol $m^{-2}\ s^{-1}$) applied through a thin optic fiber in addition to permanent whole cell illumination of intermediate intensity (28 μmol $m^{-2}\ s^{-1}$). Curves 1 and 2 represent F_m' changes in AOI when the optic fiber was positioned 1 mm upstream and downstream of AOI, respectively, with regard to the direction of cytoplasmic flow. In the case of delivery of "irradiated" cytoplasm to AOI from the illuminated upstream area, the narrow beam induced strong quenching of F_m' after a distinct lag period. When the optic fiber was shifted downstream of AOI, F_m' remained unaffected.

The origin of this asymmetry for distant interactions between illuminated and shaded chloroplasts is similar to that of pH patch formation around the light spot. Apparently, the chloroplasts of brightly illuminated area release or absorb some ion or substance that acts like a messenger and moves vectorially with the cytoplasmic flow along the cell. When the modified cytoplasm arrives to remote chloroplasts in AOI residing at moderate irradiance, F_m' is quenched (curve 1). The background irradiance did not quench F_m' when the modified cytoplasm streamed away from AOI (curve 2).

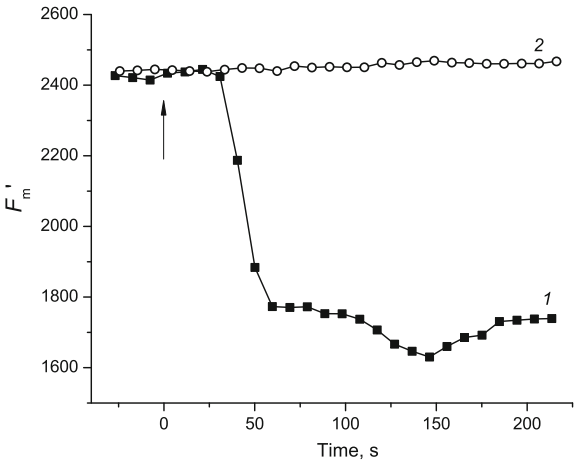

Fig. 12.2 Asymmetric changes in chlorophyll fluorescence F_m' on a microscopic area of the chloroplast layer in *C. corallina* cell upon the onset of localized illumination (500 μmol m^{-2} s^{-1}) directed through a 0.4 mm-wide optic fiber adjusted in two different positions: (*1*) 1 mm upstream of analyzed cell region (AOI) with regard to the direction of cytoplasmic flow and (*2*) 1 mm downstream of AOI. The spot light was superimposed on permanent background illumination of the whole cell (28 μmol m^{-2} s^{-1}). The *arrow* marks the moment when localized light was switched on

12.4.2 Inhibition of Photosynthesis by Inflow of "Irradiated Cytoplasm"

The F_m' changes induced by continuous localized light applied upstream of AOI showed complex nonmonotonic kinetics. Short light pulses induced smaller F_m' transients of a simpler shape. These F_m' changes can be expressed after recalculation as changes in NPQ that increases with lowering of F_m'. The plot of NPQ as a function of light pulse duration fits to an S-shaped Boltzmann curve. The initial concave portion of the fitting curve contains information on the period (15–20 s) during which some effector substance is produced inside brightly illuminated chloroplasts and released into the flow. Alternatively, it may reflect the period during which some metabolite essential for photosynthesis is depleted in chloroplasts and starts declining in the cytoplasm.

Comparatively short light pulses applied upstream of AOI (20–45 s) induced the F_m' changes that started and developed after the end of light pulse. The time lapse as long as 100 s between the end of a light pulse and the peak of NPQ could be observed at large separation distances between the light spot and AOI.

The light pulses of 30–60 s duration, applied upstream of AOI, induced F_m' responses with roughly symmetrical front and rear slopes. Such responses, reminiscent of peaks in elution chromatography, can be fitted to Gaussian curves. Figure 12.3 shows the peak position on the F_m'-fitting curves as a function of

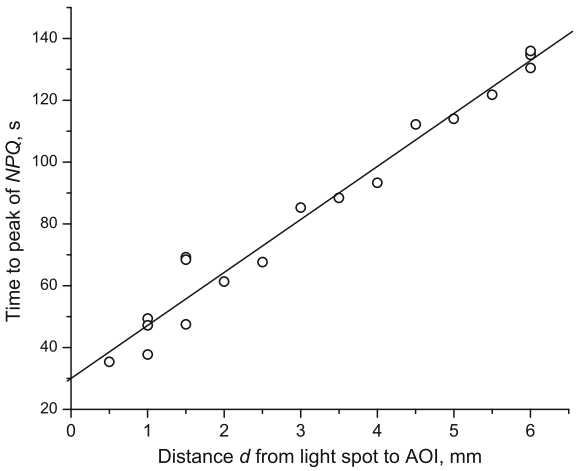

Fig. 12.3 Position of NPQ peak (F_m' minimum) on fitted curves of the pulse-induced quenching response as a function of distance between AOI and 0.4 mm optic fiber located upstream of AOI. The light pulse duration was 30 s, the intensity of permanent background light was 25 μmol m^{-2} s^{-1}. The inverse of the slope for the given internode (≈60 μm/s) falls into the range of streaming velocities. The time is given relative to the time point at which the light pulse was switched on

distance *d* between AOI and the irradiation point. The larger was the distance between the light spot and AOI, the longer time was needed to observe the F_m' dip (NPQ peak). The inverse of the slope of this linear plot (expressed in μm/s) was in the range of velocities typical of cytoplasmic streaming in Characean cells. The velocity of mediator movement was calculated with a simplifying assumption of linear, rather than the helical flow. The actual traveling distance along the helical path of cytoplasmic flow is higher than the separation distance *d* by the factor defined from the helix pitch distance and the cell diameter. The calculated rate of the mediator movement with the allowance for helical path will be respectively higher.

The ordinate segment corresponding to zero distance *d* in Fig. 12.3 (30 s) represents the time of the complete stimulus–response cycle except for the step of mediator migration with the streaming cytoplasm. About half of this time is attributed to the release of the messenger from brightly illuminated chloroplasts to the liquid flow or, alternatively, to the depletion of some essential metabolite from the cytoplasm. Another half represents the exchange of the intermediate between streaming cytoplasm and chloroplasts in the shaded area, which is followed by NPQ development.

The amplitude of cyclosis-mediated F_m' change was lowered with increasing distance *d* between AOI and the light guide position. Nevertheless, at a distance of 6 mm between the light spot and AOI, the cyclosis-mediated F_m' changes constituted about 25% of the response observed at a 1 mm distance.

12.4.3 Stimulation of Photosynthesis by Inflow of "Darkened Cytoplasm"

The drop of F_m' in AOI in Fig. 12.2 implies that the PSII efficiency declines upon the inflow of "irradiated" cytoplasm, because the cytoplasmic composition promotes the dissipation of excess excitation energy to heat. On the other hand, the inflow of cytoplasm from darkened regions to moderately lit cell areas was found to promote the PSII activity. Evidence on this point was obtained by comparing light-response curves of the effective quantum yield of PSII-driven electron flow $\Delta F/F_m'$ when the whole cell or a small cell part were exposed to light of the same quality and intensity under conditions of active cyclosis and after inhibition of streaming with the actin inhibitor, CB (Bulychev and Dodonova 2011).

In the untreated cell the gradual increase of PFD to 100 μmol m^{-2} s^{-1} was accompanied by the sigmoid decrease in $\Delta F/F_m'$ under illumination of entire cell, but had little effect on $\Delta F/F_m'$ when the major cell part was screened while only a 2 mm cell portion with AOI in the center was irradiated. After inhibition of cyclosis with CB, the light-response curve of $\Delta F/F_m'$ assessed under overall illumination remained almost unchanged, whereas the light curve obtained with the narrow light beam was modified and became similar to that observed under whole-cell lighting.

Thus, the light-response curves for PSII quantum yield of electron flow differed substantially under conditions of general and localized illumination but these differences vanished upon the cessation of cyclosis. It means that the interruption of cyclosis-mediated communication between shaded and illuminated cell regions diminishes the photosynthetic activity of locally illuminated chloroplasts at elevated irradiances. It also suggests that the arrival of cytoplasm from darkened cell regions is beneficial for photosynthetic efficiency (increase in $\Delta F/F_m'$), whereas the flow of cytoplasm from irradiated regions reduces $\Delta F/F_m'$. The effect of CB on the light-response curves was reversed upon the recovery of cyclosis after cell washing with a fresh medium.

It should be noted that cyclosis-mediated interactions are only evident when the cell parts communicating through lateral transport are metabolically nonuniform, e.g., exhibit dark and photosynthetic metabolism, as it probably occurs under the imposed light gradient or natural mosaic illumination. Conversely, the lateral transport of uniformly composed cytoplasm along evenly illuminated cells is analogous in many respects to the lack of lateral exchange. It is presently unknown whether the cytoplasm modified by strong light is depleted in some essential component (e.g., inorganic carbon or phosphate) or enriched with some messenger substance or metabolite. The occurrence of chloroplast responses far away (up to 6 mm) from the illumination site and a long delay of their appearance (up to 100 s) after the extinguished flash are relevant to photosynthesis under flickering light commonly encountered by charophytes in natural environments.

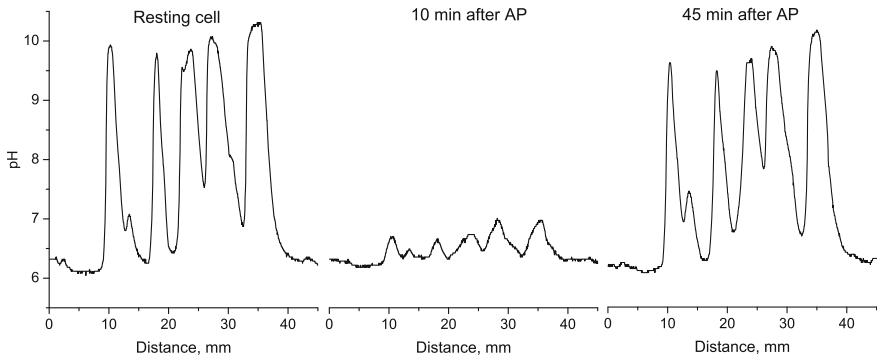

Fig. 12.4 Transient inhibition of light-dependent pH banding in a *C. corallina* cell after the propagation of an electrically triggered action potential (AP). Longitudinal pH profiles near the cell surface were measured (*left*) before AP, (*central*) 10 min after the propagation of a single AP, and (*right*) 45 min after the AP propagation

12.5 Effects of Membrane Excitation on Photosynthetic and pH Patterns

The light–dark transitions are the main factors causing reversible elimination and restoration of pH bands in Characean cells. However, the electrical excitation of cell membranes (action potential, AP) was found to override the influence of continuous light, causing the pH pattern to collapse temporarily despite the ongoing illumination (Bulychev et al. 2004; Krupenina et al. 2008). Although the duration of individual AP is only 3–5 s, the effects of this signal on H^+ transport and photosynthesis persist for 15–30 min.

12.5.1 Transient Collapse of the pH Pattern

The pH_o profile along the internodal cell of *C. corallina* undergoes striking changes upon the electrical excitation of PM with a short pulse of electric current. In the resting cell the pH profile is composed of few alkaline peaks and acidic zones with pH_o shifts as large as 3.5 units (Fig. 12.4). Within about 10 min after the AP generation, the alkaline peaks diminished strongly and the pH profile was largely flattened. The banding profile was restored almost completely within 40 min after the AP generation. Using serial pH profiles, acquired at regular intervals before and after triggering the AP, 3D (time–space) diagrams were plotted to visualize the dynamics of pH patterns after electrical excitation of PM (Krupenina et al. 2008). The decay of pH pattern after AP was similar to that upon darkening but it started with a shorter lag period (Bulychev and Kamzolkina 2006). The decay of pH bands is controlled by diffusion in the unstirred layers

between the acid and alkaline zones and between the unstirred layers and the bulk medium (Bulychev and Krupenina 2010). The recovery of alkaline bands after the AP-induced decline started earlier at higher PFD and elevated concentrations of external Ca^{2+} (Eremin et al. 2007).

The pH_o changes in the acid zone are comparatively small and not resolved in Fig. 12.4. However, when the pH sensor was positioned in the acid zone, it recorded the pH_o increase after AP generation with the amplitude of 0.3–0.35 pH units. Particularly large AP-induced pH changes in the acid zones (up to 0.9 unit) were observed in cells treated with dithiothreitol (DTT) known to reduce disulfide bonds (Dodonova et al. 2010). Based on the notion that the acid cell regions possess H^+-pump activity while the alkaline zones feature high passive conductance for H^+ or OH^-, it was supposed that the AP inhibits temporally both the ATPase-driven H^+ efflux and the passive H^+ influx (OH^- efflux) in different cell regions.

Ionic fluxes during AP in plants comprise the Ca^{2+} influx into the cytoplasm through voltage-gated PM channels, which is followed by the Cl^- efflux through Ca^{2+}-activated channels, and the delayed K^+ efflux (Lunevsky et al. 1983; Beilby 2007). The increase in cytosolic Ca^{2+} content is greatly contributed by the release of Ca^{2+} from intracellular stores (Thiel et al. 2002). The role of AP in osmotic regulation is related to large Cl^- and K^+ effluxes from the cytoplasm to the apoplast during cell excitation. During AP plant cells may lose appreciable quantities of these osmolytes and undergo turgor movements. However, on a relative scale the changes in cytoplasmic Cl^- and K^+ levels during excitation are incomparably smaller than the change in Ca^{2+} level, which increases from the resting level of $\sim$0.1 to the order of 10 μM (Williamson and Ashley 1982; Berestovsky and Kataev 2005). High levels of cytosolic Ca^{2+} were reported to inhibit H^+ extrusion by the PM H^+-ATPase (Sehnke et al. 2002), which is in line with the inhibitory effect of AP on acid bands.

12.5.2 Inactivation of High pH Channels

The origin of temporal elimination of alkaline bands after membrane excitation was partly clarified from parallel measurements of AP-induced changes in pH_o, membrane resistance (R_m), and membrane potential (V_m) in electrically insulated alkaline cell areas (Bulychev and Krupenina 2009). The R_m values in these cell regions at rest were low, corresponding to a high membrane conductance ($\sim$8.3 S/m^2), which falls into the reported range of 5–15 S/m^2 (Smith and Walker 1985). After the AP generation, R_m was found to increase several fold (by a factor of 7.5 in Fig. 12.5a) within about 40 s. The membrane conductance, G_m decreased accordingly. The increase in R_m was paralleled by a large (50–60 mV) hyperpolarization of V_m and by lowering of pH_o. The AP-induced changes in R_m, V_m, and pH_o returned to their initial values within 15 min or longer depending on the irradiance.

Comparison of R_m and pH_o kinetics in alkaline zones after AP (Fig. 12.5b) showed that the peak of R_m was attained much earlier than the minimum of pH_o

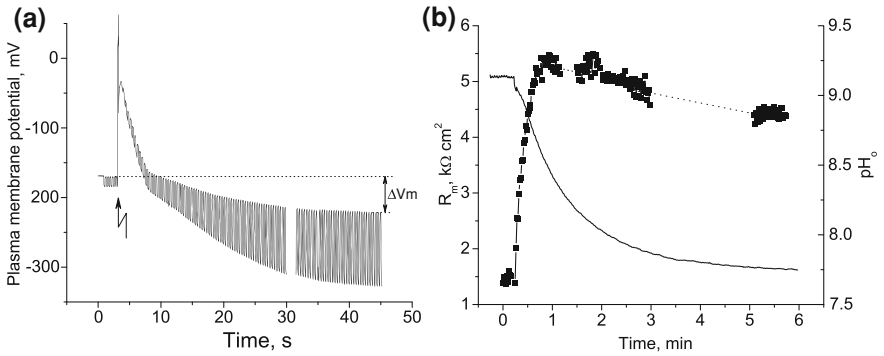

Fig. 12.5 Changes in plasmalemma potential (V_m), resistance (R_m), and surface pH (pH$_o$) in space-clamped alkaline region of *C. corallina* cell upon triggering the AP. The AP was evoked after 20-min rest period in continuous blue light (100 μE m^{-2} s^{-1}). The membrane resistance was tested by passing a train of rectangular hyperpolarizing current pulses (1 μA, 160 ms, 3 Hz). **a** The AP-induced increase in R_m concurrent with the V_m hyperpolarization. The R_m values are proportional to V_m shifts induced by pulses of electric current. The double-headed arrow indicates the post-excitation hyperpolarization. **b** Kinetics of AP-induced R_m changes and pH near the outer cell surface

and that the initial stages of R_m recovery proceeded concurrently with the ongoing pH$_o$ decrease. Hence, the conductance inactivation is not the consequence of pH$_o$ decrease but, most probably, is the cause of H^+ flux cessation. The AP-induced drop of pH$_o$, paralleled by a hyperpolarizing shift of V_m and by a profound G_m decrease, suggests that the collapse of pH pattern after AP generation involves the suppression of passive electrogenic H^+ (OH^-) transport in the alkaline cell areas, which might be considered as a rapid inactivation of the high pH channels. Furthermore, it is becoming clear that the origin of high pH$_o$ in alkaline zones of *Chara* cells cannot be attributed to functioning of H^+/HCO_3^- symport or OH^-/HCO_3^- antiport, as is often suggested. In the case of electroneutral symport or antiport, the cessation of H^+ (OH^-) transport and the respective pH$_o$ changes would have occurred without the decrease in G_m.

The AP-induced pH shifts in separate zones differed substantially in untreated and DTT-treated cells, indicating that the pattern of extracellular currents depends on the oxidoreduction state of SH-groups. The AP-sensitive inward H^+ fluxes, confined normally to alkaline cell regions, became small after the treatment of cell with DTT, despite the enhanced H^+ efflux in the acid regions (Dodonova et al. 2010). This modified pattern of H^+ flows would mean that the conductance of alkaline cell regions ceased to be the main load for the electrogenic H^+-pump after reduction of disulfide bonds. In this case the pump, which remained active and AP-sensitive, could drive not only the HCO_3^-/CO_2 conversion but also the accumulation of mineral nutrients, e.g., K^+, which enters the cell through ion channels distributed uniformly over PM.

12.5.3 Transient Enhancement of Photosynthetic Pattern

Surprisingly, the elimination of pH pattern after triggering the AP is accompanied by temporal enhancement of spatial heterogeneity of fluorescence and electron flow in chloroplasts (Krupenina et al. 2008). The pattern becomes more contrast because the operating PSII efficiency $\Delta F_m/F_m'$ is hardly influenced by AP in the acidic cell regions, whereas $\Delta F_m/F_m'$ drops in alkaline cell regions where it was already low in the resting state.

The obvious dissimilarity in AP-induced changes of photosynthetic and pH bands provide evidence that the AP affects chloroplast functions and the PM H^+-transport through different pathways initiated by the rise in cytoplasmic Ca^{2+} as a common cause. A possible explanation for the enhancement of photosynthetic pattern is that inhibition of H^+-ATPase in the acidic bands and the concurrent cessation of H^+ influx in the alkaline cell areas after AP produce opposite shifts in the cytosolic pH (pH_c) in different cell regions.

The arrest of continuous H^+ inflow after AP would shift the balance toward higher pH_c in alkaline cell regions, while the arrest of H^+ pump would lower pH_c in the acidic cell regions. According to Muto et al. (1982), the shift of pH from 6.5 to 8.0 in suspensions of intact chloroplasts stimulated the light-induced Ca^{2+} uptake by 80%. Therefore, one may expect that the stromal Ca^{2+} concentration would increase to a larger extent after AP in the alkaline cell regions than in the acidic regions. This may account for the stronger inhibition of CO_2 fixation and ATP consumption in the alkaline cell regions compared to acidic areas (Krupenina et al. 2008). These changes would result in thylakoid energization (ΔpH increase) and energy-dependent quenching, provided some form of ΔpH-generating electron transport (e.g., electron transport to O_2 and monodehydroascorbate) is maintained.

In addition to influence on PSII electron flow, the AP generation was found to affect the photoreactions of PSI. Such influence was evident from the redox transients of chlorophyll P700 reflected by photoinduced absorbance changes $\Delta A_{810–870}$ in resting cells exposed to dim light and in the same cells subjected to excitatory electric stimulus prior to measurement (Bulychev and Krupenina 2010).

12.5.4 Impact of AP on Photosynthesis Through Gated Permeation of Xenobiotics

In the presence of biologically active exogenous compounds, like herbicides, growth regulators, etc., the AP generation may influence the photosynthetic pattern via an alternative mechanism, through changes in compartmentation of added chemicals. Water-soluble charged substances whose permeation is strongly hindered by the PM are especially interesting in this respect. A cationic redox mediator methyl viologen (MV) is an example of xenobiotics generating reactive oxygen species (ROS) (Dodge 1989). The herbicidal action of MV is due to its

efficient reduction by electrons received from PSI, which is followed by reaction with oxygen and ROS production. The oxidized and reduced forms are recycled during MV operation, so that very low catalytic amounts of MV are quite effective.

Chlorophyll fluorescence measurements in *Chara* cells showed that the divalent cation of MV (MV^{2+}) does not pass across the permeability barriers (plasmalemma and chloroplast envelope) in the resting cell, but gains an immediate access to the sites of its interaction with PSI after the AP generation (Bulychev and Krupenina 2008a). Hence, the onset of herbicide action on chloroplasts in vivo coincides with the moment of AP stimulation. This notion was confirmed by the lack of any MV effect on light-induced redox changes of P700 (PSI reaction center chlorophyll and primary electron donor) in the resting cell and by drastic irreversible alteration of P700 photoreduction kinetics after triggering a single AP (Bulychev and Krupenina 2008b)

A better understanding of the AP action in the presence of MV came from analysis of spatiotemporal dynamics of chlorophyll fluorescence (Krupenina et al. 2011). The PM excitation was found to exert different influence on photosynthetic patterns of electron flow and NPQ in the absence and presence of MV in the external medium. Under physiological conditions the AP-induced NPQ and $\Delta F/F_m'$ changes were reversible and manifested mostly in the alkaline regions. By contrast, the quenching evoked by a single AP in the presence of MV was irreversible and was stronger in the acid regions than in the alkaline areas. The spatial heterogeneity of $\Delta F/F_m'$ and NPQ was transiently enhanced after the AP generation in the absence of MV, but the patterns were irreversibly smoothed after evoking an AP in the presence of MV. These findings emphasize different processes underlying the AP-induced NPQ in the absence and in the presence of the redox-cycling agent MV.

The physiological Ca^{2+}-mediated pathway, leading to fluorescence quenching after AP generation (see Sect. 12.5.3), comprises the increase in cytoplasmic Ca^{2+} level, Ca^{2+} entry into the stroma of illuminated chloroplasts, inhibition of the Calvin cycle reactions and ATP consumption, the replacement of CO_2-dependent electron pathway with O_2-dependent electron flow, and the resulting increase in ΔpH as the cause of NPQ increase (Krupenina and Bulychev 2007; Krupenina et al. 2008). Unlike this natural mechanism, the AP-triggered quenching in the presence of MV arises because the AP opens a gate for rapid penetration of the MV into the cell and into the chloroplast stroma where it catalyzes the reduction of O_2 by PSI. The products of this reaction are superoxide anions, converted by superoxide dismutase to H_2O_2. The subsequent enzymatic decomposition of H_2O_2 catalyzed by ascorbate peroxidase produces monodehydroascorbate, which is an effective electron acceptor from PSI (Asada 1999). The increase in NPQ is caused by inhibition of CO_2 fixation and by enhanced ΔpH due to the decrease in ATP demand and stimulation of O_2-dependent electron flow ("water–water cycle"). The critical step in this mechanism is the passage of MV through the membrane pores turned open during the electrical excitation.

The calcium-permeable channel of PM is not strictly selective: the pore diameter of 0.8 nm (Berestovsky, personal communication) is sufficiently large to

pass MV whose ionic radius is 0.33 nm. Therefore Ca^{2+} and MV may compete for the entry into the cytoplasm during the AP. In accord with this notion, the elevated Ca^{2+} concentration (2 mM instead of 0.1 mM) in the external medium prevented the AP-triggered permeation of MV, which was evident from the lack of F_m' quenching. After subsequent lowering of external Ca^{2+} level, the MV-mediated quenching of F_m' appeared immediately after the AP generation. It is possible that the Ca^{2+} binding to PM near the channel at elevated Ca^{2+} level affects the electrostatic field around the pore, thus preventing the permeation of MV^{2+}.

The results demonstrate the potential possibility for the control over MV toxicity in plants and show that permeation of MV through the membrane cell barriers might be promoted by the electric signals propagated over the plants. The electric pulses in plants arise upon injuries, heating, rapid cooling, mechanical agitation, and ionic changes in the environment (Shepherd et al. 2008). Judging from experiments with Characean internodes as a model plant system, it is not excluded that stimulatory impact of AP on the effectiveness of MV treatment can be enhanced or suppressed by adjusting the ionic composition of the external medium.

12.5.5 *Effects of Membrane Excitation on Fluorescence Under Localized Lighting*

The AP-induced changes in fluorescence and photosynthetic electron transport under uniform illumination occur at a narrow range of light intensities. They are not observed in darkness because linear electron transport coupled with H^+ pumping into the thylakoid is a precondition of their appearance. On the other hand, when the light intensity exceeds a certain threshold, nonphotochemical quenching develops, which diminishes $\Delta F/F_m'$ and F_m' and their sensitivity to AP generation. By contrast, in cells exposed to narrow light beam, $\Delta F/F_m'$ remained high and NPQ remained low even at high light intensities (Sect. 12.4.3), pointing to the possibility that the AP-induced responses may occur at a wider PFD range.

Effects of AP generation on F_m' fluorescence under localized lighting might differ from those under overall illumination because the cytoplasmic flow in the resting cell and the streaming stoppage on the peak of AP become additional factors affecting the chloroplast–PM interactions under spot illumination. When the whole cell is illuminated, the effects of streaming and of its cessation on $\Delta F/F_m'$ and F_m' are not so much evident (Sect. 12.4.3).

Indeed, the F_m' changes caused by the electrical excitation of PM differed substantially depending on the illumination pattern (whole-cell versus partial illumination), even though the wavelengths and irradiance were identical in both cases (Bulychev and Dodonova 2011). In a cell exposed to PFD of 45 and 71 μmol m^{-2} s^{-1}, the AP triggered at lower irradiance was followed by the F_m' decrease under whole-cell illumination but was without effect in the case of small area illumination (Fig. 12.6). At elevated PFD, the electrical excitation

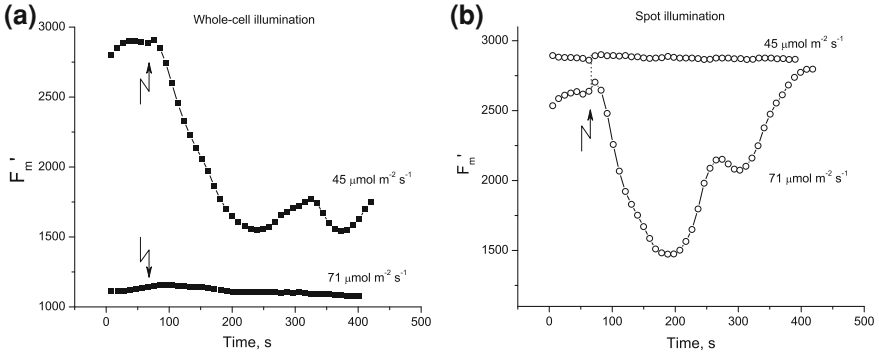

Fig. 12.6 Changes in F_m' chlorophyll fluorescence triggered by generation of the AP (*zigzag arrows*) under **a** whole-cell illumination (*solid symbols*), and **b** illumination of a 2 mm wide cell area (*open circles*) at PFD of 45 and 71 μmol m^{-2} s^{-1}

resulted in F_m' quenching under illumination of a small cell area but had no effect on F_m' under overall illumination, since F_m' was already quenched by light at this PFD.

When an intense narrow beam was applied to AOI through the optic fiber, while the rest part of the cell was kept in darkness, the initial rapid quenching of F_m' was followed by the release of quenching within about 3 min, indicating the activation of CO_2 fixation. A surprising point is that NPQ was low under steady state despite the intense incident light. This was apparently due to continuous inflow of "dark" cytoplasm to AOI. By contrast, when the spot beam was applied in addition to weak illumination of the whole cell, it caused a sustained decrease in F_m', even though the background light was almost 20 times weaker than the spot beam. It means that the composition of cytoplasm arriving from dimly illuminated cell parts differed from that arriving from darkened areas and sufficed to quench fluorescence after the AP propagation.

In the area of intense local illumination, the F_m' response to AP generation was manifested even at a high intensity light directed through the 0.4 mm optic fiber (Bulychev and Dodonova 2011). Thus, a continuous flow of cytoplasm from the darkened to illuminated cell regions not only enhanced the chloroplast photosynthetic activity but also shifted and broadened the range of F_m' responses to membrane excitation.

It appears that NPQ induced by AP in locally illuminated cells originates from two basic causes. One is the onset of the Ca^{2+}-mediated pathway, also operative when the AP is generated under overall illumination. The other is a sudden cessation of cytoplasmic streaming, which arrests the permanent renewal of the cytoplasm around the chloroplasts in the illuminated area. This would immediately affect the substrate and metabolite exchange across the chloroplast envelope, giving rise to NPQ and suppression of electron flow.

Nevertheless, the effect of AP on F_m' and $\Delta F/F_m'$ cannot be entirely assigned to the stoppage of streaming. Such effects of membrane excitation are readily observed under whole-cell illumination, at which the cessation of cytoplasmic streaming had a minor effect on PSII efficiency (Sect. 12.4.3). The basic similarity of electrical signal-induced fluorescence responses in *Chara* and in small-sized cells of plant leaves also argues against such possibility, because influence of streaming on photosynthesis is presumably weaker in mesophyll cells, where cyclosis rates and the light heterogeneity at the cell level are lower than in Characean cells.

The shift of AP-induced F_m' transients toward the elevated PFD range under localized lighting is possibly due to the existence of some laterally transportable cytoplasmic component whose level is modulated by both photosynthetic metabolism and by the electrical excitation of PM. Calcium is one of the candidates for this role because its cytoplasmic level is modulated by light (Johnson et al. 2006; Harada and Shimazaki 2009) and by the electrical excitation of the cell. At variance with earlier reports, the photosynthetically active light was found to induce rapid transient increase in cytosolic Ca^{2+} level (Harada and Shimazaki 2009), which is similar to the cytosolic Ca^{2+} rise upon the electrical membrane excitation in plant cells.

12.6 Conclusion

Internodal cells of *Chara corallina* represent a unique model system to study interactions between photosynthesis, membrane excitation, and cytoplasmic streaming, as well as the role of these processes in generation and regulation of functional patterns in green cells and tissues. It is established that the inflow of cytoplasm from darkened cell parts promotes photosynthetic activity of chloroplasts residing at intermediate irradiance, whereas the delivery of cytoplasm from illuminated regions suppresses this activity and enhances nonphotochemical quenching. The vectorial movement of the "irradiated" cytoplasm induces functional asymmetry (pattern formation) both in the chloroplast layer and in the PM. The signal transferred between illuminated and shaded cell parts was found to move at the velocity of cytoplasmic streaming. The effects of membrane excitation (action potential) on photosynthesis and membrane H^+ transport are area specific; they are also mediated by different mechanisms under physiological conditions and in the presence of some redox-cycling compounds. The influence of action potential on chlorophyll fluorescence under spot illumination appears to involve both the activation of Ca^{2+}-mediated pathways and the stoppage of cyclosis. The cytoplasmic flow from darkened to illuminated cell parts enhances interactions between respiratory and light-dependent metabolism, which promotes photosynthesis and protects chloroplasts from photooxidative damage under excess light.

Acknowledgments This work was supported by the Russian Foundation of Basic Research

References

Asada K (1999) The water–water cycle in chloroplasts: scavenging of active oxygen and dissipation of excess photons. Ann Rev Plant Physiol Plant Mol Biol 50:601–639

Baker NR (2008) Chlorophyll fluorescence: a probe of photosynthesis in vivo. Annu Rev Plant Biol 59:89–113

Beilby MJ (2007) Action potential in charophytes. Int Rev Cytol 257:43–82. doi:10.1016/S0074-7696(07)57002-6

Beilby MJ, Mimura T, Shimmen T (1993) The proton pump, high pH channels, and excitation: voltage clamp studies of intact and perfused cells of *Nitellopsis obtusa*. Protoplasma 175:144–152

Berestovsky GN, Kataev AA (2005) Voltage-gated calcium and Ca^{2+}-activated chloride channels and Ca^{2+} transients: voltage-clamp studies of perfused and intact cells of *Chara*. Eur Biophys J 34:973–986. doi:10.1007/s00249-005-0477-9

Bisson MA, Walker NA (1980) The *Chara* plasmalemma at high pH. Electrical measurements show rapid specific passive uniport of H^+ or OH^-. J Membr Biol 56:1–7

Borowitzka MA (1987) Calcification in algae: mechanisms and the role of metabolism. Crit Rev Plant Sci 6:1–45

Bradley MO (1973) Microfilaments and cytoplasmic streaming: inhibition of streaming with cytochalasin. J Cell Sci 12:327–343

Braun M, Foissner I, Lühring H, Schubert H, Thiel G (2007) Characean algae: still a valid model system to examine fundamental principles in plants. Progr Bot 68:193–220

Bulychev AA, Dodonova SO (2011) Effects of cyclosis on chloroplast–cytoplasm interactions revealed with localized lighting in characean cells at rest and after electrical excitation. Biochim Biophys Acta 1807:1221–1230. doi:10.1016/j.bbabio.2011.06.009

Bulychev AA, Kamzolkina NA (2006) Differential effects of plasma membrane electric excitation on H^+ fluxes and photosynthesis in characean cells. Bioelectrochemistry 69:209–215. doi:10.1016/j.bioelechem.2006.03.001

Bulychev AA, Krupenina NA (2008a) Action potential opens access for the charged cofactor to the chloroplasts of *Chara corallina* cells. Russ J Plant Physiol 55:175–184. doi:10.1134/S1021443708020039

Bulychev AA, Krupenina NA (2008b) Facilitated permeation of methyl viologen into chloroplasts in situ during electric pulse generation in excitable plant cell membranes. Biochem (Moscow), Suppl Series A: Membr Cell Biol 2:387–394. doi:10.1134/S1990747808040132

Bulychev AA, Krupenina NA (2008c) Effects of plasma membrane excitation on spatially distributed H^+ fluxes, photosynthetic electron transport and non-photochemical quenching in the plant cell. In: Bernstein EM (ed) Bioelectrochemistry research developments. Nova Science Publishers, New York

Bulychev AA, Krupenina NA (2009) Transient removal of alkaline zones after excitation of *Chara* cells is associated with inactivation of high conductance in the plasmalemma. Plant Signal Behav 4:727–734

Bulychev AA, Krupenina NA (2010) Physiological implications of action potential in characean cell: effects on pH bands and spatial pattern of photosynthesis. In: DuBois ML (ed) Action potential: biophysical and cellular context, initiation, phases and propagation. Nova Science Publishers, New York

Bulychev AA, Vredenberg WJ (2003) Spatio-temporal patterns of photosystem II activity and plasma-membrane proton flows in *Chara corallina* cells exposed to overall and local illumination. Planta 218:143–151. doi:10.1007/s00425-003-1084-6

Bulychev AA, Cherkashin AA, Rubin AB, Vredenberg WJ, Zykov VS, Müller SC (2001a) Comparative study on photosynthetic activity of chloroplasts in acid and alkaline zones of *Chara corallina*. Bioelectrochemistry 53:225–232

Bulychev AA, Polezhaev AA, Zykov SV, Pljusnina TY, Riznichenko GY, Rubin AB, Jantoss W, Zykov VS, Müller SC (2001b) Light-triggered pH banding profile in *Chara* cells revealed with a scanning pH microprobe and its relation to self-organization phenomena. J Theor Biol 212:275–294. doi:10.1006/jtbi.2001.2375

Bulychev AA, Zykov SV, Rubin AB, Müller SC (2003) Transitions from alkaline spots to regular bands during pH pattern formation at the plasmalemma of *Chara* cells. Eur Biophys J 32: 144–153. doi:10.1007/s00249-003-0280-4

Bulychev AA, Kamzolkina NA, Luengviriya J, Rubin AB, Müller SC (2004) Effect of a single excitation stimulus on photosynthetic activity and light-dependent pH banding in *Chara* cells. J Membr Biol 202:11–19. doi:10.1007/s00232-004-0716-5

Bulychev AA, Van den Wijngaard PWJ, De Boer AH (2005) Spatial coordination of chloroplast and plasma membrane activities in *Chara* cells and its disruption through inactivation of 14-3-3 proteins. Biochemistry (Moscow) 70:55–61

Coelho SMB, Brownlee C, Bothwell JHF (2008) A tip-high, Ca^{2+}-interdependent, reactive oxygen species gradient is associated with polarized growth in *Fucus serratus* zygotes. Planta 227:1037–1046. doi:10.1007/s00425-007-0678-9

Davies E (2006) Electrical signals in plants: facts and hypotheses. In: Volkov A (ed) Plant electrophysiology theory and methods. Springer, Berlin

Dodge A (1989) Herbicides interacting with photosystem I. In: Dodge A (ed) Herbicides and plant metabolism. Cambridge University Press, Cambridge

Dodonova SO, Bulychev AA (2011) Cyclosis-related asymmetry of chloroplast–plasma membrane interactions at the margins of illuminated area in *Chara corallina* cells. Protoplasma 248(4):737–749. doi:10.1007/s00709-010-0241-6

Dodonova SO, Krupenina NA, Bulychev AA (2010) Suppression of the plasma membrane H^+-conductance on the background of high H^+-pump activity in dithiothreitol-treated *Chara* cells. Biochem (Moscow), Suppl Series A Membr Cell Biol 4:389–396. doi:10.1134/S1990747810040094

Dorn A, Weisenseel MH (1984) Growth and the current pattern around internodal cells of *Nitella flexilis* L. J Exp Bot 35:373–383

Eremin A, Bulychev A, Krupenina NA, Mair T, Hauser MJB, Stannarius R, Müller S, Rubin AB (2007) Excitation-induced dynamics of external pH pattern in *Chara corallina* cells and its dependence on external calcium concentration. Photochem Photobiol Sci 6:103–109. doi:10.1039/b607602e

Feijo JA, Sainhas J, Hackett GR, Kunkel JG, Hepler PK (1999) Growing pollen tubes possess a constitutive alkaline band in the clear zone and a growth-dependent acidic tip. J Cell Biol 144:483–496

Felle HH (1998) The apoplastic pH of the *Zea mays* root cortex as measured with pH-sensitive microelectrodes: aspects of regulation. J Exp Bot 49:987–995

Finazzi G, Johnson GN, Dallosto L, Joliot P, Wollman F-A, Bassi R (2004) A zeaxanthin-independent nonphotochemical quenching mechanism localized in the photosystem II core complex. Proc Natl Acad Sci U S A 101:12375–12380. doi:10.1073/pnas.0404798101

Foissner I (2004) Microfilaments and microtubules control the shape, motility, and subcellular distribution of cortical mitochondria in characean internodal cells. Protoplasma 224:145–157. doi:10.1007/s00709-004-0075-1

Foissner I, Wasteneys GO (2007) Wide-ranging effects of eight cytochalasins and latrunculin A and B on intracellular motility and actin filament reorganization in characean internodal cells. Plant Cell Physiol 48:585–597. doi:10.1093/pcp/pcm030

Fromm J (2006) Long-distance electrical signaling and physiological functions in higher plants. In: Volkov A (ed) Plant electrophysiology theory and methods. Springer, Berlin

Fromm J, Lautner S (2007) Electrical signals and their physiological significance in plants. Plant, Cell Environ 30:249–257. doi:10.1111/j.1365-3040.2006.01614.x

Goldstein RE, Tuval I, Van de Meent J-W (2008) Microfluidics of cytoplasmic streaming and its implications for intracellular transport. Proc Natl Acad Sci U S A 105:3663–3667. doi:10.1073/pnas.0707223105

Gow NAR, Kropf DL, Harold FM (1984) Growing hyphae of *Achlya bisexualis* generate a longtitudinal pH gradient in the surrounding medium. J Gen Microbiol 130:2967–2974

Grams TEE, Lautner S, Felle HH, Matyssek R, Fromm J (2009) Heat-induced electrical signals affect cytoplasmic and apoplastic pH as well as photosynthesis during propagation through the maize leaf. Plant, Cell Environ 32:319–326. doi:10.1111/j.1365-3040.2008.01922.x

Hager A (2003) Role of the plasma membrane H^+-ATPase in auxin-induced elongation growth: historical and new aspects. J Plant Res 116:483–505. doi:10.1007/s10265-003-0110-x

Hansen U-P, Moldaenke C, Tabrizi H, Ramm D (1993) The effect of transthylakoid proton uptake on cytosolic pH and the imbalance of ATP and NADPH/H^+ production as measured by CO_2− and light-induced depolarization of the plasmalemma. Plant Cell Physiol 34:681–695

Harada A, Shimazaki K (2009) Measurement of changes in cytosolic Ca^{2+} in *Arabidopsis* guard cells and mesophyll cells in response to blue light. Plant Cell Physiol 50:360–373. doi:10.1093/pcp/pcn203

Jansson C, Northen T (2010) Calcifying cyanobacteria—the potential of biomineralization for carbon capture and storage. Curr Opin Biotechnol 21:1–7. doi:10.1016/j.copbio.2010.03.017

Johnson CH, Shingles R, Ettinger WF (2006) Regulation and role of calcium fluxes in the chloroplast. In: Wise RR, Hoober JK (eds) The structure and function of plastids. Springer, Dordrecht

Kamiya N (1959) Protoplasmic streaming. Springer, Wien

Koziolek C, Grams TEE, Schreiber U, Matyssek R, Fromm J (2003) Transient knockout of photosynthesis mediated by electrical signals. New Phytol 161:715–722. doi:10.1046/j.1469-8137.2003.00985.x

Krol E, Dziubinska H, Trebacz K (2010) What do plants need action potentials for? In: DuBois ML (ed) Action potential: biophysical and cellular context, initiation, phases and propagation. Nova Science Publisher, New York

Krupenina NA, Bulychev AA (2007) Action potential in a plant cell lowers the light requirement for non-photochemical energy-dependent quenching of chlorophyll fluorescence. Biochim Biophys Acta 1767:781–788. doi:10.1016/j.bbabio.2007.01.004

Krupenina NA, Bulychev AA, Roelfsema MRG, Schreiber U (2008) Action potential in *Chara* cells intensifies spatial patterns of photosynthetic electron flow and non-photochemical quenching in parallel with inhibition of pH banding. Photochem Photobiol Sci 7:681–688. doi:10.1039/b802243g

Krupenina NA, Bulychev AA, Schreiber U (2011) Chlorophyll fluorescence images demonstrate variable pathways in the effects of plasma membrane excitation on electron flow in chloroplasts of *Chara* cells. Protoplasma 248:513–522. doi:10.1007/s00709-010-0198-5

Lucas WJ (1975a) The influence of light intensity on the activation and operation of the hydroxyl efflux system of *Chara corallina*. J Exp Bot 26:347–360

Lucas WJ (1975b) Photosynthetic fixation of ^{14}carbon by internodal cells of *Chara corallina*. J Exp Bot 26:331–346

Lucas WJ, Dainty J (1977) Spatial distribution of functional OH^- carriers along a characean internodal cell: determined by the effect of cytochalasin B on $H^{14}CO_3^-$ assimilation. J Membr Biol 32:75–92

Lucas WJ, Nuccitelli R (1980) HCO_3^- and OH^- transport across the plasmalemma of *Chara*: spatial resolution obtained using extracellular vibrating probe. Planta 150:120–131

Lunevsky VS, Zherelova OM, Vostrikov IY, Berestovsky GN (1983) Excitation of characeae cell membranes as a result of activation of calcium and chloride channels. J Membr Biol 72:43–58

Marten I, Deeken R, Hedrich R, Roelfsema MRG (2010) Light-induced modification of plant plasma membrane ion transport. Plant Biol 12:64–79. doi:10.1111/j.1438-8677.2010.00384.x

McConnaughey T (1991) Calcification in *Chara corallina*: CO_2 hydroxylation generates protons for bicarbonate assimilation. Limnol Oceanogr 36:619–628

Metraux JP, Richmond PA, Taiz L (1980) Control of cell elongation in *Nitella* by endogeneous cell wall pH gradients. Multiaxial extensibility and growth studies. Plant Physiol 65:204–210

Muto S, Izawa S, Miyachi S (1982) Light-induced Ca^{2+} uptake by intact chloroplasts. FEBS Lett 139:250–254

Nobel PS (2005) Physicochemical and environmental plant physiology. Academic, London
Ogata K, Toko K, Fujiyoshi T, Yamafuji K (1987) Electric inhomogeneity in membrane of characean internode influenced by light-dark transition, O_2, N_2, CO_2-free air and extracellular pH. Biophys Chem 26:71–81
Palmgren MG (1998) Protein gradients and plant growth: role of the plasma membrane H^+-ATPase. Adv Bot Res 28:1–70
Pavlovic A, Slovakova L, Pandolfi C, Mancuso S (2011) On the mechanism underlying photosynthetic limitation upon trigger hair irritation in the carnivorous plant Venus flytrap (*Dionaea muscipula* Ellis). J Exp Bot 62:1991–2000. doi:10.1093/jxb/erq404
Pickard WF (2003) The role of cytoplasmic streaming in symplastic transport. Plant, Cell Environ 26:1–15
Plieth C, Tabrizi H, Hansen U-P (1994) Relationship between banding and photosynthetic activity in *Chara corallina* as studied by the spatially different induction curves of chlorophyll fluorescence observed by an image analysis system. Physiol Plant 91:205–211
Plyusnina TY, Lavrova AI, Riznichenko GY, Rubin AB (2005) Modeling the pH and the transmembrane potential banding along the cell membrane of alga *Chara corallina*. Biophysics 50:434–440
Prins HBA, Snel JFH, Zanstra PE, Helder RJ (1982) The mechanism of bicarbonate assimilation by the polar leaves of *Potamogeton* and *Elodea*. CO_2 concentrations at the leaf surface. Plant, Cell Environ 5:207–214
Rayle DL, Cleland DL (1992) The acid growth theory of auxin-induced cell elongation is alive and well. Plant Physiol 99:1271–1274
Schmölzer PM, Höftberger M, Foissner I (2011) Plasma membrane domains participate in pH banding of *Chara* internodal cells. Plant Cell Physiol 52:1274–1288. doi:10.1093/pcp/pcr074
Schreiber U (2004) Pulse-amplitude (PAM) fluorometry and saturation pulse method. In: Papageorgiou G, Govindjee (eds) Chlorophyll a fluorescence: a signature of photosynthesis. Kluwer Academic Publishers, Dordrecht
Schurr U, Walter A, Rascher U (2006) Functional dynamics of plant growth and photosynthesis—from steady-state to dynamics—from homogeneity to heterogeneity. Plant, Cell Environ 29:340–352. doi:10.1111/j.1365-3040.2005.01490.x
Sehnke PC, DeLille JM, Ferl RJ (2002) Consummating signal transduction: the role of 14-3-3 proteins in the completion of signal-induced transitions in protein activity. Plant Cell 14:S339–S354. doi:10.1105/tpc.010430
Shepherd VA, Beilby MJ, Khazaaly SAS, Shimmen T (2008) Mechano-perception in *Chara* cells: the influence of salinity and calcium on touch-activated receptor potentials, action potentials and ion transport. Plant, Cell Environ 31:1575–1591
Shimmen T, Wakabayashi A (2008) Involvement of membrane potential in alkaline band formation by internodal cells of *Chara corallina*. Plant Cell Physiol 49:1614–1620. doi:10.1093/pcp/pcn136
Shimmen T, Yamamoto A (2002) Induction of a new alkaline band at a target position in internodal cells of *Chara corallina*. Plant Cell Physiol 43:980–983
Shimmen T, Yokota E (2004) Cytoplasmic streaming in plants. Curr Opin Cell Biol 16:68–72. doi:10.1016/j.ceb.2003.11.009
Siebke K, Weis E (1995) Assimilation images of leaves of *Glechoma hederacea*: analysis of non-synchronous stomata related oscillations. Planta 196:155–165
Smith JR, Walker NA (1985) Effects of pH and light on the membrane conductance measured in the acid and basic zones of *Chara*. J Membr Biol 83:193–205
Spear DG, Barr JK, Barr CE (1969) Localization of hydrogen ion and chloride ion fluxes in *Nitella*. J Gen Physiol 54:397–414
Stahlberg R, Cosgrove DJ (1997) The propagation of slow wave potentials in pea epicotyls. Plant Physiol 113:209–217
Takakura T, Fang W (2002) Climate under cover. Kluwer, Dordrecht
Tazawa M (2003) Cell physiological aspects of the plasma membrane electrogenic H^+ pump. J Plant Res 116:419–442. doi:10.1007/s10265-003-0109-3

Thiel G, Wacke M, Foissner I (2002) Ca^{2+} mobilization from internal stores in electrical membrane excitation in *Chara*. Progr Bot 64:217–233

Van Sambeek JW, Pickard BG (1976) Mediation of rapid electrical, metabolic, transpirational, and photosynthetic changes by factors released from wounds. III. Measurements of CO_2 and H_2O flux. Can J Bot 54:2662–2671

Verchot-Lubicz J, Goldstein RE (2010) Cytoplasmic streaming enables the distribution of molecules and vesicles in large plant cells. Protoplasma 240:99–107. doi:10.1007/s00709-009-0088-x

Walker NA, Smith FA, Cathers IR (1980) Bicarbonate assimilation by fresh-water charophytes and higher plants. I. Membrane transport of bicarbonate ions is not proven. J Membr Biol 57:51–58

Williamson RE, Ashley CC (1982) Free Ca^{2+} and cytoplasmic streaming in the alga *Chara*. Nature 296:647–650

Chapter 13
Functional Characterization of Plant Ion Channels in Heterologous Expression Systems

Yi Wang

Abstract Plant ion channels have been confirmed as the most important membrane proteins mediating ion fluxes across the plant cell membrane, which play crucial roles in many physiological processes in living plant cells. According to the structural and functional diversity, plant ion channels can be divided into several distinct families and exhibit the great variation in ion permeability, gating property, tissue expression pattern, subcellular localization, physiological function, and regulatory mechanism. The genetic identification and functional characterization of plant ion channels have been considered as important aspects to investigate the plant physiological processes. Along with the development of molecular genetics and plant genome sequencing, more and more plant ion channel genes have been identified according to the structure alignment with animal ion channels. Although part of them have been characterized, the physiological functions of most plant ion channels are still obscure and need further studies. The electrophysiology is the special approach to investigate the ion channels, which help the researchers to understand the channel features and functions. The ionic currents mediated by plant ion channels could be recorded in the isolated protoplasts or organelles from various plant cells by using electrophysiological techniques. However, most of the plant cells simultaneously express a great number of diverse channels. It is extremely difficult to distinguish the currents which are mediated by the channel of interest. Therefore, the heterologous expression systems with few endogenous ionic conductances are employed to express and functionally characterize plant ion channel of interest. To data, a great number of heterologous expression systems have been developed for the ion channel characterization. Each system exhibits the unique features and is used for the characterization of different kinds of ion

Y. Wang (✉)
State Key Lab of Plant Physiology and Biochemistry, College of Biological Sciences, China Agricultural University, #2 West Yuan Ming Yuan Road, Beijing 100193, China
e-mail: yiwang@cau.edu.cn

A. G. Volkov (ed.), *Plant Electrophysiology*,
DOI: 10.1007/978-3-642-29119-7_13,

channels. The electrophysiology combining with heterologous expression systems has become the most important tool to characterize the functions of plant ion channels as well as their regulatory mechanisms. In this chapter, several commonly used heterologous expression systems are discussed, meanwhile their application in characterization of plant ion channels is also referred.

13.1 Plant Ion Channels

As the transmembrane proteins, plant ion channels locate at the plasma membrane or intracellular membrane (e.g., tonoplast, plastid, mitochondrial membranes) of living plant cells and mediate the ion fluxes across the membrane. The hydrophilic pore structures of plant ion channels form the passages which allow the solute ions to pass through at extremely high rates (10^6–10^8 ions per second through one channel protein) driven by transmembrane electrochemical potentials (Maathuis et al. 1997). Plant ion channels are expressed in various tissues and diverse cell types, and differ in terms of gating mechanisms, ion selectivity, activation kinetics as well as regulatory mechanisms (Barbier-Brygoo et al. 2000; White 2000; Lebaudy et al. 2007; Ward et al. 2009). Different plant ion channels are selectively expressed in specific tissues or cells, where they perform the appointed functions to facilitate the physiological processes of these tissues or cells. These ion channels, together with their accessory components as well as other ion transporters, establish a complicated transmembrane transport systems and play crucial roles in almost all of the plant physiological processes, including nutrition uptake, ion transport, cell growth, cell movement, signal transduction, ion homeostasis, osmoregulation, pathogen response, etc. (White 2000; Roberts 2006; Kaplan et al. 2007; Lebaudy et al. 2007; Isayenkov et al. 2010).

13.1.1 Ion Selectivity

Generally, plant ion channels could be classified into different categories according to their ion selectivity or permeability. The channels that allow the cations (e.g., K^+, Ca^{2+}) to get across are nominated as cation channels (Véry and Sentenac 2002). Correspondingly, the anion channels only mediate the anion (e.g., Cl^-, NO_3^-, malate) fluxes across the cell membrane (Barbier-Brygoo et al. 2000; De Angeli et al. 2007). Furthermore, some channels show the strict ion selectivity, which exclusively mediate the fluxes of specific ions, such as K^+ channels (Lebaudy et al. 2007), whereas a large number of plant channels are found as nonselective ion channels which compatibly permit several kinds of ions to transit (Demidchik et al. 2002).

13.1.1.1 Cation Channels

In plant cells, the most important cation channels include K^+ channels and Ca^{2+} channels. The K^+ absorption from soils as well as K^+ translocation in plants are mainly conducted by K^+ channels and transporters (Lebaudy et al. 2007). The Ca^{2+} channels are regarded as the crucial components generating the Ca^{2+} signals in plant cells (Hamilton et al. 2000; Miedema et al. 2008).

So far, a great number of genes encoding K^+ channels have been widely cloned and identified in many plant species (Véry and Sentenac 2003; Lebaudy et al. 2007; Chen et al. 2008). In *Arabidopsis*, totally 15 K^+ channels have been identified, which belong to three families according to their structures, including *Shaker*, TPK, and Kir-like families (Lebaudy et al. 2007). The Shaker family is the most important K^+ channel family in plants containing nine members in *Arabidopsis*. Most of them have been functionally characterized (except AKT5), and play crucial roles in K^+ uptake and translocation in plants (Reviewed in Gambale and Uozumi 2006). The plant TPK (tandem-pore K^+ channel) and Kir-like (K^+ inward rectifier) channels were all called KCO channels previously, which are now considered as two distinct families according to their channel structures. In *Arabidopsis*, Kir-like family has one single member (formerly called KCO3) without functional characterization. TPK family harbors five members, in which all are located at tonoplast (Voelker et al. 2006) except TPK4 at the plasma membrane (Becker et al. 2004). The TPK K^+ channels mainly participate in vacuolar K^+ transport, K^+ homeostasis, stomatal function, and pollen tube growth (Becker et al. 2004; Gobert et al. 2007).

Plenty of data have reported that the Ca^{2+} currents can be recorded in many kinds of plant cells. But most of the Ca^{2+}-permeable channels have not yet been molecularly characterized in plants. However, in *Arabidopsis* it is proposed that 41 genes (1 *TPC*, 20 *CNGCs* and 20 *GLRs*) encoding non-selective cation channels might be permeable to Ca^{2+} ions. According to the investigation of Ca^{2+} channels in animals, the unique voltage-dependent Ca^{2+} channel homolog (*TPC*1) was identified in plants, which encodes a slow vacuolar (SV) channel at tonoplast (Peiter et al. 2005). AtTPC1 is confirmed as a plant Ca^{2+}-permeable channel and plays roles in ABA signaling pathway (Peiter et al. 2005). With regard to *CNGC* and *GLR* families in *Arabidopsis*, AtCNGC1, AtCNGC2, and AtCNGC18 have proved the permeability to Ca^{2+} ions, when they were characterized in heterologous expression systems (Leng et al. 1999; Ali et al. 2006; Frietsch et al. 2007). Recently, the GLR1.1 and GLR3.7 were also shown to form Ca^{2+} channels and control Ca^{2+} fluxes across the plasma membrane of *Arabidopsis* pollen tubes (Michard et al. 2011).

13.1.1.2 Anion Channels

Compared with the cation channels, the genetic characterization of plant anion channels is still limited. However, the members in several gene families are considered to encode plant anion channels (Barbier-Brygoo et al. 2000; De Angeli et al. 2007). Generally, plant anion channels can be divided into two groups according to their activating times, the rapid (R-type) anion channels, and the slow (S-type) activating channels (Roberts 2006). The members in aluminum-activated malate transporter (ALMT) family are regarded as R-type anion channels in plant cells, which have been identified in many plant species (wheat, maize, *Arabidopsis*) and mainly function in the Al^{3+} resistance by releasing malate into rhizosphere (Sasaki et al. 2004; Hoekenga et al. 2006; Pineros et al. 2008). Recently, an S-type channel named SLAC1 was identified in *Arabidopsis* guard cells, involving in stomatal movement (Negi et al. 2008; Vahisalu et al. 2008). In addition, the members in chloride channel (CLC) family are also considered as the putative anion channels. However, the AtCLCa channel has been confirmed to behave as a NO_3^-/H^+ antiporter rather than a channel (De Angeli et al. 2006).

13.1.2 Gating Property

The ion channels cannot be opened or activated all the time, otherwise the cell transmembrane potentials will collapse. The opening and closing of ion channels should be precisely controlled in order to fulfill their correct physiological functions in living plant cells. This control is called "gating". According to the gating mechanism, the plant ion channels can be classified into three main categories: voltage-gated, ligand-gated, and stretch-activated ion channels (Blatt and Thiel 1993; Krol and Trebacz 2000).

13.1.2.1 Voltage-Gated Channels

The voltage-gating is the most common gating mechanism of plant channels. Most of the plant ion channels belong to this category, whose activation is dependent on the voltages across the cell membrane (membrane potential). Some of them are activated by membrane hyperpolarization (membrane potentials more negative than threshold potential); while some other channels can be opened when the membrane potential is depolarized (positive than threshold potential). Taking K^+ channels as an example, the hyperpolarization-activated K^+ channels mainly mediate the K^+ ions fluxing into the plant cells, which are also called the inwardly rectifying K^+ channels, such as AKT1 in *Arabidopsis* root cells (Hirsch et al. 1998). Comparatively, the outwardly rectifying K^+ channels are activated at membrane depolarization and lead to the K^+ release from plant cells, like GORK in *Arabidopsis* guard cells (Ache et al. 2000). As for Ca^+ channels, most of the Ca^{2+} currents

recorded at plasma membrane of plant cells are activated under hyperpolarized conditions (Gelli and Blumwald 1997; Véry and Davies 2000; Hamilton et al. 2000). However, some depolarization-activated Ca^{2+} channels were still found in plant cells (Huang et al. 1994; Thuleau et al. 1994; Miedema et al. 2008).

13.1.2.2 Ligand-Gated Channels

This type of channels harbors the special domain that could bind various chemical messengers usually called ligand, such as amino acids, monoamines, and other biogenic amines. The channel opening and closing are controlled by the binding of ligand. The ligand-gated ion channels are first investigated in animals. Two main kinds of ligand-gated ion channels are found in animal cells including cyclic nucleotide-gated channel (CNG) family and ionotropic glutamate receptor (iGluR) family (Dingledine et al. 1999; Kaupp and Seifert 2002). Along with the accomplishment of *Arabidopsis* genome sequencing, it seems that the ligand-gated channels also exist in plant cells. By using the sequence alignment, the cyclic nucleotide-gated channel (CNGC) family and GLR (glutamate receptor-like) family are identified in plants. In *Arabidopsis*, each of these two families harbors 20 members, which show the sequence similarity with their homolog CNG and iGluR in animals (Davenport 2002; Talke et al. 2003; Kaplan et al. 2007).

The results of electrophysiological experiments in heterologous systems have showed that some CNGC channels could be activated by cyclic nucleotides (Leng et al. 1999, 2002), which suggest CNGCs might be the downstream targets of cyclic nucleotide signals. In addition, some CNGCs could mediate the Ca^{2+} currents across the plasma membrane and generate the cytoplasmic Ca^{2+} signals (Leng et al. 1999; Ali et al. 2006). Therefore, the CNGCs are considered as the prime components which connect the cyclic nucleotide signals and Ca^{2+} signals in plants (Talke et al. 2003). Compared with CNGC channels, the functional identification of GLR channels in plants is still scarce. A recent report has revealed that some GLR channels may also control the Ca^{2+} fluxes across the plasma membrane in plant cells (Michard et al. 2011).

13.1.2.3 Stretch-Activated Channels

This kind of channels could be activated by the stretch force applied on the cell membrane, and are usually called mechanosensitive channels (MS channels) as well (Sachs 2010). Although the stretch-activated currents have been recorded in various types of plant cells (Qi et al. 2004; Dutta and Robinson 2004; Zhang et al. 2007), the genetic identification of these channels is still obscure. Recently, a new gene family *MSL* containing 10 members has been reported to encode the MS channels in *Arabidopsis* (Haswell and Meyerowitz 2006). And some of them have been shown the MS channel activities (Haswell et al. 2008). So far, a

number of putative MS channel genes have also been predicted in other plant species, six genes in rice and at least seven genes in poplar tree (Haswell 2007). However, the characterization of these MS channels is still devoid, which needs further studies.

13.2 Functional Characterization of Plant Ion Channels in Heterologous Expression Systems

The expression and characterization of ion channels in heterologous expression systems are prevalent, but important approaches to analyze ion channel functions and their biophysical properties, such as ion selectivity, gating property, pivotal amino acid loci, structure–function relationship, regulatory mechanism, etc. This approach together with electrophysiological techniques provides the opportunity to study the ion channel of interest in vitro. But why do researchers employ the heterologous systems for the investigation of ion channels? The main reason is to exclude the interference of any other unconcerned channels in native cells. Generally, one plant cell expresses different kinds of ion channels, which often work together and jointly participate in plant physiological processes. The ionic currents recorded in native plant cells are composed of various kinds of currents from different ion channels. It is hard to distinguish the different channel currents and seek out the currents mediated by the channel of interest. Therefore, the expression and characterization of a given channel in heterologous systems with clean background could avoid from the interference of other channels. Second, the channel currents in native cells may be too small to be analyzed. The expression of channel in heterologous systems will amplify the channel currents by increasing the number of expressed channel proteins, which facilitates the current recording and analysis. Besides, the heterologous systems also show the remarkable advantages when they are utilized to study the channel pivotal amino acid loci, structure–function relationship, channel assembling, and stoichiometry of channel subunits, etc.

However, the disadvantages of heterologous systems should also be noticed. After all, they are in vitro systems; the data from heterologous systems cannot substitute the in vivo experiments. The functional expression of a channel in native cells requires a large number of regulatory proteins or accessory proteins which are involved in channel trafficking, targeting, assembling, and post-translational modification. The heterologous systems may lack these native regulatory proteins, which sometimes leads to the incorrect expression or distorted channel features compared with native cells.

So far, a series of heterologous expression systems has been developed for the characterization of ion channels. All these systems possess their own features and could be selectively used according to the experimental demands. However, these heterologous systems also show some common characters: (1) lack endogenous

ion transport activity ("electrically silent"); (2) permit the expression of various foreign genes; (3) foreign genes can be transferred into the systems with high rates; (4) can be used for electrophysiological recording; etc. In this section, several commonly used heterologous expression systems are described, whose features as well as application examples are also referred.

13.2.1 Xenopus Oocytes

The *Xenopus* oocytes perhaps is the most important heterologous expression system used for ion channel characterization, which is based on oocytes of South African clawed frog (*Xenopus laevis*) and two-electrode voltage clamp (TEVC) technique. Since the first ion channel was expressed in *Xenopus* oocytes (Gundersen et al. 1984), this expression system has been extensively used and well developed in ion channel investigation. To be an optimal heterologous expression system for channel characterization, it possesses many unique advantages (Weber 1999; Goldin 2006).

First of all, the experimental operations of this expression system are relatively easy, including oocyte isolation, RNA (or DNA) injection, oocyte incubation, and current recording. One donor frog can provide hundreds of oocytes each time, which are surgically isolated but without sacrificing the frog. So one frog can be used for several times. The isolated oocytes are extraordinarly huge (up to 1.3 mm in diameter). Therefore, it is very easy to handle the oocytes, such as oocyte transfer, RNA (or DNA) injection as well as impalement with electrodes. When recording the channel currents using TEVC in oocytes, it requires two electrodes impaling into one oocyte for voltage recording and current injection, respectively. This operation is much easier than patch-clamping which uses one electrode to get a patch on the surface of cell membrane.

Second, the oocytes are so hard that the isolated oocytes can survive in the liquid solution for upto 2 weeks, as long as the incubating temperature is under control. Furthermore, one oocyte can endure the impalement with multiple electrodes at the same time. This makes it possible to test the rapid responses of channels (e.g., ligand-gated channels) by injecting the reagent (e.g., channel activator, blocker) into oocyte when recording the currents. Once starting to record currents, the TEVC recording is very stable, which prolongs the recording time. It might be useful to analyze the slowly activated/inactivated channels.

Third, oocyte is a high efficient protein expression system, which can generate much more channel proteins than any other heterologous expression systems. Therefore, the large currents can be recorded in oocytes, which may facilitate the current analysis. In addition, the oocytes faithfully express injected RNA in a dose-dependent manner. It is feasible to control the current amplitude within a proper range by adjusting the amount of injected RNA. Besides, multiple proteins or channels can be expressed in one oocyte at the same time, which makes it convenient to analyze the channel assembling or regulation. The expression levels of

different proteins can be easily controlled by adjusting the ratio of different RNA samples.

Fourth, several different electrophysiological techniques including TEVC, cut-open oocyte voltage clamp, macropatch voltage clamp, and patch-clamp (for single channel recording) have been developed for *Xenopus* oocytes in order to obtain the low-noise, fast-clamp recordings. These different techniques can be all carried out in this system to meet diverse experimental demands.

Although *Xenopus* oocyte is an optimal heterologous expression system, it still has some disadvantages. Nevertheless, these drawbacks can be partially avoided by means of methods. Generally, the oocytes are electrically silent, but sometimes partial oocytes express a few endogenous channels that cause endogenous currents. However, these endogenous currents are relatively small. Usually, the heterologous currents mediated by expressed channels are much larger than the endogenous currents; therefore, this problem could be ignored. Another disadvantage is quality variations of oocytes owing to the seasonal factor and temperature. Summer or high temperature may affect the status of frogs and deteriorate the oocytes rapidly. Sometimes, the oocytes from different frogs might show the great variation. Therefore, it is important to breed the frogs and perform experiments at proper environmental temperature (18–20°C). In addition, the membrane capacitance of oocyte is extremely large due to the huge size of oocyte, which increases the clamping time when the pulse voltage is changed. It is difficult to record the currents of rapidly activated channels (some voltage-gated channels in animals). Nevertheless, most of the voltage-gated channels in plant cells are slowly activated, so that the large capacity transient would not be a problem for plant channel characterization in oocytes.

The *Xenopus* oocyte is first used to identify animal ion channels and receptors in 1980s (Miledi et al. 1982; Gundersen et al. 1984). Almost 10 years later, the plant channels and receptors were initially characterized in this system (Boorer et al. 1992; Cao et al. 1992; Schachtman et al. 1992), which has become the primary approach for plant ion channel investigations. The *Arabidopsis* K^+ channel KAT1 is the first characterized plant channel in *Xenopus* oocytes (Schachtman et al. 1992). After that, more and more plant ion channels have been expressed and functionally characterized in this system. Taking plant K^+ channels as an example, most of the *Shaker* K^+ channels (except SPIK and AKT5) and one TPK channel (AtTPK4) have been functionally identified as voltage-dependent channels in *Xenopus* oocytes (Becker et al. 2004; Gambale and Uozumi 2006; Xu et al. 2006; Wang et al. 2010). With regard to the ligand-gated channels, only few CNGC channels have been identified in *Xenopus* oocyte. AtCNGC2 and AtCNGC4 were both identified as cNMP-activated K^+ channels in oocytes, whereas AtCNGC4 showed the permeability to Na^+, but AtCNGC2 did not (Leng et al. 1999; Balague et al. 2003).

The first identified plant anion channel in *Xenopus* oocytes is a voltage-dependent chloride channel CLC-Nt1 from tobacco, which elicits slowly activating inward currents upon membrane hyperpolarization condition in oocytes (Lurin et al. 1996). After that, some R-type anion channels from ALMT family were also

characterized in *Xenopus* oocytes, including TaALMT1, AtALMT1, AtALMT9, and AtALMT12 (Sasaki et al. 2004; Hoekenga et al. 2006; Kovermann et al. 2007; Meyer et al. 2010). Interestingly, AtALMT9 was confirmed as a tonoplast-located channel; however, it could still be functionally expressed in oocytes (Kovermann et al. 2007). It is suggesting that the channel localization of AtALMT9 in oocytes might be totally changed (Kovermann et al. 2007). For the S-type anion channels, the SLAC1 was recently characterized in oocytes, but whose functional expression in oocytes needs the presence of protein kinase OST1 and calcium-dependent protein kinases (CPKs) (Geiger et al. 2009a, 2010).

13.2.2 Mammalian Cells

Mammalian cell is another extensively used heterologous expression system, which is an alternative when the channel could not be functionally expressed in *Xenopus* oocytes. A series of mammalian cell lines have been developed as host cells for the expression of heterologous channels, including human embryonic kidney (HEK) (HEK epithelial cell line), COS (African Green Monkey kidney fibroblast cell line), Chinese hamster ovary (CHO) (CHO cell line), etc. Usually, the channel cDNA is constructed into a plasmid vector, and then transfected into cell lines. According to the experimental demands, the transient expression or stable expression of ion channels in host cells can be selected and used. The former is commonly utilized for the identification of plant channels. As a popular transient expression system, the advantages of mammalian cells are obvious (Thomas and Smart 2005; Clare 2006). First of all, the propagation rate of cell lines is extremely high, which could generate a mass of cells for experiments. The high transfection efficiency and high protein yield could fulfill the demands of biochemical studies as well as electrophysiological experiments. Second, the operations for cell transfection, reproduction, and maintenance have been well developed, so that it is very quick and easy to start the research. A wide variety of expression vectors and transfection methods are available for cell transfection. In many cases, the same plasmid vector can be compatibly used for different cell lines, which may facilitate the investigation in several cell lines simultaneously. In addition, the mammalian cells are appropriate for patch-clamping experiments because of two main reasons. Compared with plant protoplasts, the mammalian cells have clean surface which makes it much easier to obtain the high seal resistance between capillary and cell surface. Small cell size reduces the clamping time when the pulse voltage is changed, which is more suitable for the characterization of fast activated channels.

Nevertheless, the disadvantages of mammalian cells should also be noticed (Thomas and Smart 2005; Clare 2006). Despite the high transfection efficiency, the host cells cannot be transfected at 100%, which causes a little difficulty to choose cells for patch-clamping without marker proteins. It is the common phenomenon that the transient transfection efficiency is highly dependent on the selected vector and cell type. The cell-to-cell variation of gene expression levels seems to be

another inevitable problem that results in the variation of electrophysiological data. In some cases, overexpression of channels may lead to the cytotoxicity which depresses the cell growth and viability. The cytotoxicity is probably caused by two reasons, including energy over exhausting of host cells and accumulation of misfolded proteins in host cells. Furthermore, it is not convenient to co-express multi proteins in one mammalian cell using transient transfection approach. And the expression levels of different proteins in one cell are also out of control compared with *Xenopus* oocytes. This might be a drawback when the regulatory mechanisms of channel subunits or accessary proteins are investigated in mammalian cells.

As an alternative system, a number of plant ion channels have been characterized in mammalian cells. Some of these channels can be functionally expressed in both *Xenopus* oocytes and mammalian cells, such as KAT1 (Schachtman et al. 1992; Szabo et al. 2000), KAT2 (Pilot et al. 2001; Ivashikina et al. 2005), AKT2 (Cao et al. 1995; Ivashikina et al. 2005), and AtCNGC2 (Leng et al. 1999, 2002). These channels showed the similar channel activities and gating properties in these two expression systems. It is demonstrated that these channels may possess the similar regulatory mechanisms. *Xenopus* oocytes and mammalian cells both contain the regulators or accessory proteins of these channels which are similar as those regulators in native plant cells. On the other hand, a few of plant channels are only expressed in mammalian cells, but not in *Xenopus* oocytes. SPIK is a pollen-specific K^+ channel mediating K^+ fluxes across the plasma membrane of pollen tubes in *Arabidopsis*, whose channel activity was identified in COS7 cells rather than *Xenopus* oocytes (Mouline et al. 2002). The SPIK channels expressed in COS7 cells displayed the similar channel properties as in pollen protoplasts, including activation kinetics, gating charge, sensitivity to external pH (Mouline et al. 2002). However, the activation threshold of SPIK was negatively shifted in COS7 cells (−125 mV) compared with pollen protoplasts (−100 mV) (Mouline et al. 2002). It is speculated that the channel activities in heterologous systems are sensitive and alterable, which is heavily dependent on the host processing machineries for channel proteins such as translation, trafficking, protein modification, and regulation (Mouline et al. 2002).

13.2.3 Insect Cells

The insect cell, similar to mammalian cell, is another available system for the heterologous expression of foreign proteins by infection of recombinant baculovirus (King and Possee 1992). The most used insect cell line Sf9 (*Spodoptera frugiperda*) exhibits the similar characters as mammalian cell lines when used for channel characterization. Therefore, it is an alternative method when the identification of channels in mammalian cells failed. For example, K^+ channels AKT1 and SKT1 both belong to the plant *Shaker* family and show the high similarity of amino acid sequence (Gambale and Uozumi 2006). The initial attempts to express

these two channels in either *Xenopus* oocytes or mammalian cells are both unsuccessful (Gaymard et al. 1996; Dreyer et al. 1997; Zimmermann et al. 1998), whereas by using baculovirus-infected insect cells, AKT1, and SKT1 are successfully expressed and functionally characterized in Sf9 cells (Gaymard et al. 1996; Zimmermann et al. 1998). It is suggested that the particular regulators or accessory proteins of these two channels exist in insect cells rather than in *Xenopus* oocytes or mammalian cells. The insect cells have been proved as an available system for the characterization of plant K^+ channels; however, this system still has an obvious disadvantage. The Sf9 cells usually could not sustain the hyperpolarized voltage and collapse down when the membrane potential is beyond −100 mV (Gaymard et al. 1996). Reducing the expression level of K^+ channels in cells could partially avoid this problem, whereas, Sf9 cells might not be the optimal system for the electrophysiological characterization of voltage-dependent channels, especially for the hyperpolarization-activated channels (Gaymard et al. 1996). Due to this drawback, the insect cell is rarely used for the identification of plant ion channels.

13.2.4 Microorganism Cells

In many investigations, the microorganisms such as yeast (*Saccharomyces cerivisiae*) and *Escherichia coli* were also employed as heterologous expression systems for the identification of plant ion channels. These two systems have been extensively used for the genetic manipulation, production of heterologous proteins, and functional analysis of foreign genes, due to their several advantages: small cell size, rapid growth and reproduction rates, easy transformation methods, high yield of protein production, etc. For the functional characterization of plant ion channels, two methods using these two systems are developed, including complement experiment in mutant strains and electrophysiological recording in spheroplasts.

Owing to the facility of genetic manipulation in microorganism cells, a great number of mutant strains of yeast and *E. coli* have been obtained. The heterologous ion channels can be functionally characterized in the appropriate mutant strains whose endogenous channels (or transporters) are deleted or lost. For example, the yeast mutant strain *trk*1Δ *trk*2Δ (deletion of two K^+ transporters *TRK*1 and *TRK*2) is first utilized to identify plant K^+ channels by using the complement experiments. When the plant K^+ channels AKT1 and KAT1 were, respectively, expressed in *trk*1Δ *trk*2Δ strain, the K^+ transport-deficient phenotype of *trk*1Δ *trk*2Δ was significantly suppressed (Anderson et al. 1992; Sentenac et al. 1992) so that, the K^+ transport activities of AKT1 and KAT1 were confirmed. Furthermore, the K^+ uptake-deficient *E. coli* mutant strain LB2003 was also employed to characterize plant K^+ channels (Uozumi et al. 1998). AKT2 and KAT1 could functionally complement the K^+ uptake-deficient phenotype of LB2003 strain and remarkably rescue the growth of LB2003 strain at low K^+ concentrations (Uozumi et al. 1998).

On the other hand, the yeast cells and *E. coli* cells can also be used for the electrophysiological characterization of ion channels. Originally, these two systems are not suitable to apply the standard electrophysiological techniques. First, the main disadvantage is the extremely small size of cells which makes it difficult to patch a cell. The diameter of yeast cell usually is smaller than 10 μm; an *E. coli* cell is only 1 μm in diameter and 2 μm long. However, this problem can be partially resolved by means of approaches. By improving the nutrition in medium and choosing multiploid strain, the yeast cells with larger diameters could be obtained, which are big enough for the electrophysiological experiments (Bertl et al. 1998). For the *E. coli* cells, the cephalexin is employed to block the cell septation but without inhibiting cell growth. As a result, the long filamentous cells are obtained, which can be used to isolate the giant spheroplasts (5–10 μm in diameter) for patch-clamping (Martinac et al. 1987). Second, the yeast cells as well as *E. coli* cells are both covered with cell walls which must be removed before the electrophysiological experiments. For this reason, the spheroplasts isolated from yeast or *E. coli* cells are more difficult to form gigaseal between cell surface and capillary than mammalian cells.

Since both these systems have obvious drawbacks, why do the researchers still utilize them? It is because these two systems could be used for the specific purposes in channel characterization which cannot be achieved in any other heterologous expression systems. Similar to plant cells, the yeast cells also have vacuoles, therefore not only the PM-located channels, but also the tonoplast-located channels can be expressed and characterized in yeast cells by using patch-clamping experiments. For example, the *trk*1Δ *trk*2Δ yeast cells which lack the fast-activating inward currents across the PM provide the clean background for the electrophysiological characterization of plant PM-located inward K^+ channels AKT1 and KAT1 (Bertl et al. 1995, 1997). Besides, some tonoplast-located plant channels, such as AtTPK1 (*Arabidopsis*) and NtTPK1 (tobacco), were also characterized as K^+-selective channels when functionally expressed in yeast vacuoles (Hamamoto et al. 2008; Latz et al. 2007). This special character makes yeast cells as the unique heterologous system for the molecular identification of tonoplast-located plant channels in future.

With regard to *E. coli* cells, it is a special heterologous system used for the characterization of stretch-activated channels (or MS channels). The endogenous MS channels of *E. coli* have been extensively investigated already (Martinac 2001; Strop et al. 2003). The *E. coli* mutant strains lacking endogenous MS channel genes could be employed to express and characterize the heterologous MS channels (Levina et al. 1999). To date, several MS channels from archaebacteria and protists have been successfully characterized in this system (Kloda and Martinac 2001; Nakayama et al. 2007). Recently, a great number of putative MS channels have been predicted in higher plants (*Arabidopsis*, rice, poplar tree) (Haswell and Meyerowitz 2006; Haswell 2007), and a few of them were confirmed as MS channels (Haswell et al. 2008). However, most of these putative plant MS channels have not been functionally identified yet. Therefore, the heterologous expression

and electrophysiological characterization of these channels in *E. coli* cells will be an important approach to reveal the functions and properties of plant MS channels.

13.2.5 Plant Cells

The expression systems referred above are all derived from animals or microorganisms, which would not be appropriate for the characterization of plant ion channels in some cases. Part of plant channels could not be functionally expressed in these systems due to many unpredictable problems, such as RNA translation, protein targeting, protein modification, regulator interacting, and so on. Therefore, a new expression system with plant native background is demanded, which may conquer these problems of compatibility between animals and plants. In recent years, the tobacco mesophyll cells have become the very new expression system for the characterization of plant channels relying on the transient transformation of tobacco leaves (Bei and Luan 1998; Hosy et al. 2005). Because of lacking inward K^+ currents, tobacco mesophyll protoplasts are regarded as a fine system to characterize the plant inward K^+ channels, even some other channels (Bei and Luan 1998; Hosy et al. 2005). In addition, the tonoplast-located channels can also be identified in this system by using the isolated vacuoles from mesophyll protoplasts. Several K^+ channels from plant *Shaker* family have been already expressed and characterized in this systems, including AKT1, AKT2, KAT1, AtKC1, and KDC1 (Bei and Luan 1998; Hosy et al. 2005; Latz et al. 2007; Bregante et al. 2008; Duby et al. 2008).

It is noticeable that one plant channel sometimes exhibits the different properties when identified in various systems (animal cells and tobacco mesophyll protoplasts) (Hosy et al. 2005; Latz et al. 2007). It is suggested that plant channel features may be distorted when identified in animal cells. In this case, the characterization of a plant channel in tobacco mesophyll protoplasts become important, and may provide the correct channel information. Nevertheless, a minor drawback of this system is also observed. The transient transformation efficiency and channel expression levels in protoplasts showed significant cell-to-cell variations (Duby et al. 2008), which brings a little difficulty to statistically analyze the electrophysiological data.

13.3 Investigation of Channel Regulatory Mechanisms in Heterologous Expression Systems

The natural activities of ion channels in plant cells require the presence of correct regulators or accessory proteins which participate in many important processes, including channel trafficking, targeting, assembling, post-translational modification, etc. Lack of native regulators may lead to the incorrect channel activities even if their is no activity when the channel is expressed in heterologous systems. This is perhaps the main reason why many plant ion channels often display the

distorted features in heterologous systems compared with native cells. Therefore, the identification of these channel regulators would be a crucial approach to investigate the regulatory mechanisms of plant ion channels.

In plants, a number of channel regulators have been identified, which play important roles in facilitating the ion channels with correct activities. More and more data have confirmed that the plant ion channels are regulated in several different aspects, including trafficking, assembling, and phosphorylation status (Chérel et al. 2002; Li et al. 2006; Xu et al. 2006; Lee et al. 2007; Geiger et al. 2009a, b; Honsbein et al. 2009; Wang et al. 2010; Held et al. 2011). And these regulatory mechanisms have already been investigated in heterologous systems. Interestingly, all these regulators were characterized in *Xenopus* oocytes. It is suggested that *Xenopus* oocytes would be a perfect system used for the characterization of plant ion channel regulators. According to their functions, the regulators could be divided into two main groups. Some of them positively regulate the channels by activating or increasing channel activities. Meanwhile others perform as negative modulators that inhibit or inactivate the channel activities. Choosing a proper heterologous expression system would be a pivotal premise when the positive or negative regulators are identified in vitro.

13.3.1 Positive Regulatory Mechanisms

Some plant ion channels cannot be functionally expressed in heterologous systems alone, perhaps due to lack of proper positive regulators in the systems. Although it is unfortunate that the channel properties cannot be studied in this system, this system on the contrary could be considered as an optimal tool for the characterization of channel positive regulators. The candidate protein, which elicits the channel currents when co-expressed with the channel protein in this system, would be regarded as a positive regulator of this channel.

Plenty of data have revealed that the phosphorylation status is a vital factor controlling the plant channel activities. Many protein kinases have been confirmed as positive regulators of plant ion channels. Taking K^+ channel AKT1 as an example, the former studies found that AKT1 itself cannot form a functional channel when expressed in *Xenopus* oocytes alone (Gaymard et al. 1996). This problem was not solved until AKT1 positive regulators were found. Xu et al. 2006 identified the candidate regulators of AKT1 channel, including a Ser/Thr protein kinase CIPK23 (CBL-interacting protein kinase) as well as its interacting proteins CBL1, and CBL9 (calcineurin B-like protein). The CIPK23 interacts with AKT1 and phosphorylates AKT1 protein at the plasma membrane together with CBL1 or CBL9. Only in circumstances where AKT1, CIPK23, and CBL1 (or CBL9) were co-expressed in *Xenopus* oocytes, the AKT1-mediated inward K^+ currents could be observed (Li et al. 2006; Xu et al. 2006). This is a successful example to characterize the positive regulators of plant ion channels in heterologous system. After that, this system was also used to determine the anion channel regulators.

The anion channel SLAC1 can be phosphorylated and activated by two protein kinases OST1 (open stomata 1, SnRK2.6) and CPK23. SLAC1-mediated anion currents were also recorded in *Xenopus* oocytes when co-expressed with OST1 or CPK23, respectively (Lee et al. 2009; Geiger et al. 2009a, 2010). Although many protein kinases were found as positive regulators of ion channels, it does not mean that protein kinases regulate ion channel via phosphorylation at all time. Recent report showed that AKT2-mediated K^+ currents in *Xenopus* oocytes were remarkably increased when co-expressed with CIPK6 and CBL4 (Held et al. 2011). The protein kinase CIPK6 could interact with AKT2, but do not phosphorylate AKT2. The CIPK6/CBL4 complex increased AKT2 currents by enhancing the translocation of AKT2 channel from ER to PM in a kinase interaction-dependent, but phosphyorylation-independent way (Held et al. 2011).

13.3.2 Negative Regulatory Mechanisms

The plant channel activities must be strictly controlled during the plant growth and development processes, or under the various environmental conditions. In some circumstances, the channel activities should even be inhibited for the accurate physiological processes. Therefore, the negative regulators of ion channels are also important for the living plant cells. To study a negative regulator in heterologous systems, it is a precondition that the ion channel should be functionally expressed in the heterologous system first. Then the inhibition of the negative regulator can be determined when the channel and regulator are co-expressed in the heterologous system.

It has been known that the channel activities can be controlled by phosphorylation status. Since the protein kinases could activate the channel via phosphorylation, there must be a series of protein phosphatases in plant cells which negatively modulate the channel activity through dephosphorylation. So far, two protein phosphatases from 2C-type protein phosphatase (PP2C) family have been identified in plants, whose regulatory functions on K^+ channels were subsequently confirmed in *Xenopus* oocytes. The protein phosphatase AIP1, as the opposite of CIPK23, was found to inhibit AKT1-mediated K^+ currents and inactivate AKT1 channel in *Xenopus* oocytes via dephosphorylation in the presence of CIPK23 and CBL1/9 (Lee et al. 2007). CIPK23 and AIP1 interact with each other and regulate AKT1 activity interchangeably by modifying the phosphorylation status of AKT1 channel (Lee et al. 2007). In addition, the similar inhibitory regulation was also identified between AKT2 and AtPP2CA, which was validated in *Xenopus* oocytes (Chérel et al. 2002).

Besides the phosphorylation regulation, the channel assembling or heteromerization of different channel subunits was shown as another important regulatory mechanism. It is well-known that many animal K^+ channels could assemble together and form heteromeric K^+ channels (Salinas et al. 1997). This regulation was also detected in plant cells. AtKC1 is reported as an α-subunit of *Shaker* K^+

channel family, and AtKC1 alone do not form functional K^+ channel in heterologous expression systems (Reintanz et al. 2002). However, when co-expressed with AKT1 in *Xenopus* oocytes (together with CIPK23 and CBL1/9), AtKC1 remarkably inhibited AKT1-mediated inward K^+ currents and negatively shifted the voltage dependence of AKT1 channel (Geiger et al. 2009b; Wang et al. 2010). It is suggested that AtKC1 interacts with AKT1 and inhibits AKT1 channel activity by forming the AKT1/AtKC1 heteromeric K^+ channels in plant cells (Geiger et al. 2009b; Wang et al. 2010).

13.4 Conclusion

In summary, the heterologous expression systems combining with electrophysiological techniques have become the most powerful tools for expression and characterization of plant ion channels. Along with the development of plant genome sequencing, more and more plant ion channels have been identified, and subsequently characterized in various heterologous systems using reverse genetics approach. This chapter attempts to highlight the features of different heterologous expression systems when used for plant ion channel characterization. Each of them exhibits their own advantages as well as disadvantages. It is common that many plant channels cannot be functionally expressed in every heterologous system. Although the channel could be simultaneously expressed in several systems, the channel properties derived from different systems may be still diverse. Therefore, choosing a proper expression system would be the sticking point to successfully characterize a plant ion channel of interest and obtain the correct features of the channel. Actually, it is usually impossible to predict a particular system that will be the proper one for functional characterization of a given channel, especially for a novel channel. The attempts in different heterologous systems in parallel are worth to carry out, and then the optimal system should be found. Although the heterologous systems have been successfully used for the channel identification, there is still an important issue that should be noticed. The channel characterization in heterologous systems is the in vitro experiments after all, which cannot completely imitate the status of channel in native plant cells. Therefore, the results derived from heterologous systems should be carefully analyzed and interpreted when the channel features are investigated.

References

Ache P, Becker D, Ivashikina N, Dietrich P, Roelfsema RG, Hedrich R (2000) GORK, a delayed outward rectifier expressed in guard cells of *Arabidopsis thaliana*, is a K^+-selective, K^+-sensing ion channel. FEBS Lett 486:93–98

Ali R, Zielinski RE, Berkowitz GA (2006) Expression of plant cyclic nucleotide-gated cation channels in yeast. J Exp Bot 57:125–138

Anderson JA, Huprikar SS, Kochian LV, Lucas WJ, Gaber RF (1992) Functional expression of a probable *Arabidopsis thaliana* potassium channel in *Saccharomyces cerevisiae*. Proc Nat Acad Sci USA 89:3736–3740

Balague C, Lin B, Alcon C, Flottes G, Malmstrom S, Kohler C, Neuhaus G, Pelletier G, Gaymard F, Roby D (2003) HLM1, an essential signaling component in the hypersensitive response, is a member of the cyclic nucleotide gated channel ion channel family. Plant Cell 15:365–379

Barbier-Brygoo H, Vinauger M, Colcombet J, Ephritikhine G, Frachisse J-M et al (2000) Anion channels in higher plants: functional characterization, molecular structure and physiological role. BBA-Biomembr 1465:199–218

Becker D, Geiger D, Dunkel M, Roller A et al (2004) AtTPK4, an *Arabidopsis* tandem-pore K^+ channel, poised to control the pollen membrane voltage in a pH- and Ca^{2+}-dependent manner. Proc Nat Acad Sci USA 101:15621–15626

Bei Q, Luan S (1998) Functional expression and characterization of a plant K^+ channel in a plant cell model. Plant J 13:857–865

Bertl A, Anderson JA, Slayman CL, Gaber RF (1995) Use of *Saccharomyces cerevisiae* for patch-clamp analysis of heterologous membrane proteins: characterization of Kat1, an inward-rectifying K^+ channel from *Arabidopsis thaliana*, and comparison with endogeneous yeast channels and carriers. Proc Nat Acad Sci USA 92:2701–2705

Bertl A, Reid JD, Sentenac H, Slayman CL (1997) Functional comparison of plant inward-rectifier channels expressed in yeast. J Exp Bot 48:405–413

Bertl A, Bihler H, Kettner C, Slayman CL (1998) Electrophysiology in the eukaryotic model cell *Saccharomyces cerevisiae*. Pflugers Arch 436:999–1013

Blatt MR, Thiel G (1993) Hormonal control of ion channel gating. Annu Rev Plant Physiol Plant Mol Biol 44:543–567

Boorer KJ, Forde BG, Leigh RA, Miller AJ (1992) Functional expression of a plant plasma membrane transporter in *Xenopus* oocytes. FEBS Lett 302:166–168

Bregante M, Yang Y, Formentin E, Carpaneto A, Schroeder J et al (2008) KDC1, a carrot Shaker-like potassium channel, reveals its role as a silent regulatory subunit when expressed in plant cells. Plant Mol Biol 66:61–72

Cao Y, Anderova M, Crawford NM, Schroeder JI (1992) Expression of an outward-rectifying potassium channel from maize mRNA and complementary RNA in *Xenopus* oocytes. Plant Cell 4:961–969

Cao Y, Ward JM, Kelly WB, Ichida AM, Gaber RF, Anderson JA, Uozumi N, Schroeder JI, Crawford NM (1995) Multiple genes, tissue specificity, and expression dependent modulation contribute to the functional diversity of potassium channels in *Arabidopsis thaliana*. Plant Physiol 109:1093–1106

Chen YF, Wang Y, Wu WH (2008) Membrane transporters for nitrogen, phosphate and potassium uptake in plants. J Integr Plant Biol 50:835–848

Chérel I, Michard E, Platet N, Mouline K, Alcon C, Sentenac H, Thibaud JB (2002) Physical and functional interaction of the *Arabidopsis* K^+ channel AKT2 and phosphatase AtPP2CA. Plant Cell 14:1133–1146

Clare JJ (2006) Functional expression of ion channels in mammalian systems. In: Clare JJ, Trezise DJ (eds) Expression and analysis of recombinant ion channels. WILEY-VCH Verlag GmbH & Co. KGaA, Weinheim

Davenport R (2002) Glutamate receptors in plants. Ann Bot 90:549–557

De Angeli A, Monachello D, Ephritikhine G, Frachisse J, Thomine S et al (2006) The nitrate/proton antiporter AtCLCa mediates nitrate accumulation in plant vacuoles. Nature 442: 939–942

De Angeli A, Thomine S, Frachisse J, Ephritikhine G, Gambale F et al (2007) Anion channels and transporters in plant cell membranes. FEBS Lett 581:2367–2374

Demidchik V, Davenport RJ, Tester M (2002) Nonselective cation channels in plants. Annu Rev Plant Biol 53:67–107

Dingledine R, Borges K, Bowie D, Traynelis SF (1999) The glutamate receptor ion channels. Pharmacol Rev 51:7–62

Dreyer I, Antunes S, Hoshi T, Müller-Röber B, Palme K, Pongs O, Reintanz B, Hedrich R (1997) Plant K^+ channel α-subunits assemble indiscriminately. Biophys J 72:2143–2150

Duby G, Hosy E, Fizames C, Alcon C, Costa A, Sentenac H, Thibaud JB (2008) AtKC1, a conditionally targeted Shaker-type subunit, regulates the activity of plant K^+ channels. Plant J 53:115–123

Dutta R, Robinson KR (2004) Identification and characterization of stretch-activated ion channels in pollen protoplasts. Plant Physiol 135:1398–1406

Frietsch S, Wang Y-F, Sladek C, Poulsen LR, Romanowsky SM et al (2007) A cyclic nucleotide-gated channel is essential for polarized tip growth of pollen. Proc Nat Acad Sci USA 104:14531–14536

Gambale F, Uozumi N (2006) Properties of Shaker-type potassium channels in higher plants. J Membr Biol 210:1–19

Gaymard F, Cerutti M, Horeau C et al (1996) The baculovirus/insect cell system as an alternative to *Xenopus* oocytes: first characterization of the AKT1 K^+ channel from *Arabidopsis thaliana*. J Biol Chem 271:22863–22870

Geiger D, Becker D, Vosloh D, Gambale F, Palme K et al (2009a) Heteromeric AtKC1-AKT1 channels in *Arabidopsis* roots facilitate growth under K^+-limiting conditions. J Biol Chem 284:21288–21295

Geiger D, Scherzer S, Mumm P, Stange A, Marten I et al (2009b) Activity of guard cell anion channel SLAC1 is controlled by drought-stress signaling kinase-phosphatase pair. Proc Nat Acad Sci USA 106:21425–21430

Geiger D, Scherzer S, Mumm P, Marten I, Ache P et al (2010) Guard cell anion channel SLAC1 is regulated by CDPK protein kinases with distinct Ca^{2+} affinities. Proc Nat Acad Sci USA 107:8023–8028

Gelli A, Blumwald E (1997) Hyperpolarization-activated Ca^{2+}-permeable channels in the plasma membrane of tomato cells. J Membr Biol 155:35–45

Gobert A, Isayenkov S, Voelker C, Czempinski K, Maathuis FJM (2007) The two-pore channel *TPK1* gene encodes the vacuolar K^+ conductance and plays a role in K^+ homeostasis. Proc Nat Acad Sci USA 104:10726–10731

Goldin AL (2006) Expression of ion channels in *Xenopus* oocytes. In: Clare JJ, Trezise DJ (eds) Expression and analysis of recombinant ion channels. WILEY-VCH Verlag GmbH & Co. KGaA, Weinheim

Gundersen CB, Miledi R, Parker I (1984) Messenger RNA from human brain induces drug- and voltage-operated channels in *Xenopus* oocytes. Nature 308:421–424

Hamamoto S, Marui J, Matsuoka K, Higashi K, Igarashi K et al (2008) Characterization of a tobacco TPK-type K^+ channel as a novel tonoplast K^+ channel using yeast tonoplasts. J Biol Chem 283:1911–1920

Hamilton DW, Hills A, Kohler B, Blatt MR (2000) Ca^{2+} channels at the plasma membrane of stomatal guard cells are activated by hyperpolarization and abscisic acid. Proc Nat Acad Sci USA 97:4967–4972

Haswell ES (2007) MscS-like proteins in plants. In: Hamill OP (ed) Mechanosensitive ion channels. Academic, San Diego

Haswell ES, Meyerowitz EM (2006) MscS-like proteins control plastid size and shape in *Arabidopsis thaliana*. Curr Biol 16:1–11

Haswell ES, Peyronnet R, Barbier-Brygoo H, Meyerowitz EM, Frachisse J-M (2008) Two MscS homologs provide mechanosensitive channel activities in the *Arabidopsis* root. Curr Biol 18:730–734

Held K, Pascaud F, Eckert C et al (2011) Calcium-dependent modulation and plasma membrane targeting of the AKT2 potassium channel by the CBL4/CIPK6 calcium sensor/protein kinase complex. Cell Res 21:1116–1130

Hirsch RE, Lewis BD, Spalding EP, Sussman MR (1998) A role for the AKT1 potassium channel in plant nutrition. Science 280:918–921

Hoekenga OA, Maron LG, Pineros MA et al (2006) *AtALMT1*, which encodes a malate transporter, is identified as one of several genes critical for aluminum tolerance in *Arabidopsis*. Proc Nat Acad Sci USA 103:9738–9743

Honsbein A, Sokolovski S, Grefen C, Campanoni P, Pratelli R et al (2009) A tripartite SNARE-K^+ channel complex mediates in channel-dependent K^+ nutrition in *Arabidopsis*. Plant Cell 21:2859–2877

Hosy E, Duby G, Very AA, Costa A, Sentenac H, Thibaud JB (2005) A procedure for localisation and electrophysiological characterisation of ion channels heterologously expressed in a plant context. Plant Methods 1:1–14

Huang JW, Grunes DL, Kochian LV (1994) Voltage-dependent Ca^{2+} influx into right-side-out plasma membrane vesicles isolated from wheat roots: characterization of a putative Ca^{2+} channel. Proc Nat Acad Sci USA 91:3473–3477

Isayenkov S, Isner JC, Maathuis FJM (2010) Vacuolar ion channels: roles in plant nutrition and signalling. FEBS Lett 584:1982–1988

Ivashikina N, Deeken R, Fischer S, Ache P, Hedrich R (2005) AKT2/3 subunits render guard cell K^+ channels Ca^{2+} sensitive. J Gen Physiol 125:483–492

Kaplan B, Sherman T, Fromm H (2007) Cyclic nucleotide-gated channels in plants. FEBS Lett 581:2237–2246

Kaupp UB, Seifert R (2002) Cyclic nucleotide-gated ion channels. Physiol Rev 82:769–824

King LA, Possee RD (1992) The baculovirus expression system: a laboratory guide. Chapman and Hall, London

Kloda A, Martinac B (2001) Molecular identification of a mechanosensitive channel in archaea. Biophys J 80:229–240

Kovermann P, Meyer S, Hortensteiner S, Picco C, Scholz-Starke J, Ravera S, Lee Y, Martinoia E (2007) The *Arabidopsis* vacuolar malate channel is a member of the ALMT family. Plant J 52:1169–1180

Krol E, Trebacz K (2000) Ways of ion channel gating in plant cells. Ann Bot 86:449–469

Latz A, Becker D, Hekman M, Müller T, Beyhl D et al (2007) TPK1, a Ca^{2+} -regulated *Arabidopsis* vacuole two-pore K^+ channel is activated by 14–3–3 proteins. Plant J 52:449–459

Lebaudy A, Véry AA, Sentenac H (2007) K^+ channel activity in plants: genes, regulations and functions. FEBS Lett 581:2357–2366

Lee SC, Lan WZ, Kim BG, Li L, Cheong YH et al (2007) A protein phosphorylation/dephosphorylation network regulates a plant potassium channel. Proc Nat Acad Sci USA 104:15959–15964

Lee SC, Lan W, Buchanan BB, Luan S (2009) A protein kinase-phosphatase pair interacts with an ion channel to regulate ABA signaling in plant guard cells. Proc Nat Acad Sci USA 106:21419–21424

Leng Q, Mercier RW, Yao W, Berkowitz GA (1999) Cloning and first functional characterization of a plant cyclic nucleotide-gated cation channel. Plant Physiol 121:753–761

Leng Q, Mercier RW, Hua B-G, Fromm H, Berkowitz GA (2002) Electrophysiological analysis of cloned cyclic nucleotide-gated ion channels. Plant Physiol 128:400–410

Levina N, Totemeyer S, Stokes NR, Louis P, Jones MA et al (1999) Protection of *Escherichia coli* cells against extreme turgor by activation of MscS and MscL mechanosensitive channels: identification of genes required for MscS activity. EMBO J 18:1730–1737

Li L, Kim B-G, Cheong YH, Pandey GK, Luan S (2006) A Ca^{2+} signaling pathway regulates a K^+ channel for low-K response in *Arabidopsis*. Proc Nat Acad Sci USA 103:12625–12630

Lurin C, Geelen D, Barbier-Brygoo H, Guern J, Maurel C (1996) Cloning and functional expression of a plant voltage-dependent chloride channel. Plant Cell 8:701–711

Maathuis FJ, Ichida AM, Sanders D, Schroeder JI (1997) Roles of higher plant K^+ channels. Plant Physiol 114:1141–1149

Martinac B (2001) Mechanosensitive channels in prokaryotes. Cell Physiol Biochem 11:61–76

Martinac B, Buechner M, Delcour AH, Adler J, Kung C (1987) Pressure-sensitive ion channel in *Escherichia coli*. Proc Nat Acad Sci USA 84:2297–2301

Meyer S, Mumm P, Imes D, Endler A, Weder B et al (2010) AtALMT12 represents an R-type anion channel required for stomatal movement in *Arabidopsis* guard cells. Plant J 63:1054–1062

Michard E, Lima PT, Borges F, Silva AC, Portes MT et al (2011) Glutamate receptor-like genes form Ca^{2+} channels in pollen tubes and are regulated by pistil D-serine. Science 332:434–437

Miedema H, Demidchik V, Véry AA, Bothwell JH, Brownlee C, Davies JM (2008) Two voltage-dependent calcium channels co-exist in the apical plasma membrane of *Arabidopsis thaliana* root hairs. New Phytol 179:378–385

Miledi R, Parker I, Sumikawa K (1982) Properties of acetylcholine receptors translated by cat muscle mRNA in *Xenopus* oocytes. EMBO J 1:1307–1312

Mouline K, Véry AA, Gaymard F, Boucherez J, Pilot G, Devic M, Bouchez D, Thibaud JB, Sentenac H (2002) Pollen tube development and competitive ability are impaired by disruption of a Shaker K^+ channel in *Arabidopsis*. Genes Dev 16:339–350

Nakayama Y, Fujiu K, Sokabe M, Yoshimura K (2007) Molecular and electrophysiological characterization of a mechanosensitive channel expressed in the chloroplasts of *Chlamydomonas*. Proc Nat Acad Sci USA 104:5883–5888

Negi J, Matsuda O, Nagasawa T, Oba Y, Takahashi H et al (2008) CO_2 regulator SLAC1 and its homologues are essential for anion homeostasis in plant cells. Nature 452:483–486

Peiter E, Maathuis FJM, Mills LN, Knight H, Pelloux J et al (2005) The vacuolar Ca^{2+}-activated channel TPC1 regulates germination and stomatal movement. Nature 434:404–408

Pilot G, Lacombe B, Gaymard F, Cherel I, Boucherez J, Thibaud JB, Sentenac H (2001) Guard cell inward K^+ channel activity in *Arabidopsis* involves expression of the twin channel subunits KAT1 and KAT2. J Biol Chem 276:3215–3221

Pineros MA, Cancado GM, Maron LG, Lyi SM, Menossi M, Kochian LV (2008) Not all ALMT1-type transporters mediate aluminum-activated organic acid responses: the case of ZmALMT1 - an anion-selective transporter. Plant J 53:352–367

Qi Z, Kishigami A, Nakagawa Y, Iida H, Sokabe M (2004) A mechanosensitive anion channel in *Arabidopsis thaliana* mesophyll cells. Plant Cell Physiol 45:1704–1708

Reintanz B, Szyroki A, Ivashikina N, Ache P, Godde M, Becker D, Palme K, Hedrich R (2002) AtKC1, a silent Arabidopsis potassium channel α-subunit modulates root hair K^+ influx. Proc Nat Acad Sci USA 99:4079–4084

Roberts SK (2006) Plasma membrane anion channels in higher plants and their putative functions in roots. New Phytol 169:647–666

Sachs F (2010) Stretch-activated ion channels: What are they? Physiology 25:50–56

Salinas M, Duprat F, Heurteaux C, Hugnot JP, Lazdunski M (1997) New modulatory alpha subunits for mammalian *shab* K^+ channels. J Biol Chem 272:24371–24379

Sasaki T, Yamamoto Y, Ezaki B, Katsuhara M, Ahn SJ, Ryan PR, Delhaize E, Matsumoto H (2004) A wheat gene encoding an aluminum-activated malate transporter. Plant J 37:645–653

Schachtman DP, Schroeder JI, Lucas WJ, Anderson JA, Gaber RF (1992) Expression of an inward-rectifying potassium channel by the *Arabidopsis* KAT1 cDNA. Science 258:1654–1658

Sentenac H, Bonneaud N, Minet M, Lacroute F, Salmon JM, Gaymard F, Grignon C (1992) Cloning and expression in yeast of a plant potassium ion transport system. Science 256:663–665

Strop P, Bass R, Rees DC (2003) Prokaryotic mechanosensitive channels. In: Rees DC (ed) Advances in protein chemistry. Membrane proteins, vol 63. Academic, Amsterdam, pp 177–209

Szabo I, Negro A, Downey PM, Zoratti M, Lo Schiavo F, Giacometti GM (2000) Temperature-dependent functional expression of a plant K^+ channel in mammalian cells. Biochem Biophys Res Commun 274:130–135

Talke IN, Blaudez D, Maathuis FJM, Sanders D (2003) CNGCs: prime targets of plant cyclic nucleotide signalling? Trends Plant Sci 8:286–293

Thomas P, Smart TG (2005) HEK293 cell line: a vehicle for the expression of recombinant proteins. J Pharmacol Toxicol Methods 51:187–200

Thuleau P, Ward JM, Ranjeva R, Schroeder JI (1994) Voltage-dependent calcium-permeable channels in the plasma membrane of a higher plant cell. EMBO J 13:2970–2975

Uozumi N, Nakamura T, Schroeder JI, Muto S (1998) Determination of transmembrane topology of an inward-rectifying potassium channel from *Arabidopsis thaliana* based on functional expression in *Escherichia coli*. Proc Nat Acad Sci USA 95:9773–9778

Vahisalu T, Kollist H, Wang Y-F, Nishimura N, Chan W-Y et al (2008) SLAC1 is required for plant guard cell S-type anion channel function in stomatal signalling. Nature 452:487–491

Véry AA, Davies JM (2000) Hyperpolarization-activated calcium channels at the tip of *Arabidopsis* root hairs. Proc Nat Acad Sci USA 97:9801–9806

Véry AA, Sentenac H (2002) Cation channels in the *Arabidopsis* plasma membrane. Trends Plant Sci 7:168–175

Véry AA, Sentenac H (2003) Molecular mechanisms and regulation of K^+ transport in higher plants. Annu Rev Plant Biol 54:575–603

Voelker C, Schmidt D, Mueller-Roeber B, Czempinski K (2006) Members of the *Arabidopsis* AtTPK/KCO family form homomeric vacuolar channels in planta. Plant J 48:296–306

Wang Y, He L, Li HD, Xu J, Wu WH (2010) Potassium channel α-subunit AtKC1 negatively regulates AKT1-mediated K^+ uptake in *Arabidopsis* roots under low-K^+ stress. Cell Res 20:826–837

Ward JM, Mäser P, Schroeder JI (2009) Plant ion channels: gene families, physiology, and functional genomics analyses. Annu Rev Physiol 71:59–82

Weber W (1999) Ion currents of *Xenopus laevis* oocytes: state of the art. Biochim Biophys Acta 1421:213–233

White PJ (2000) Calcium channels in higher plants. BBA-Biomembr 1465:171–189

Xu J, Li HD, Chen LQ, Wang Y, Liu LL, He L, Wu WH (2006) A protein kinase, interacting with two calcineurin B-like proteins, regulates K^+ transporter AKT1 in *Arabidopsis*. Cell 125:1347–1360

Zhang W, Fan LM, Wu WH (2007) Osmo-sensitive and stretch-activated calcium-permeable channels in *Vicia faba* guard cells are regulated by actin dynamics. Plant Physiol 143:1140–1151

Zimmermann S, Talke I, Ehrhardt T, Nast G, Müller-Röber B (1998) Characterization of SKT1, an inwardly rectifying potassium channel from potato, by heterologous expression in insect cells. Plant Physiol 116:879–890

Chapter 14
Mechanism of Passive Permeation of Ions and Molecules Through Plant Membranes

Alexander G. Volkov, Veronica A. Murphy and Vladislav S. Markin

Abstract The Gibbs free energy of ion and molecule transfer $\Delta G(\mathrm{tr})$ from the aqueous phase to a hydrophobic part of a biomembrane can be calculated as a sum of all contributions $\Delta G(\mathrm{tr}) = \Delta G(\mathrm{el}) + \Delta G(\mathrm{hph}) + \Delta G(\mathrm{si})$, where $\Delta G(\mathrm{el})$ is electrostatic contribution, $\Delta G(\mathrm{hph})$ is the hydrophobic effect, and $\Delta G(\mathrm{si})$ is determined by specific interactions of the transferred particle (ion, dipole) with solvent molecules, such as hydrogen bond formation, donor–acceptor, and ion–dipole interactions. The electrostatic component of the Gibbs energy of ion transfer from medium *w* into the medium *m* was found from conventional Born expression corrected for the image energy in a thin membrane. The hydrophobic contribution to the Gibbs free energy of solute resolvation with surface area *S* can be calculated using the equation, $\Delta G_s = -N_A S\gamma$, where γ is the surface tension in the cavity formed by the transferred particle in the media and N_A is the Avogadro's number. A significant point is that the free energy of the hydrophobic effect is opposite in sign to the electrostatic effect. As a result, the sum of electrostatic and hydrophobic components of the Gibbs free energy decreases with a solute size, so that $\Delta G(\mathrm{tr}) > 0$ only for small ions. The specific energy of ion/dipolar layer interaction depend on the dipolar membrane surface potential ϕ_s as $\Delta G(\mathrm{si}) = -zF\phi_s$, where *ze* is the charge of ions and *F* is the Faraday constant. These calculations yielded the permeability of different ions and neutral molecules through plant membranes in good agreement with experimental data.

A. G. Volkov (✉) · V. A. Murphy
Department of Chemistry, Oakwood University, 7000 Adventist Blvd, Huntsville, AL 35896, USA
e-mail: agvolkov@yahoo.com

V. S. Markin
Department of Neurology, University of Texas Southwestern Medical Center at Dallas, Dallas, TX 75390-8813, USA

A. G. Volkov (ed.), *Plant Electrophysiology*,
DOI: 10.1007/978-3-642-29119-7_14,

14.1 Introduction

The physiological processes inside plants and the primary and secondary metabolism involve membrane transport of molecules and ions across membranes, which is essential for plant growth and cellular homeostasis (Collander 1937, 1941, 1949, 1954; Becker et al. 1986; Ksenzhek and Volkov 1984; Marschner 1999; Mohr and Schopfer 1994; O'Neil et al. 1986; Ray 1960; Volkov 2006, 2008a, 2008b; Volkov et al. 2011d). The cell membrane acts as a barrier, separating the cell contents from the external medium (Volkov et al. 1997a, b). The barrier is selectively permeable and regulates the transport of ions and neutral molecules into and out of the cell. Biomembranes have sufficiently low permeability so that transport systems in the membrane can maintain suitable gradients of ions or polar solutes against a substantial leak (Mueller et al. 1962; Nobel 1999; Volkov et al. 1997a).

The mechanism by which solutes permeate the plasma membrane and their regulation is a key problem in plant physiology (Buchanan et al. 2000; Taiz and Zeiger 1999). The permeation of solutes across membranes depends on concentration gradients. Solute transport across plant membranes is essential for a number of cellular functions. In cells, this process is aided by ion and water channels, carriers, and pumps which lower the free energy barrier associated with the transfer of solutes from the polar aqueous environment to the nonpolar interior of the membrane. However, ions and small molecules can permeate membranes, even in the absence of special proteins, to assist the transport (Tien 1974; Tien and Ottova-Leitmannova 2000; Volkov and Deamer 1994; Volkov et al. 1997a, b).

The transport across membranes can be passive or active. Active transport is an energy-requiring process that moves ions across the membrane. Passive transport, unlike active transport, does not involve the input of the Gibbs energy and is dependent on the permeability of the cell membrane. Passive transport operates on the existing electrochemical potential gradients of the permeant, and its work leads to the disappearance of this gradient. Subsequently, understanding the mechanism of passive ion and dipole transport at a molecular level could offer valuable insight into the induced charge transport.

The balance between maintenance and dissipation of concentration gradients across biomembranes is crucial for the function of biological systems. Processes such as photosynthetic phosphorylation require membranes that provide effective barriers to passive diffusion of protons (Volkov 1989). In other cases, the rapid exchange of molecules such as water across a cell membrane is essential which demands aquaporins that increase the intrinsic water permeability of the membrane. Permeability coefficients of many ions and small neutral molecules have been determined experimentally and vary over a remarkably broad range. Two alternative mechanisms are commonly used to explain ion permeation of biological membranes in the absence of channel or transport proteins. One is referred to as the partition-diffusion mechanism, in which it is proposed that ions and molecules may diffuse across the hydrophobic interior of the membrane (Volkov and Deamer 1994; Volkov et al. 1997a, b). The other is the pore mechanism, in which the ion transport is assumed to be supported by transient aqueous pores in the membrane (Leontiadou et al. 2004;

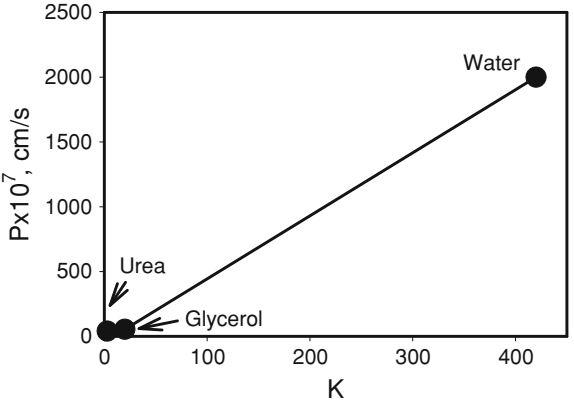

Fig. 14.1 Dependence of permeability coefficient of bilayer membranes from egg phosphatidylcholine on partition coefficient between hexdecane and water. Experimental points are taken from Gennis (1989)

Marrink and Berendsen 1994, 1996). Ions may be expected to permeate more easily via such pores, because the water molecules of the pore can reduce the repulsive hydrophobic interaction of the membrane to the penetrated ion (Markin and Kozlov 1985; Volkov et al. 1997a, b).

Generally, the most commonly used models for describing the passive transport of ions across biological membranes is the partition-diffusion model, which relates a given solute's permeability coefficient to its ability to partition into and diffuse across the phospholipid membrane. This model treats the membrane as a thin static slab of hydrophobic matter embedded in an aqueous environment. In order to cross the membrane, the permeating particle must dissolve in the hydrophobic region, diffuse across, and leave by re-dissolving into the second aqueous phase. If the membrane thickness and the diffusion and partition coefficients of the permeating species are known, the permeability coefficient can be calculated.

The barrier of the biological membrane is selectively permeable and able to regulate what enters and exits the cell. The partition coefficients of ions and neutral molecules are usually determined by experiment and estimated theoretically (Abramson 1981; Becker et al. 1986; Bemporad et al. 2004; Chiou et al. 2001; Collander 1937, 1941, 1949, 1950, 1954; Dordas et al. 2000; Haas and Schönherr 1979; Hsu et al. 1990; Kornyshev and Volkov 1984; Markin and Volkov 1987a, b, c; Markin and Volkov 1989a, b; Pohorille and Wilson 1996; Poznansky et al. 1976; Trapp 2000, 2004; Tyerman and Steude 1984; Volkov et al. 1997a; Volkov and Deamer 1994). Mechanisms of ions, water, and small neutral molecules permeation across membranes will be discussed in this chapter.

14.2 Overton Rule and Transport of Neutral Compounds Across Plant Membranes

At the end of the nineteenth century, Overton (1895, 1899) postulated a rule that the permeability of plant and animal cell membranes is proportional to the partition coefficient of solutes between oil and water (Fig. 14.1), which is known as

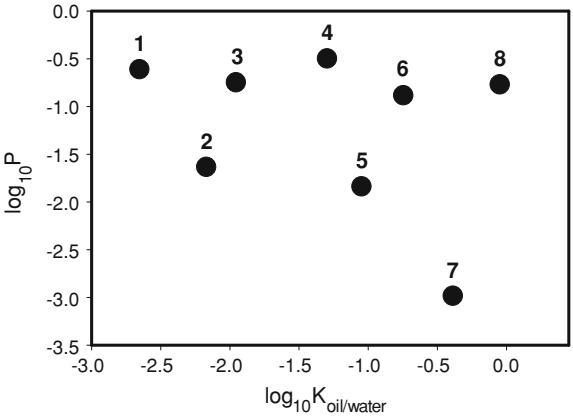

Fig. 14.2 Dependence of permeability coefficient of *Chara tomentosa* cells on partition coefficient between olive oil and water: *1*—ethylene glycol, *2*—urea, *3*—diethylurea, *4*—dimethylurea, *5*—thiourea, *6*—diacetine, *7*—glycerol, *8*—butylamide. Experimental points are taken from Collander (1949)

the "Overton Rule". Plant membranes behave as a solubility membrane in which the hydrophobic bulk structure plays a significant role.

Colander (1937, 1949, 1951 1954) analyzed the relationships between lipophilicity and membrane permeability for plant cells of *Nitella* and *Chara*. Briggs et al. (1982) found the relationship between lipophilicity and root uptake and translocation of non-ionized chemicals by using barley. Many authors measured partition coefficients of different compounds between water and organic solvents such as octanol, liquid hydrocarbons, esters, and vegetable oil and compared them with membrane permeability in plants (Bellaloui et al. 1999; Dordas et al. 2000; Hsu et al. 1990; Trap 2000). Collander (1937, 1949, 1954) published data on permeability of *Chara tomentosa* and *Nitella* cells to small molecules and found that there is significant dispersion and considerable scattering of experimental points on the dependence of membrane permeability on partition coefficient (Figs. 14.2 and 14.3). Collander (1937) measured the permeability of 16 different kinds of plant cells to different molecules and found that the membrane permeability for the same molecules varies from one plant to another. This deviation from Overton "rule" can be caused by different thicknesses of plasma membranes (Collander 1937) and surface potential, different diffusion coefficient and dipolar moments of solutes, or active transport, for which Overton proposed the term "adenoid activity" at the end of the nineteenth century. Benga (1989) found that membrane permeability of some solutes do not correlate with the partition coefficient in the octanol/water system (Fig. 14.4).

We will discuss in this chapter the main effects which influence the membrane permeability and cause a deviation from the Overton "rule". The divergence between experimental data and prediction from the Overton "rule" can be caused by specific interactions of the transferred particle (ion, dipole) at the membrane–water interface, such as hydrogen bond formation, donor–acceptor, dipole–dipole, and ion–dipole interactions (Kornyshev and Volkov 1984; Markin and Volkov 1987a, b, c). The higher plant membrane permeability in a comparison with predictions from the Overton "rule" can be explained by facilitated transport by membrane transporters, transient aqueous pores, aquaporins, ion channels and pumps.

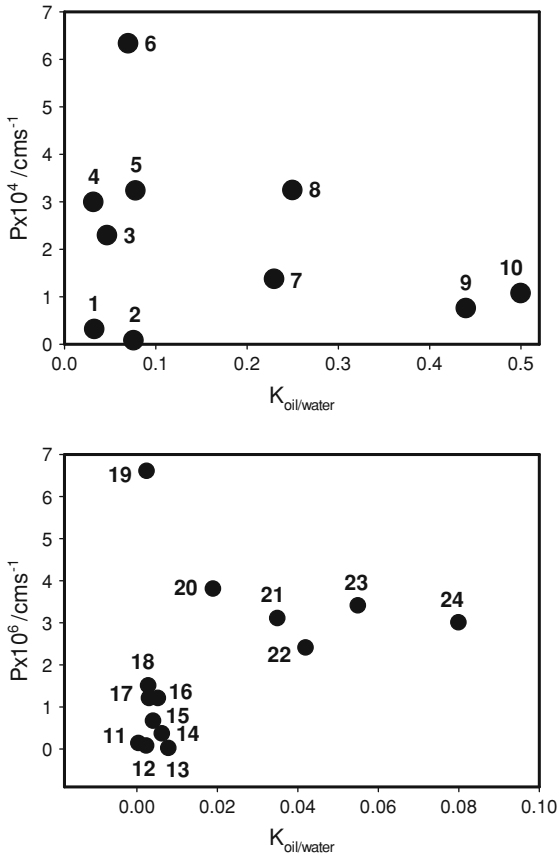

Fig. 14.3 Dependence of permeability coefficient of *Nitella* cells on partition coefficient between olive oil and water: *1*—caffeine, *2*—formamid, *3*—isopropanol, *4*—ethanol, *5*—methanol, *6*—D_2O, *7*—tert-butanol, *8*—sec.-butanol, *9*—triacetin, *10*—triethyl citrate, *11*—urea, *12*—tetraethylene glycol,*13*—polyethylene glycol monoethyl ether, *14*—thiourea, *15*—ethyl-urea, *16*—ethylene–glycol, *17*—N,N'-dimethyl-urea; *18*—N,N-dimethyl-urea, *19*—acetamide, *20*—N,N-diethyl-urea, *21*—dipropylene glycol, *22*—1,3-butanediol, *23*—1,5-pentanediol, *24*—glycerol monochlorhydrin. Experimental points are taken from Collander (1954)

14.3 Partition

The Gibbs energy of solute resolvation is a key concept intimately related to the ion and neutral molecule transport across biological and artificial membranes, the mechanisms of interfacial and phase transfer catalysis, the kinetics of ion transfer across liquid membranes, the coupling of heterogeneous reactions in bioenergetics, extraction, drug delivery in pharmaceutical chemistry, and the design and manufacture of ion-selective electrodes and sensors (Markin and Volkov 1987a, b, c, 1989a, b, 1990, 2004; Volkov 2001, 2003; Volkov et al. 1997a).

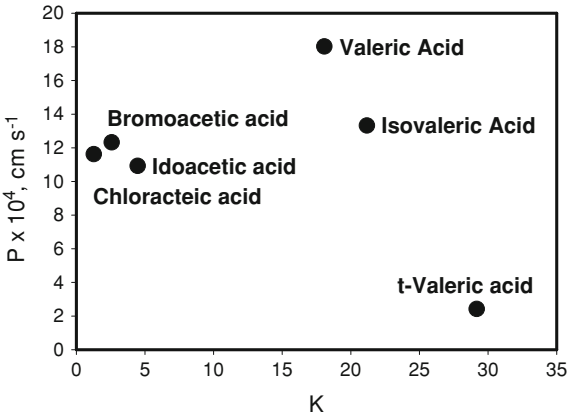

Fig. 14.4 Dependence of permeability coefficient of bilayer membranes from egg lecitins on partition coefficient between octanol and water. Experimental points are taken from Benga (1989) and Tien and Ottova-Leitmanova (2000)

By solvation, we mean the sum of all structural and energy changes occurring in a system when ions pass from the gaseous phase into solution. It has become customary to divide the interaction between ion and solvent and the corresponding energy, into several components (Kornyshev and Volkov 1984; Markin and Volkov 1987a, b, c). To understand the energies involved in transferring an ion or dipole between two solvent phases, one must take the following effects into account:

1. Formation in a medium of a cavity to accommodate the ion or molecule also known as the hydrophobic effect;
2. Electrostatic polarization of the medium;
3. Changes in the structure of the solvent that involve the breakdown of the initial structure and the production of a new structure in the immediate vicinity of the ion or molecule;
4. Specific interactions of ions or molecules with solvent molecules, such as hydrogen bond formation, donor–acceptor, dipole–dipole, and ion–dipole interactions;
5. Annihilation of defects: a small ion or molecule may be captured in a "statistical micro-cavity" within the local solvent structure so far releasing energy of this defect;
6. The correction term for different standard states.

This subdivision is purely conditional since many of these different effects may overlap, for example, electric polarization of the medium may significantly influence its structure. Assigning such a division does permit analysis of the individual components. However, sometimes components can be grouped into "blocks". For example, one may speak about the hydrophobic effect which combines the formation of a cavity and structural changes of the solvent in the vicinity of the new particle. This is quite justifiable because the hydrophobic effect, together with the electrostatic effect, provides the major contribution to the solvation energy. On the other hand, sometimes it becomes necessary to consider each individual component of a given effect (Markin and Volkov 1987a, b, 1987c).

For example, the total solvation (or resolvation) energy can be divided into electrostatic $\Delta G(\text{el})$ and non-electrostatic parts $\Delta G(\text{hpb})$:

$$\Delta_{\beta}^{\alpha} G_i^0 = \Delta_{\beta}^{\alpha} G_i^0(\text{el}) + \Delta_{\beta}^{\alpha} G_i^0(\text{hph}) \tag{14.1}$$

To find the Gibbs standard resolvation energy, one needs to compare the Gibbs energies for a given solute in each media. If one of the phases (β) is a vacuum (vac), the difference

$$\Delta_{\text{vac}}^{\alpha} G_i^0 = G_i^{0,\alpha} + G_i^{0,\text{vac}} \tag{14.2}$$

is called the solvation energy of the solute i in the α phase. The resolvation energy can be represented as the difference of two solvation energies:

$$\Delta_{\beta}^{\alpha} G_i^0 = \Delta_{\text{vac}}^{\alpha} G_i^0 - \Delta_{\text{vac}}^{\beta} G_i^0 \tag{14.3}$$

If two immiscible liquids α and β are mutually saturated, a certain amount of one solvent will be dissolved in the other solvent and vice versa. The corresponding energy of resolvation between two mutually balanced solvents is called the Gibbs partition energy. For most ions and solvents the standard Gibbs energies of transfer and partition coincide within experimental error. However, for some solvents and ions these quantities may differ significantly.

When considering the standard Gibbs resolvation energy, attention should be paid to whether one deals with ion transfer between pure or mutually saturated solvents (Markin and Volkov 1987a, b, c; Volkov et al. 1997a).

14.4 Hydrophobic Effect

The calculation of the hydrophobic interaction is a focus of intense interest in the context of plant membrane science. Contemporary approaches to such problems are based on phenomenological, semi-phenomenological, and microscopic statistical-mechanics models (Abramson 1981; Flewelling and Hubbel 1986a, 1986b; Macdonald 1976; Tanford 1980). All of these use several poorly defined parameters to characterize solute interaction with the solvent. To avoid uncertainty, the hydrophobic contribution to the Gibbs energy of solute resolvation can be calculated using the hydrophobic equation (Markin and Volkov 1987a, b, c; Volkov and Kornyshev 1985; Sisskind and Kazarnowsky 1933; Ulig 1937; Volkov et al. 1997a, b). The surface energy of a solute with surface area S, when expressed in terms of surface tension at the solute–solvent interface $\gamma_{o,m}$, is equal to $S\gamma_{o,m}$, and the difference in the surface energies in the media w and m is $S(\gamma_{m,w} - \gamma_{m,m})$. According to the Antonov rule (Antonov 1907),

$$\gamma_{o,w} - \gamma_{o,m} = \gamma_{w,m}\,\text{sign}(\gamma_w - \gamma_m), \tag{14.4}$$

where $\gamma_{w,m}$ is the interfacial tension at the planar boundary between the media w and m. The surface tensions at the boundaries between air o and the solvents

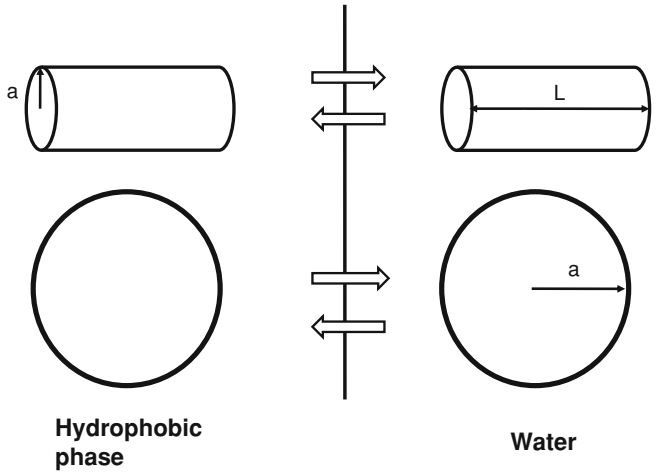

Fig. 14.5 Hydrophobic effect: partition of solutes between two phases

w and *m,* respectively, at the same pressure and temperature are $\gamma_{o,w}$ and $\gamma_{o,m}$. Here the equation for the hydrophobic contribution to the energy of resolvation has the form (Markin and Volkov 1987a, b, c; Volkov and Kornyshev 1985):

$$\Delta_{\beta}^{\alpha}G^{0}(\text{hph}) = -N_A S\gamma_{wm}\text{sgn}(\gamma_w - \gamma_m), \tag{14.5}$$

where N_A is the Avogadro number. This relation (14.5) infers that the molecules of the two solvents *w* and *m* do not mix or react chemically with each other. The hydrophobic contribution to the Gibbs energy of a solute transfer from water to hydrocarbon phase is negative and the absolute value is obviously greater for particles with larger surface area.

In many cases the shape of a solute can be approximated by a sphere with a radius *a* or by a cylinder with radius *a* and length *L* (Fig. 14.5). For a spherical solute, Eq. 14.5 can be written as

$$\Delta_{\beta}^{\alpha}G^{0}(\text{hph}) = -4\pi a^2 N_A\gamma_{wm}\text{sgn}(\gamma_w - \gamma_m) \tag{14.6}$$

and for a cylindrical solute

$$\Delta_{\beta}^{\alpha}G^{0}(\text{hph}) = -2\pi a(a+L)N_A\gamma_{wm}\text{sgn}(\gamma_w - \gamma_m). \tag{14.7}$$

Figure 14.6 shows the dependence of Gibbs energy on radius *a* and interfacial tension γ_{wm} for a spherical solute. Interfacial tension at liquid hydrocarbon/water interface varies from 49 to 52 mNm^{-1} for saturated hydrocarbons and from 34 to 38 mNm^{-1} for hydrocarbons with double bonds. It means that the hydrophobic contribution to the Gibbs energy of a solute transfer from water to hydrocarbon decreases about 30% in the presense of a double bond. Although the interfacial tension at the liquid hydrocarbon/water interface is about 49–52 mNm^{-1} for

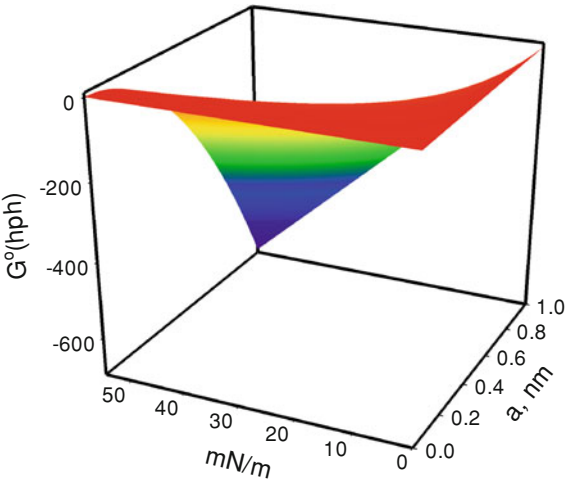

Fig. 14.6 Dependence of hydrophobic contribution to the energy of resolvation of a spherical solute on its radius a and interfacial tension γ

saturated alkanes, it is much lower in unsaturated hydrocarbons, which in turn should be reflected in the related hydrophobic effect. It is clear that the presence of double bonds should decrease the hydrophobic effect. On the other hand, experimental measurements show that double bonds generally increase permeability of membranes to ions and polar molecules. This is presumably due to the fact that although alkanes have a dielectric moment equal to zero, the double bond in alkenes induces a dielectric moment of about half a Debye unit that can cause specific ion–dipole and dipole–dipole interactions among solvent molecules. This in turn produces a higher dielectric permittivity and increased partition coefficient, with the end result being that unsaturated lipid bilayers are more permeable than saturated lipid bilayers.

Figure 14.7 shows the dependence of the hydrophobic contribution to the Gibbs energy of a solute transfer for molecules with cylindrical shapes.

The effect of curvature on the surface tension at a molecularly sized sphere was calculated by Tolman (1949). The surface tension at radius a can be written as

$$\gamma_a = \gamma \frac{1}{1 + \frac{2\delta}{a}}, \tag{14.8}$$

where δ is a parameter, which according to Tolman (1949) is the distance from the surface of tension to the dividing surface for which the surface excess of fluid vanishes. Parameter δ can vary between zero and a few angstroms.

From the theoretical point of view, the limits of applicability of the hydrophobic formula are not quite clear. Nonetheless, it works surprisingly well for calculation of the partition coefficients of a system of two immiscible liquids (Abramson 1981; Kornyshev and Volkov 1984; Markin and Volkov 1987a, b, c; Volkov and Kornyshev 1985; Volkov et al. 1997a). Some deviation from the hydrophobic formula is observed if the interfacial tension of two pure immiscible solvents is less than

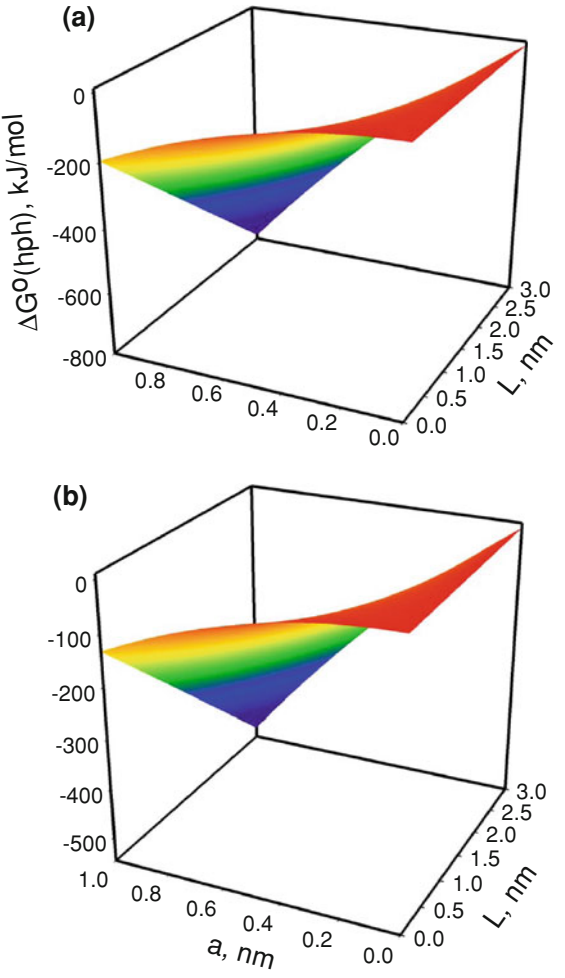

Fig. 14.7 Dependence of hydrophobic contribution to the energy of resolvation of a cylindrical solute on its radius a and length L. (**a**) $\gamma = 52$ mN/m, (**b**) $\gamma = 35$ mN/m

10 mNm^{-1} and if the size of the dissolved particle is less than 0.2 nm (Abramson 1981). An important advantage of the hydrophobic formula is that it does not involve fitting parameters because $\gamma_{\alpha\beta}$ is determined experimentally. A significant point is that the free energy of the hydrophobic effect is opposite in sign to the electrostatic effect. As a result, the sum of electrostatic and hydrophobic components of Gibbs energy decreases with ionic size, so that $\Delta G(\text{tr}) > 0$ only for small ions. For ions with radii larger than 0.45 nm, $\Delta G(\text{tr}) < 0$. This prediction is consistent with experimental data.

Using the hydrophobic equation in the form of Eq. 14.5, we can calculate the hydrophobic energy of a solute transfer from water to a liquid hydrocarbon. The results are presented graphically in Figs. 14.5 and 14.6. The hydrophobic contribution to the Gibbs energy of ion or molecule transfer from water to

hydrocarbon is negative and the absolute value is obviously greater for particles with larger radii, a. It has been surprisingly useful for calculations of partition coefficients in systems consisting of two immiscible liquids (Abramson 1981; Kornyshev and Volkov 1984; Markin and Volkov 1987a, b, c; Volkov and Kornyshev 1985; Volkov et al. 1997a).

14.5 Electrostatics

Polarization of the medium consists of a number of components, which can be divided into three main groups: electronic, atomic, and orientational. Two sets of models exist to calculate the electrostatic portion of the solvation energy (Born 1920; Dogonadze and Kornyshev 1974; Markin and Volkov 1987a, b, c; Kornyshev 1981; Volkov and Kornyshev 1985). In the first set (Born 1920) the medium is considered as a structureless continuum, while in the second set it is represented by a set of individual particles having either realistic or simplified properties (Dogonadze and Kornyshev 1974). In early works the solvent structure was taken into account by directly calculating the energies of particular configurations of solvent molecules in the vicinity of the ion. The configuration and the number of molecules in it were chosen with a certain degree of arbitrariness, proceeding from some physical considerations, which ensured an excellent fit between experimental and theoretical data. Such models completely ignored the statistical properties of the solution which are very important for obtaining a correct description of solvation. The modern approach lies in developing a statistical theory of ion–dipole plasma which describes both the energy and the statistical aspects of the phenomenon (Kornyshev 1981; Kornyshev and Volkov 1984; Volkov and Kornyshev 1985).

It is also necessary to take into account the differences between larger and smaller ions in the short range interaction of the ion with each solvent. With larger ions, such a contribution is concerned primarily with the work spent on creating a cavity in the medium in which the ion will be placed. Entropy effects related to the disordering induced by the structure-breaking ion also fall in this category. The opposite effect may occur in the case of smaller ions, a process we will refer to as defect annihilation. For instance, an ion may be captured in a statistically probable micro-cavity in the local structure of solvent, thereby releasing the energy of this defect. Other examples are the energy release due to ion–solvent hydrogen bonding via individual protons, and the entropy effect of structure-making ions. Contributions of this kind are very sensitive to the nature of both the ion and the solvent.

There is also an intermediate approach, in which, while remaining within the framework of continuum theories, attempts are made to take account of the influence of the discrete nature of the solvent on the effective parameters of the model. For this purpose, account is taken of nonlinear dielectric effects, and the mutual correlation of the polarization vectors of the solvent molecules, situated at short distances from one another, is analyzed using the theory of non-local electrostatics. Each of these approaches, reflecting the role of different effects, has its own advantages.

In general, for smaller ions of low chemical activity, the electrostatic contribution dominates. With increasing an ionic radius, the electrostatic contribution decreases, becoming comparable to the rising hydrophobic contribution. We can now discuss electrostatic considerations in more detail.

Electrostatic interactions play a central role in a variety of biophysical processes in plants (Markin et al. 2008; Volkov 1989, 2000, 2006, 2008a, b; Volkov et al. 2007, 2008a, b, c, 2009a, b, 2010a, b, c, d, 2011a, b, c). The electrostatic contribution to the Gibbs energy of ion resolvation has often been estimated with the aid of Born's continuum model in which the ion is described as a sphere of a radius a with charge q distributed uniformly over its surface, while the solvent is considered a structureless medium with a macroscopic dielectric constant ε. The Born model is assuming that it is only the charge on the ion that is responsible for ion–solvent interactions. The interactions between the solvent and the ion are considered to be electrostatic in origin. Born model considered ion as equivalent to a charged sphere and structured solvent as a structureless continuum with dielectric constant Fig. 14.8. In this model free energy of ion transfer between two phases is considered as a sum of work of discharging an equivalent sphere in one phase and work of charging an equivalent sphere in other solvent. The work of charging of an uncharged sphere of a radius a is

$$A = \int_0^q \varphi \, dq = \int_0^q \frac{q}{4\pi\varepsilon_0\varepsilon a} \, dq = \frac{q^2}{8\pi\varepsilon_0\varepsilon a} \tag{14.9}$$

and work of discharging can be written as

$$A = \int_q^0 \varphi \, dq = \int_q^0 \frac{q}{4\pi\varepsilon_0\varepsilon a} \, dq = -\frac{q^2}{8\pi\varepsilon_0\varepsilon a} \, . \tag{14.10}$$

The relationship between an ionic radius a and the electrostatic (Born) component of the Gibbs energy of ion transfer from medium w into the medium m is calculated from the expression

$$\Delta_m^w G(\text{Born}) = -N_A \frac{q^2}{8\pi\varepsilon_0 a}\left(\frac{1}{\varepsilon_w} - \frac{1}{\varepsilon_m}\right). \tag{14.11}$$

For hydrated ion transfer from medium w into the medium m, Gibbs energy is equal to:

$$\begin{aligned}\Delta_m^w G(\text{Born}) &= -N_A \frac{q^2}{8\pi\varepsilon_0}\left[\left(1-\frac{1}{\varepsilon_s}\right)\left(\frac{1}{a}-\frac{1}{b}\right) + \left(1-\frac{1}{\varepsilon_m}\right)\frac{1}{b} - \left(1-\frac{1}{\varepsilon_s}\right)\left(\frac{1}{a}-\frac{1}{b}\right) - \left(1-\frac{1}{\varepsilon_w}\right)\frac{1}{b} -\right] \\ &= -N_A \frac{q^2}{8\pi\varepsilon_0 b}\left(\frac{1}{\varepsilon_w} - \frac{1}{\varepsilon_m}\right)\end{aligned} \tag{14.12}$$

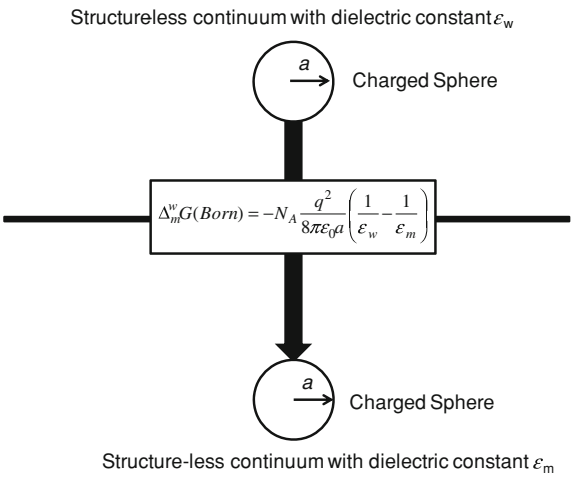

Fig. 14.8 The Born model for electrostatic contribution to ion–solvent interactions considers ion as a charged sphere and the solvent as a structureless continuum

where ε_w, ε_m and ε_s are dielectric permittivities of phases w, m, and a hydrated shell; a is bare ion radius; b is hydrated ion radius. From Eq. 14.12 it follows that Born component of free energy of ion transfer between two immiscible liquid phases strongly depends on dielectric permittivities of both phases.

The main weakness of the Born continuum model is that all of the information about the dielectric properties of a pure solvent is contained in the dielectric constant ε, which treats the solvent as a structureless screening background. However, Born formulated his model in 1920 on the basis of Lorentz macroscopic electrostatics, assuming that they could be extrapolated to localized induction and electric field effects of the ion. In calculations of fields produced by microscopic sources such as ions, it is necessary to take into account the microscopic structure of the medium. One way to do this is to apply non-local electrostatics, which is now widely used both in solid-state theory and in the theory of liquid solution.

The solvation energies calculated by the Born formula differ noticeably from experimental values. Since, in most of the cases, the resolvation energy is the difference between two comparatively large solvation energies, even a relatively small error in each energy may give rise to considerable error in the resolvation energy, even an incorrect sign. For example, Eq. 14.11 implies that if $\varepsilon_w > \varepsilon_m$ there is a higher probability for the ion to reside in solvent w, irrespective of ion size. In practice this is not always the case. It is known that small ions of radius $a < 0.2$ nm reside mainly in a polar solvent of high permittivity, while large organic ions reside preferably in the hydrophobic phase. Data on the partition coefficients, extraction, solubility, and current–voltage characteristics show that the standard free energy of ion transfer from water into a less polar solvent is positive for small radius ions and negative for large radius ions, while Eq. 14.11 implies that the sign of this energy does not depend on the ion radius.

The Born relation overestimates the solvation energy and provides values which are too negative (Markin and Volkov 1987a, b, c). However, when particular

energy values are compared with experimental data, a certain radius must be assigned to each ion. This procedure is arbitrary to a certain extent because an ion is not a hard sphere of a definite radius. The ion radius is solely an effective parameter which enables a convenient description of different properties of an ionic system. It is frequently the case that different properties of a system are best described in terms of different ion radii. Although there are reasonable physical restrictions on the range within which an ion radius value can be selected, it is meaningless to consider that one radius is better than another.

The difficulty encountered in selection of an ion radius is confirmed by the existence of at least four ion radius scales which have been calculated using different assumptions: namely the Pauling (1927) scale; the Goldschmidt (1926) scale; the Waddington (1966) scale; the Gourary and Adrian (1960) scale. There is minimal variation between the first three scales; however, the fourth scale is very different. Blandamer and Symons (1963) have attempted to choose the most relevant scales of ion radii by comparing the Gibbs energy with the ion hydration entropy. They demonstrated that if any of these quantities is plotted as a function of $1/a$, all the points corresponding to alkali cations and anions of halide compounds fit the same smooth curve, provided the Gourary–Adrian scale is used. Other sets of ionic radii lead to two different curves: one for cations and the other for anions. It is difficult to say whether much attention should be paid to this fact since it does not have a theoretical explanation. For the Gourary–Adrian scale experimental data points ideally fit an ideal straight line (Markin and Volkov 1987a, b, c), thereby confirming the conclusion of Blandamer and Symons. We believe this fact undoubtedly deserves attention. For the other three scales, the fit is not very good, although deviation from a straight line is noticeable only for the smallest ions: Li^+; Na^+; K^+, but not for Cl^-, Br^- and I^- deviation is small (Markin and Volkov 1987a, b, c).

The electrostatic part of the hydration energy, as calculated by the Born relation, is shown by curve 1 in Fig. 14.9. It can be seen that the calculated values are indeed lower (by approximately 50%) than experimental $\Delta^{w}_{vac}G^0$ values. Thus, the Born theory requires improvement. Equation 14.11 includes only two experimental parameters: the ion radius and dielectric permittivity ε. By appropriately changing one of these parameters, one can, in principle, achieve satisfactory agreement with experimental results. However, this formal "fitting" of the ion radius leads to unreasonable values which fall onto none of the four acceptable scales. Therefore, although such a fitting provides an empirical relation which is in good agreement with experiment, it still cannot constitute a physical explanation of the solvation phenomenon.

Another rapidly developing semi-macroscopic approach is to calculate the electrostatic part of the solvation energy using the non-local electrostatics method (Dogonadze and Kornyshev 1974; Kornyshev 1981; Landau and Lifshitz 1984; Volkov and Kornyshev 1985; Vorotyntsev and Kornyshev 1993). Non-local electrostatics takes into account that fluctuations of solvent polarization are correlated in space, since liquid has a structure caused by quantum interaction

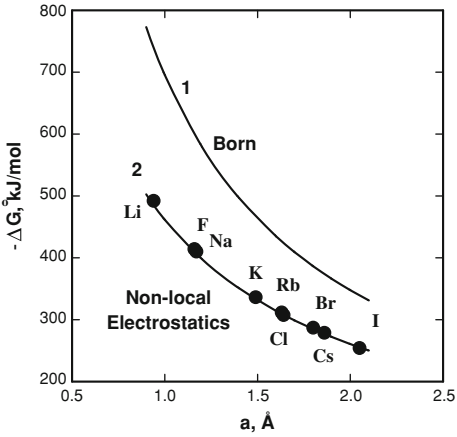

Fig. 14.9 Gibbs energy of ionic hydration as a function of an ionic radius. *Line 1* was calculated from the Born theory. *Line 2* was calculated from non-local electrostatic theory. The points are experimental data with hydrated ionic radii taken from Gourary and Adrian (1960); $\lambda = 0.1$ nm, $\Lambda = 0.7$ nm

between its molecules. This means that the average polarization at each point depends on the electric displacement at all other points of the space correlated with a given point. As a result of this correlation, the response of polarization to external field at distances of the order of a correlation radius proves to be less than that in a simple model of local electrostatics, because the effective dielectric constant decreases. Kornyshev and Volkov (1984) used a generalization of the Born model to describe the electrostatic contribution to the free energy of resolvation. In this approach, nonlocal electrostatics were used to describe the dielectric response of a solvent in terms of the static dielectric function $\varepsilon(\mathbf{k})$. This function contains information about special features of screening at short distances associated with liquid structure.

In nonlocal electrostatics the electric displacement D and electric field E are related by the tensor $\varepsilon_{mn}(\mathbf{r})$:

$$D^m(\mathbf{r}) = \sum_n \int d\mathbf{r}' \varepsilon_0 \varepsilon_{mn}(\mathbf{r} - \mathbf{r}') E^n(\mathbf{r}'), \quad (m, n = x, y, z). \tag{14.13}$$

It should be noted that although this relation is spatially complicated, it is linear. Further calculations are carried out in terms of the Fourier transform of the tensor $\varepsilon_{mn}(\mathbf{r})$ which is called the static dielectric function $\varepsilon(\mathbf{k})$:

$$\varepsilon(\mathbf{k}) = \sum_{m,n} \frac{k_m k_n}{k^2} \int d(\mathbf{r} - \mathbf{r}') e^{-ik(\mathbf{r}-\mathbf{r}')} \varepsilon_{mn}(\mathbf{r} - \mathbf{r}'). \tag{14.14}$$

Approximations for $\varepsilon_{(\alpha)}(\mathrm{k})$ $\varepsilon_{(\beta)}(\mathrm{k})$ and must be used to obtain an analytical function for $\Delta_\beta^\alpha G(\mathrm{el})$. To this end, we can apply the results of an analysis by Dogonadze and Kornyshev (1974) according to which the expression

$$\frac{1}{\varepsilon(k)} = \frac{1}{\varepsilon_{\mathrm{opt}}} - \left(\frac{1}{\varepsilon_{\mathrm{opt}}} - \frac{1}{\varepsilon_*}\right) \frac{1}{1 + k^2\lambda^2} + \left(\frac{1}{\varepsilon_*} - \frac{1}{\varepsilon}\right) \frac{1}{1 + k^2\Lambda^2} \tag{14.15}$$

can serve as a reasonable approximation for $\varepsilon(\mathbf{k})$ of polar liquids. It corresponds to provisional splitting of the medium polarization fluctuations $\vec{P}(\vec{r})$ into three modes $\vec{P} = \vec{P}_e + \vec{P}_i + \vec{P}_D$ associated with the excitation of electronic (e), vibrational (i), and orientational (Debye, D) degrees of freedom. Since these are marked separately in frequency, we can write

$$\left\langle \vec{P}(\vec{r})\,\vec{P}(0) \right\rangle \approx \left\langle \vec{P}_e(\vec{r})\,\vec{P}_e(0) \right\rangle + \left\langle \vec{P}_i(\vec{r})\,\vec{P}_i(0) \right\rangle + \left\langle \vec{P}_D(\vec{r})\,\vec{P}_D(0) \right\rangle. \quad (14.16)$$

Equation 14.15 corresponds to an exponential attenuation of these correlations in space with correlation radii Λ and λ for the Debye and vibrational polarization, respectively, and with a negligibly small correlation radius for the electronic polarization. Quantities ε_{opt} and ε^* are the values of the liquid's dielectric permittivities at frequencies corresponding to the transparent bands separating the electronic and vibrational and orientational (ε^*) regions of the spectrum, respectively. Although the values of λ and Λ are rather uncertain, they cannot be regarded as purely adjustable parameters of the theory. By its physical meaning, λ is of the order of the radius of a water molecule. Λ is comparable with the characteristic length of the hydrogen–bonding chain which, according to diffraction data, is of the order of 0.7 nm.The potential produced in a medium by a charged sphere of radius a at a distance r from its center is given by:

$$\varphi(\mathbf{r}) = \frac{ze_0}{2\pi^2\varepsilon_0}\int_0^\infty \frac{dk}{\varepsilon(k)}\frac{\sin kr}{kr}\frac{\sin ka}{ka}. \quad (14.17)$$

Hence, we can easily find the electrostatic contribution to the solvation energy:

$$\Delta^{\alpha}_{\text{vac}}G^0(\text{el}) = N_A\frac{ze_0}{4\pi^2\varepsilon_0}\int_0^\infty dk\frac{\sin ka}{k^2a^2}\left[1-\frac{1}{\varepsilon(k)}\right]. \quad (14.18)$$

Polarization of the medium can be divided into three main groups: optical, vibrational and orientational. To evaluate Eq. 14.18, one has to specify the function $\varepsilon(\mathbf{k})$. This can be done, for example, by subdividing fluctuations of the medium polarization into three modes relating to different degrees of freedom: namely, (1) electronic or optical; (2) vibrational or infra-red; and (3) orientational or Debye. If the radius of the correlation of the ith mode of a fluctuation is λ_i, then

$$1-\frac{1}{\varepsilon(k)} = 1-\frac{1}{\varepsilon_{\text{opt}}} + \left(\frac{1}{\varepsilon_{\text{opt}}}-\frac{1}{\varepsilon_2}\right)\frac{1}{1+k^2\lambda_2^2} + \left(\frac{1}{\varepsilon_2}-\frac{1}{\varepsilon_3}\right)\frac{1}{1+k^2\lambda_3^2} \quad (14.19)$$

In this expression the correlation length of the electronic mode is set equal to zero. The exact values of the correlation lengths λ_2 and λ_3 cannot be determined a priori but they can be approximated from physical considerations. In the infra red region, the length λ_3 depends on liquid type. In the case of non-associated liquids

the correlation length for orientational vibration is approximately equal to the intermolecular distance; while for associated liquids (water for example) λ_3 is equal to the characteristic length of the hydrogen bond chain, i.e., 0.5–0.7 nm.

Integration of Eq. 14.19 with [1–1/ε(k)] expressed by Eq. 14.18 yields:

$$\Delta^{\text{vacuum}}_{\text{water}} G(\text{el}) = N_A \frac{q^2}{8\pi\varepsilon_0 a}\left\{1 - \frac{1}{\varepsilon_{\text{opt}}} + \left(\frac{1}{\varepsilon_{\text{opt}}} - \frac{1}{\varepsilon_2}\right)\phi\left(\frac{2a}{\lambda_2}\right) + \left(\frac{1}{\varepsilon_2} - \frac{1}{\varepsilon_3}\right)\phi\left(\frac{2a}{\lambda_3}\right)\right\}, \tag{14.20}$$

where:

$$\psi(x) = 1 - (1 - e^{-x})\frac{1}{x}\,. \tag{14.21}$$

It is important to note that Eqs. 14.11 and 14.20 predict an essentially different dependence of the solvation energy on the dielectric properties of the solvent. The result obtained in calculations of the electrostatic component of the Gibbs energy of ion hydration with relation (14.20) are plotted in Fig. 14.9 together with data for the measured free energy of hydration of individual ions. The fit is remarkably good for both cations and anions (Kornyshev and Volkov 1984; Volkov and Kornyshev 1985). A minor deviation is seen for the very small Li^+ ion, which could be due to entropy effects in structure formation or to defect annihilation effects described earlier. That is, the ion could be trapped in a statistically probable microcavity in the water structure, and this would liberate the energy of the defect microcavity. The obvious differences between theory and experiment, found in the case of large ions, provide evidence for the importance of hydrophobic effects in creating a cavity in the medium able to accommodate the ion.

Figure 14.10 shows the dependence of the Gibbs energy of hydration for an ion with radius equal to 0.149 nm (for example, K^+) on correlation lengths λ and Λ. The largest value for the hydration energy is obtained in the Born limit $\lambda = 0$, that is, in a structureless solvent. The finiteness of λ and Λ reduces the contribution of any one of the three modes P_i, P_e or P_D. In Eq. 14.20, the correlation length of the electronic mode P_e is set equal to zero. The exact values of the correlation lengths λ and Λ cannot be determined a priori, but they can be estimated from infrared spectral characteristics. In the infrared region, the length Λ depends on the properties of the liquid. In the case of non-associated liquids the correlation length for orientational vibration is approximately equal to the intermolecular distance, while for associated liquids Λ is equal within an order of magnitude to the characteristic length of the hydrogen bond chain (Kornyshev and Volkov 1984; Volkov and Kornyshev 1985).

The non-electrostatic portion of the total Gibbs energy is usually assumed to arise from the energy of solvation of a hypothetical ion that lacks electrical charge, but with all other characteristics unchanged. This can be estimated by comparison with a proper neutral analog, such as a noble gas, and it is assumed that for particles of the same shape and size the energies needed to form a cavity and modify the solvent structure are equal, irrespective of the particle charge. This

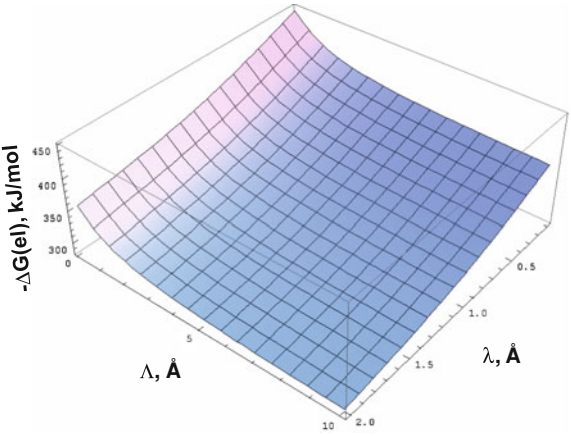

Fig. 14.10 Electrostatic contribution to the Gibbs energy of Na^+ hydration (ΔG(el)) as a function of correlation radii λ and Λ

approach has an important advantage. If the ion and analog neutral particle are assumed to be in identical standard states in the gaseous phase and solution, then a comparison of the theoretical results with experimental data no longer requires a correction for the loss of translational entropy of ions in the solution.

The electrostatic contribution to the hydration energy calculated by these relations is shown in Fig. 14.8, together with experimental data for small monovalent ions (Kornyshev and Volkov 1984; Volkov and Kornyshev 1985). The correlation lengths were chosen to provide the best fit between theoretical and experimental data: $\lambda_2 = 0.1$ nm and $\lambda_3 = 0.7$ nm. As can be seen from Fig. 14.8, the agreement between theory and experiment obtained by Kornyshev and Volkov (1984) is more than satisfactory. The nonlocal electrostatics method refers to the continuum models, but the effective parameters needed for calculation are chosen by analyzing the solvent structure. This method gives rather accurate values for the solvation energy for small ions and also permits calculation, by virtue of Eq. 14.1, of the resolvation energy. For large ions there remains considerable discrepancy between theory and experiment, which makes it necessary to take into account other effects. In our case, these effects are the work done in the formation of a cavity in the solvent and the hydrophobic effect. The largest value for the solvation energy is obtained in the Born limit $\lambda_2 = \lambda_3 = 0$, i.e., in a structureless solvent (Kornyshev and Volkov 1984; Volkov and Kornyshev 1985).

The major disadvantage of the continuum and semi-continuum approaches to the solvation problem lies in the solvent model itself. An allowance for dielectric saturation or dipole correlation is an attempt to partially describe the discrete properties of the solvent within the framework of the continuum model (Markin and Volkov 1987a, b, c). Other analogous approaches attempt to take into account the unknown effect of the solvent molecular structure on the thermodynamic properties of a system. However, the problem can only be solved correctly using a statistical model of the solvent and taking into account its discrete structure.

14.6 Membrane Transport and Partition Energy

In the preceding sections we considered different effects which contribute to the energy of ion and neutral molecule resolvation. However, for most solvents which are of practical interest the greatest contribution is due to the electrostatic and hydrophobic effects. Therefore, the resolvation energy can be presented as a sum of all contributions:

$$G(\mathrm{tr}) = G(\mathrm{el}) + G(\mathrm{hph}) + G(\mathrm{si}), \tag{14.22}$$

where $\Delta G(\mathrm{el})$ is electrostatic contribution, $\Delta G(\mathrm{hph})$ is the hydrophobic effect, and $\Delta G(\mathrm{si})$ is caused by specific interactions of the transferred particle (ion, dipole) with solvent molecules, such as hydrogen bond formation, donor–acceptor, and ion–dipole interactions (Kornyshev and Volkov 1984; Markin and Volkov 1987a, b, c; Volkov and Markin 2002).

Figure 14.6 shows that the hydrophobic effect can make the resolvation energy change sign as the ion radius varies. The calculation results are in excellent agreement with experimental data. The discrepancy observed for small radius anions may be attributed to the formation of hydrogen bonds between anion and solvent or to defect annihilation. The energy corresponding to this discrepancy is on the same order of magnitude as the energy gain obtained in the formation of a weak hydrogen bond between anion and solvent. It should, however, be noted that for small anions resolvation energies reported by different authors differ considerably.

The transfer of small inorganic ions with radii less then 0.3 nm through the interface between two immiscible liquids is impeded, because it requires considerable energy for the resolvation and penetration of small charged particles into nonpolar or low polar solvents. It is possible to facilitate the ion transfer from water to a nonpolar solvent using complexing agents or chelators, which have relatively large sizes and can screen the charge of ion. Chelators are well soluble in organic solvent due to a large hydrophobic effect and small electrostatic contribution and thereby facilitate the ion transfer between two contacting liquid phases.

14.7 Image Forces at Plant Membranes

The image forces acting on charged particles near interfaces are defined as the forces of interaction between these particles and the "image" of free and bound charges induced by them in the region next to the interface, minus the analogous quantity in one bulk phase. As a rule, positive or negative adsorption of ions arises at the oil/water interface due to the effect of image forces. This effect is caused by different dielectric bulk properties of contact phases and by the inhomogeneous transition region where the ions and their solvation shells have a different size. As a result, different planes of closest approaches arise where ions and dipolar molecules can interact specifically with the interfacial region.

The electrostatic Gibbs energy for an ion in the vicinity of a boundary between two liquid phases with dielectric constants ε_1 and ε_2 is determined by the Born ion

solvation energy and by the interaction with its image charge (Fig. 14.8). In research dealing with the energy of image forces and with the interactions of charges at the oil/water interface, approximate models of the interface are often employed which are based on the traditional description of the interface between two local dielectrics.

In the water/hydrocarbon system the force of attraction (or repulsion) of charge in the oil phase with its image in the aqueous phase is given by

$$f(x) = -\frac{\varepsilon_w - \varepsilon_m}{\varepsilon_w + \varepsilon_m} \frac{q^2}{16\pi\varepsilon_0\varepsilon_m x^2}, \tag{14.23}$$

where x is the distance from the interface. If $\varepsilon_w > \varepsilon_m$, the charge in the nonpolar phase is attracted to its image, but if $\varepsilon_w < \varepsilon_m$, there is repulsion between the charge in a hydrocarbon phase and its image. In the case of a plant membrane placed in a medium with high dielectric permittivity, the sum from an infinite number of images must be calculated. The combined Born and image energy of an ion in a thin membrane can be estimated (Neumke and Lauger 1969) as follows:

$$\Delta G(\text{el}) = \Delta G(\text{Born}) - N_A \frac{q^2}{16\pi\varepsilon_0\varepsilon_w} \left\{\frac{1}{x} + \frac{1}{d}\sum\nolimits_{n=1}^{\infty}\left[\frac{\theta^{2n}}{n + x/d} + \frac{\theta^{2n-2}}{n - x/d} - \frac{\theta^{2n}}{n + a/d} - \frac{\theta^{2n-2}}{n - a/d}\right]\right\} \tag{14.24}$$

$$\Delta G(\text{el}) = \Delta G(\text{Born}) - N_A \frac{q^2}{16\pi\varepsilon_0\varepsilon_w} \left\{\frac{1}{x} + \frac{1}{d}\sum\nolimits_{n=1}^{\infty}\left[\frac{\theta^{2n}}{n + x/d} + \frac{\theta^{2n-2}}{n - x/d} - \frac{\theta^{2n}}{n + a/d} - \frac{\theta^{2n-2}}{n - a/d}\right]\right\},$$

where

$$\theta = -\frac{\varepsilon_m - \varepsilon_w}{\varepsilon_m + \varepsilon_w}. \tag{14.25}$$

The effect of image forces is small compared with Born electrostatic effects and depends on the ion size and membrane thickness (Fig. 14.11).

We can calculate the Gibbs energy of ion or dipole transfer $\Delta G(\text{tr})$ from an aqueous phase to a hydrocarbon phase according to the Eq. 14.22. For small ions, the electrostatic contribution is predominant in $\Delta G(\text{tr})$, so that the discrepancies of the hydrophobic relation, which becomes evident with small ions, are negligible. At large ionic radii the hydrophobic term predominates, so that calculations according to the hydrophobic equations are consistent with experimental results.

14.8 Dipolar Potential

Plant membranes differ from water/liquid hydrocarbon membranes by the presence of a 2D dimensional layer of adsorbed water dipoles and lipid heads. Even if lipids are neutral there is a positive dipolar potential within the membrane surface layer,

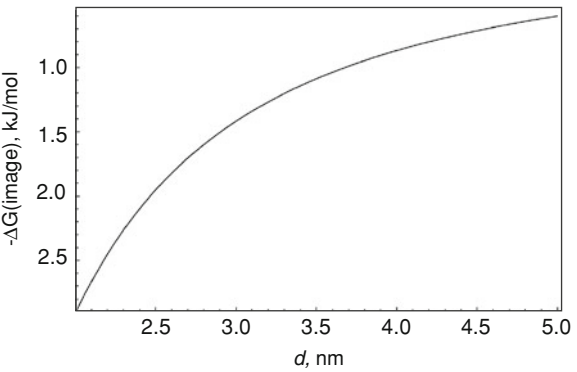

Fig. 14.11 Contribution of the image forces to electrostatic Gibbs energy of hydrated K^+ transfer on membrane thickness d calculated according to Eq. 14.24

which should be taken into account when describing specific interaction of ions with the membrane surface. For instance, the dipole–dipole specific interactions create different concentrations of cations and anions at water/membrane interfaces. Rusanov et al. (1984) and Rusanov and Kuni (1982) calculated this energy as $4\pi q\Delta P_S$, where P_S is a characteristic of the surface excess polarization, which is defined as

$$P_S = \int_a^\infty [P - P(\infty)]dr. \tag{14.26}$$

P is the local polarization vector, and the sign Δ denotes a change in the quantity upon the passage of the sphere from one medium to another.

We can estimate the specific energy of ion/dipolar layer interaction as a function of a dipole potential

$$G(\text{si}) = -zeF\phi_s, \tag{14.27}$$

where ze is the charge of ions, F is the Faraday potential, and ϕ_s is dipolar membrane surface potential. Usually ϕ_s is estimated for bilayers to be between -100 and -200 mV (Flewelling and Hubbell 1986b; Gawrish et al. 1992). At nitrobenzene/water and 1,2-dichloroethane/water interfaces dipolar potential, measured directly at the point of zero free charge, is about -20 to -50 mV (Volkov 1996) in the absence of phospholipids and -100 to -200 mV in the presence of phospholipid monolayer (Ikonen et al. 2007; Mälkiä et al. 2004; Murtomaki et al. 2001). The direct method of dipolar potential determination at membranes is to measure the dependence of membrane permeabilities of two opposite charged hydrophobic ions having the same ionic radius. Such ions can be, for example, tetraphenylphosphonium ($TPhP^+$) and tetraphenylborate ($TPhB^-$) (Volkov et al. 1997a). They have the same electrostatic and hydrophobic effects, but opposite effects as to a dipole potential sign. Figure 14.12 shows the difference of membrane permeability coefficient for $TPhP^+$ and $TPhB^-$ due to the dipolar potential.

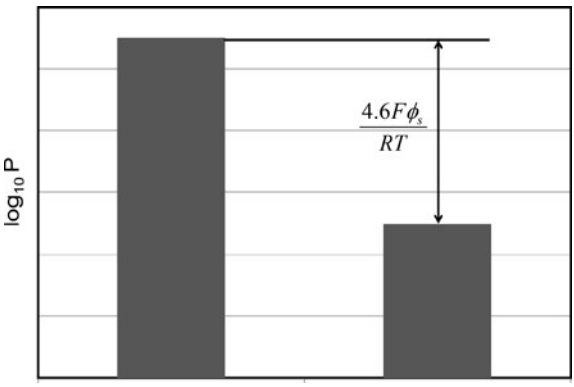

Fig. 14.12 The method of a membrane dipolar potential determination from the measurement of the difference in membrane permeabilities of a hydrophobic cation tetraphenylphosphate ($TPhP^+$) and hydrophobic anion tetraphenylborate ($TPhB^-$) of the same radius

It is possible to calculate the permeability of membranes for the partition model of ion or molecule transfer. The partition coefficient of an ion (K_i) is equal (Markin and Volkov 1987a, b, c) to:

$$K_i = \exp(-\Delta G_i^0(\mathrm{tr})/RT). \tag{14.28}$$

A permeability coefficient (*Pi*) is the number of ions or molecules of crossing in unit time a unit area of the membrane, when a unit concentration difference is applied across the membrane. The permeability coefficient is a directly measurable quantity and it is related to the partition coefficient by the expression

$$P_i = D_i K_i / d, \tag{14.29}$$

where D_i is ion diffusion coefficient and d is the membrane thickness. Substituting K_i from Eqs. 14.28 into 14.29 allows P_i to be calculated directly. The partition coefficient and calculated permeability coefficient have extreme parameter sensitivity with respect to an ionic radius. Substituting radii of bare (nonhydrated) ions such as sodium and potassium in this calculation gives values that are too small for mermbrane permeability when compared with experimental data, and the radius of a bare proton leads to absurd values. On the other hand, substituting hydrated radii gives permeability values surprisingly close to those measured experimentally (Table 14.1).

14.9 Dipole Partition

It is important to analyze the energetic profile of dipole molecules at the interface between two immiscible liquids. Let us consider that molecule has dipolar moment μ_1 and it is located in phase w with dielectric permittivity ε_w. Its image μ_2 is located in phase m with the dielectric permittivity ε_m. The dipole μ_1 has angle Θ with an axis x. The interface is located at $x = 0$. The force of an interaction of a dipole with its image is (Volkov et al. 1997a):

Table 14.1 Bare and hydrated radii of ions

Ion	Bare ion radius (nm)	Hydrated radius (nm)
$H3O^+$	0.115	0.28
$H9O4^+$	0.395	0.395
Li^+	0.094	0.382
Na^+	0.117	0.358
Ag^+	0.126	0.341
$NH4^+$	0.148	0.331
K^+	0.149	0.331
Rb^+	0.163	0.329
Cs^+	0.186	0.329
Be^{2+}	0.031	0.459
Mg^{2+}	0.072	0.428
Zn^{2+}	0.074	0.430
Cd^{2+}	0.097	0.426
Ca^{2+}	0.100	0.412
Pb^{2+}	0.132	0.401
Al^{3+}	0.053	0.480
OH^-	0.133	0.300
F^-	0.116	0.352
Cl^-	0.164	0.332
Br^-	0.180	0.330
I^-	0.205	0.331
$NO3^-$	0.179	0.340

$$f(x) = -\frac{3(\varepsilon_w - \varepsilon_m)\vec{\mu}_1^2}{4\pi\varepsilon_0(\varepsilon_w + \varepsilon_m)\varepsilon_m(2x)^4}(1 + \cos^2\Theta). \tag{14.30}$$

Function $f(x)$ is positive if $\varepsilon_w > \varepsilon_m$ and there exists a repulsion of the dipole from the interface.

Energy of the dipole interaction with its image can be calculated as

$$E(x, \Theta) = \int_0^\infty f(x)dx \tag{14.31}$$

and substituting (14.30) into (14.31) gives the equation:

$$E(x, \Theta) = -\frac{(\varepsilon_w - \varepsilon_m)\mu_1^2}{8\pi\varepsilon_0(\varepsilon_w + \varepsilon_m)\varepsilon_m(2x)^3}(1 + \cos^2\Theta). \tag{14.32}$$

There are two equilibrium conditions $\Theta = 0$ and $\Theta = \pi/2$ and the stable state occurs when the dipole is perpendicular to the interface. It is possible to determine the thickness of a layer in which dipoles are oriented perpendicular to the interface supposing that $E(x,0)$–$E(x,\pi/2)$ exceeds kT:

$$x \approx \sqrt[3]{\frac{(\varepsilon_w - \varepsilon_m)\mu_1^2}{64\pi\varepsilon_0(\varepsilon_w + \varepsilon_m)\varepsilon_m kT}}. \tag{14.33}$$

For the water/decane interface, $x = 0.14$ nm and this result means that only one monolayer of water is oriented at the interface by image forces.

When a molecule with a permanent dipole moment μ is surrounded by other particles, the inhomogeneous field of the permanent dipole polarizes its environment. In the surrounding particles moments proportional to the polarizability are induced, and if these particles have a permanent dipole moment their orientation is influenced. An exact calculation of the consequences of these two effects may be made using nonlocal electrostatics.

Bell (1932) considered an ideal dipole in the center of a spherical cavity and calculated the Gibbs energy of a dipole molecule transferred from vacuum to a medium of dielectric constant ε

$$\Delta^i_{\text{vac}}G = -N_A \frac{\mu^2}{12\pi\varepsilon_0 a^3}\left(\frac{\varepsilon - 1}{2\varepsilon + 1}\right). \tag{14.34}$$

Bell's model consists of a spherical cavity with radius a in a continuous dielectric of dielectric constant ε. Situated in the center of the cavity is a nonpolarizable point dipole with moment μ. In this simplified picture of the interaction between a permanent dipole and its surroundings, the value has chosen for a influences the result. Bell took a about equal to the radius of the molecule.

The electrostatic Gibbs energy of an ideal dipole transfer from the phase w to the solvent m can be calculated using the thermodynamic cycle (Volkov et al. 1997a):

$$\Delta G_{\text{dip}} = -\frac{N_A v_1^2}{12\pi\varepsilon_0 a^3}\left(\frac{\varepsilon_m - 1}{2\varepsilon_m + 1} - \frac{\varepsilon_w - 1}{2\varepsilon_w + 1}\right) = \frac{N_A \mu_1^2}{4\pi\varepsilon_0 a^3}\left(\frac{\varepsilon_w - \varepsilon_m}{(2\varepsilon_w + 1)(2\varepsilon_m + 1)}\right), \tag{14.35}$$

where μ_1 is the dipole moment and a is the effective dipole size. The dipole moment μ_1 can vary from solvent to solvent. For simplicity, we will discuss the case when the dipolar moment of a solute is the same in phases w and m.

The Gibbs energy of image forces for dipole in membrane (Arakelyan and Arakelyan 1983; Arakelyan et al. 1985) is

$$\Delta G_{I(\text{dip})} = -\frac{N_A \mu_1^2}{6\pi\varepsilon_0\varepsilon_m d^3}\sum_{i=1}^{\infty}\left(\frac{\Theta^{2i-1}}{(2i - 1 - \alpha)^3} + \frac{\Theta^{2i-1}}{(2i - 1 + \alpha)^3}\right), \tag{14.36}$$

where

$$\Theta = (\varepsilon_w - -\varepsilon_m)/(\varepsilon_w + \varepsilon_m) \text{ and } \alpha = 2x/d. \tag{14.37}$$

In Eq. 14.37, x is the distance between dipole and the middle of the membrane.

The total electrostatic Gibbs energy of the dipole profile can be evaluated from Eqs. 14.35 and 14.36:

$$\Delta G_{\text{dip}} = \frac{N_A \mu_1^2}{4\pi\varepsilon_0 a^3}\left(\frac{\varepsilon_w - \varepsilon_m}{(2\varepsilon_w + 1)(2\varepsilon_m + 1)}\right) - \frac{N_A \mu_1^2}{6\pi\varepsilon_0 \varepsilon_m d^3}\sum_{i=1}^{\infty}\left(\frac{\Theta^{2i-1}}{(2i - 1 - \alpha)^3} + \frac{\Theta^{2i-1}}{(2i - 1 + \alpha)^3}\right). \tag{14.38}$$

The image energy strongly depends on the membrane thickness and decreases with increasing thickness.

The water concentration in a hydrophobic region of a membrane can be calculated from the estimated Gibbs energy of water molecule transfer from water to the liquid hydrocarbon as

$$c_m = c_w \exp(-\Delta G(\text{tr})/RT). \tag{14.39}$$

Figure 14.13 shows the dependence of water concentration on liquid membrane thickness.

Using Eqs. 14.28 and 14.38, it is possible to calculate the permeability of molecules across a membrane. ΔG(si) is approximated by 19 kJ/mol for the breakage of a hydrogen bond between water molecules.

Figure 14.14 illustrates how the water permeability coefficient is affected by the thickness of the membrane. Although permeability becomes noticeably smaller with increasing membrane thickness, the magnitude of this decrease is much smaller than that observed for protons. The permeability coefficient for the longest lipid (2.4×10^{-2} cm/s) is only about five times lower than for the shortest (5.0×10^{-3} cm/s) (Paula et al. 1996; Volkov et al. 1997b). Furthermore, the slope of the curve is roughly constant which is in sharp contrast to the biphasic behavior observed for potassium ions.

Glycerol and urea display quite similar permeabilities, with glycerol being slightly more permeable than urea. The values were in the range of 1.1×10^{-6}–6.2×10^{-6} cm/s and 3.4×10^{-6}–6.0×10^{-7} cm/s, for glycerol and urea, respectively (Paula et al. 1996). This indicates that the membrane represents a significantly higher diffusion barrier to these molecules than to water or protons. The slope of permeability coefficient plotted against bilayer thickness resembles that of water with permeability values for the longest and shortest lipid differing by roughly 5-fold.

Despite the interesting results arising from considerations of both electrostatic and hydrophobic contributions to ionic permeation, we must be careful in applying them uncritically to ionic permeation events in membranes. The main difficulty is that plant membranes are not ideal slabs of a hydrocarbon with uniform dielectric properties, but instead are highly dynamic, with considerable fluctuation around the means of thickness and intermolecular distance within the bilayer. In the section to follow, we will examine an alternative mechanism for permeation of ions across membranes, and then compare experimental results with theoretical predictions from both models.

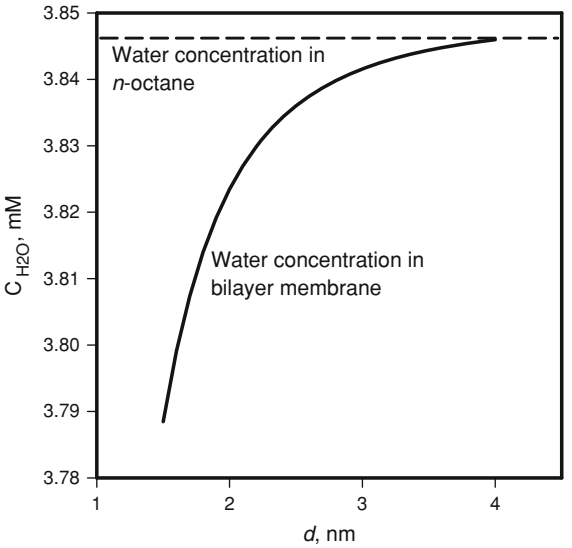

Fig. 14.13 Dependence of the water concentration on the thickness of a bilayer phospholipid membrane

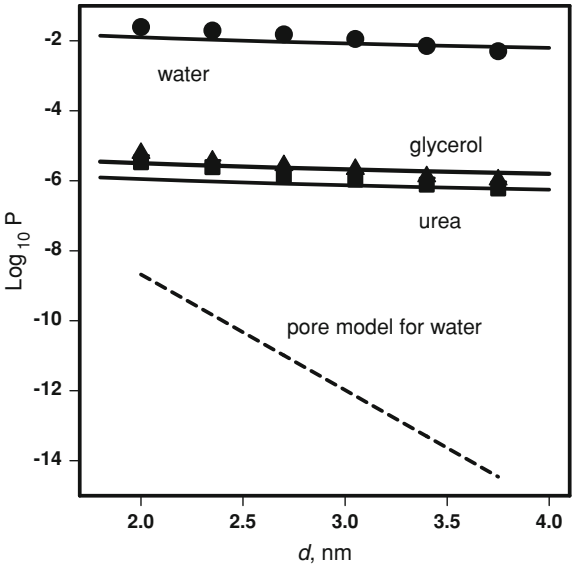

Fig. 14.14 Dependence of water, urea, and glycerol permeability on membrane thickness d. Points are experimental data, solid lines are calculated according to the solubility-diffusion model. Parameters: $r_{water} = 0.12$ nm, $r_{urea} = 0.28$ nm, $r_{glycerol} = 0.29$ nm, $\gamma_{\alpha/\beta} = 51$ mN m^{-1}, $p_{water} = 1.85$ D, $a_{water} = 1.38$ Å, $\Delta G(\text{si})_{(water)} = 33$ kJ mol^{-1}, $\Delta G(\text{si})_{(urea/glycerol)} = 3 \times 25$ kJ mol^{-1}, $D_{water} = 4.59 \times 10^{-5}$ cm^2 s^{-1}, $D_{urea} = 1.38 \times 10^{-5}$ cm^2 s^{-1}, $D_{glycerol} = 1.06 \times 10^{-5}$ cm^2 s^{-1} (after Volkov et al. 1998)

14.10 Passive Membrane Transport by Partition or Transient Pore Mechanism

Although the partition model can describe the barrier property of membranes under specified conditions, certain assumptions regarding the hydrated radius of the permeating species are required. We will now consider an alternative hypothesis, in which fluctuations in membrane structure produce rare transient defects that allow solutes to bypass the electrostatic and hydrophobic energy barriers.

For the barrier function to operate, the lipid bilayer forming the basis of the membrane must be continuous and devoid of structural defects. If the membrane is rearranged so that the defects of the through type appear, the membrane properties change. If pores that are small relative to the cell radius appear, an elevated background conductance of the membrane can arise for ions from both extra- and intracellular solutions. If the pore size is comparable with that of the intracellular protein molecules, cell lysis takes place, i.e., all the cell contents are released into the external medium.

Two types of pore structures in the membranes are possible. They can be roughly classified as hydrophobic and hydrophilic defects. During formation of a transient hydrophobic defect, lipid molecules are moved apart by thermal fluctuations so that the membrane hydrophobic core makes contact with and is penetrated by the aqueous bulk phase. Hydrophilic defects are formed if the lipid molecules are tilted into the transient defect so that it is lined with lipid polar head groups. In both the hydrophobic and hydrophilic defects pore formation results from dynamic properties of the membranes and the equilibrium pore distribution is relatively constant over time. However, formation of hydrophilic pores is more likely. Hydrophilic pores can arise due to membrane thermal fluctuation or as a result of external stimuli, such as membrane extension by osmotic pressure, reactions with chemical compounds, and electrical field effects. Pore formation results in dynamic changes of the membrane properties, but thermal fluctuations in the bilayer lead to an equilibrium pore distribution in the membrane.

Markin and Kozlov (1985) analyzed the distribution of hydrophilic pore radii in a membrane at thermodynamic equilibrium from the point of view of the elasticity or flexure of the lipid bilayer and its spontaneous curvature. The pore size distribution was calculated for three model membranes: uniform membranes with a constant spontaneous curvature, membranes with clusters of high spontaneous curvature, and membranes composed of two types of lipids, one with a high spontaneous curvature. Their calculations showed that the presence of asymmetric lipid molecules with positive spontaneous curvature should increase the number of pores in the membrane. The pore-related membrane permeability to uncharged molecules was estimated on the basis of this theory. The calculated values for water permeability were distinctly lower than the experimentally estimated values, suggesting that the mechanism of water transport across the membrane is mainly due to the direct passage of water molecules across the membrane hydrophobic layer.

Although small, neutral substances like water generally move across membranes by diffusion of individual molecules, there is still the possibility that water is occasionally involved in the formation of transient hydrated defects. A pertinent model was recently presented by Benjamin (1993) who used molecular dynamics and computer simulations to investigate the interface between water and a non-polar phase. An intriguing property of the interface is that it is surprisingly rough, with "fingers" of several water molecules occasionally entering the non-polar phase. Benjamin (1993) showed that ion permeation of the interface is linked to the presence of such water fingers. Wilson and Pohorille (1996) performed molecular dynamics simulations of the transport of Na^+ and Cl^- across a lipid bilayer located between two water lamellae. The ion located in water has no influence on the structure of the membrane. Permeation of hydrated ions into membrane is accompanied by the formation of deep, asymmetric thinning defects in the bilayer. As the hydrated ion crosses the midplane of the membrane, the deformation switches sides. The initial defect slowly relaxes, and a defect forms in the outgoing side of the membrane.

Thermal fluctuations in bilayers produce transient pores lined with lipid head groups (Hamilton and Kaller 1990a, b). The formation of pores considerably lowers the free Gibbs energy barrier to transfer of the ions across the membrane and increases the permeabilities of membranes to ions. Ion flux was calculated from the collision frequency of the ions with the bilayer surface and the total area of pores in the bilayer that are large and deep enough to allow an ion to cross the bilayer. The total number of pores, f_p can be expressed as the following integral:

$$fp = \int_{s_i}^{\infty} sn(s)\,\mathrm{d}s, \tag{14.40}$$

where $n(s)\mathrm{d}s$ is the number of pores per membrane area between pore area s and $s + ds$. The pore area distribution can be written as

$$n(s) = n_0 \exp(-k_1 s/RT) \exp(-k_2 d/RT), \tag{14.41}$$

where n_o is the maximum number of discrete pores in the bilayer (taken to be half the number of lipid molecules in the bilayer), and the exponential terms are related to the probabilities of forming a pore of area s and depth d, respectively. If an ion of a given radius can permeate the bilayer, s is taken to be the area of that ion, and d is the bilayer thickness. Given these assumptions the ionic permeability P_i (Hamilton and Kaller 1990a,b) is

$$P_i = \frac{Di\sigma n_0 RT}{R_{\mathrm{avg}} A_{\mathrm{mem}} k_1} \left[s_i + \frac{RT}{k_1}\right] \exp[-k_1 s_i/RT] \exp[-k_2 d/RT]\,. \tag{14.42}$$

Here, D_i is the ion diffusion coefficient, $\exp(-k_1 s/RT)$ is the probability of forming a pore of area s, $\exp(-k_2 d/RT)$ is the probability of forming a pore of depth d, σ is the concentration enhancement at the membrane surface due to the electrical double

layer effects, R_{avg} is the vesicle radius, A_{mem} is the membrane area per mL of solution, R is the gas constant, and T the absolute temperature. Pores can be induced in membranes by applying mechanical stress or an electric field.

The two models described above were tested (Deamer and Volkov 1995; Paula et al. 1996, 1998; Volkov et al. 1997b). An important variable under experimental control is bilayer thickness, which can be changed by choosing lipids with longer or shorter hydrocarbon chains. Proton and potassium fluxes across liposomes composed of phospholipids with fatty acid chain lengths varying from 14 to 24 carbons were measured. Permeability decreased logarithmically as membrane thickness increased in the shorter chain lipids, following the slope of the line predicted by the transient pore mechanism. However, permeability tended to level off in the thicker bilayers (C16 and C18 lipids) approaching the lines predicted by the partition model. The results suggest that the mechanism of ionic permeation may depend on membrane thickness: thinner bilayers have many transient defects that allow rapid permeation of small ionic species, while in thicker bilayers defects become so rare that partitioning mechanisms dominate ionic flux.

The permeability of lipid bilayers to protons is five to six orders of magnitude greater than to other monovalent cations. This result is consistent with the partitioning model only if every proton carries at least four waters of hydration into the bilayer phase (Deamer and Volkov 1995). The alternative proposed here is that transient hydrated defects occur in the membrane. Figure 14.15 summarizes the Grotthuss mechanism: an excess proton is incorporated at one end of a single file of water molecules, and a series of proton transfers takes place between adjacent water molecules until a proton is released at the other end. If water in the defects has significant hydrogen bonding, as it does in the bulk phase, hydrogen bond exchange could account for the vastly greater proton permeation rates without any assumptions regarding water of hydration. That is, protons could cross the membrane by "hopping" along hydrogen bonded chains of water in the defect. This concept was proposed by Nagle and Morowitz (1978) who coined the term "proton wire" for hydrogen bonded networks of amino acid side chains. Nagle and Tristram-Nagle (1983) extended this concept to more general proton transport mechanisms, including water, and developed the concept of "transient hydrogen bonded chains" (tHBC) to describe proton transport in clusters of water molecules associated through hydrogen bonds.

Both models, partition and transient aqueous pores, contribute to the membrane permeability. Zahn and Brickman (2001) studied proton transport across BLM according to diffusive permeation and transport via aqueous pores using a mixed quantum–classical molecular dynamics simulation technique. Authors found that proton diffusion through BLM requires the permeation of an $H^+(H_2O)_n$ complex with $n \geq 4$.

Marrink et al. (1996) studied proton transport across transient single-file water pores in lipid membrane by molecular dynamics simulations and found that the nature of the pore is very transient, with a mean lifetime of a few picoseconds. The total excess free energy for the full water pore is 108 ± 10 kJ/mol and this value indicates that such a complete water pore spanning the membrane is a rare

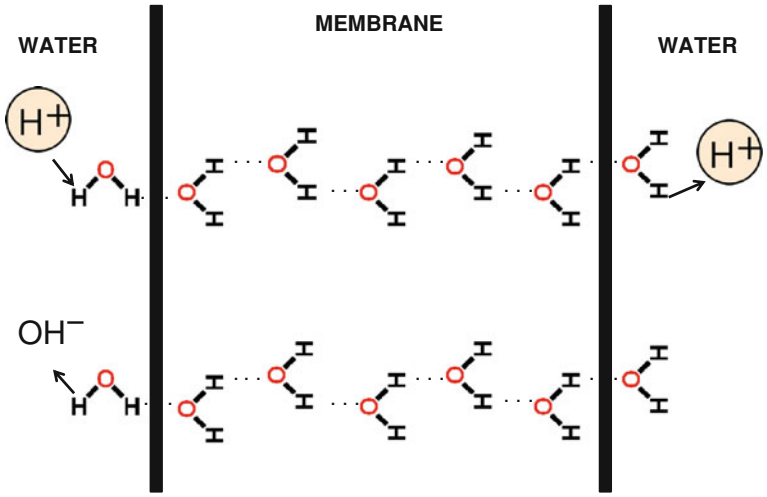

Fig. 14.15 Grotthuss (1806) mechanism of proton transfer through a transient aqueous chain

phenomenon. The rapid translocation of protons along a chain of hydrogen-bonded water molecules, or proton wire, is thought to be an important mechanism for proton permeation through transmembrane channels or thin lipid membranes. Proton transfer in the wire is a semi-collective process that results from the subtle interplay of rapid hydrogen-bond length fluctuations along the water chain.

Two mechanisms have been discussed to account for solute permeation of lipid bilayers. Partitioning into the hydrophobic phase of the membrane, followed by diffusion is accepted by many for the permeation of water and other small neutral solutes, but transient pores have also been proposed to account for both water and ionic solute permeation. These two mechanisms make distinctively different predictions about the permeability coefficient as a function of membrane thickness. Whereas the solubility-diffusion mechanism predicts only a modest variation related to bilayer thickness, the pore model predicts an exponential relationship. The results for water and the neutral permeating solutes are best explained by the solubility-diffusion mechanism. The results for protons and potassium ions in shorter chain lipids are consistent with the transient pore model but better fit the theoretical line predicted by the solubility-diffusion model at longer chain lengths (Deamer and Volkov 1995; Paula et al. 1996; 1998; Volkov et al. 1997a, b).

14.11 Conclusions

Membranes have important structural and functional roles in the plant physiology. Membrane permeability is extremely sensitive to size of a solute. The Gibbs energy of partitioning has two primary contributing factors, which were described

in terms of electrostatic and hydrophobic effects. The electrostatic term dominates permeation of smaller ions, but the hydrophobic effect becomes significant for larger ions to the extent that the Gibbs energy can be negative for ions larger than 0.45 nm diameter. A significant point is that the free energy of the hydrophobic effect is opposite in sign to the electrostatic effect.

The effect of image forces is small compared with hydrophobic and Born electrostatic effects. Additionally, they depend on the ion size and membrane thickness. Even if the lipids are neutral, there is a dipolar potential within the membrane surface layer, which should be taken into account when describing the specific interaction of ions with the membrane interface. For instance, the ion–dipole- and dipole–dipole-specific interactions create different concentrations of cations and anions at water/membrane interfaces.

Surface potentials represent a potential difference between the membrane interface and the bulk aqueous phase. These potentials are responsible for ion binding at the membrane/water interface and significant difference between cation and anion membrane permeabilities.

In order to partition into hydrophobic region of the membrane, penetrating molecules must be hydrophobic enough to overcome the enegy losses that occur in breaking the hydrogen bonds with water or the lipid head groups. This process has a considerable energy barrier for water and other molecules, which exhibit strong hydrogen bonding tendencies.

Acknowledgments This work was supported by the grant CBET-1064160 from the National Science Foundation.

References

Abramson AA (1981) Surface active compounds. Properties and applications. Khimiya, Leningrad

Antonow G (1907) Sur la tension superficielle a la limite de deux couches. J Chim Phys 5: 372–385

Arakelyan VB, Arakelyan SB (1983) Energetic profile of a dipole molecule in the thin membrane. Biol Zh Armenii 36:775–779

Arakelyan VB, Arakelyan SB, Avakyan TsM, Aslanyan VM (1985) Electrostatic effects on transport of water across bilayer lipid membranes. Biofizika 30:170–171

Becker M, Kerstiens G, Schönherr J (1986) Water permeability of plant cuticles: permeance, diffusion and partition coefficients. Trees 1:54–60

Bell RP (1932) The electrical energy of dipole molecules in solution and solubilities of ammonia, hydrogen chloride, and hydrogen sulfite in various solvents. J Chem Soc 32:1371–1382

Bellaloui N, Brown PH, Dandekar AM (1999) Manipulation of in vivo sorbitol production alters boron uptake and transport in tobacco. Plant Physiol 119:735–741

Bemporad D, Luttmann C, Essex JW (2004) Computer simulation of small molecule permeation across a lipid bilayer: dependence on bilayer properties and solute volume, size, and cross-sectional area. Biophys J 87:1–13

Benga G (1989) Water transport in biological membranes. CRC Press, Boca Raton, pp 41–75

Benjamin I (1993) Mechanism and dynamics of ion transfer across a liquid–liquid interface. Science 261:1558–1560

Blandamer MJ, Symons MCR (1963) Significance of new values for ionic radii to solvation phenomena in aqueous solution. J Phys Chem 67:1304–1306
Born M (1920) Volumen und hydrationswärme der ionen. Z Phys 1:45–48
Briggs GG, Bromilow RH, Evans AA (1982) Relationship between lipophilicity and root uptake and translocation of non-ionized chemicals by barley. Pestic Sci 13:495–504
Buchanan BB, Gruissem W, Jones RL (2000) Biochemistry and molecular biology of plants. American Society of Plant Physiologists, Rockville
Chiou CT, Sheng G, Manes M (2001) A partition-limited model of the plant uptake of organic contaminants from soil and water. Environ Sci Technol 35:1437–1444
Collander R (1937) The permeability of plant protoplasts to non-electrolytes. Trans Faraday Soc 33:985–990
Collander R (1941) Selective absorption of cations by higher plants. Plant Physiol 16:691–720
Collander R (1949) The permeability of plant protoplasts to small molecules. Physiol Plant 2:300–311
Collander R (1950) The distribution of organic compounds between iso-butanol and water. Acta Chem Scand 4:1085–1098
Collander R (1951) The partition of organic compounds between higher alcohols and water. Acta Chem Scand 5:774–780
Collander R (1954) The permeability of *Nitella* cells to non-eleetrolytes. Physiol Plant 7:420–445
Deamer DW, Volkov AG (1995) Proton permeation of lipid bilayers. In: Disalvo EA, Simon SA (eds) Permeability and stability of lipid bilayers. CRC Press, Boca Raton
Dogonadze RR, Kornyshev AA (1974) Polar-solvent structure in theory of ion solvation. J Chem Soc, Faraday Trans 2(70):1121–1132
Dordas C, Chrispeels MJ, Brown PH (2000) Permeability and channel-mediated transport of boric acid across membrane vesicles isolated from squash roots. Plant Physiol 124:1349–1361
Flewelling RF, Hubbell WL (1986a) Hydrophobic ion interactions with membranes: thermodynamic analysis of tetraphenylphosphonium binding to vesicles. Biophys J 49:531–540
Flewelling RF, Hubbell WL (1986b) The membrane dipole potential in a total membrane potential model. Biophys J 49:541–552
Gawrish K, Ruston D, Zimmerberg J, Parsegian VA, Rand RP, Fuller N (1992) Membrane dipole potentials, hydration forces, and the ordering of water at membrane surfaces. Biophys J 61:1213–1223
Gennis RB (1989) Biomembranes: molecular structure and function. Springer Verlag, NY
Goldschmidt VM (1926) Geochem Vert Ges der Elemente, Oslo
Gourary BS, Adrian FS (1960) Wave functions for electron-excess color centers in alkali halide crystals. Solid State Phys 10:127–247
Grotthus CJT (1806) Sur la décomposition de l'eau et des corps qu'elle tient en dissolution à l'aide de l'électricité galvanique. Ann Chim 58:54–73
Haas K, Schönherr J (1979) Composition of soluble cuticular lipids and water permeability of cuticular membranes from citrus leaves. Planta 146:399–403
Hamilton RT, Kaler EW (1990a) Alkali metal ion transport through thin bilayers. J Phys Chem 94:2560–2566
Hamilton RT, Kaler EW (1990b) Facilitated ion transport through thin bilayers. J Membr Sci 54:259–269
Hsu FC, Marxmiller RL, Yang AYS (1990) Study of root uptake and xylem translocation of cinmethylin and related compounds in detopped soybean roots using a pressure chamber technique. Plant Physiol 93:1573–1578
Ikonen M, Murtomaki L, Kontturi K (2007) An electrochemical method for the determination of liposome–water partition coefficients of drugs. J Electroanal Chem 602:189–194
Kornyshev AA (1981) Nonlocal screening of ions in a structurized polar liquid. New aspects of solvent description in electrolyte theory. Electrochim Acta 26:1–20
Kornyshev AA, Volkov AG (1984) On the evaluation of standard Gibbs energies of ion transfer between two solvents. J Electroanal Chem 180:363–381
Ksenzhek OS, Volkov AG (1998) Plant energetics. Academic, San Diego

Landau LD, Lifshitz EM (1984) Electrodynamics of continuous media, 2nd edn. Pergamon, NY
Leontiadou H, Mark AE, Marrink SJ (2004) Molecular dynamics simulation of hydrophobic pores in lipid bilayers. Biophys J 86:2156–2164
Macdonald RC (1976) Energetics of permeation of thin lipid membranes by ions. Biochim Biophys Acta 448:193–198
Mälkiä A, Murtomäki L, Urtti A, Kontturi K (2004) Drug permeation in biomembranes in vitro and in silico prediction and influence of physicochemical properties. Eur J Pharm Sci 23: 13–47
Markin VS, Kozlov MM (1985) Pores statistics in bilayer lipid membranes. Biol Membr 2:205–223
Markin VS, Volkov AG (1987a) The standard Gibbs energy of ion resolvation and non-linear dielectric effects. J Electroanal Chem 235:23–40
Markin VS, Volkov AG (1987b) Theoretical description of Gibbs energy of ion transfer. Russ Chem Rev 56:1953–1972
Markin VS, Volkov AG (1987c) The standard Gibbs free energy of ion transfer. Sov Electrochem 23:1105–1112
Markin VS, Volkov AG (1989a) Interfacial potentials at the interface between two immiscible electrolyte solutions–some problems in definitions and interpretation. J Colloid Interface Sci 131:382–392
Markin VS, Volkov AG (1989b) The Gibbs energy of ion transfer between two immiscible liquids. Electrochim Acta 34:93–107
Markin VS, Volkov AG (1990) Potentials at the interface between two immiscible electrolyte solution. Adv Colloid Interface Sci 31:111–152
Markin VS, Volkov AG (2004) Distribution potential in small liquid–liquid systems. J Phys Chem B 108:13807–13812
Markin VS, Volkov AG, Jovanov E (2008) Active movements in plants: mechanism of trap closure by *Dionaea muscipula* ellis. Plant Signal Behav 3:778–783
Marrink SJ, Berendsen HCJ (1996) Permeation process of small molecules across lipid membranes studied by molecular dynamics simulations. J Phys Chem 100:16729–16738
Marrink SJ, Berendsen HJC (1994) Simulation of water transport through a lipid membrane. J Phys Chem 98:4155–4168
Marrink SJ, Jahnig F, Berendsen HJC (1996) Proton transport across transient single-file water pores in a lipid membrane studied by molecular dynamics simulations. Biophys J 71:632–647
Marschner H (1999) Mineral nutrition of higher plants. Academic, San Diego
Mohr H, Schopfer P (1994) Plant physiology. Springer, Berlin
Mueller P, Rudin DO, Ti Tien H, Wescott WC (1962) Reconstitution of cell membrane structure in vitro and its transformation into an excitable system. Nature 194:979–980
Murtomaki L, Manzanares JA, Mafe S, Kontturi K (2001) Phospholipids at liquid–liquid interfaces and their effect on charge transfer. In: Volkov AG (ed) Liquid interfaces in chemical, biological, and pharmaceutical applications, surfactant science series, vol 95. M Dekker, NY
Nagle JF, Morowitz HJ (1978) Molecular mechanisms for proton transport in membrane. Proc Natl Acad Sci U S A 75:298–302
Nagle JF, Tristram-Nagle S (1983) Hydrogen bonded chain mechanisms for proton conduction and proton pumping. J Membr Biol 74:1–14
Neumke B, Lauger P (1969) Nonlinear electrical effects in lipid bilayer membranes II. Integration of the generalized Nernst–Plank equations. Biophys J 9:1160–1170
Nobel PS (1999) Physicochemical and environmental plant physiology. Academic, San Diego
O'Neill SD, Keith B, Rappaport L (1986) Transport of gibberellin A1 in cowpea membrane vesicles. Plant Physiol 80:81–817
Overton E (1895) Über die osmotishen Eigenschaften der lebenden Pflanzen und Tierzelles. Vierteljahrsschr Naturforch Ges Zuerich 40:159–201
Overton E (1899) Über die allgemeinen osmotishen Eigenschaften der Zelle, ihre vermutlichen Ursachen und ihre Bedeutung fur die physiologie. Vierteljahrsschr Naturforch Ges Zuerich 44:88–114

Paula S, Volkov AG, Van Hoek AN, Haines TH, Deamer DW (1996) Permeation of protons, potassium ions, and small polar molecules through phospholipid bilayers as a function of membrane thickness. Biophys J 70:339–348
Paula S, Volkov AG, Deamer DW (1998) Permeation of halide anions through phospholipid bilayers occurs by the solubility-diffusion mechanism. Biophys J 74:319–327
Pauling L (1927) The sizes of ions and the structure of ionic crystals. J Amer Chem Soc 49: 765–790
Pohorille A, Wilson MA (1996) Excess chemical potential of small solutes across water-membrane and water-hexane interfaces. J Chem Phys 104:3760–3773
Poznansky M, Tong S, Perrin WC, Milgram JM, Solomon AK (1976) Nonelectrolyte diffusion across lipid bilayer systems. J Gen Physiol 67:45–66
Ray P (1960) On the theory of osmotic water movement. Plant Physiol 35:783–795
Rusanov AI, Dukhin SS, Yaroshchuk AE (1984) Problem of the surface layer in liquid mixtures and the electric double layer. Kolloidnyi Zh 46:490–494
Rusanov AI, Kuni FM (1982) Theory of nucleation on charged nuclei 1. General thermodynamic relationships. Kolloidnyi Zh 44:934–941
Sisskind B, Kasarnowsky J (1933) Studying of gases solubilities 2. The solubility of argon. Zh Fiz Khim 4:683–690
Taiz L, Zeiger E (1999) Plant physiology. Sinauer Associates, Sunderland
Tanford C (1980) The hydrophobic effect: formation of micelles and biological membranes. Wiley, NY
Tien TH (1974) Bilayer lipid membranes (BLM) theory and practice. M Dekker, NY
Tien TH, Ottova-Leitmannova A (2000) Membrane biophysics as viewed from experimental bilayer lipid membranes. Elsevier, Amsterdam
Tolman R (1949) The effect of droplet size on surface tension. J Chem Phys 17:333–337
Trapp S (2000) Modeling uptake into roots and subsequent translocation of neutral and ionisable organic compounds. Pest Manag Sci 56:767–778
Trapp S (2004) Plant uptake and transport models for neutral and ionic chemicals. Environ Sci Pollut Res 11(1):33–39
Tyerman SD, Steudle E (1984) Determination of solute permeability in *Chara* internodes by a turgor minimum method. Plant Physiol 74:464–468
Uhlig HH (1937) The solubilities of gases and surface tension. J Phys Chem 41:1215–1225
Volkov AG (1989) Oxygen evolution in the course of photosynthesis. Bioelectrochem Bioenerg 21:3–24
Volkov AG (1996) Potentials of thermodynamic and free zero charge at the interface between two immiscible electrolytes. Langmuir 12:3315–3319
Volkov AG (2000) Green plants: electrochemical interfaces. J Electroanal Chem 483:150–156
Volkov AG (ed) (2001) Liquid interfaces in chemical, biological, and pharmaceutical applications, surfactant science series, vol 95. M Dekker, NY
Volkov AG (ed) (2003) Interfacial catalysis. M Dekker, NY
Volkov AG (ed) (2006) Plant electrophysiology. Springer, Berlin
Volkov AG (2008a) Gibbs energy of ion and dipole transfer. In: Bard AJ, Inzelt G, Scholz F (eds) Electrochemical dictionary. Springer, Berlin, p 305
Volkov AG (2008b) Ion transport through membranes and ion channels. In: Bard AJ, Inzelt G, Scholz F (eds) Electrochemical dictionary. Springer, Berlin, pp 369–370
Volkov AG, Adesina T, Markin VS, Jovanov E (2008a) Kinetics and mechanism of *Dionaea muscipula* trap closing. Plant Physiol 146:694–702
Volkov AG, Adesina T, Markin VS, Jovanov E (2007) Closing of Venus flytrap by electrical stimulation of motor cells. Plant Signal Behav 2:139–144
Volkov AG, Baker K, Foster JC, Clemmons J, Jovanov E, Markin VS (2011a) Circadian variations in biologically closed electrochemical circuits in *Aloe vera* and *Mimosa pudica*. Bioelectrochem 81:39–45
Volkov AG, Carrell H, Adesina T, Markin VS, Jovanov E (2008b) Plant electrical memory. Plant Signal Behav 3:490–492

Volkov AG, Carrell H, Baldwin A, Markin VS (2009a) Electrical memory in Venus flytrap. Bioelectrochem 75:142–147
Volkov AG, Carrell H, Markin VS (2009b) Biologically closed electrical circuits in Venus flytrap. Plant Physiol 149:1661–1667
Volkov AG, Coopwood KJ, Markin VS (2008c) Inhibition of the *Dionaea muscipula* ellis trap closure by ion and water channels blockers and uncouplers. Plant Sci 175:642–649
Volkov AG, Deamer DW (1994) Mechanisms of the passive ion permeation of lipid bilayers: partition or transient aqueous pores. In: Allen MJ, Cleary SF, Sowers AE (eds) Charge and field effects in biosystems-4. World Scientific, Singapore
Volkov AG, Deamer DW, Tanelian DI, Markin VS (1997a) Liquid interfaces in chemistry and biology. Wiley, NY
Volkov AG, Foster JC, Ashby TA, Walker RK, Johnson JA, Markin VS (2010a) *Mimosa pudica*: electrical and mechanical stimulation of plant movements. Plant Cell Environ 33:163–173
Volkov AG, Foster JC, Baker KD, Markin VS (2010b) Mechanical and electrical anisotropy in *Mimosa pudica*. Plant Signal Behav 5:1211–1221
Volkov AG, Foster JC, Markin VS (2010c) Molecular electronics in pinnae of *Mimosa pudica*. Plant Signal Behav 5:826–831
Volkov AG, Foster JC, Markin VS (2010d) Signal transduction in *Mimosa pudica*: biologically closed electrical circuits. Plant Cell Environ 33:816–827
Volkov AG, Foster JC, Markin VS (2011b) Anisotropy and nonlinear properties of electrochemical circuits in leaves of *Aloe vera* L. Bioelectrochem 81:4–9
Volkov AG, Wooten JD, Waite AJ, Brown CR, Markin VS (2011c) Circadian rhythms in electrical circuits of *Clivia miniata*. J Plant Physiol 168:1753–1760
Volkov AG, Kornyshev AA (1985) Dependence of the free Gibbs energy of resolvation during ion transfer from one solvent to another on the ion size. Sov Electrochem 21:814–817
Volkov AG, Markin VS (2002) Electrochemical double layers: liquid–liquid interfaces. In: Bard AJ, Stratmann M (eds) Encyclopedia of electrochemistry: thermodynamics of electrified interfaces, vol 1. Wiley-VCH, Weinheim
Volkov AG, Paula S, Deamer DW (1997b) Two mechanisms of permeation of small neutral molecules and hydrated ions across phospholipid bilayers. Bioelectrochem Bioenerg 42: 153–160
Volkov AG, Pinnock MR, Lowe DC, Gay MS, Markin VS (2011d) Complete hunting cycle of dionaea muscipula: consecutive steps and their electrical properties. J Plant Physiol 168: 109–120
Vorotyntsev MA, Kornyshev AA (1993) Electrostatics of a medium with the spatial dispersion. Nauka, Moscow
Waddington TC (1966) Ionic radii and the method of the undetermined parameter. Trans Faraday Soc 62:1482–1492
Wilson MA, Pohorille A (1996) Mechanism of unassisted ion transport across membrane bilayers. J Am Chem Soc 118:6580–6587
Zahn D, Brickmann J (2001) Quantum-classical simulation of proton transport via a phospholipid bilayer. Phys Chem Chem Phys 3:848–852

Index

A. G. Volkov (ed.), *Plant Electrophysiology*,
DOI: 10.1007/978-3-642-29119-7, © Springer-Verlag Berlin Heidelberg 2012